NASA Contractor Report 3248

Rotary Balance Data for a Typical Single-Engine General Aviation Design for an Angle-of-Attack Range of 20° to 90°

III—Influence of Control Deflection on Predicted Model D Spin Modes

John N. Ralston and Billy P. Barnhart

CONTRACT NAS1-16205
JUNE 1984

NASA

NASA Contractor Report 3248

Rotary Balance Data for a Typical Single-Engine General Aviation Design for an Angle-of-Attack Range of 20° to 90°

III—Influence of Control Deflection on Predicted Model D Spin Modes

John N. Ralston and Billy P. Barnhart
Bihrle Applied Research, Inc.
Jericho, New York

Prepared for
Langley Research Center
under Contract NAS1-16205

National Aeronautics
and Space Administration

Scientific and Technical Information Office

1984

SUMMARY

The influence of control deflections on the rotational flow aerodynamics and on predicted spin modes is discussed for a 1/6-scale general aviation airplane model. The model was tested for various control settings at both zero and ten degree sideslip angles. Data were measured, using a rotary balance, over an angle-of-attack range of 20° to 90°, and for clockwise and counter-clockwise rotations covering an $\Omega b/2V$ range of 0 to 0.5.

With pro-spin controls, a steep spin is predicted for this airplane that agrees reasonably well with preliminary free-spinning model results. However the predicted spin mode was somewhat steeper than the preliminary unpublished flight test spin results. This difference is most likely due to the effect of Reynolds number on the dynamic stalling characteristics of a rotating wing. High Reynolds number rotary balance tests are needed to quantify this effect.

The basic model, as tested, indicated that the airplane would be damped in yaw but would generally exhibit propelling rolling moments. The rudder effectiveness began to diminish above 40° angle of attack and was ineffective above 60° angle of attack. The ailerons were effective in roll up to 80° angle of attack and produced adverse yaw only at angles of attack above 50°.

INTRODUCTION

The NASA Langley Research Center is conducting a broad general

aviation stall/spin research program, which includes spin-tunnel and free-flight radio-control model tests, as well as full-scale flight tests for a number of configurations typical of light, general aviation airplanes. As a part of this effort, rotary balance tests were conducted in the Langley Spin Tunnel to establish a rotational flow aerodynamic base for analysis of model and full-scale flight results.

Rotary balance data were obtained for a representative, single-engine, general aviation model, referred to as model D. The test results were divided into three areas, each of which is discussed in a separate report. Reference 1 discusses the influence of each airplane component, as well as body length and wing location, on the rotational aerodynamic characteristics. Reference 2 presents the effect of horizontal tail location in the presence of each of two wing locations and two body lengths. The aerodynamic effectiveness of the controls and their influence on predicted spin modes are discussed herein for the same configuration used for full-scale and free-spinning model tests. The appendices in the above references contain the data measured during the subject studies.

SYMBOLS

The units for physical quantities used herein are presented in U.S. Customary Units.

b	wing span, ft
c	mean aerodynamic chord, in.

C_N normal-force coefficient, $\frac{\text{Normal force}}{qS}$

C_A axial-force coefficient, $\frac{\text{Axial force}}{qS}$

C_Y side-force coefficient, $\frac{\text{Side force}}{qS}$

C_l rolling-moment coefficient, $\frac{\text{Rolling moment}}{qSb}$

C_m pitching-moment coefficient, $\frac{\text{Pitching moment}}{qSc}$

C_n yawing-moment coefficient, $\frac{\text{Yawing moment}}{qSb}$

q free-stream dynamic pressure, lb/ft^2

S wing area, ft^2

V free-stream velocity, ft/sec

α angle of attack, deg

β angle of sideslip, deg

δ_a aileron deflection, positive when right aileron is down

$(\delta_{a_{right}} - \delta_{a_{left}})/2$, deg

δ_H horizontal tail deflection, positive when trailing edge is down, deg

δ_r rudder deflection, positive when trailing edge is to the left, deg

Ω angular velocity about spin axis, rad/sec

$\Omega b/2V$ spin coefficient, positive for clockwise spin

Abbreviations:

cg center of gravity

SR spin radius

TEST EQUIPMENT

A rotary balance measures the forces and moments acting on a model while it is subjected to rotational flow conditions. Historical background for this testing technique is discussed in reference 3. A photograph and sketch of the rotary balance apparatus installed in the Langley Spin Tunnel are shown in figures 1 and 2, respectively. The system's rotary arm, which rotates about a vertical axis at the tunnel center, is supported by a horizontal boom and is driven by a motor mounted external to the test section.

A NASA six-component strain gauge balance, affixed to the bottom of the rotary balance apparatus and mounted inside the model, is used to measure the normal, lateral, and longitudinal forces, and the yawing, rolling, and pitching moments acting about the model body axis. Controls located outside of the tunnel are used to activate motors on the rotary rig, which position the model to the desired attitude. The angle-of-attack range of the rig is 0° to 90°, and the sideslip angle range is $\pm 15^{\circ}$. Spin radius and lateral displacement motors are used to position the moment center of the balance on, or at a specific distance from, the spin axis. (This is done for each combination of angle of attack and sideslip angle.) It is customary to mount the balance to the model such that its moment center is at the location about which the aerodynamic moments are desired. Electrical currents from the balance and to the motors on the rig are conducted through slip rings. Figure 2 shows how the rig is positioned in angle of attack and sideslip.

The system is capable of rotating up to 90 rpm in either direction.

A range of $\Omega b/2V$ values can be obtained by adjusting rotational speed and/or tunnel air flow velocity. (Static aerodynamic forces and moments are obtained when $\Omega=0$.)

The data acquisition, reduction, and presentation system is composed of a 12-channel scanner/voltmeter, a mini-computer with internal printer, a plotter, and a CRT display. This equipment permits data to be presented via on-line digital print-outs and/or graphical plots.

TEST PROCEDURES

Rotary aerodynamic data are obtained in two steps. First, the inertial forces and moments (tares) acting on the model at different attitudes and rotational speeds must be determined. Ideally, these inertial terms would be obtained by rotating the model in a vacuum, thus eliminating all aerodynamic forces and moments. As a practical approach, this is approximated closely by enclosing the model in a sealed spherical structure, which rotates with the model without touching it, such that the air immediately surrounding the model is rotated with it. As the rig is rotated at the desired attitude and rate, the inertial forces and moments generated by the model are measured and stored on magnetic tape for later use.

The second step is to record force and moment data with the air on and with the enclosure removed. The tares, measured in step one, are then subtracted from these data, leaving only the aerodynamic forces and moments, which are converted to coefficient form and stored on magnetic tape.

MODEL

A 1/6-scale model, representing a single-engine general aviation airplane, was constructed from foam/fiberglass and aluminum. A three-view drawing of the model is shown in figure 3. Dimensional characteristics of the model are given in Table I. A photograph of the model installed on the rotary balance in the Langley Spin Tunnel is presented in figure 1.

TEST CONDITIONS

The tests were conducted in the spin tunnel at a tunnel velocity of 25 ft/sec, which corresponds to a Reynolds number of 128,000 based on the model mean aerodynamic chord. All the configurations were tested through an angle-of-attack range of 20° to 90°, at 0° and 10° sideslip angles and with the spin axis through the full-scale airplane cg. At each spin attitude, measurements were obtained for nominal $\Omega b/2V$ values of 0.1, 0.2, 0.3, 0.4, and 0.5, in both clockwise and counter clockwise directions, as well as for $\Omega b/2V=0$ (static value).

DATA PRESENTATION

The data measured for this study are presented in the Appendix. Table II identifies the configurations tested and their corresponding appendix figure numbers. The body-axis aerodynamic coefficients, plotted as functions of $\Omega b/2V$, are presented in comparison format with data from selected configurations plotted on the same figure to demonstrate the

effect of varying configuration parameters (e.g., sideslip angle or control deflections). Plots for each of the aerodynamic coefficients are presented in six sequentially numbered figures in the following order: C_n, C_l, C_m, C_N, C_Y, C_A. Each figure, in turn, consists of ten pages, which present the subject coefficient plots at each of the following angles of attack: 20°, 25°, 30°, 35°, 40°, 50°, 60°, 70°, 80°, and 90°.

DISCUSSION

Rotary balance moment data indicate the behavior of the airplane with rotation and thus the possibility of departure and spinning motions. For a clockwise rotation, a positive rolling or yawing moment is propelling, because it will increase the rotation rate, whereas a negative moment will decrease it and is, therefore, a damping moment. Conversely, for a counter-clockwise rotation, negative moments are propelling and positive ones damping.

Rotation produces inertial moments about each axis that are functions of the rotation rate squared, as well as the orientation of the airplane. For steady spins to occur, the aerodynamic moments must balance the inertial moments about all three axes. Steady spins may, therefore, be predicted from rotary balance data by identifying the rotation rate, angle of attack, and sideslip angle that result in such an equilibrium. Reference 3 presents a discussion of a method for identifying steady spin modes from rotary balance data.

Basic Airplane Characteristics with Neutral Controls

The aerodynamic data with neutral controls are presented in figures A1 through A6 at -10°, 0°, and $+10^{\circ}$ sideslip angles. For the tested angle-of-attack range, the airplane exhibits damped yawing moments (figure A1). Damped yawing moments will generally prohibit spins at moderately flat to flat angles of attack. The rolling moment coefficients for this configuration are generally propelling over a significant $\Omega b/2V$ range at all tested angles of attack (figure A2), except near 30°. These propelling rolling moments were shown in reference 1 to be caused by the wing. Most airplanes exhibit propelling rolling moments above approximately 80° angle of attack, but these are not significant because here the yawing moment is the primary spin driving element about the velocity vector. At lower angles of attack, however, propelling rolling moments provide the mechanism for incipient spin motions, as well as the driving element for attaining spins.

Despite the propelling moments for this configuration, however, no steep or moderately steep spins are predicted with neutral controls, as shown in Table III. This is because the yawing and/or pitching moment equilibrium equations cannot be satisfied at the same spin parameter values required by the rolling moment equation.

The pitching moment (figure A3)becomes increasingly more nose-down with increasing angle of attack throughout the tested angle-of-attack range and generally also becomes more nose-down non-linearly with rotation. Such pitching moment characteristics imply that increasingly higher rotation rates are required for pitch equilibrium as angle of

attack increases.

The influence of sideslip angle on the rotational aerodynamics is evident in figures A1 through A6. Positive sideslip produces a positive incremental yawing moment, and negative sideslip produces a negative increment at all tested angles of attack, although the increments are small for angles of attack below 40°. For angles of attack up to 80° the increment due to sideslip is fairly symmetrical for positive and negative sideslip angles, especially at the lower $\Omega b/2V$ magnitudes, and its variation with rotation is generally insignificant. Above 80° angle of attack, however, the non-linear characteristic of the yawing moment coefficient vs $\Omega b/2V$ curves produces unsymmetrical yawing moment increments for positive and negative sideslip angles.

Whereas the pitching moment vs $\Omega b/2V$ curves are basically symmetrical for clockwise and counter-clockwise rotations at zero sideslip angle, non-zero sideslips skew the curves. As a result, a nose-up increment is usually produced for negative sideslip angles at clockwise rotations, as well as for positive sideslips at counter-clockwise rotations. For this airplane, however, the combination of a positive sideslip at clockwise rotations or a negative sideslip at counter-clockwise rotations does not produce any significant change in the pitching moment.

Effect of Control Deflections

Rudder:

The effect of rudder deflection is shown in figure A7 through A18.

At zero sideslip angle, the rudder introduces an incremental yawing moment coefficient that is virtually invarient with rotation rate for angles of attack between 20^{o} and 50^{o} (figure A7). The rudder effectiveness remains fairly constant through 40^{o} angle of attack and then decreases above 40^{o}, such that above 60^{o} angle of attack the rudder is ineffective. The rudder does not influence the rolling moment coefficient at any angle of attack (figure A8).

As shown in Table III, an extremely steep spin equilibrium is predicted with neutral stick when the rudder is deflected with the spin. Obviously, the positive (propelling) yawing moment increment produced by the rudder is responsible for the predicted spin, since no spin was predicted with neutral controls.

The incremental yawing moment available for spin recovery is evident in figure A7. In the angle-of-attack range where it is effective, reversing the rudder produces a significant damping yawing moment increment and, as with neutral controls, no spin modes are predicted with the rudder deflected against the rotation.

Pro-Spin Controls:

Table III shows that the predicted spin mode for pro-spin controls (aft stick and rudder deflected with the spin) is less steep than that predicted for rudder alone. The data for pro-spin controls is presented in figures A19 through A30. The elevator deflection does not influence the yawing or rolling moments (compare figures A19 and A20 with A7 and A8, respectively). The aft stick elevator deflection does provide a nose-up incremental pitching moment coefficient for angles of attack

below 40°, but is ineffective for higher angles of attack (compare figure A21 with A9). (It is not known whether forward stick is effective above 40° angle of attack, because this control setting was not tested.) By producing a less nose-down pitching moment in the predicted spin angle-of-attack region, the aft stick elevator alters the Ωb/2V vs angle of attack relationship required for equilibrium of the inertial and aerodynamic pitching moment terms, as shown in figure 4. As a result, the predicted spin is slightly flatter and slower than with rudder alone.

Ailerons:

The effect of aileron deflection on the rotational aerodynamic data is presented in figures A19 through A30 for right pro-spin controls. The ailerons produce significant incremental rolling moments up to 80° angle of attack, but are ineffective above 80° (figure A20).

The rolling moment coefficient vs Ωb/2V plots, at zero sideslip angle, generally have an elongated recumbent S-shape for this airplane. Aileron deflection, consequently, displaces the rolling moment coefficient curves perpendicularly along the vertical axis and also tends to displace the reflex points of the curves laterally as a function of the deflection. The lateral displacement is most evident at 50° angle of attack (figure A20f). Because of this characteristic, the incremental change in rolling moment coefficient due to aileron deflection can vary significantly with both the sign and magnitude of the control deflection and with Ωb/2V, at the lower Ωb/2V magnitudes where the curves reflex.

At larger Ωb/2V magnitudes, however, the incremental rolling moments due to aileron are fairly constant with rotation and symmetrical for positive and negative aileron deflections.

At 10° sideslip angle (figure A26), the rolling moment curves do not exhibit the pronounced reflex characteristic observed at zero sideslip (except at 20° angle of attack). Therefore, the incremental rolling moment due to aileron deflection at sideslip is, generally, more nearly constant with rotation and symmetrical for positive and negative ailerons.

Aileron deflection has no significant influence on yawing moment coefficient for angles of attack below 50° (figure A19). At 60° angle of attack and above, however, they produce adverse yaw, which increases with increasing angle of attack. The yawing moment increments produced by the ailerons at these higher angles of attack do not vary significantly with rotation rate.

Because the ailerons are effective in roll over the predicted angle-of-attack range, deflecting the ailerons alters the predicted spin mode (Table III). The predicted spin is steeper when the ailerons are deflected with the spin (right stick for a right spin), and flatter when they are deflected against the spin. These changes arise solely from the shifts in the aerodynamic rolling moment due to aileron deflection. The rolling moment shift produces a substantial change in the sideslip angle required to provide equilibrium of the aerodynamic and inertial rolling moments. The changes in sideslip, in turn, affect the pitch and yaw equilibriums, thereby altering the spin modes.

Correlation of Predicted and Experimental Spins

The angles of attack of the predicted spins correlate reasonably well with the preliminary spin tunnel results for this airplane, as shown in Table IV. The controls used during flight test spins differed from those tested on the model in that the full-scale airplane was spun with an elevator trim tab deflected. Subsequent unpublished wind tunnel results indicated that the tab, as expected, produced a pitching moment increment. To compare the predicted spin modes with the flight test spins, the incremental pitching moment due to the tab was added to the rotational pitching moments measured during these tests. As shown in Table V, with neutral ailerons and pro-spin elevator and rudder, a spin mode was predicted at 36° angle of attack and 3.5 seconds/turn. The preliminary unpublished flight test results for the same controls, showed a spin at 44° and 2.8 seconds/turn.

While both the predicted and flight test results are of similar type (i.e., one is not flat and the other steep), the flight test spin is slightly flatter and faster than the predicted. The flight test results, further, show that aileron deflection produces insignificant variations in the developed spin modes, whereas the model tests indicate a definite variation of the spin parameters with aileron deflection (Table V). What is not indicated in Table V is that, with ailerons deflected, the moments are close to equilibrium over a significant angle-of-attack range (25° to approximately 40°).

This is demonstrated in figure 5, which presents the inertial and aerodynamic yawing moment terms plotted as functions of angle of attack for ailerons neutral, against, and with the spin. Both the inertial and aerodynamic values shown in figure 5 are evaluated at the rotation rates and sideslip angles required for equilibrium of the pitching and rolling moments. Therefore, wherever the two yawing moment terms are equal, all three moments are in equilibrium, as required for a steady-state spin. (Reference 3 presents a detailed discussion of the method for generating such plots.)

With neutral ailerons (figure 5a), the inertial and aerodynamic yawing moment plots cross at approximately 36° angle of attack and then diverge. With both ailerons against and with the spin (figure 5b and 5c), however, the two curves remain close together for a 10° to 15° angle-of-attack range.

Because the yawing moment terms in these plots are evaluated at the $\Omega b/2V$ and sideslip values required for equilibrium of the other two moments, all three moments are close to equilibrium beginning at 25° and continuing for 10° to 15° for ailerons against and with, respectively. Therefore, a small change in any of the aerodynamic moments could produce a significant change in the predicted spin mode.

The difference between model and preliminary flight-test results for this airplane are most likely due to the difference in Reynolds number between the full-scale tests and the sub-scale general aviation model test. While the effects of Reynolds number on rotational aerodynamics has not yet been identified, static high and low Reynolds number testing of

another general aviation configuration (reference 4) revealed Reynolds number primarily affects the wing's contribution to the aerodynamics in the stall and immediate post-stall angle-of-attack region, as seen in figure 6. Significant differences in the normal and axial force coefficients are observed for the configurations in reference 4 beginning at the low Reynolds number stall angle of attack at 10° and continuing through approximately 35°. Since these differences are a direct result of Reynolds number induced changes on the stall angle of attack and stall characteristics, the aerodynamic effects of devices designed to influence the airplane's stall (such as wing leading-edge droops, etc.) can be particularly sensitive to Reynolds number.

These Reynolds number effects would also be expected to influence the rotational rolling and yawing moment contributions of the wing. This occurs because the angle of attack varies along a rotating wing, increasing from root to tip along the inboard (downgoing) wing and decreasing along the outboard one. Rolling and yawing moments are thus generated by differences in the normal and axial forces, respectively, between the inboard and outboard wings produced by these angle of attack differences. Therefore, Reynolds number effects can alter the rotational rolling and yawing moments whenever at least one wing plane is operating in the low Reynolds number post-stall angle-of-attack region, which is generally most of the steeper spin angle-of-attack range. Such Reynolds number effects on rolling moment are significant because rolling moment is the primary driver for steep spins and is, generally, produced entirely by the wing. The upper limit of the angle-of-attack range where Reynolds

number effects influence the spin modes depends on the wing geometry and on the spin rotation rate, because both determine how much of the outboard wing is operating where Reynolds number effects are significant. At higher angles of attack, in the more moderate to flat spin regions, little or none of the wing is operating in the angle-of-attack range where Reynolds number effects are significant and little change would be expected in the wing's aerodynamic contributions.

For the general aviation model D, the outboard panels of each wing are tapered and twisted in an effort to prevent the wing tips from stalling before the inboard portions of the wing. It was anticipated that these outboard wing panels' aerodynamic influence would be sensitive to Reynolds number, thus accounting for the observed differences in spin modes. Because the Reynolds number effect on the wing's aerodynamic contribution is the suspected source of the observed spin mode differences, data in this angle-of-attack region should be used with caution. Investigations into these effects are currently underway at the NASA Langley Research Center.

CONCLUDING REMARKS

The following observations pertaining to the flight-test configuration of general aviation model D are based on the analysis presented herein. Analysis of the predicted spin modes showed:

- With pro-spin controls, steep spin modes are predicted that agree reasonably well with preliminary free-spinning model

results. The predicted spins without an elevator trim tab were steepest when the ailerons were deflected with the spin and became flatter for ailerons neutral and against the spin.

- o No spin modes were predicted for neutral or recovery controls (rudder against the spin and stick neutral).
- o The predicted spin modes were steeper and slower than the flight-test results. These differences most likely arise from the influence of Reynolds number on the dynamic stalling characteristics of the rotating wing for this configuration and serve to illustrate the possible difficulties of low Reynolds number rotary balance testing for some general aviation configurations in this angle-of-attack region. High Reynolds number rotary balance tests are needed to quantify this effect.

Examination of the rotary aerodynamic data showed:

- o The basic T-tailed model D, considered in this report, exhibited damped yawing moments.
- o The model, however, had propelling rolling moments at all tested angles of attack, except near 30°.
- o The rudder produced incremental yawing moments throughout the lower tested angle-of-attack range, but its effectiveness began to diminish above 40° angle of attack and it was ineffective above 60° angle of attack.
- o The aft-stick elevator produced nose-up pitching moment increments only up to 40° angle of attack.

- The ailerons produced substantial incremental rolling moments up to 80^{o} angle of attack and some adverse yaw for angles of attack above 50^{o}. At zero sideslip angle, the ailerons displaced the non-linear character of the C_l vs $\Omega b/2V$ curves laterally along the $\Omega b/2V$ axis such that significant variations in the incremental rolling moment coefficient due to aileron resulted. At high $\Omega b/2V$ values, where the curves are more linear, no such variations were observed.

REFERENCES

1. Ralston, John N.: Rotary Balance Data for a Typical Single-Engine General Aviation Design for an Angle-of-Attack Range of 8° to 90°. I - Influence of Airplane Components for Model D. NASA CR-3246, 1983.

2. Barnhart,Billy: Rotary Balance Data for a Typical Single-Engine General Aviation Design for an Angle-of-Attack Range of 8° to 90°. II - Influence of Horizontal Tail Location for Model D. NASA CR-3247, 1982.

3. Bihrle,W.,Jr. and Barnhart, B.: Spin Prediction Techniques, Journal of Aircraft, Vol. 19, Number 11, November 1982.

4. Bihrle, William, Jr., Barnhart, Billy, and Pantason, Paul: Static Aerodynamic Characteristics of a Typical Single-Engine Low-Wing General Aviation Design for an Angle-of-Attack Range of -8° to 90°. NASA CR-2971, 1978.

TABLE I.- DIMENSIONAL CHARACTERISTICS

Overall length, ft	4.675
Wing:	
Span, ft	5.91
Area, ft^2	4.825
Root chord, in.	10.5
Tip chord, in.	7.03
Mean aerodynamic chord, in.	9.64
Leading edge of $\bar{c}$, distance rearward of leading edge of root chord, in.	2.14
Aspect ratio	7.24
Taper ratio	0.67
Dihedral, deg	7
Incidence:	
Root, deg	2.0
Tip, deg	-1.0
Airfoil Section:	
Root	NASA $65_2$415
Tip	NASA $65_2$415 mod
Horizontal tail	
Span, ft	1.67
Area, ft^2	0.696
Aspect ratio	4.0
Airfoil section	NACA 0012
Vertical tail	
Area, ft^2	0.328
Sweep at leading edge	33.9
Aspect ratio	1.47
Airfoil section	NASA 63A012

TABLE II.- CONFIGURATIONS TESTED AND FIGURE INDEX

(All configurations tested through $\alpha = 20^{\circ}$ to 90°)

FIGURE NO.	β deg	δ_H deg	δ_a deg	δ_r deg	REMARKS
A1-A6	0 +10 -10	0 ↓	0 ↓	0 ↓	Effect of sideslip, neutral controls
A7-A12	0 ↓	0 ↓	0 ↓	0 +26 -26	Rudder effectiveness, $\beta=0^{\circ}$
A13-A18	+10 ↓	0 ↓	0 ↓	0 +26 -26	Rudder effectiveness, $\beta=+10^{\circ}$
A19-A24	0 ↓	-10 ↓	-22 0 +22	-26 ↓	Effect of Ailerons, pro-spin controls, $\beta=0^{\circ}$
A25-A30	+10 ↓	-10 ↓	-22 0 +22	-26 ↓	Effect of Ailerons, pro-spin controls, $\beta=+10^{\circ}$

TABLE III.- PREDICTED SPIN MODES

CONTROLS			SPIN EQUILIBRIUM			
δ_H deg	δ_a deg	δ_r deg	α deg	$\frac{\text{sec}}{\text{turn}}$	$\frac{\Omega b}{2V}$	V Descent ft/sec
0	0	0	NO SPIN			
0	0	-26	23	2.1	0.28	191
-10	0	-26	29	2.8	0.23	175
-10	-22	-26	23	2.2	0.24	205
-10	+22	-26	37	2.9	0.26	151

I_X= 1770 slug-ft^2

I_Y= 2471 slug-ft^2

I_Z= 3783 slug-ft^2

Weight= 2338 lbs

cg= 26.3%c

$$\frac{I_X-I_Y}{mb^2} \times 10^4 = -77$$

$$\frac{I_Y-I_Z}{mb^2} \times 10^4 = -144$$

$$\frac{I_Z-I_X}{mb^2} \times 10^4 = 221$$

TABLE IV.- COMPARISON OF PREDICTED SPIN MODES AND SPIN TUNNEL RESULTS
($\delta_H = -10^o$ and $\delta_r = -26^o$ FOR ALL CASES)

Aileron Deflection	Predicted Spin Modes				Spin Tunnel			
	α deg	$\frac{\text{sec}}{\text{turn}}$	$\frac{\Omega b}{2V}$	V_D ft/sec	α deg	$\frac{\text{sec}}{\text{turn}}$	$\frac{\Omega b}{2V}$	V_D ft/sec
With	23	2.2	0.24	205	TOO STEEP TO HOLD			
Neutral	29	2.8	0.23	175	30	2.3	0.30	164
Against	37	2.9	0.26	151	35	2.5	0.28	159

$I_X = 1770$ slug-ft^2

$I_Y = 2471$ slug-ft^2

$I_Z = 3783$ slug-ft^2

Weight = 2338 lbs

cg= 26.3%c

$$\frac{I_X - I_Y}{mb^2} \times 10^4 = -77$$

$$\frac{I_Y - I_Z}{mb^2} \times 10^4 = -144$$

$$\frac{I_Z - I_X}{mb^2} \times 10^4 = 221$$

TABLE V.- COMPARISON OF PREDICTED SPIN MODES AND FLIGHT TEST RESULTS
($\delta_H = -10^\circ$ and $\delta_r = -26^\circ$ FOR ALL CASES)

Aileron Deflection	Predicted Spin Modes*				Flight Test			
	α deg	$\frac{\text{sec}}{\text{turn}}$	$\frac{\Omega b}{2V}$	V_D ft/sec	α	$\frac{\text{sec}}{\text{turn}}$	$\frac{\Omega b}{2V}$	V_D ft/sec
With	25	3.3	0.17	197	43	2.7	0.34	120
Neutral	36	3.5	0.21	152	44	2.8	0.33	120
Against	25	3.0	0.19	194	43	3.0	0.31	120

*C_m corrected to include elevator trim tab effect.

$I_X = 1770$ slug-ft^2

$I_Y = 2471$ slug-ft^2

$I_Z = 3783$ slug-ft^2

Weight= 2338 lbs

cg= 28%c

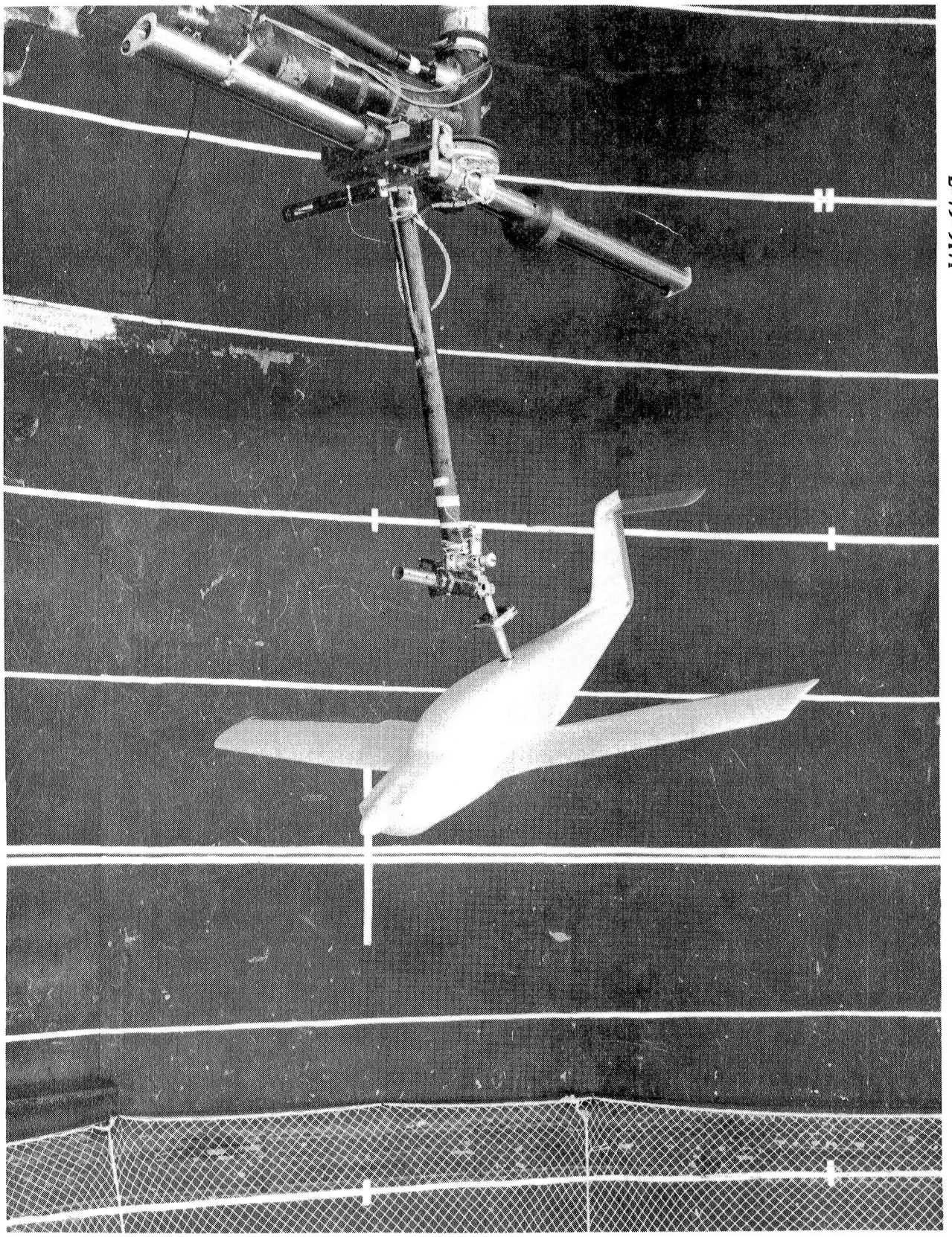

NASA
L-79-9171

Figure I. - Photograph of 1/6 scale model installed on rotary balance apparatus

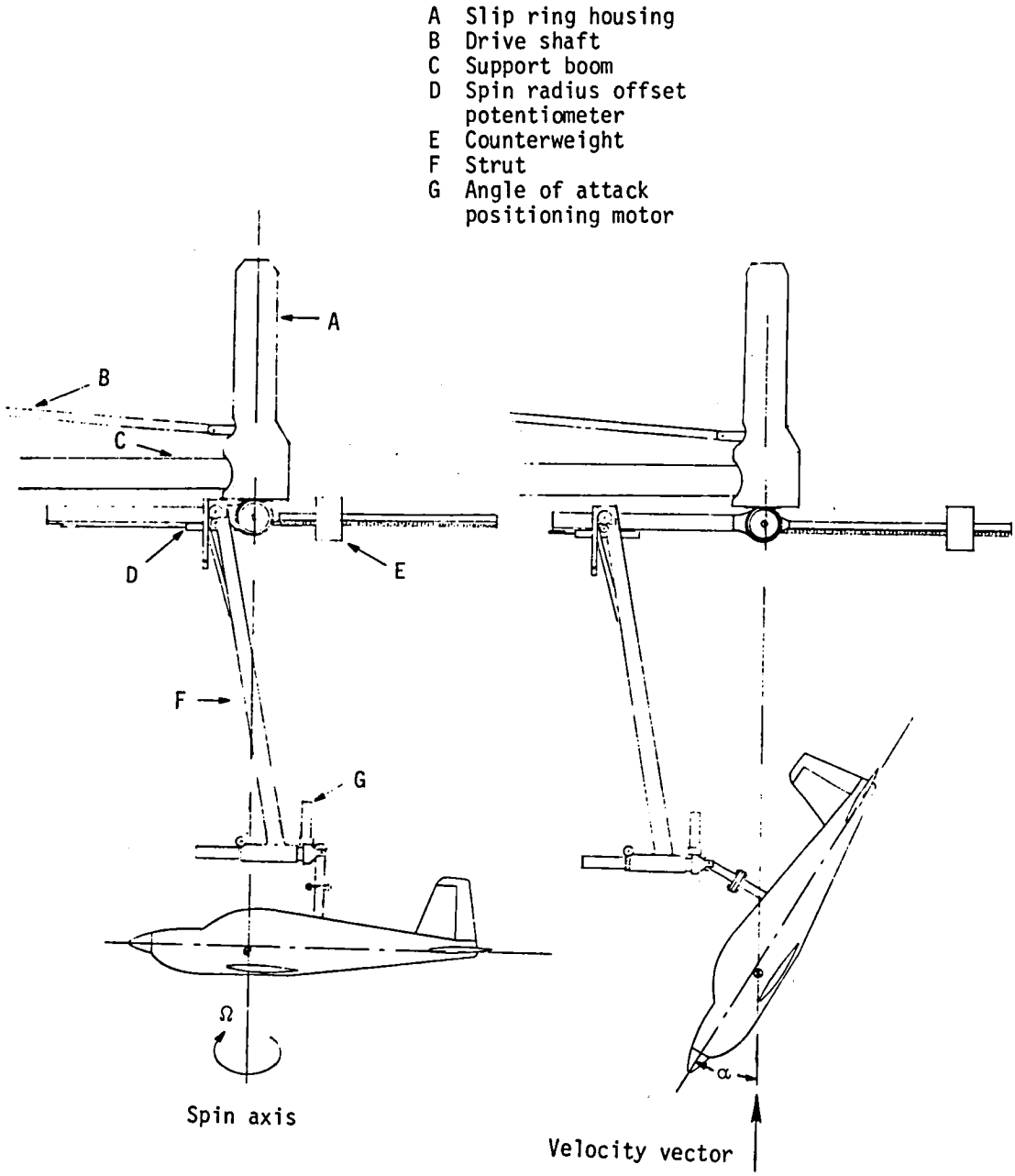

(a) Side view of model.

Figure 2.- Sketch of rotary balance apparatus.

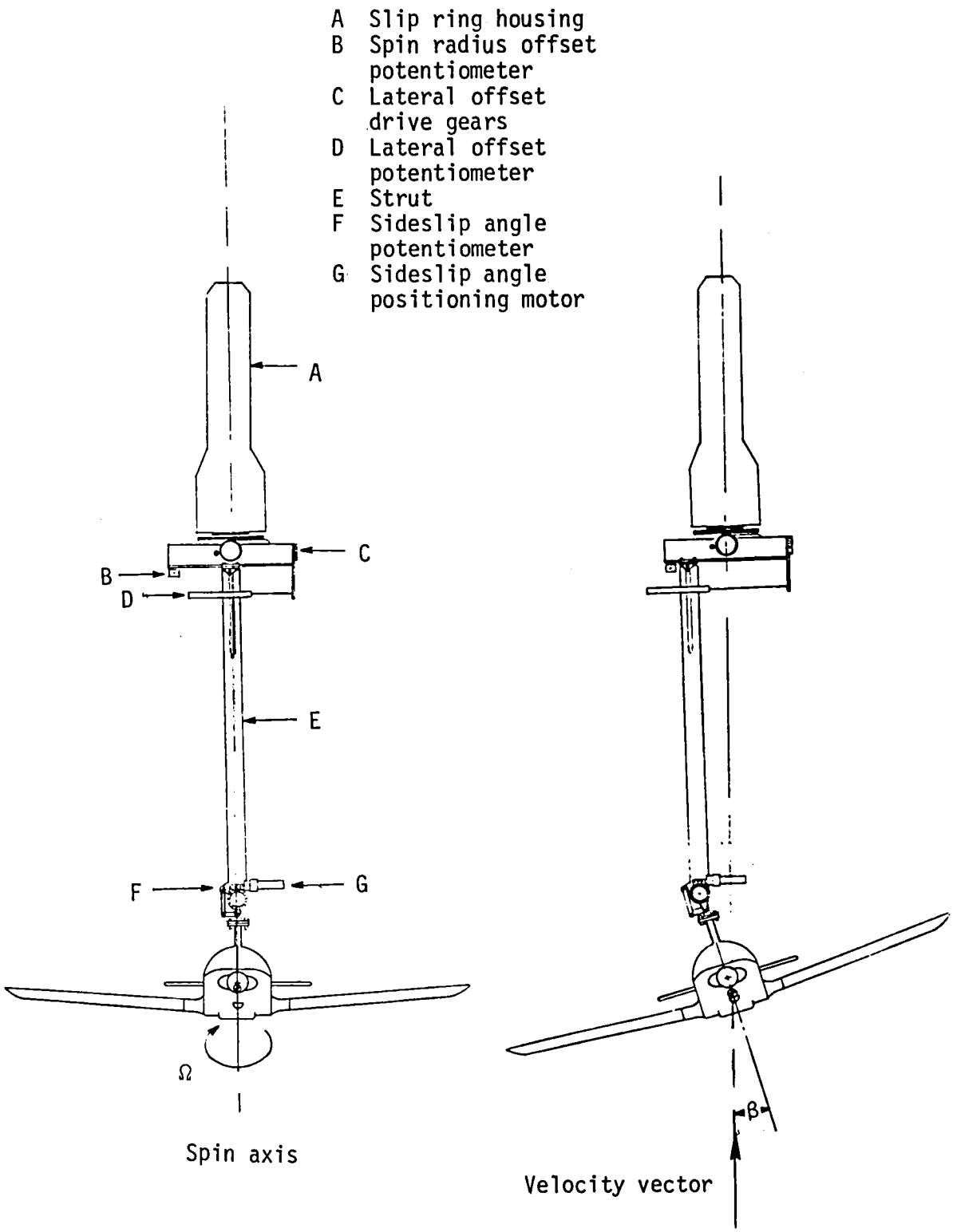

(b) Front view of model.

Figure 2.- Concluded.

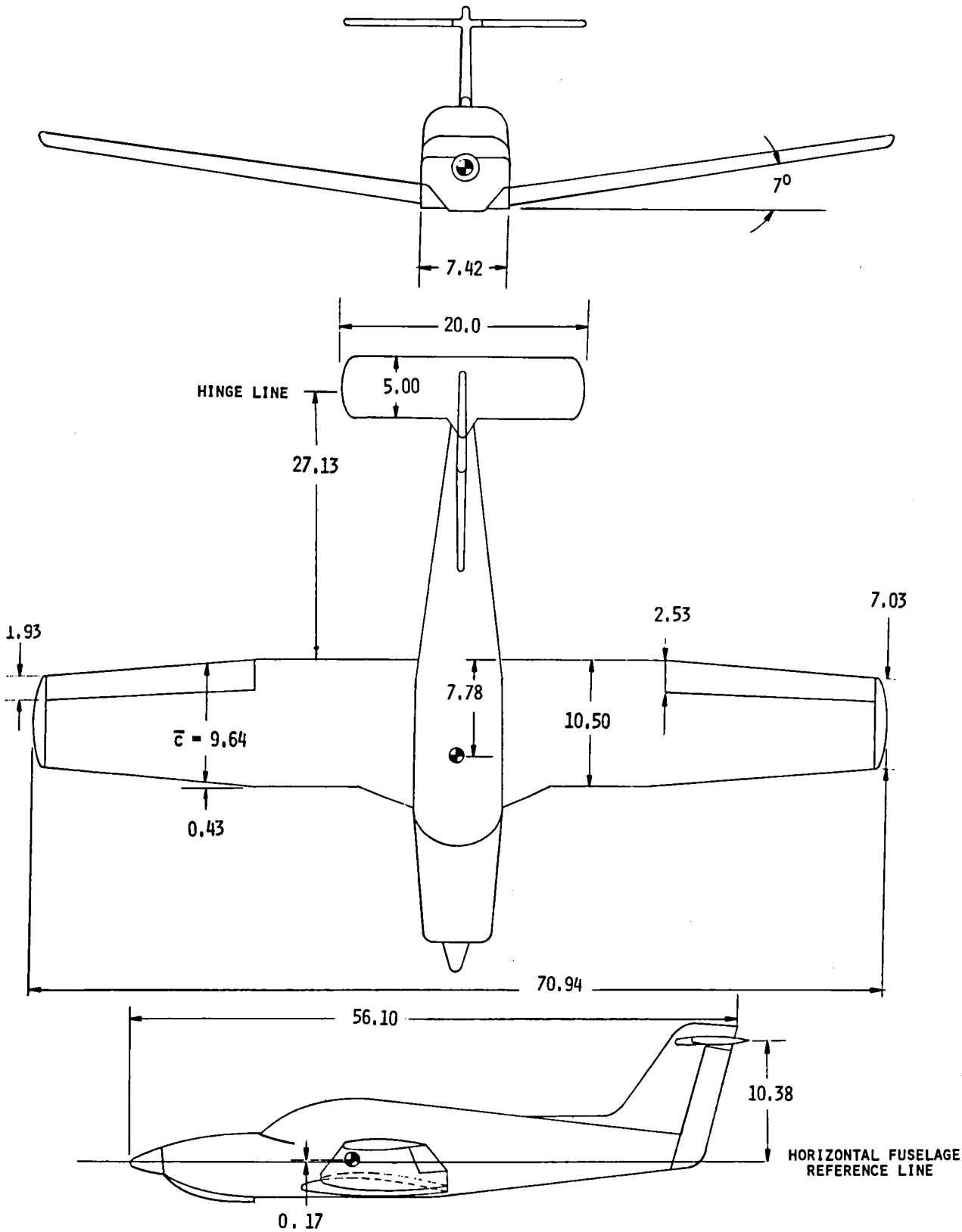

FIGURE 3.- THREE-VIEW OF 1/6-SCALE MODEL. CENTER OF GRAVITY POSITIONED AT 0.25$\bar{c}$. DIMENSIONS ARE GIVEN IN INCHES, MODEL SCALE.

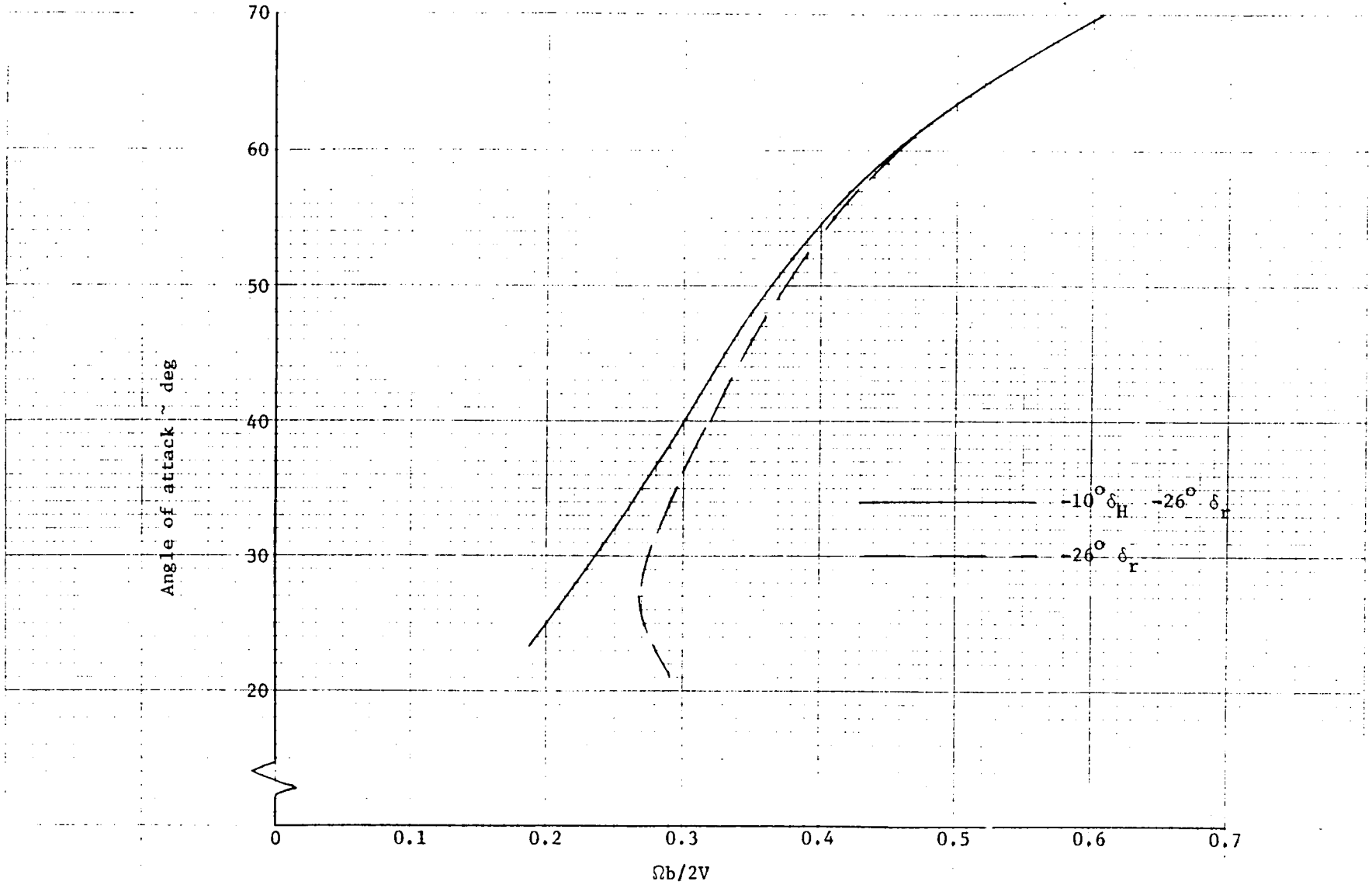

Figure 4.- Angle of attack vs. Ωb/2V relationships required for pitch equilibrium.

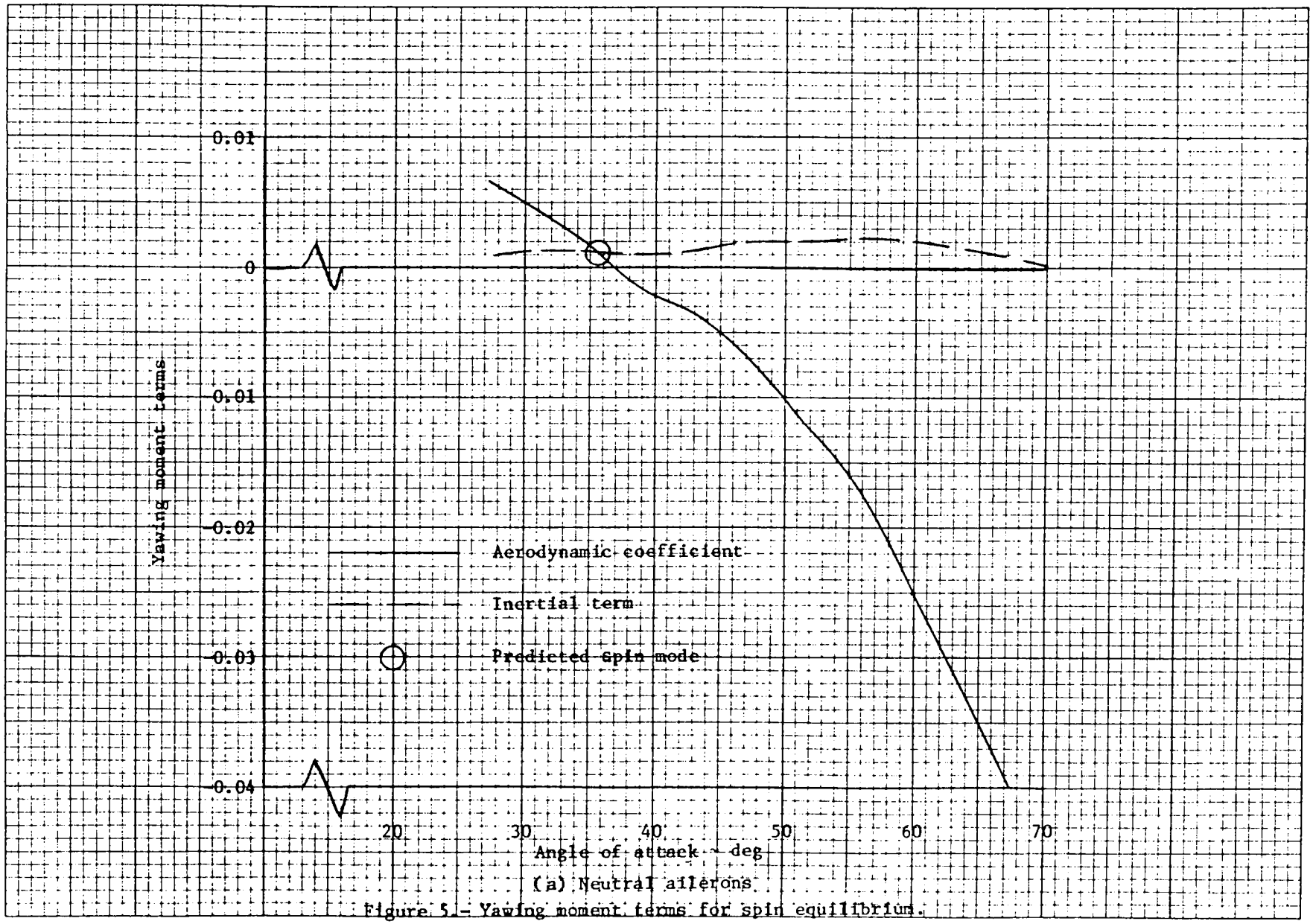

(a) Neutral ailerons

Figure 5.- Yawing moment terms for spin equilibrium.

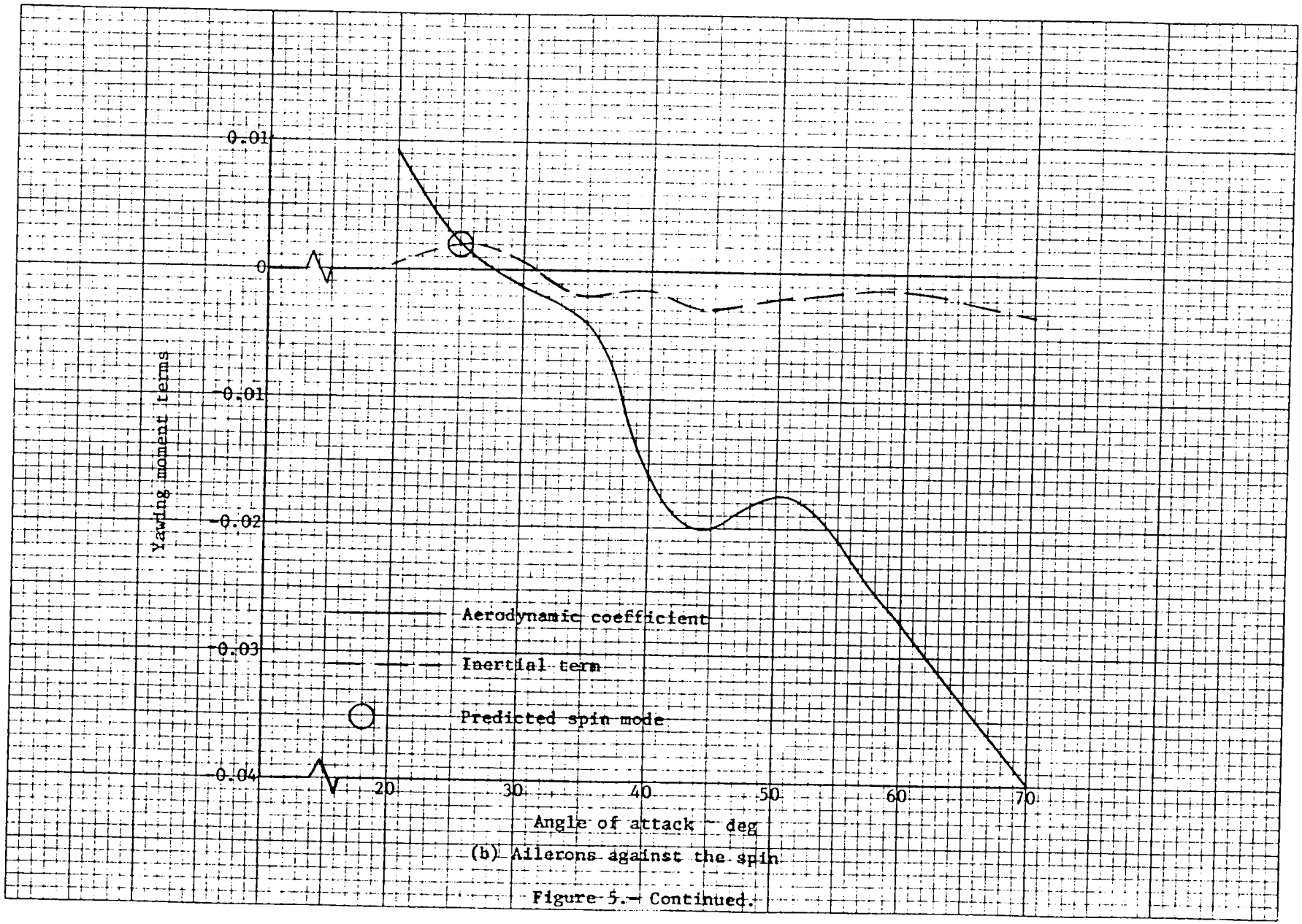

(b) Ailerons against the spin

Figure 5.– Continued.

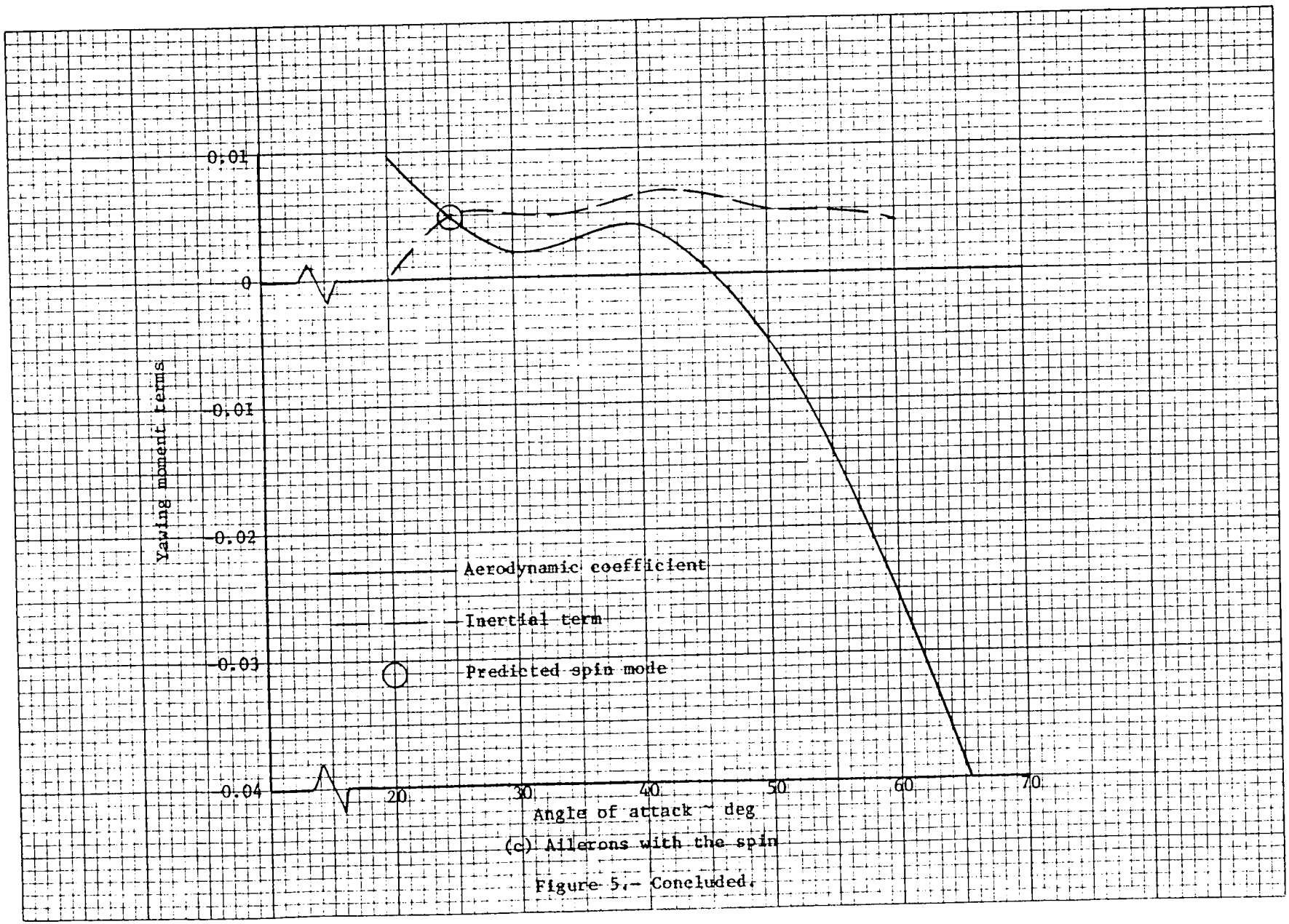

(c) Ailerons with the spin

Figure 5.- Concluded.

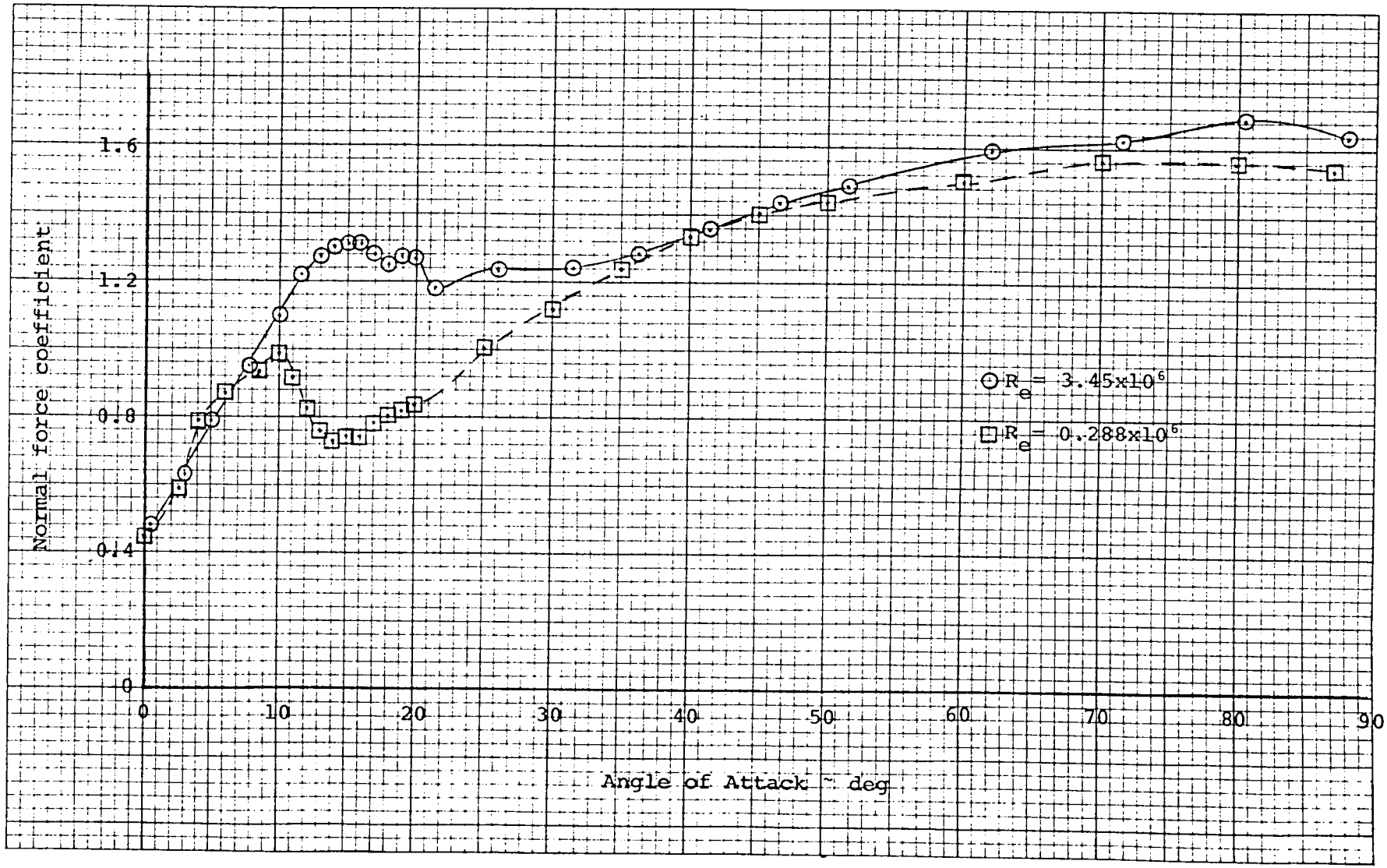

(a) Normal force coefficient

Figure 6.- Comparison of high and low Reynolds number static data for General Aviation Model A (from reference 4).

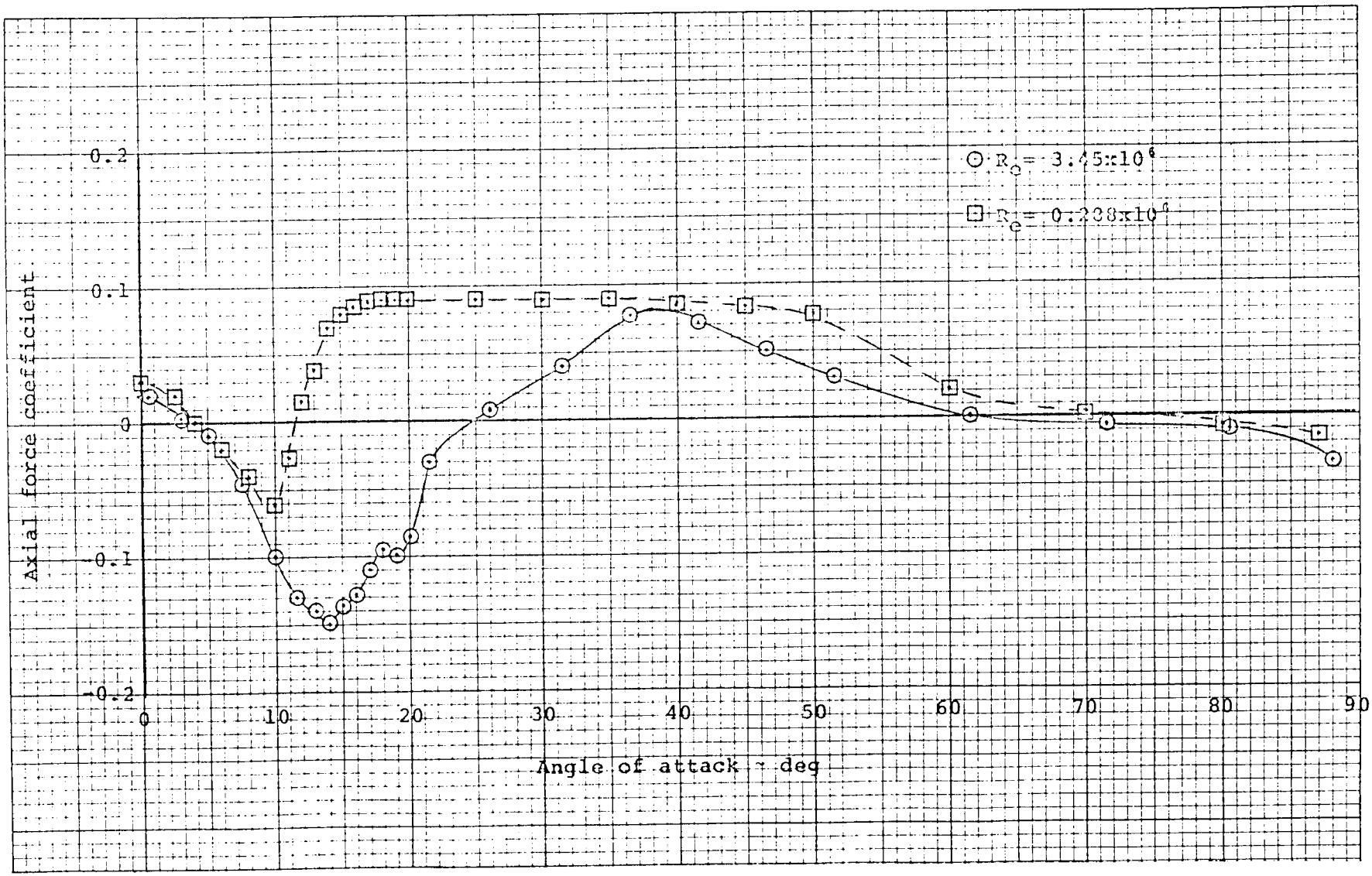

(b) Axial force coefficient

Figure 6.- Concluded.

APPENDIX

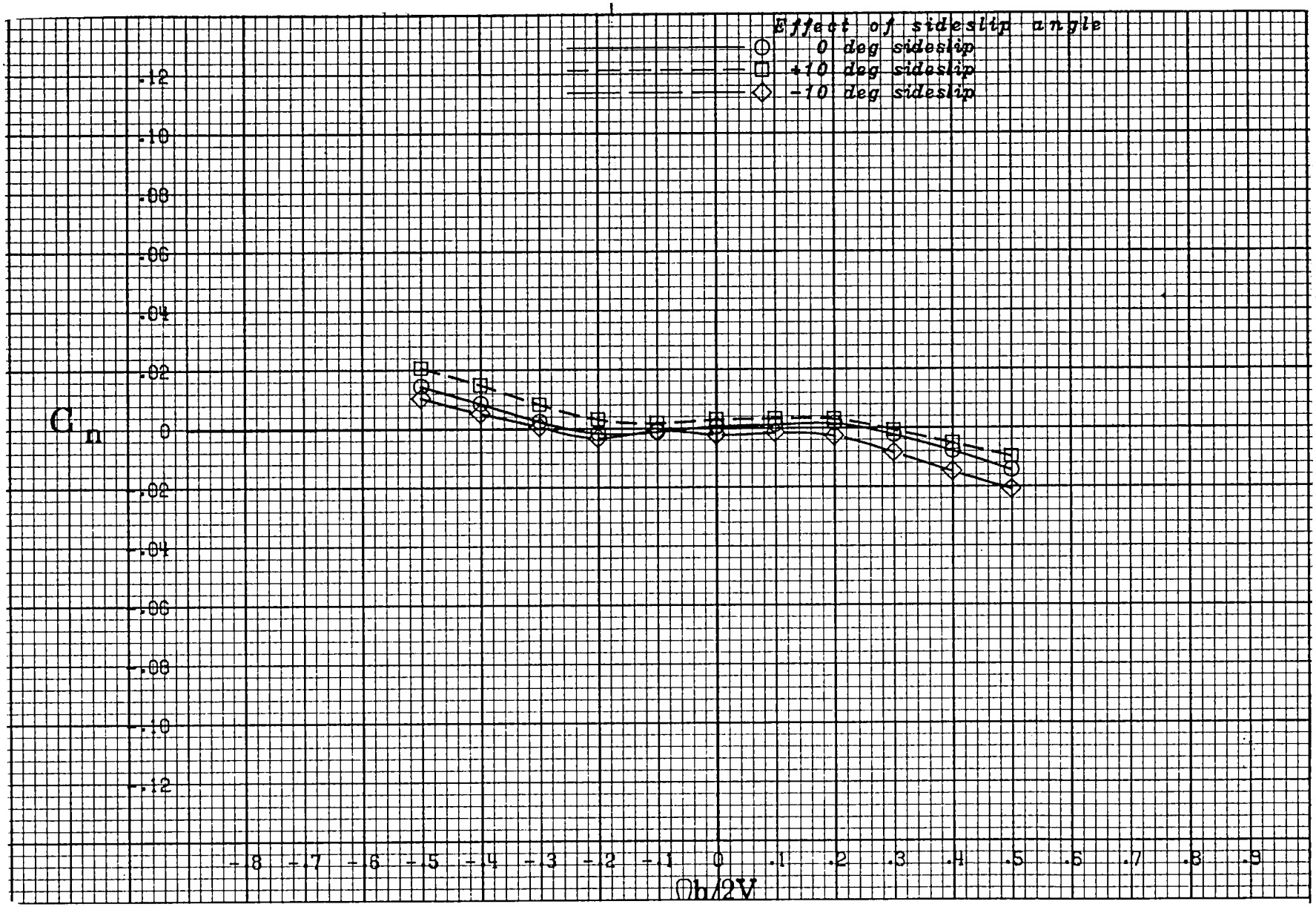

(a) α = 20 deg.

Figure A 1 .- Effect of rotation rate and sideslip angle on yawing-moment coefficient for the basic configuration with neutral controls.

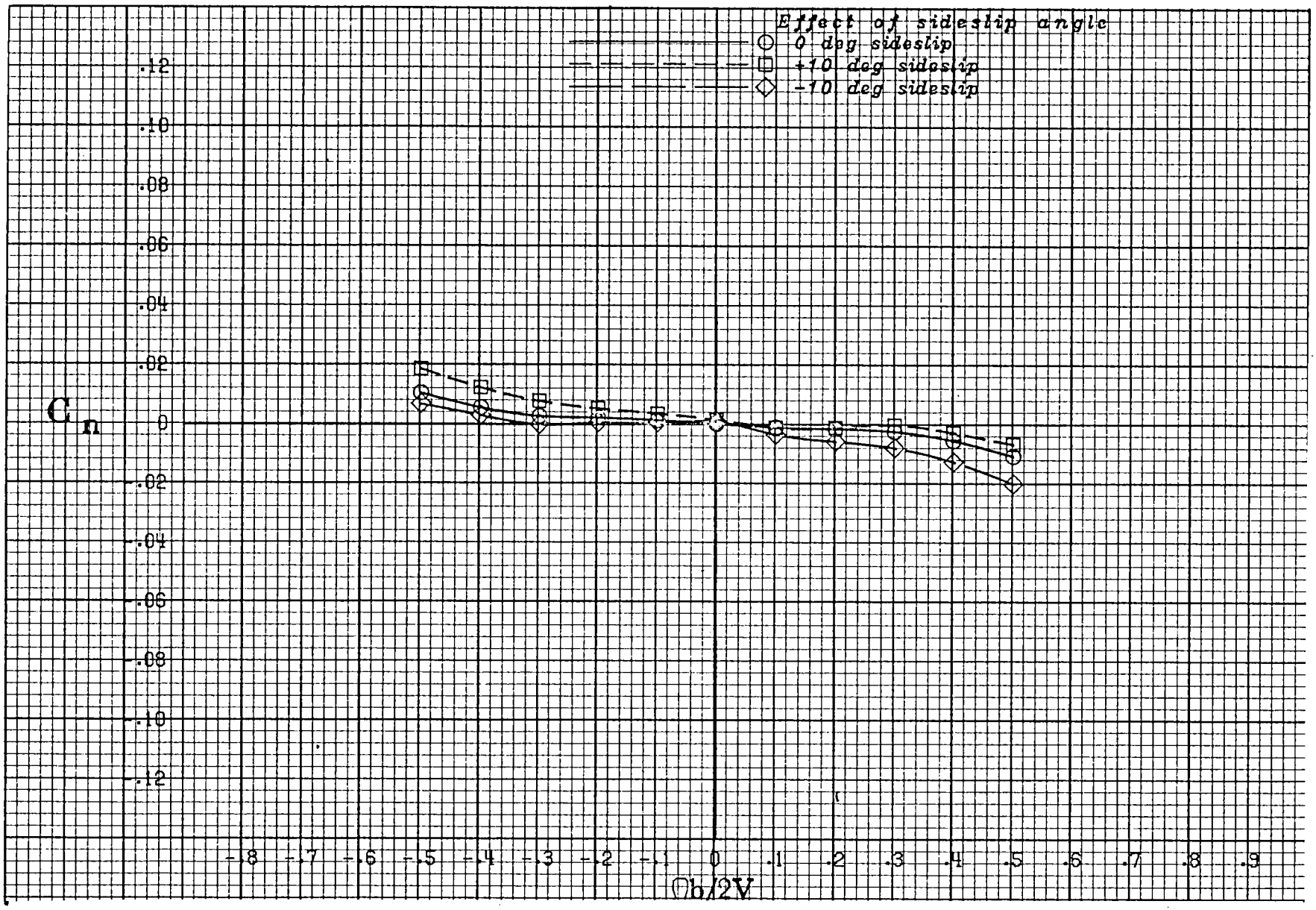

(b) α = 25 deg.

Figure A 1 .- Continued.

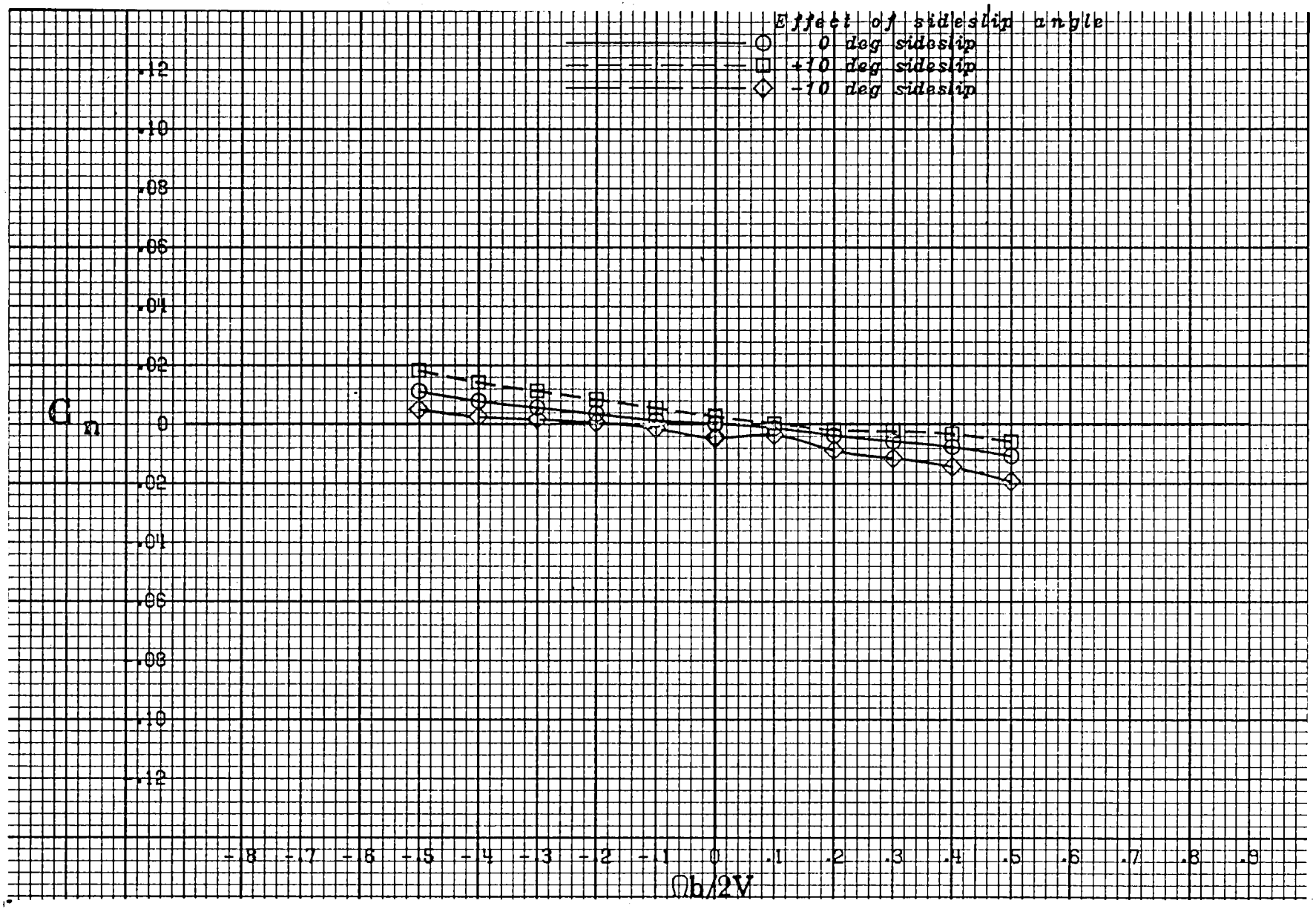

(c) α = 30 deg.

Figure A 1 .- Continued.

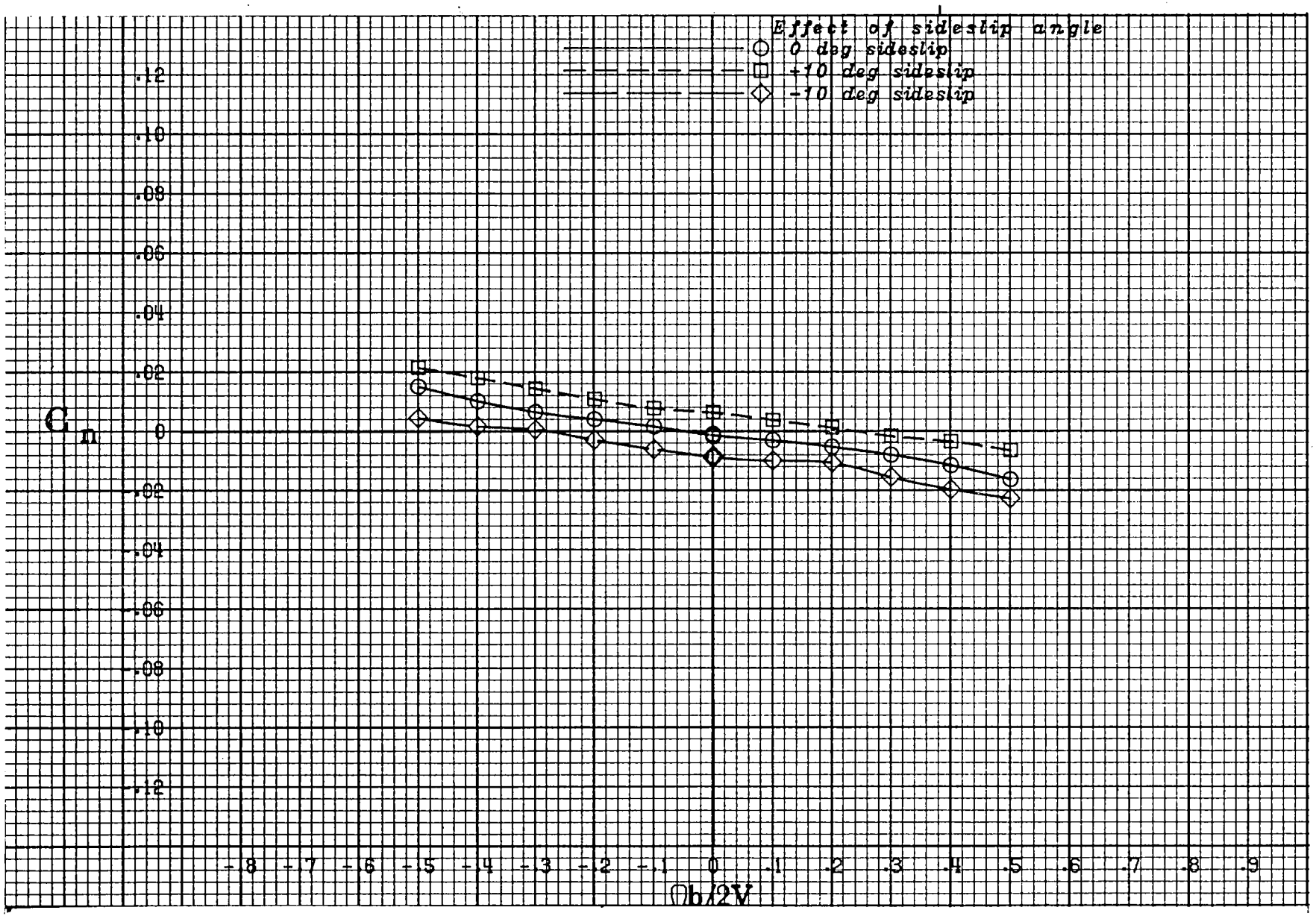

(d) α = 35 deg.

Figure A 1 .- Continued.

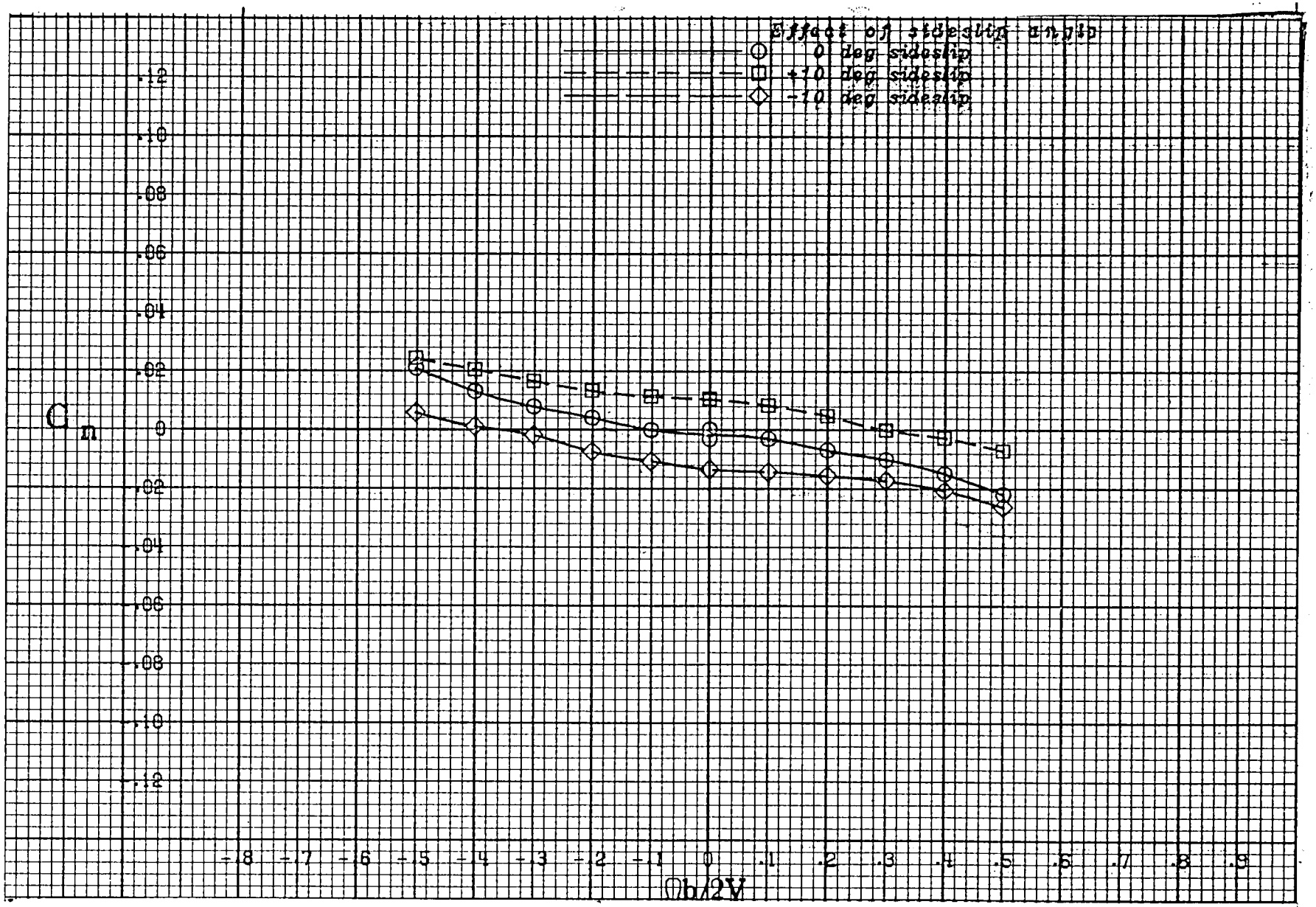

(e) α = 40 deg.

Figure A 1 .- Continued.

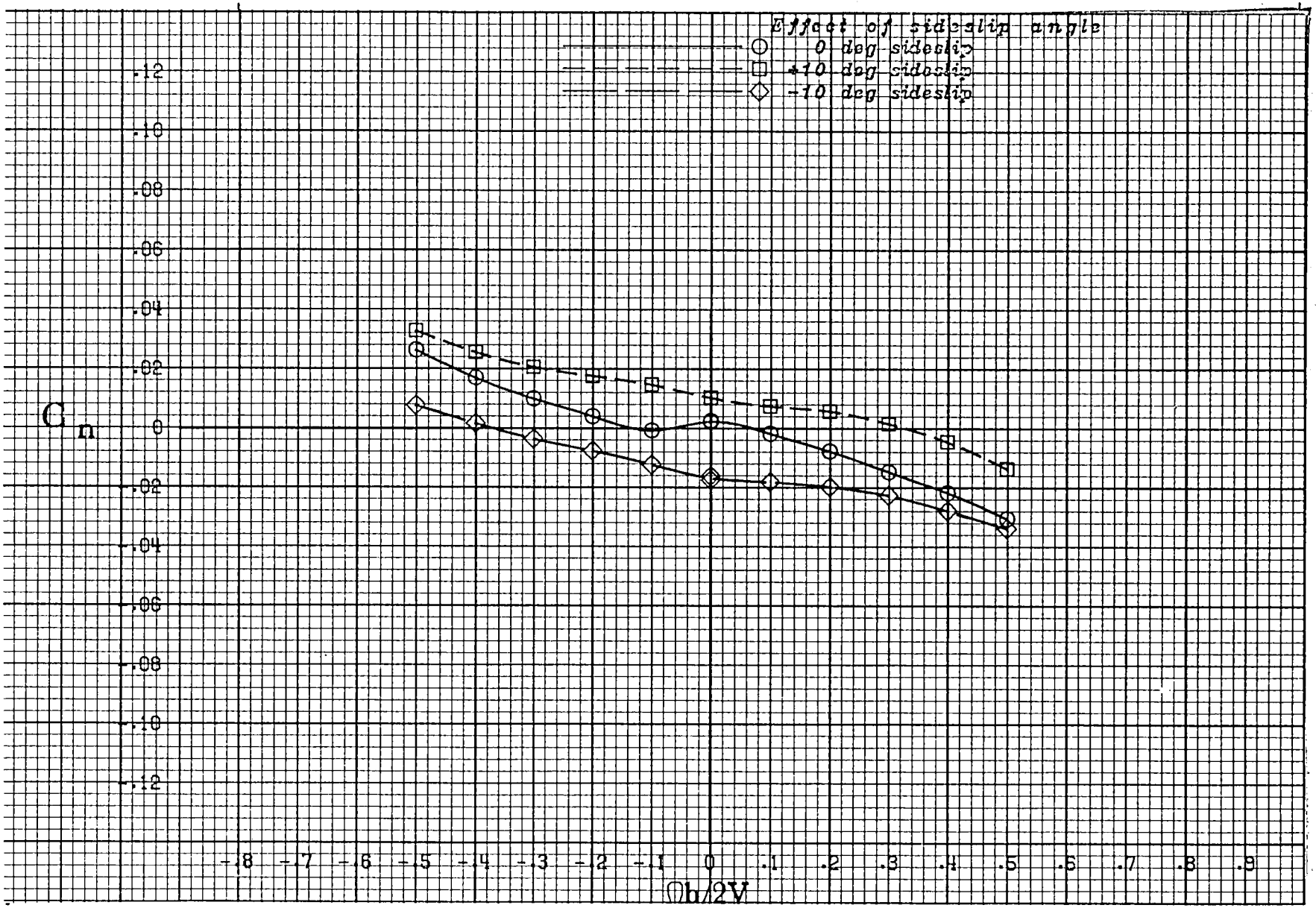

(f) α = 50 deg.

Figure A 1 .- Continued.

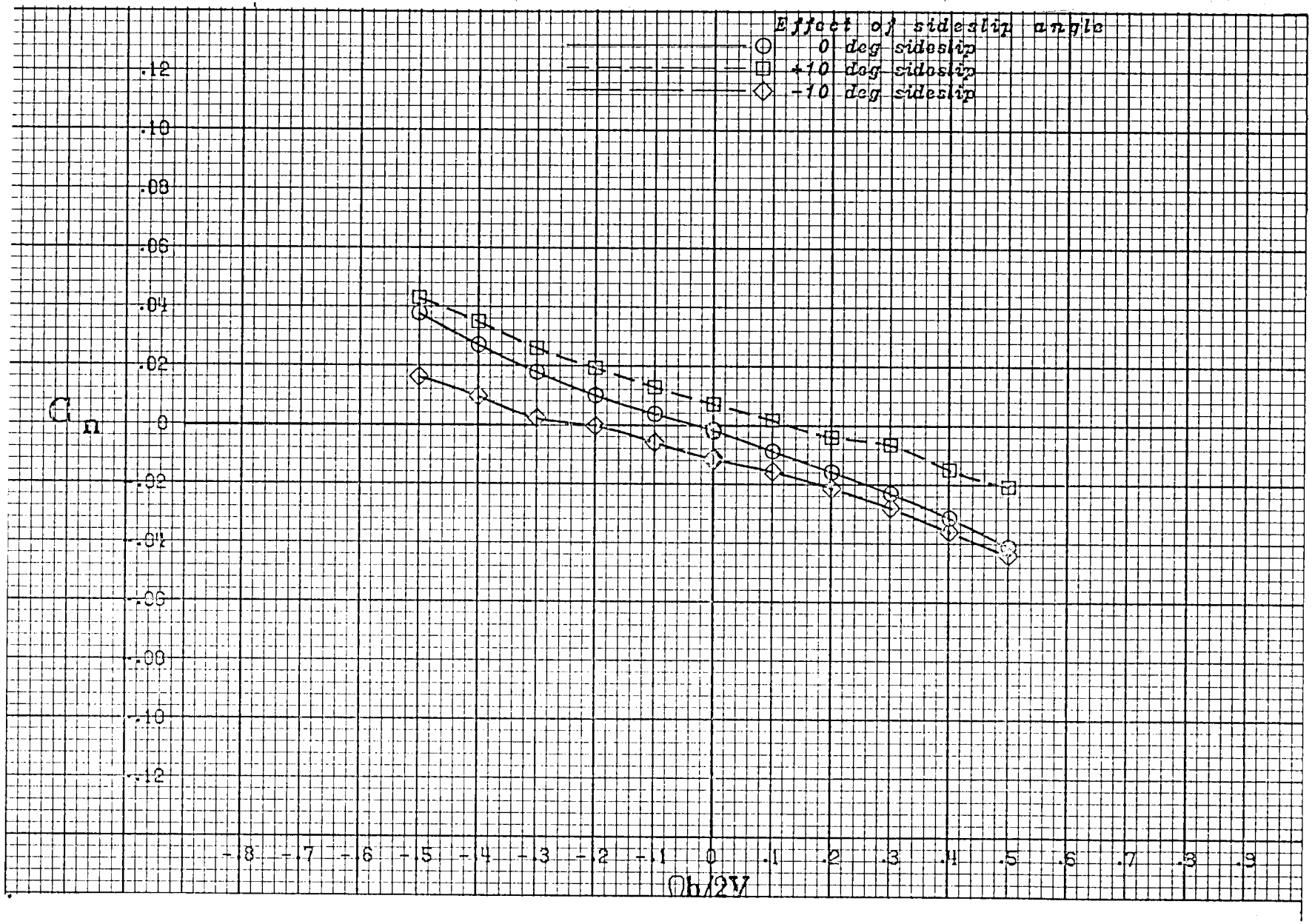

(g) α = 60 deg.

Figure A 1 .- Continued.

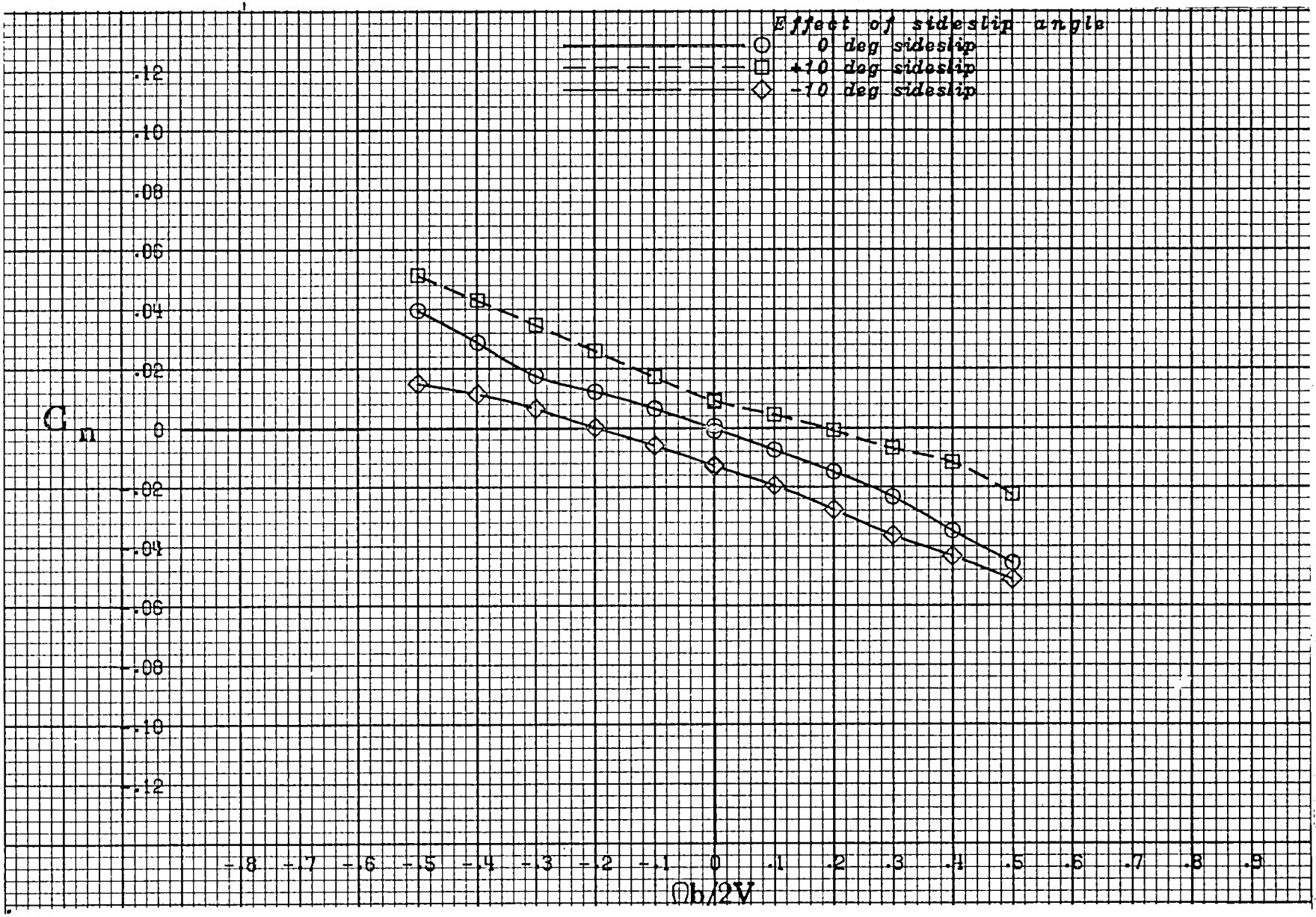

(h) α = 70 deg.

Figure A 1 .- Continued.

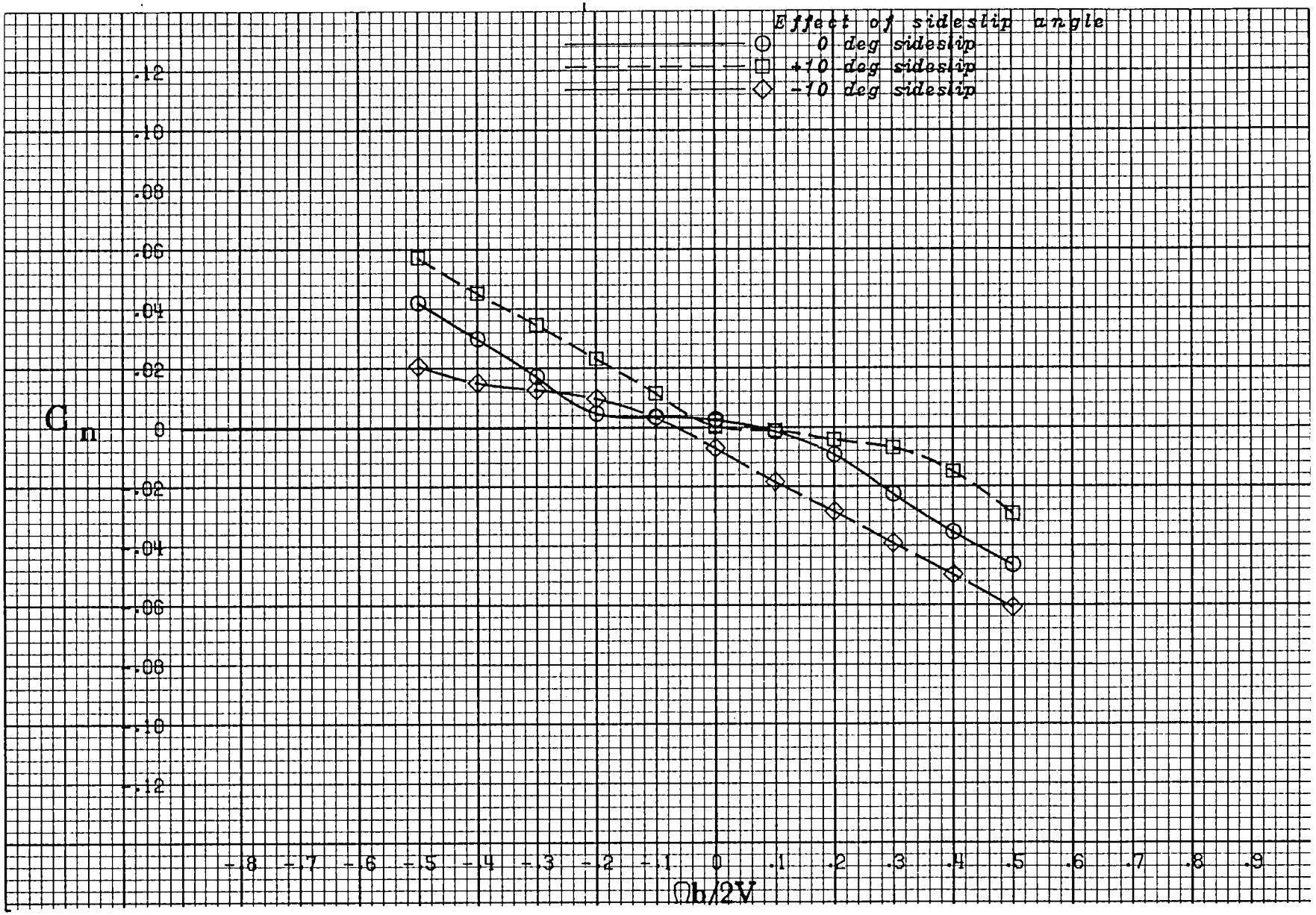

(i) α = 80 deg.

Figure A 1 .- Continued.

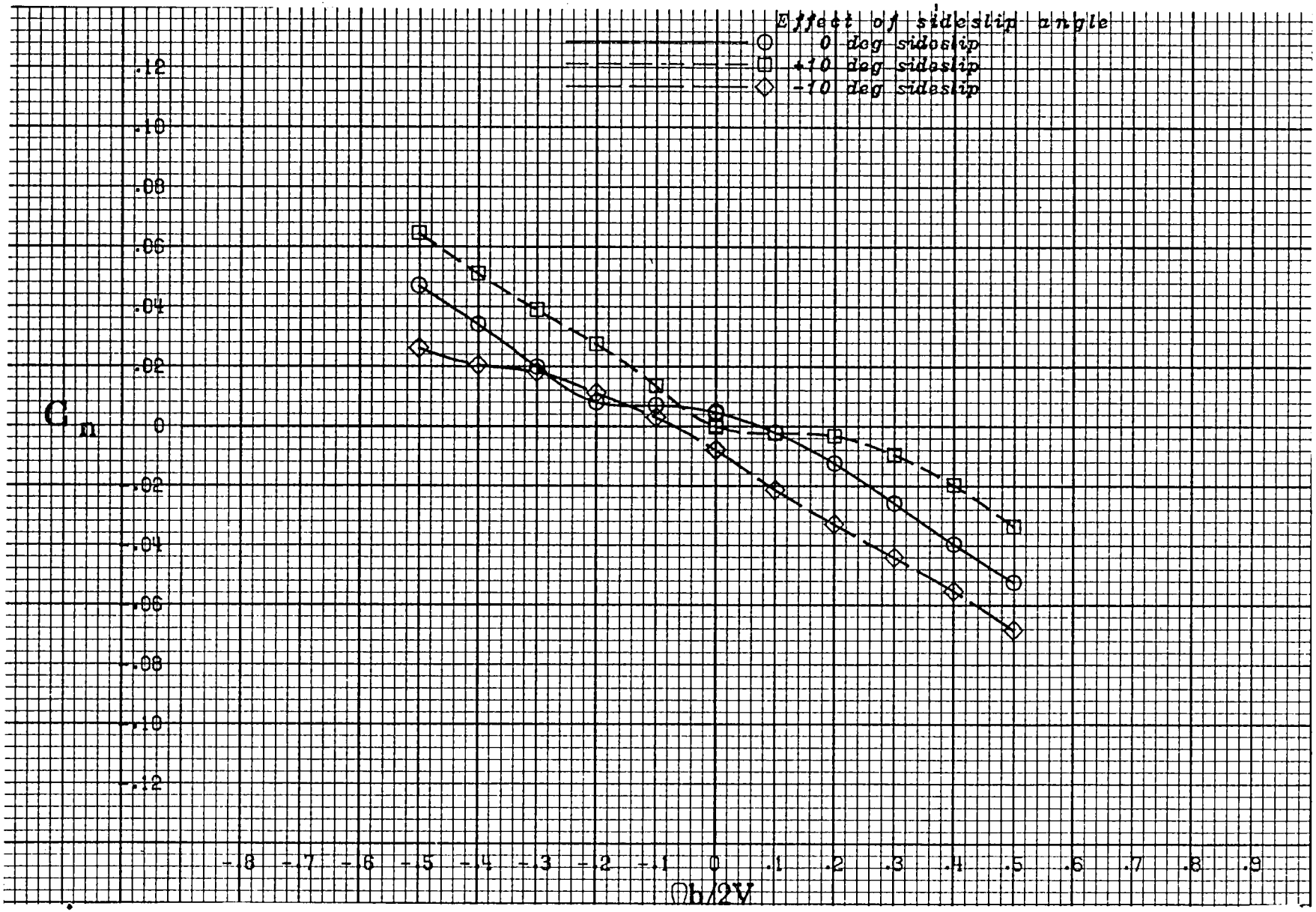

(j) α = 90 deg.

Figure A 1 .- Concluded.

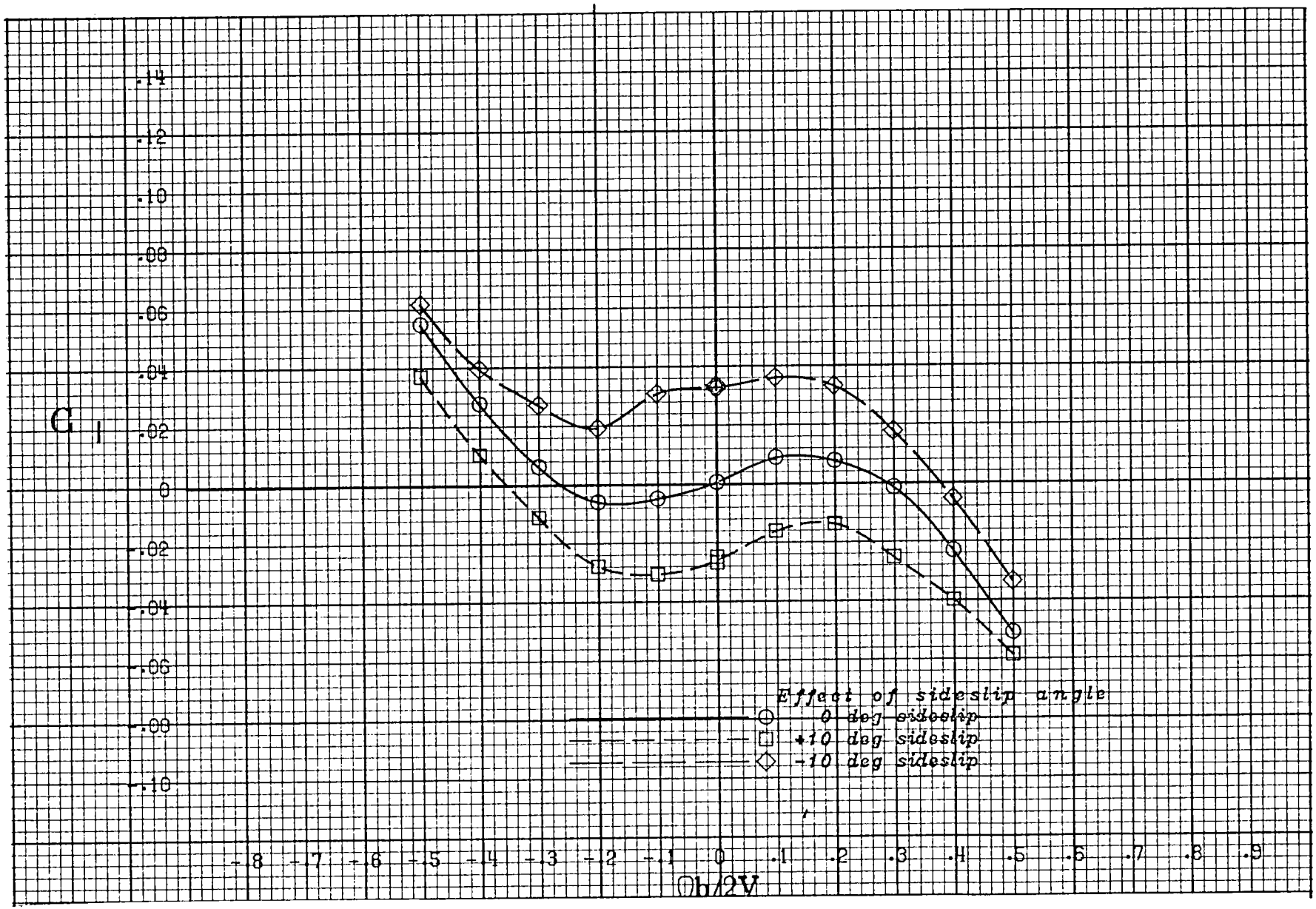

(a) α = 20 deg.

Figure A 2 .- Effect of rotation rate and sideslip angle on rolling-moment coefficient for the basic configuration with neutral controls.

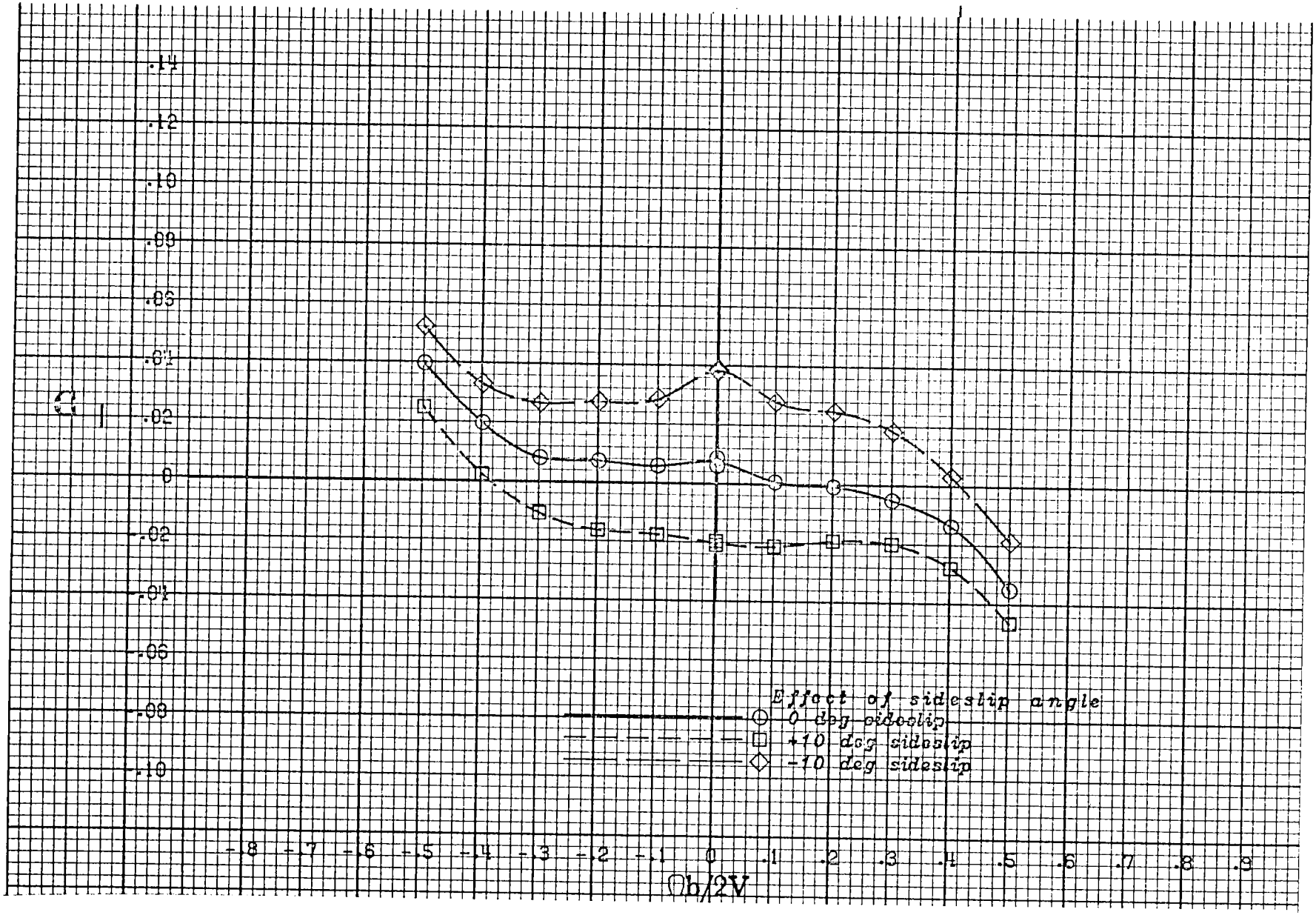

(b) α = 25 deg.

Figure A 2 .- Continued.

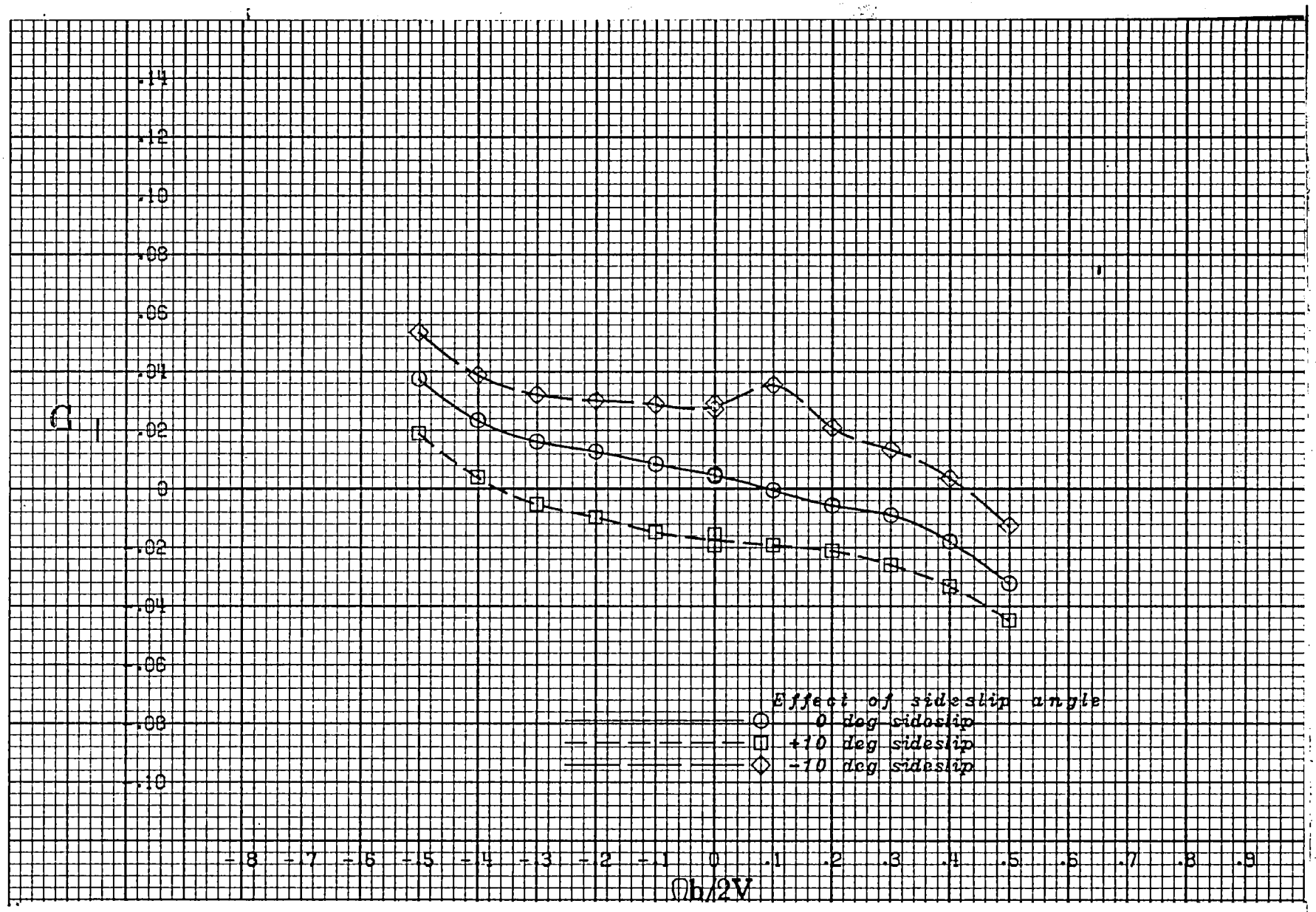

(c) α = 30 deg.

Figure A 2 .- Continued.

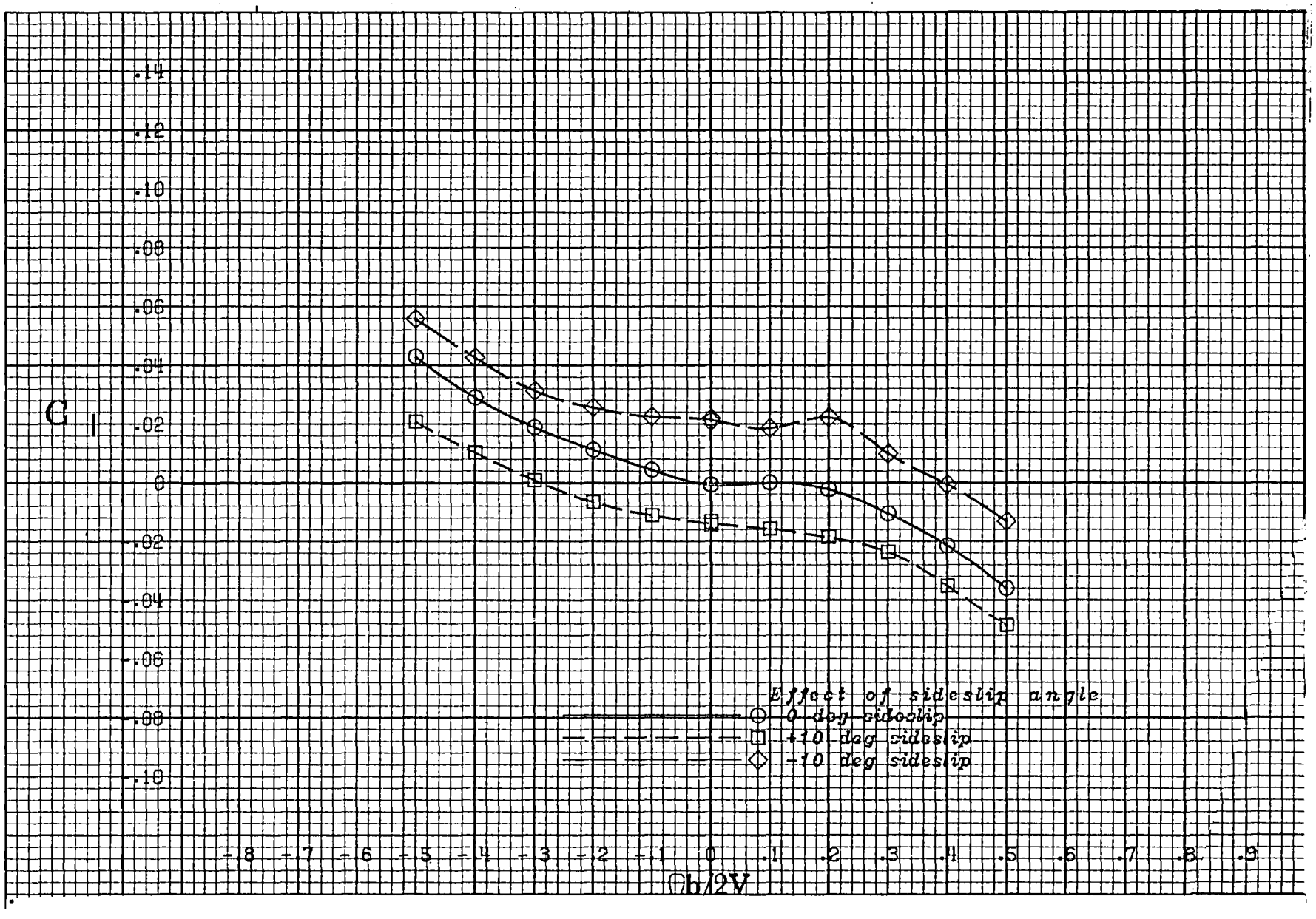

(d) α = 35 deg.

Figure A 2 .- Continued.

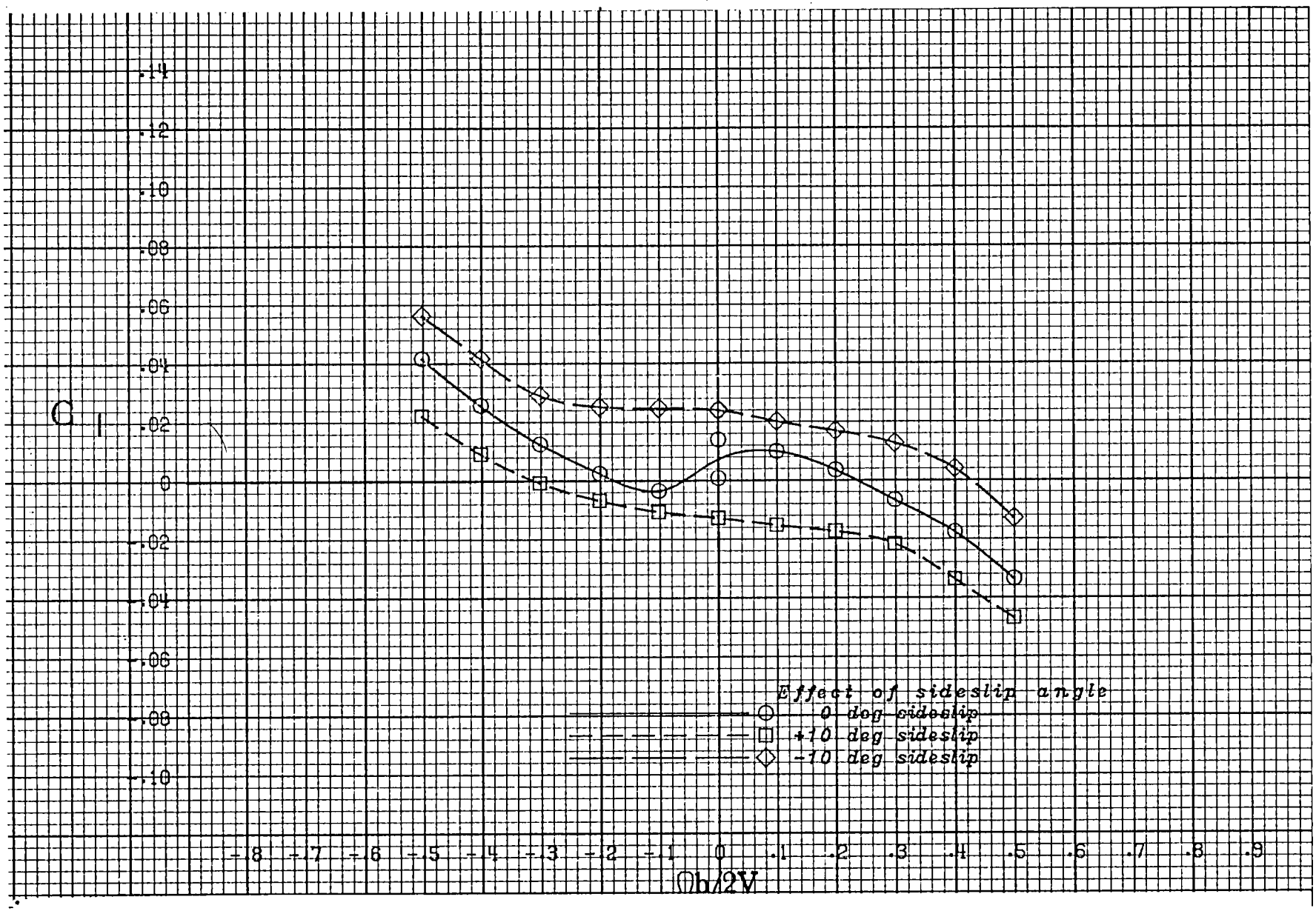

(e) α = 40 deg.

Figure A 2 .- Continued.

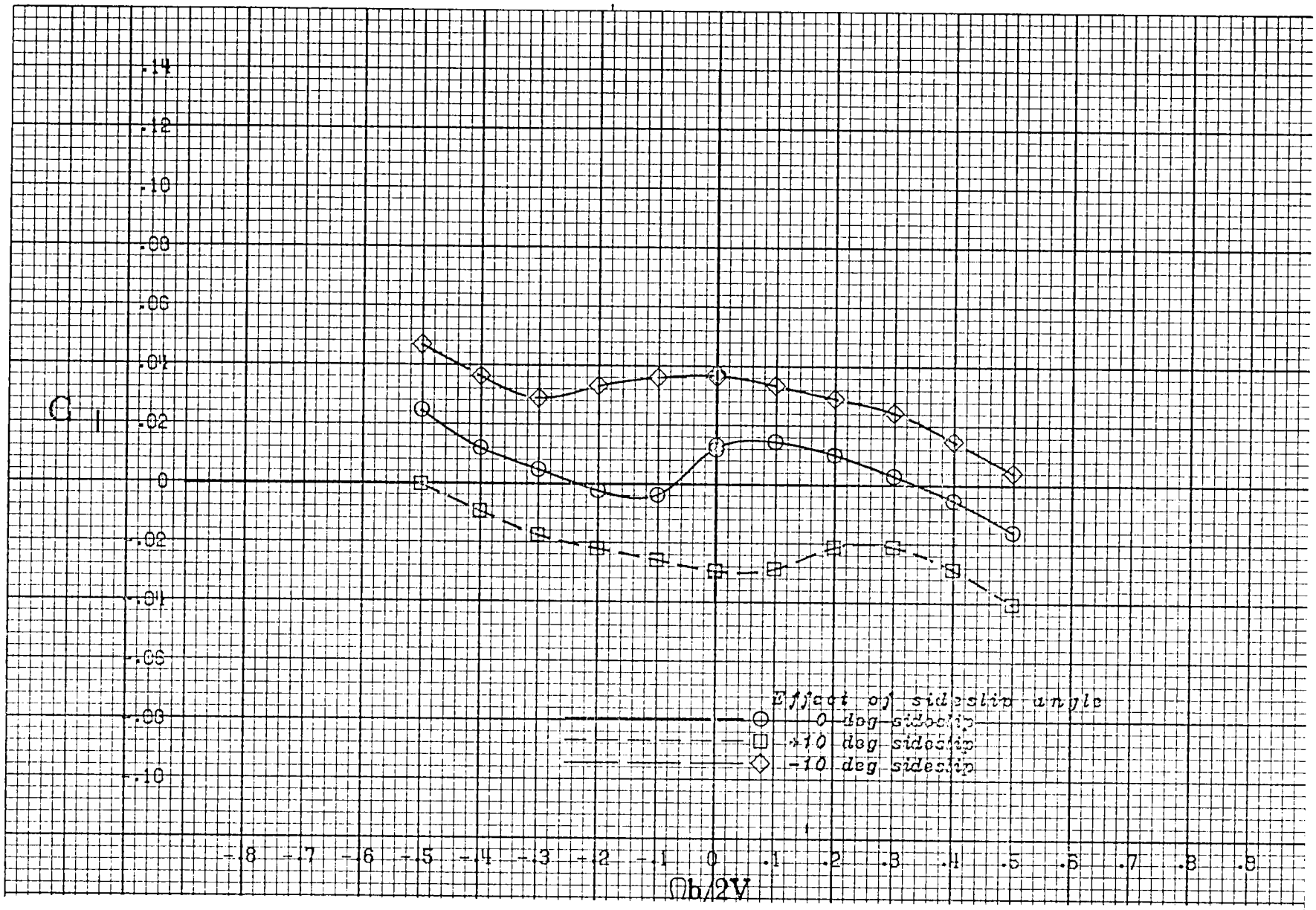

(f) α = 50 deg.

Figure A 2 .- Continued.

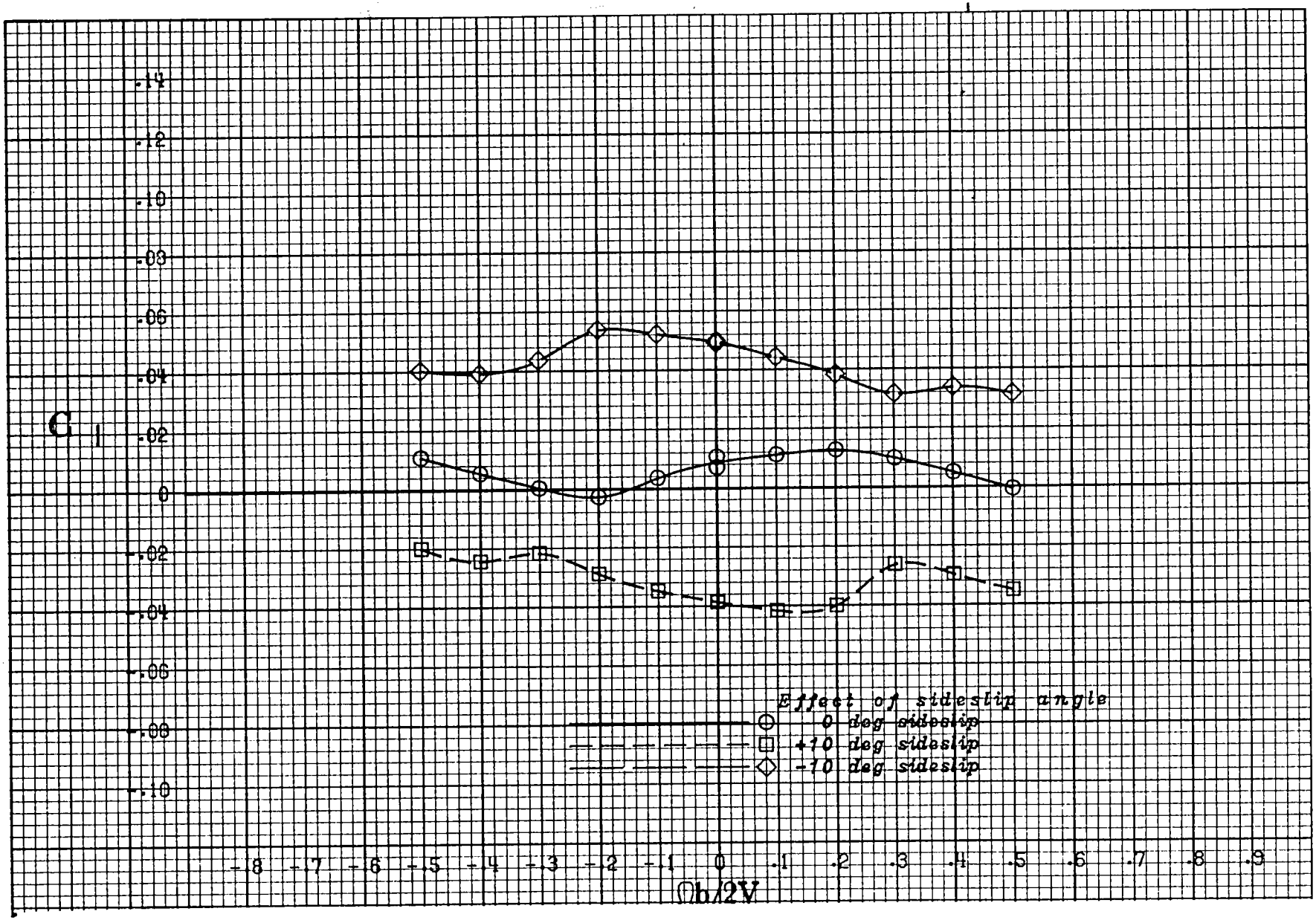

(g) α = 60 deg.

Figure A 2 .- Continued.

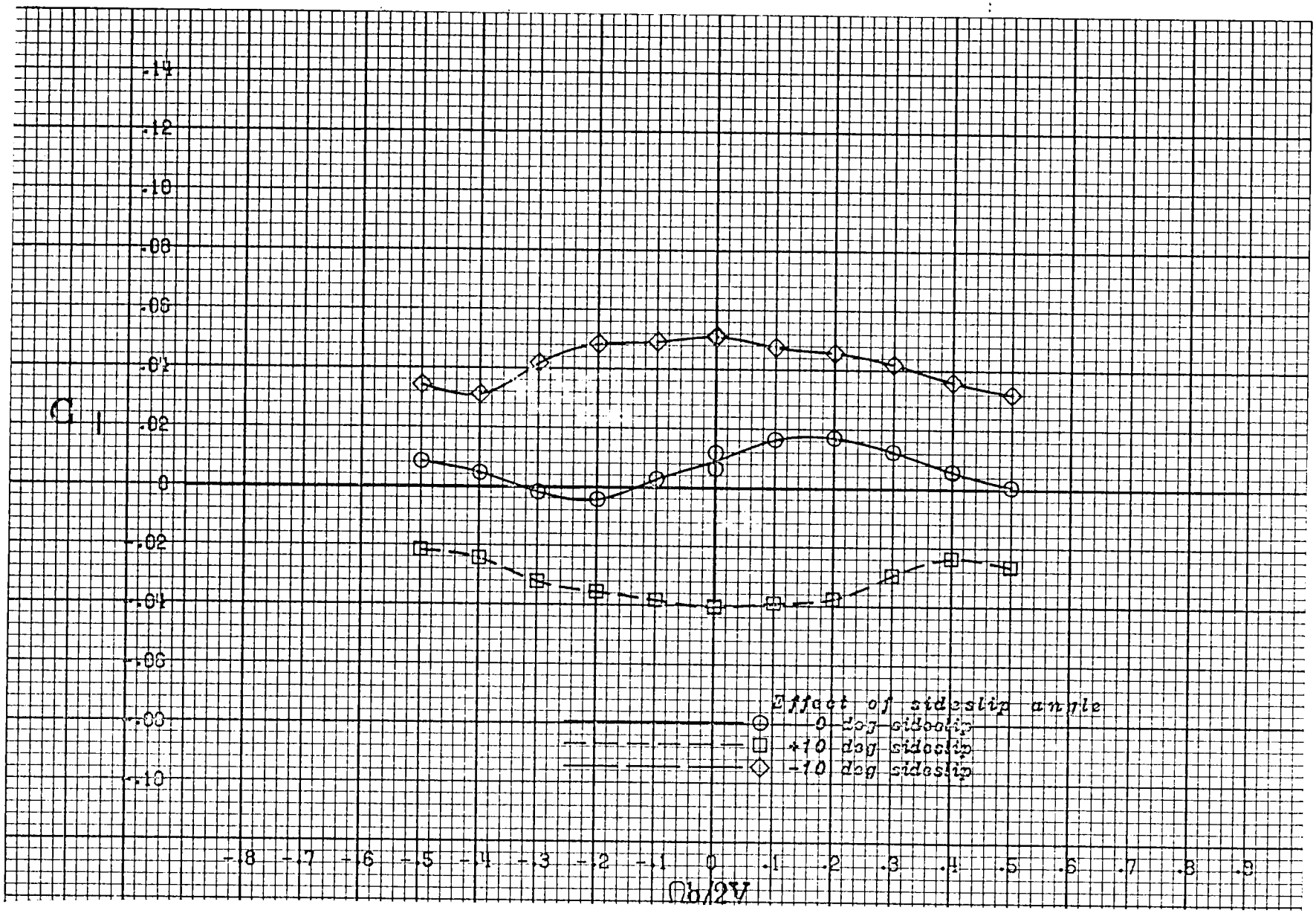

(h) α = 70 deg.

Figure A 2 .- Continued.

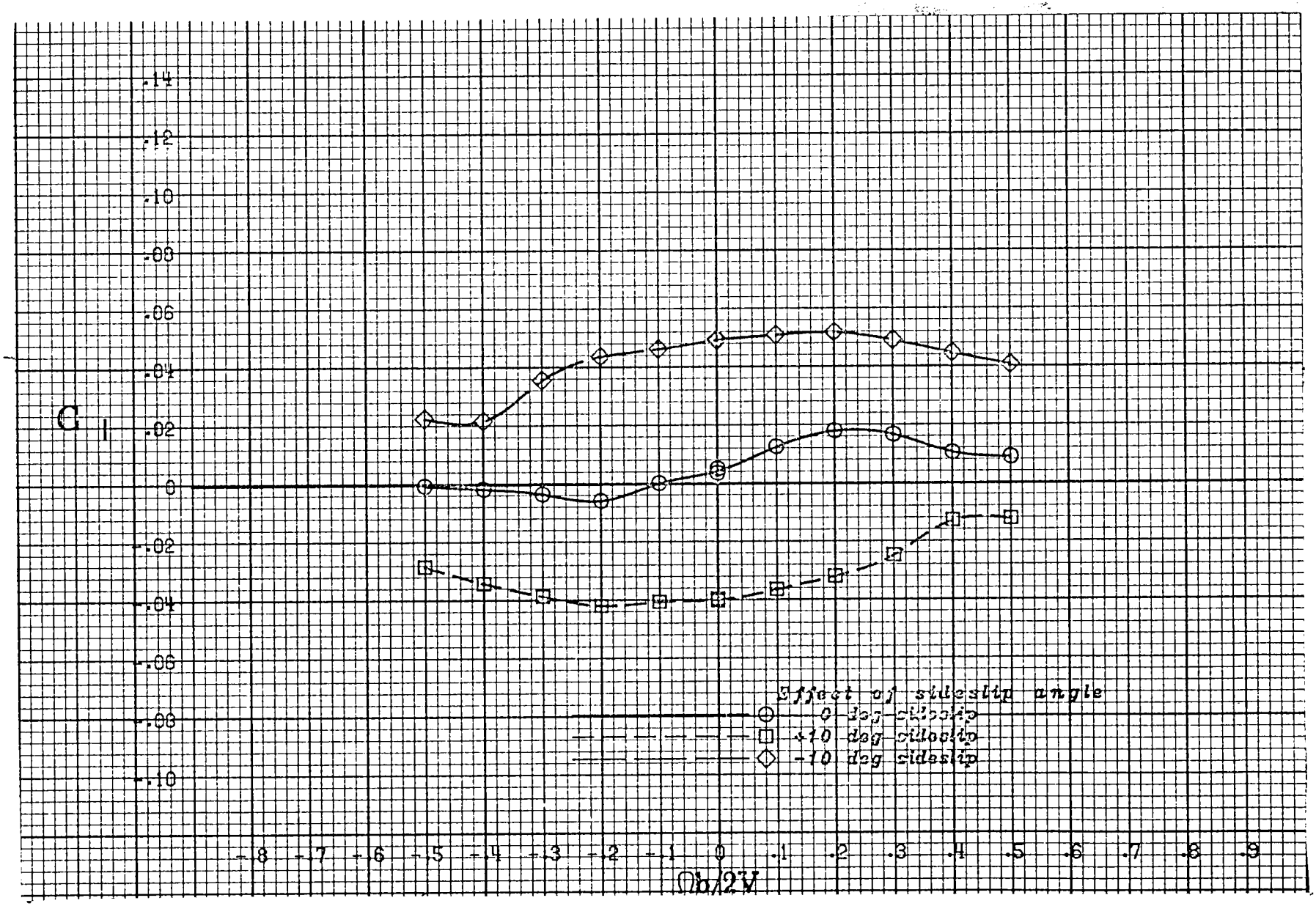

(i) α = 80 deg.

Figure A 2 .- Continued.

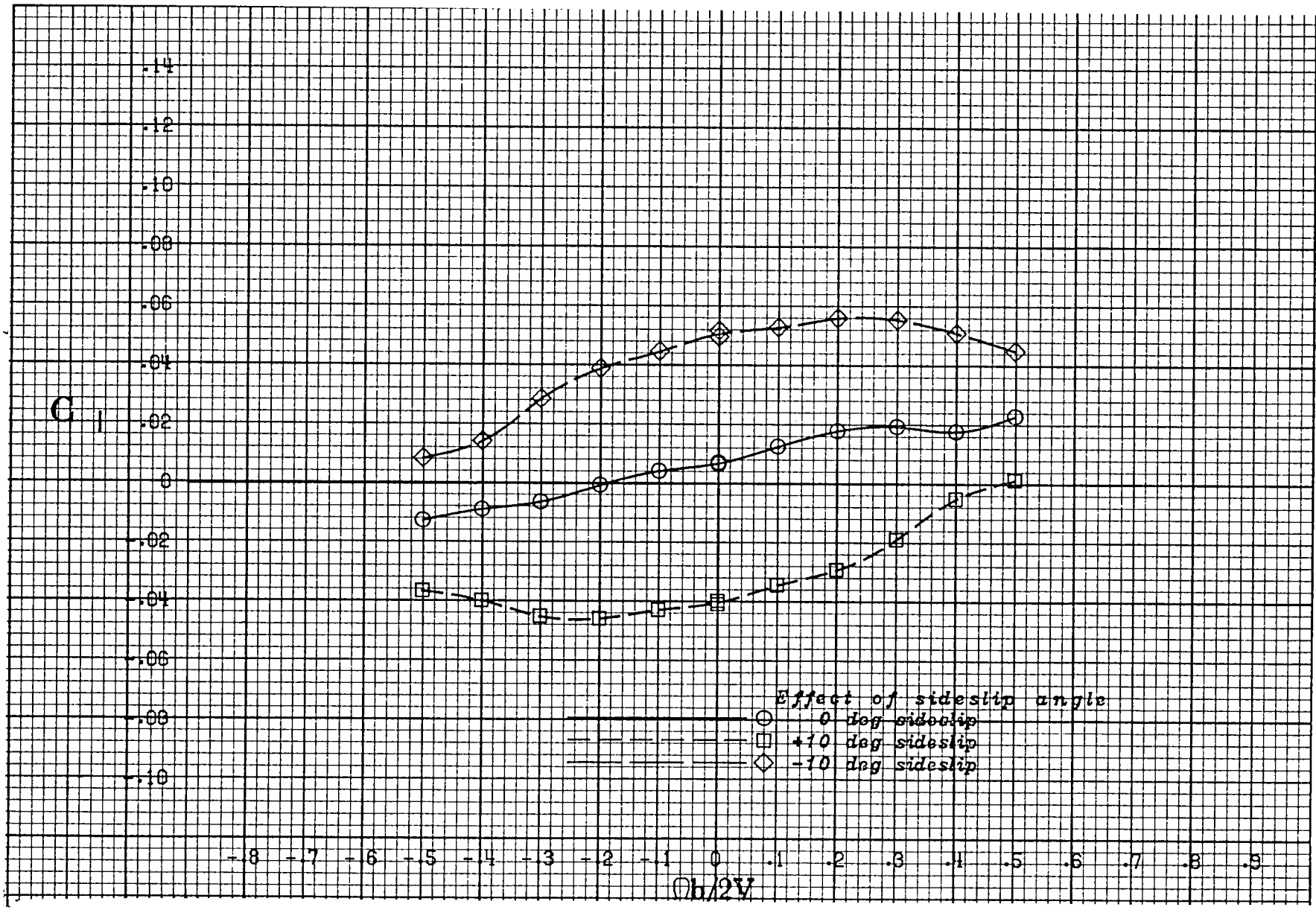

(j) α = 90 deg.

Figure A 2 .- Concluded.

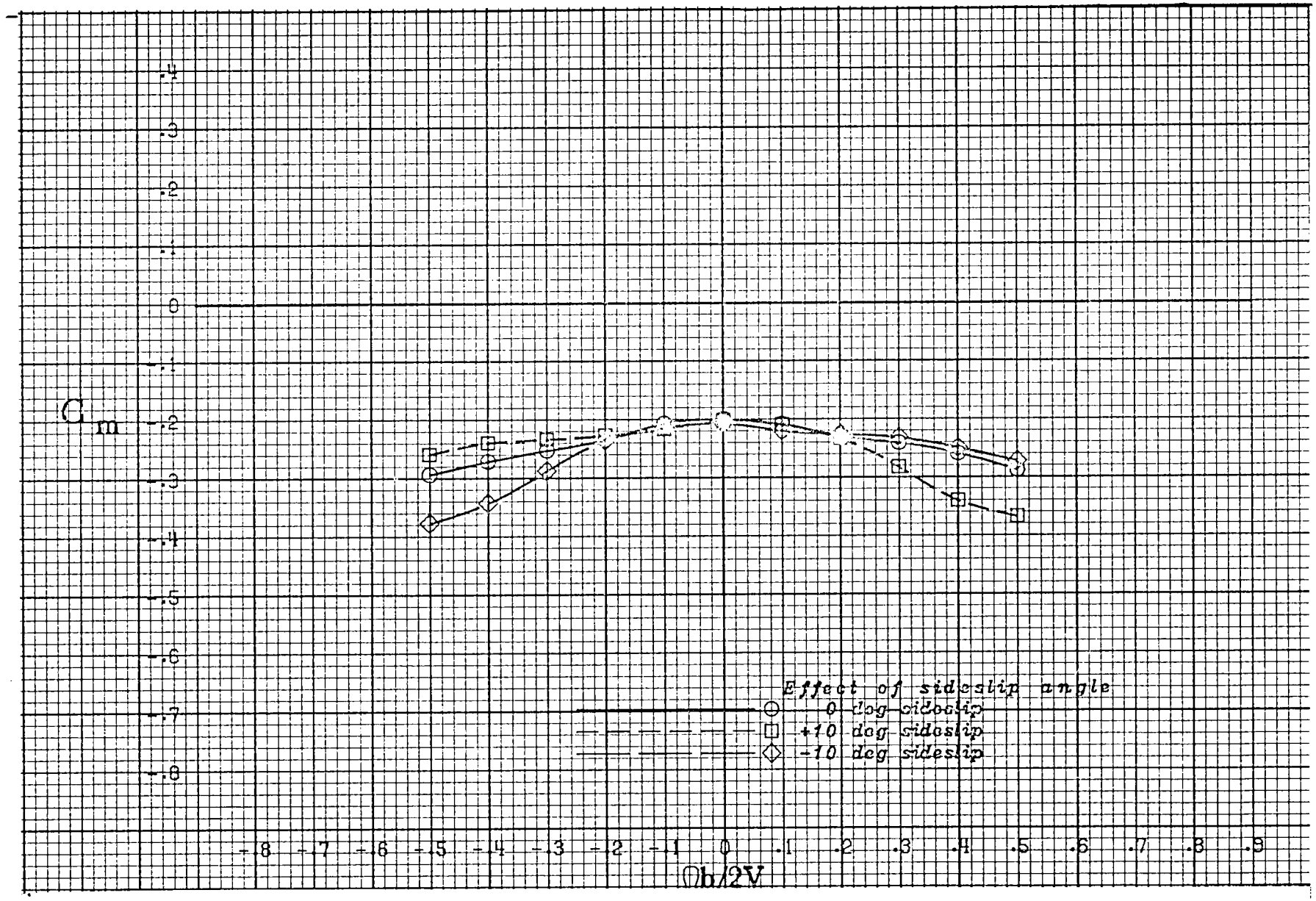

(a) α = 20 deg.

Figure A 3 .- Effect of rotation rate and sideslip angle on pitching-moment coefficient for the basic configuration with neutral controls.

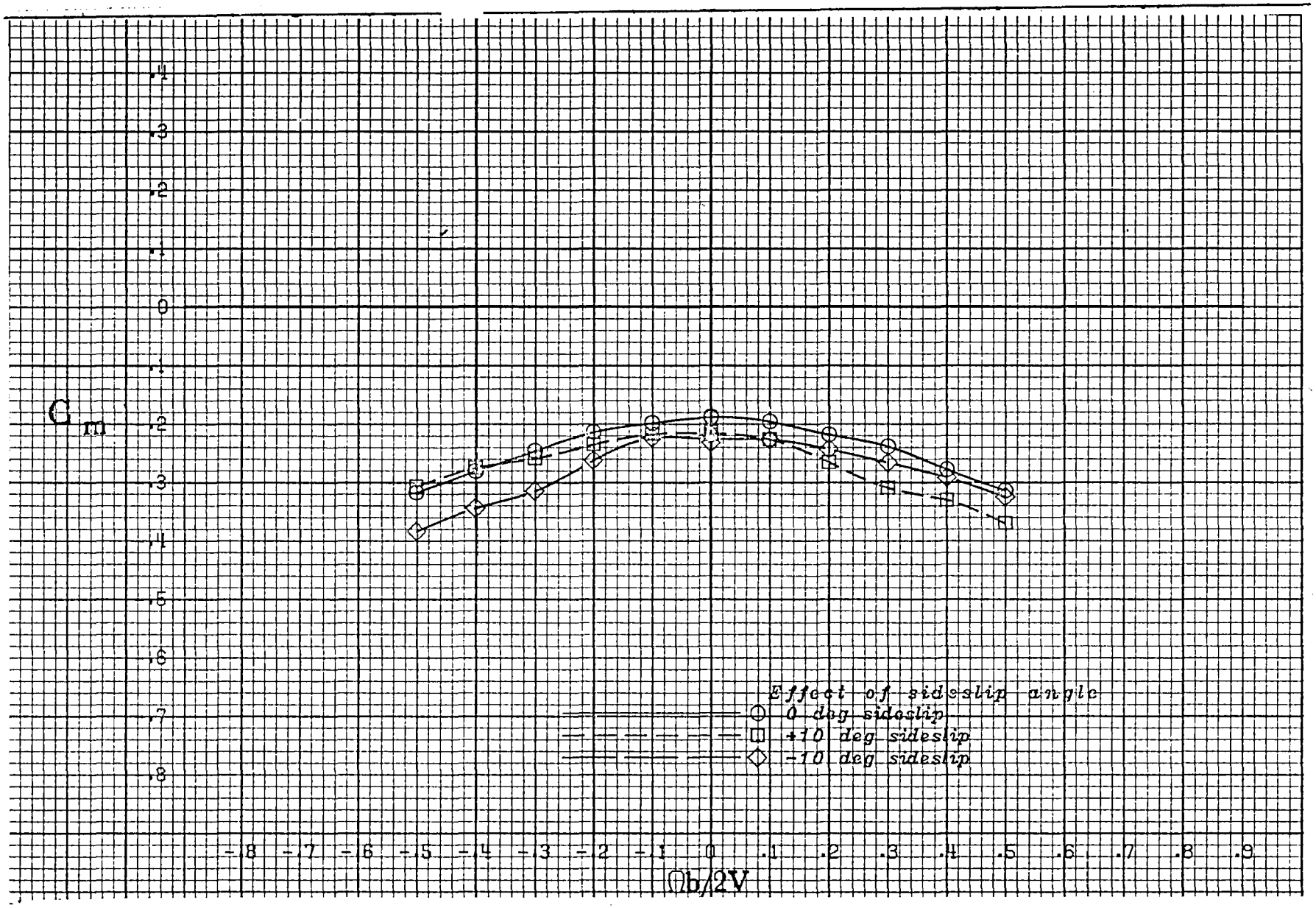

(b) α = 25 deg.

Figure A 3 .- Continued.

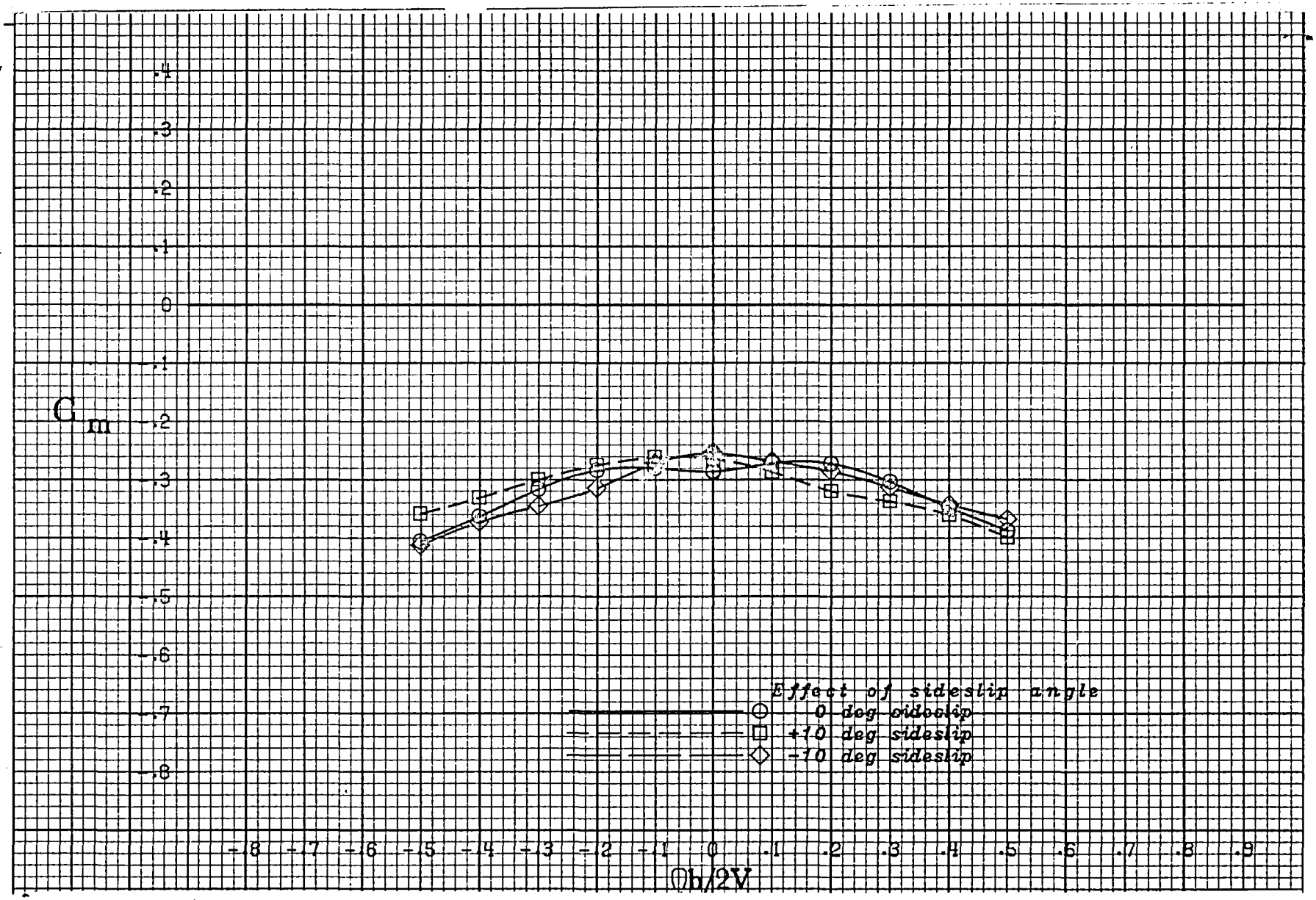

(c) α = 30 deg.

Figure A 3 .- Continued.

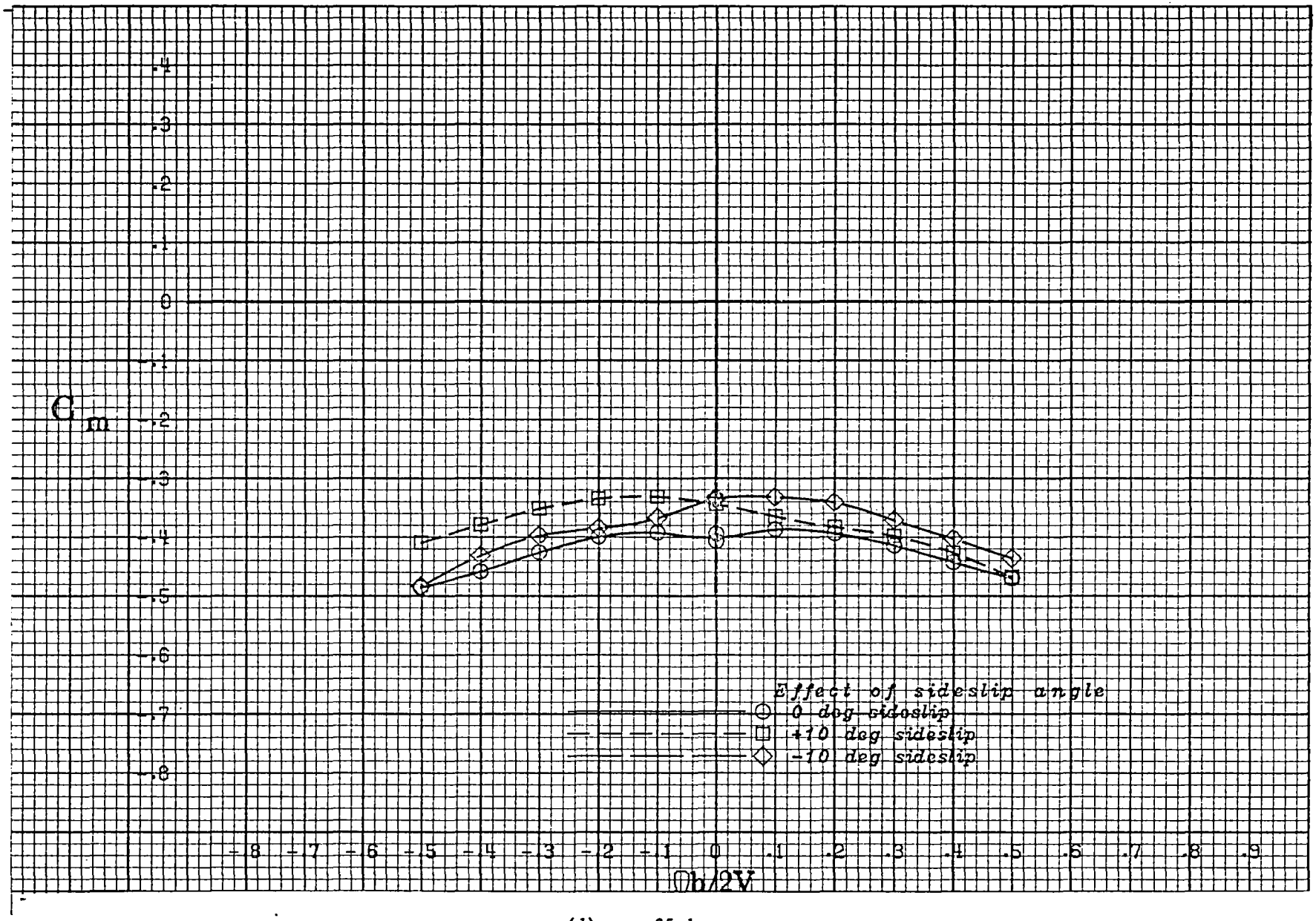

(d) α = 35 deg.

Figure A 3 .- Continued.

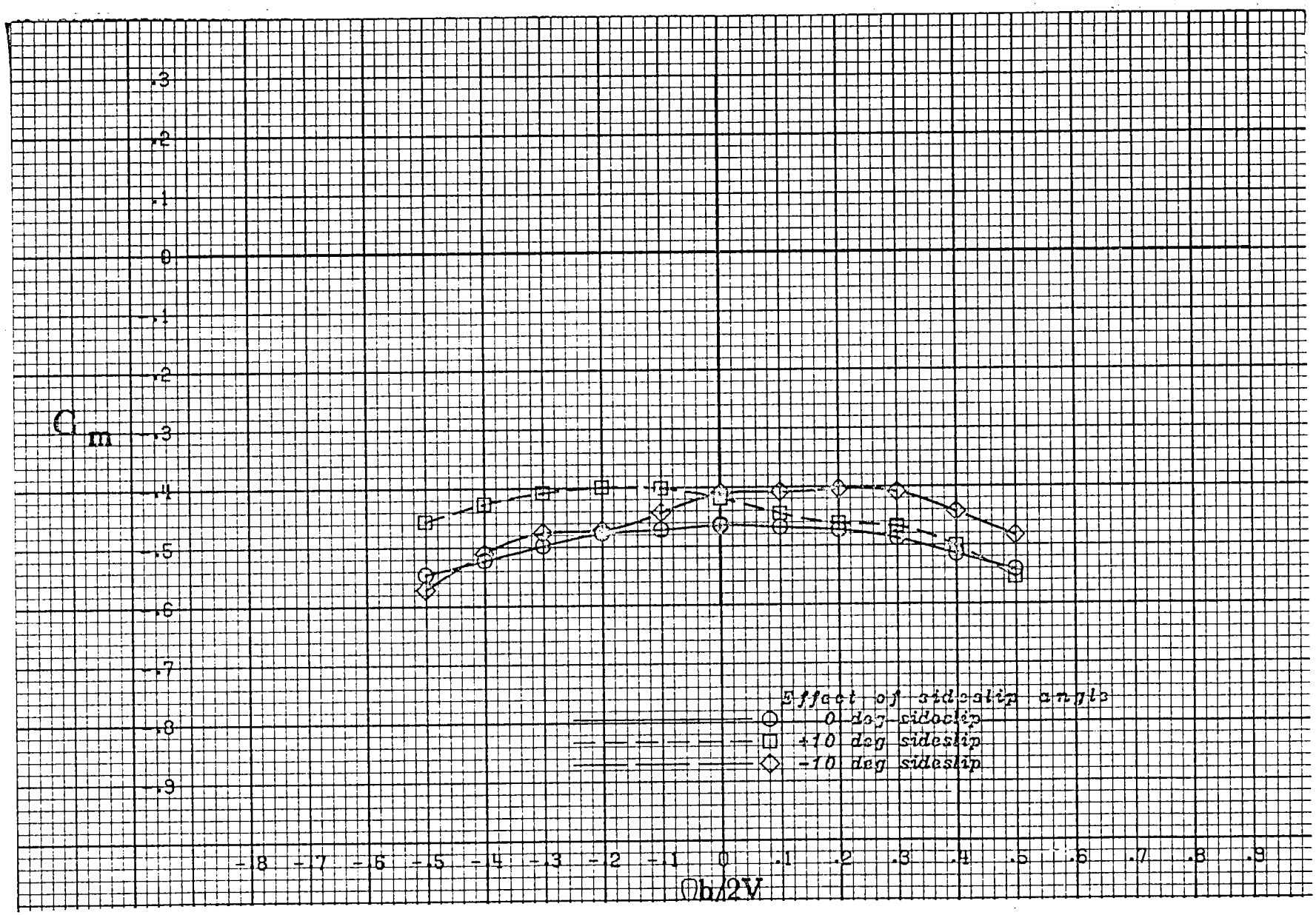

(c) α = 40 deg.

Figure A 3 .- Continued.

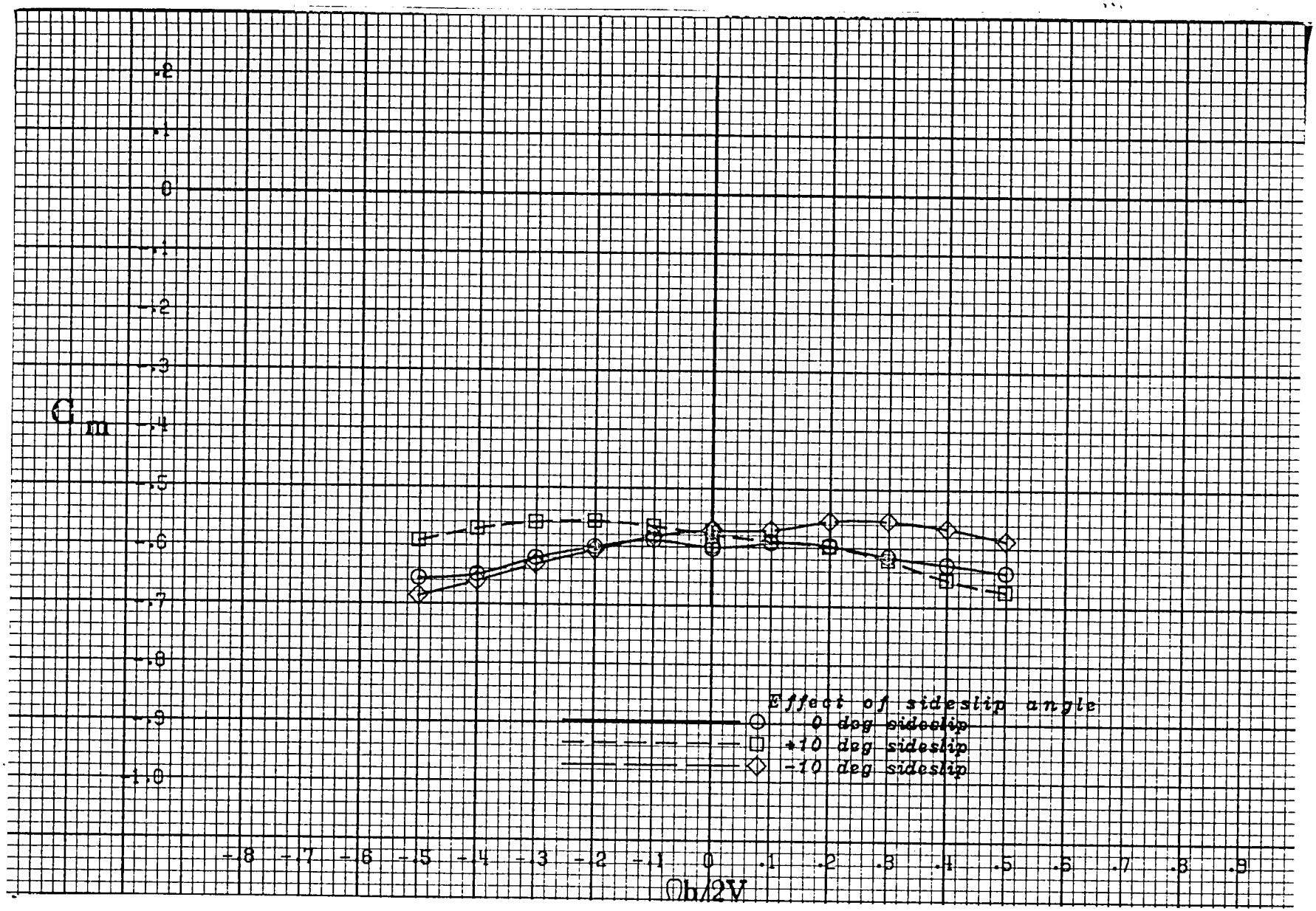

(f) α = 50 deg.

Figure A 3 .- Continued.

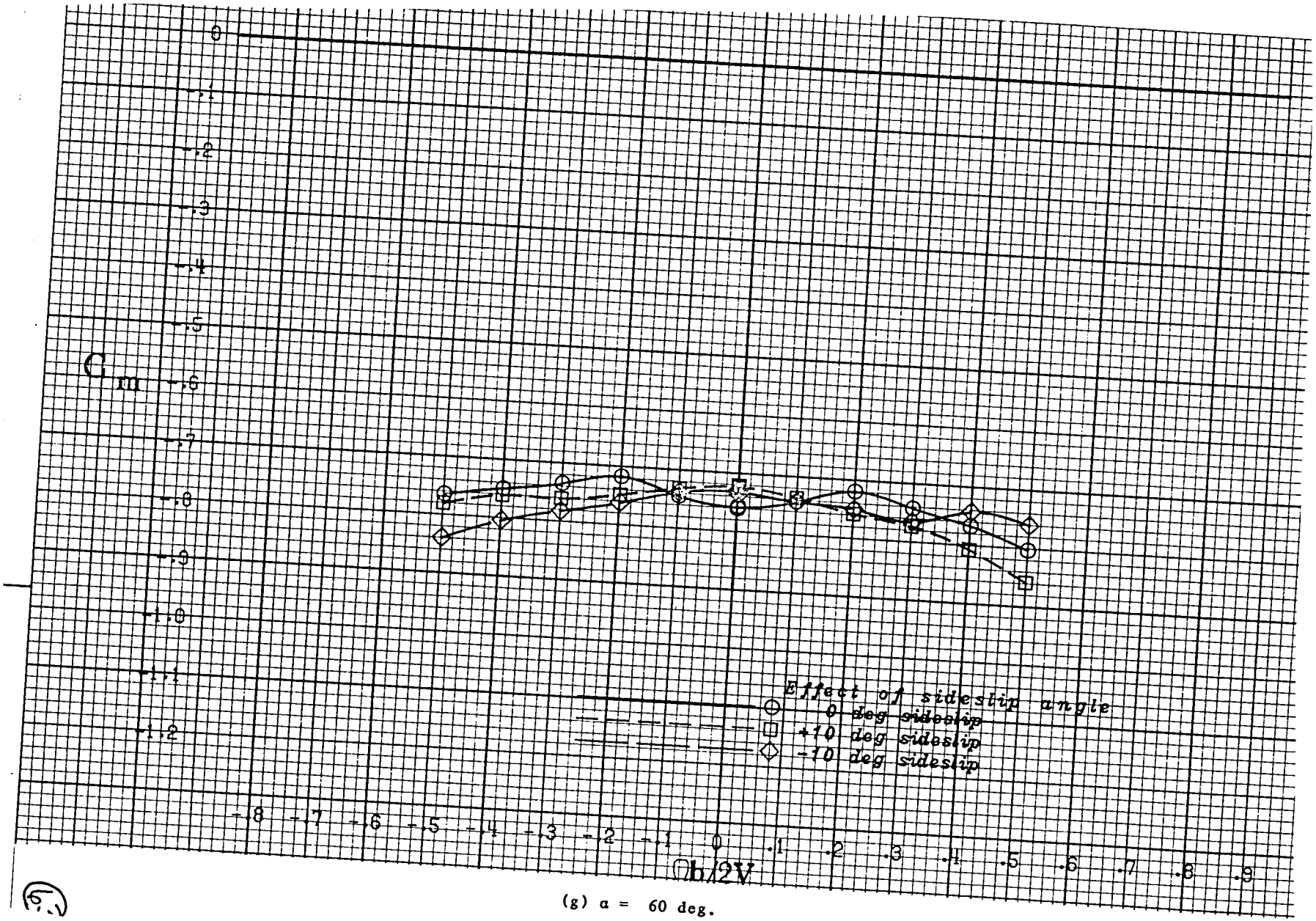

(g) α = 60 deg.

Figure A 3 .- Continued.

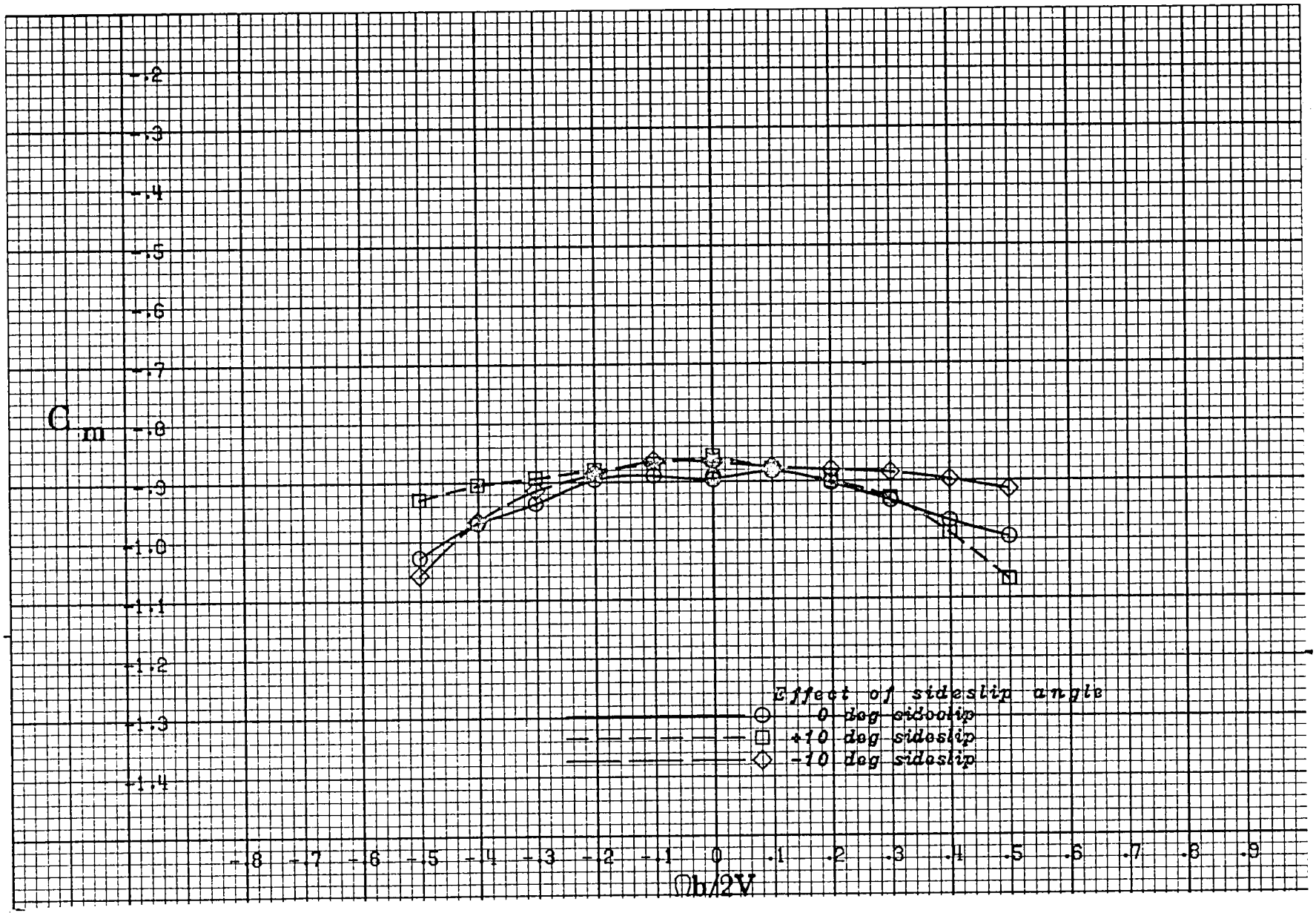

(h) α = 70 deg.

Figure A 3 .- Continued.

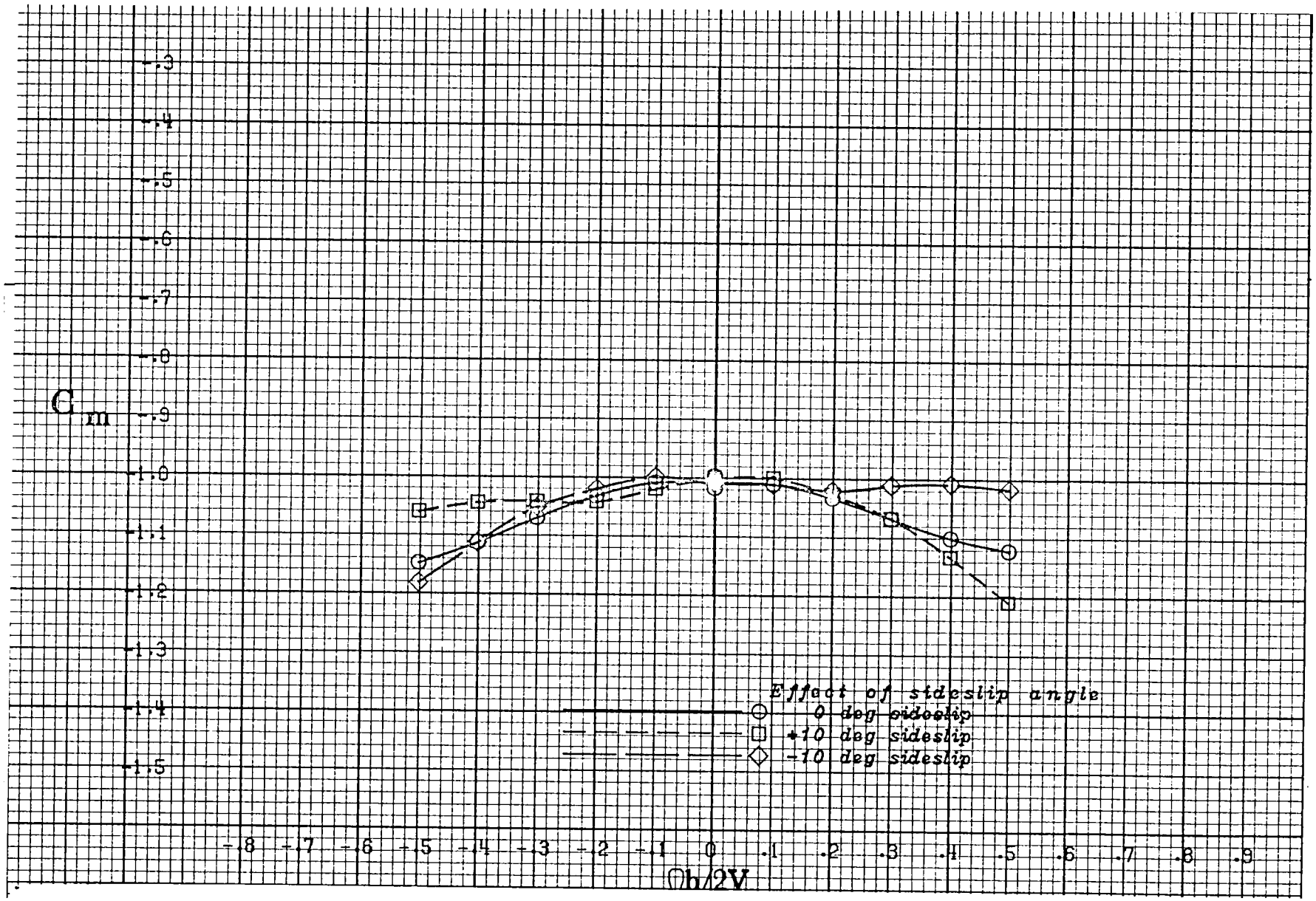

(i) α = 80 deg.

Figure A 3 .- Continued.

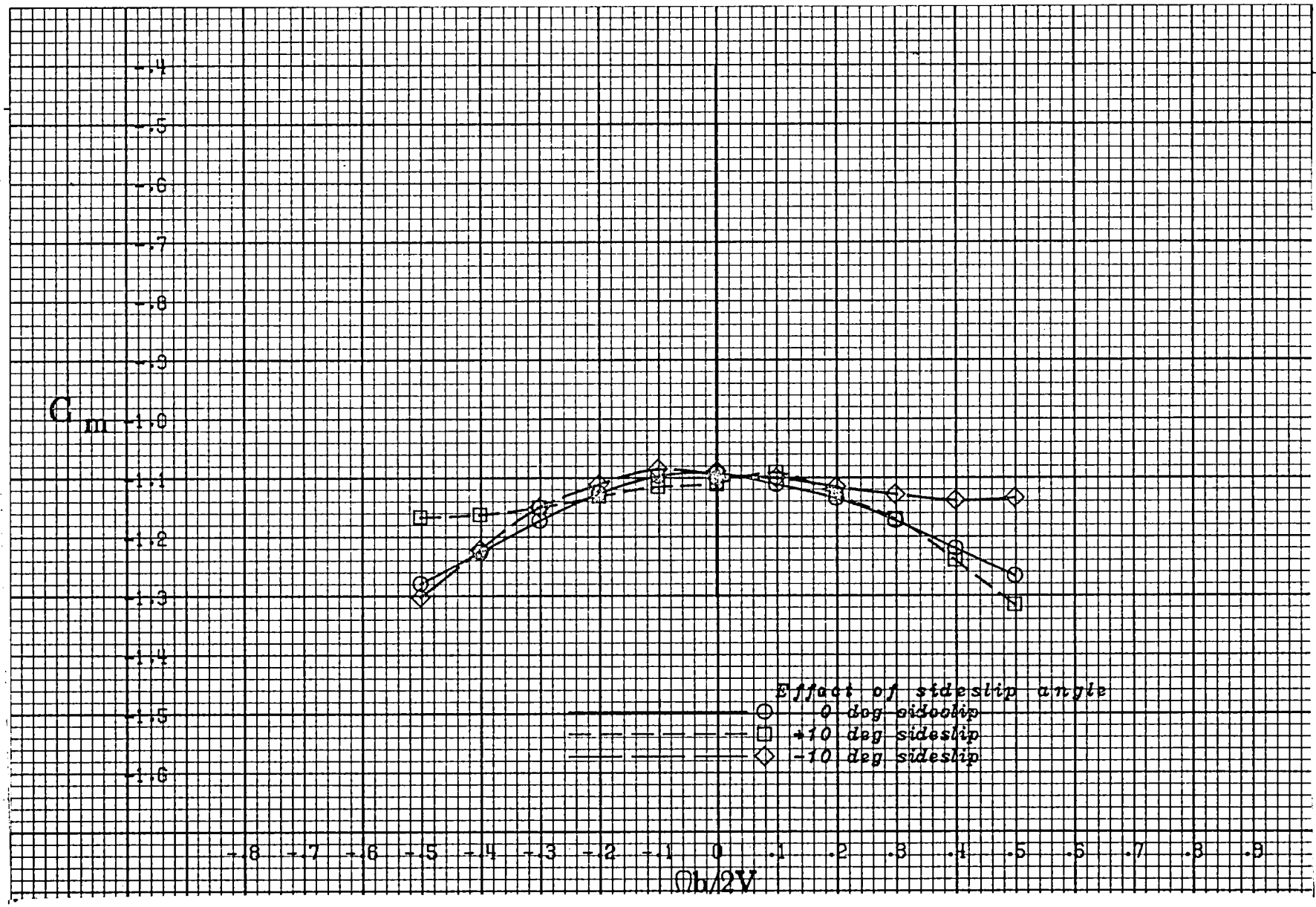

(j) α = 90 deg.

Figure A 3 .- Concluded.

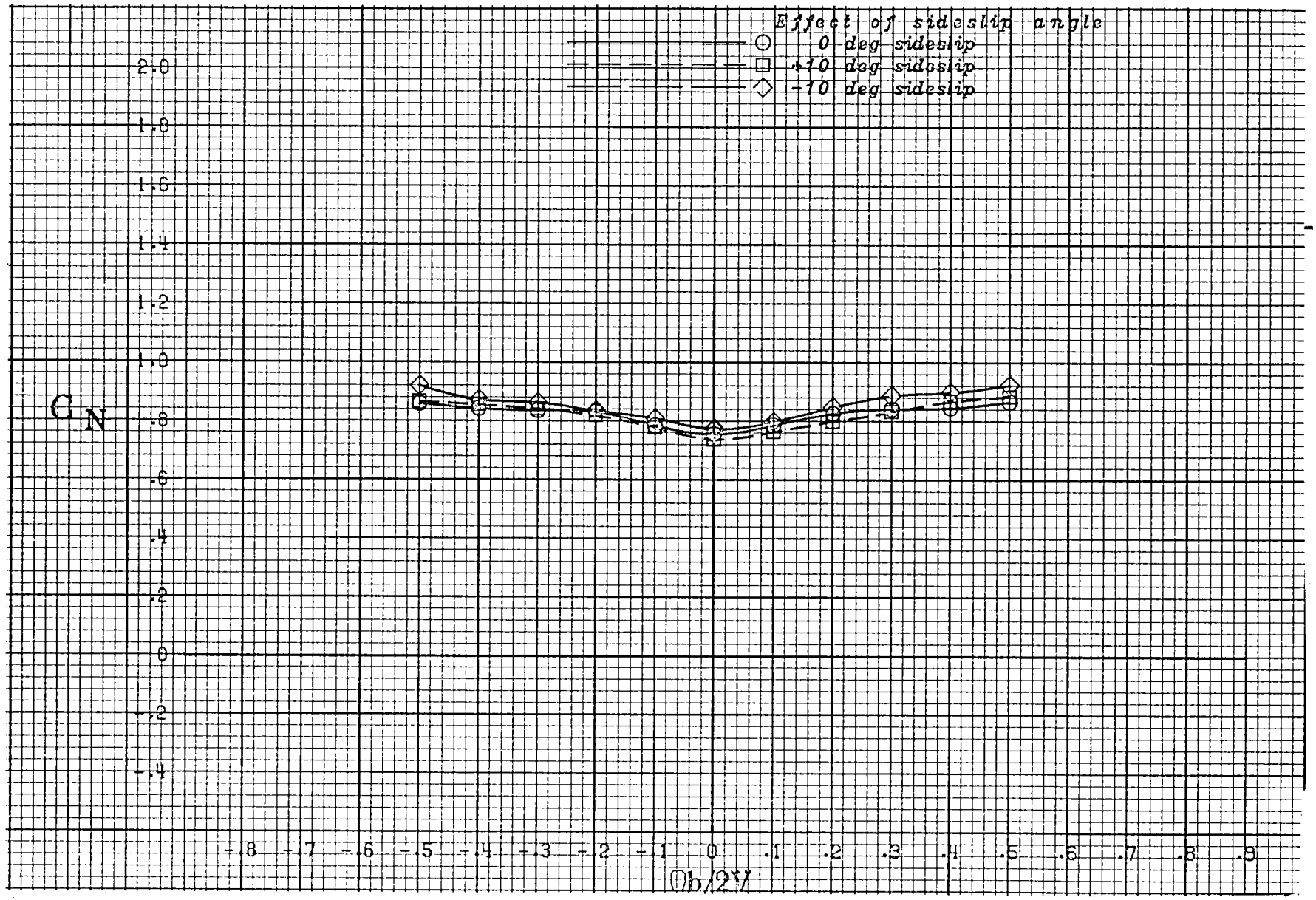

(a) α = 20 deg.

Figure A 4 .- Effect of rotation rate and sideslip angle on normal-force coefficient for the basic configuration with neutral controls.

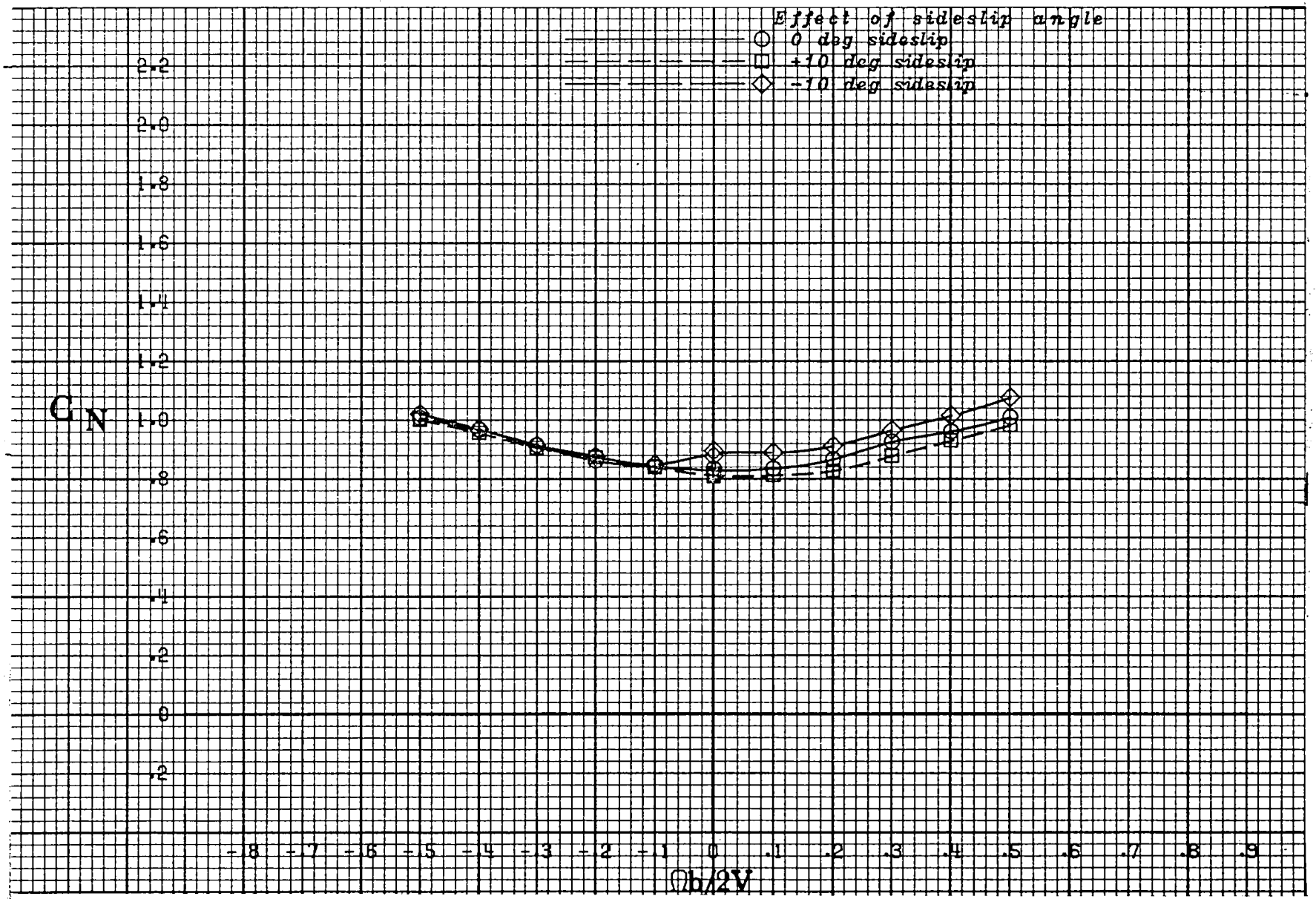

(b) α = 25 deg.

Figure A 4 .- Continued.

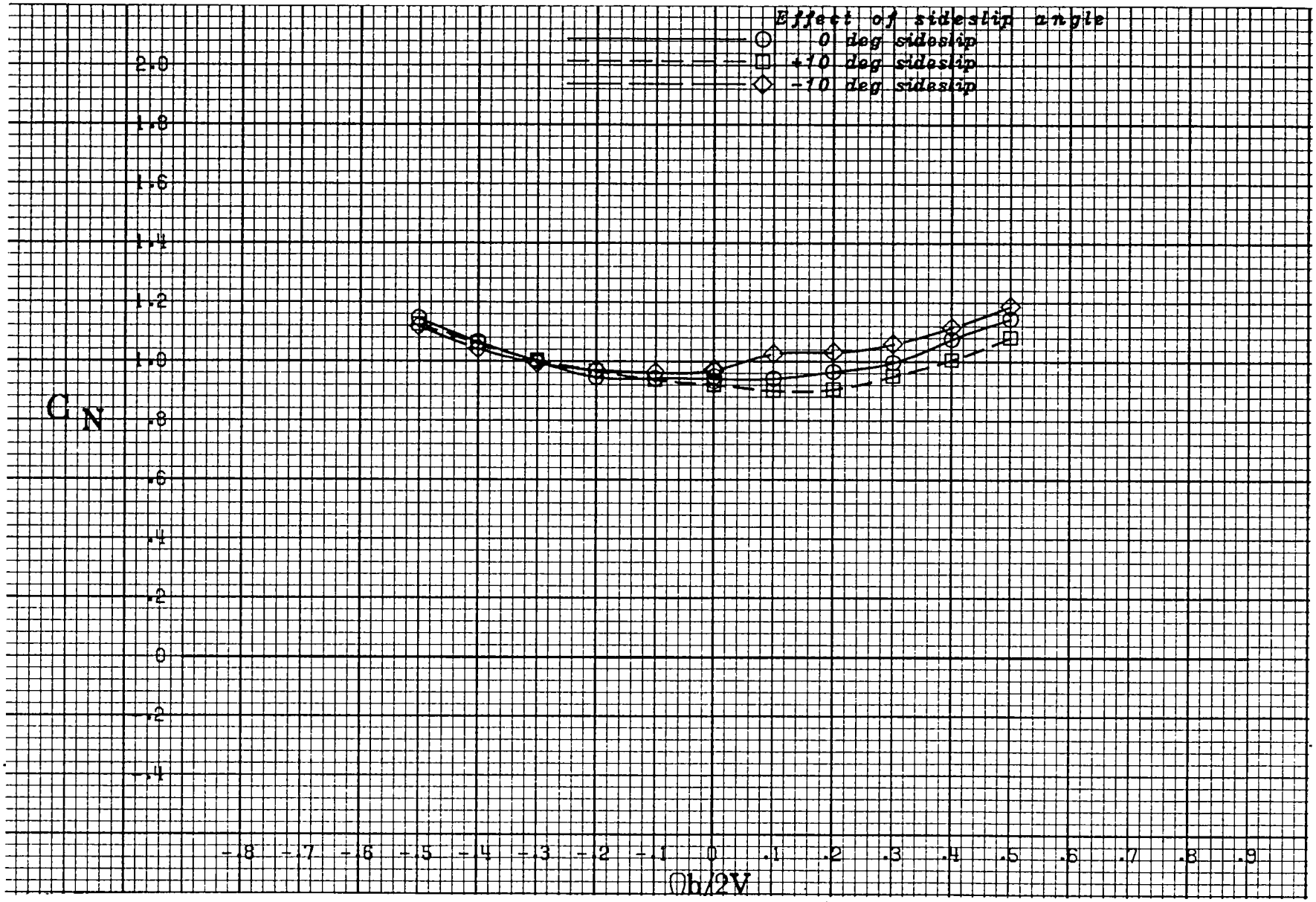

(c) α = 30 deg.

Figure A 4 .- Continued.

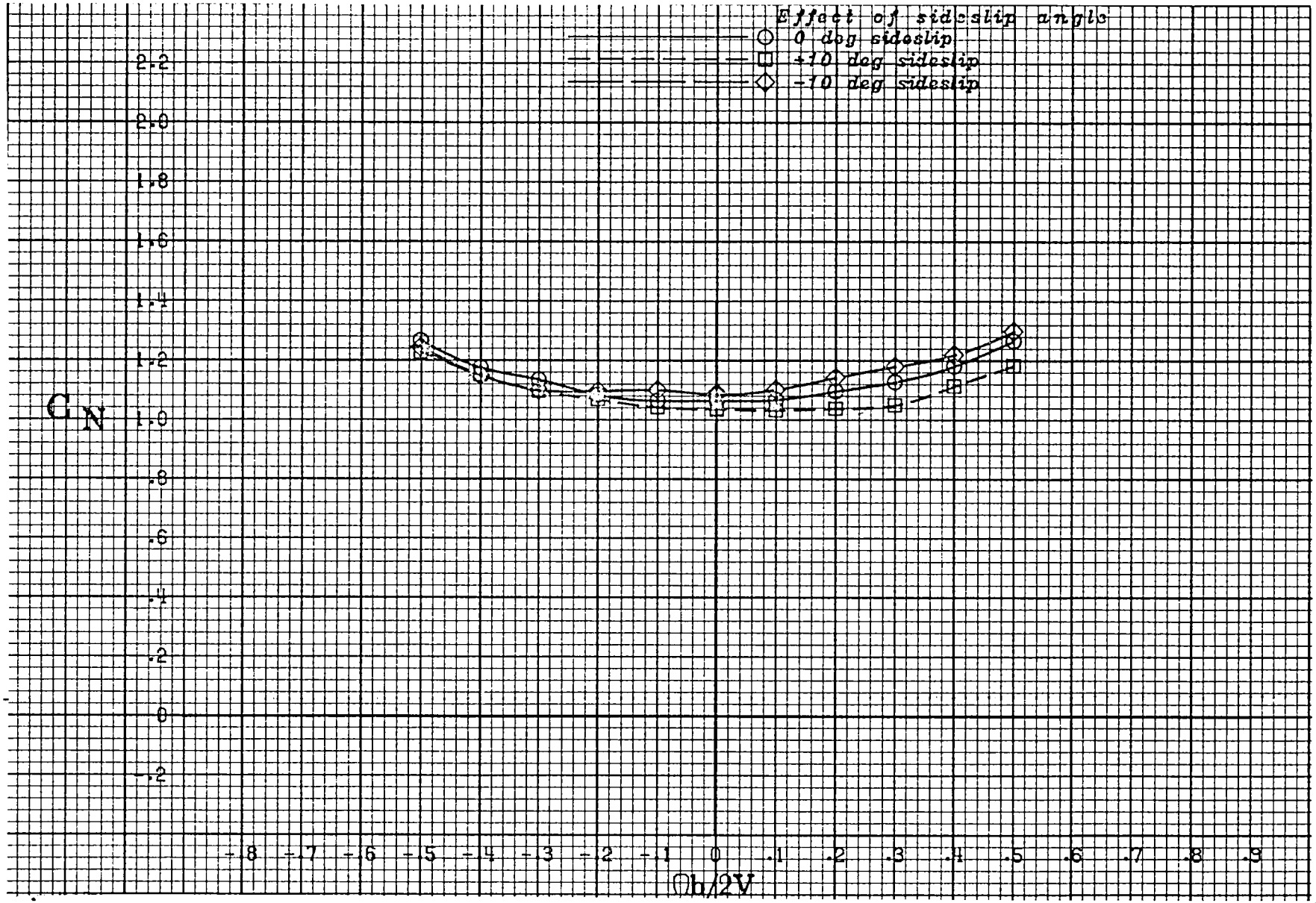

(d) α = 35 deg.

Figure A 4 .- Continued.

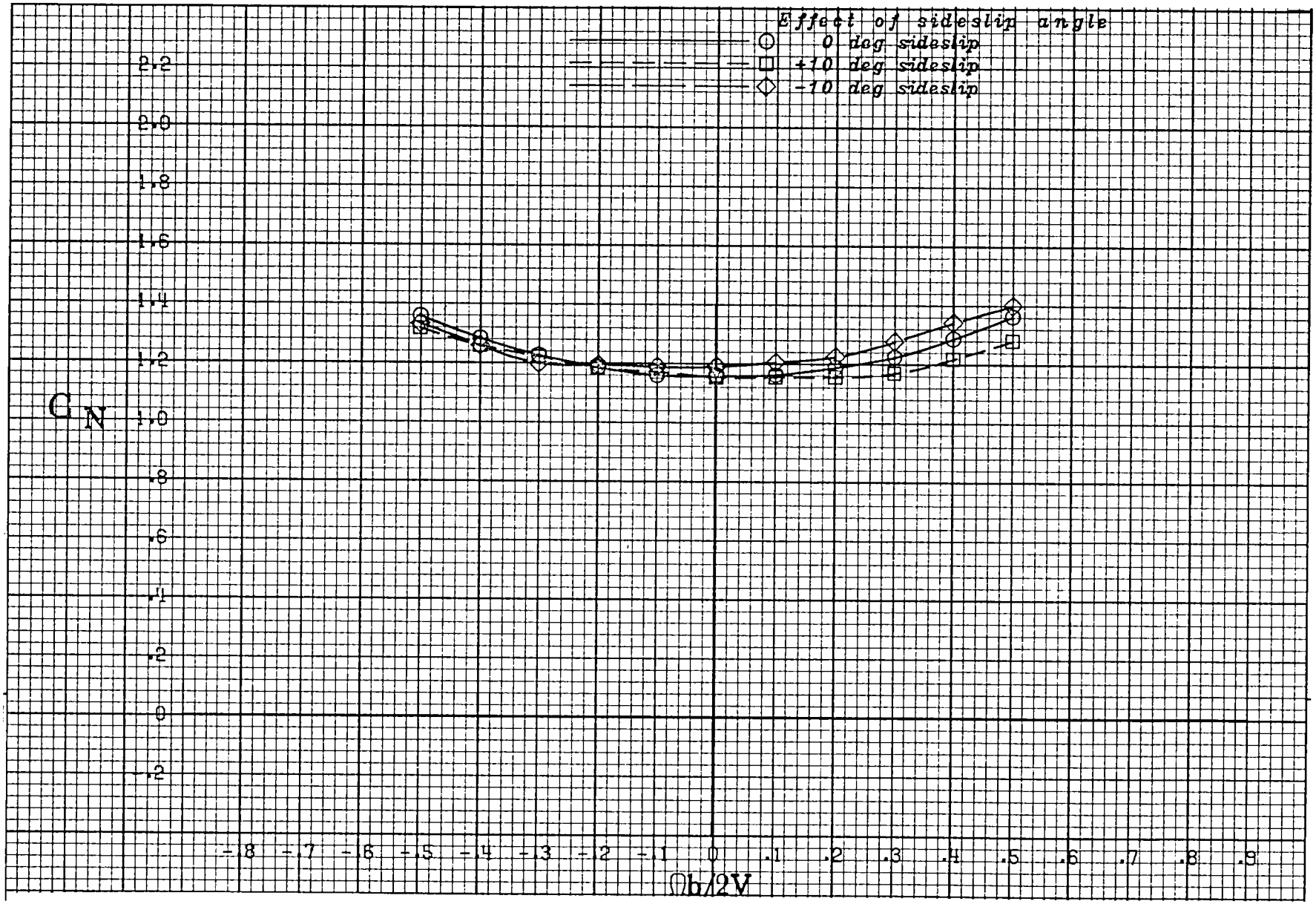

(e) α = 40 deg.

Figure A 4 .- Continued.

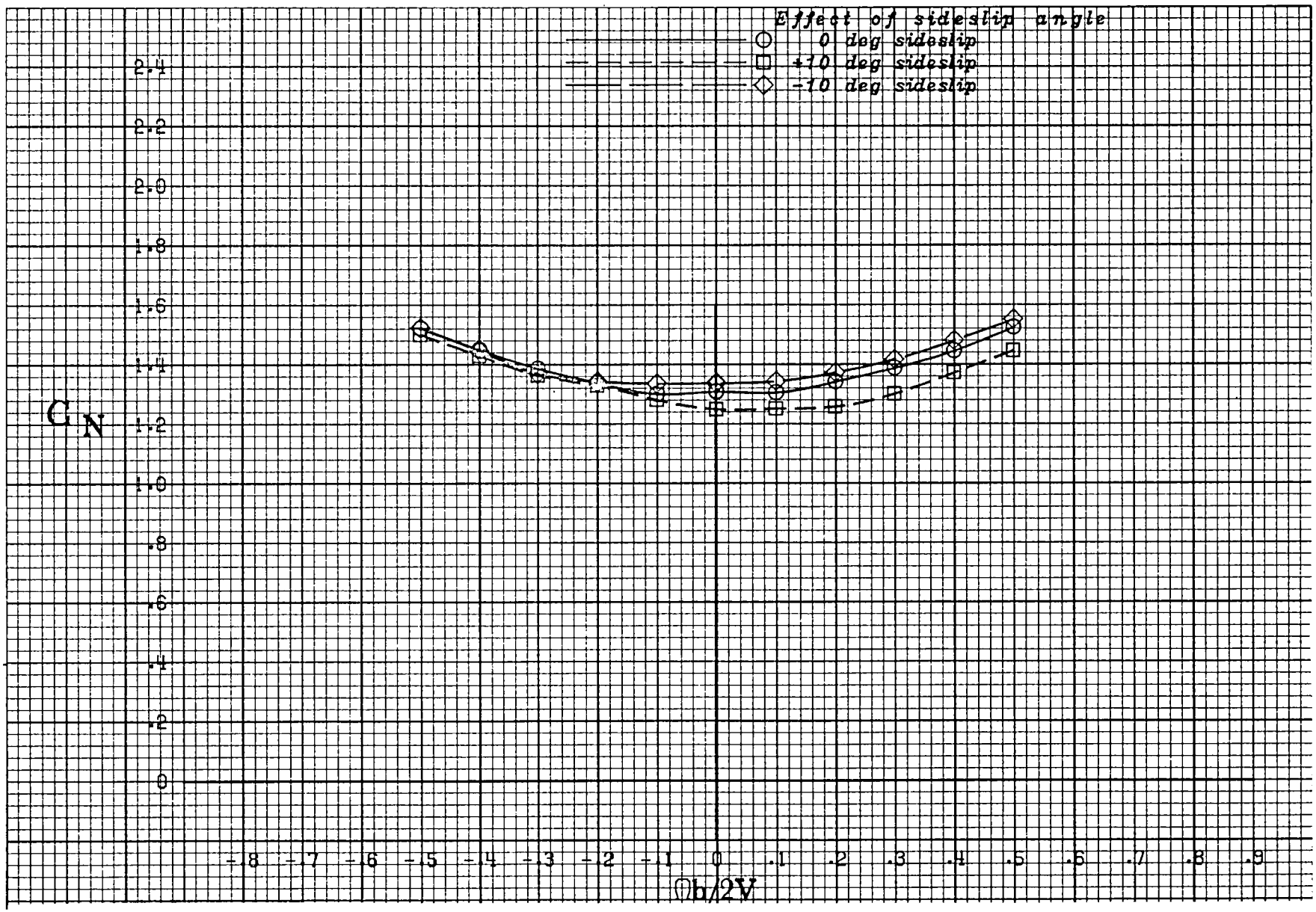

(f) α = 50 deg.

Figure A 4 .- Continued.

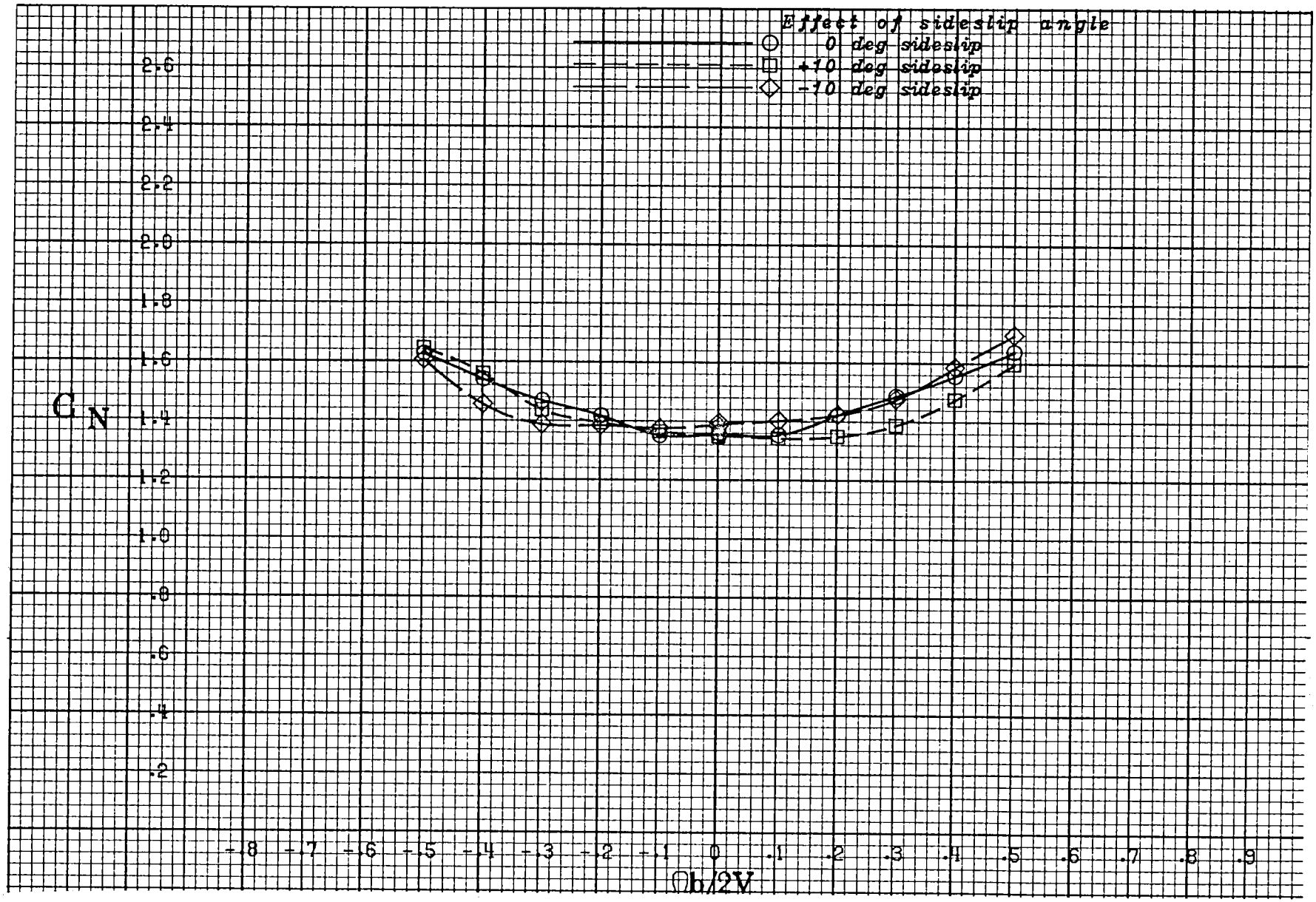

(g) α = 60 deg.

Figure A 4 .- Continued.

(h) α = 70 deg.

Figure A 4 .- Continued.

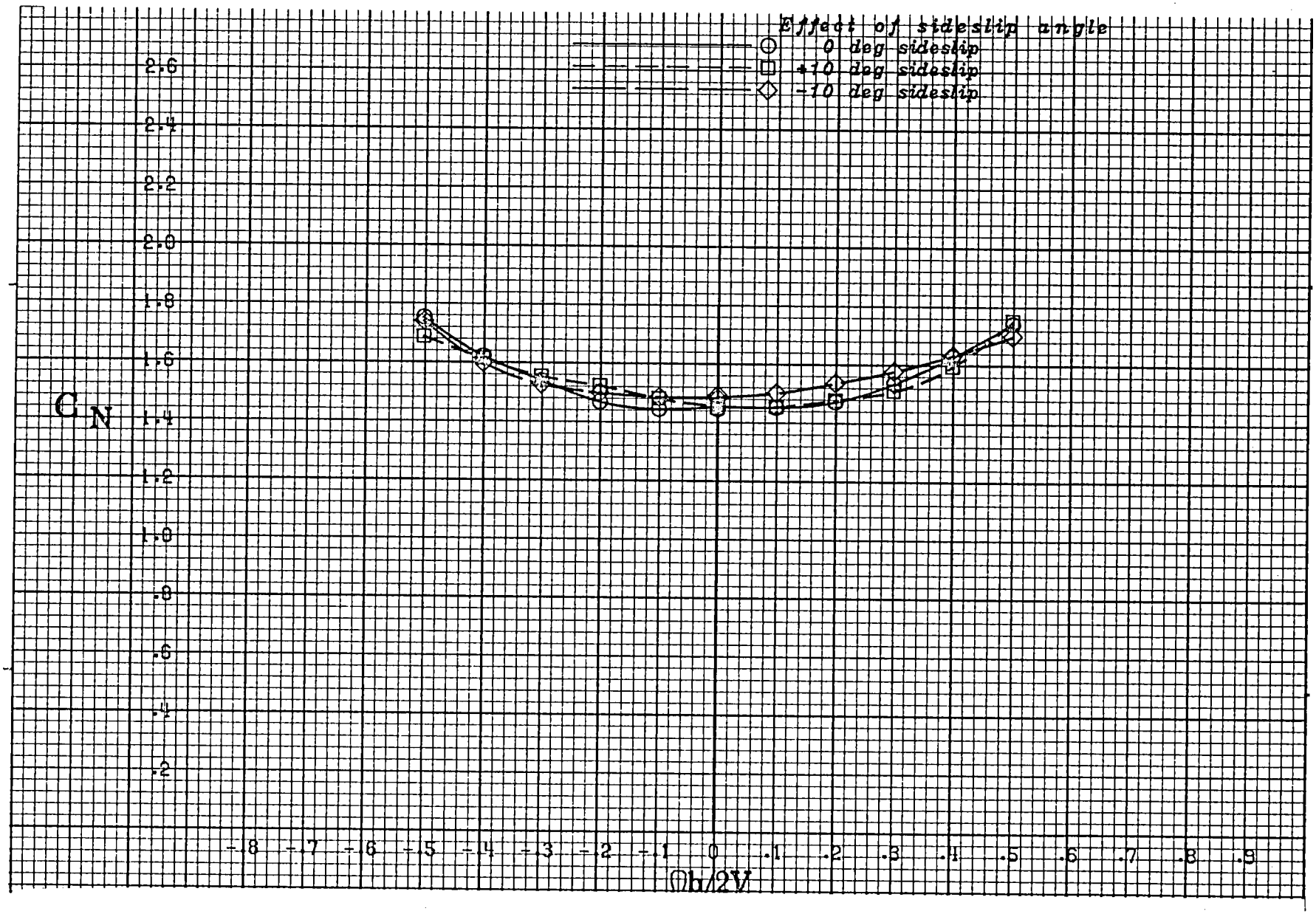

(i) α = 80 deg.

Figure A 4 .- Continued.

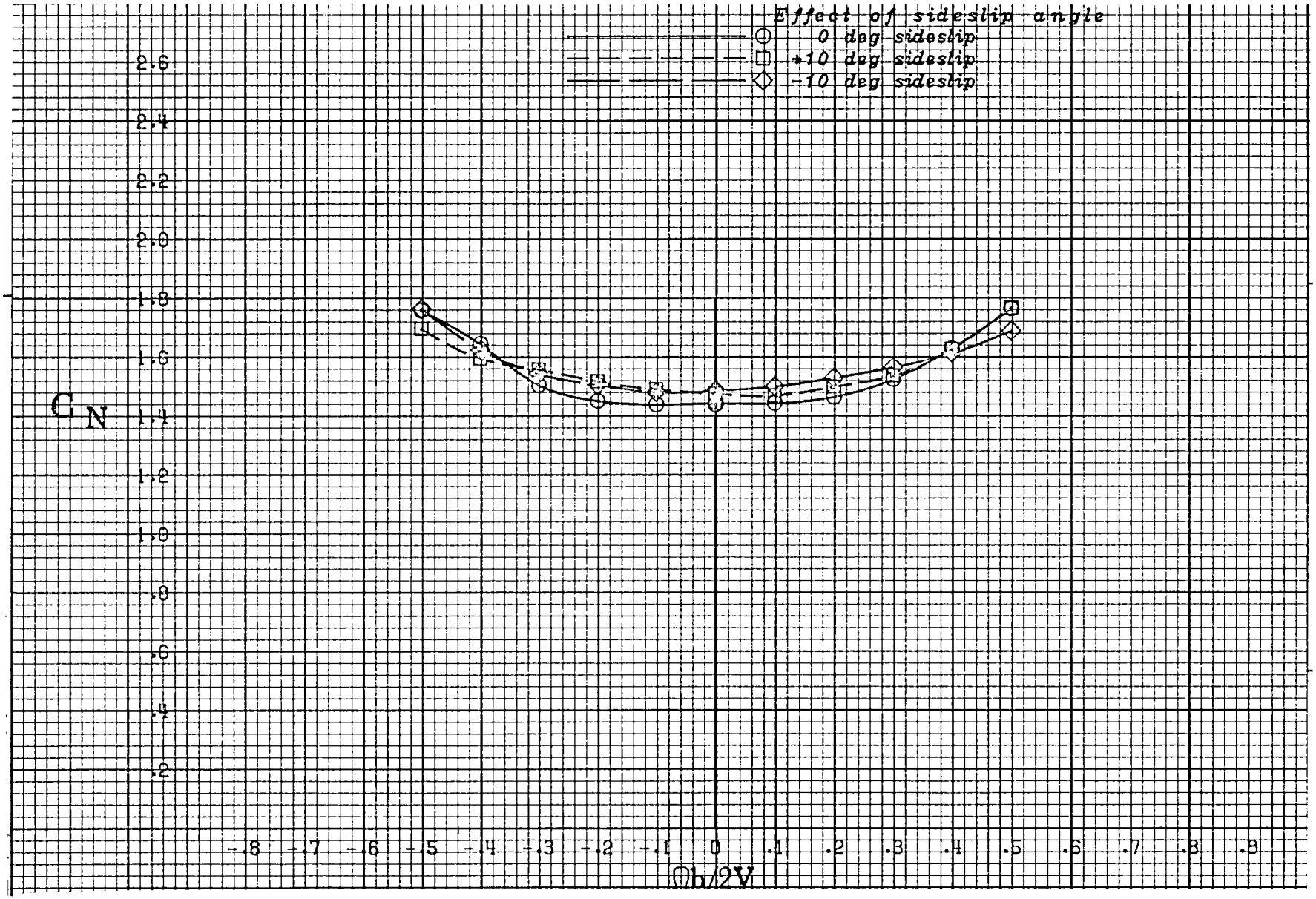

(j) α = 90 deg.

Figure A 4 .- Concluded.

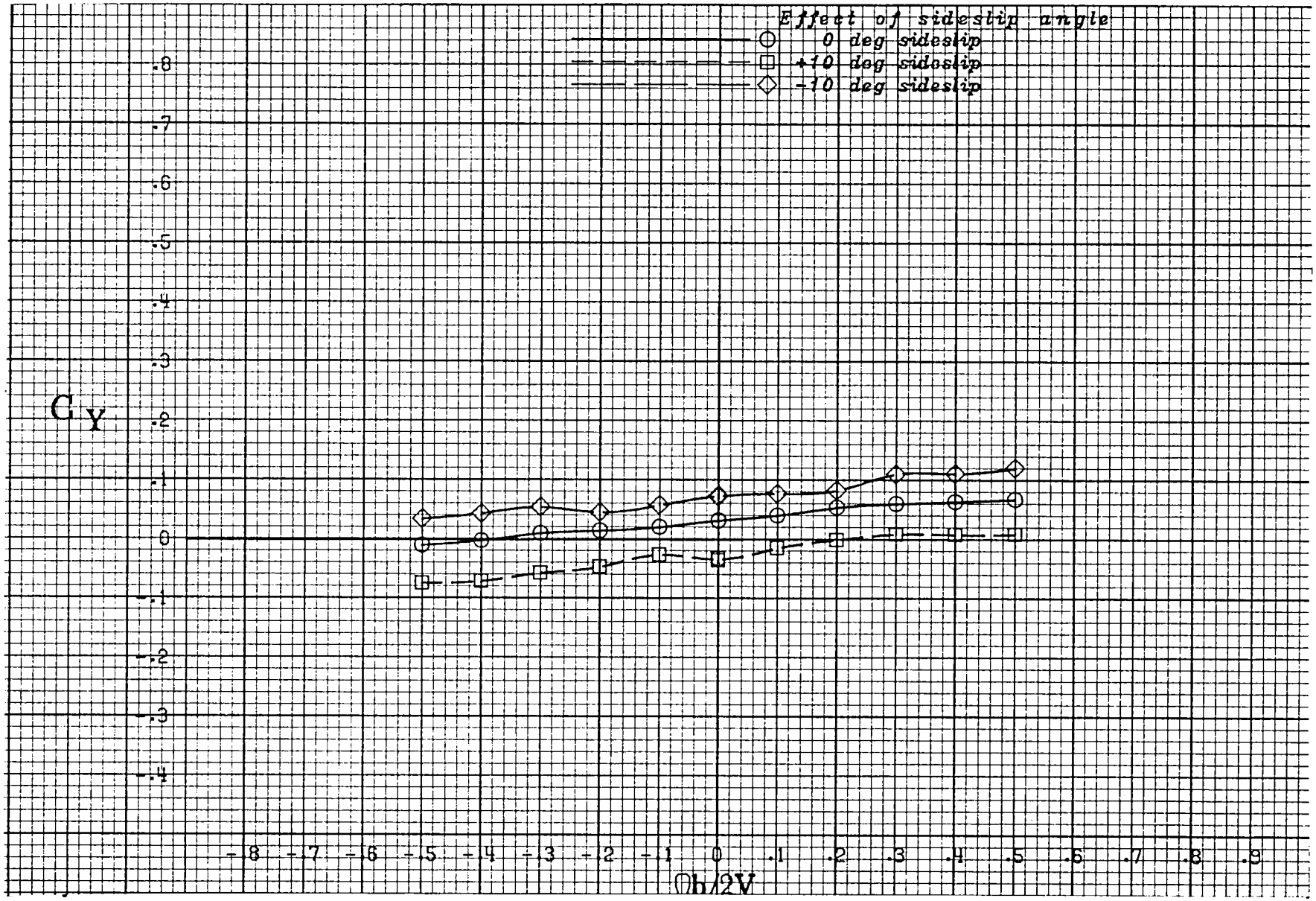

(a) α = 20 deg.

Figure A 5 .- Effect of rotation rate and sideslip angle on side-force coefficient for the basic configuration with neutral controls.

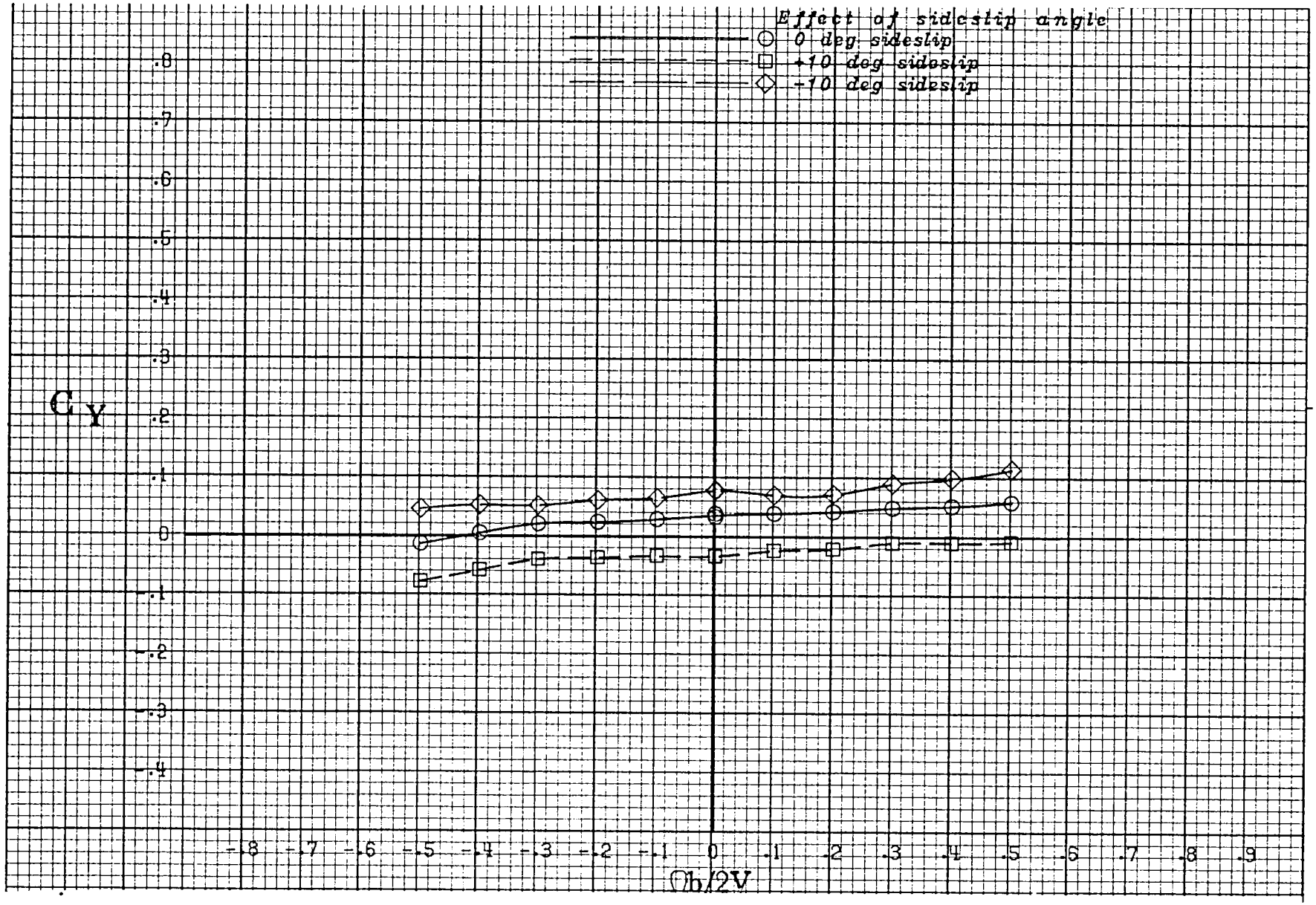

(b) α = 25 deg.

Figure A 5 .- Continued.

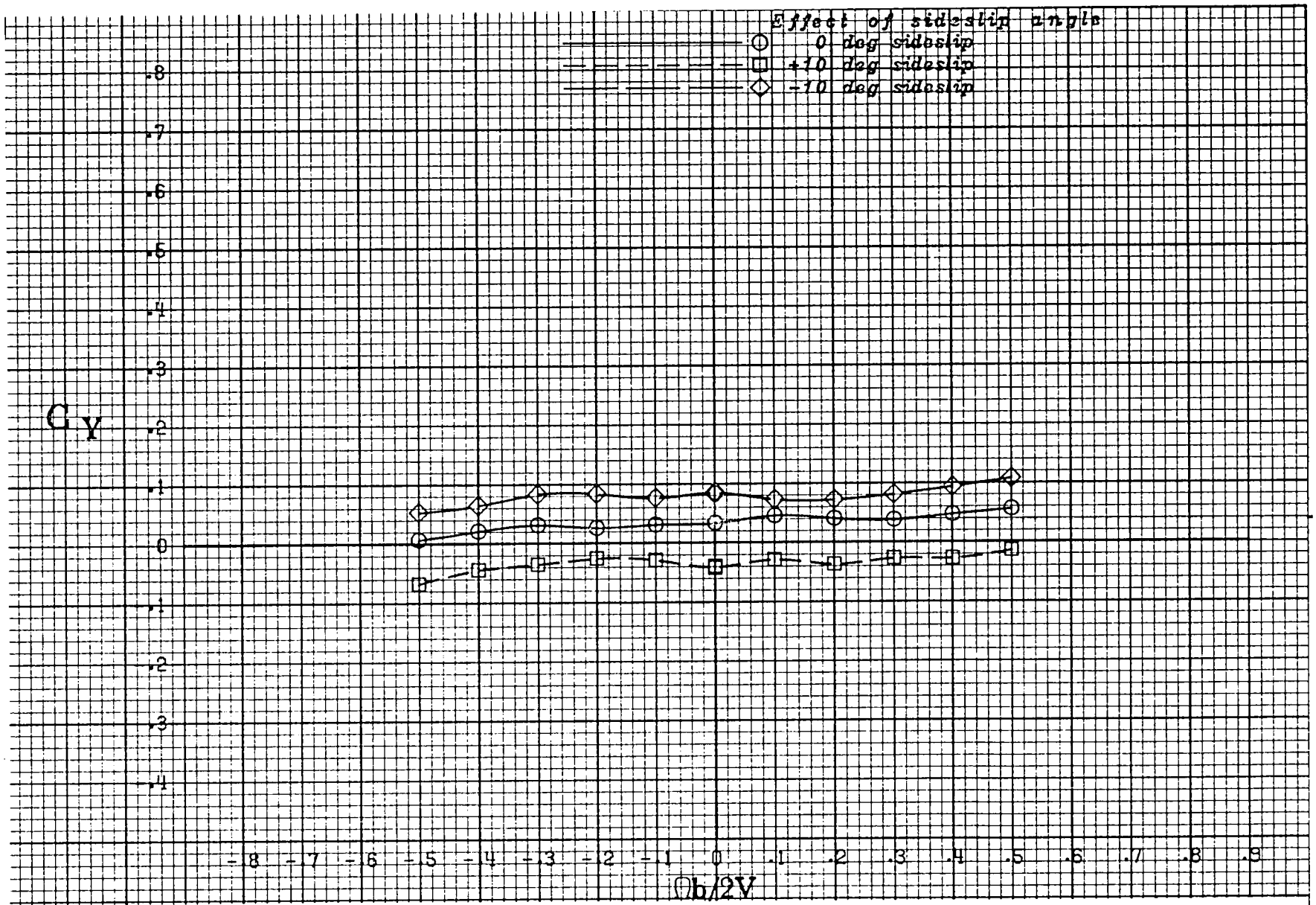

(c) α = 30 deg.

Figure A 5 .- Continued.

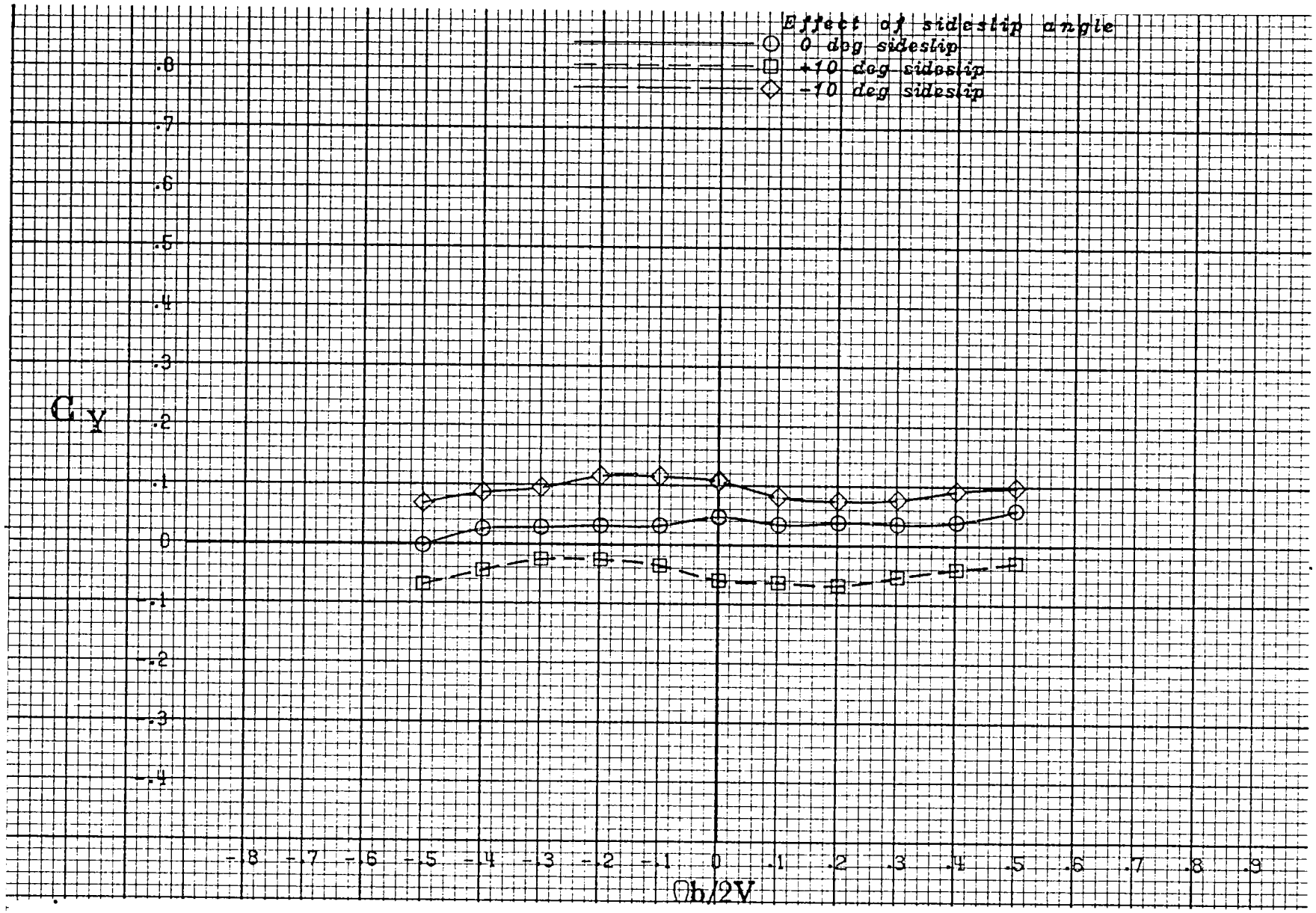

(d) α = 35 deg.

Figure A 5 .- Continued.

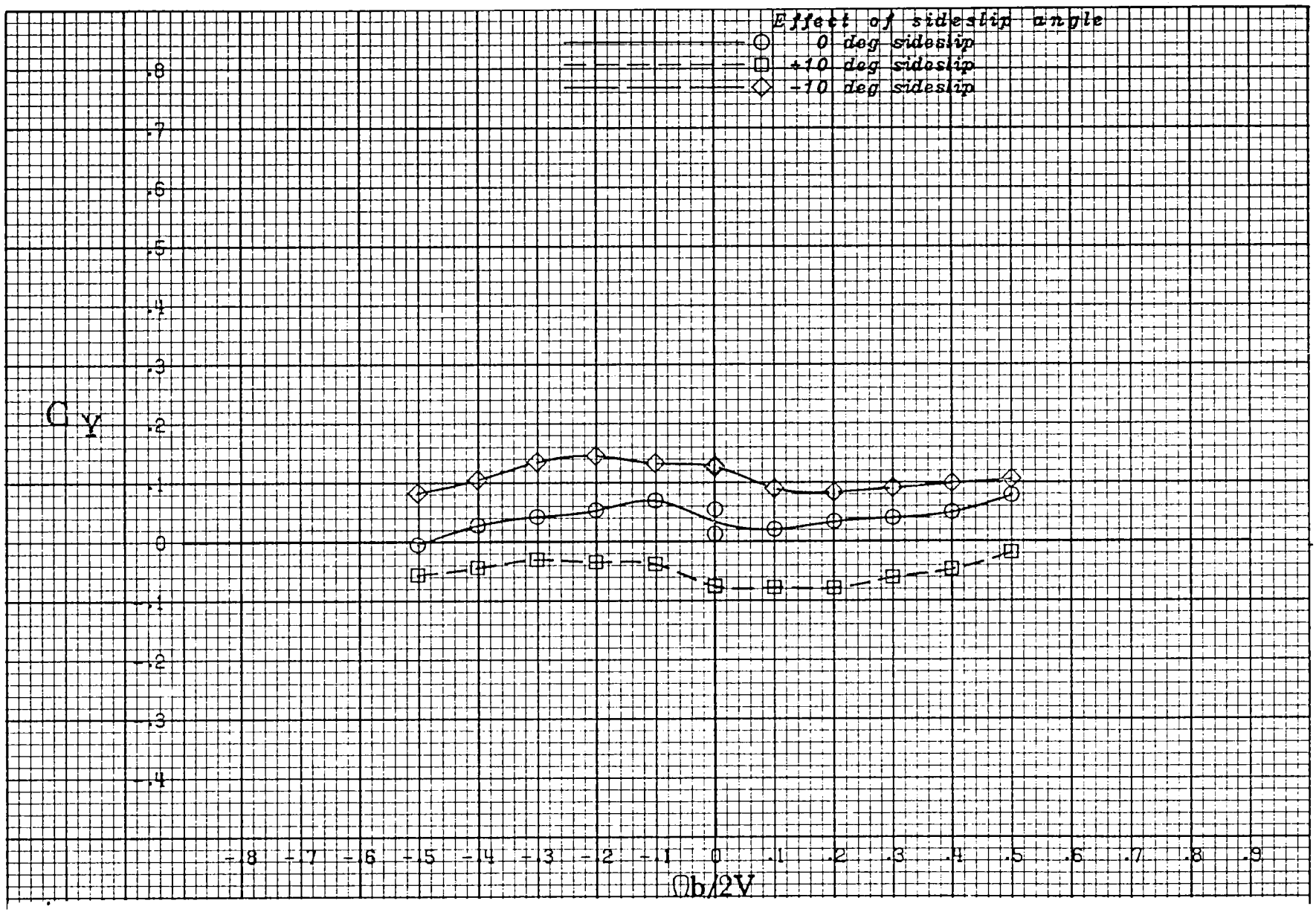

(e) α = 40 deg.

Figure A 5 .- Continued.

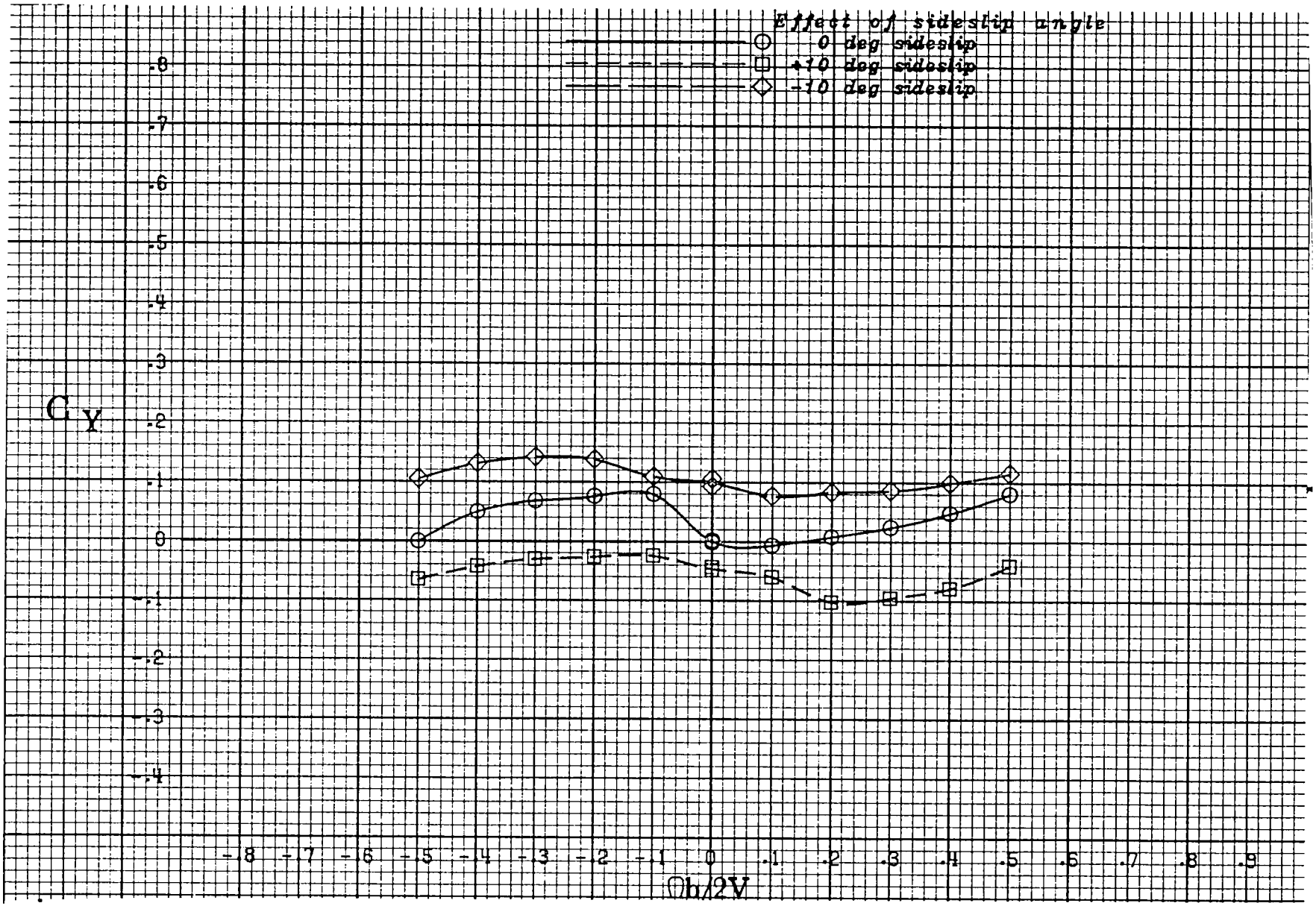

(f) α = 50 deg.

Figure A 5 .- Continued.

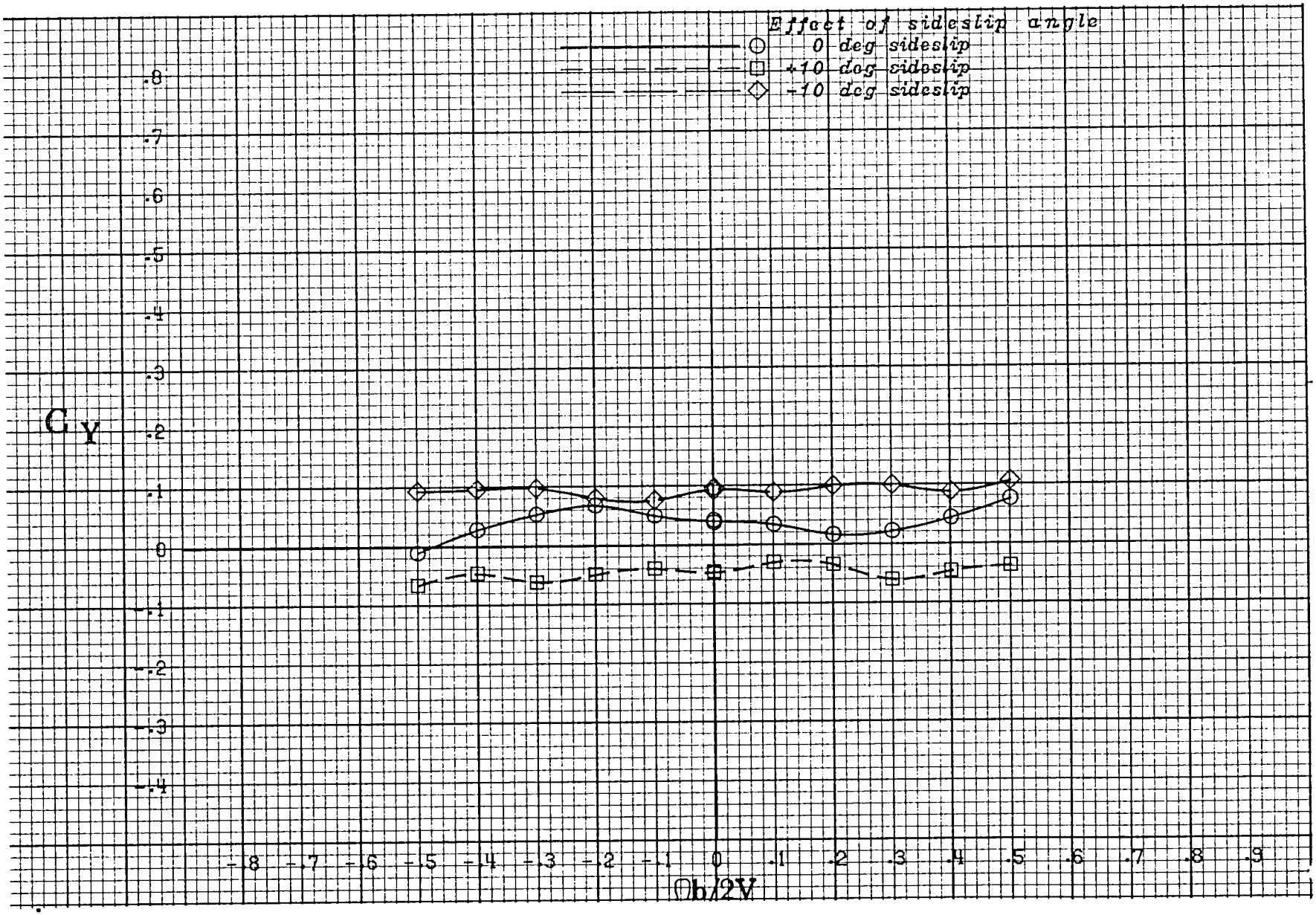

(g) α = 60 deg.

Figure A 5 .- Continued.

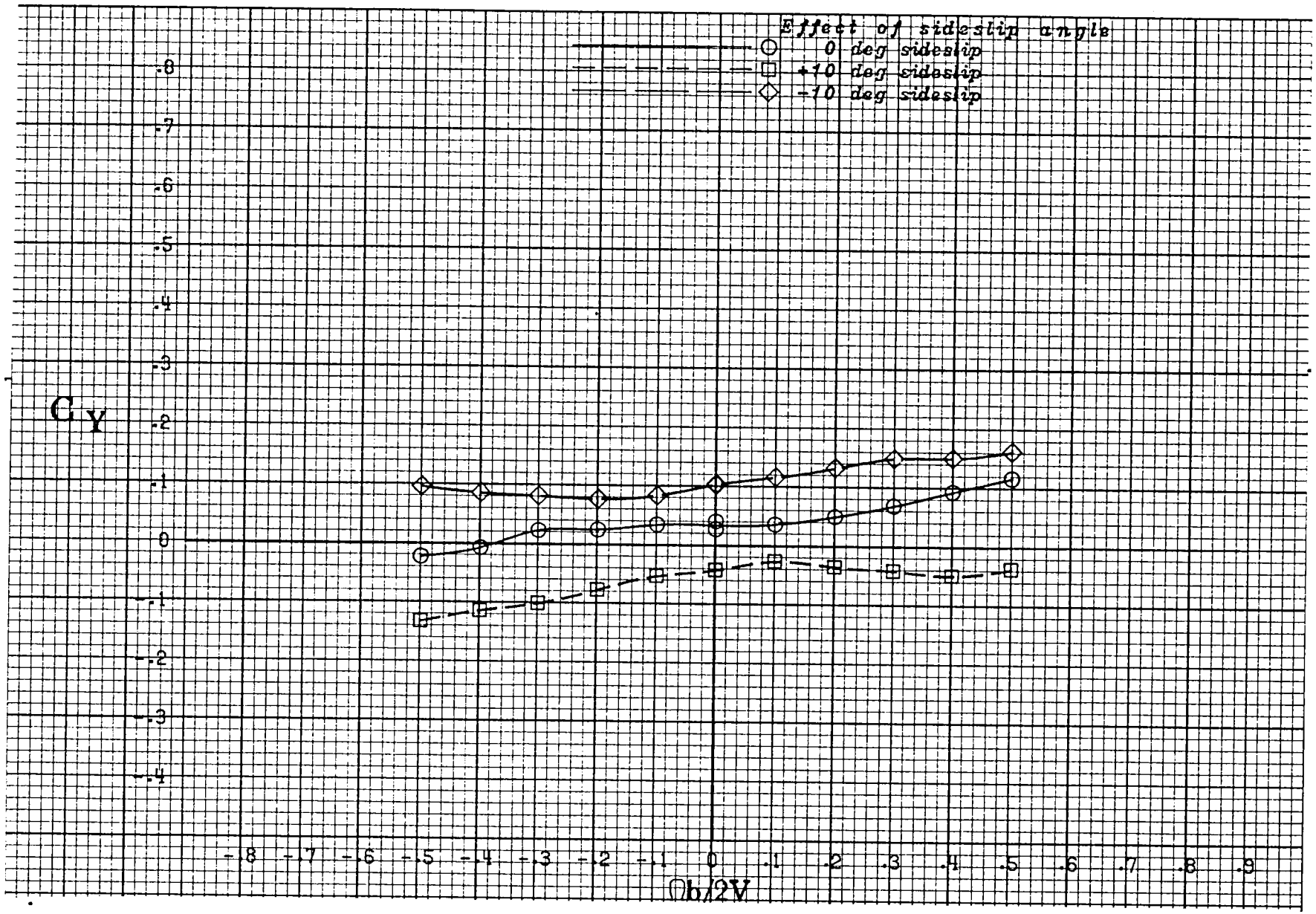

(h) α = 70 deg.

Figure A 5 .- Continued.

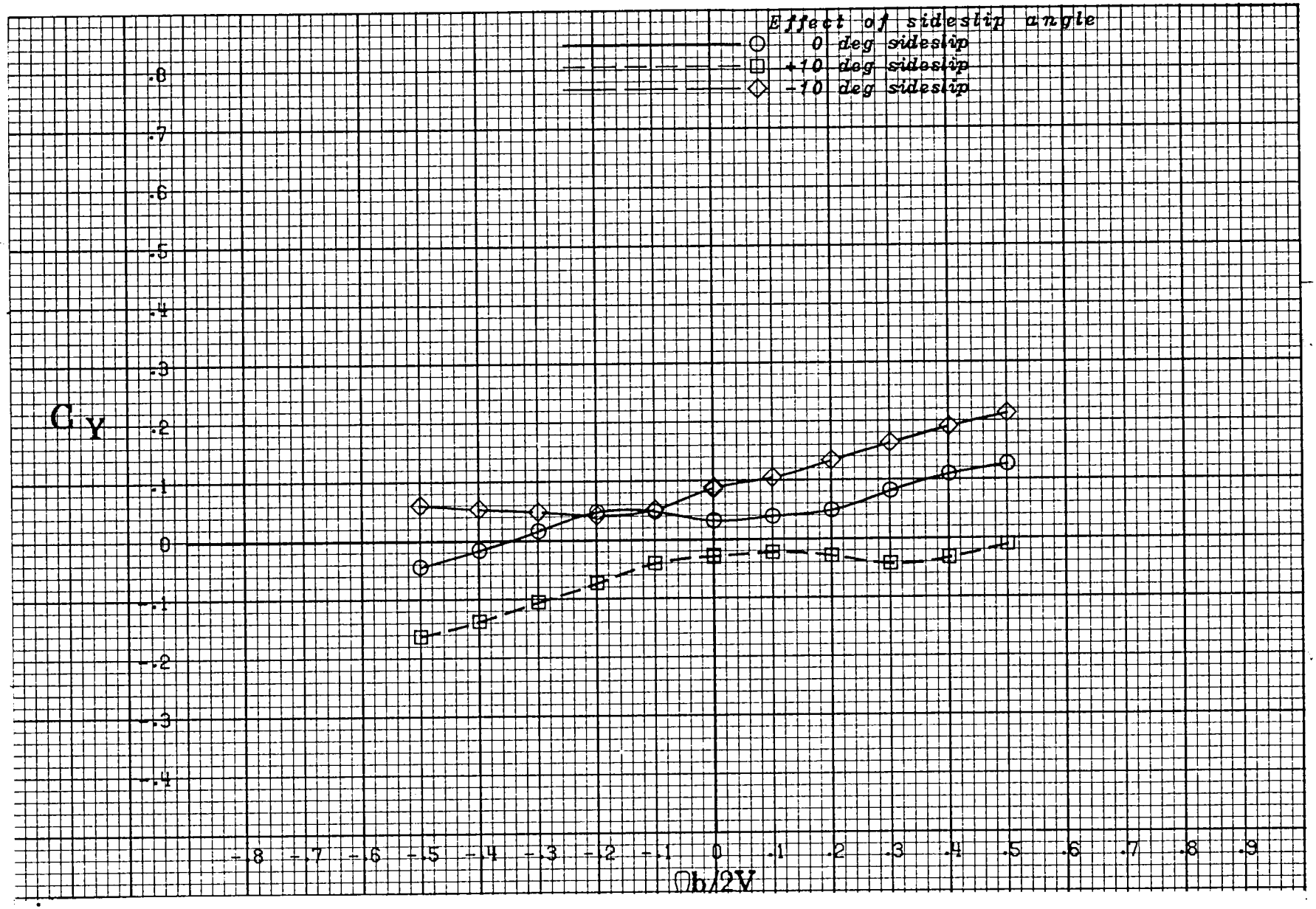

(i) α = 80 deg.

Figure A 5 .- Continued.

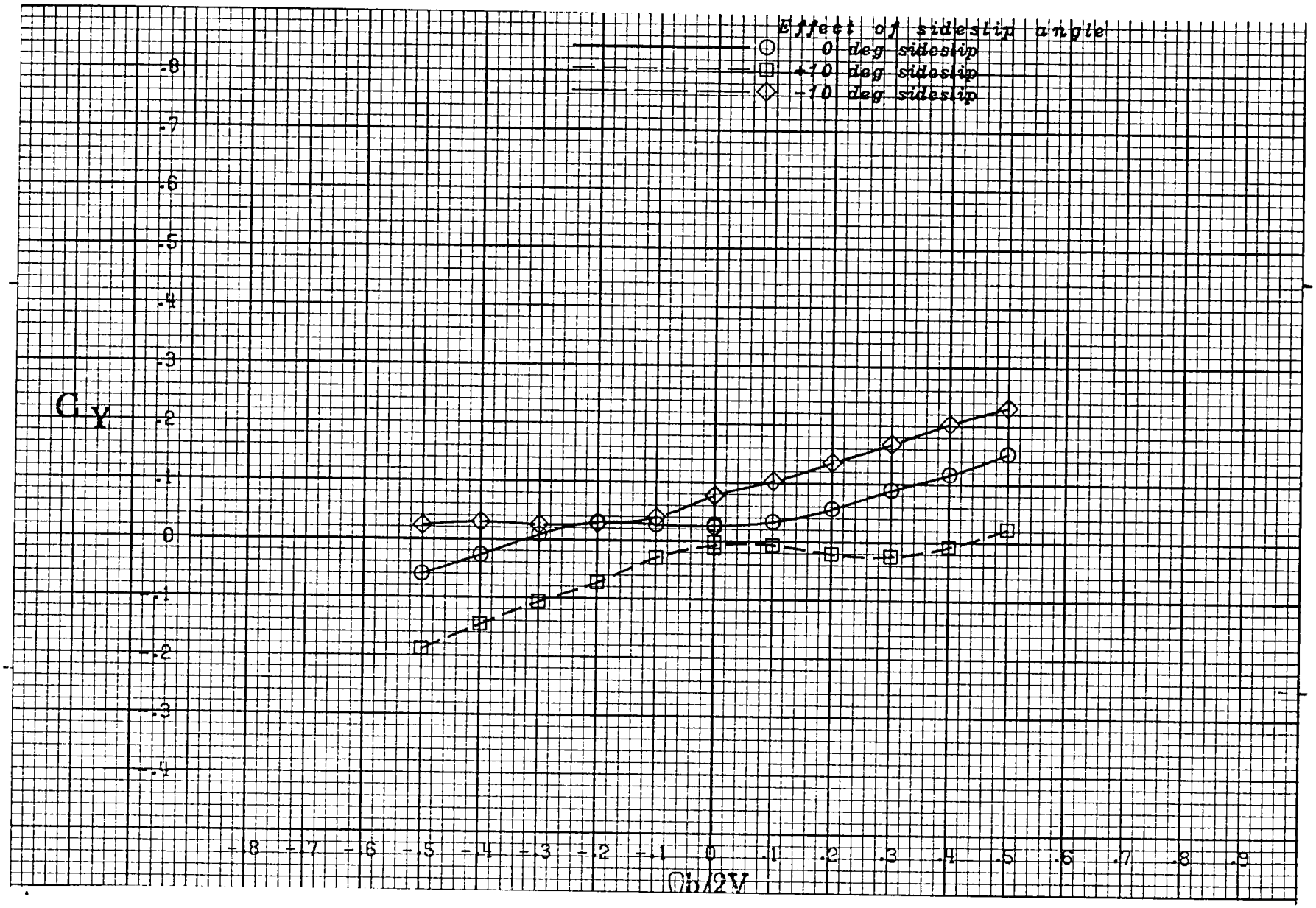

(j) α = 90 deg.

Figure A 5 .- Concluded.

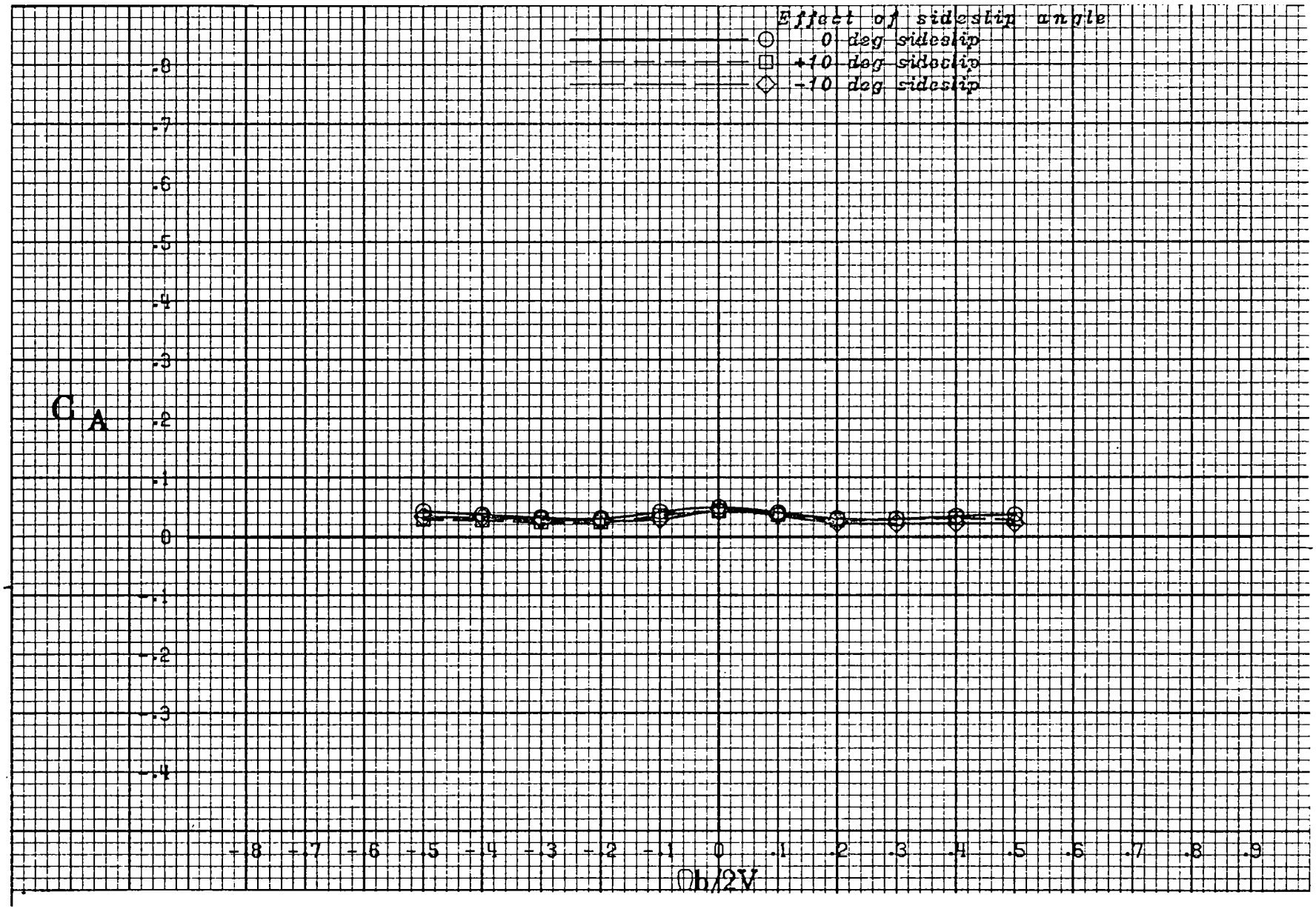

(a) α = 20 deg.

Figure A 6 .- Effect of rotation rate and sideslip angle on axial-force coefficient for the basic configuration with neutral controls.

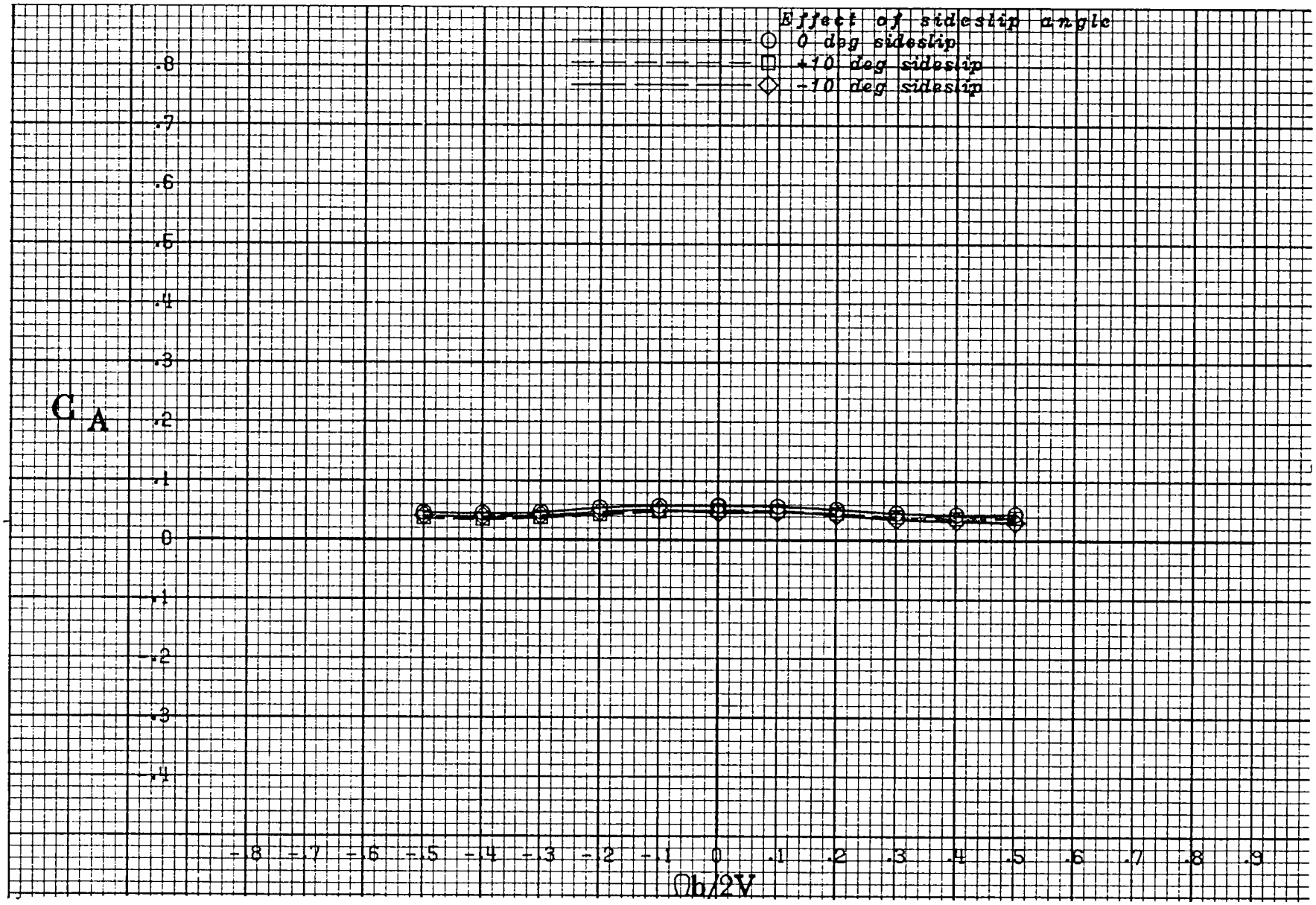

(b) α = 25 deg.

Figure A 6 .- Continued.

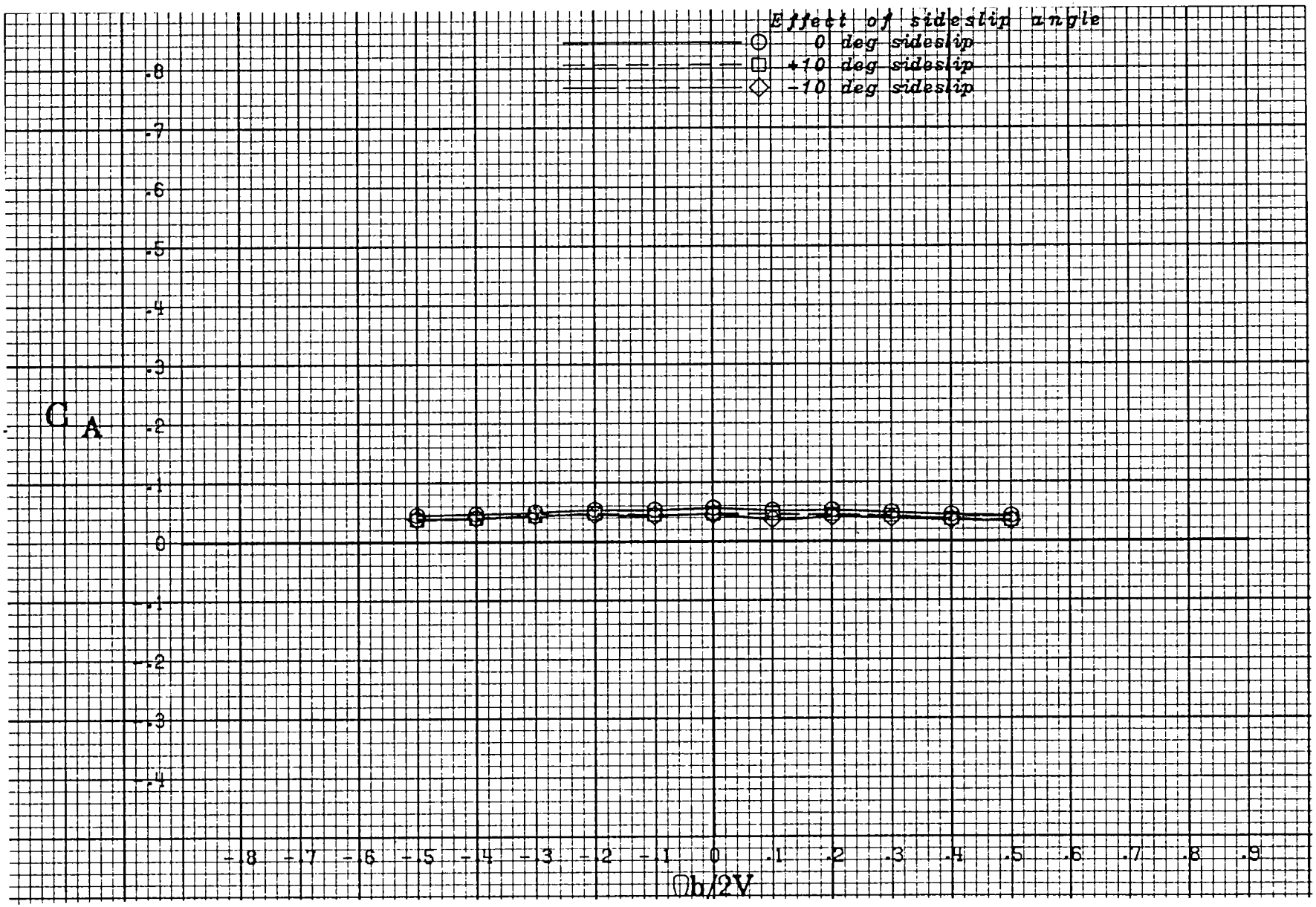

(c) α = 30 deg.

Figure A 6 .- Continued.

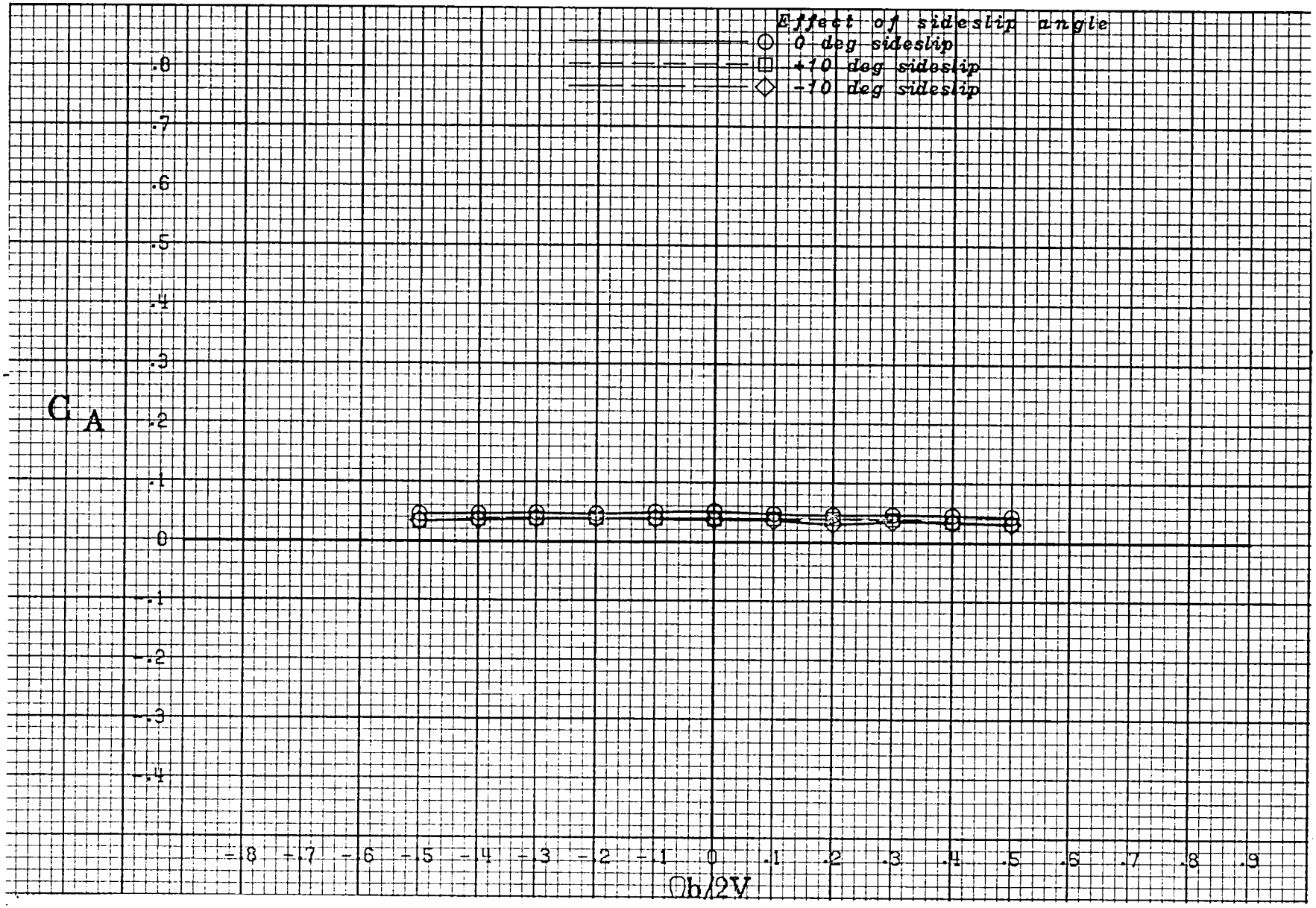

(d) α = 35 deg.

Figure A 6 .- Continued.

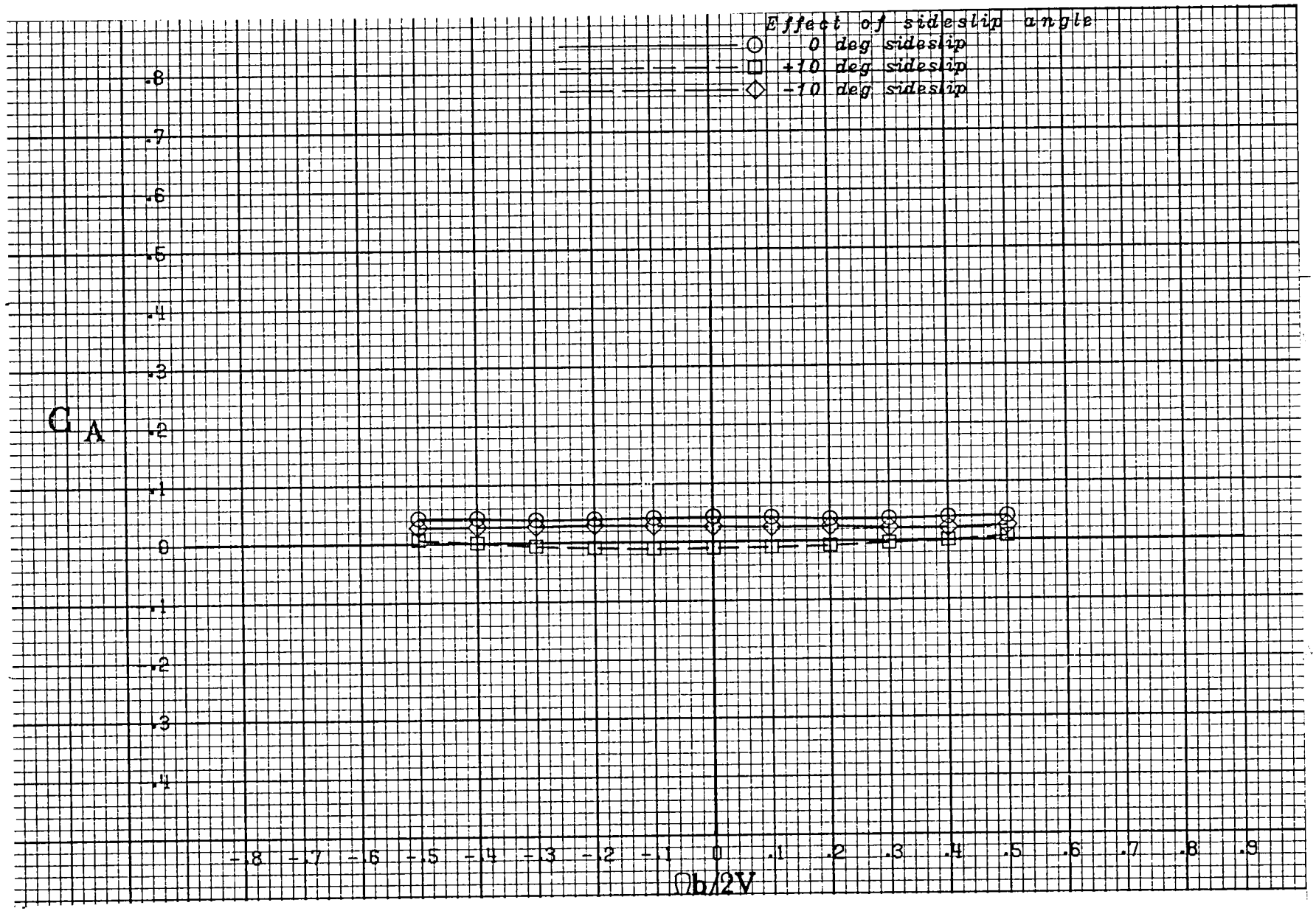

(e) α = 40 deg.

Figure A 6 .- Continued.

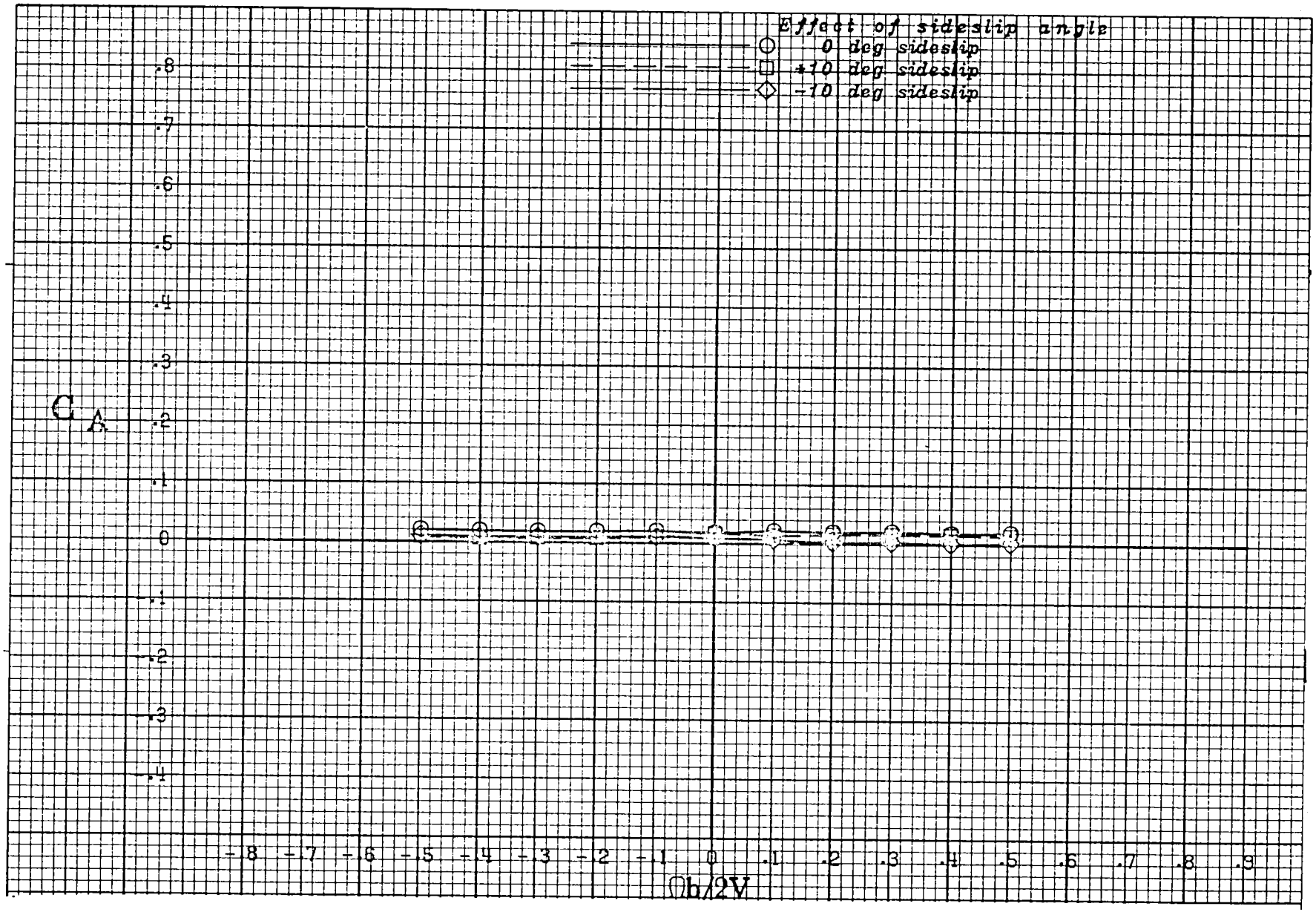

(f) α = 50 deg.

Figure A 6 .- Continued.

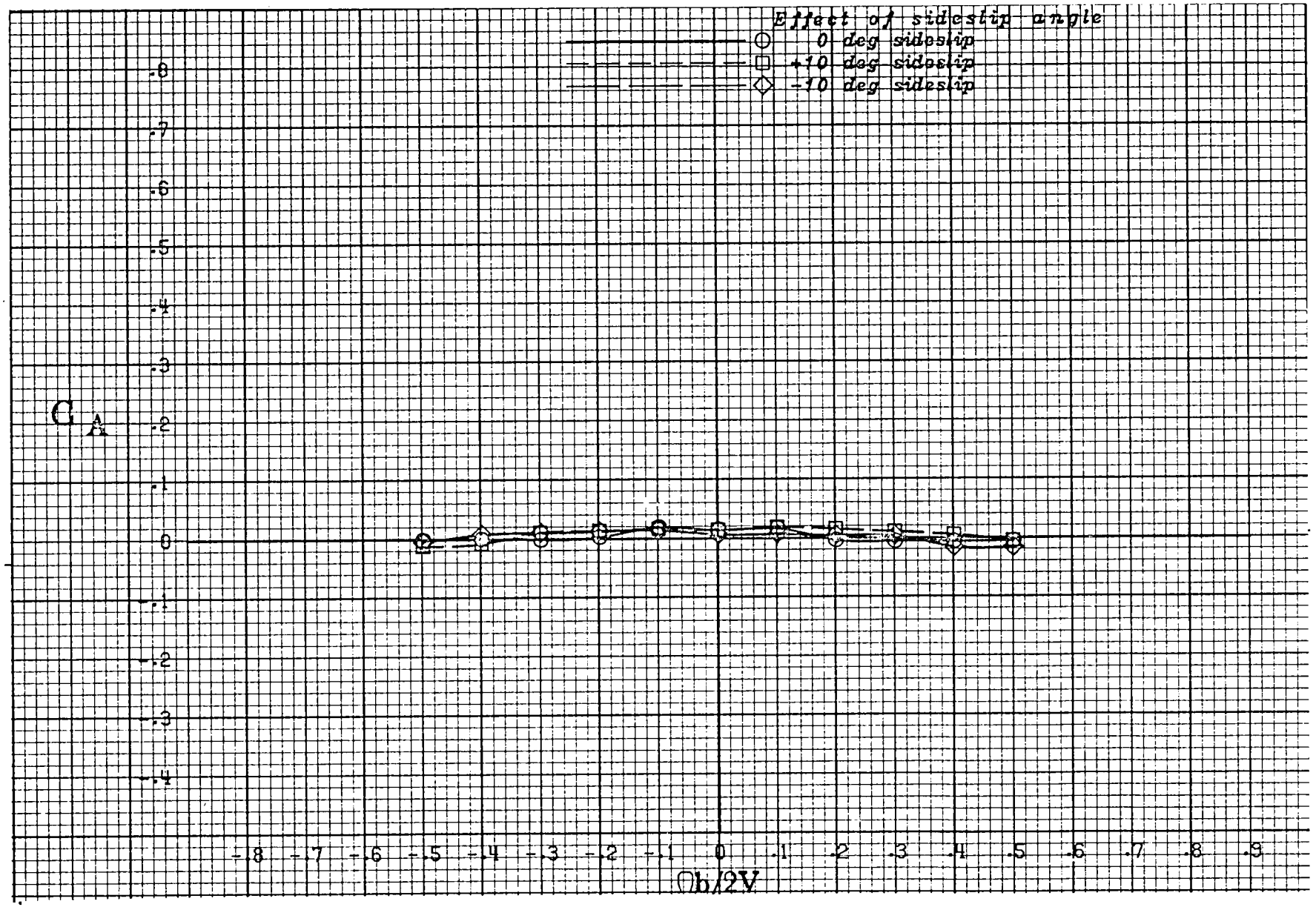

(g) α = 60 deg.

Figure A 6 .- Continued.

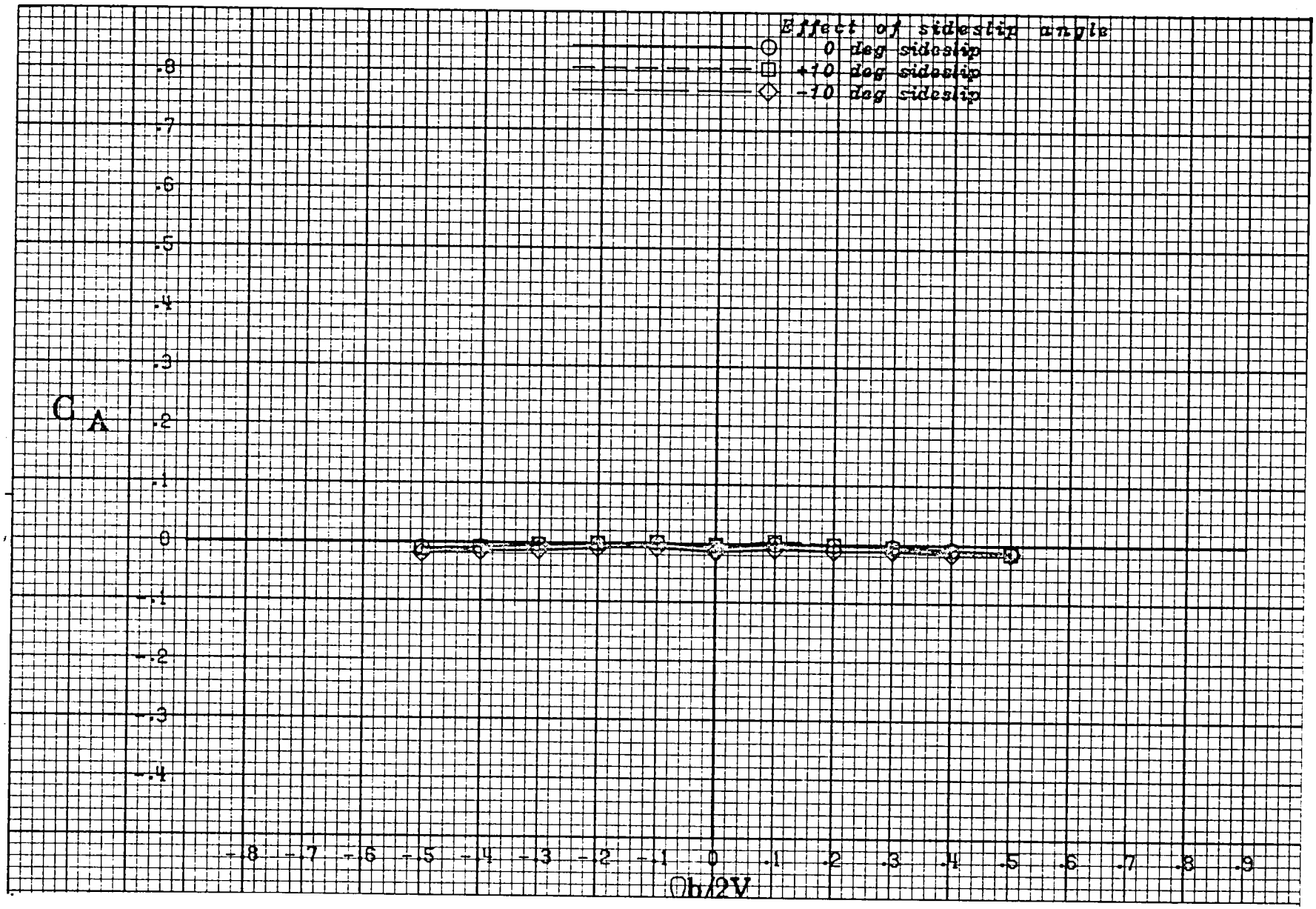

(h) α = 70 deg.

Figure A 6 .- Continued.

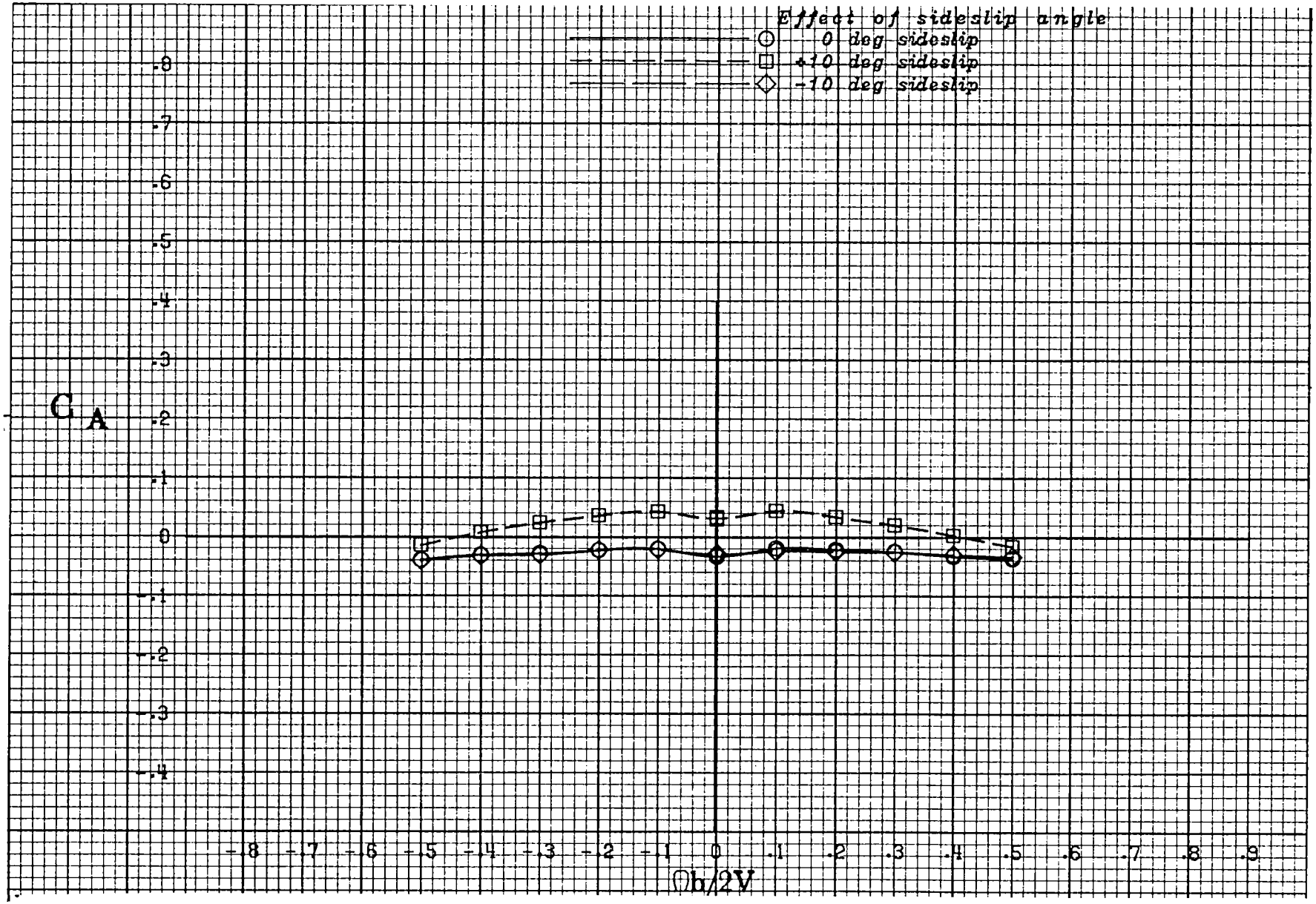

(i) α = 80 deg.

Figure A 6 .- Continued.

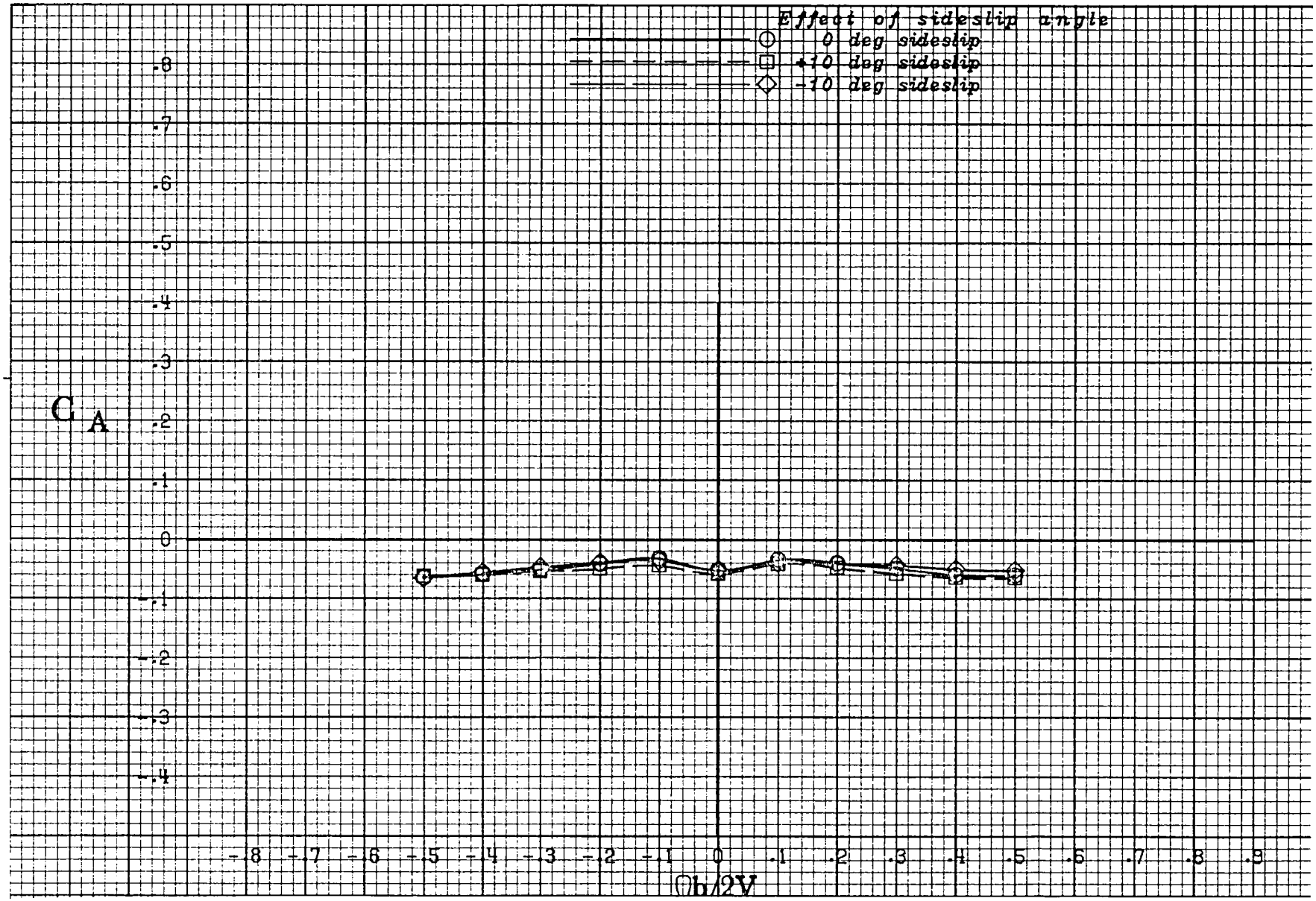

(j) α = 90 deg.

Figure A 6 .- Concluded.

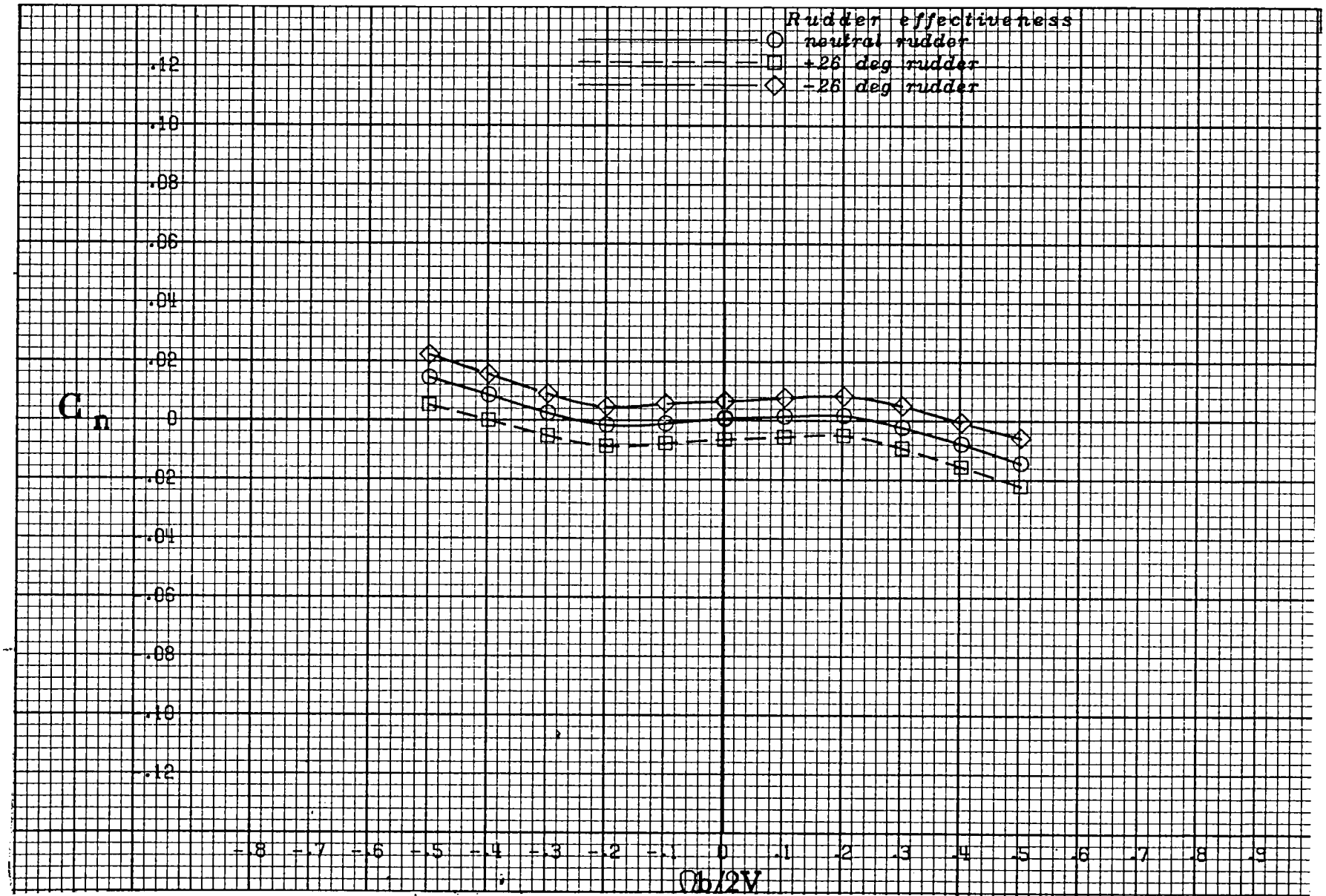

(a) α = 20 deg.

Figure A 7 .- Effect of rotation rate and rudder deflection on yawing-moment coefficient for the basic configuration with neutral elevator and ailerons at zero sideslip angle.

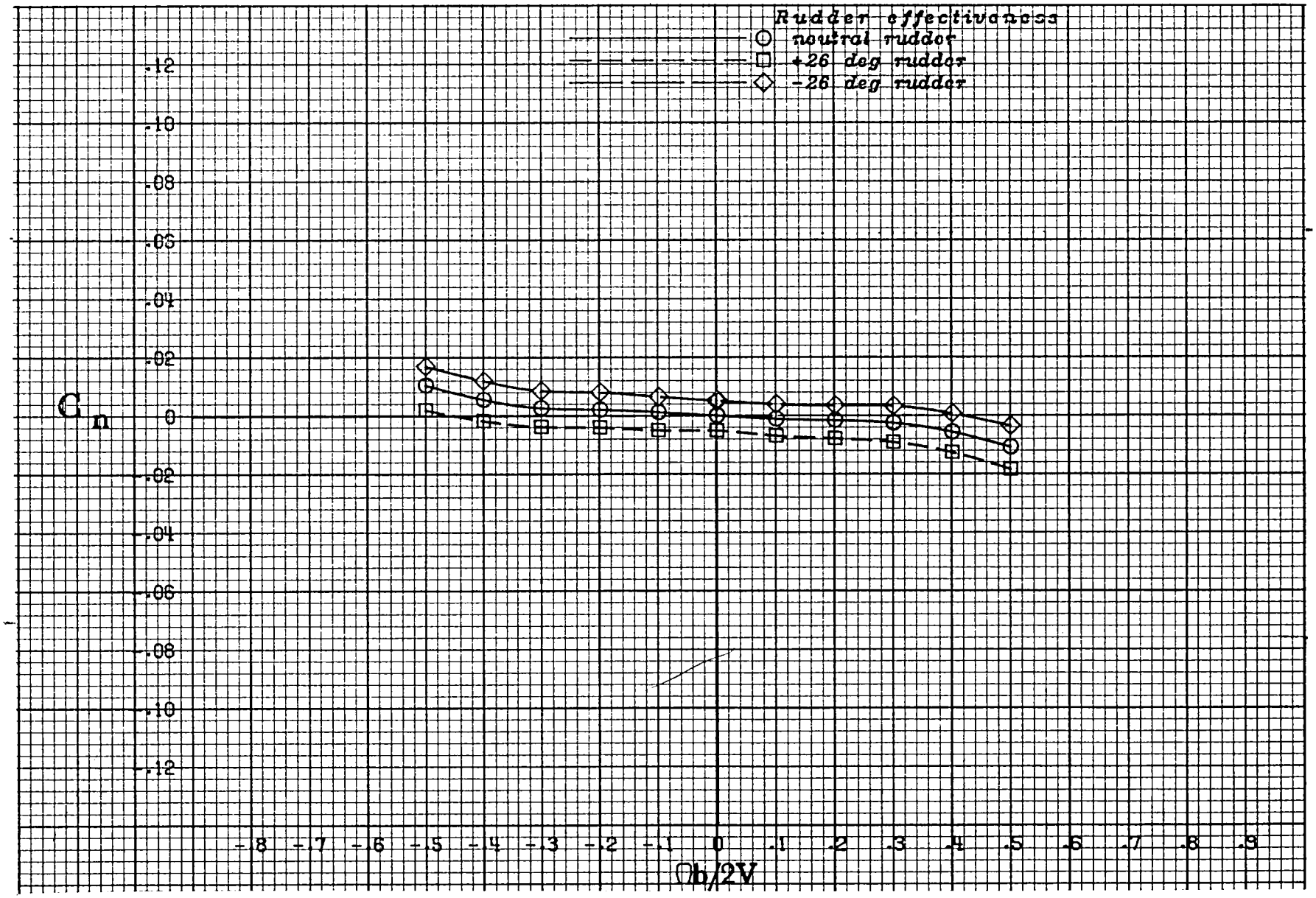

(b) α = 25 deg.

Figure A 7 .- Continued.

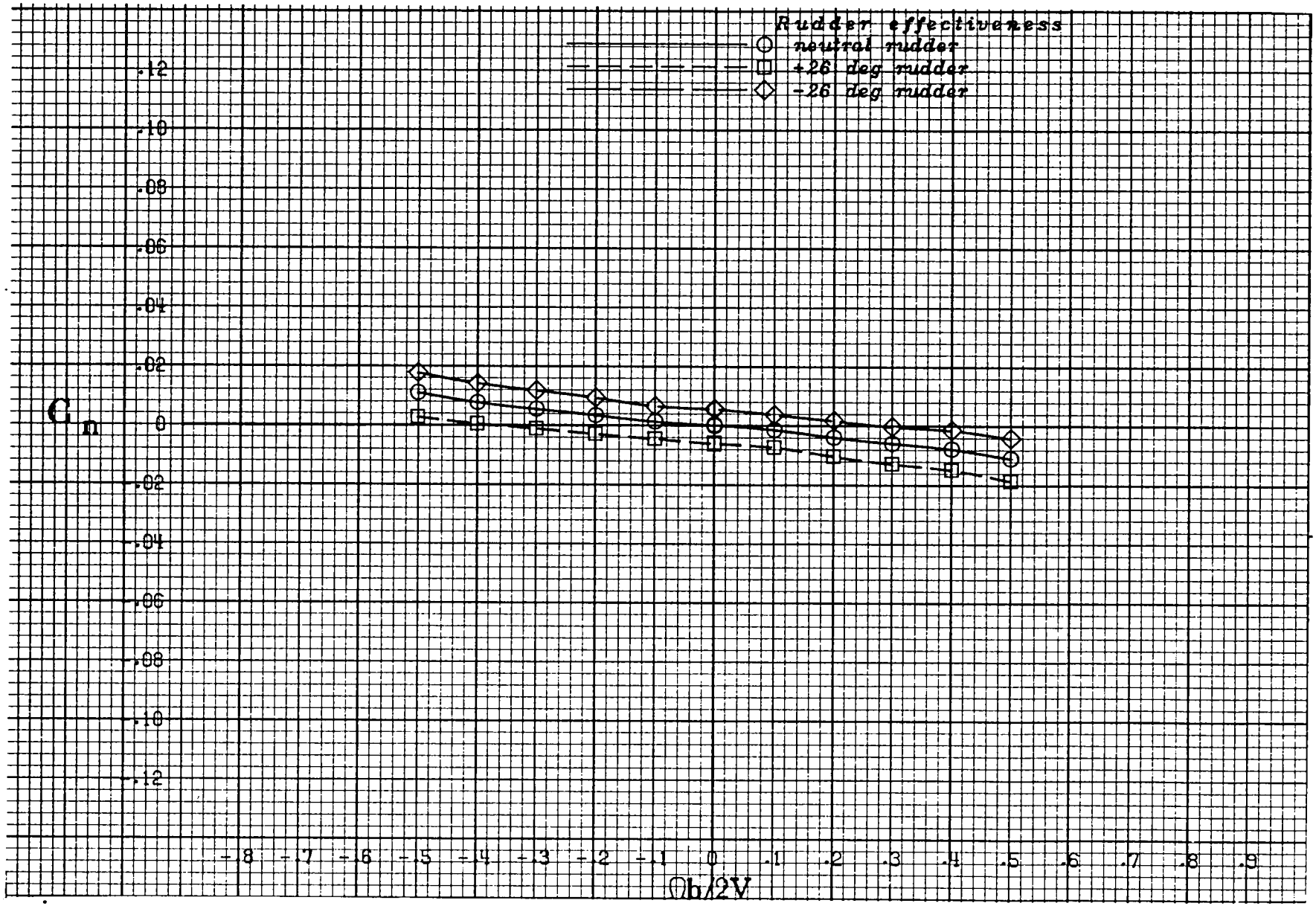

(c) α = 30 deg.

Figure A 7 .- Continued.

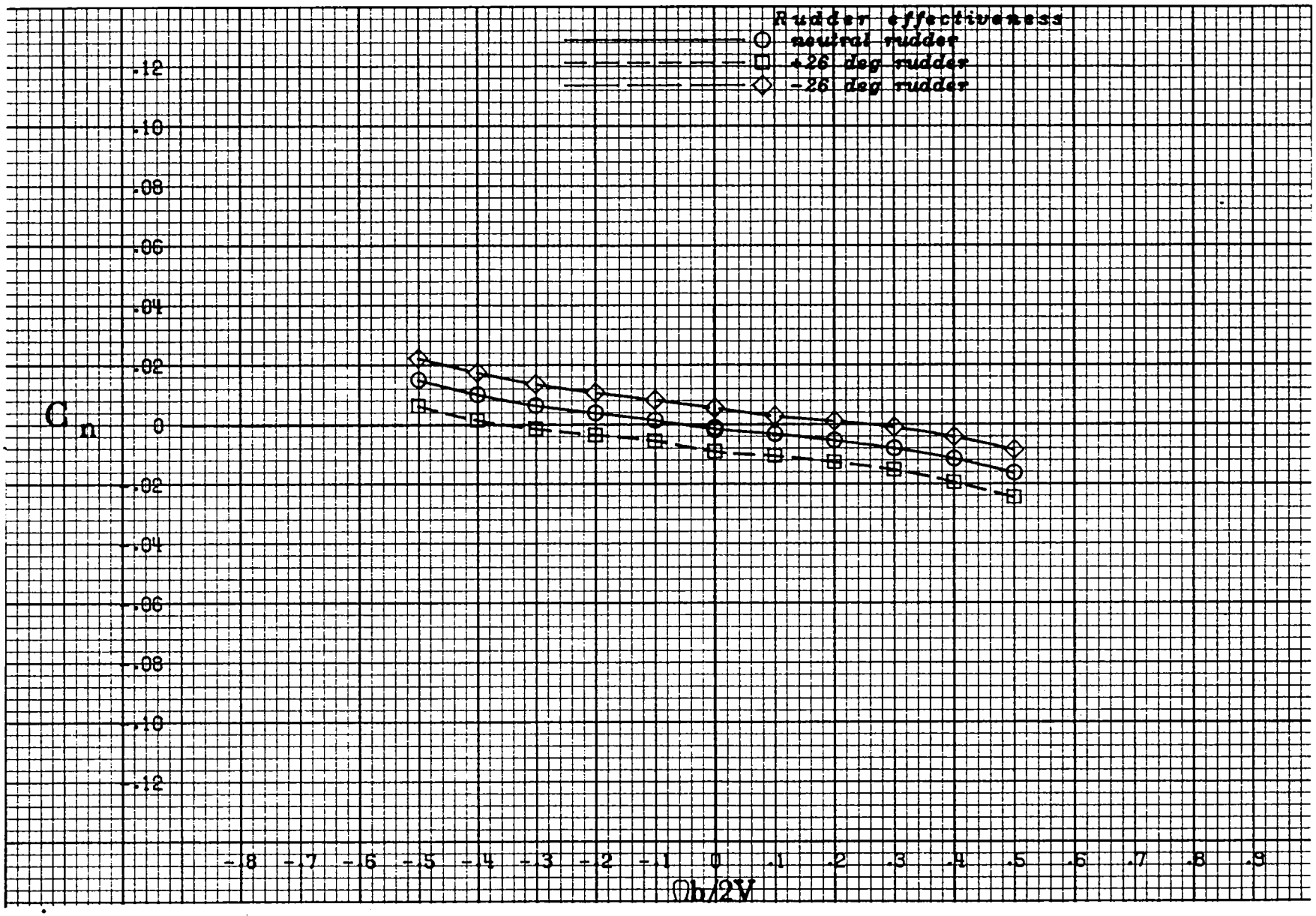

(d) α = 35 deg.

Figure A 7 .- Continued.

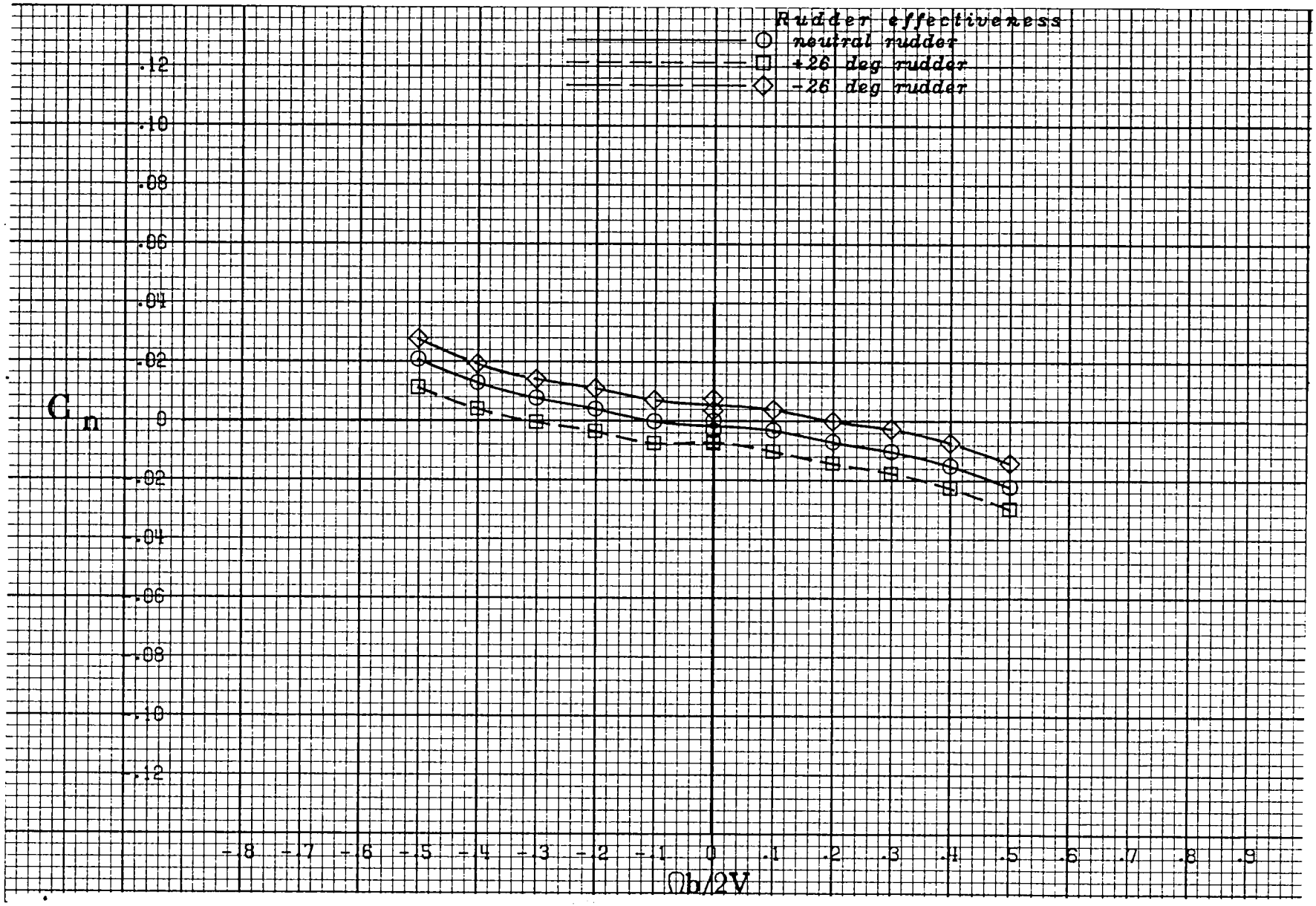

(e) α = 40 deg.

Figure A 7 .- Continued.

(f) α = 50 deg.

Figure A 7 .- Continued.

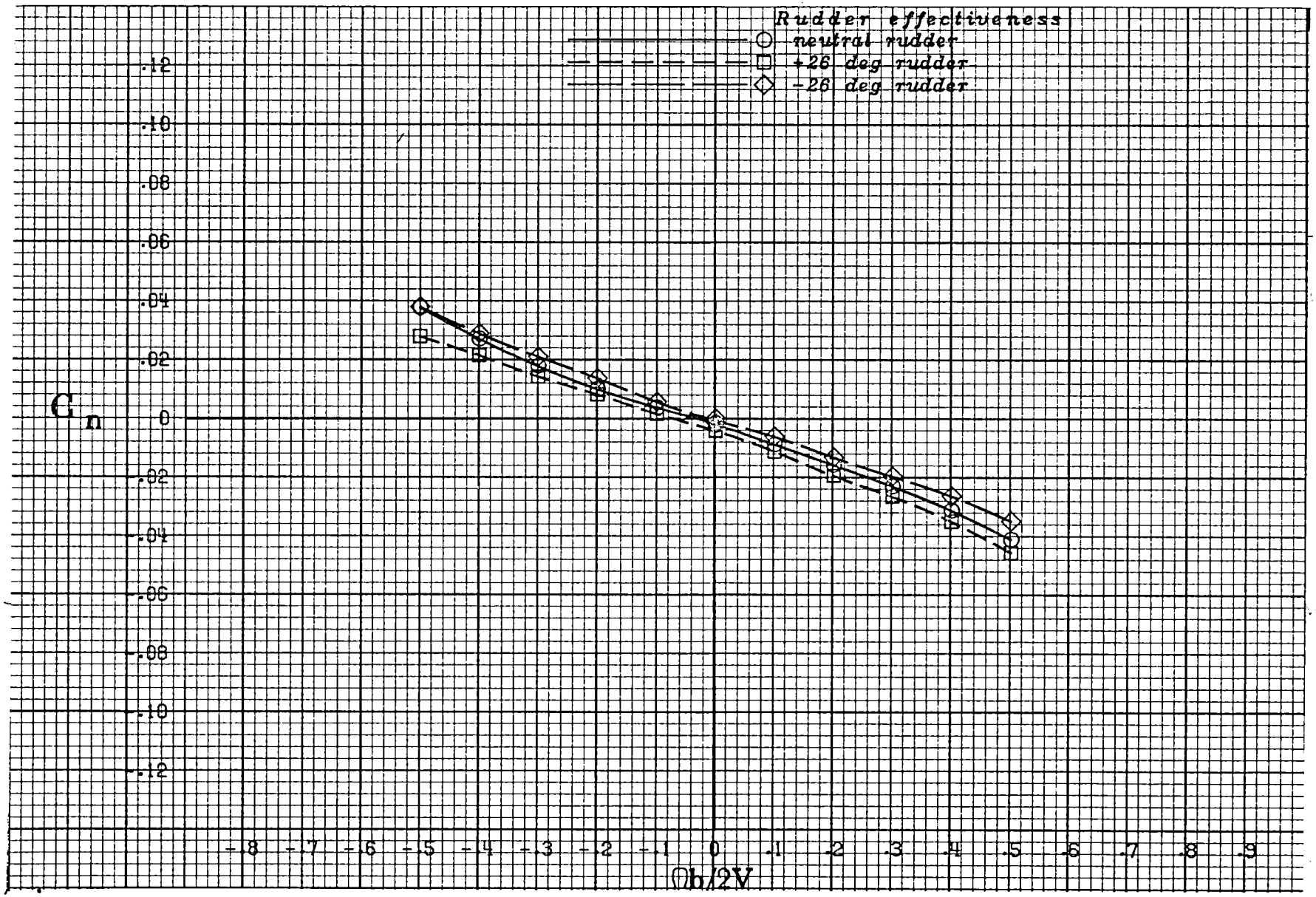

(g) α = 60 deg.

Figure A 7 .- Continued.

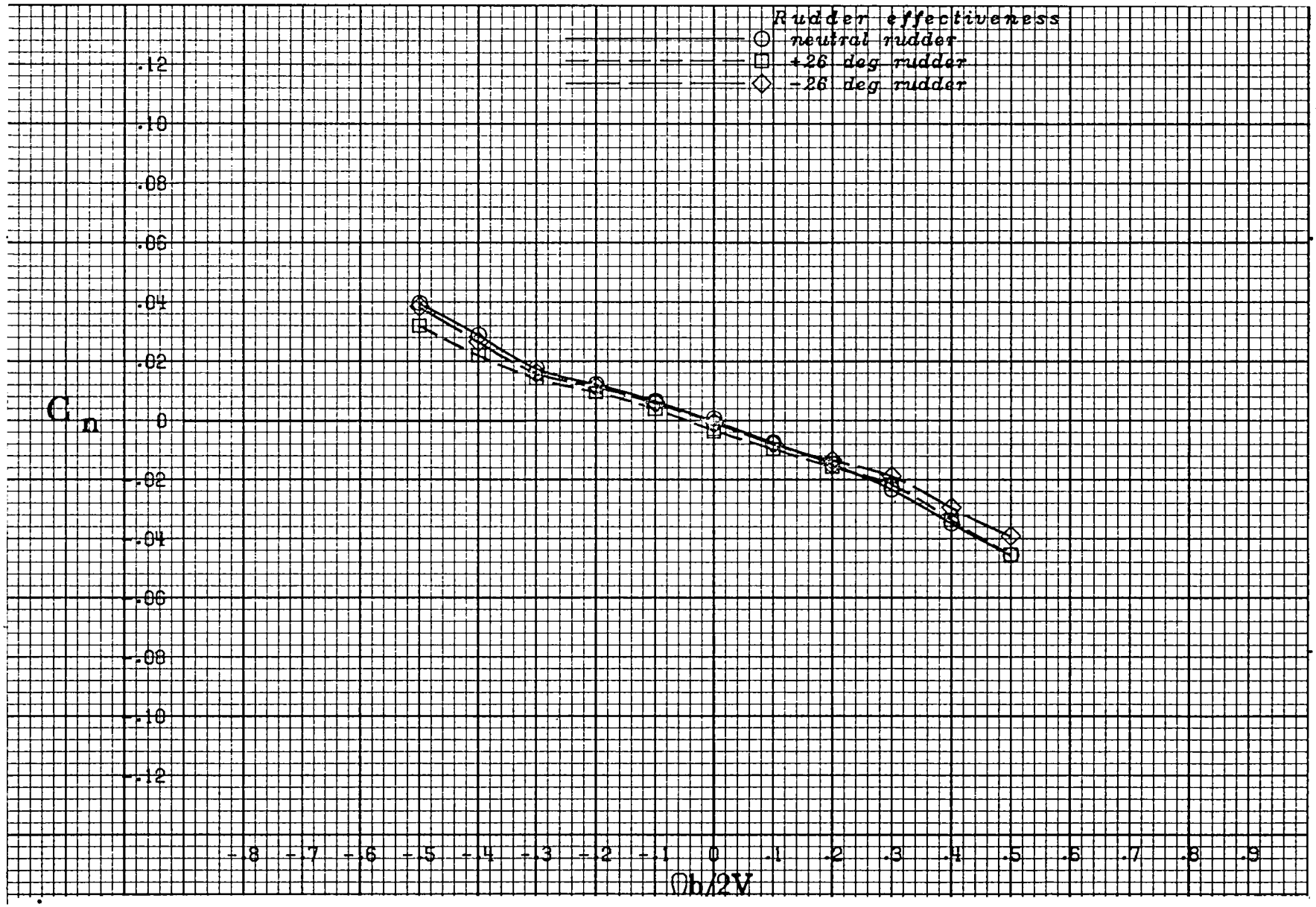

(h) α = 70 deg.

Figure A 7 .- Continued.

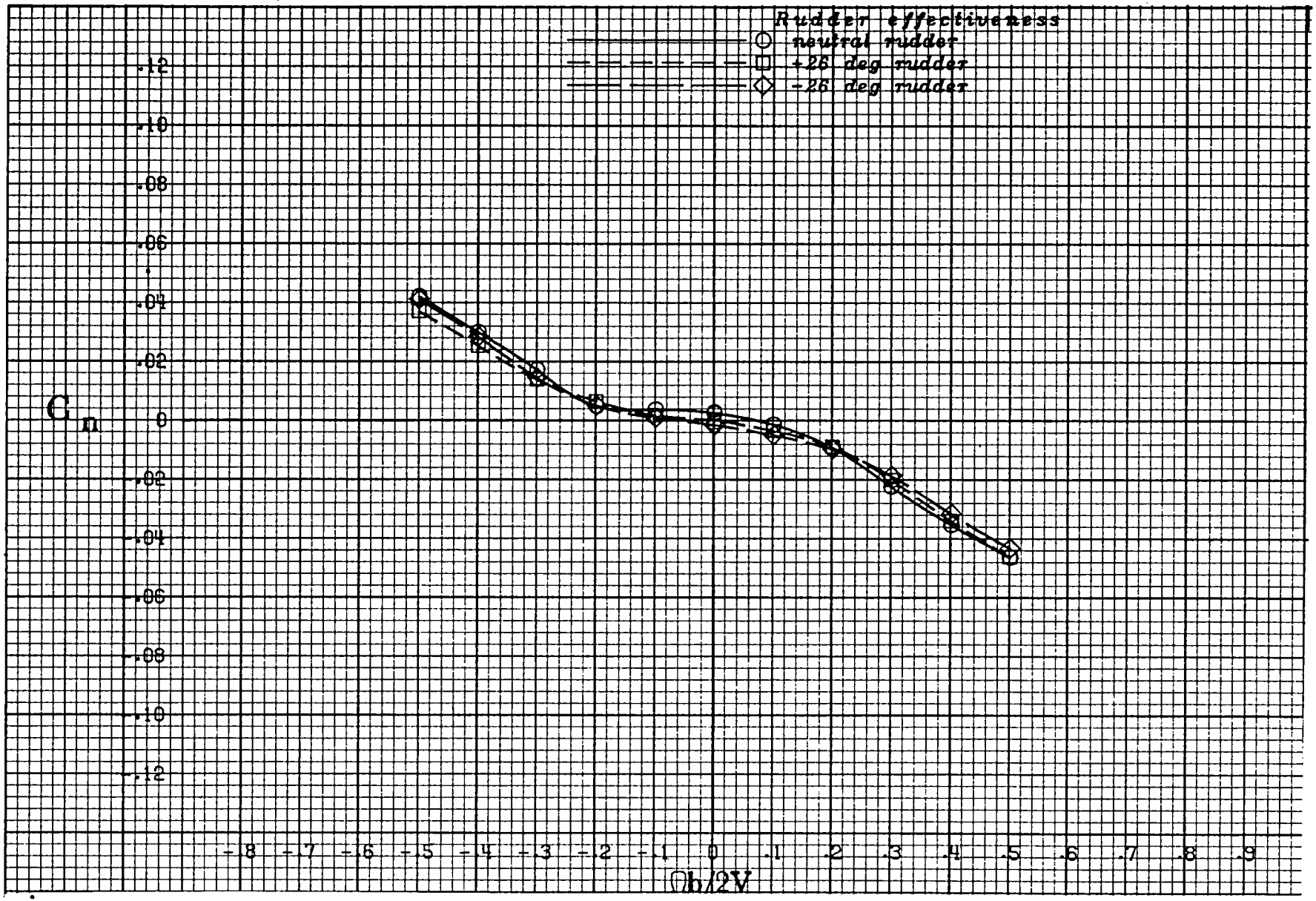

(i) α = 80 deg.

Figure A 7 .- Continued.

(j) α = 90 deg.

Figure A 7 .- Concluded.

(a) α = 20 deg.

Figure A 8 .- Effect of rotation rate and rudder deflection on rolling-moment coefficient for the basic configuration with neutral elevator and ailerons at zero sideslip angle.

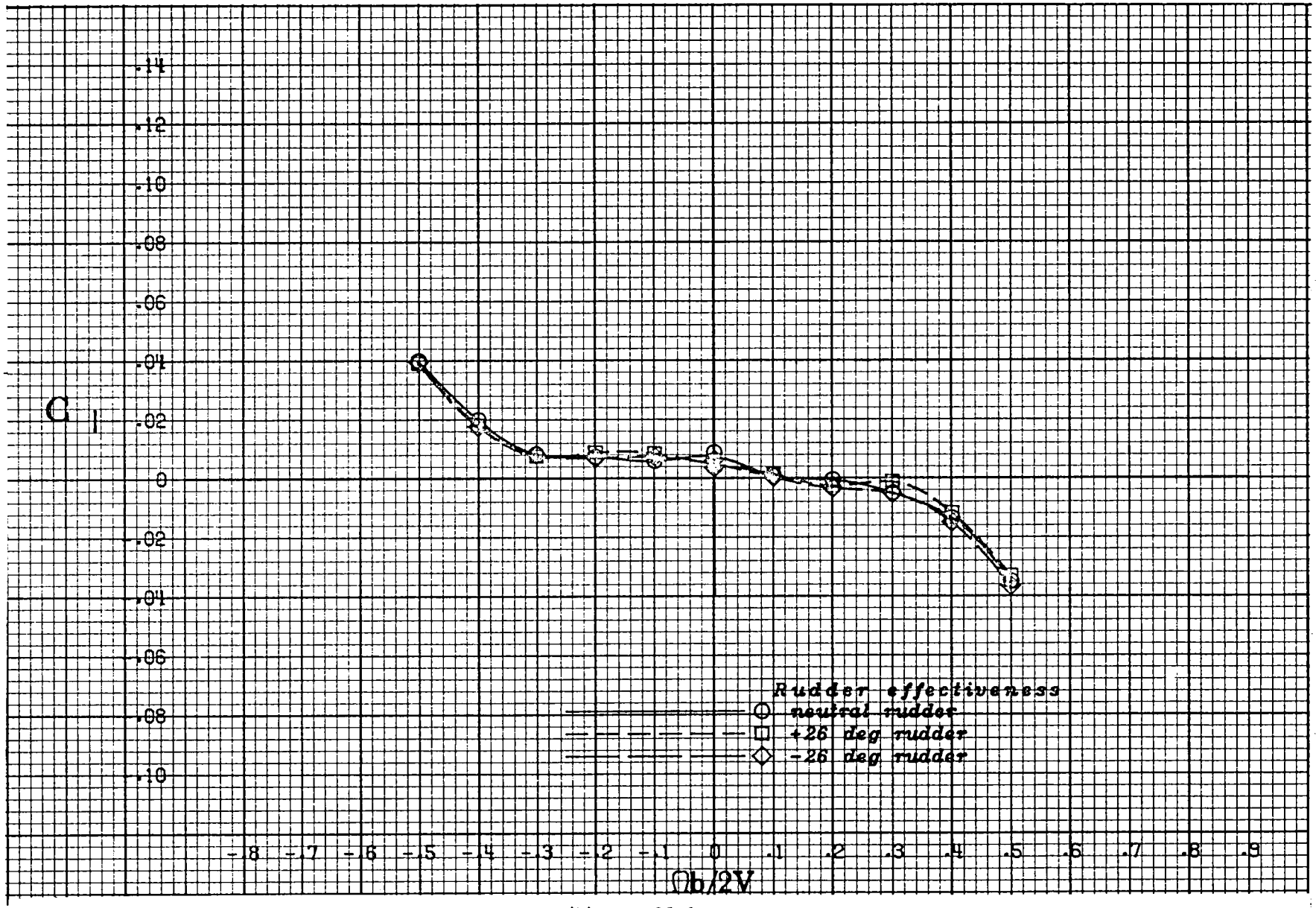

(b) α = 25 deg.

Figure A 8 .- Continued.

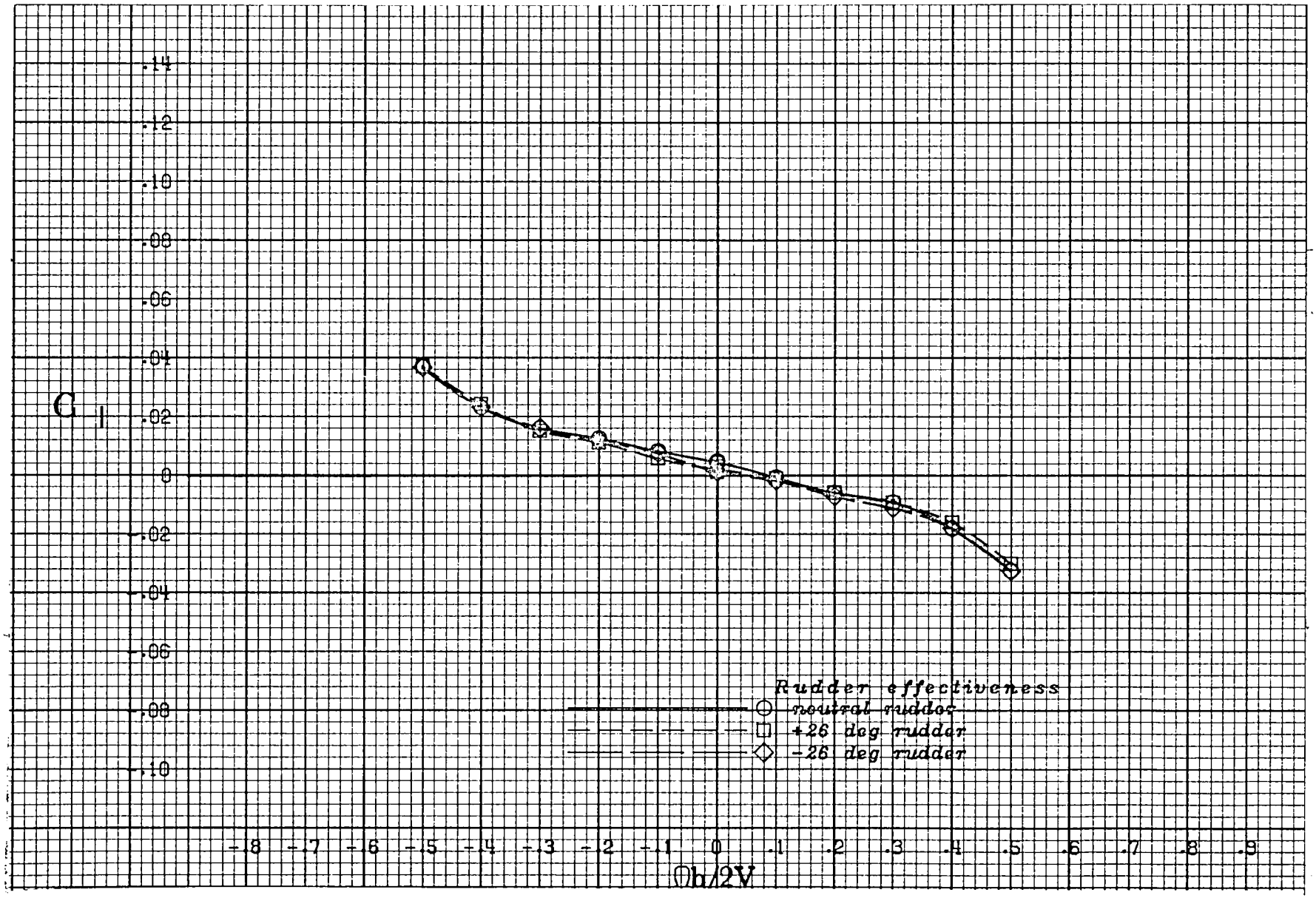

(c) α = 30 deg.

Figure A 8 .- Continued.

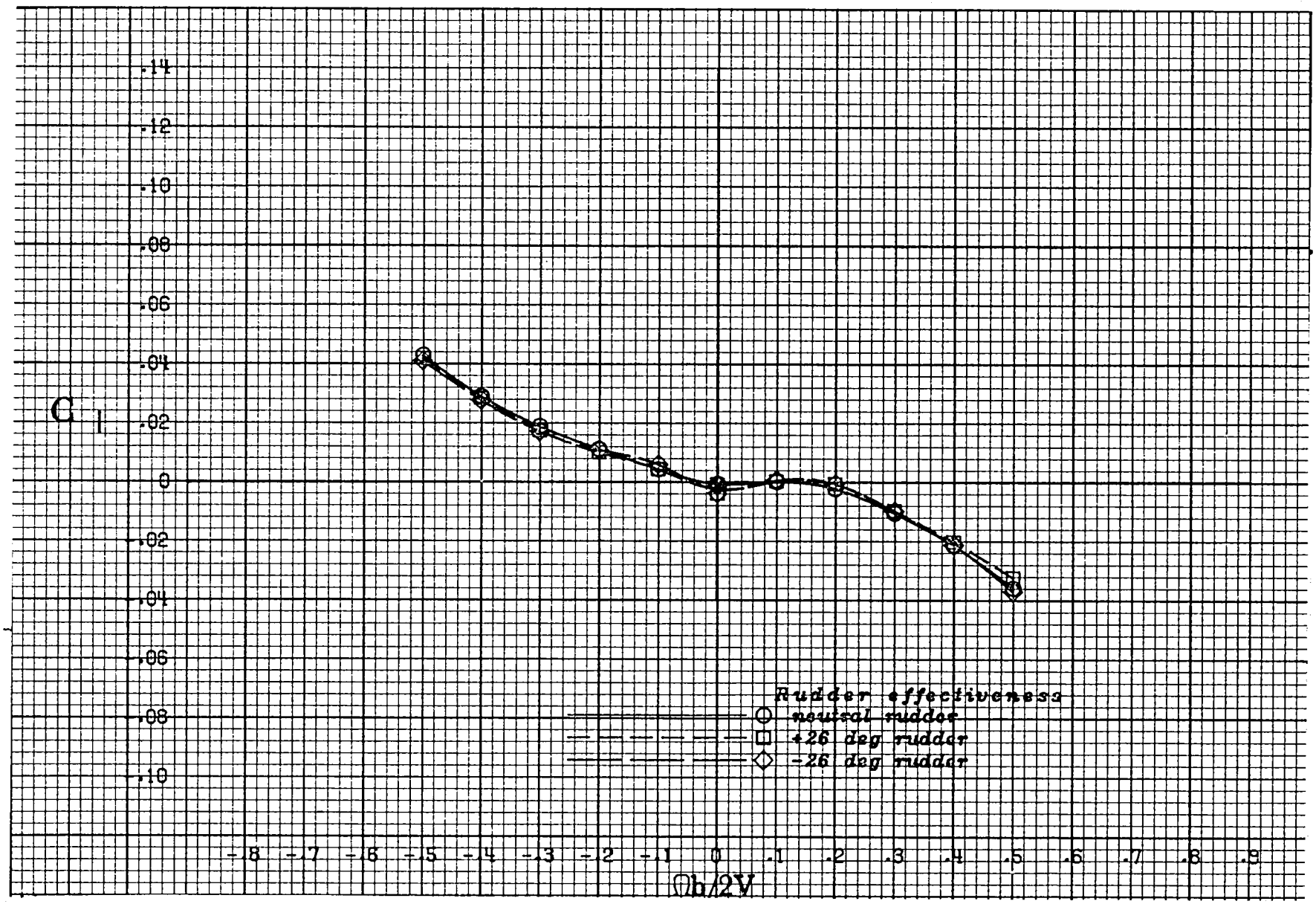

(d) α = 35 deg.

Figure A 8 .- Continued.

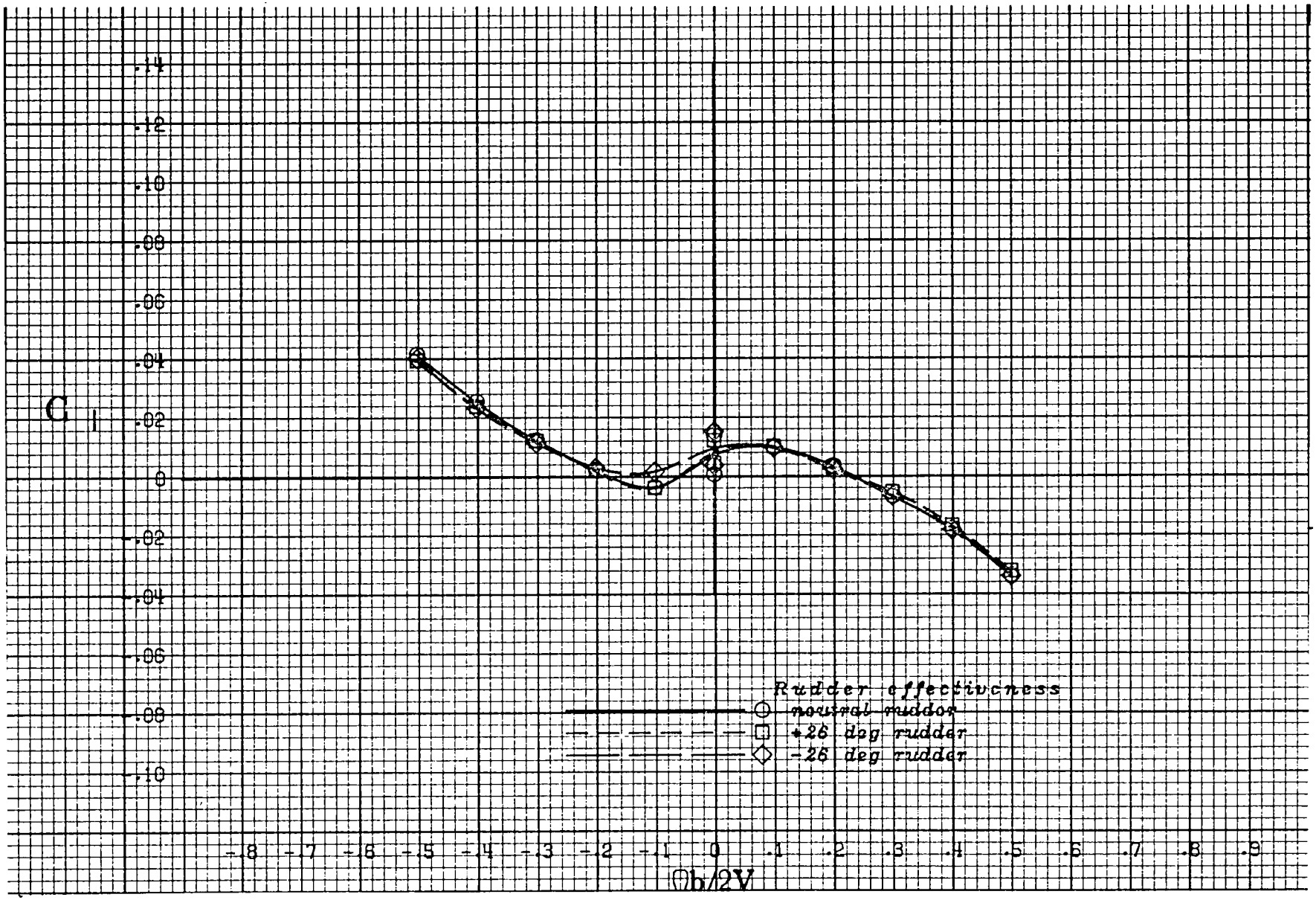

(e) α = 40 deg.

Figure A 8 .- Continued.

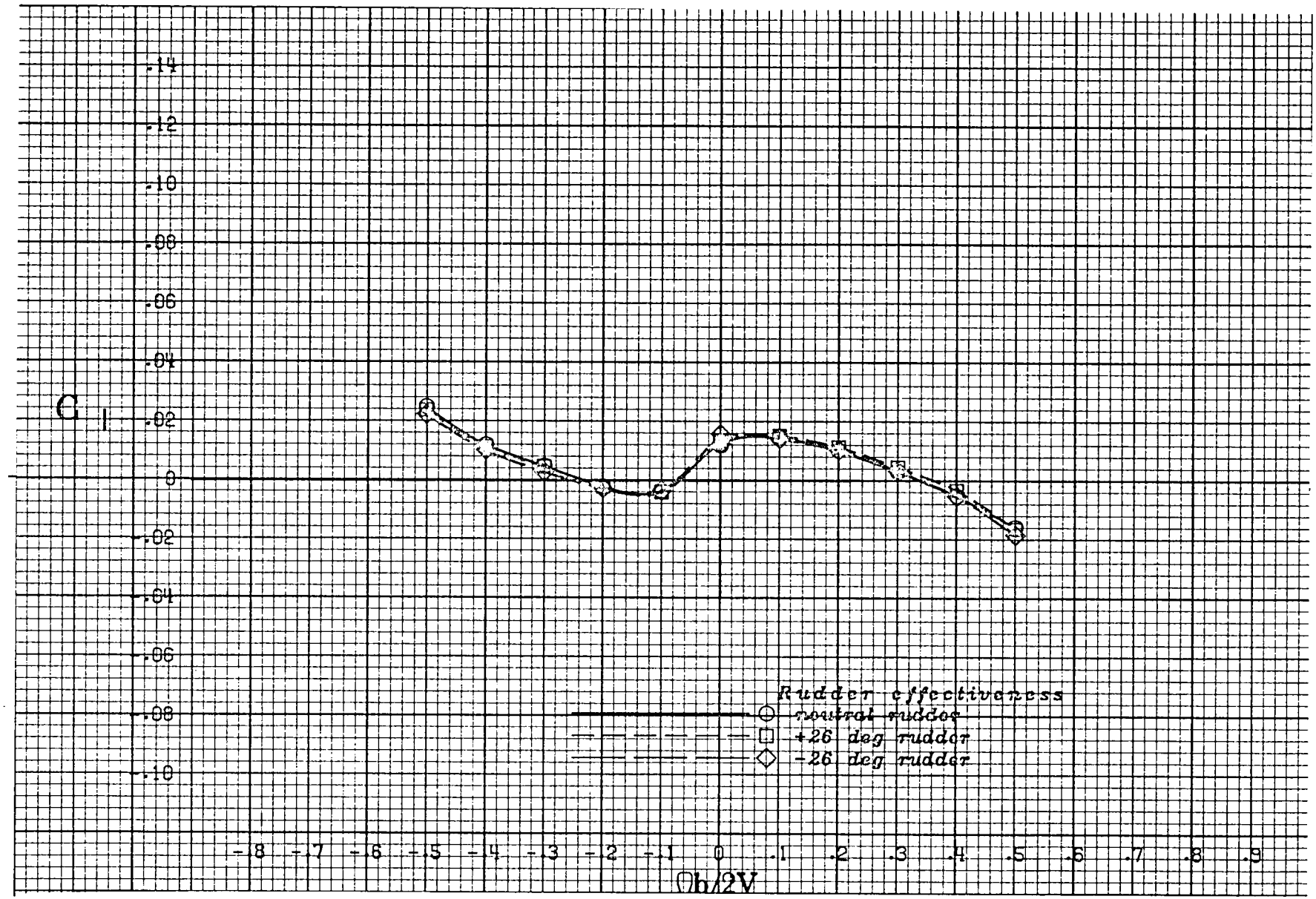

(f) α = 50 deg.

Figure A 8 .- Continued.

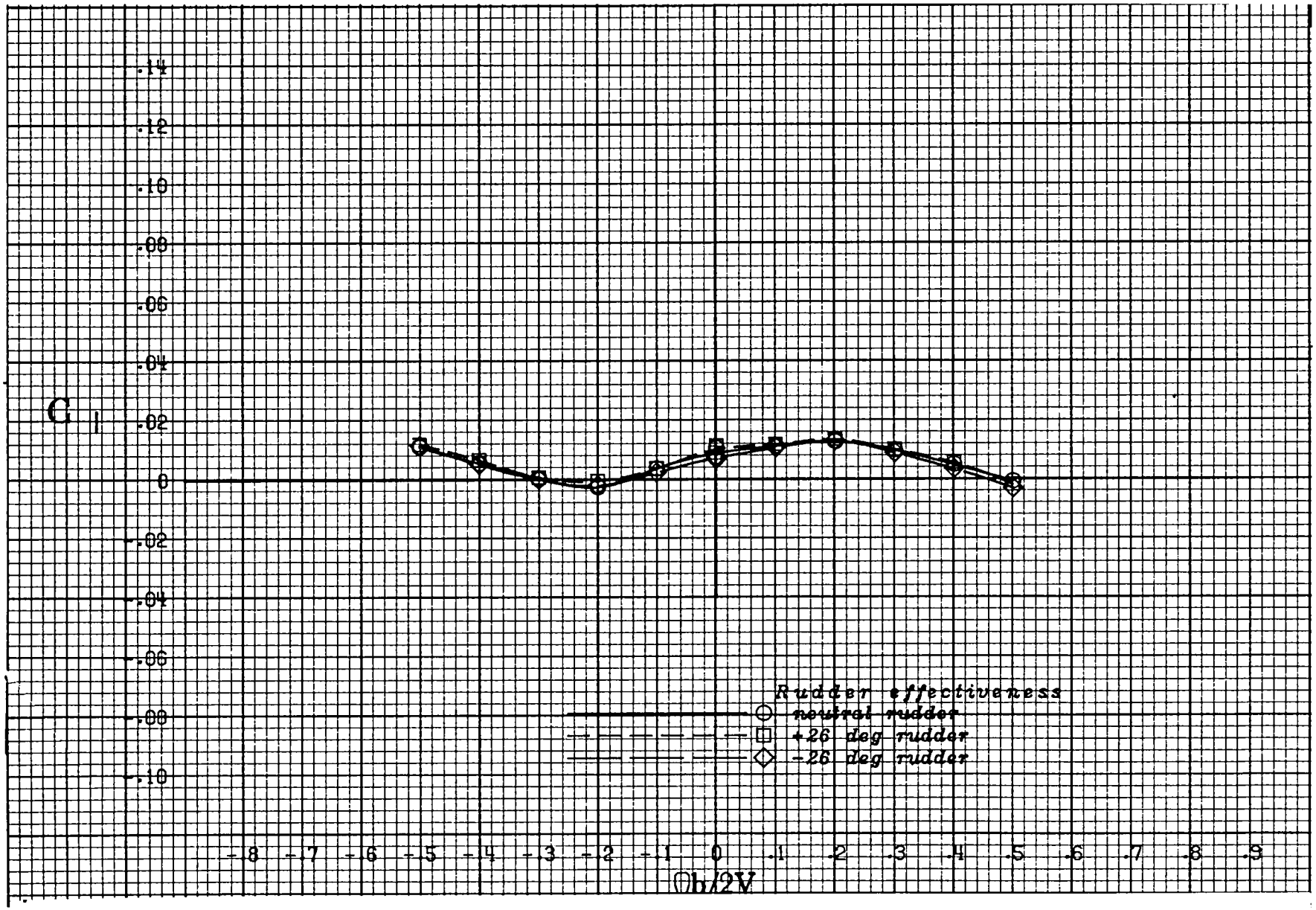

(g) α = 60 deg.

Figure A 8 .- Continued.

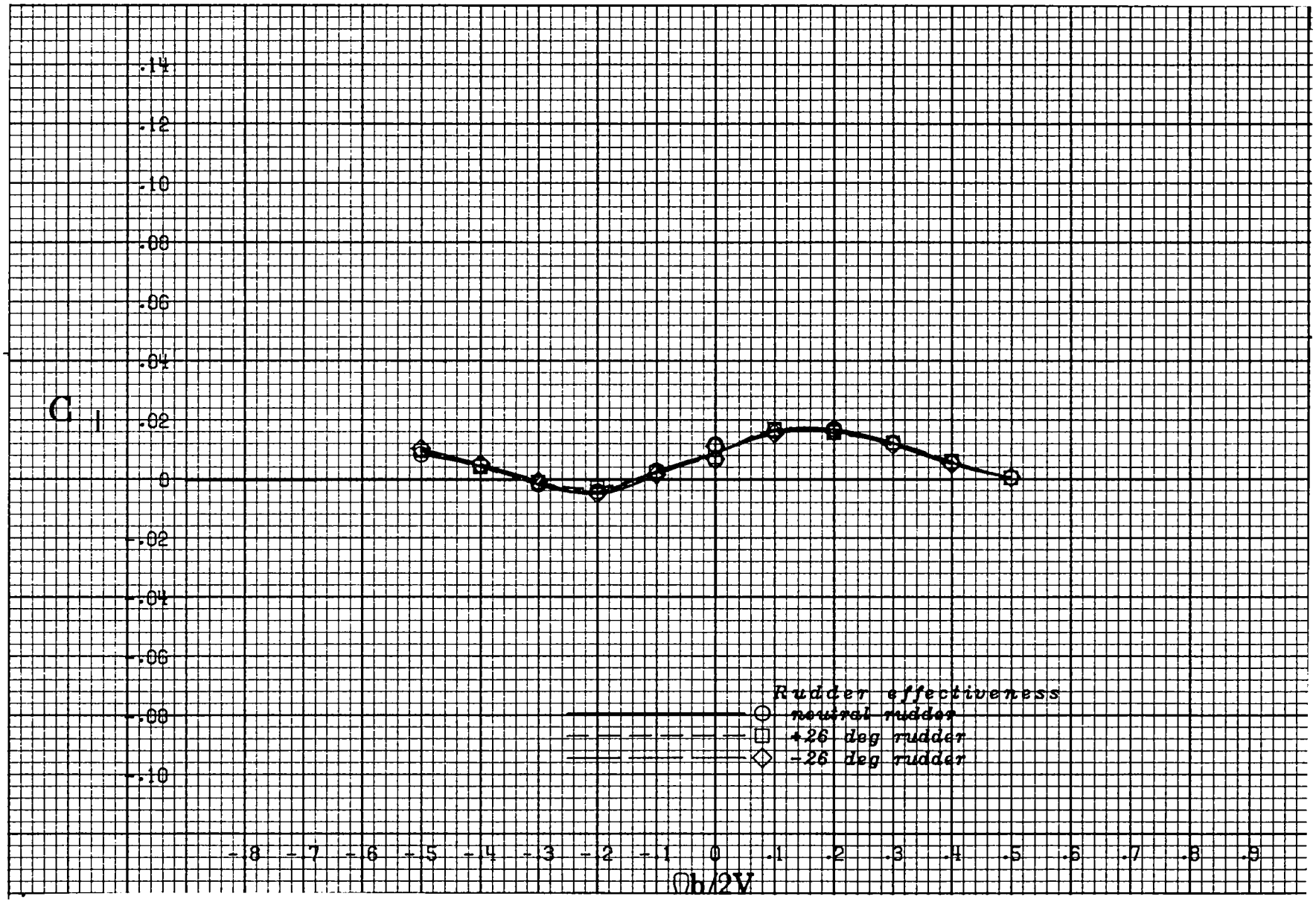

(h) α = 70 deg.

Figure A 8 .- Continued.

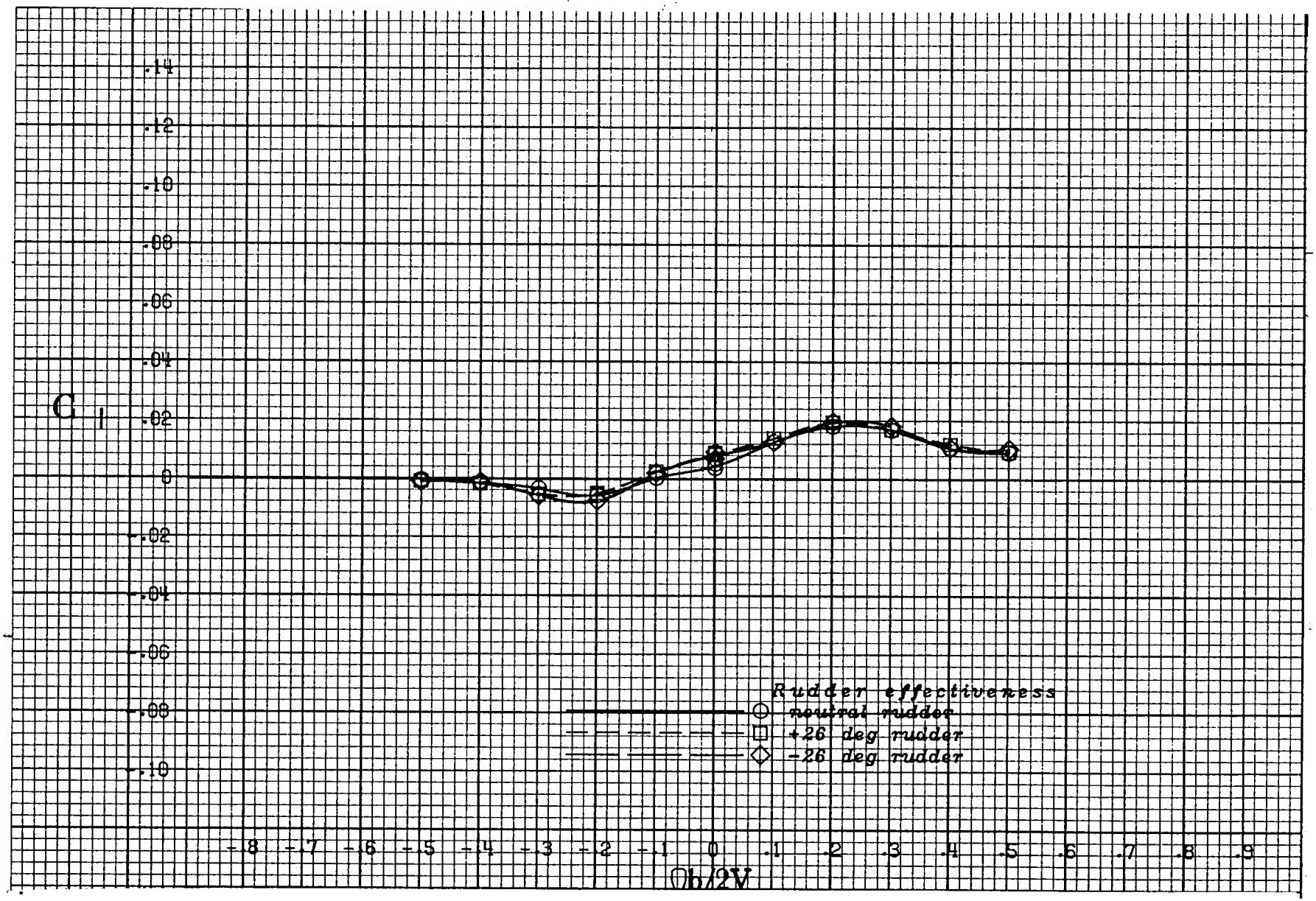

(i) α = 80 deg.

Figure A 8 .- Continued.

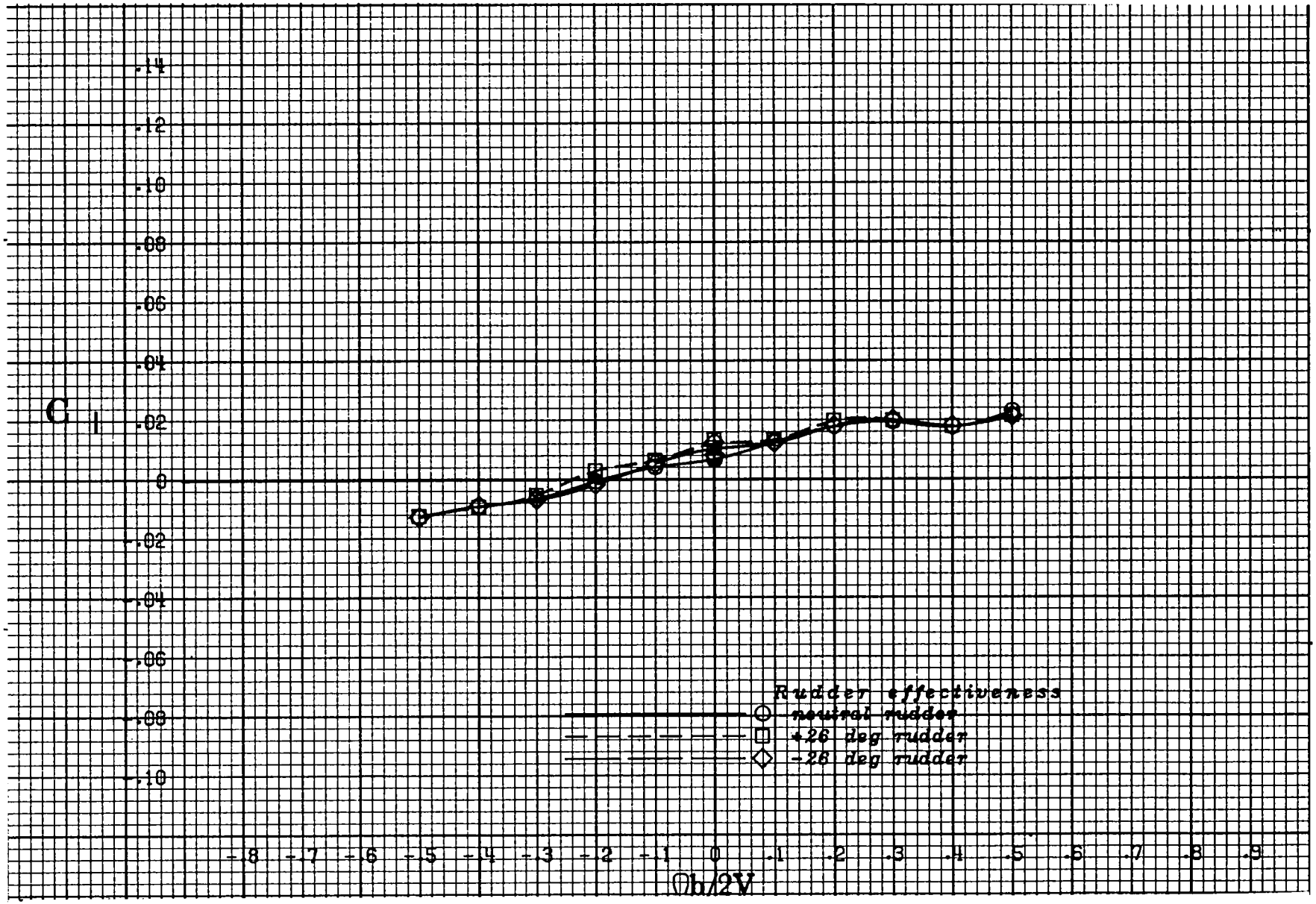

(j) α = 90 deg.

Figure A 8 .- Concluded.

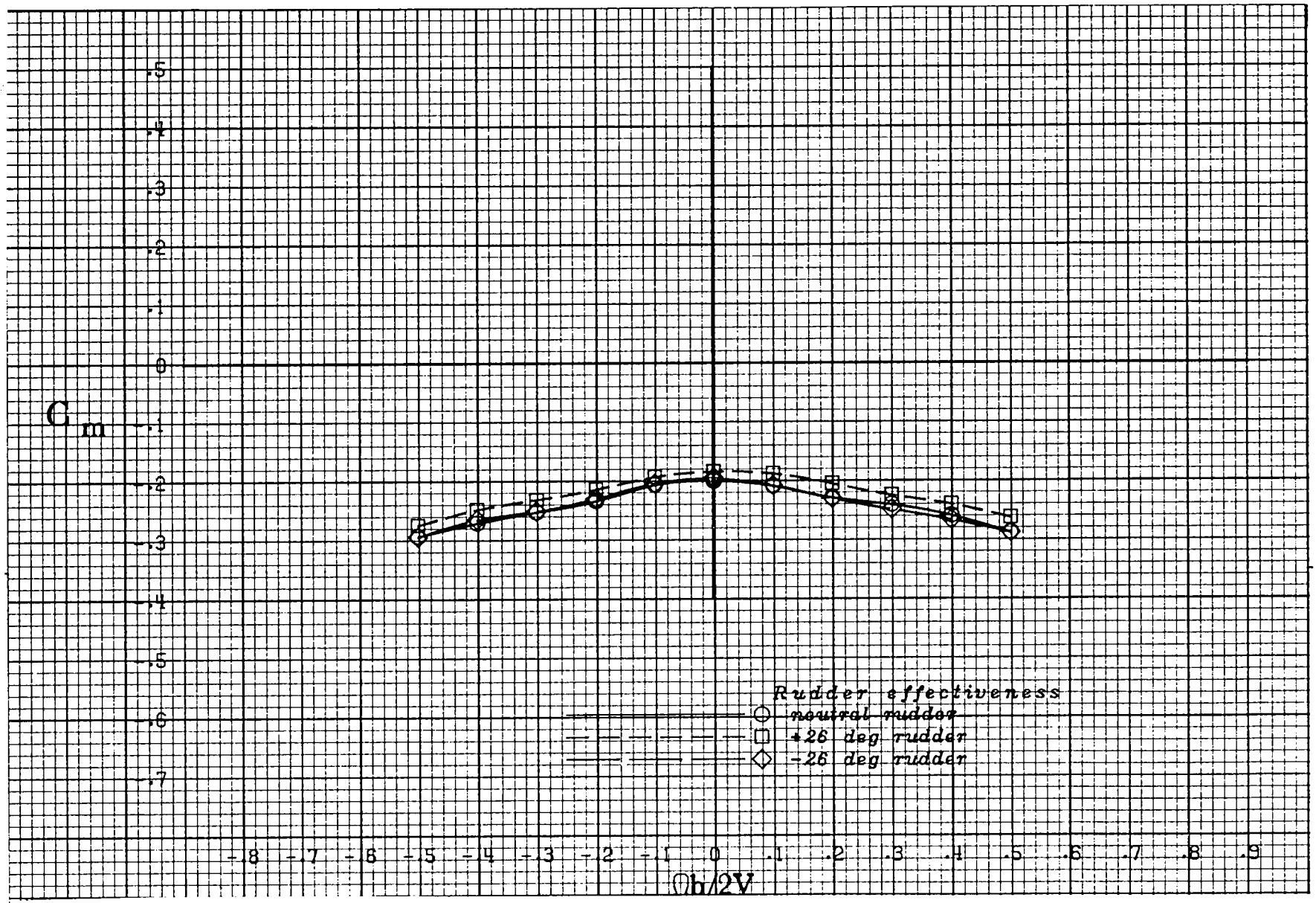

(a) α = 20 deg.

Figure A 9 .- Effect of rotation rate and rudder deflection on pitching-moment coefficient for the basic configuration with neutral elevator and ailerons at zero sideslip angle.

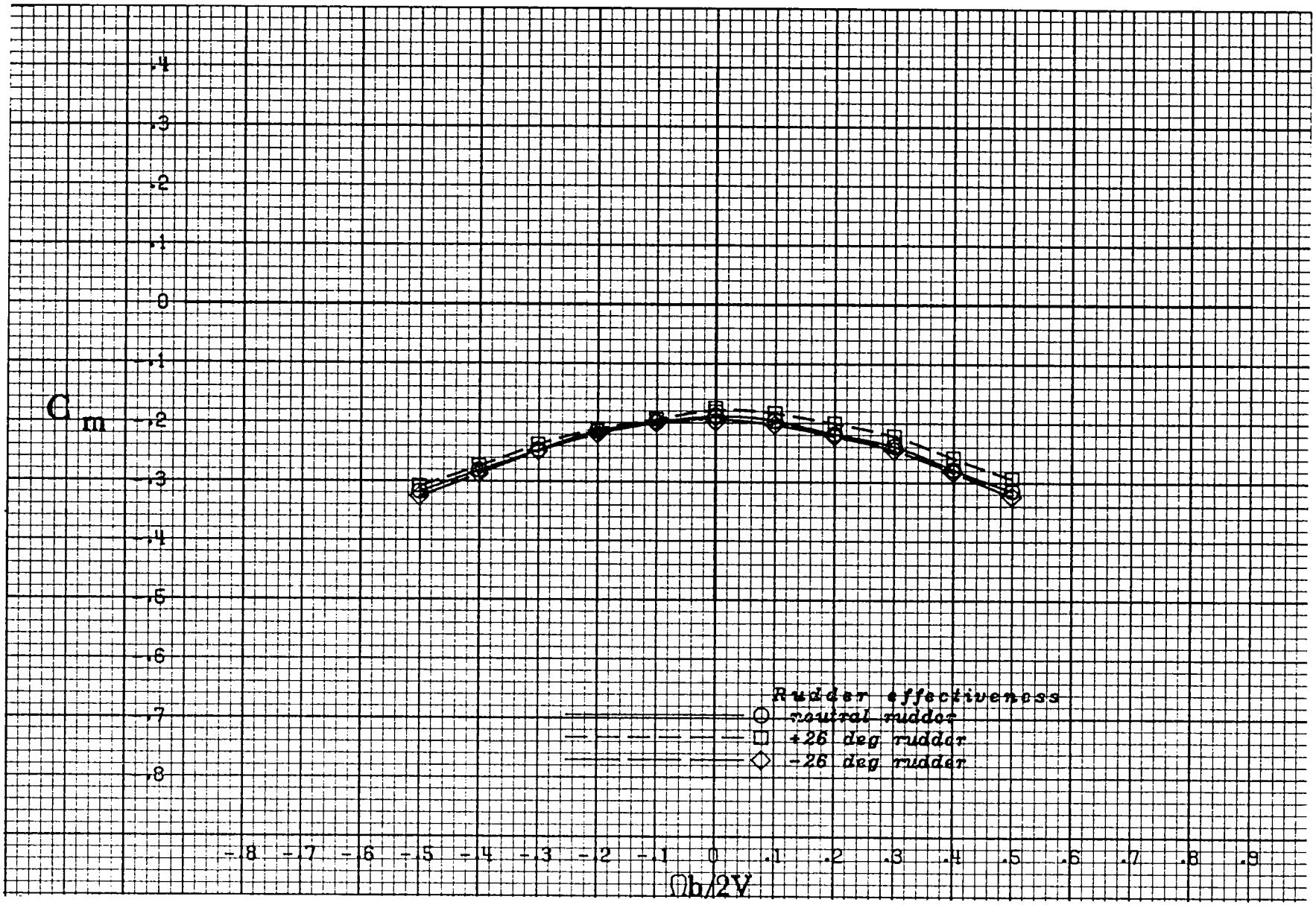

(b) α = 25 deg.

Figure A 9 .- Continued.

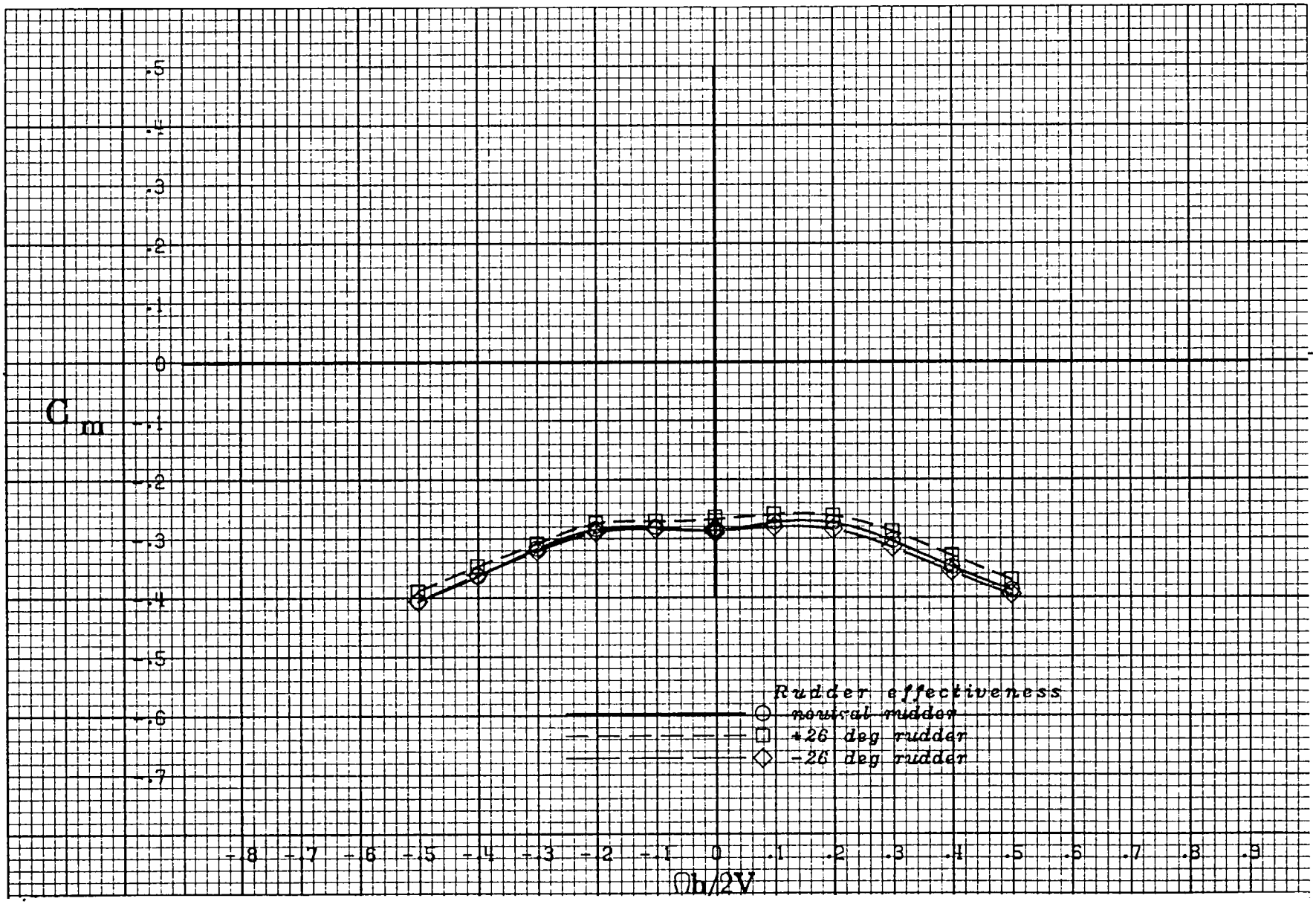

(c) α = 30 deg.

Figure A 9 .- Continued.

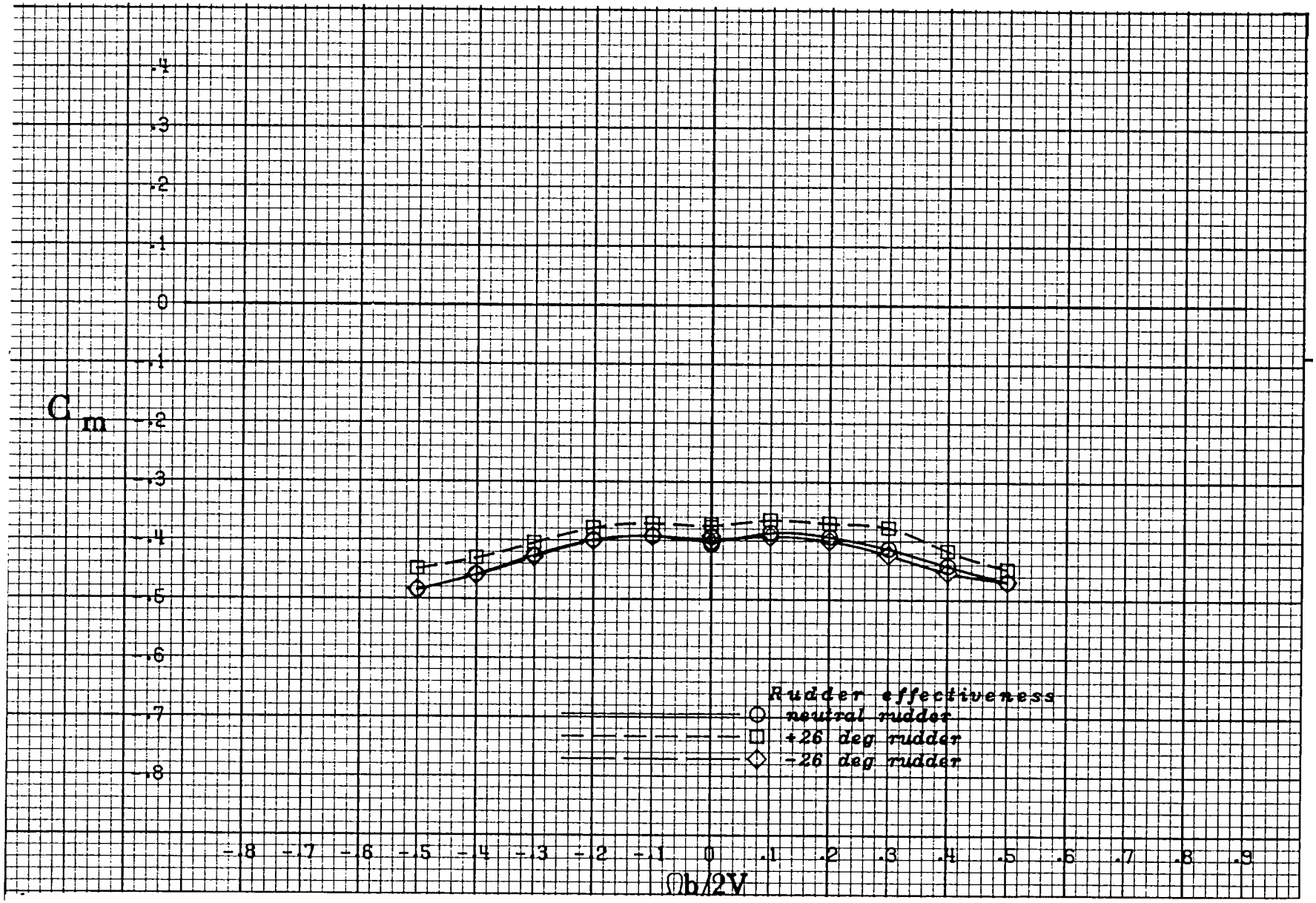

(d) α = 35 deg.

Figure A 9 .- Continued.

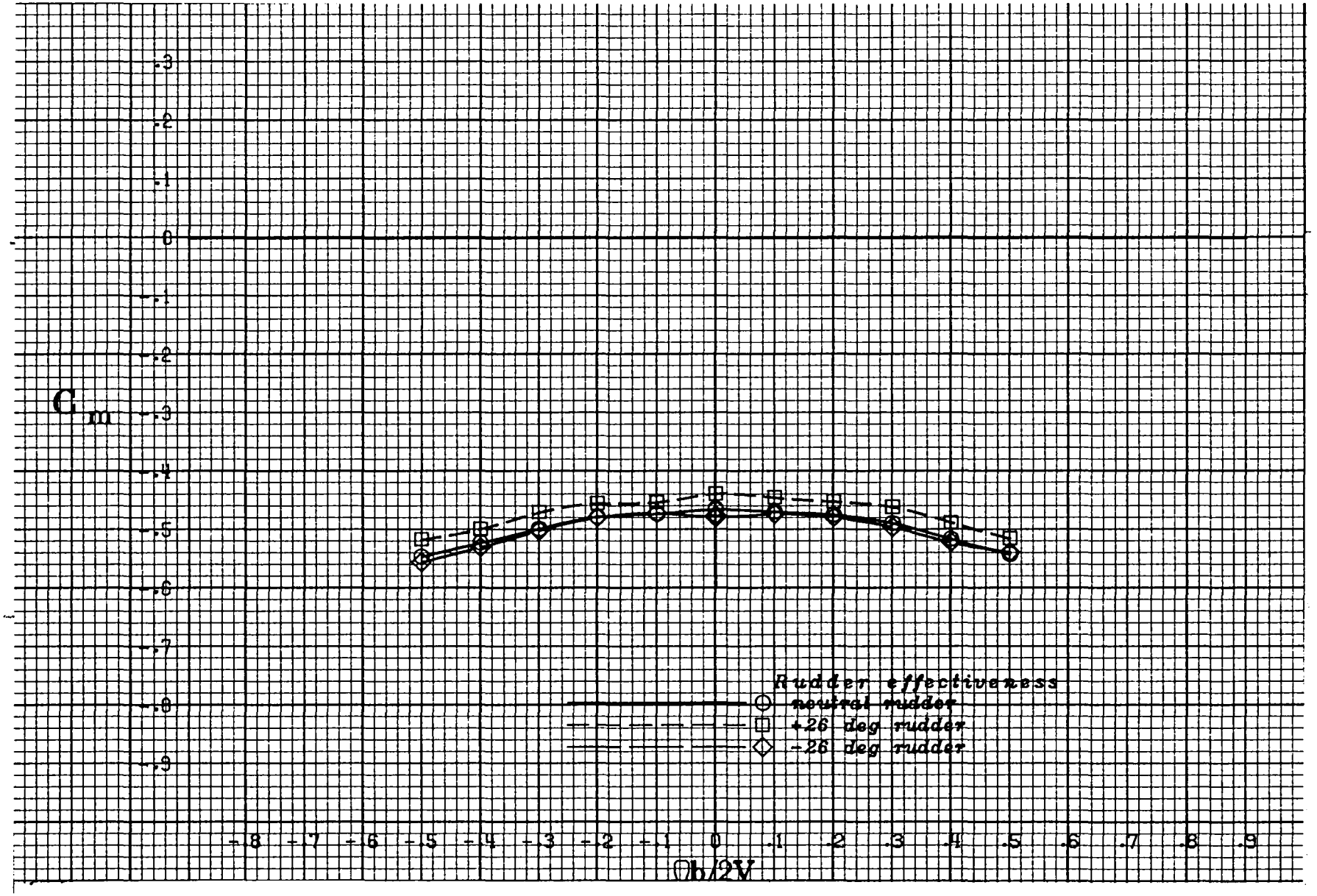

(e) α = 40 deg.

Figure A 9 .- Continued.

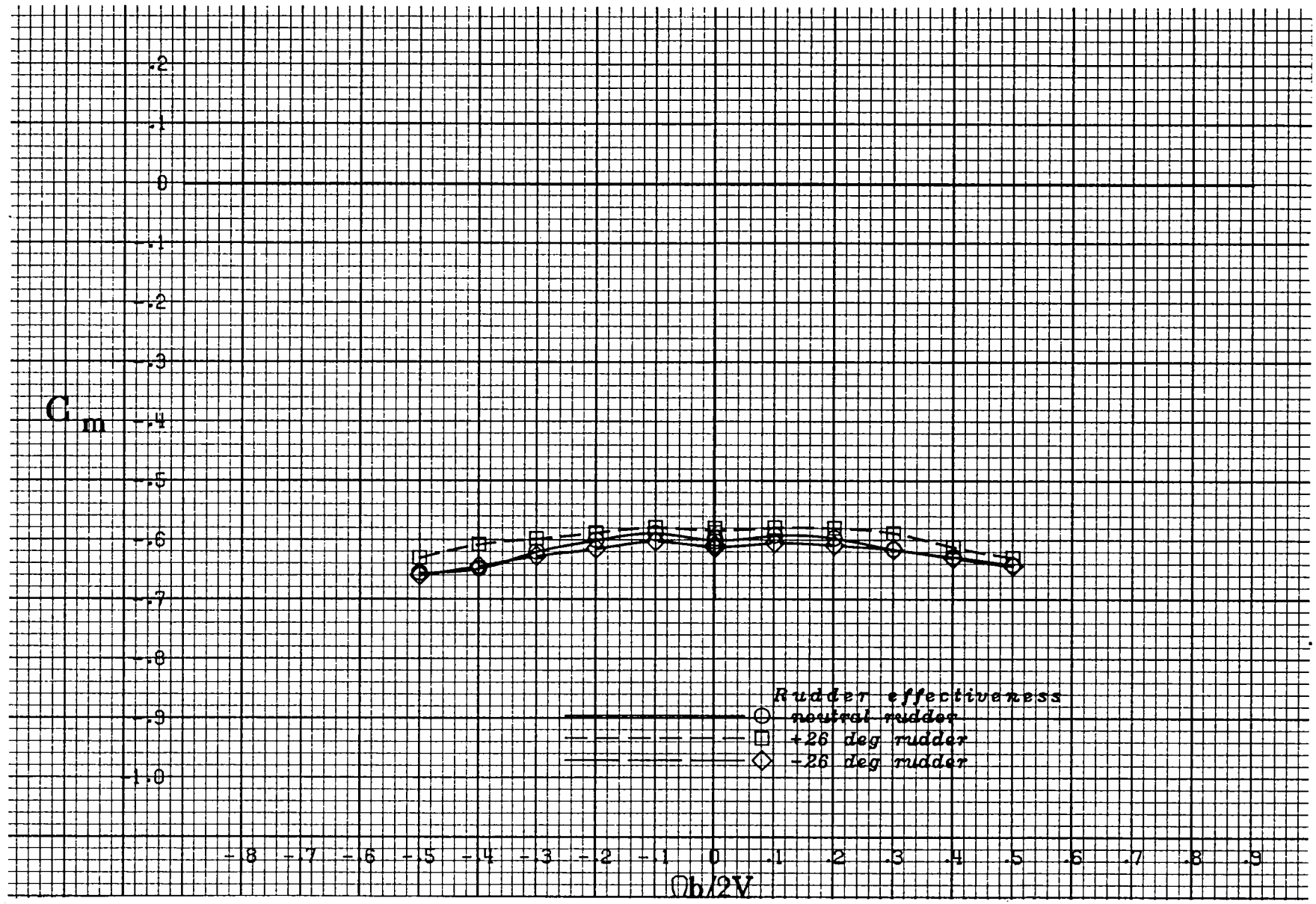

(f) α = 50 deg.

Figure A 9 .- Continued.

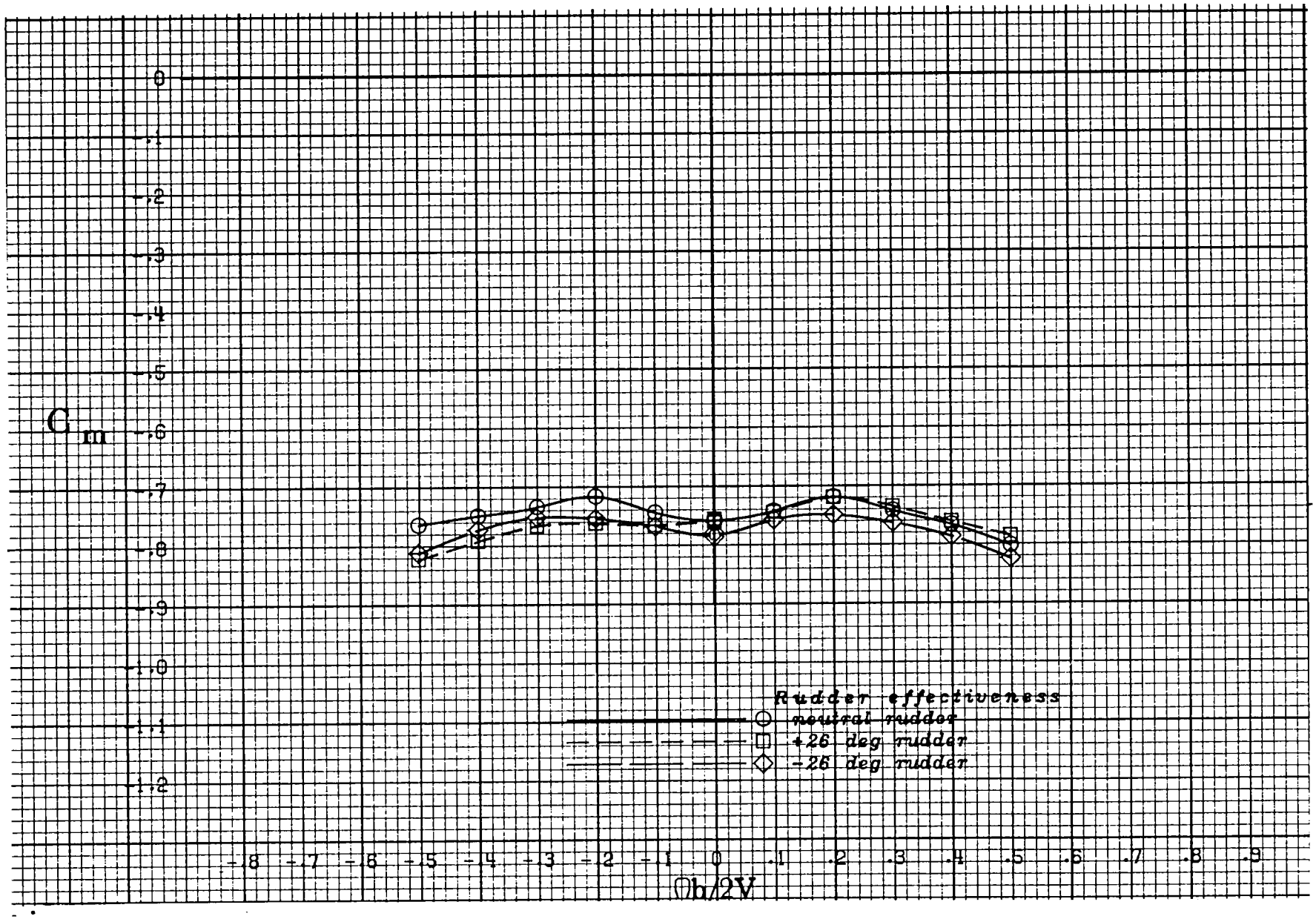

(g) α = 60 deg.

Figure A 9 .- Continued.

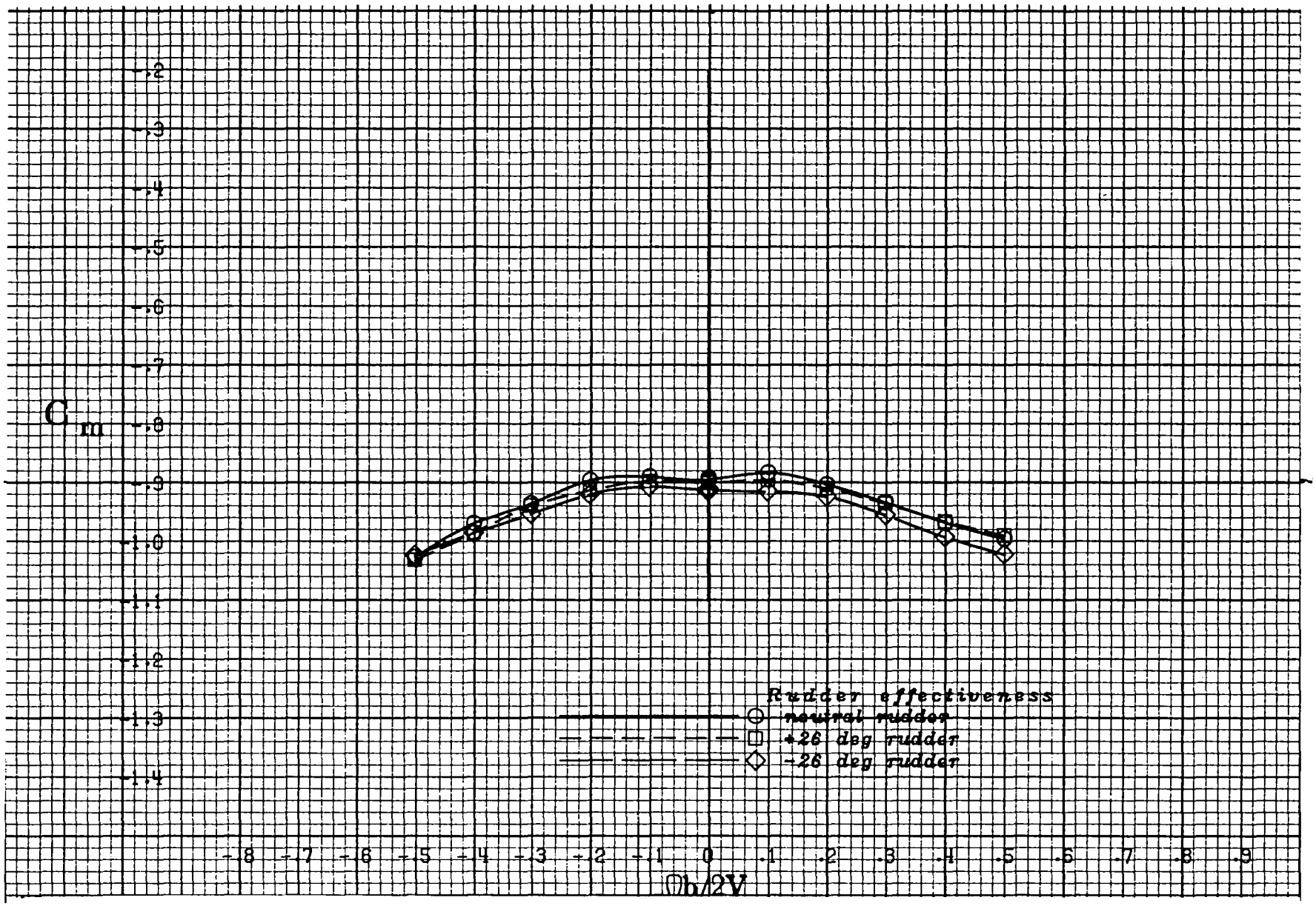

(h) α = 70 deg.

Figure A 9 .- Continued.

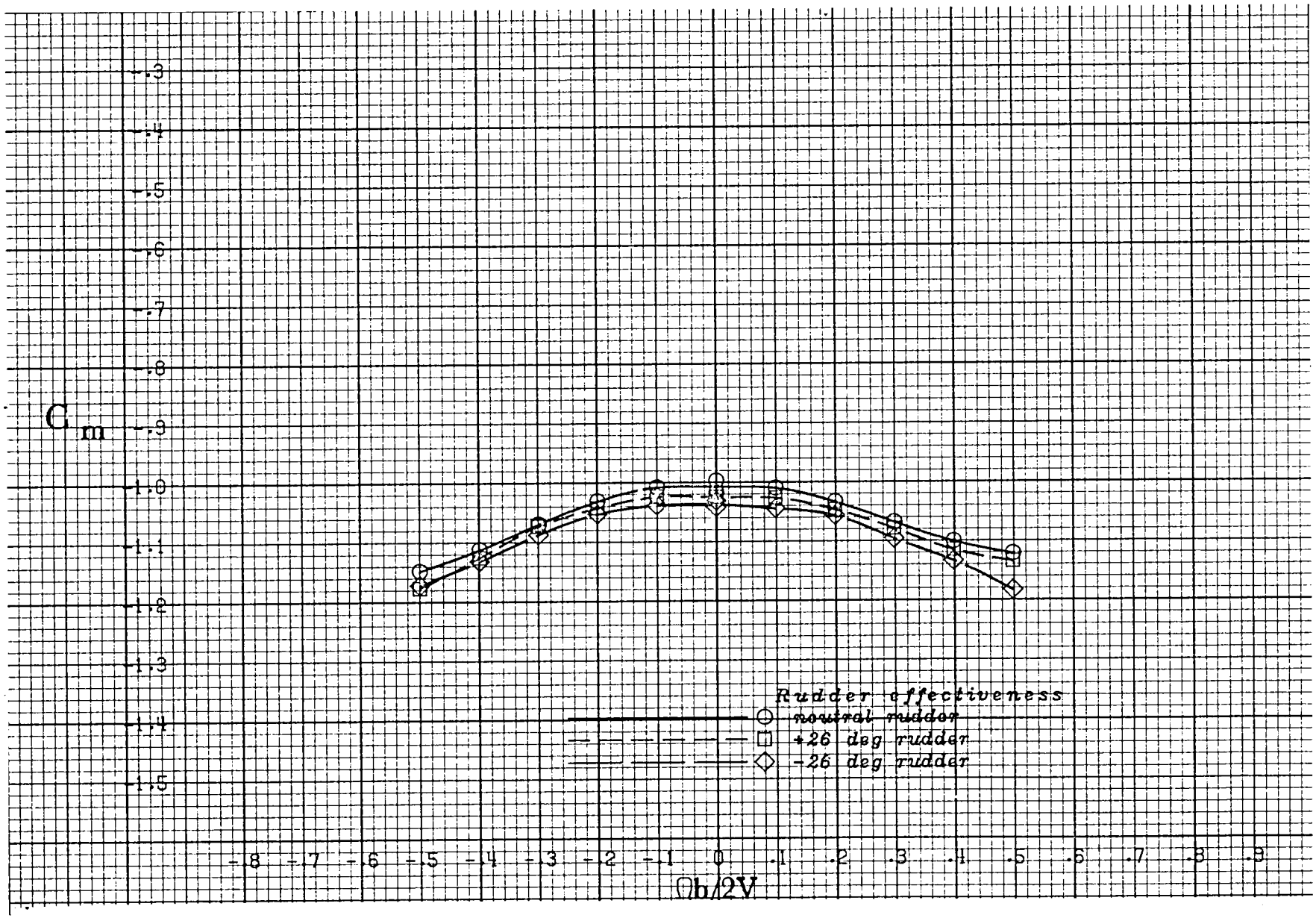

(i) α = 80 deg.

Figure A 9 .- Continued.

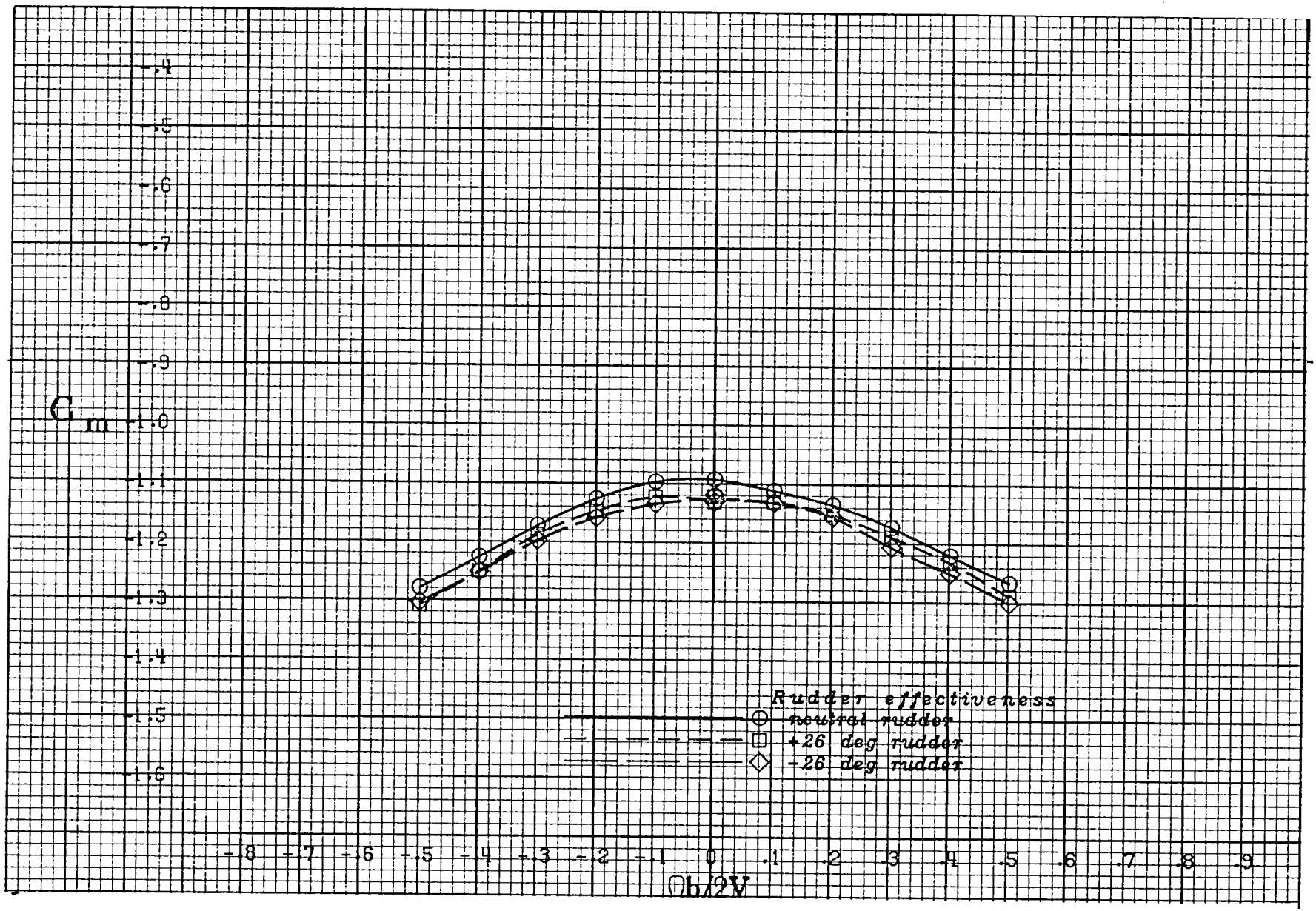

(j) α = 90 deg.

Figure A 9 .- Concluded.

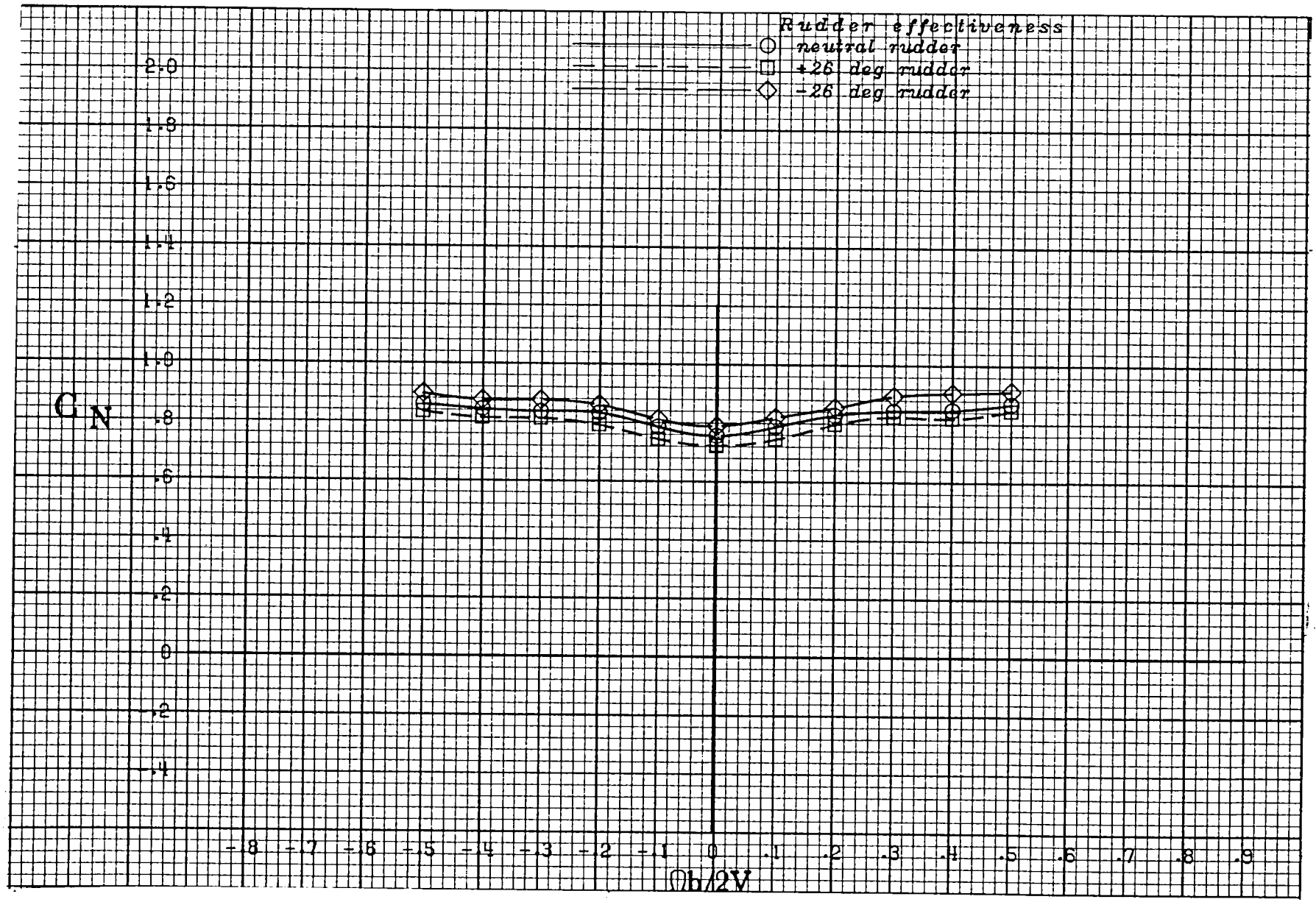

(a) α = 20 deg.

Figure A 10 .- Effect of rotation rate and rudder deflection on normal-force coefficient for the basic configuration with neutral elevator and ailerons at zero sideslip angle.

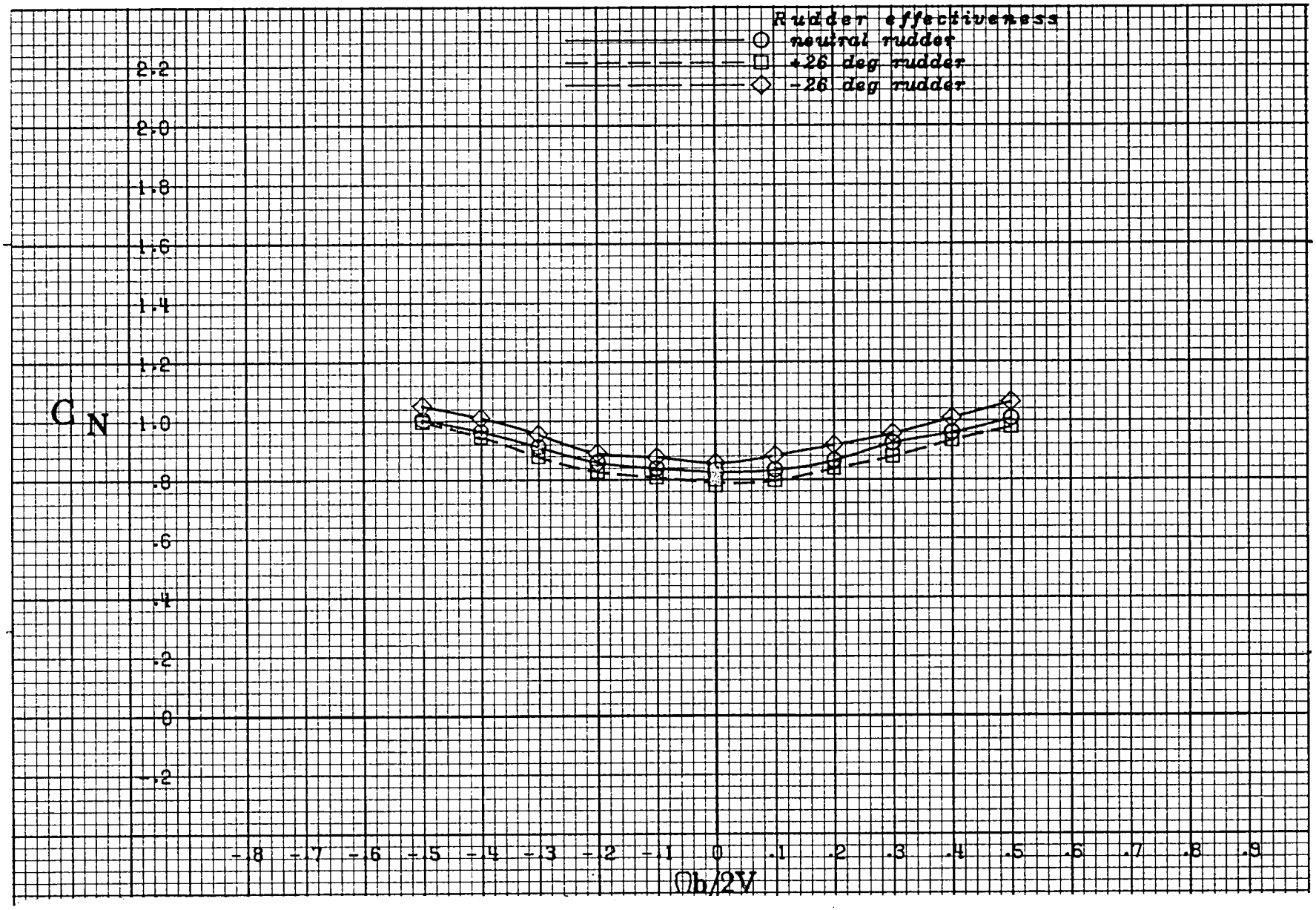

(b) α = 25 deg.

Figure A 10 .- Continued.

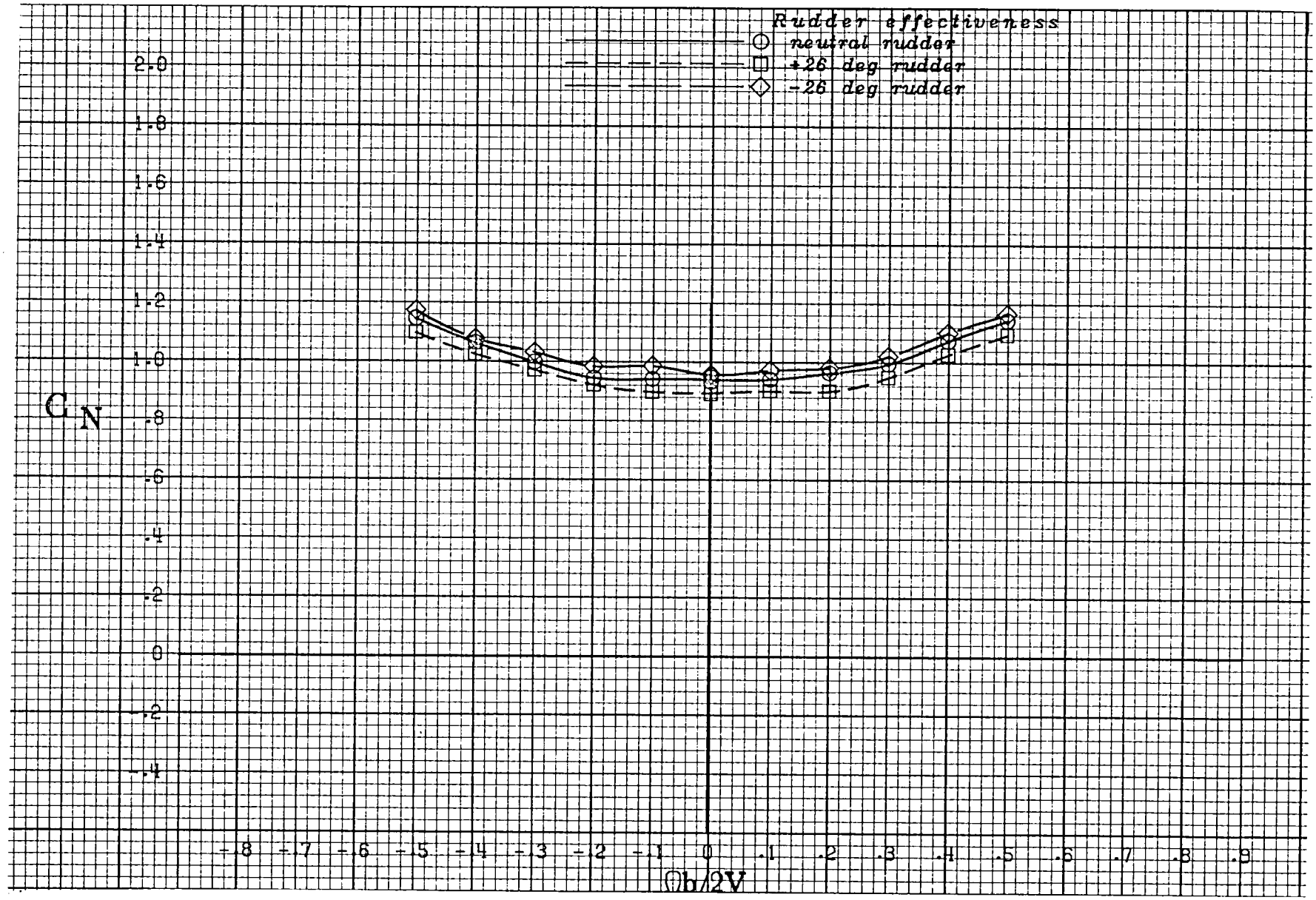

(c) α = 30 deg.

Figure A 10 .- Continued.

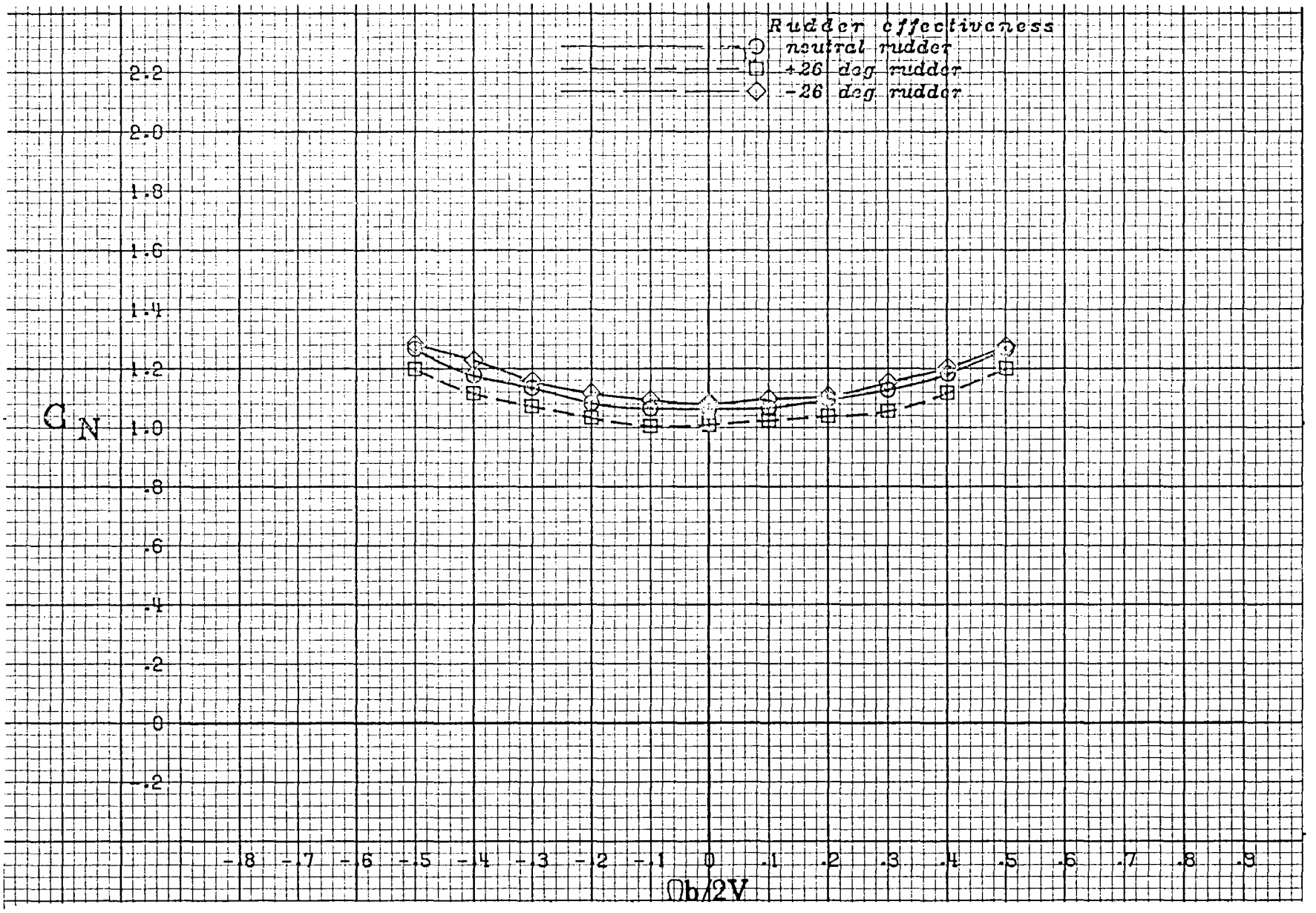

(d) α = 35 deg.

Figure A 10 .- Continued.

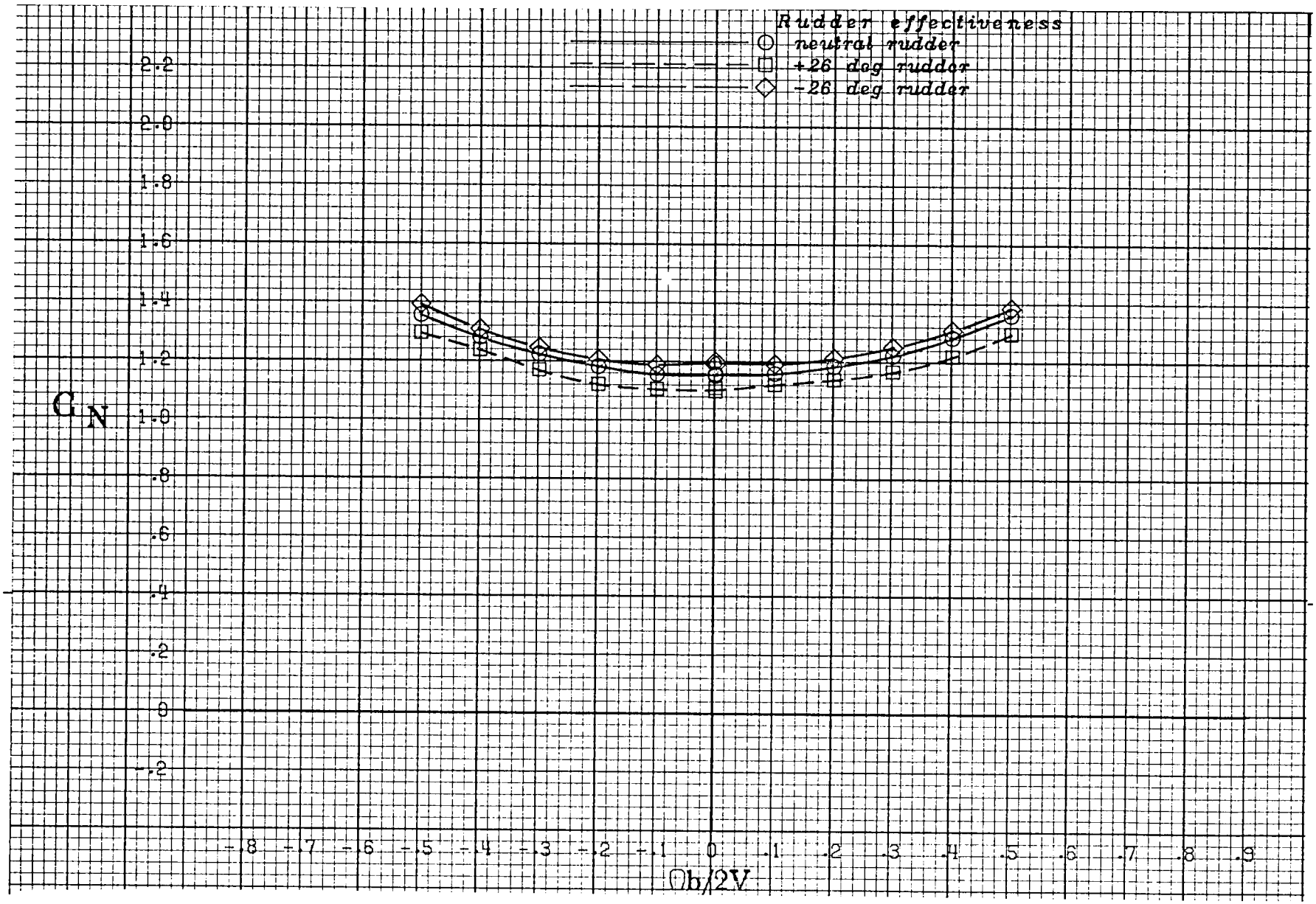

(e) α = 40 deg.

Figure A 10 .- Continued.

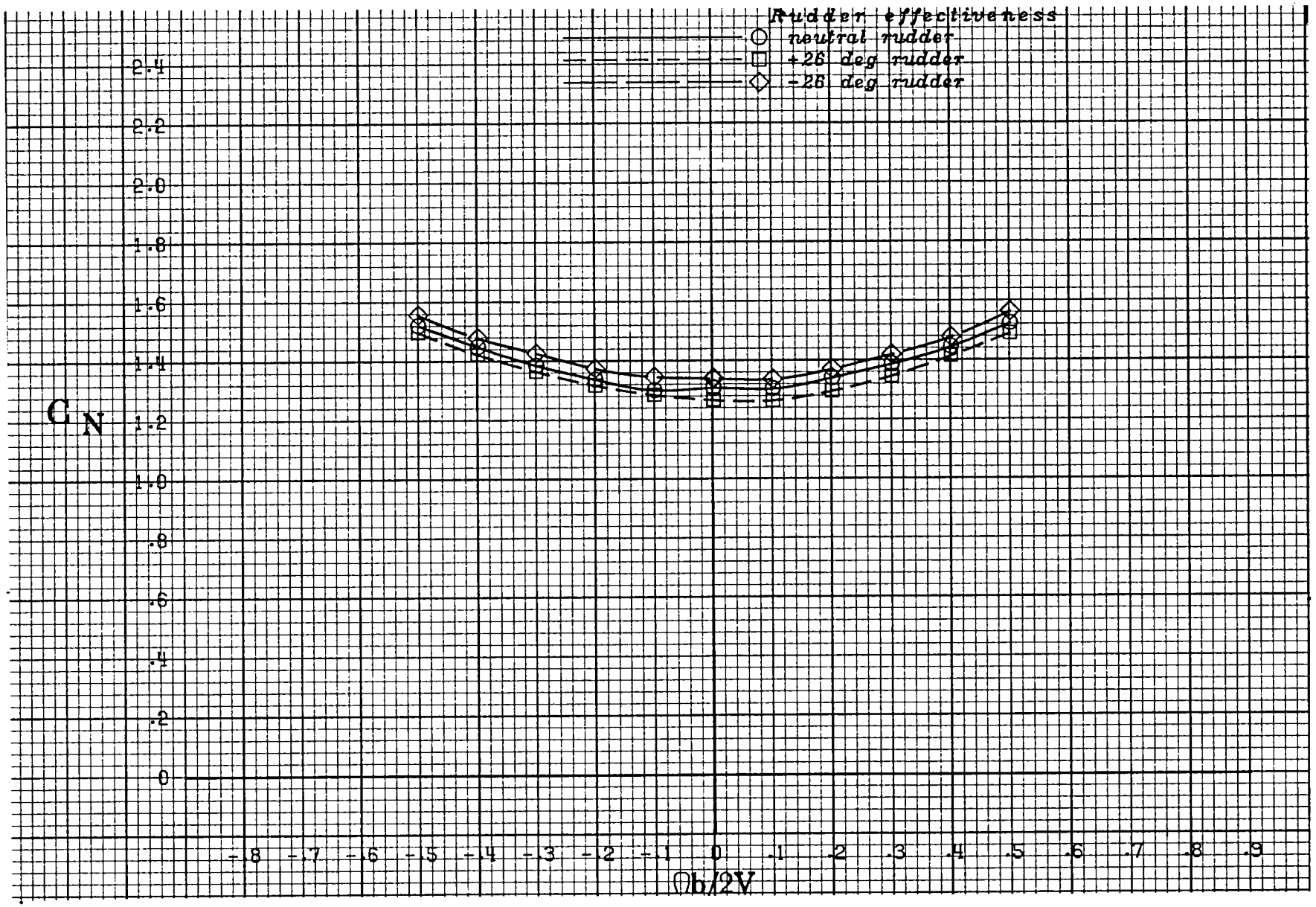

(f) α = 50 deg.

Figure A 10 .- Continued.

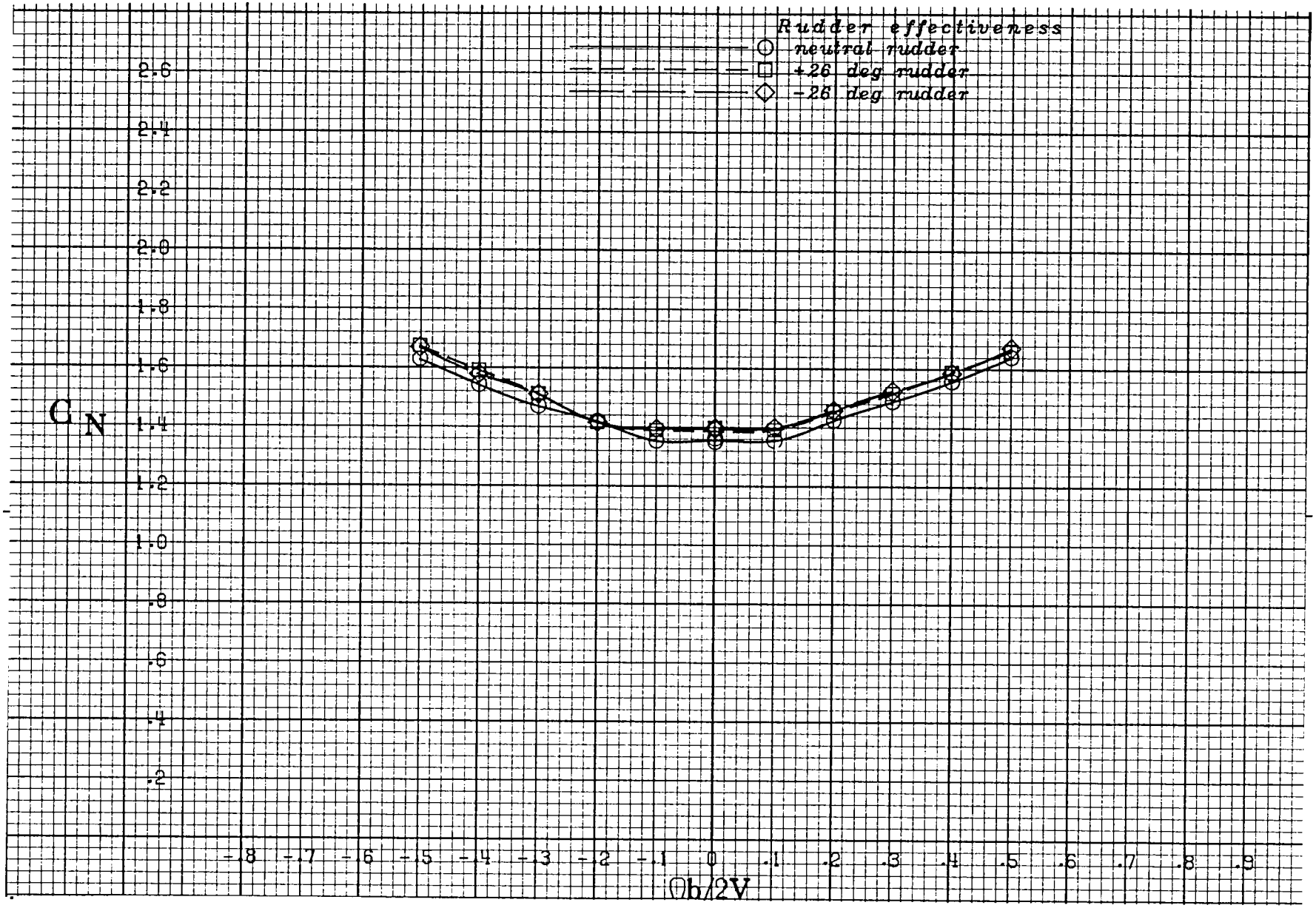

(g) α = 60 deg.

Figure A 10 .- Continued.

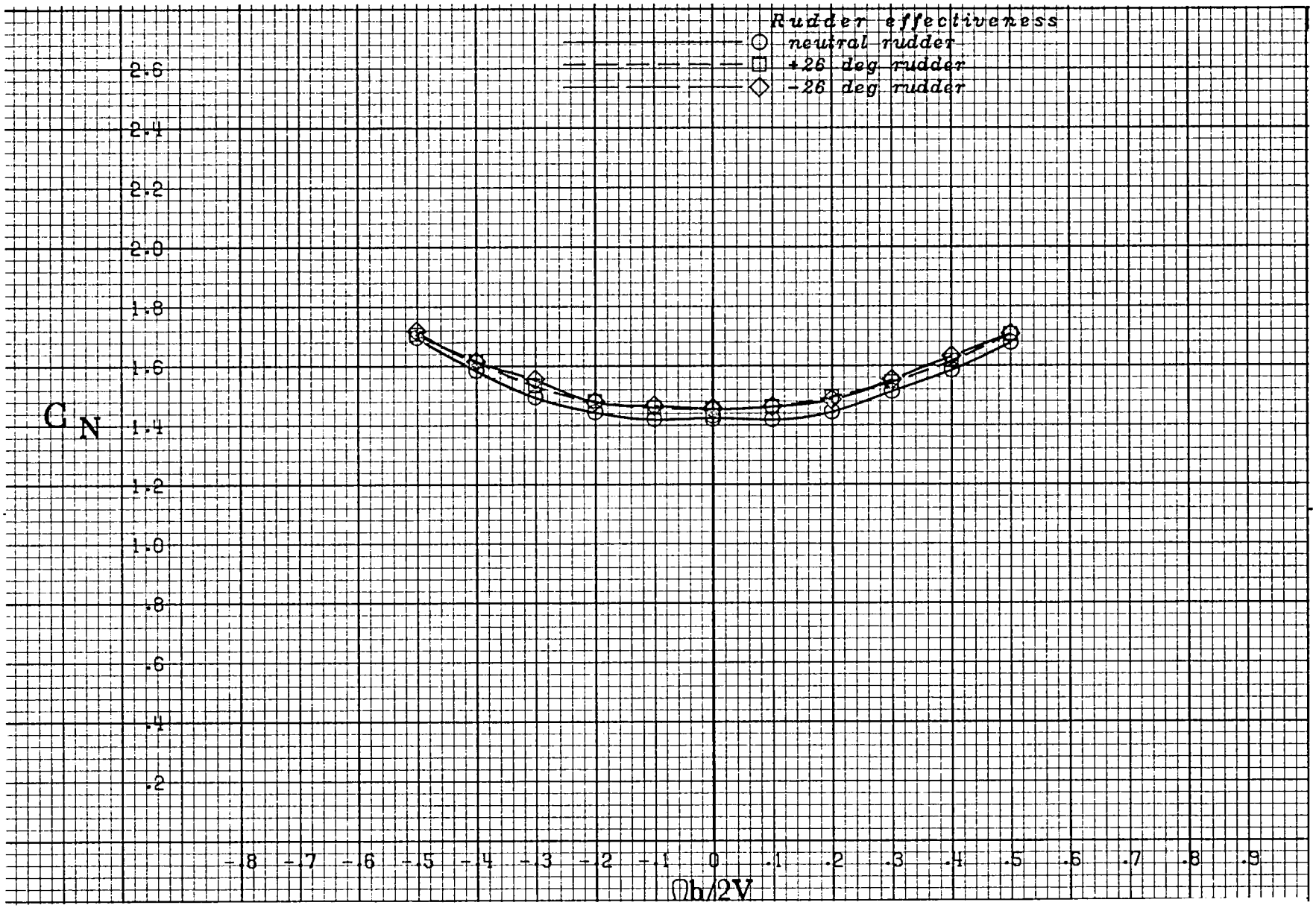

(h) α = 70 deg.

Figure A 10 .- Continued.

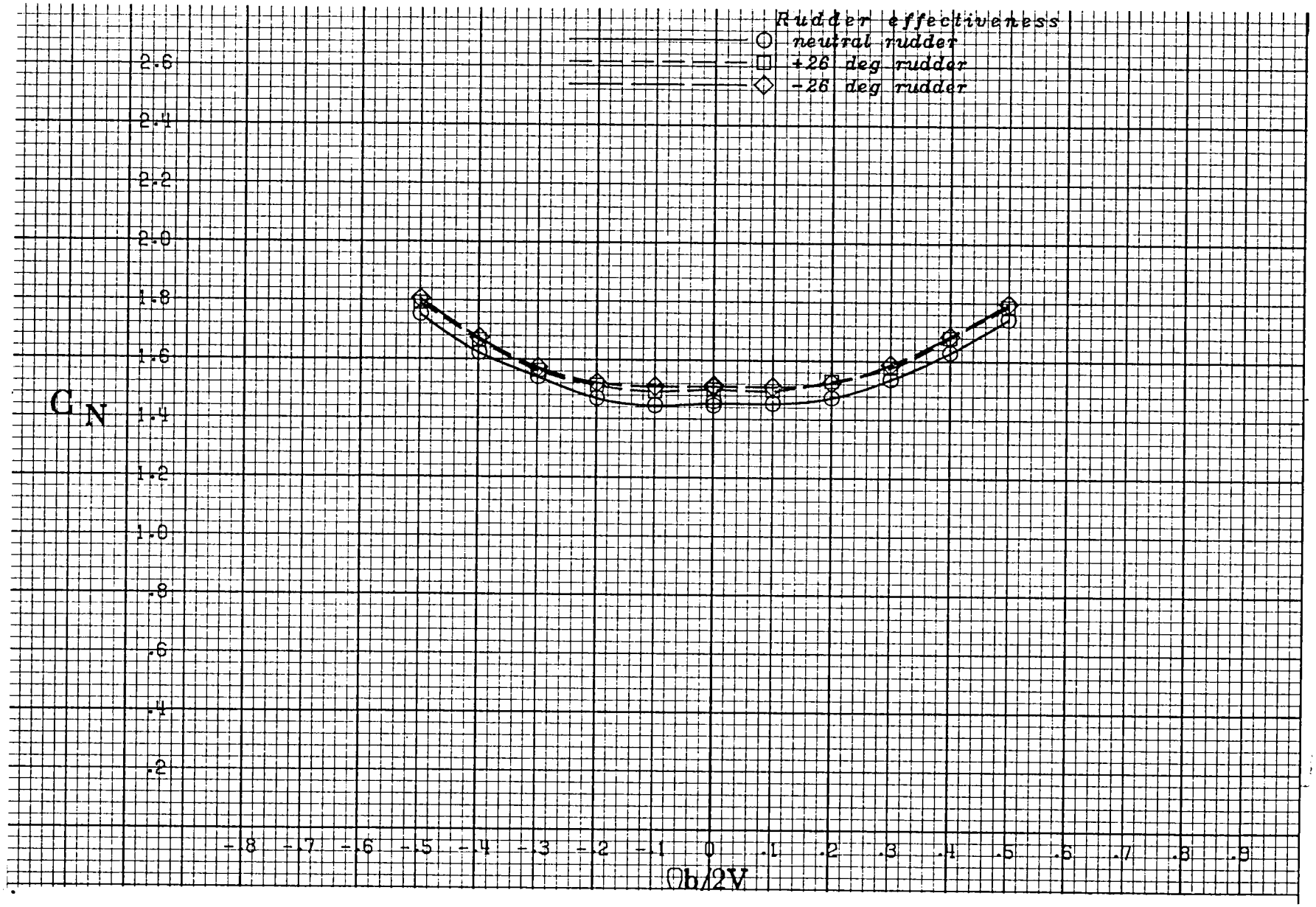

(i) α = 80 deg.

Figure A 10 .- Continued.

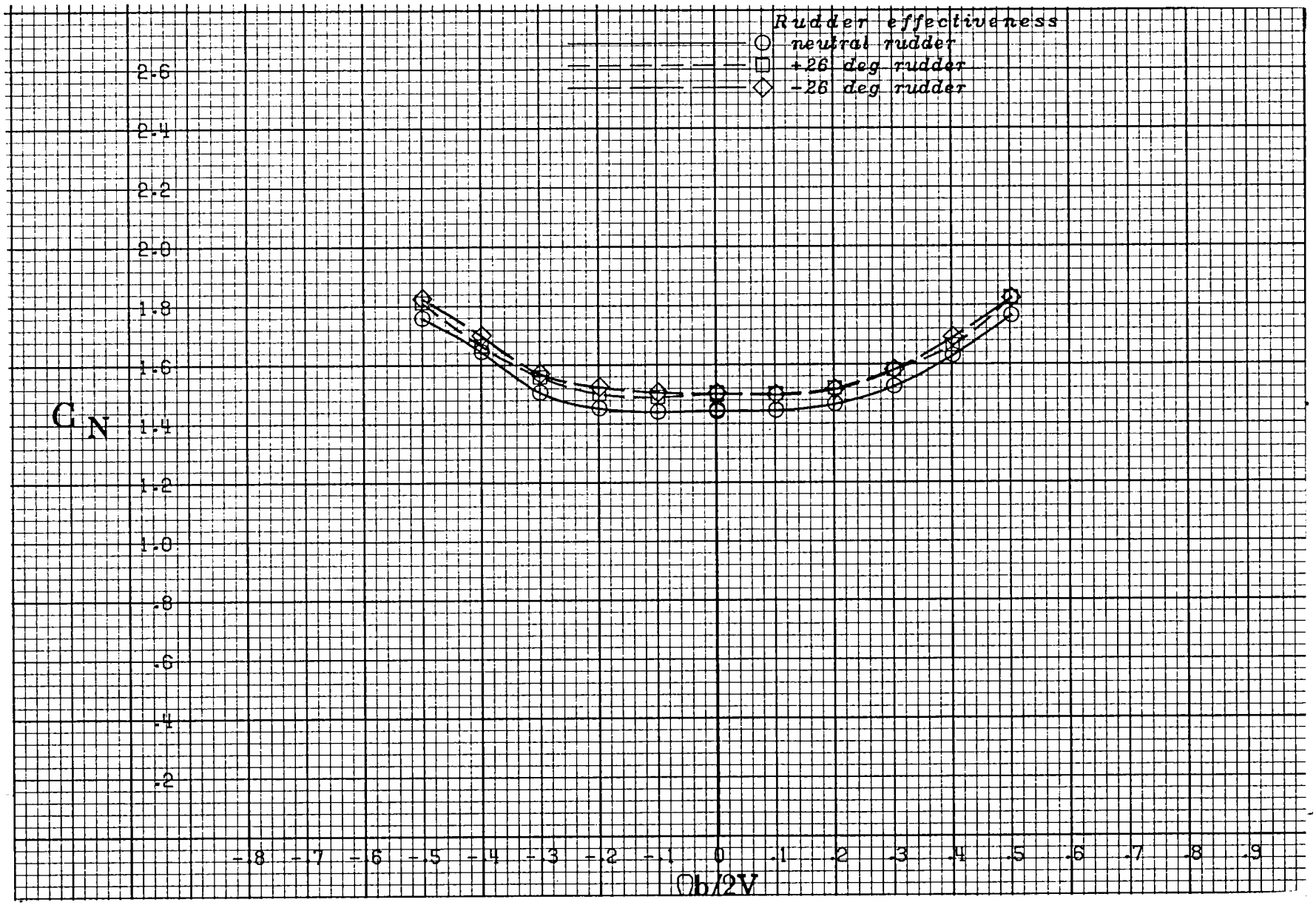

(j) α = 90 deg.

Figure A 10 .- Concluded.

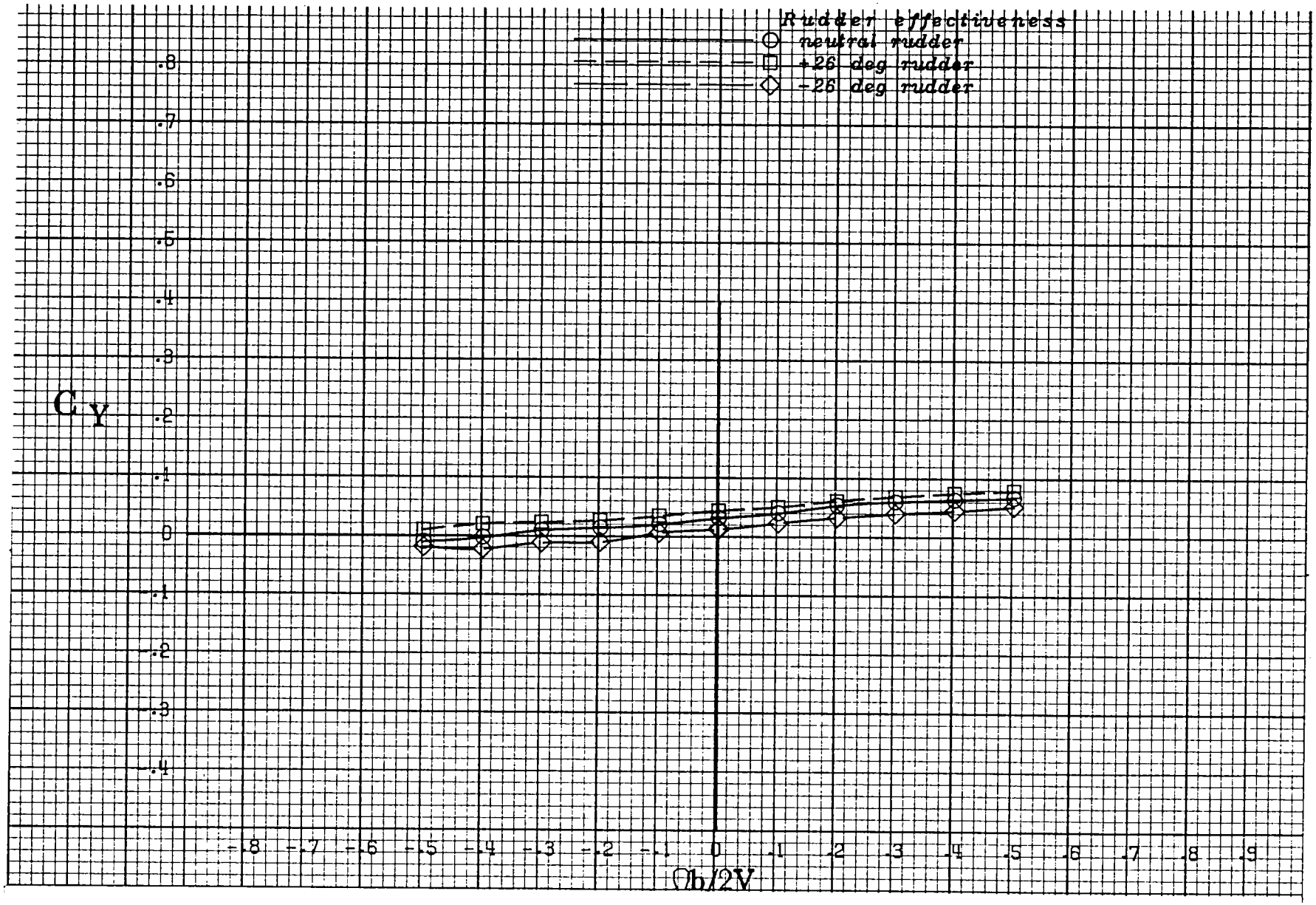

(a) α = 20 deg.

Figure A 11 .- Effect of rotation rate and rudder deflection on side-force coefficient for the basic configuration with neutral elevator and ailerons at zero sideslip angle.

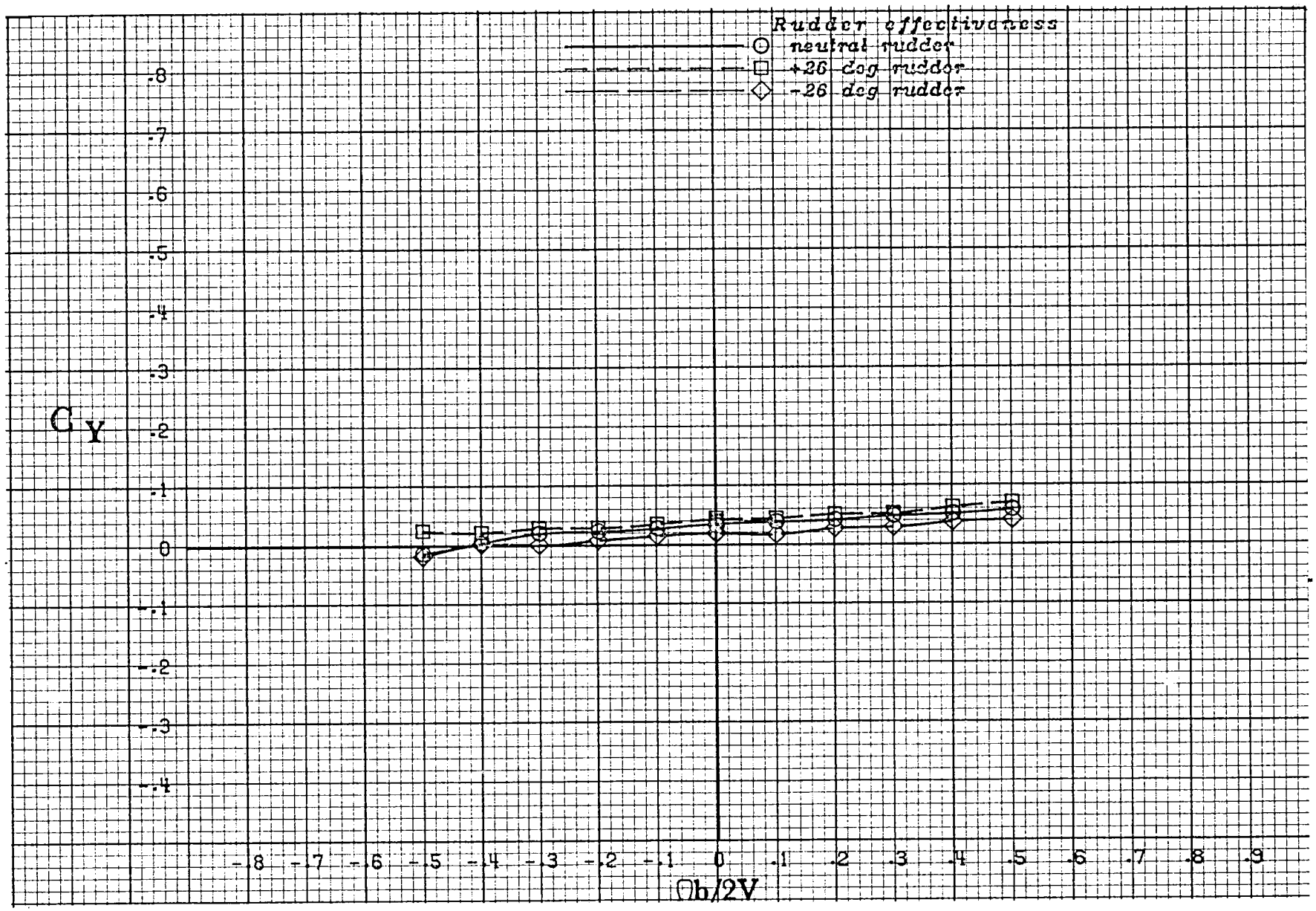

(b) α = 25 deg.

Figure A 11 .- Continued.

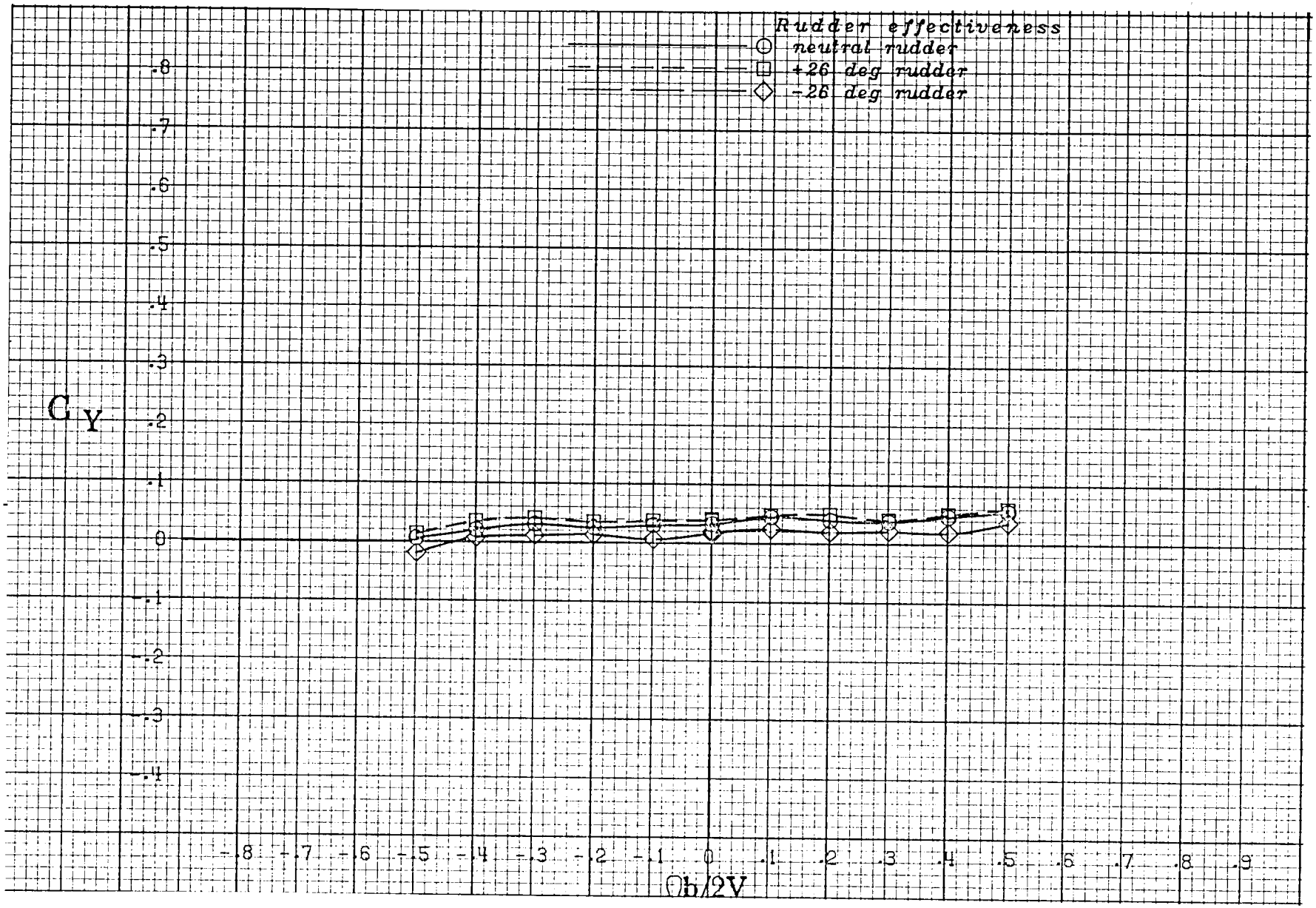

(c) α = 30 deg.

Figure A 11 .- Continued.

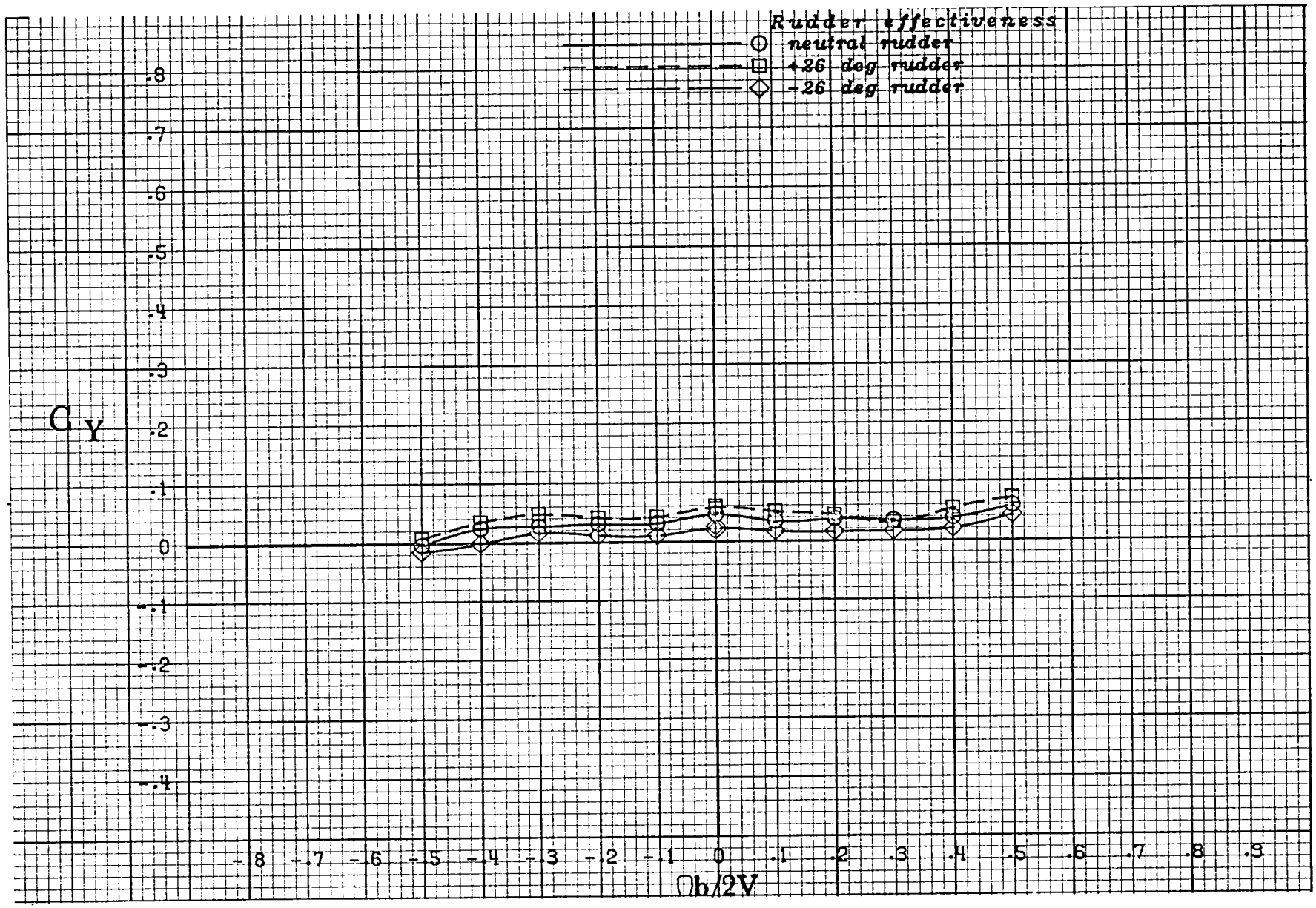

(d) α = 35 deg.

Figure A 11 .- Continued.

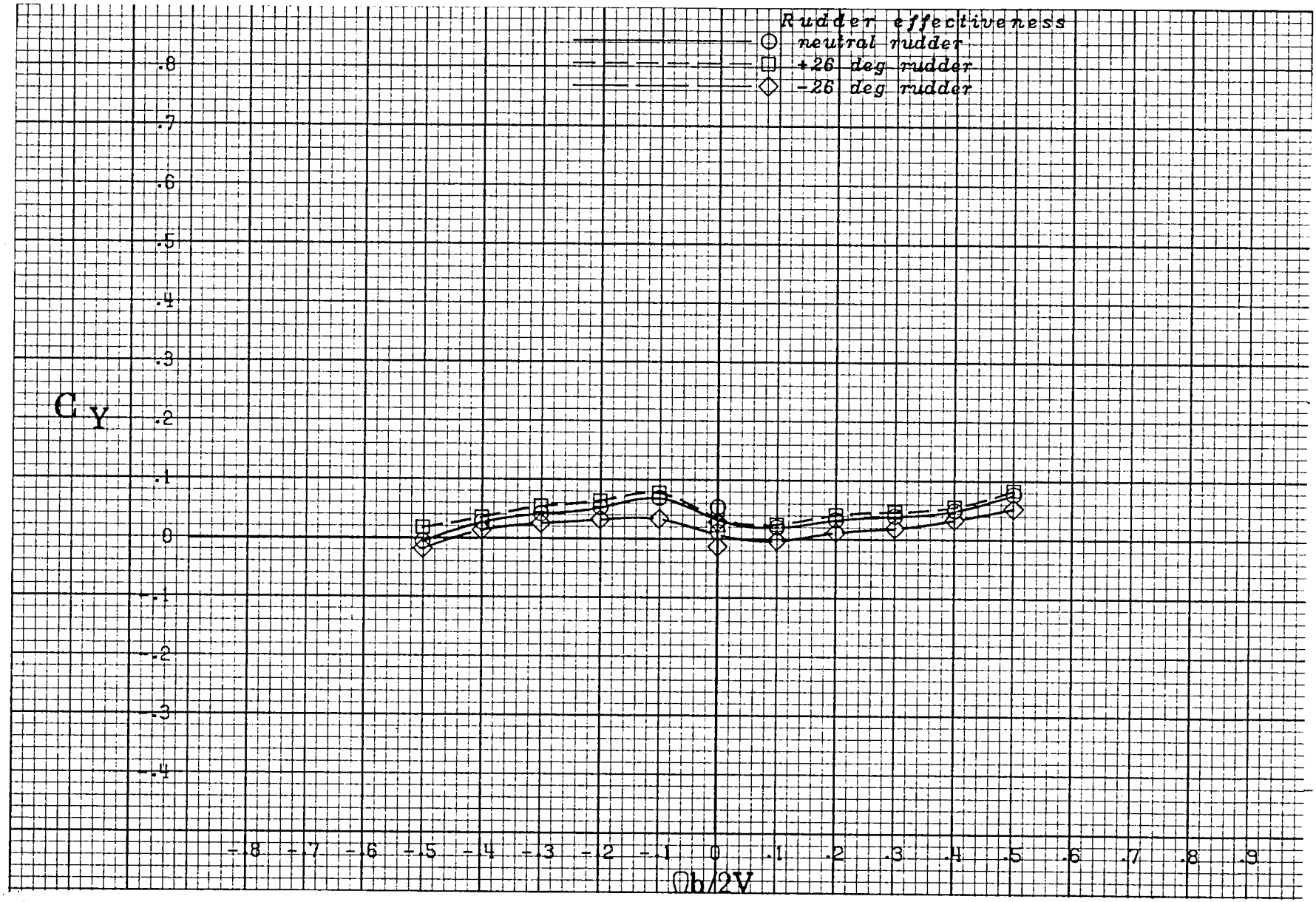

(e) α = 40 deg.

Figure A 11 .- Continued.

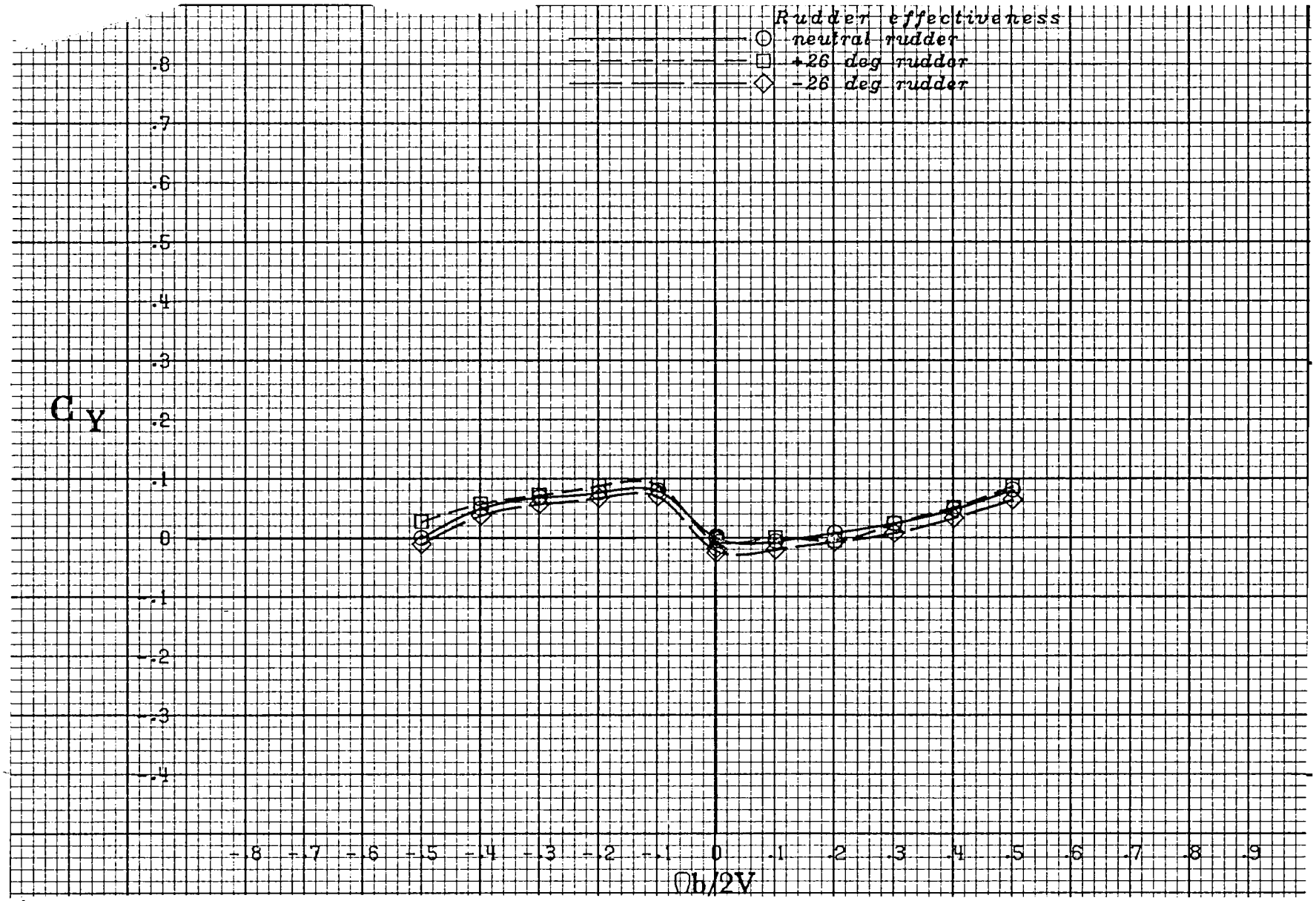

(f) α = 50 deg.

Figure A 11 .- Continued.

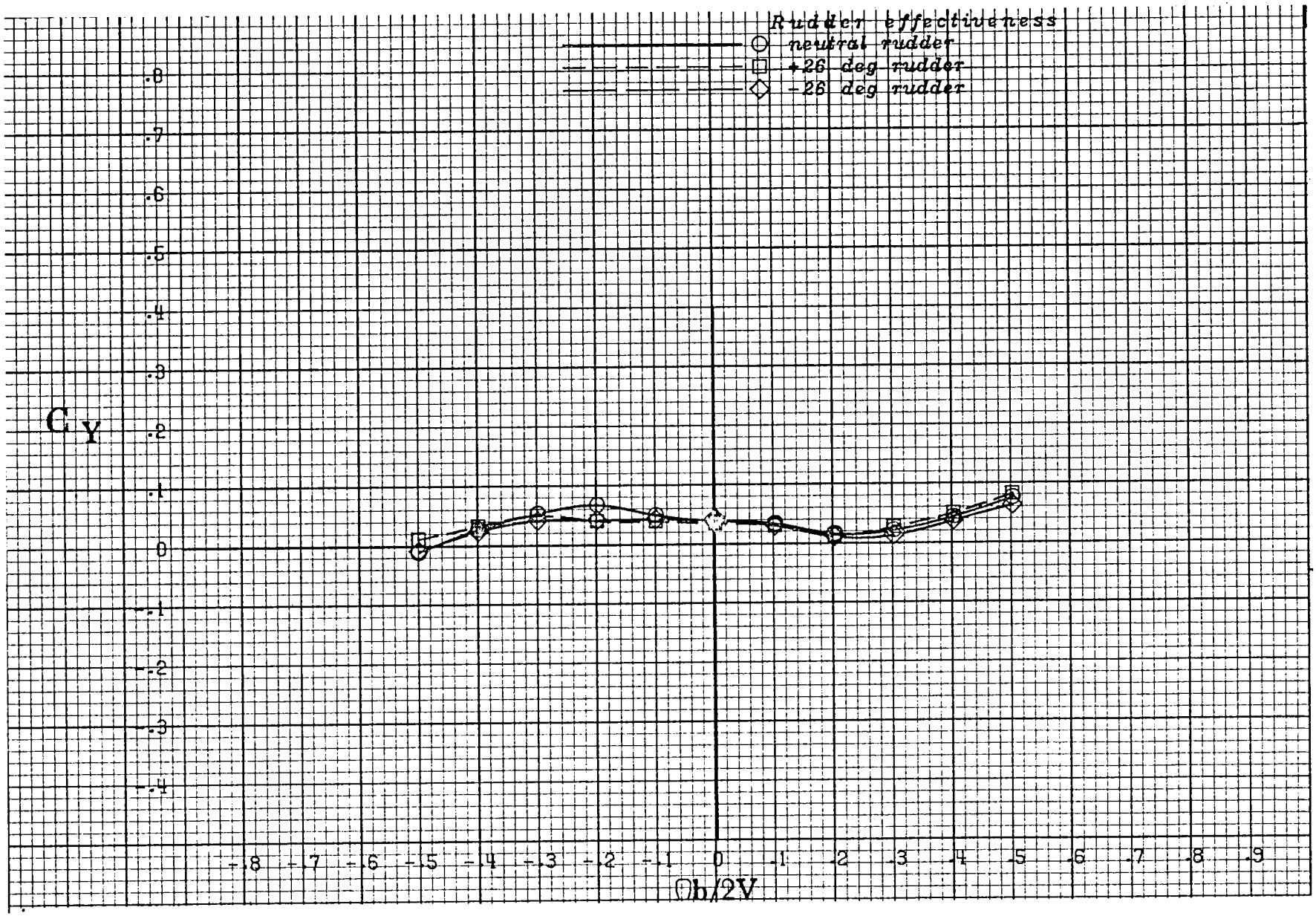

(g) α = 60 deg.

Figure A 11 .- Continued.

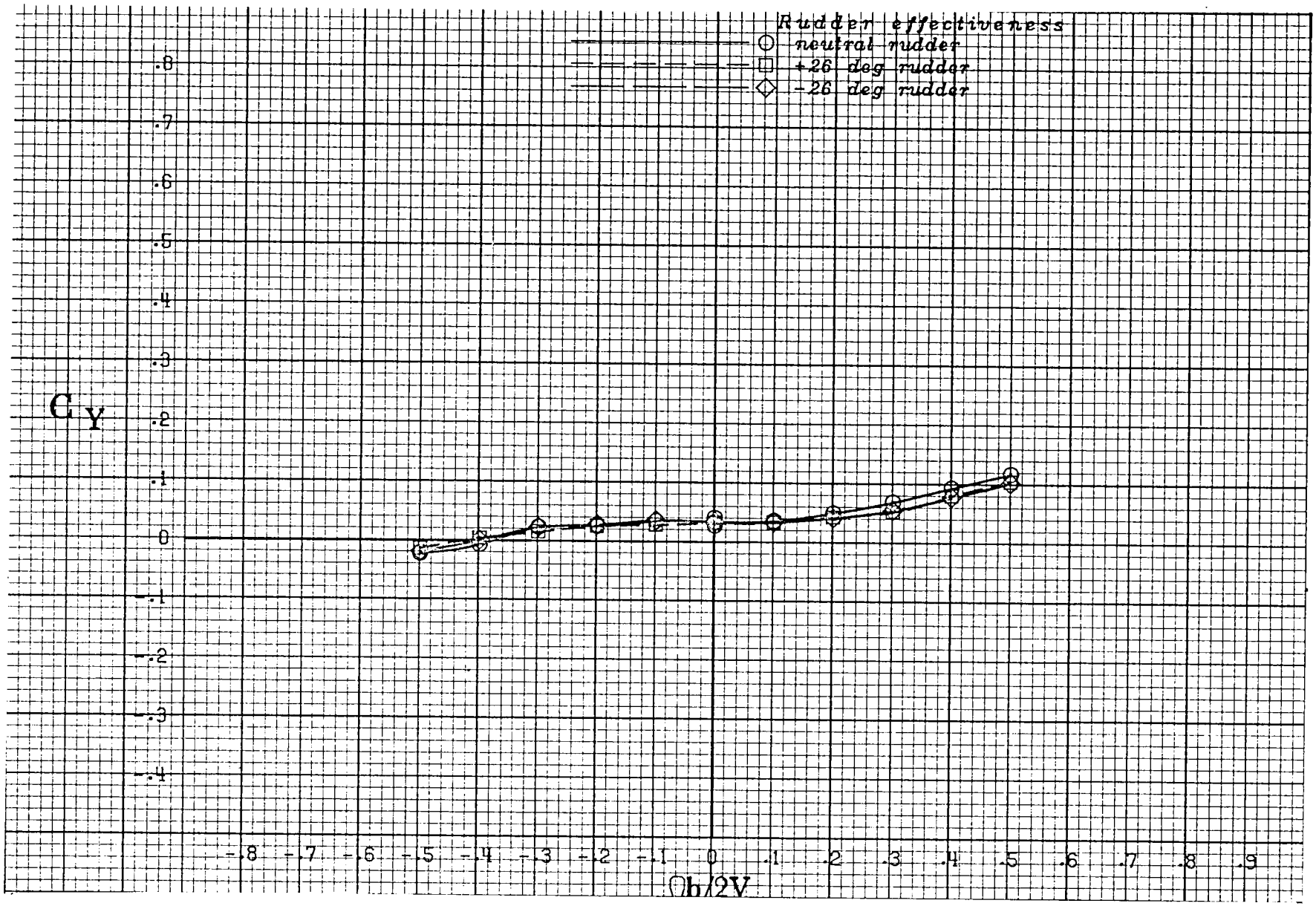

(h) α = 70 deg.

Figure A 11 .- Continued.

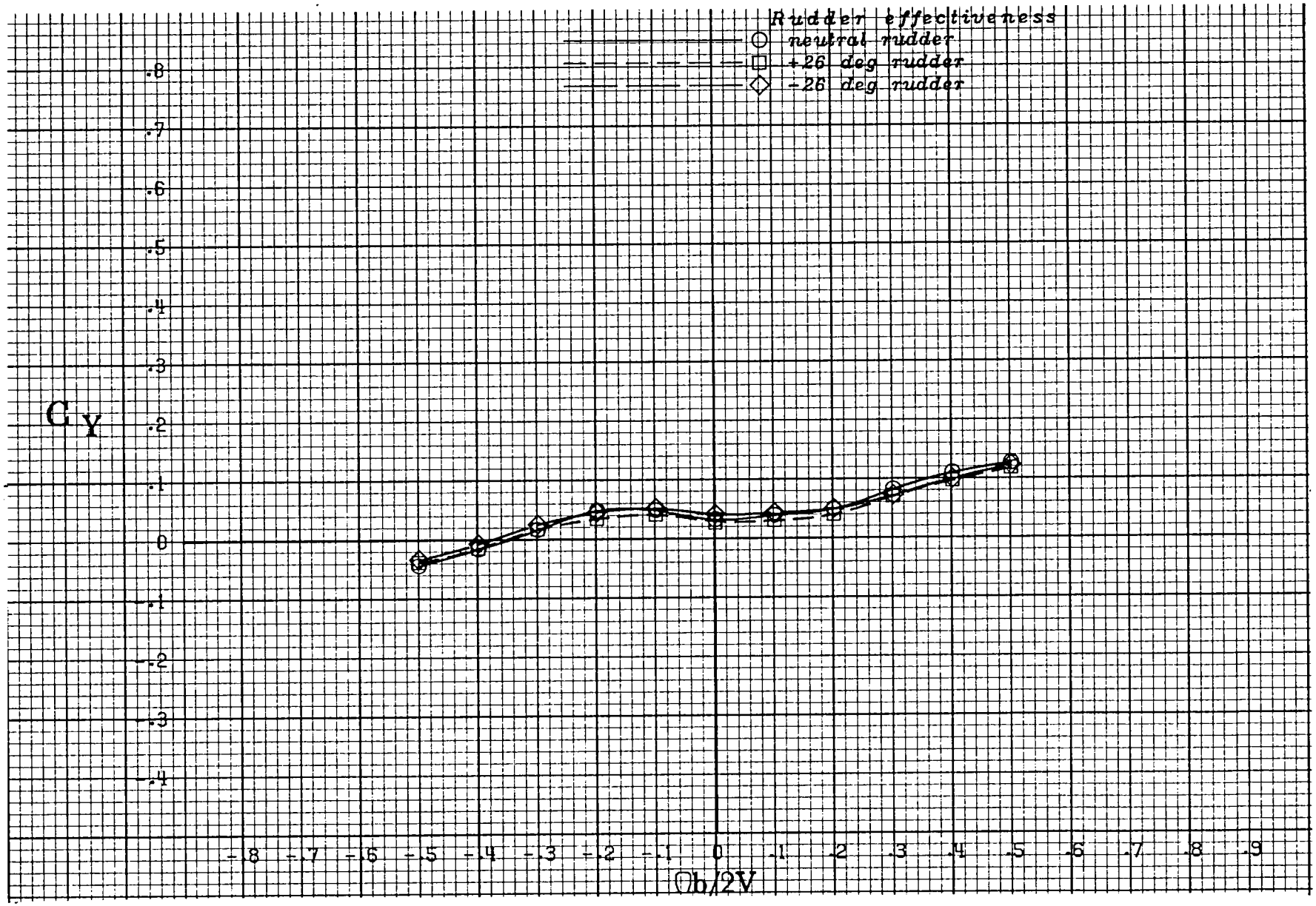

(i) α = 80 deg.

Figure A 11 .- Continued.

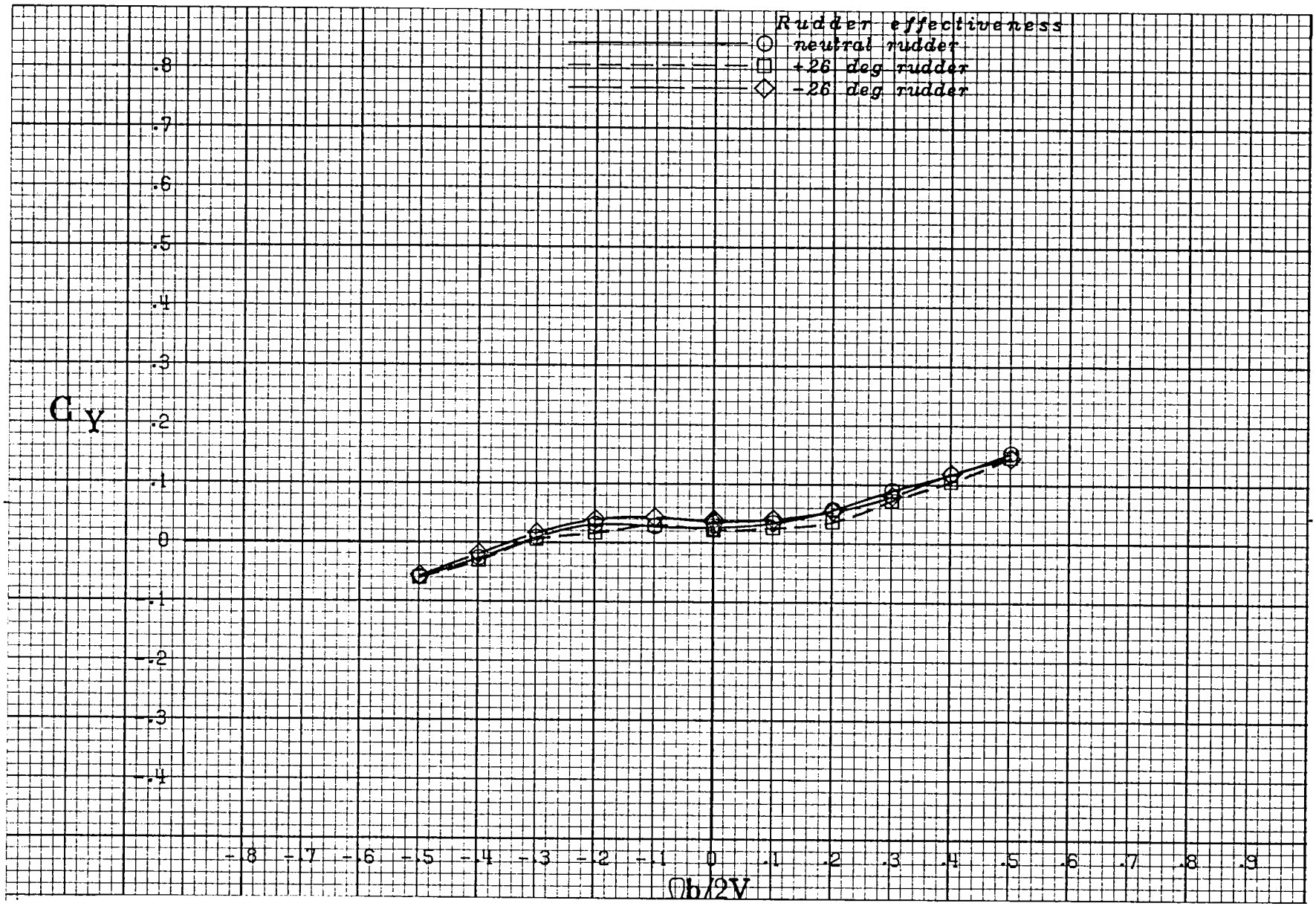

(j) α = 90 deg.

Figure A 11 .- Concluded.

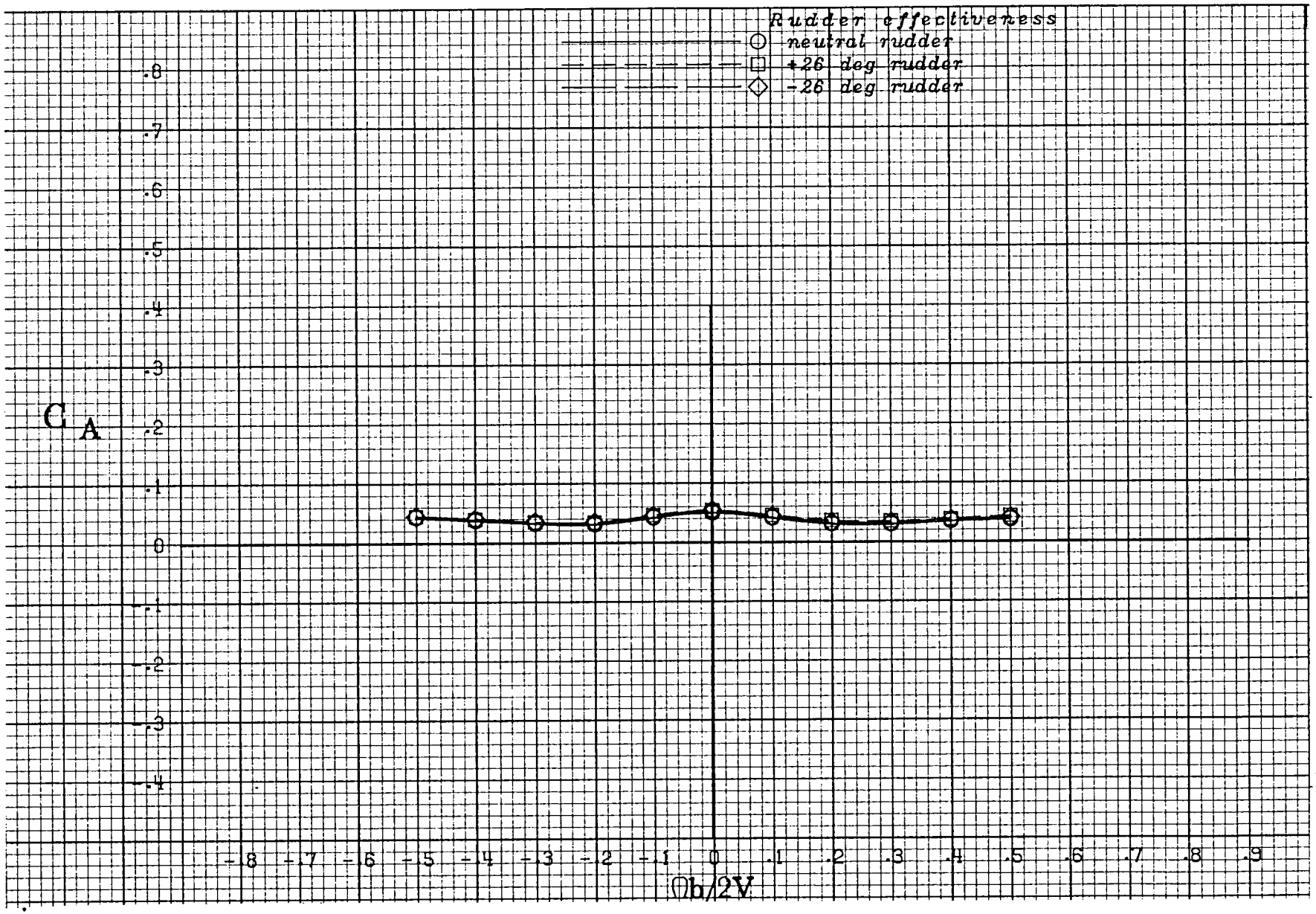

(a) α = 20 deg.

Figure A 12 .- Effect of rotation rate and rudder deflection on axial-force coefficient for the basic configuration with neutral elevator and ailerons at zero sideslip angle.

(b) α = 25 deg.

Figure A 12 .- Continued.

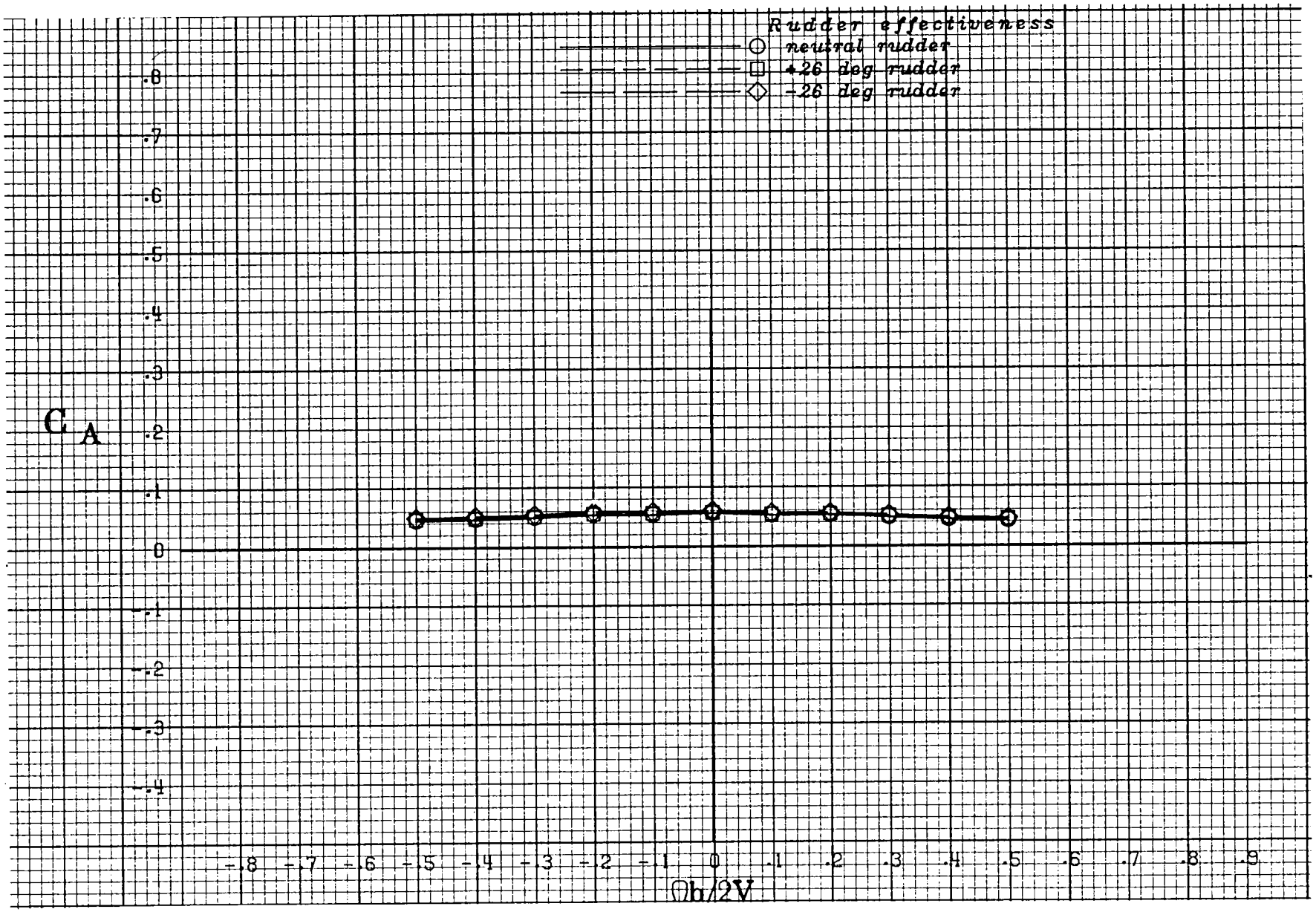

(c) α = 30 deg.

Figure A 12 .- Continued.

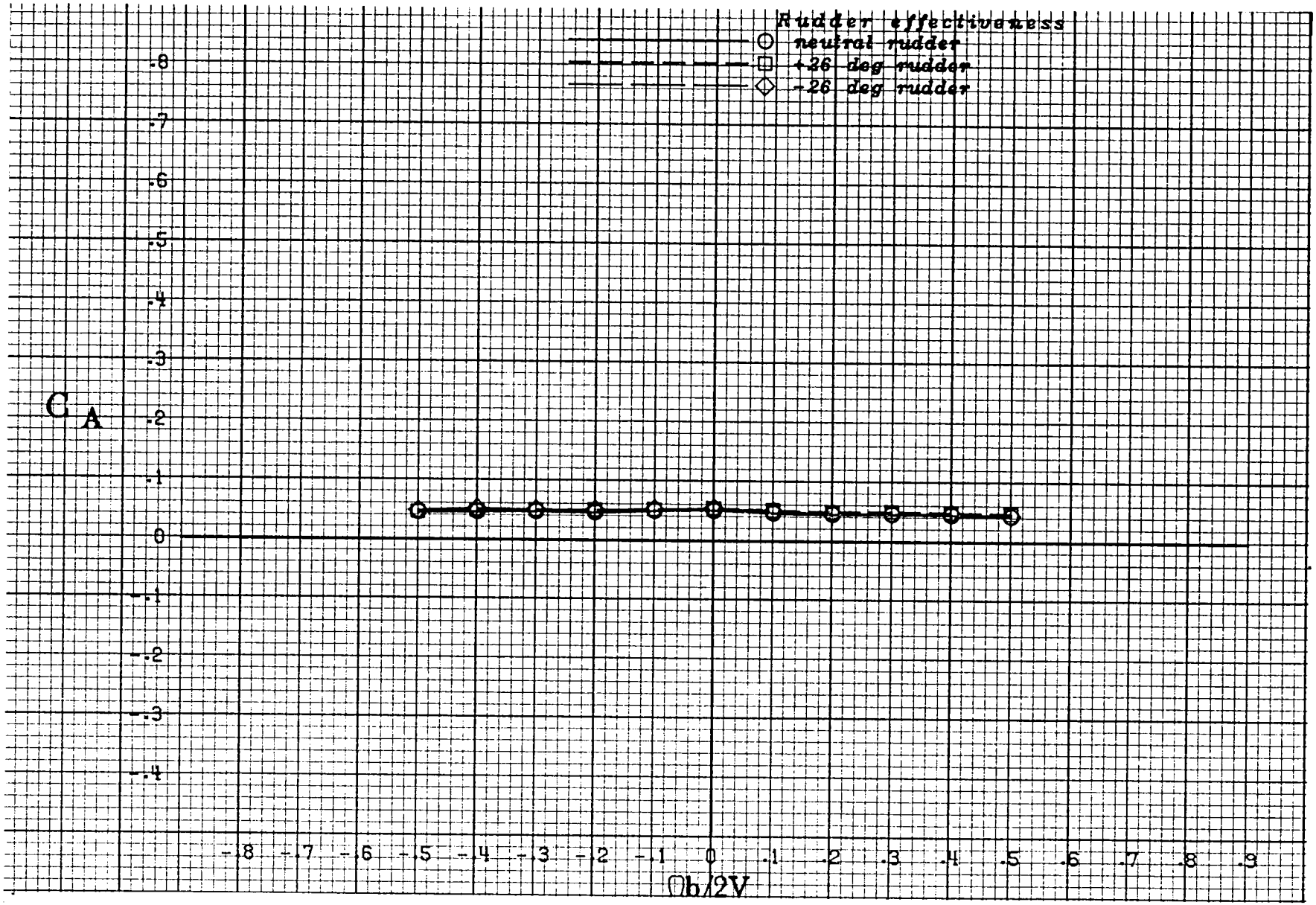

(d) α = 35 deg.

Figure A 12 .- Continued.

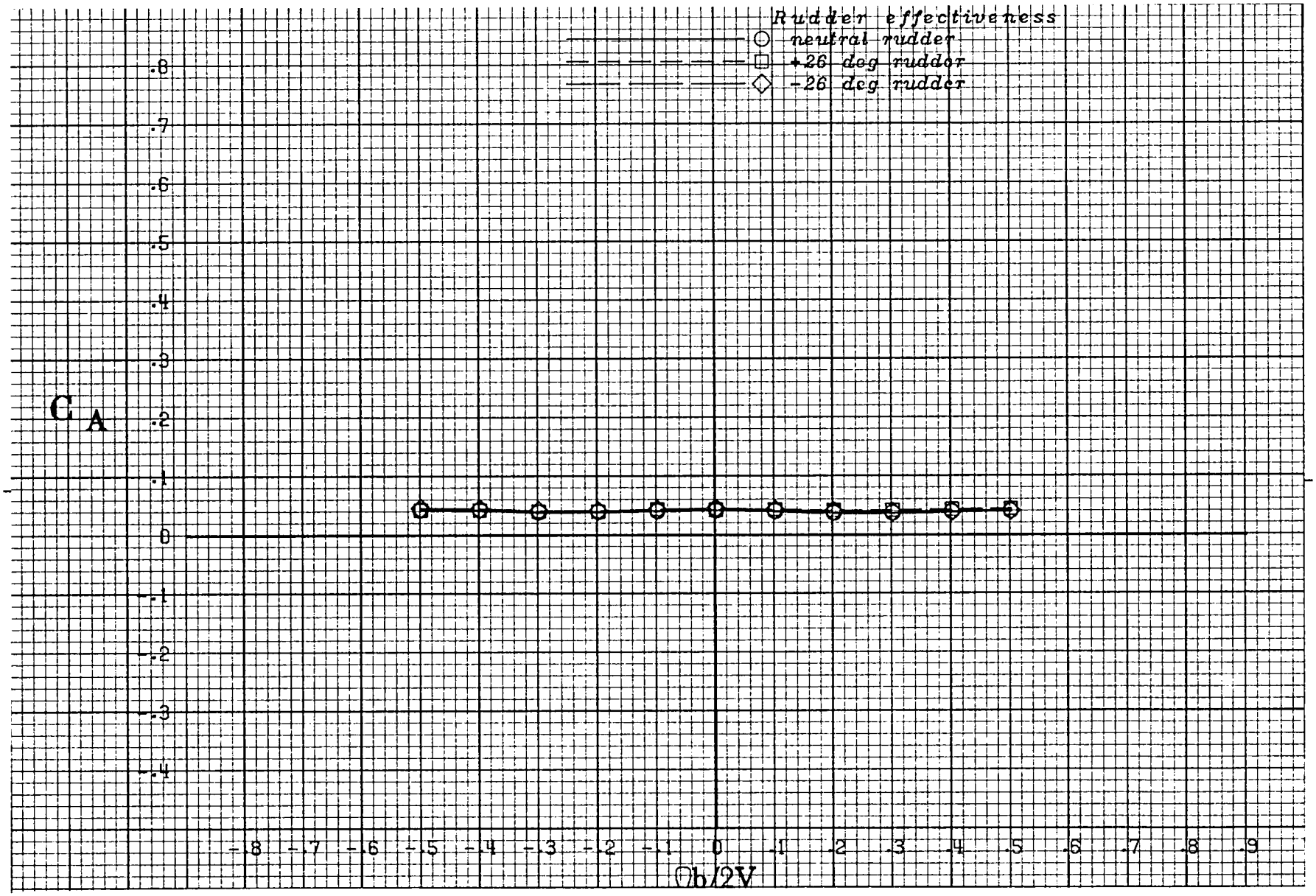

(e) α = 40 deg.

Figure A 12 .- Continued.

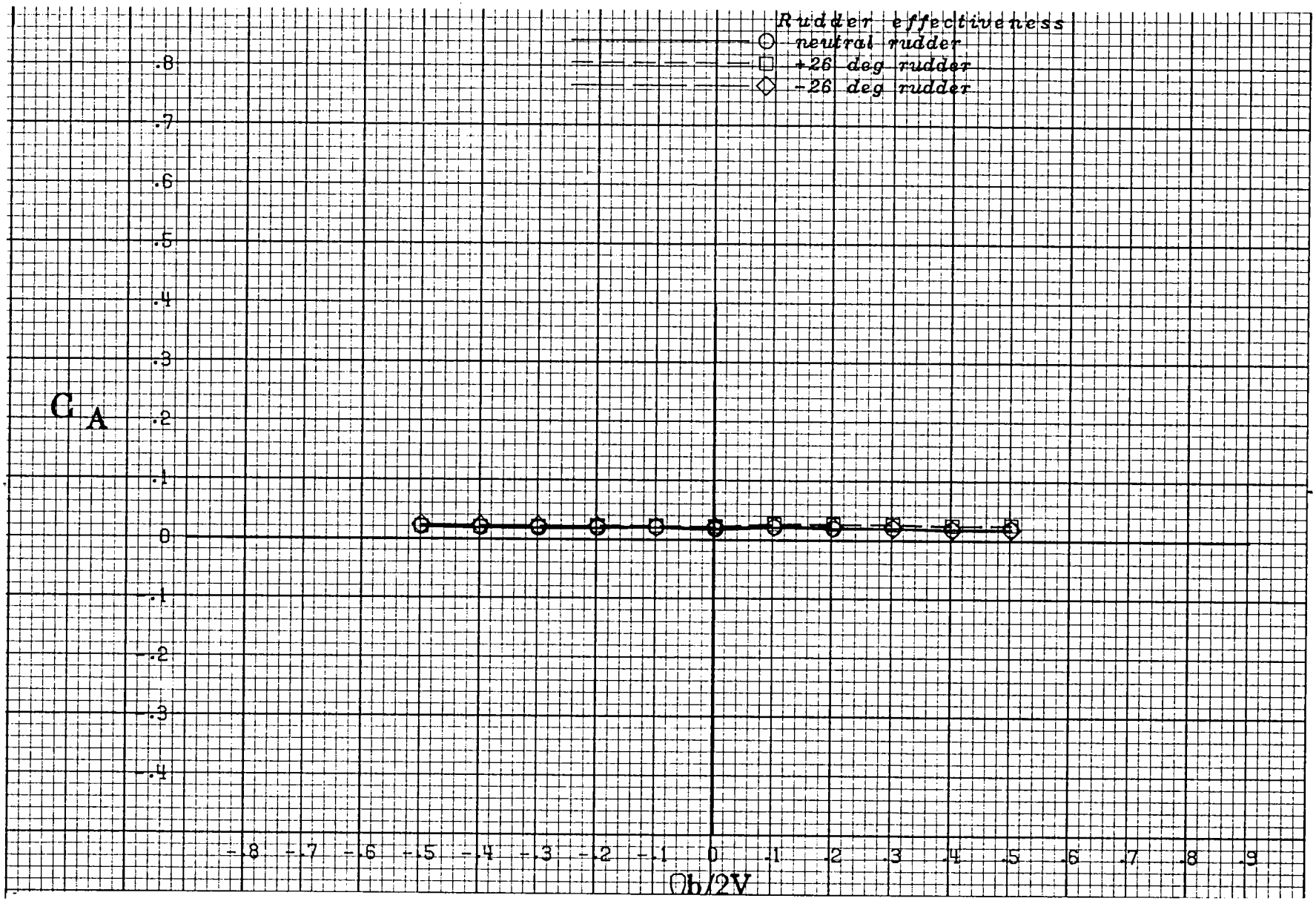

(f) α = 50 deg.

Figure A 12 .- Continued.

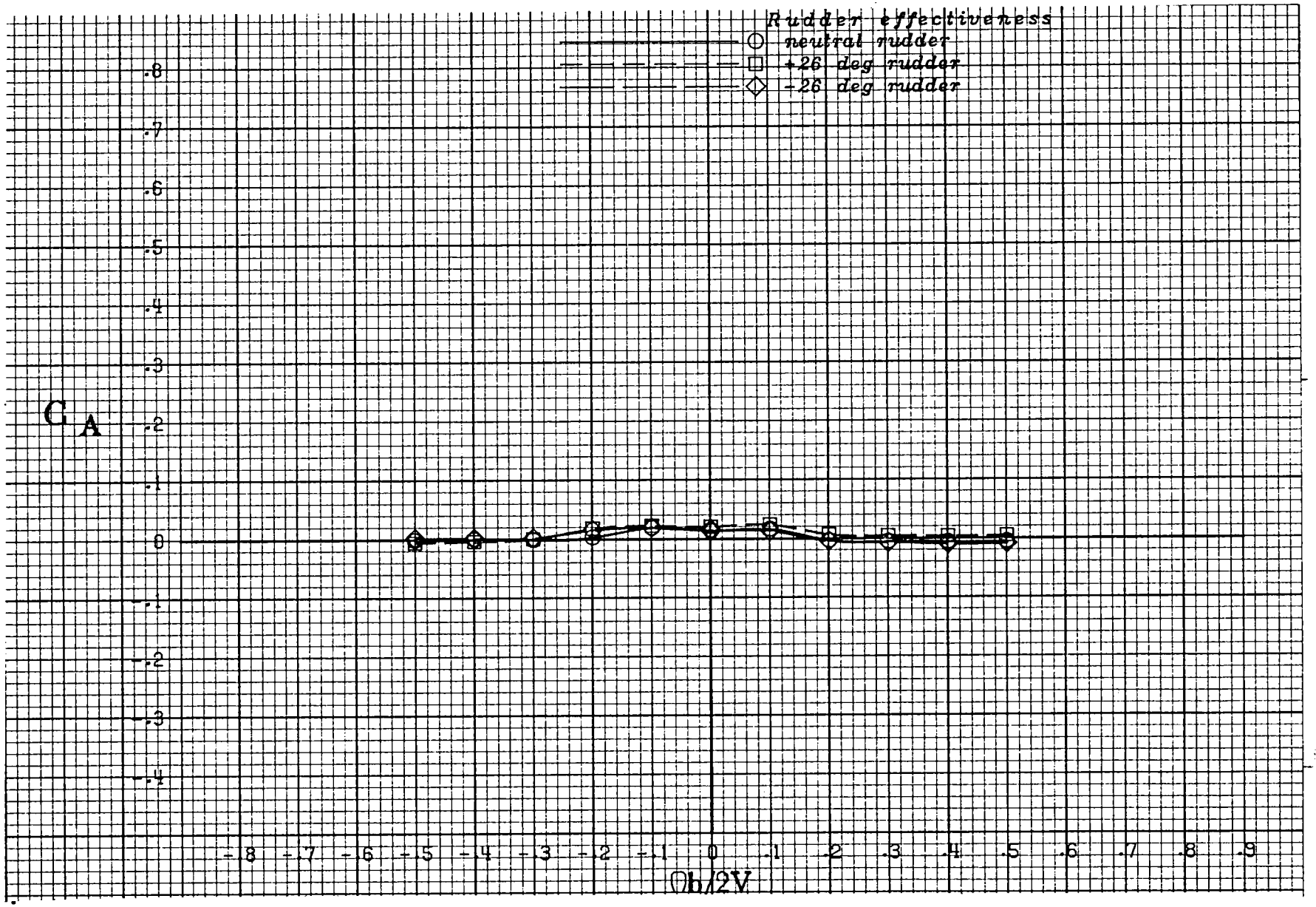

(g) α = 60 deg.

Figure A 12 .- Continued.

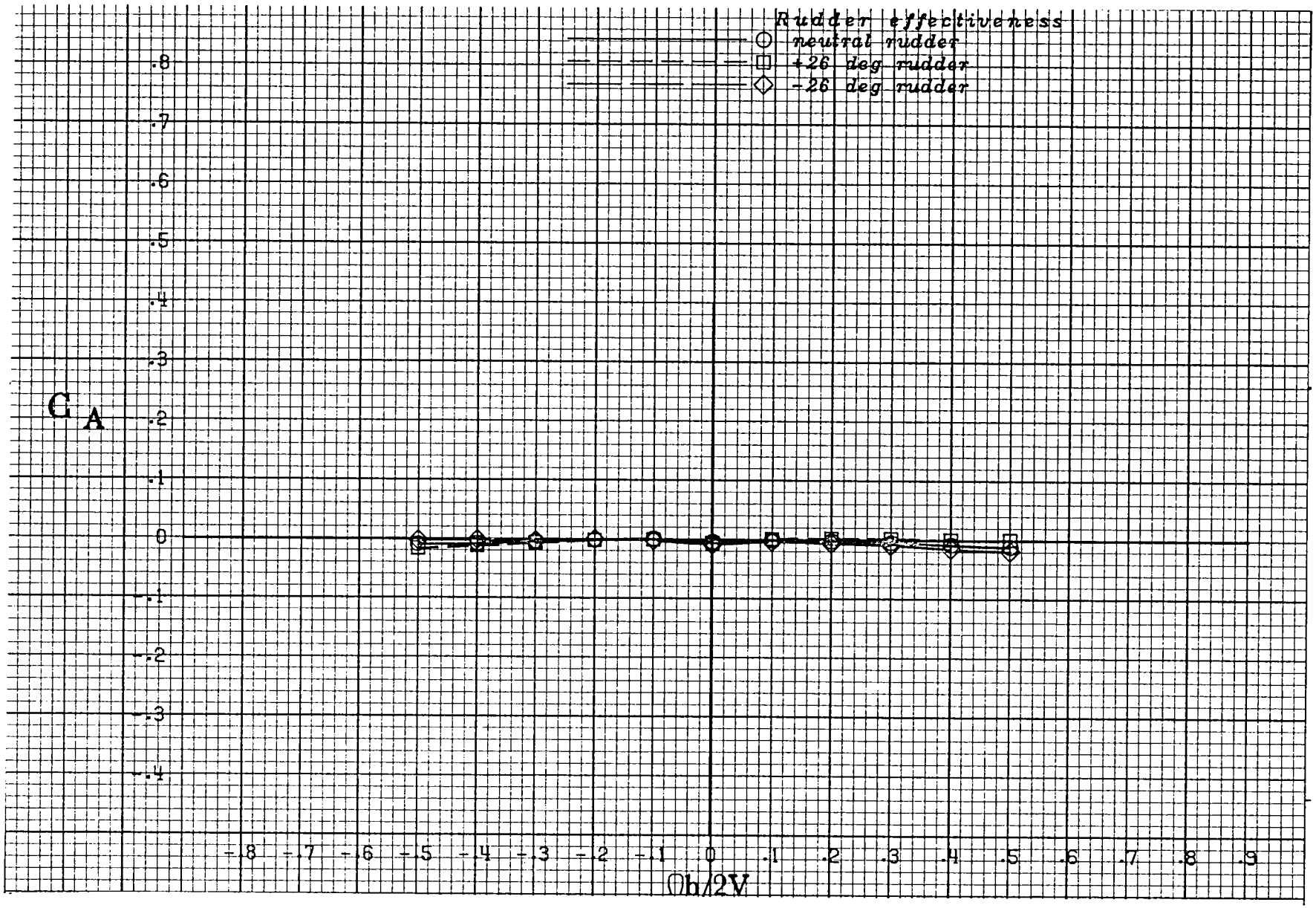

(h) α = 70 deg.

Figure A 12 .- Continued.

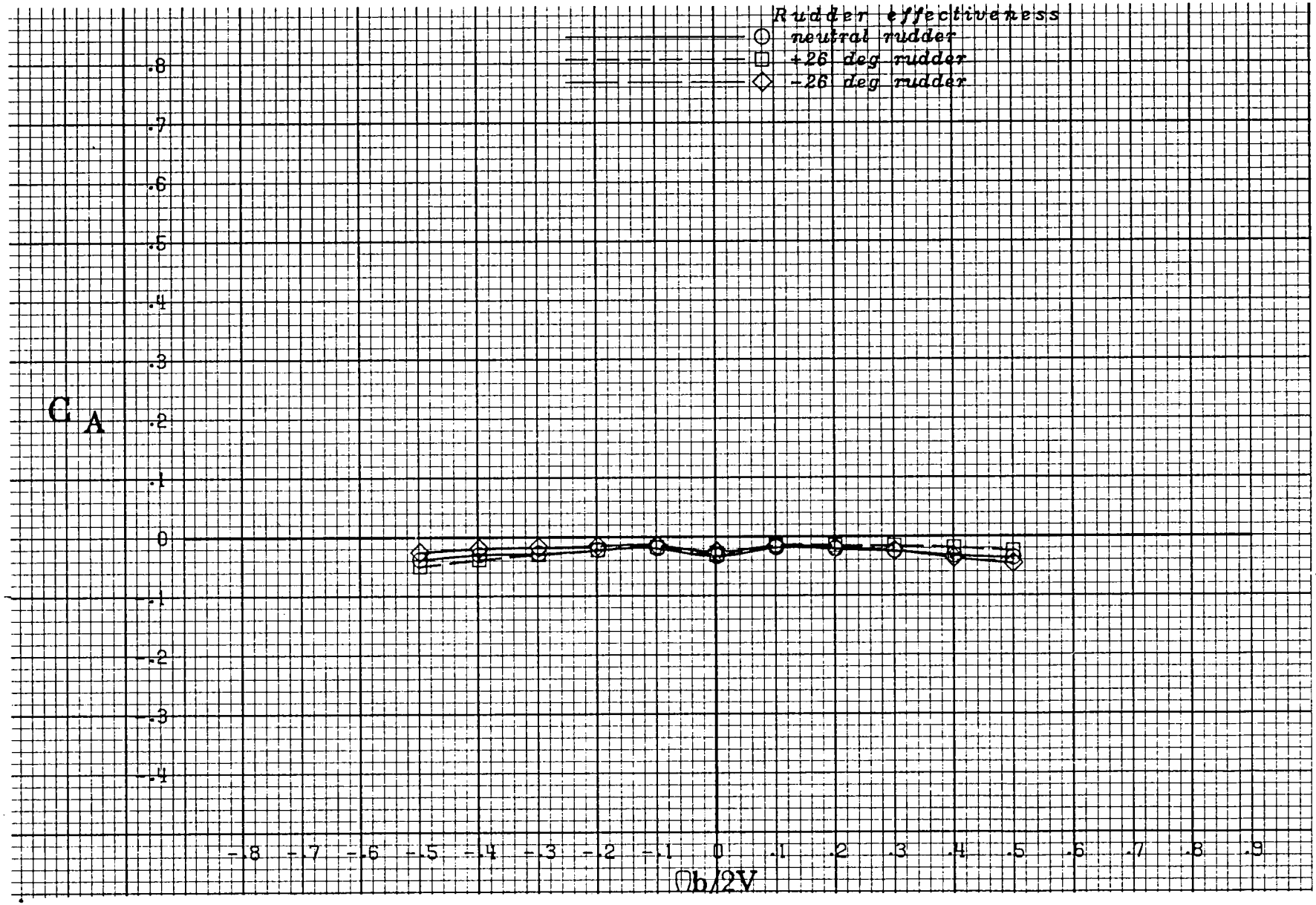

(i) α = 80 deg.

Figure A 12 .- Continued.

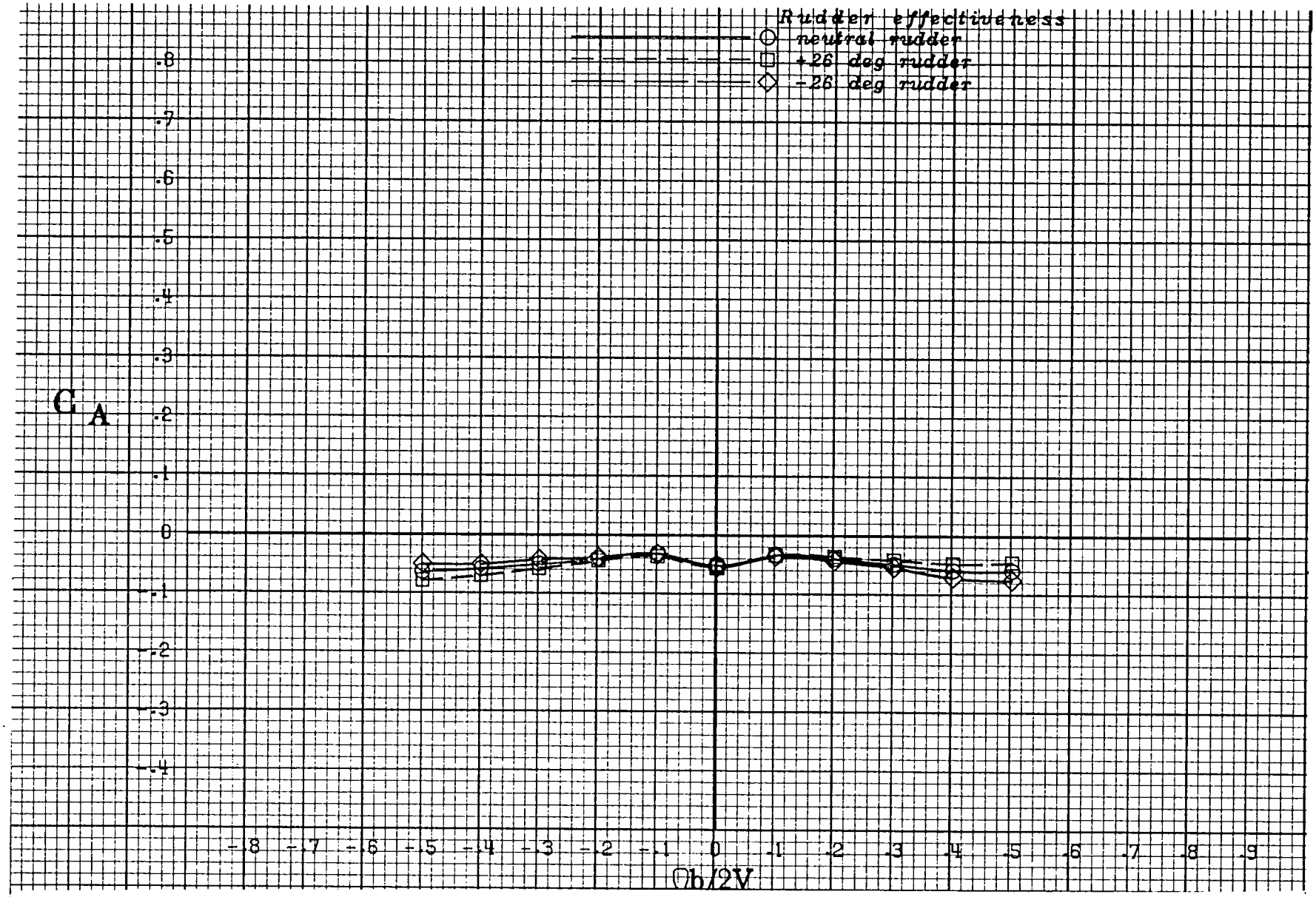

(j) α = 90 deg.

Figure A 12 .- Concluded.

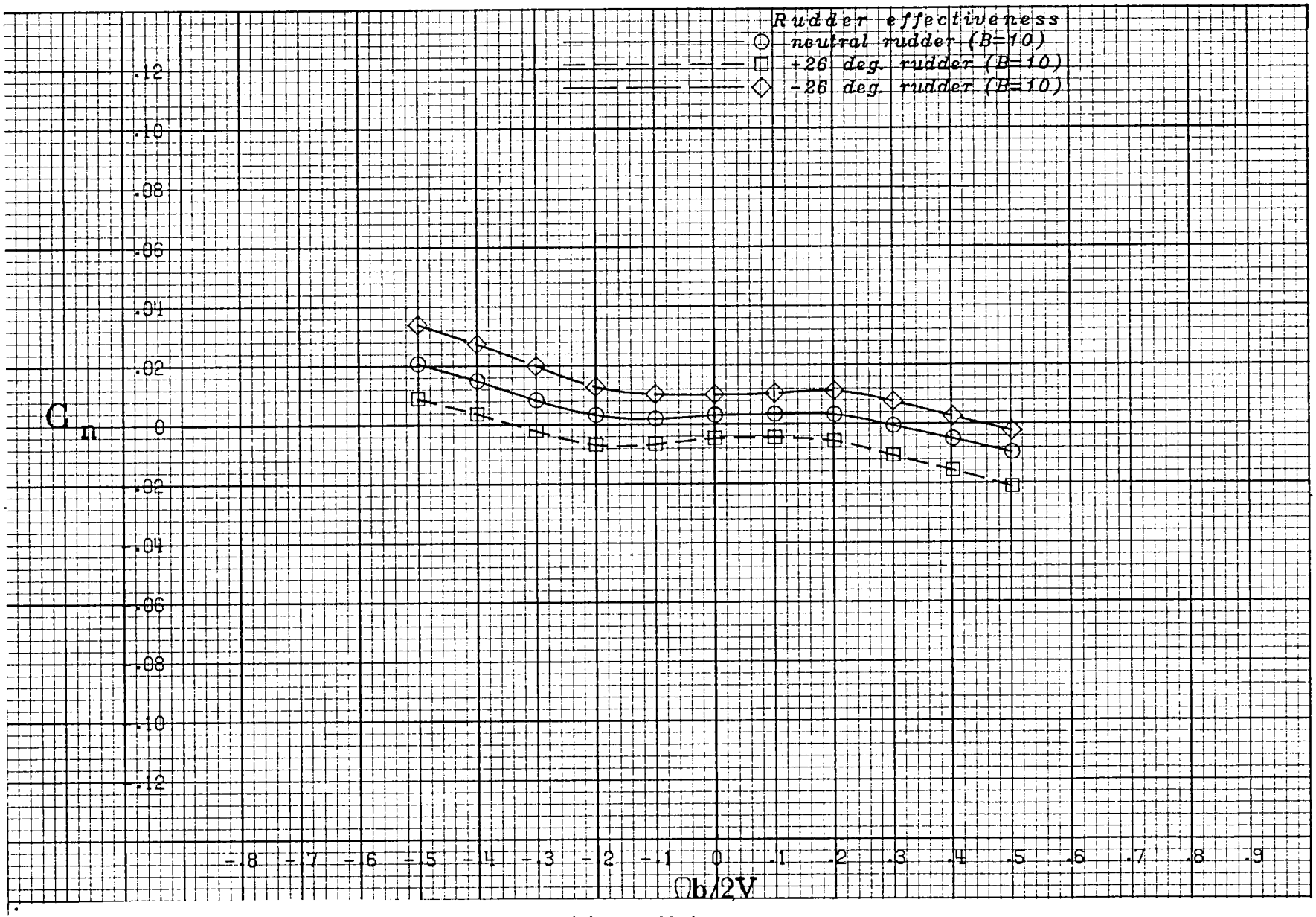

(a) α = 20 deg.

Figure A 13 .- Effect of rotation rate and rudder deflection on yawing-moment coefficient for the basic configuration with neutral elevator and ailerons at +10 deg sideslip angle.

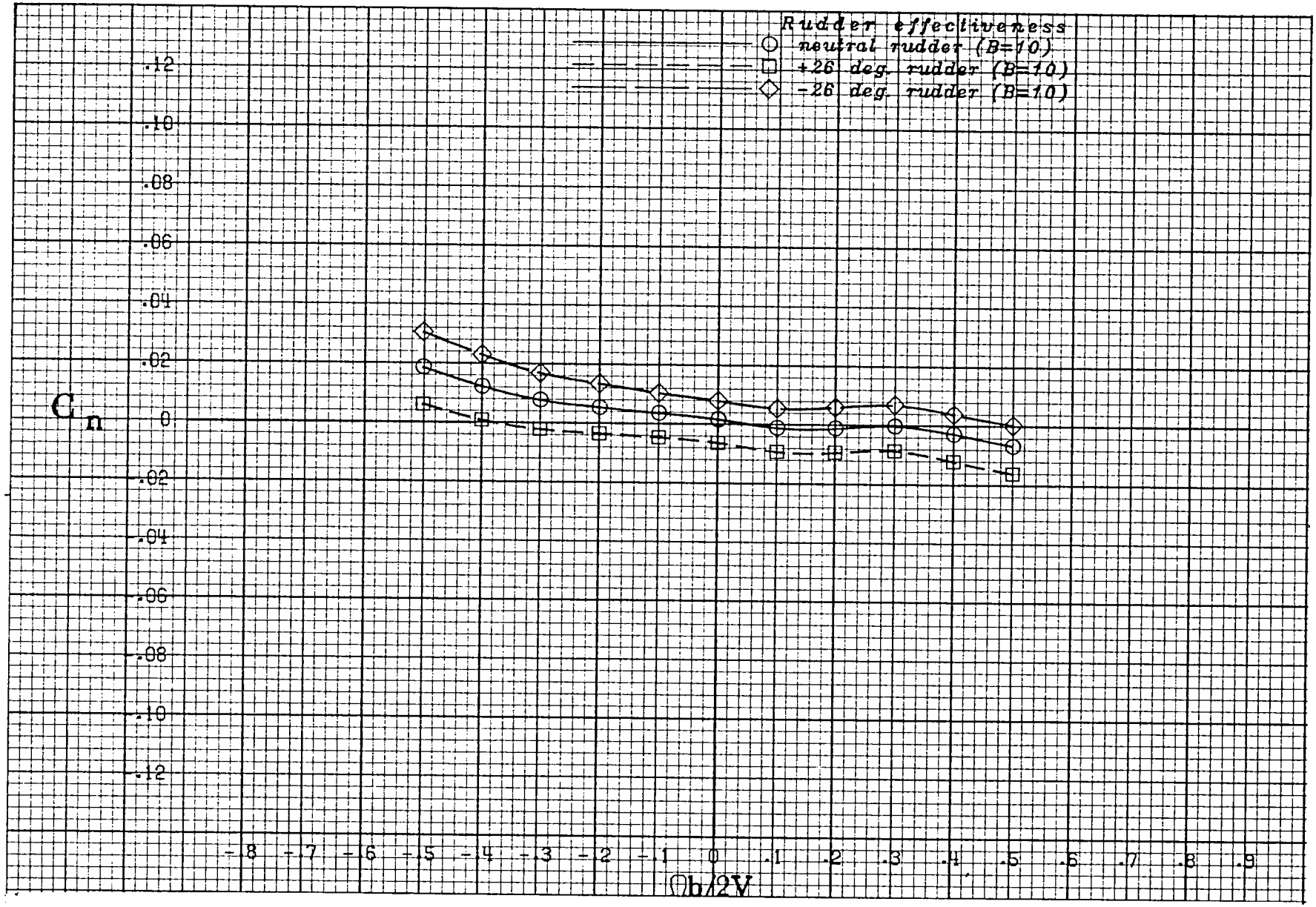

(b) α = 25 deg.

Figure A 13 .- Continued.

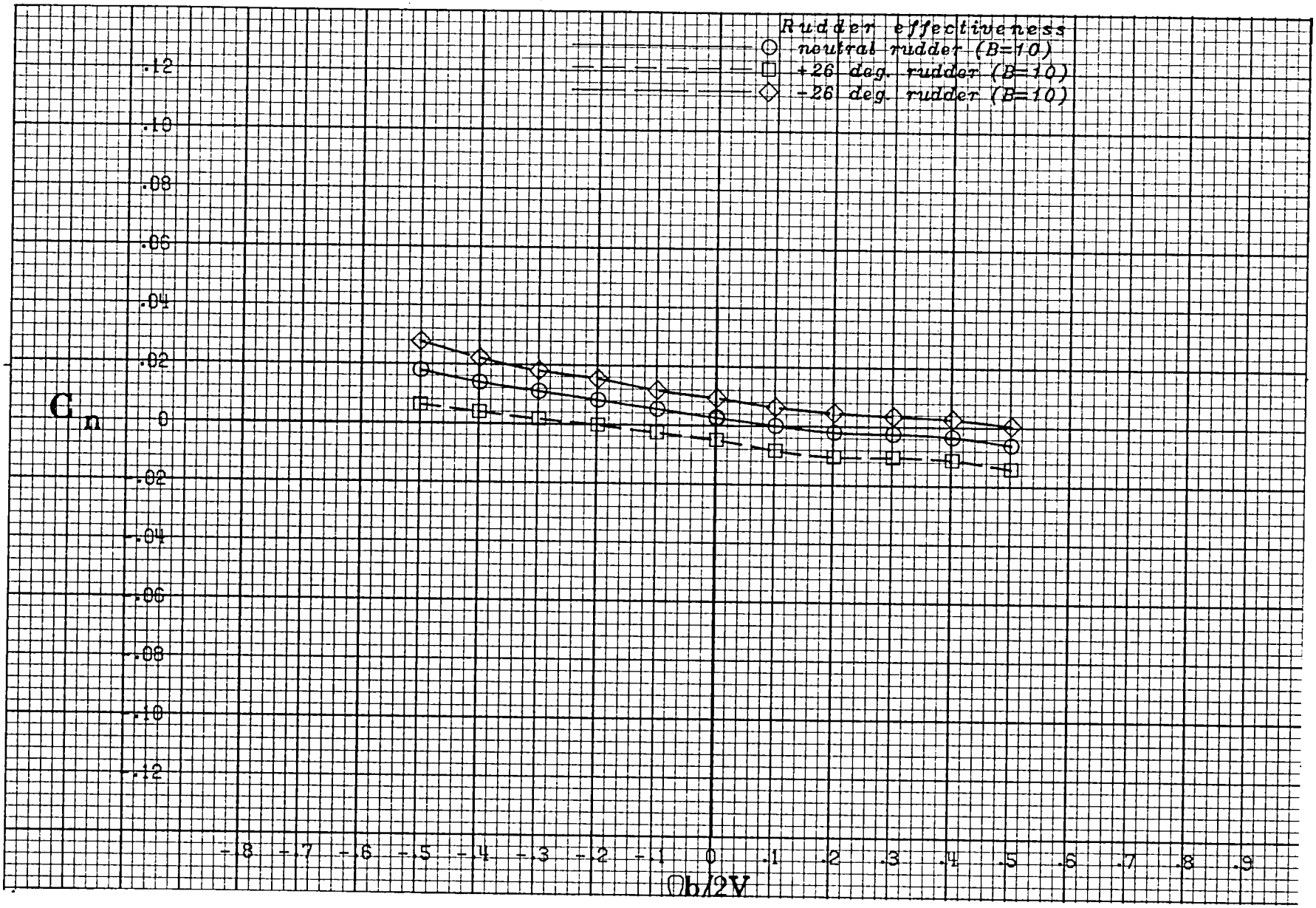

(c) α = 30 deg.

Figure A 13 .- Continued.

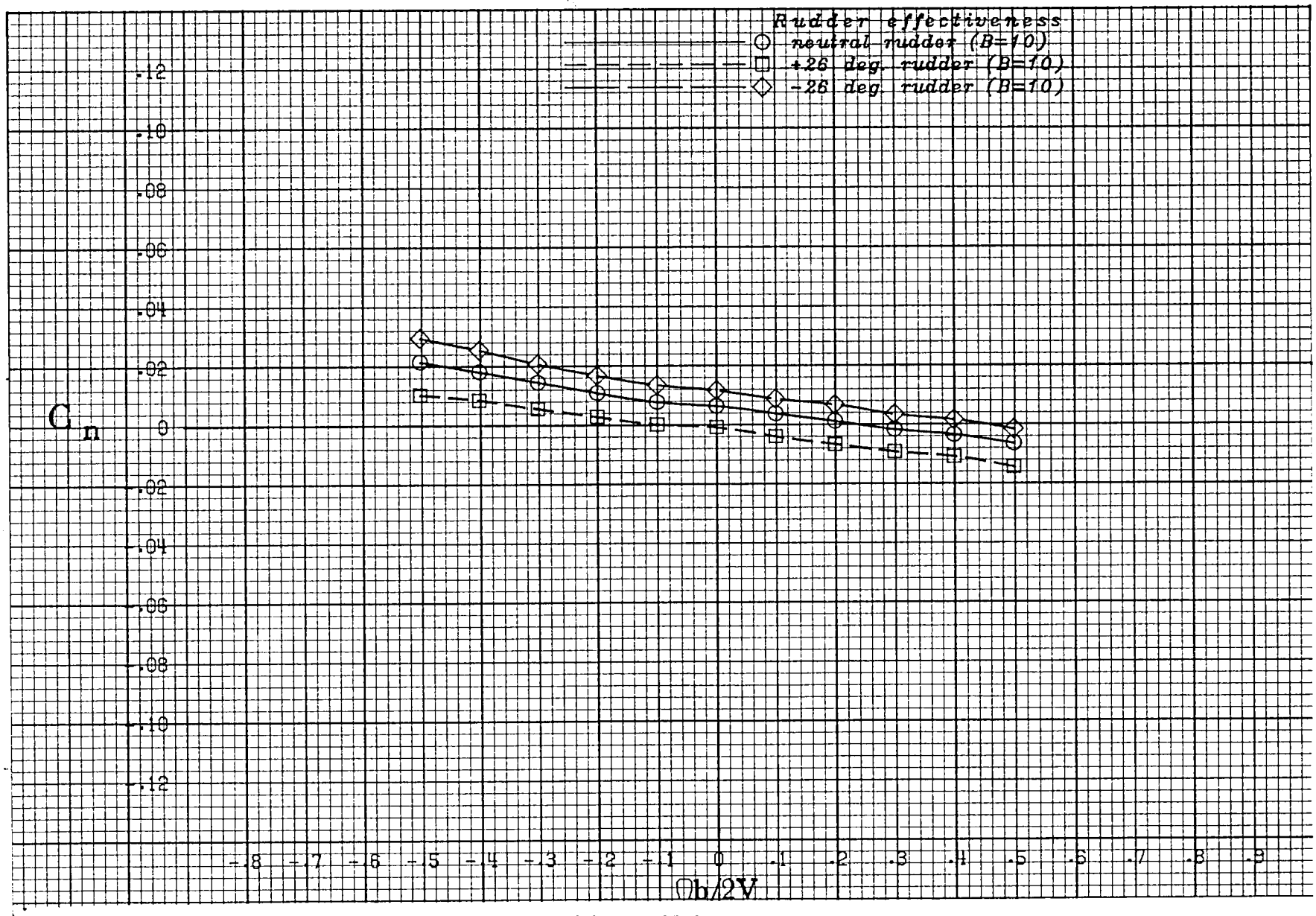

(d) α = 35 deg.

Figure A 13 .- Continued.

(e) α = 40 deg.

Figure A 13 .- Continued.

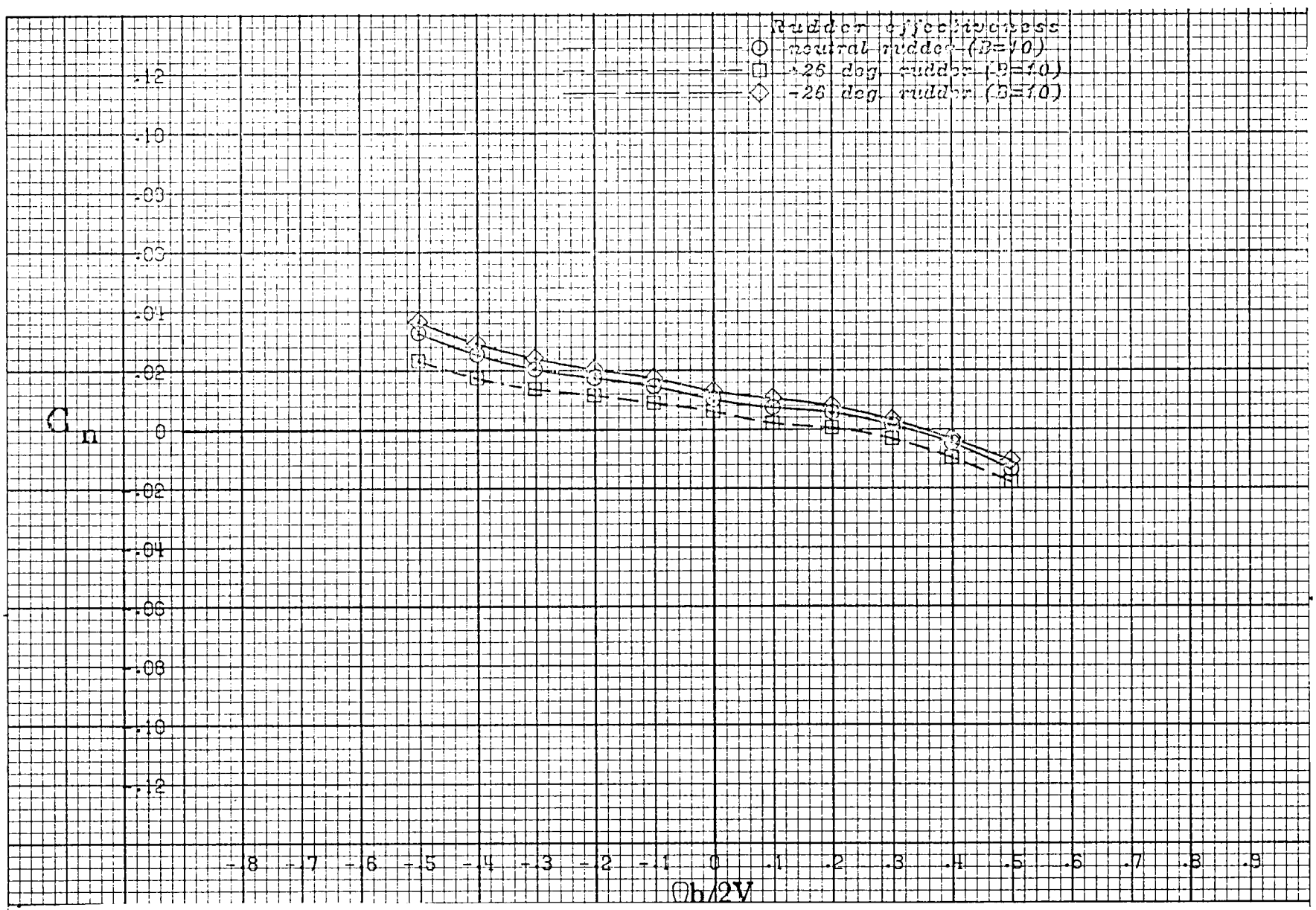

(f) α = 50 deg.

Figure A 13 .- Continued.

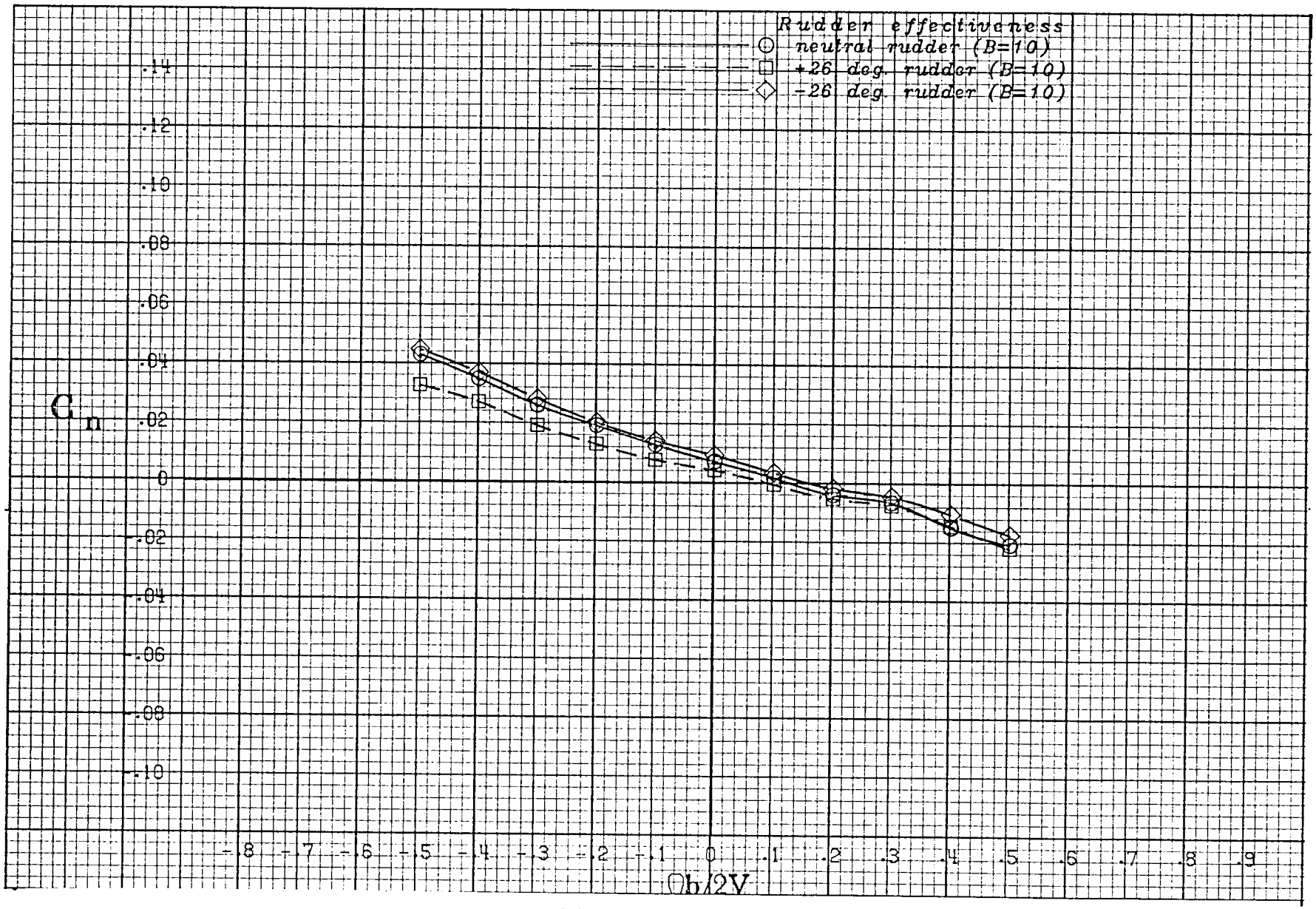

(g) α = 60 deg.

Figure A 13 .- Continued.

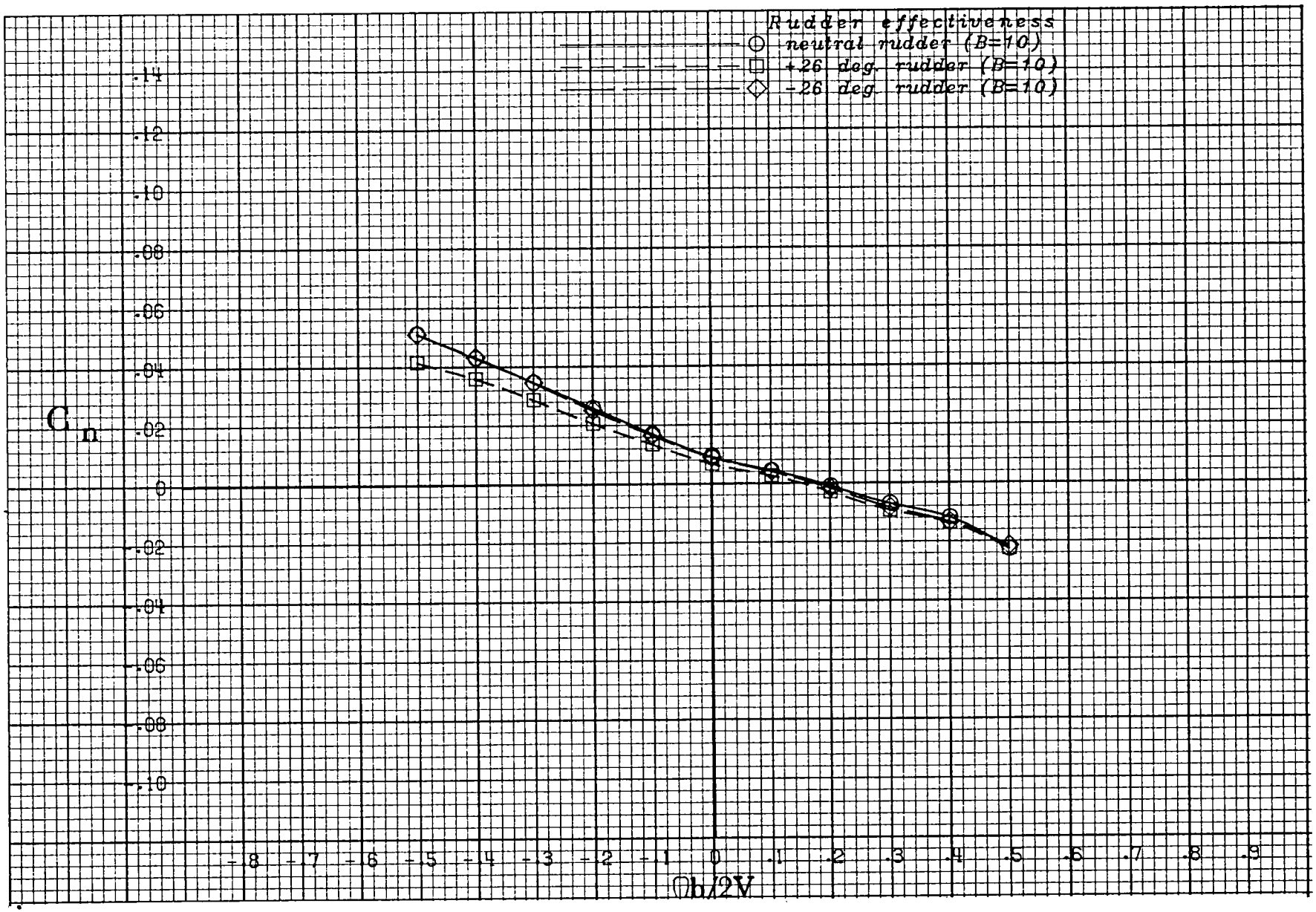

(h) α = 70 deg.

Figure A 13 .- Continued.

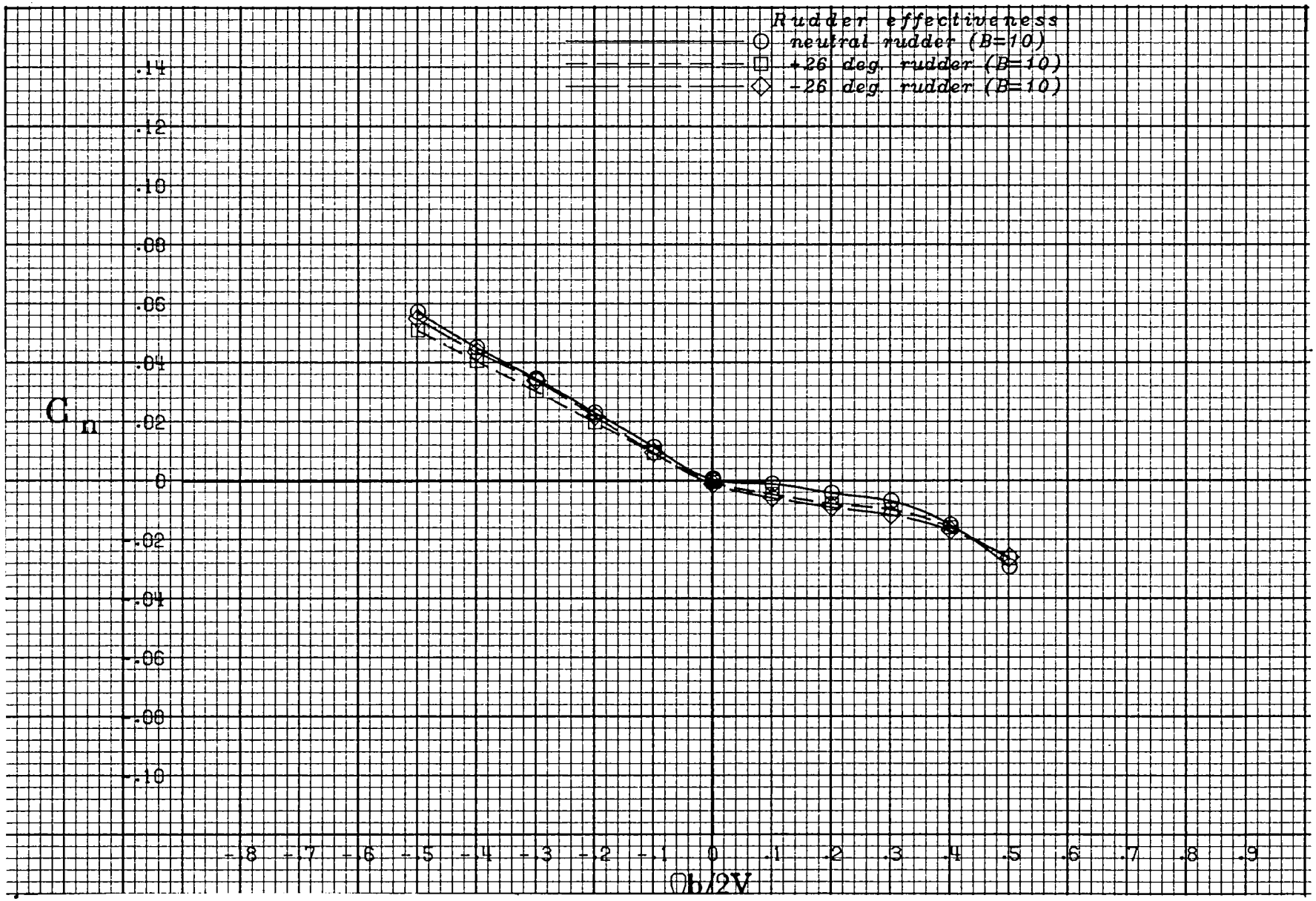

(i) α = 80 deg.

Figure A 13 .- Continued.

(j) α = 90 deg.

Figure A 13 .- Concluded.

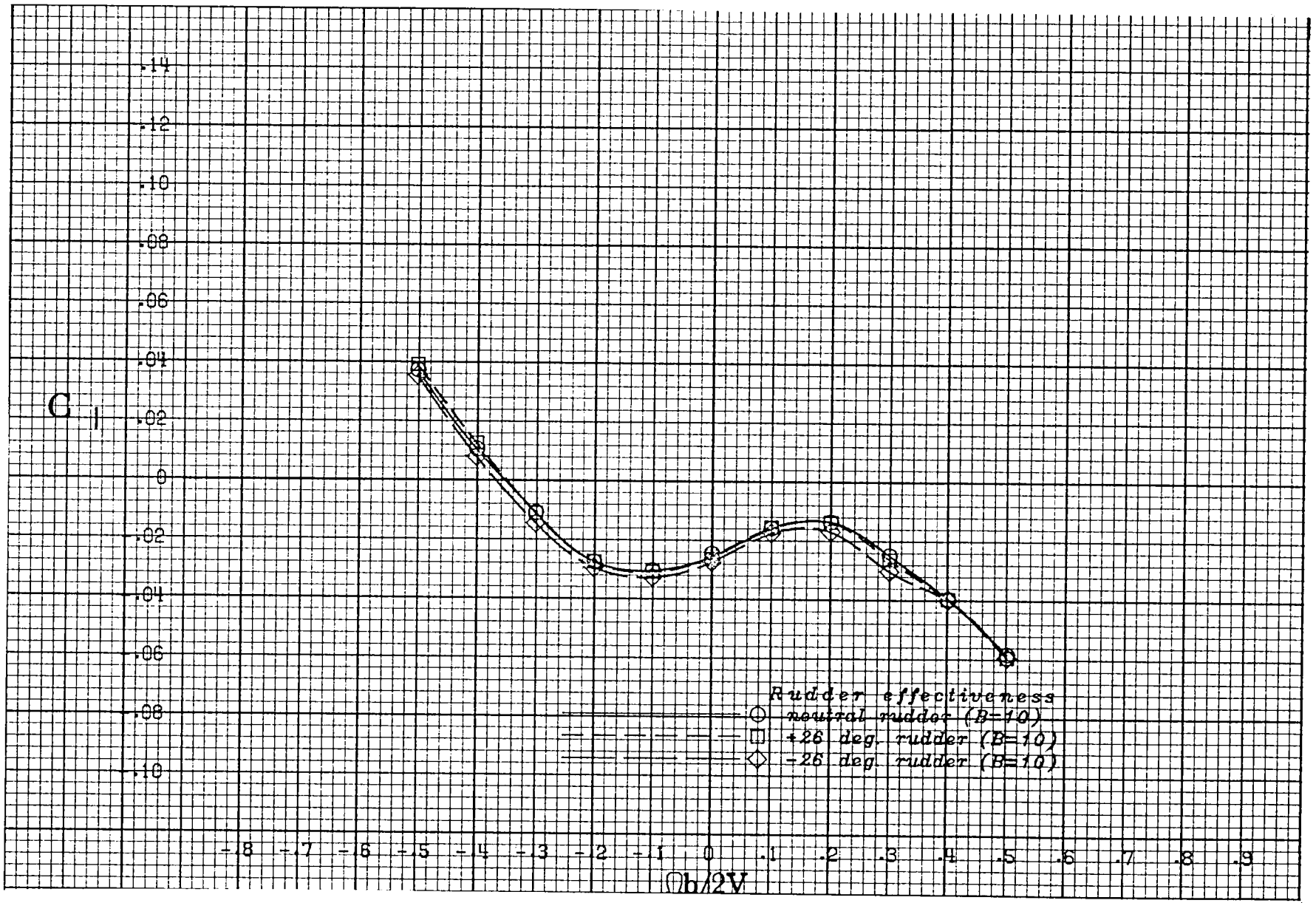

(a) α = 20 deg.

Figure A 14 .- Effect of rotation rate and rudder deflection on rolling-moment coefficient for the basic configuration with neutral elevator and ailerons at +10 deg sideslip angle.

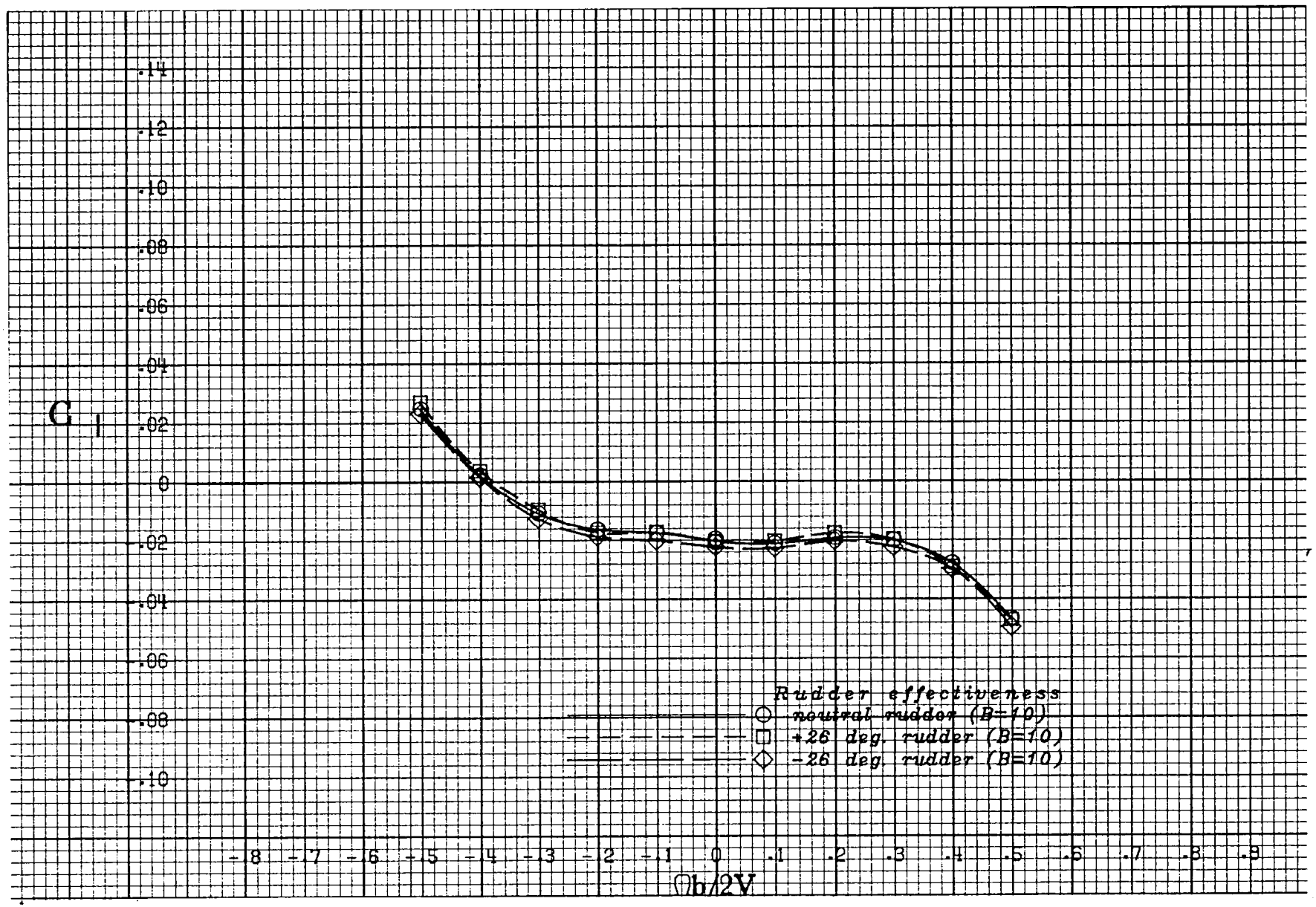

(b) α = 25 deg.

Figure A 14 .- Continued.

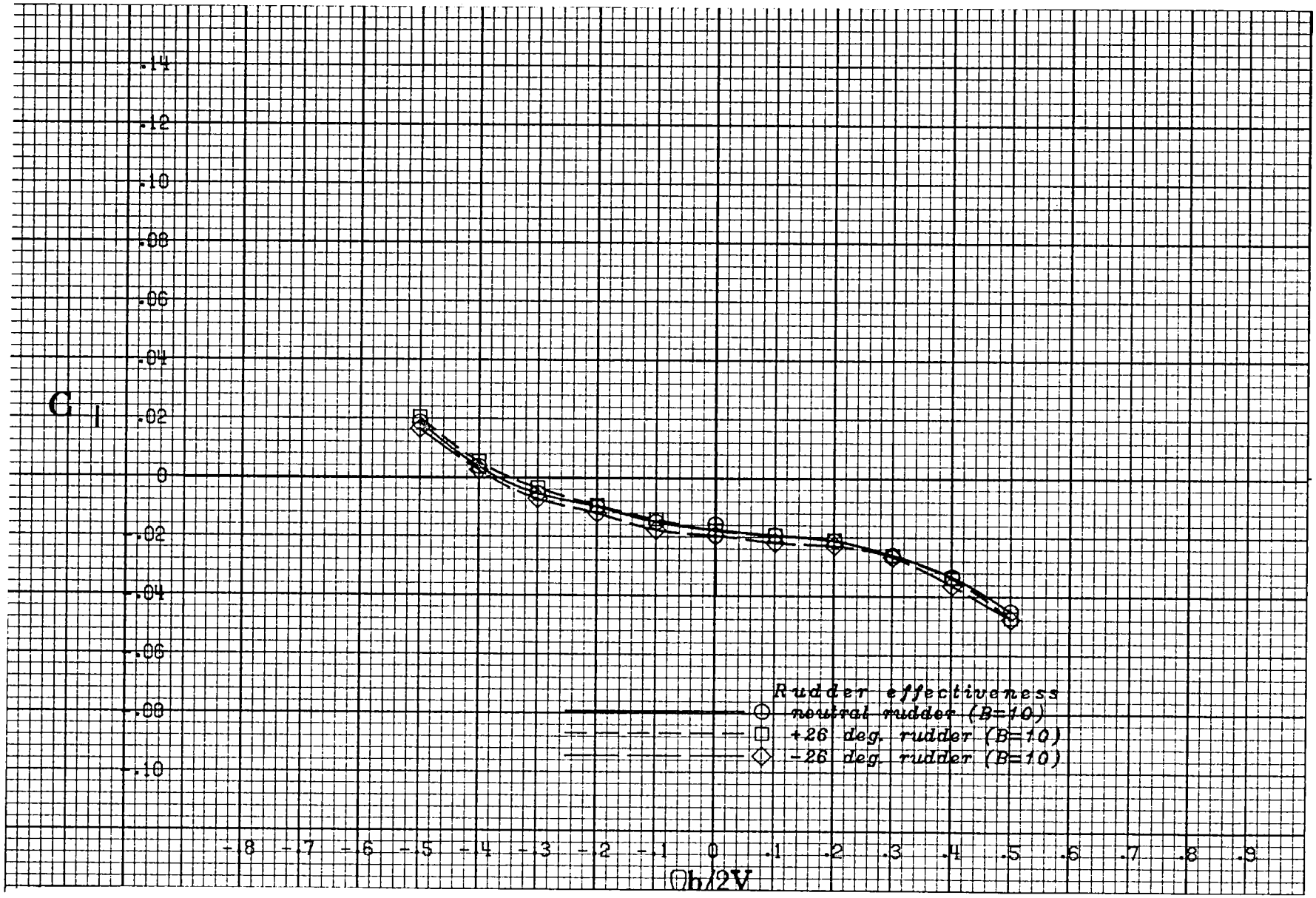

(c) α = 30 deg.

Figure A 14 .- Continued.

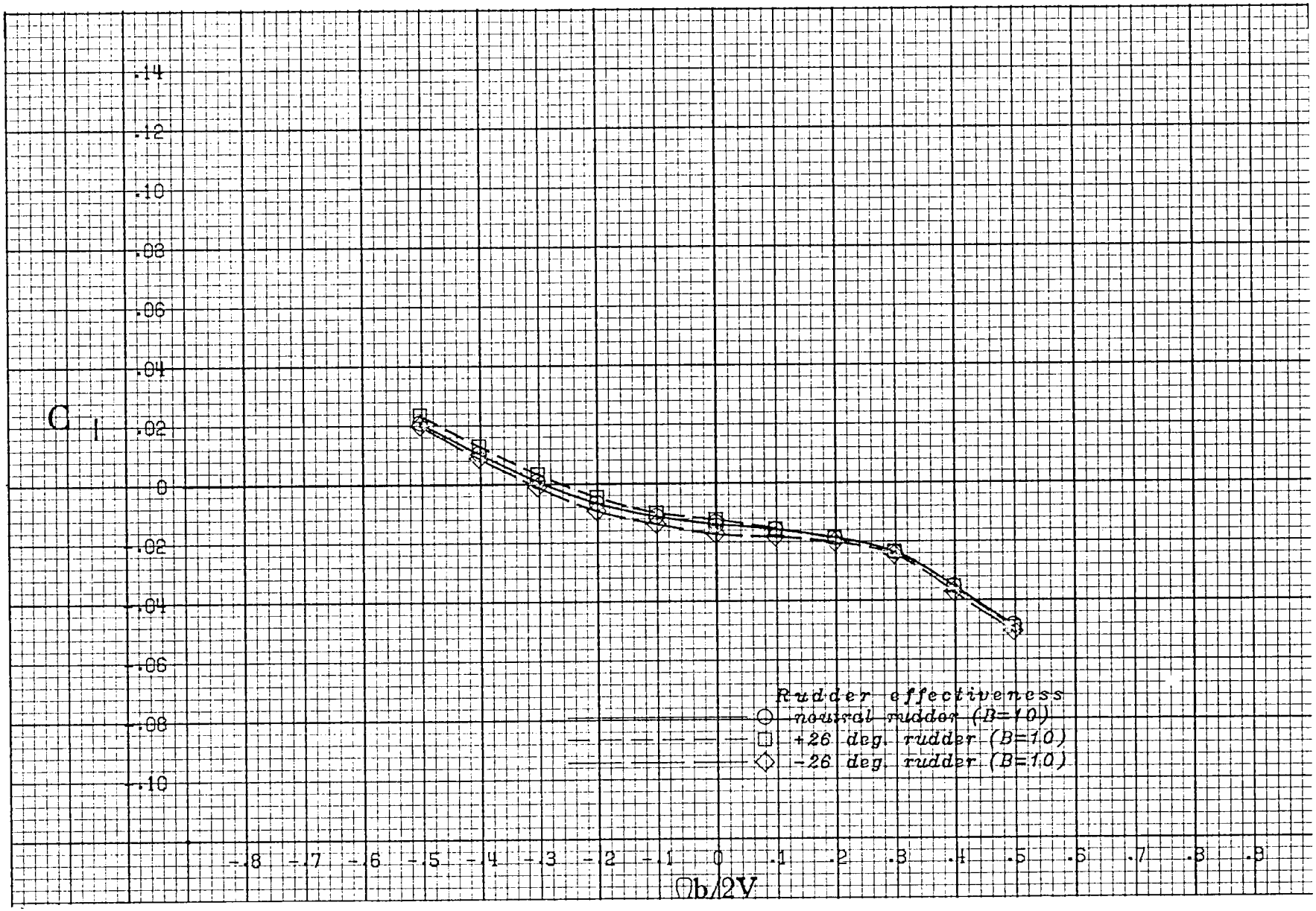

(d) α = 35 deg.

Figure A 14 .- Continued.

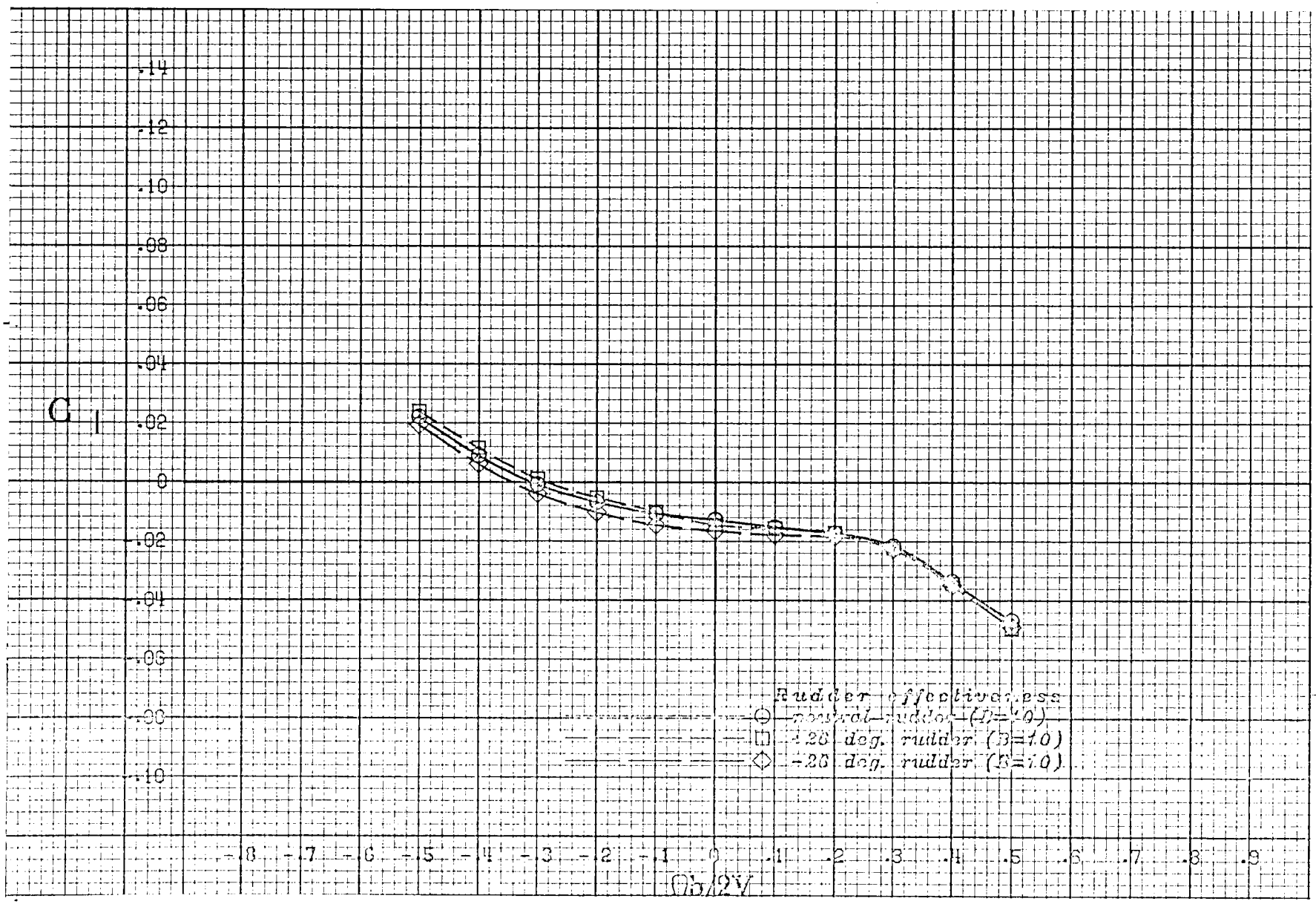

(c) α = 40 deg.

Figure A 14 .- Continued.

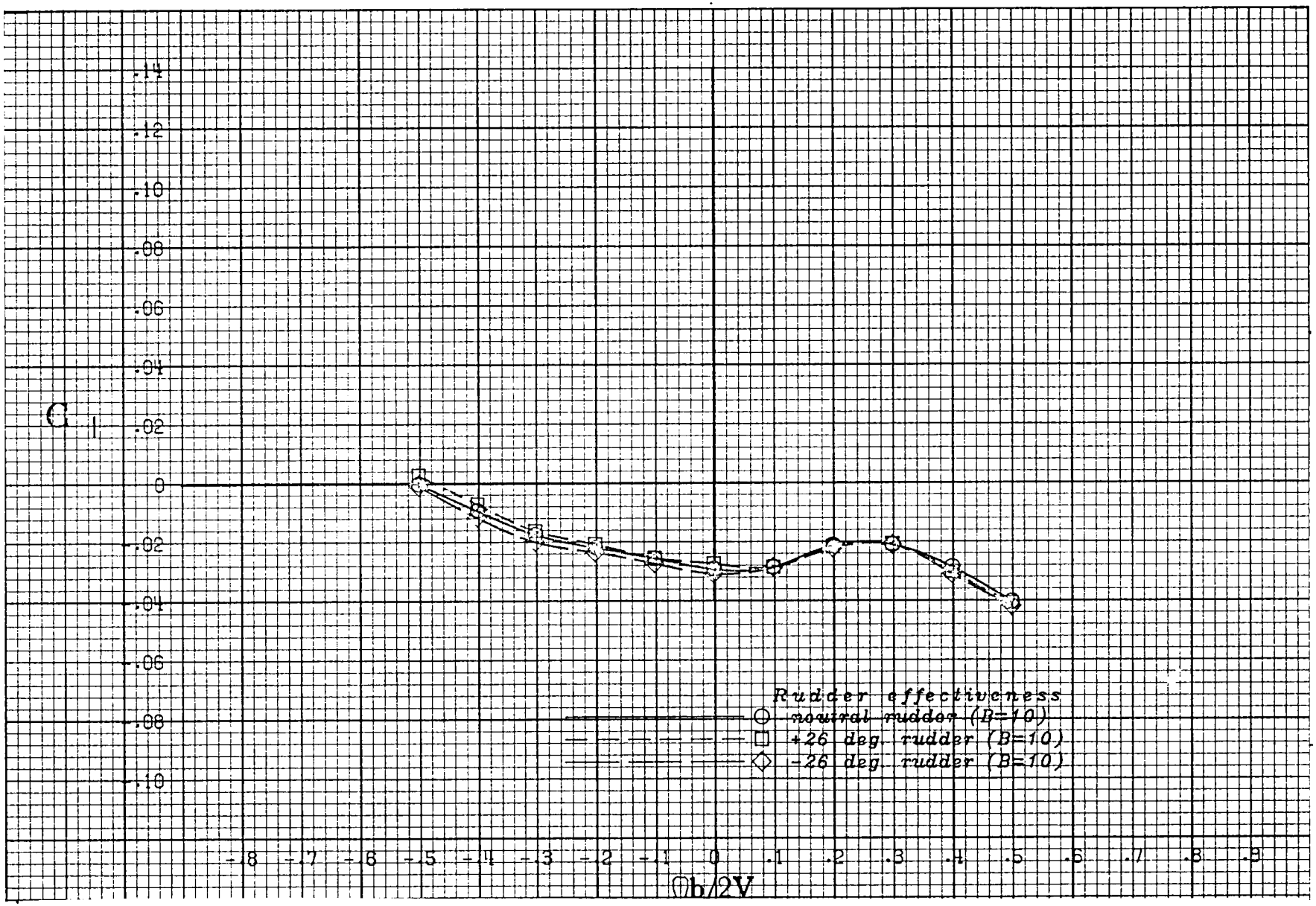

(f) α = 50 deg.

Figure A 14 .- Continued.

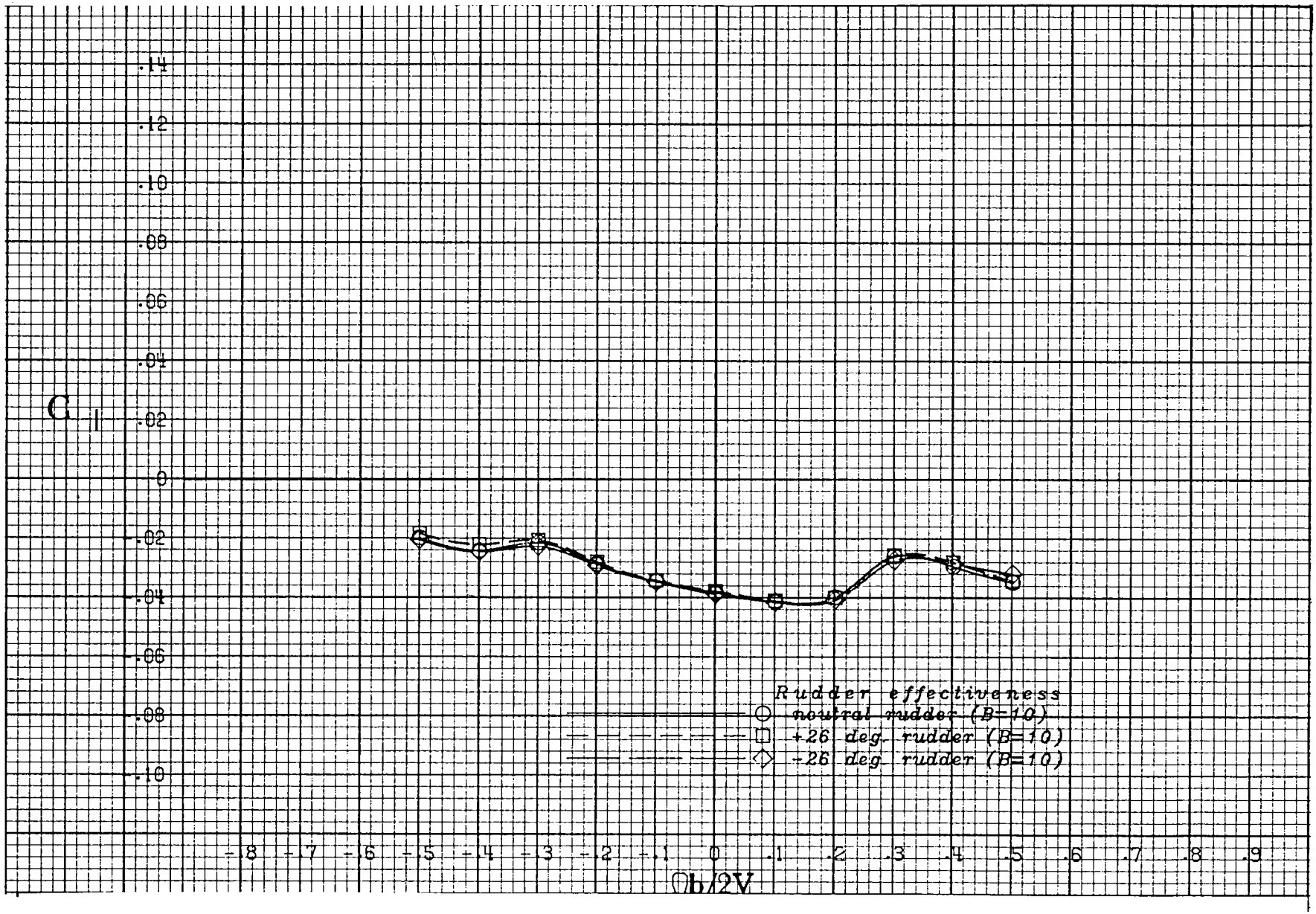

(g) α = 60 deg.

Figure A 14 .- Continued.

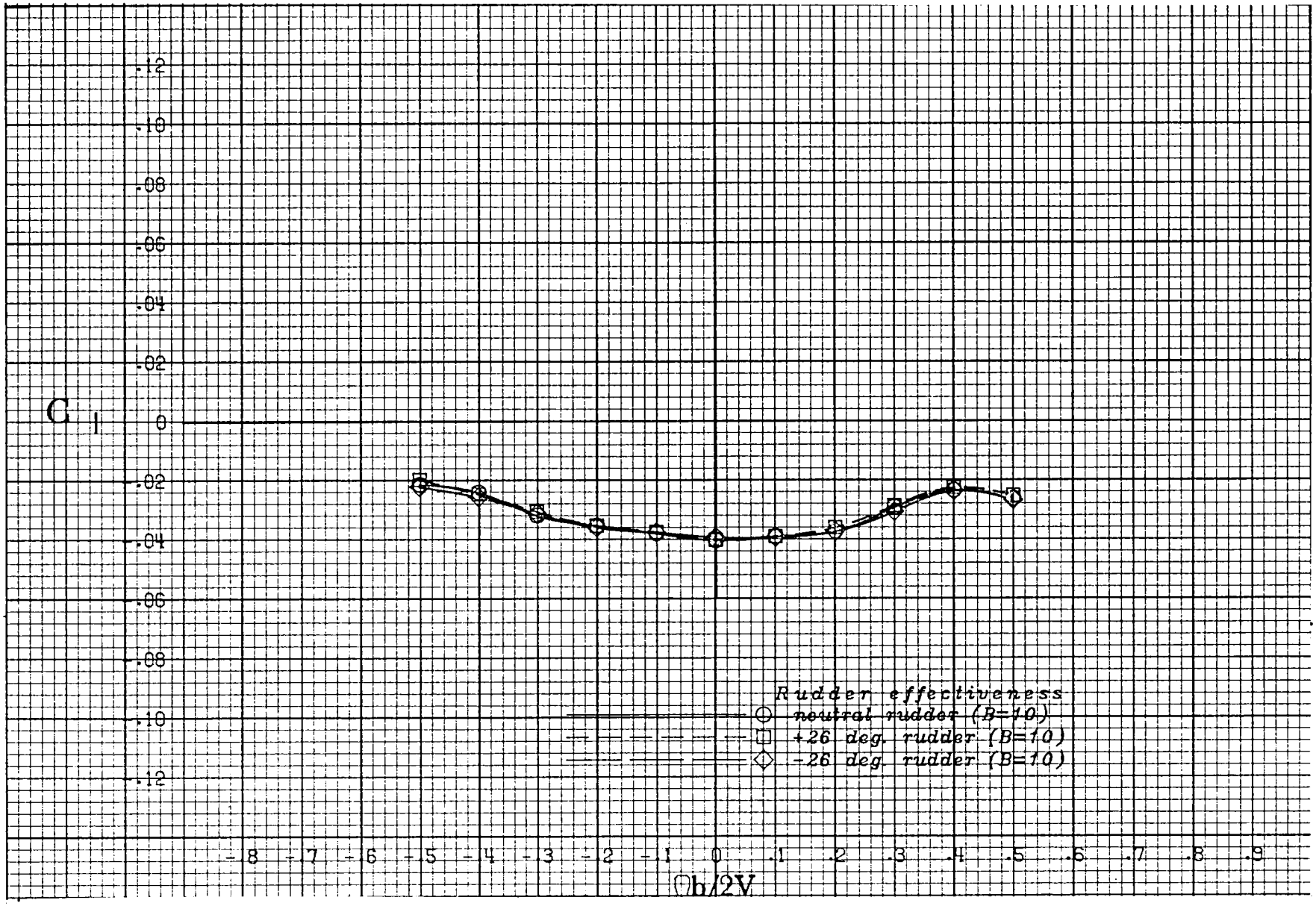

(h) α = 70 deg.

Figure A 14 .- Continued.

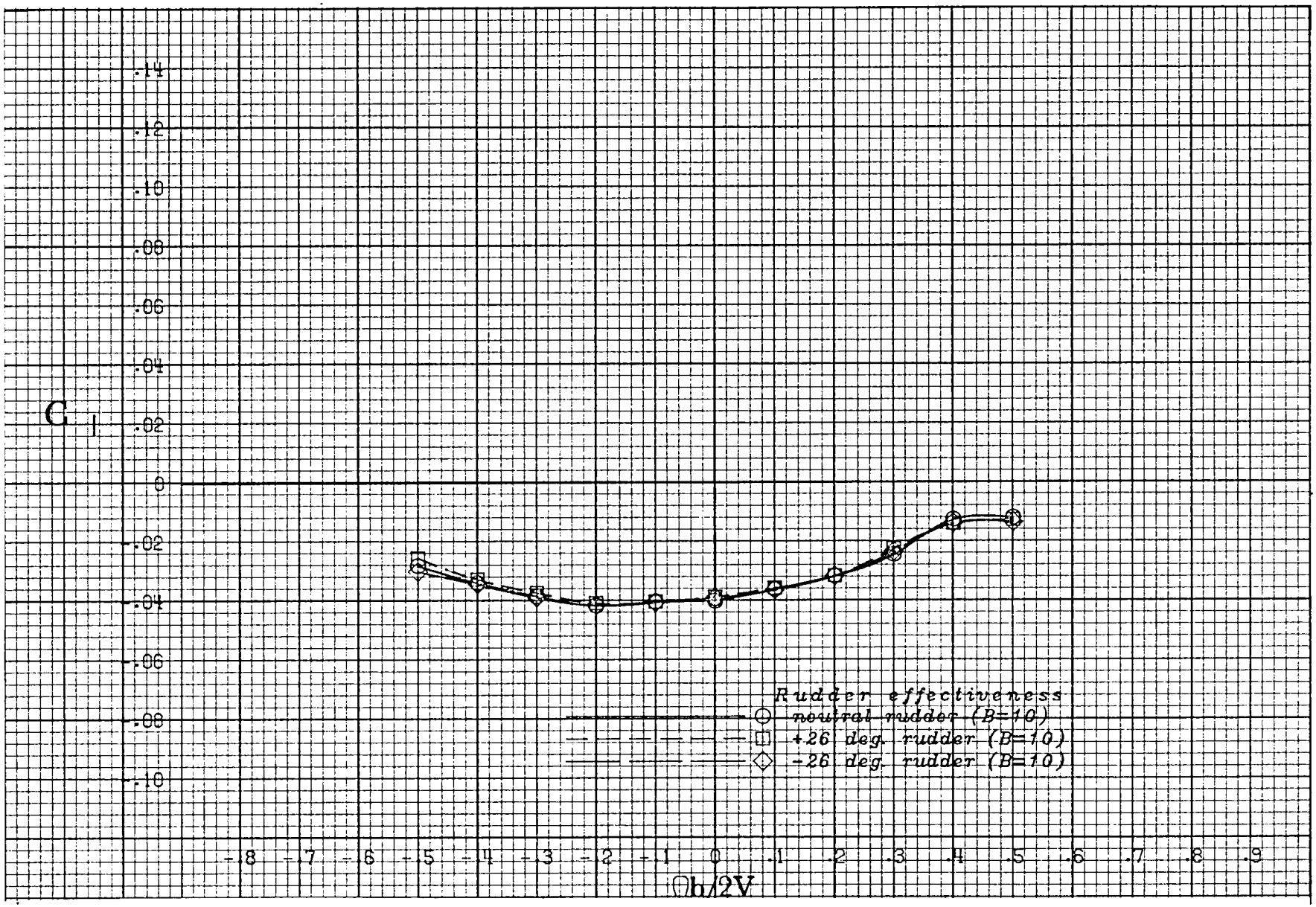

(i) α = 80 deg.

Figure A 14 .- Continued.

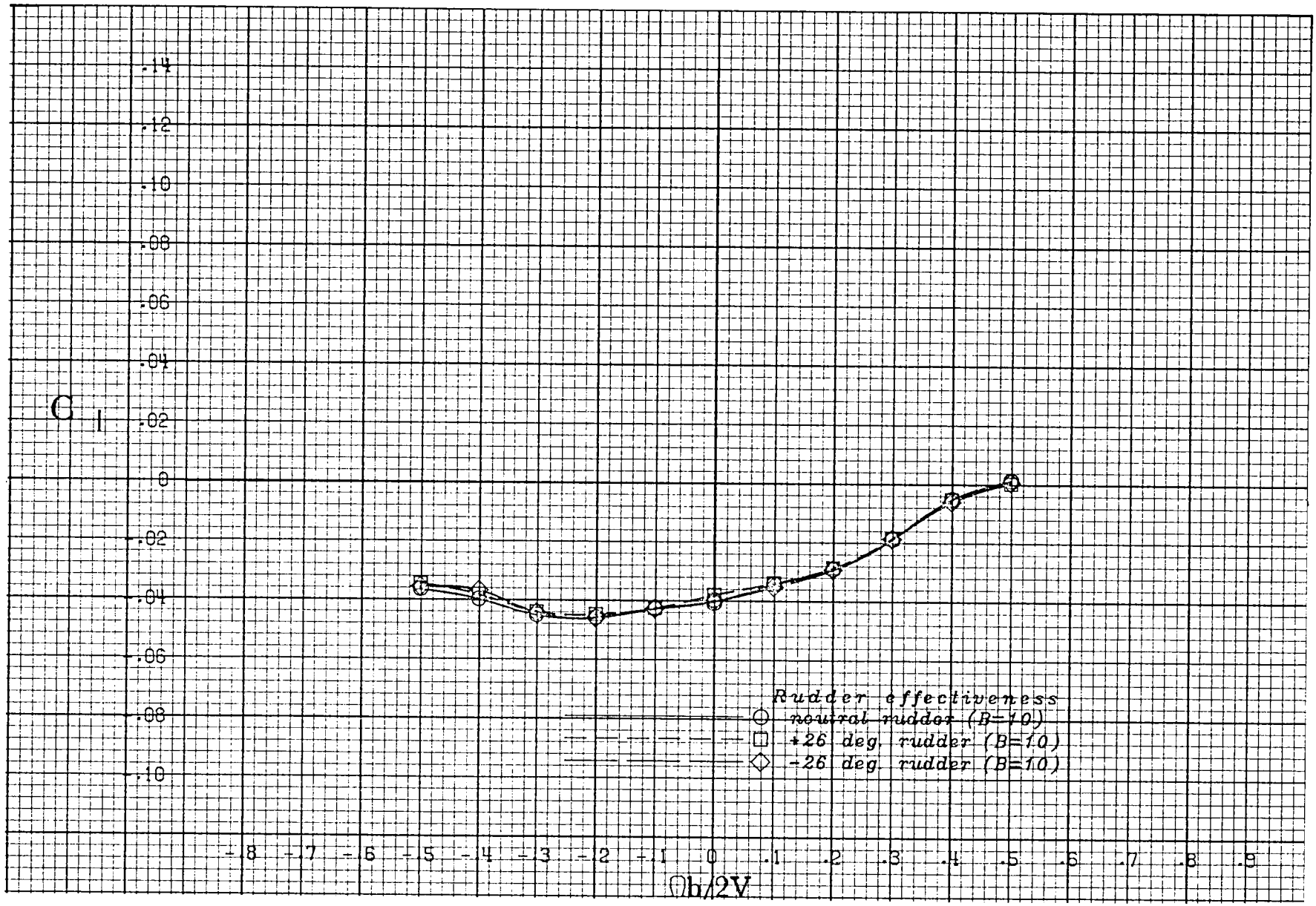

(j) α = 90 deg.

Figure A 14 .- Concluded.

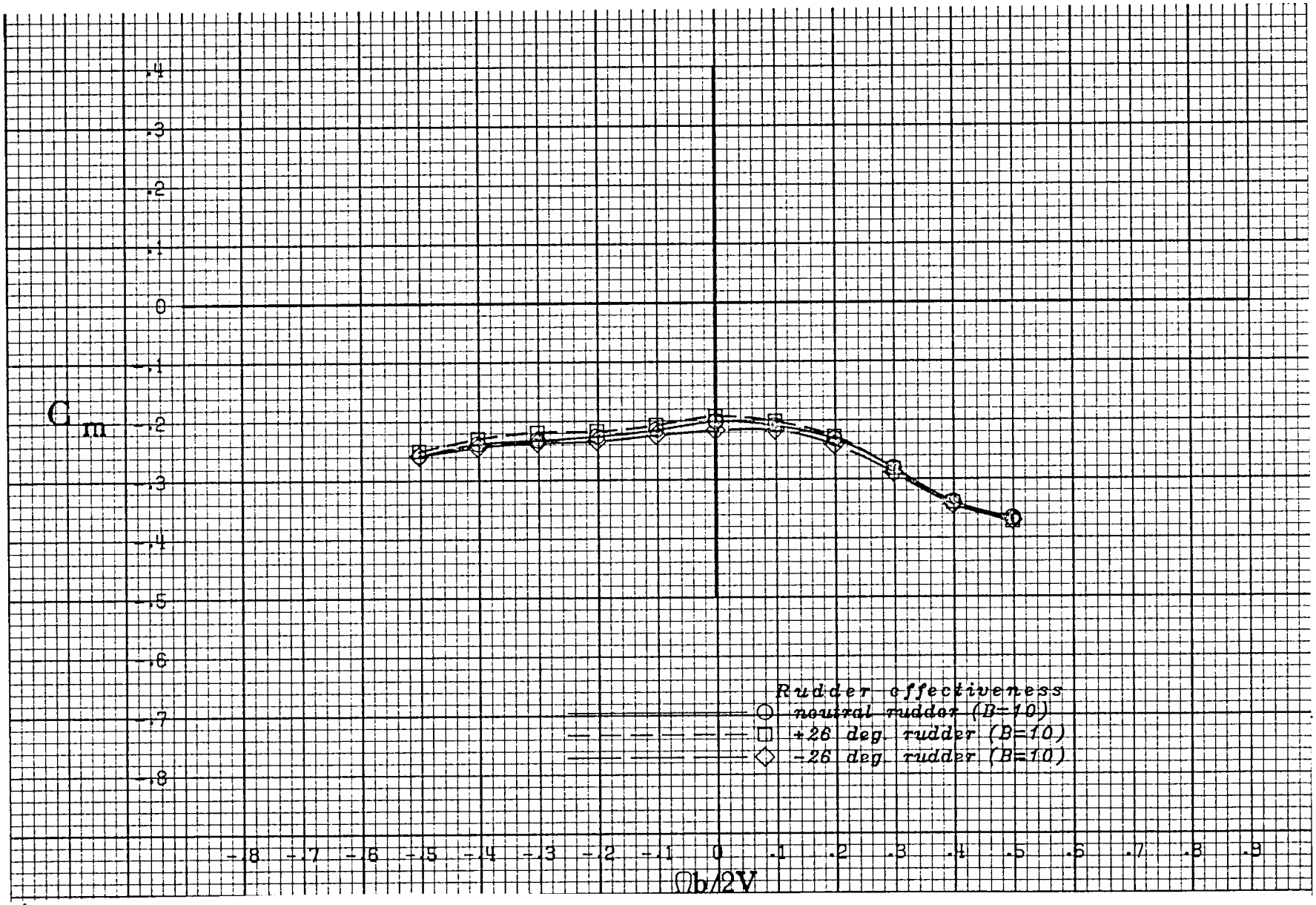

(a) α = 20 deg.

Figure A 15 .- Effect of rotation rate and rudder deflection on pitching-moment coefficient for the basic configuration with neutral elevator and ailerons at +10 deg sideslip angle.

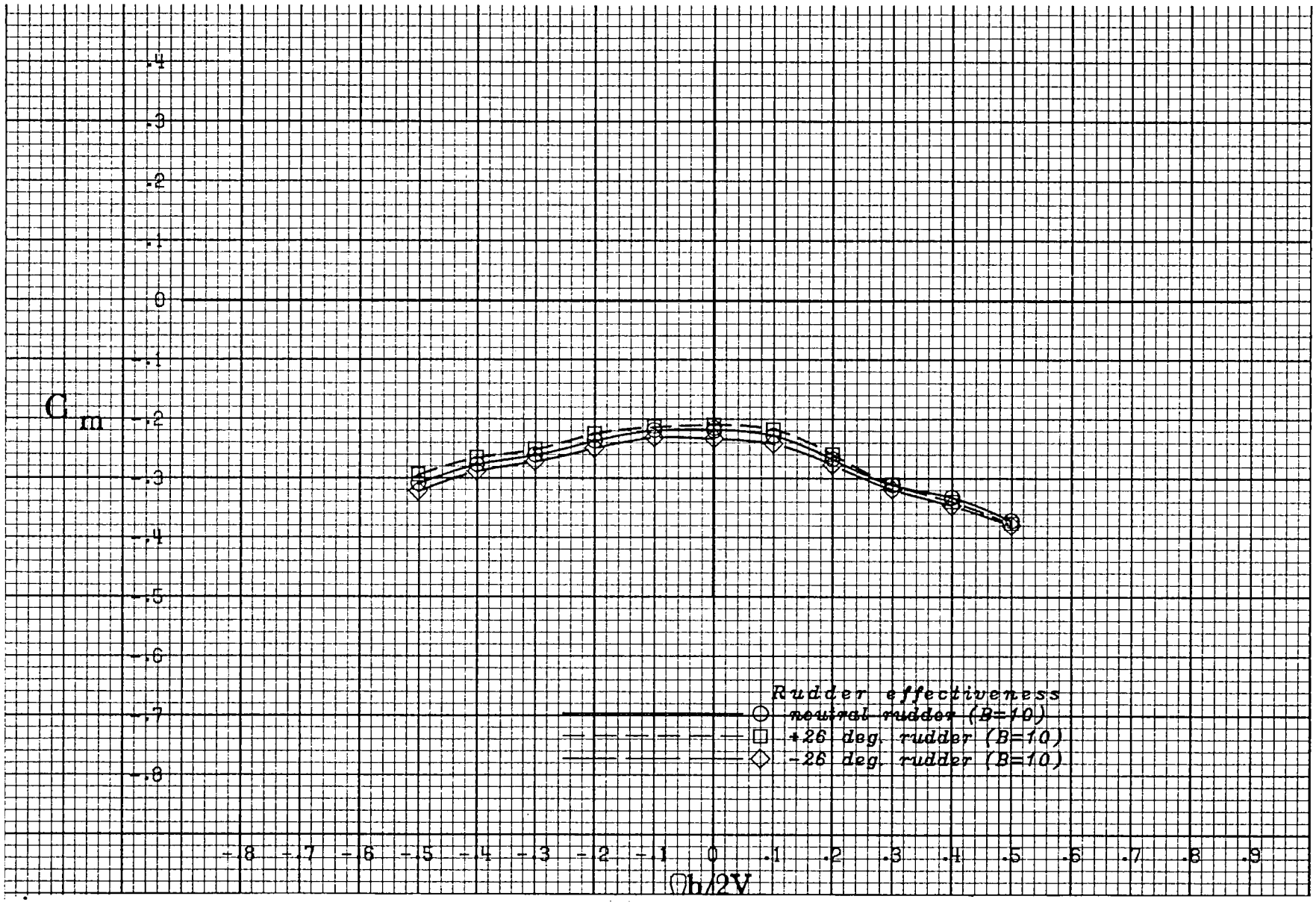

(b) α = 25 deg.

Figure A 15 .- Continued.

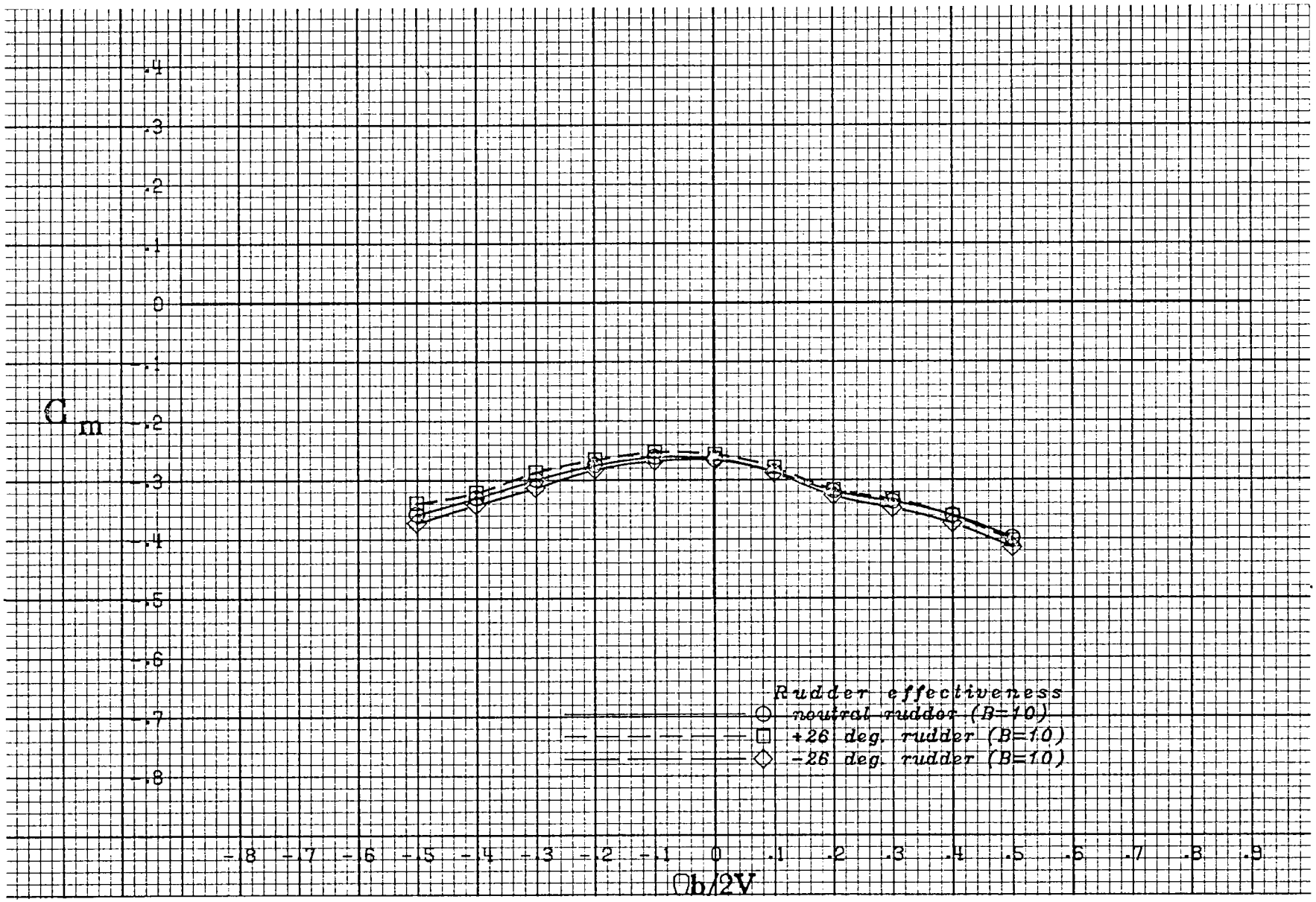

(c) α = 30 deg.

Figure A 15 .- Continued.

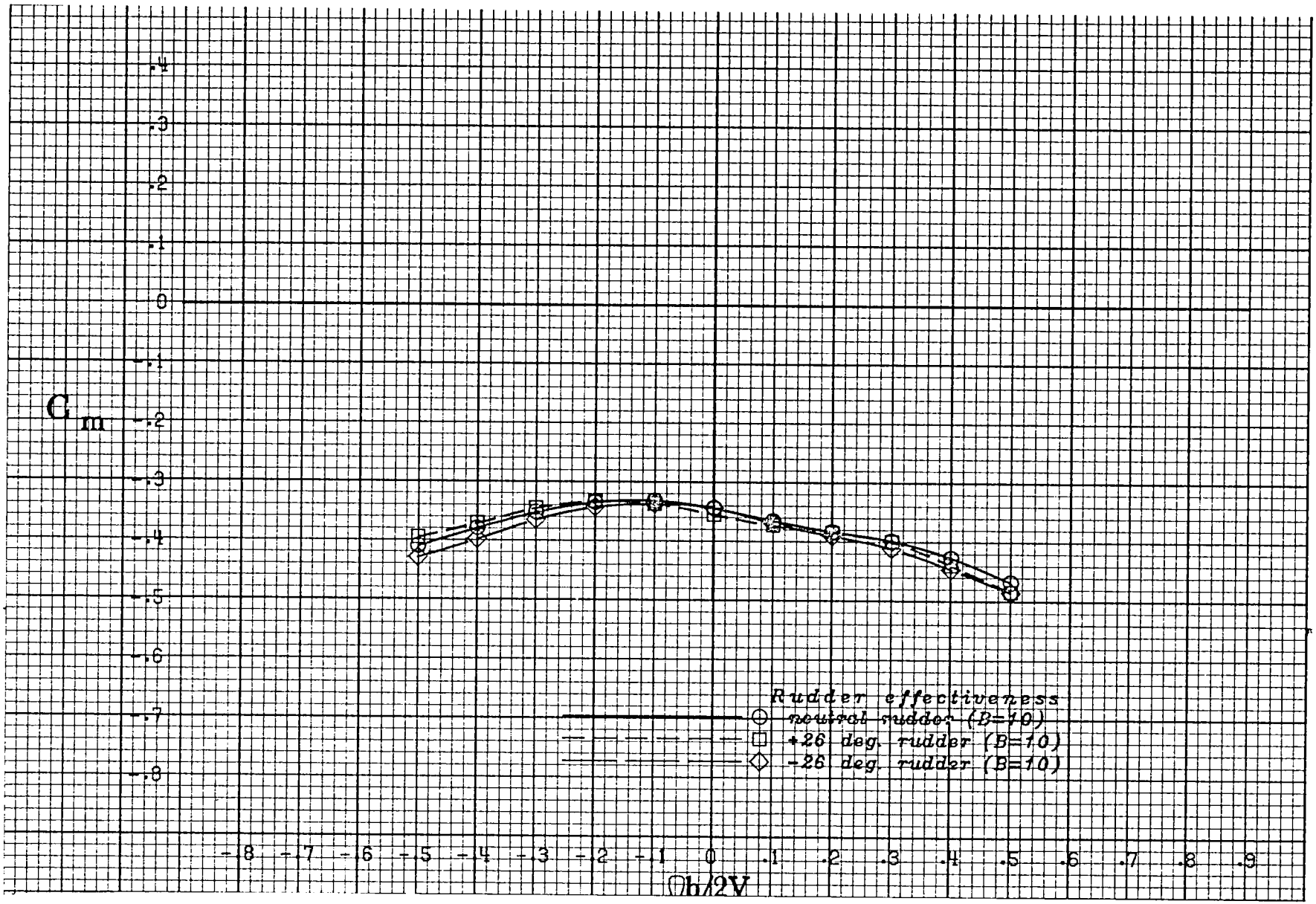

(d) α = 35 deg.

Figure A 15 .- Continued.

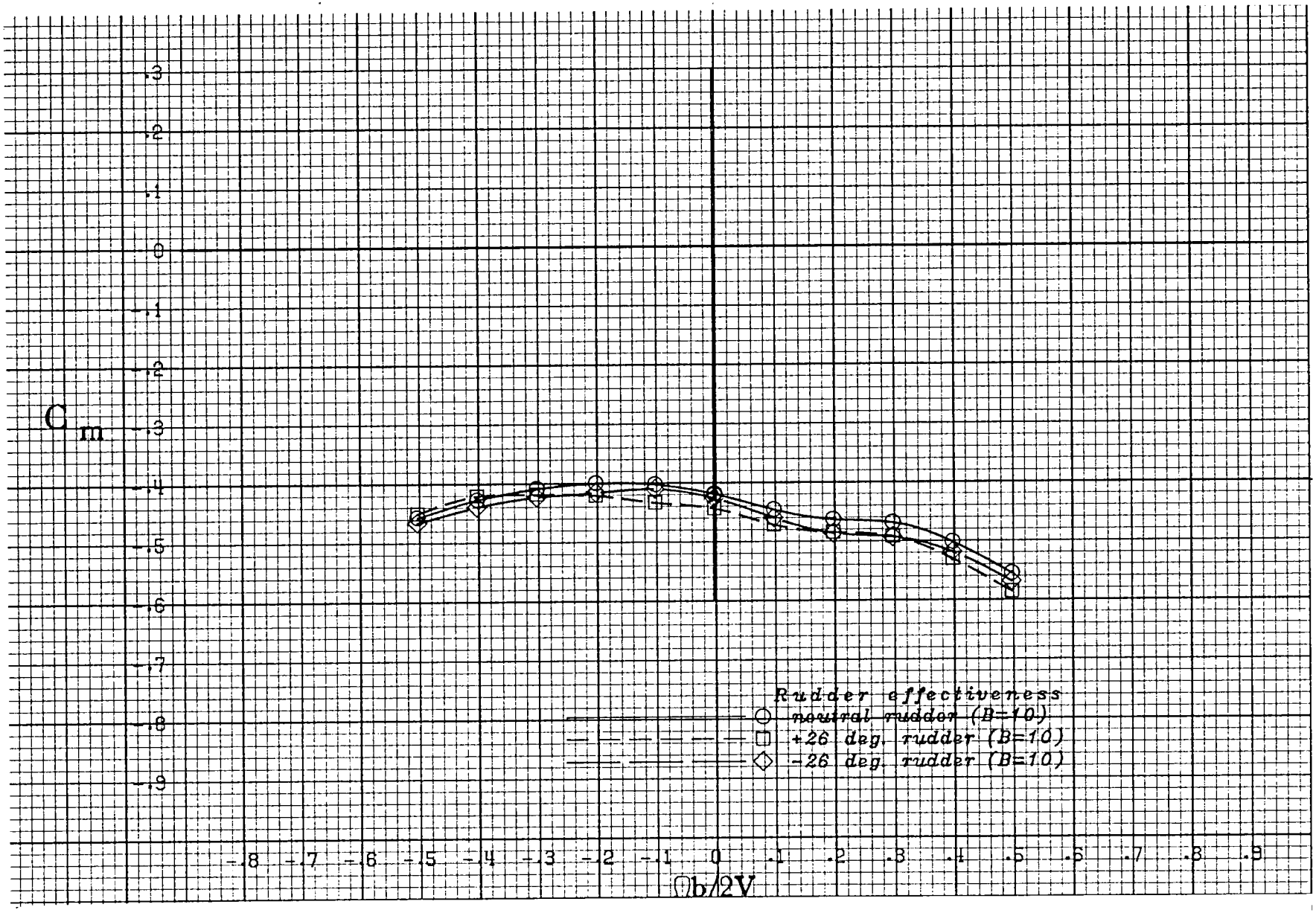

(e) α = 40 deg.

Figure A 15 .- Continued.

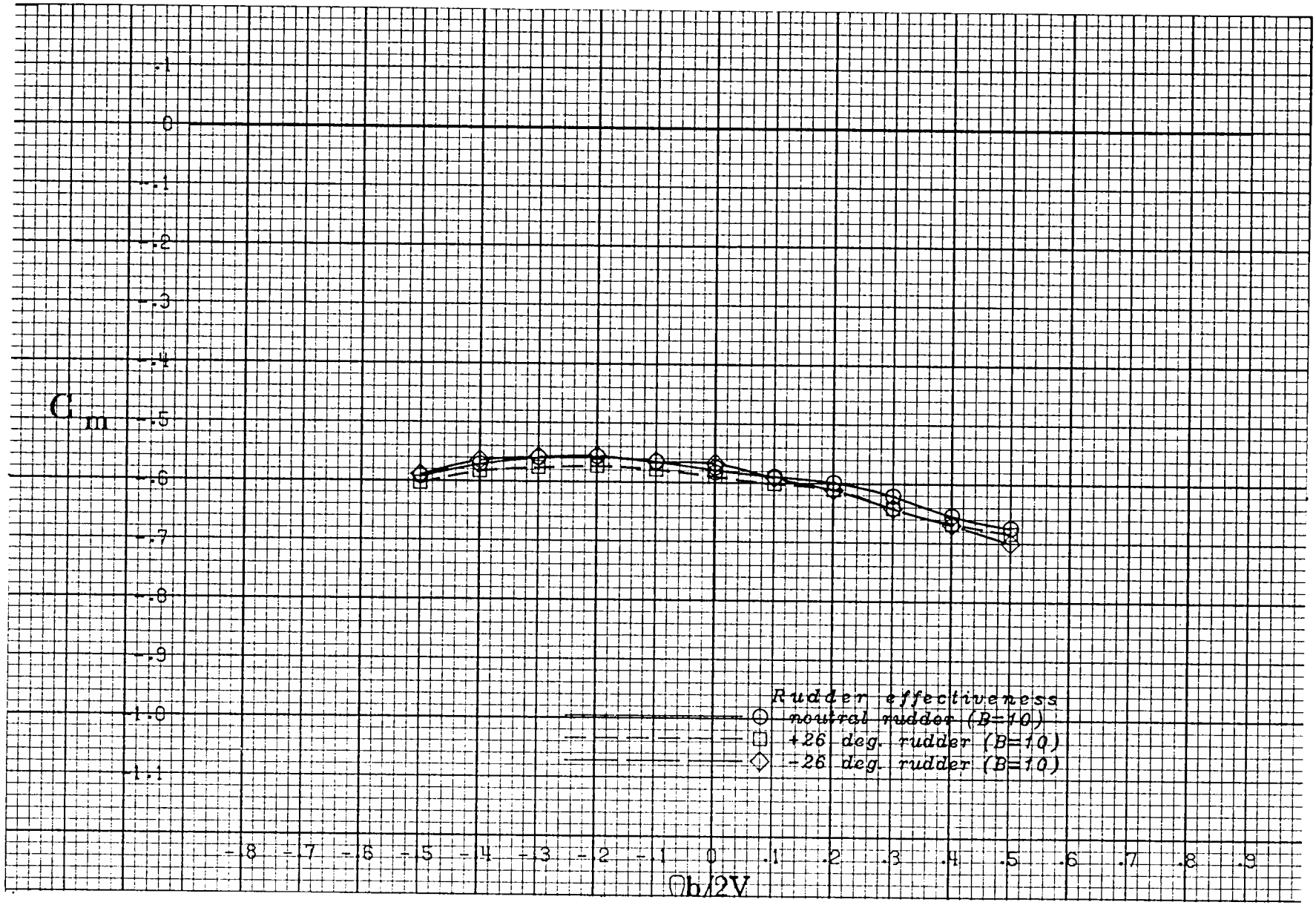

(f) α = 50 deg.

Figure A 15 .- Continued.

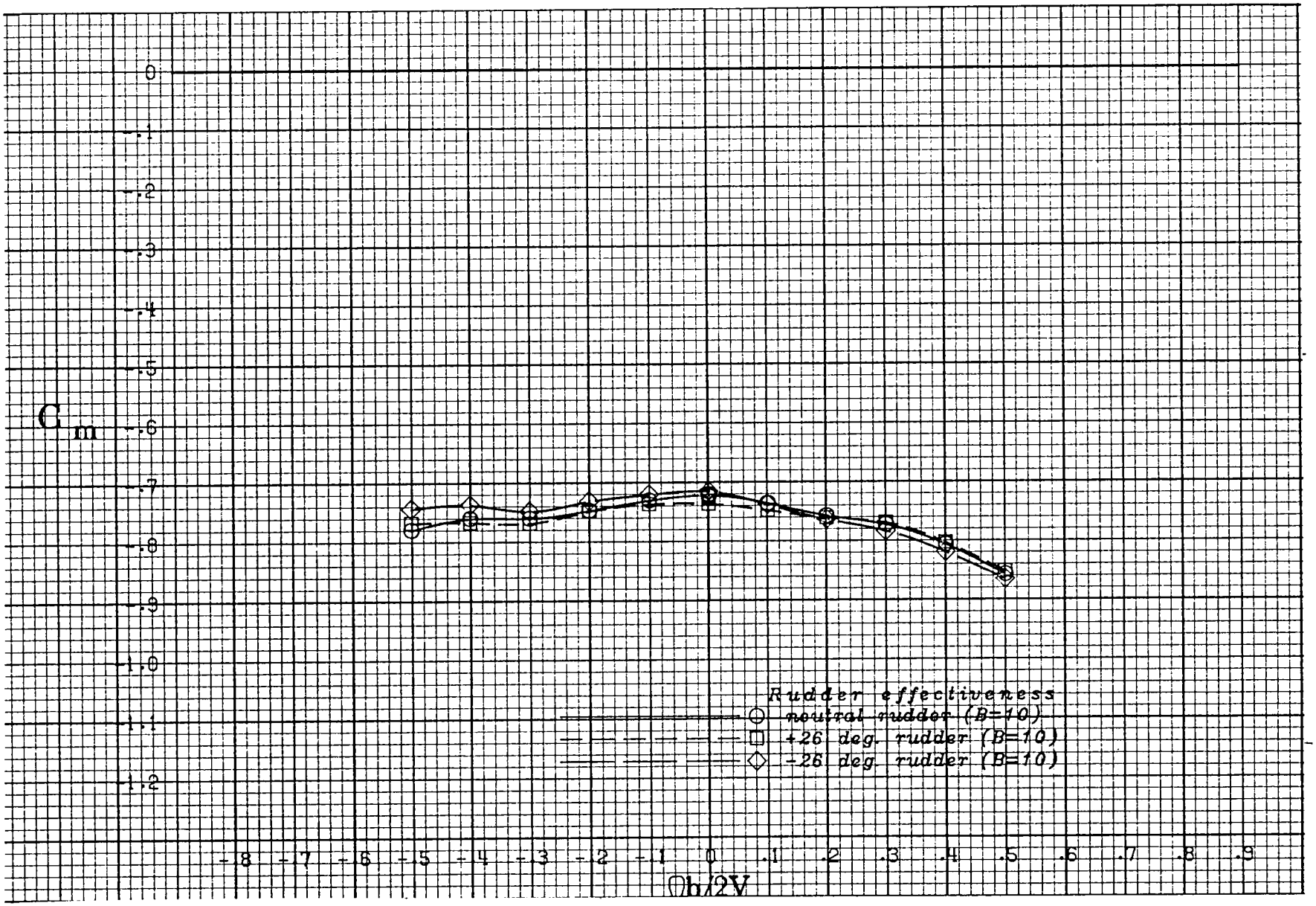

(g) α = 60 deg.

Figure A 15 .- Continued.

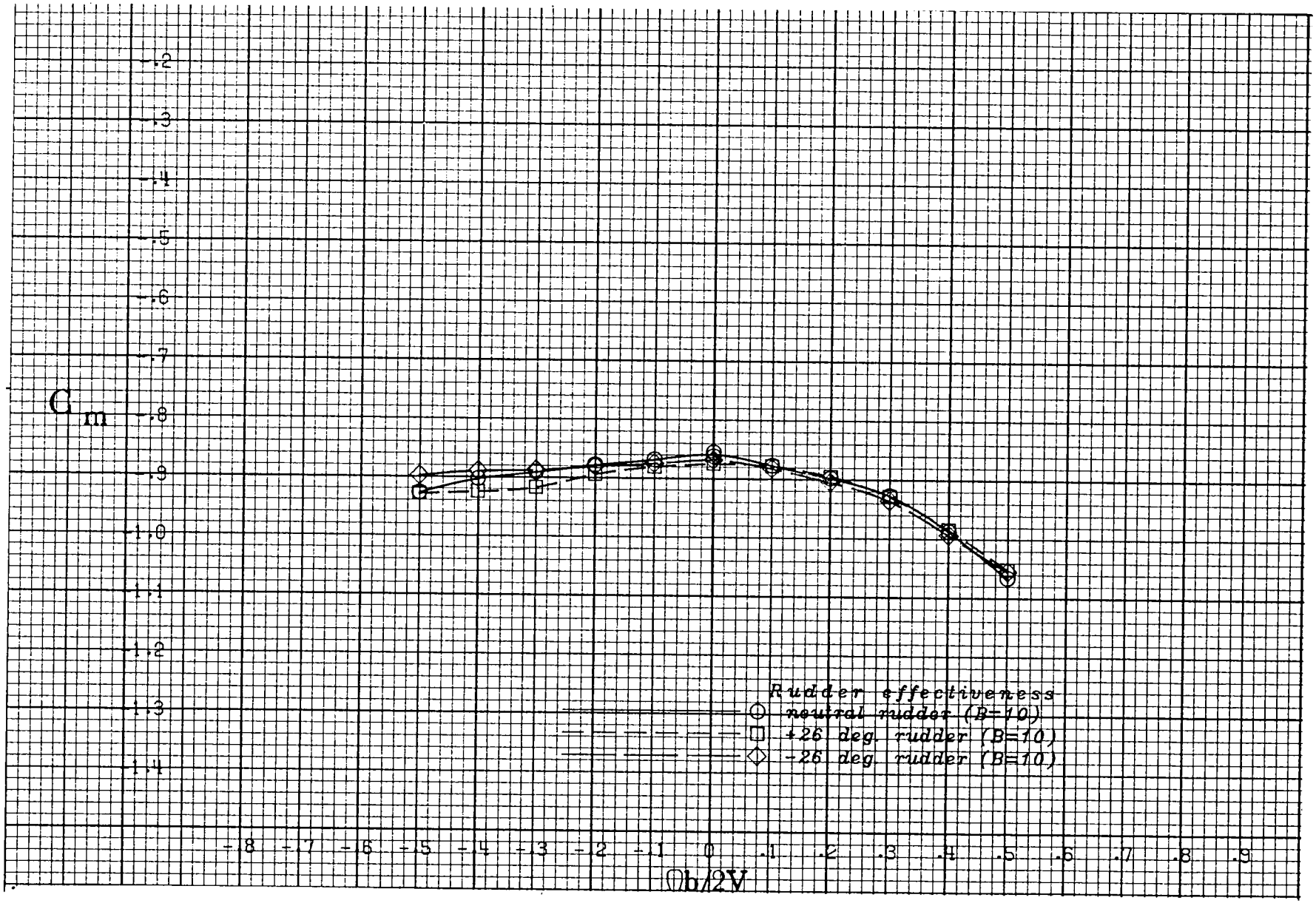

(h) α = 70 deg.

Figure A 15 .- Continued.

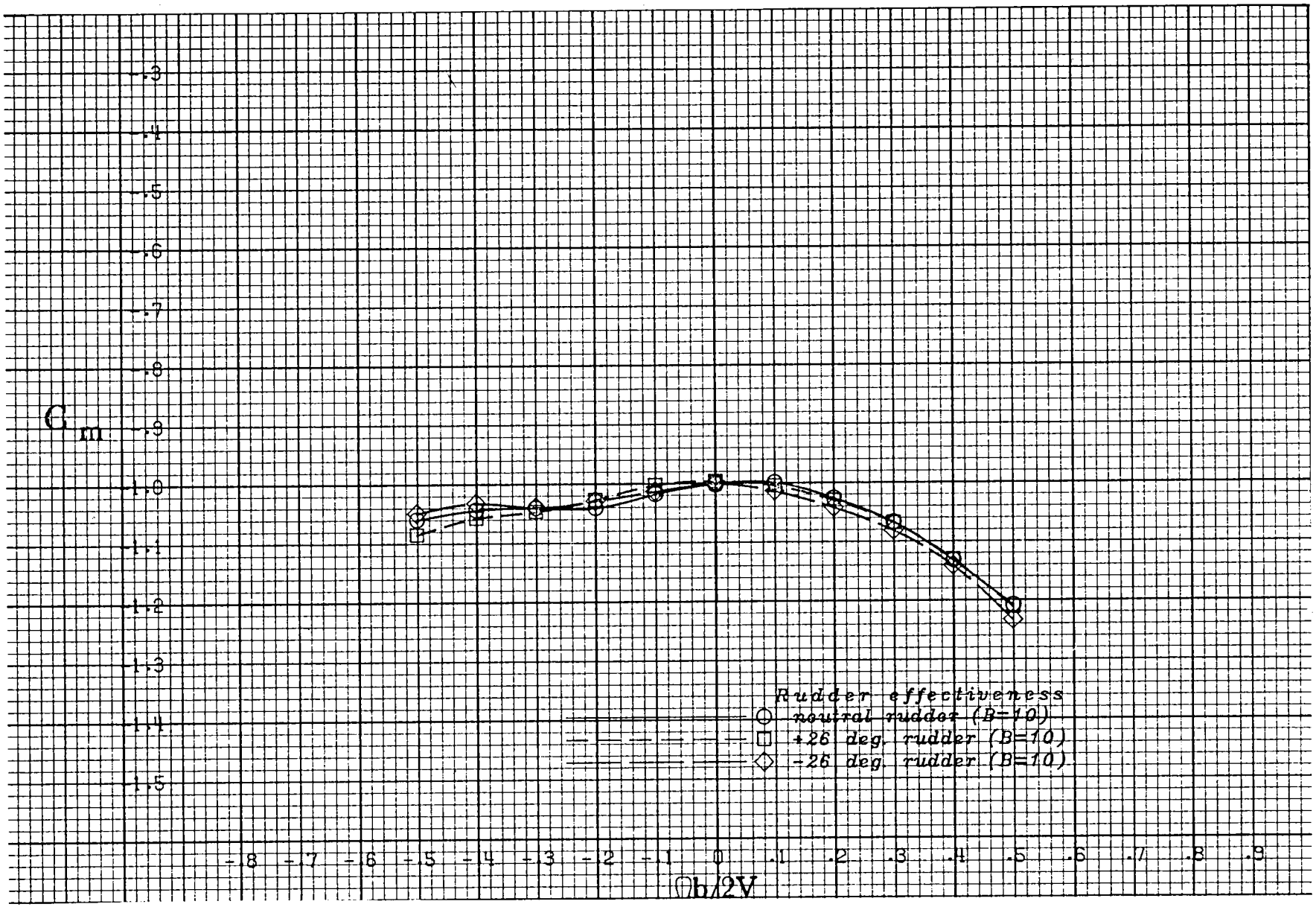

(i) α = 80 deg.

Figure A 15 .- Continued.

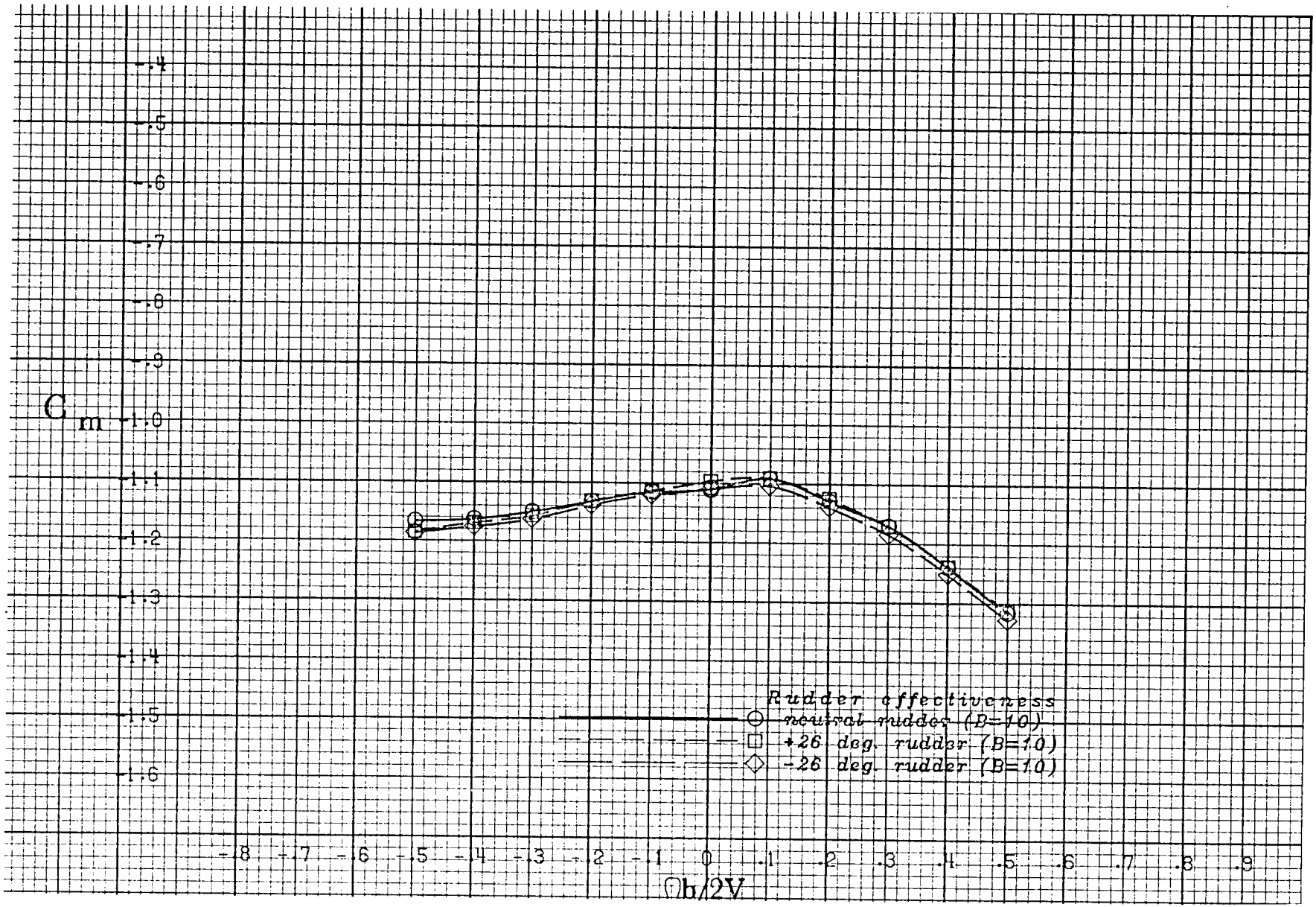

(j) α = 90 deg.

Figure A 15 .- Concluded.

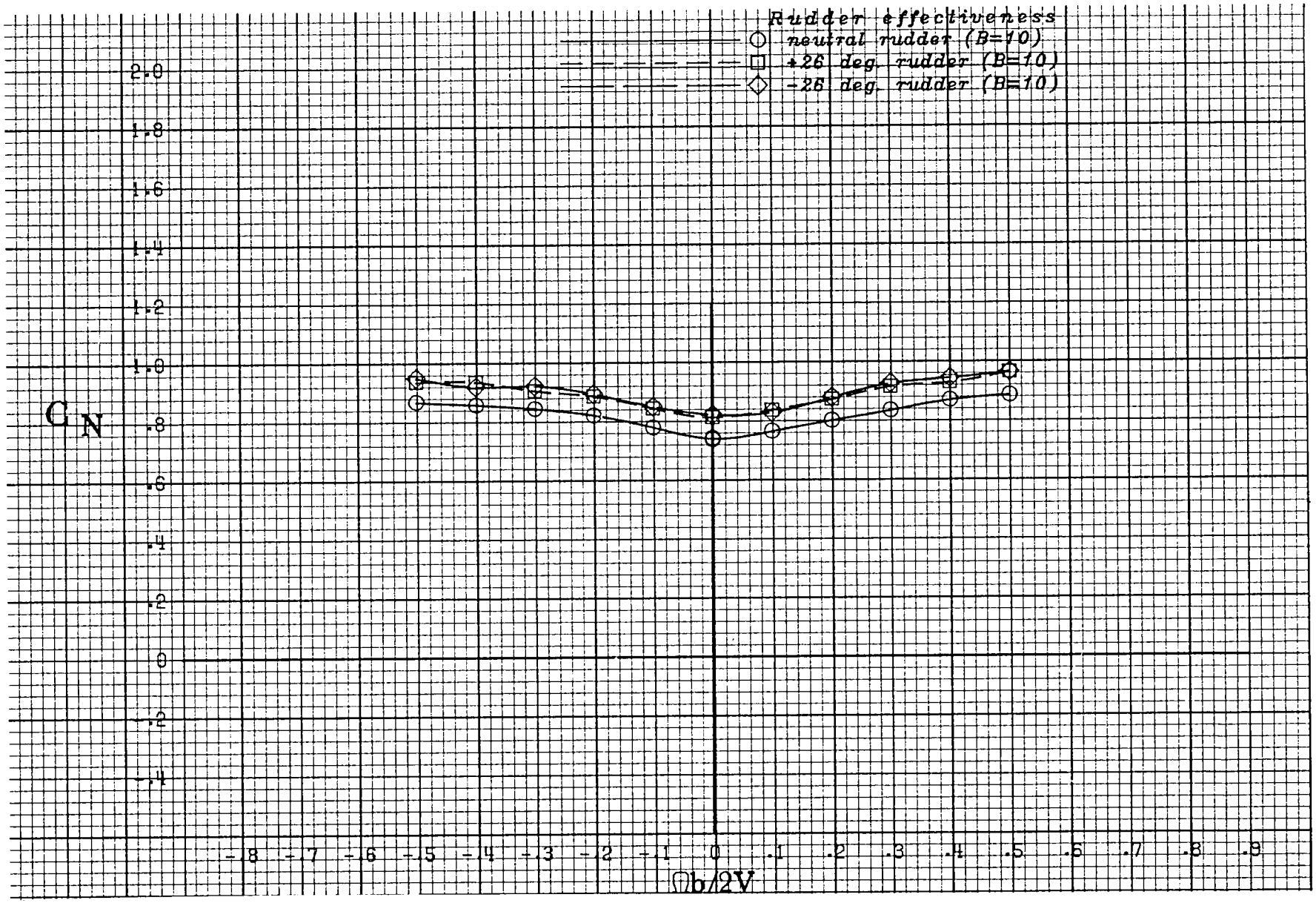

(a) α = 20 deg.

Figure A 16 .- Effect of rotation rate and rudder deflection on normal-force coefficient for the basic configuration with neutral elevator and ailerons at +10 deg sideslip angle.

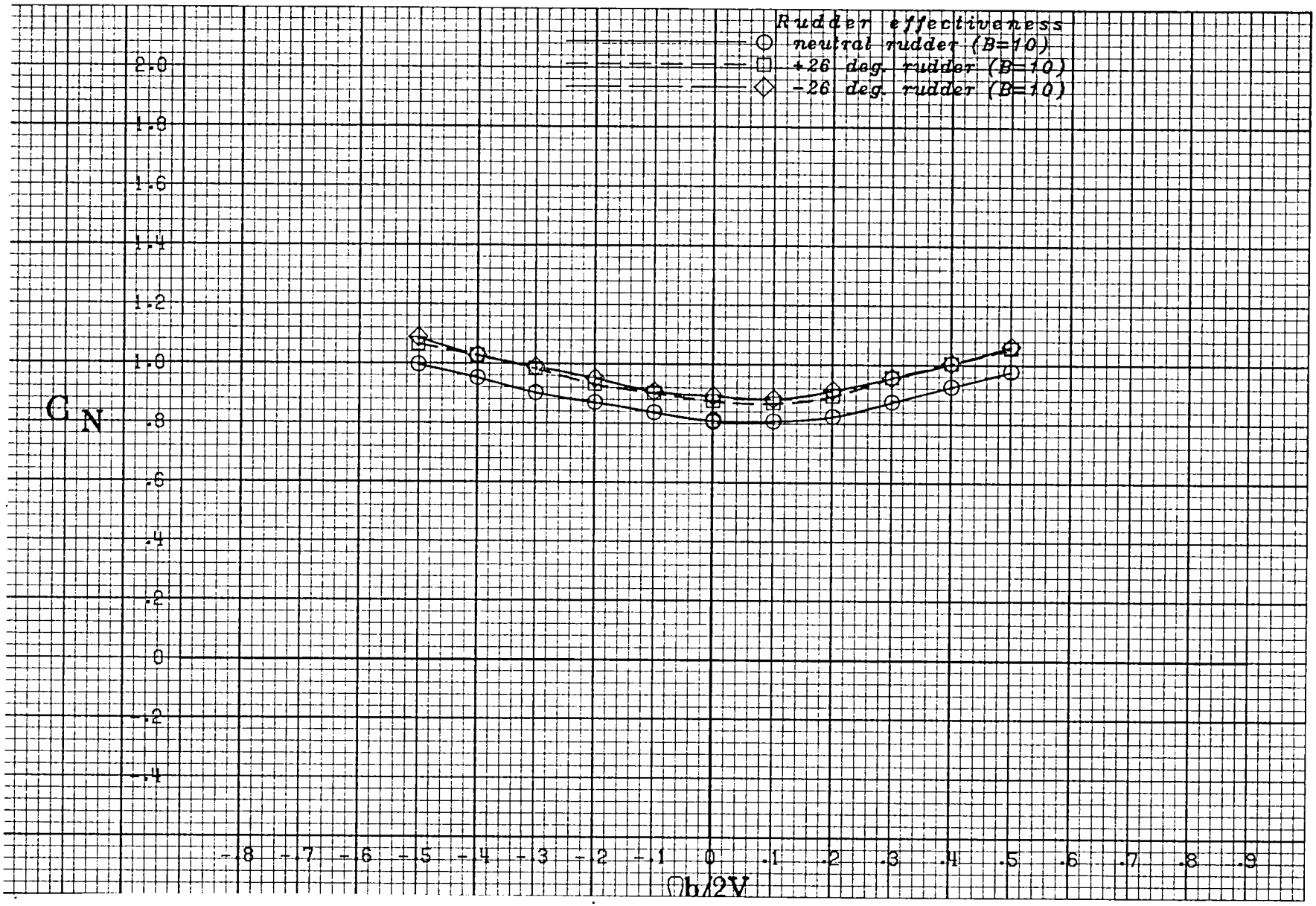

(b) α = 25 deg.

Figure A 16 .- Continued.

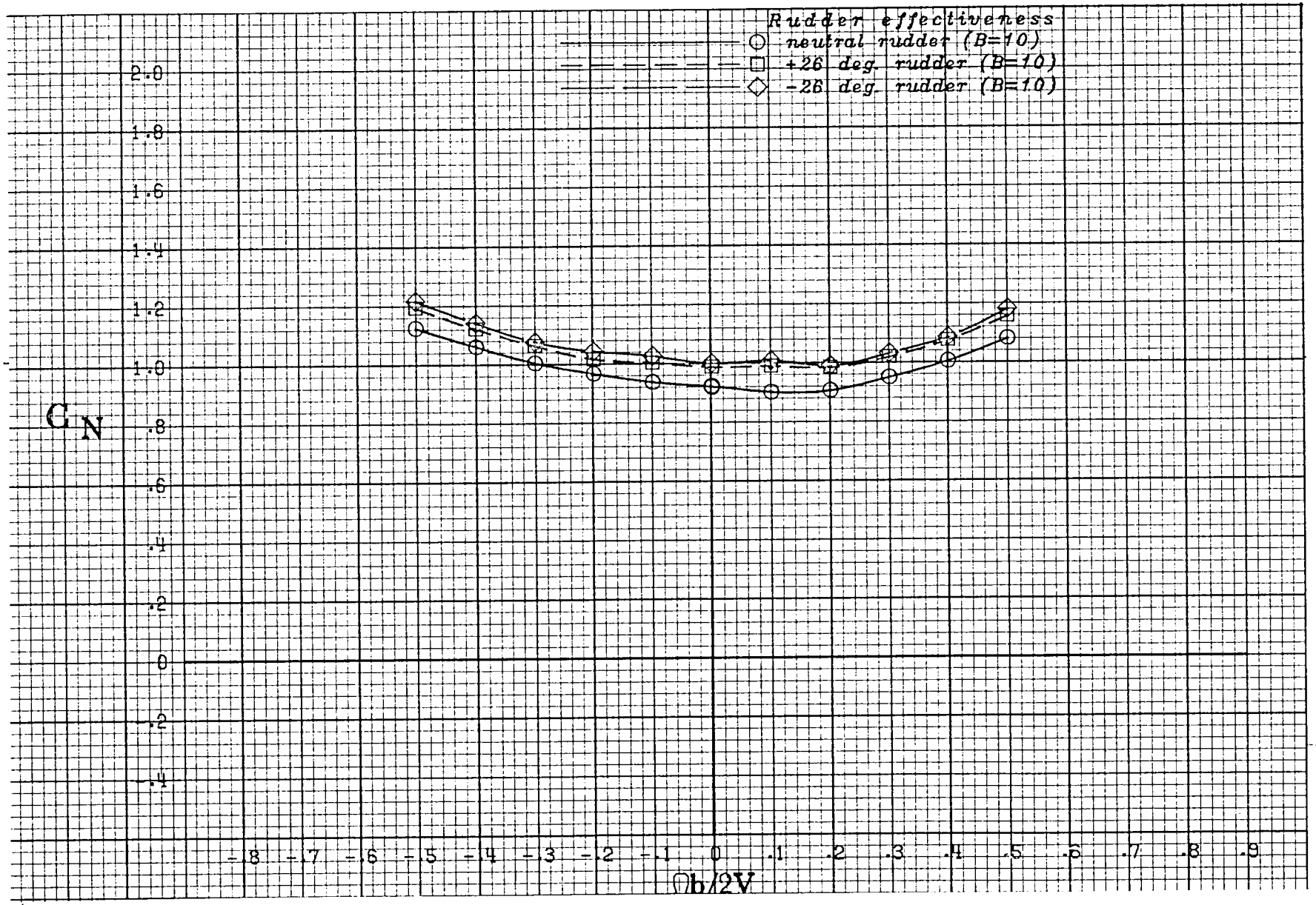

(c) α = 30 deg.

Figure A 16 .- Continued.

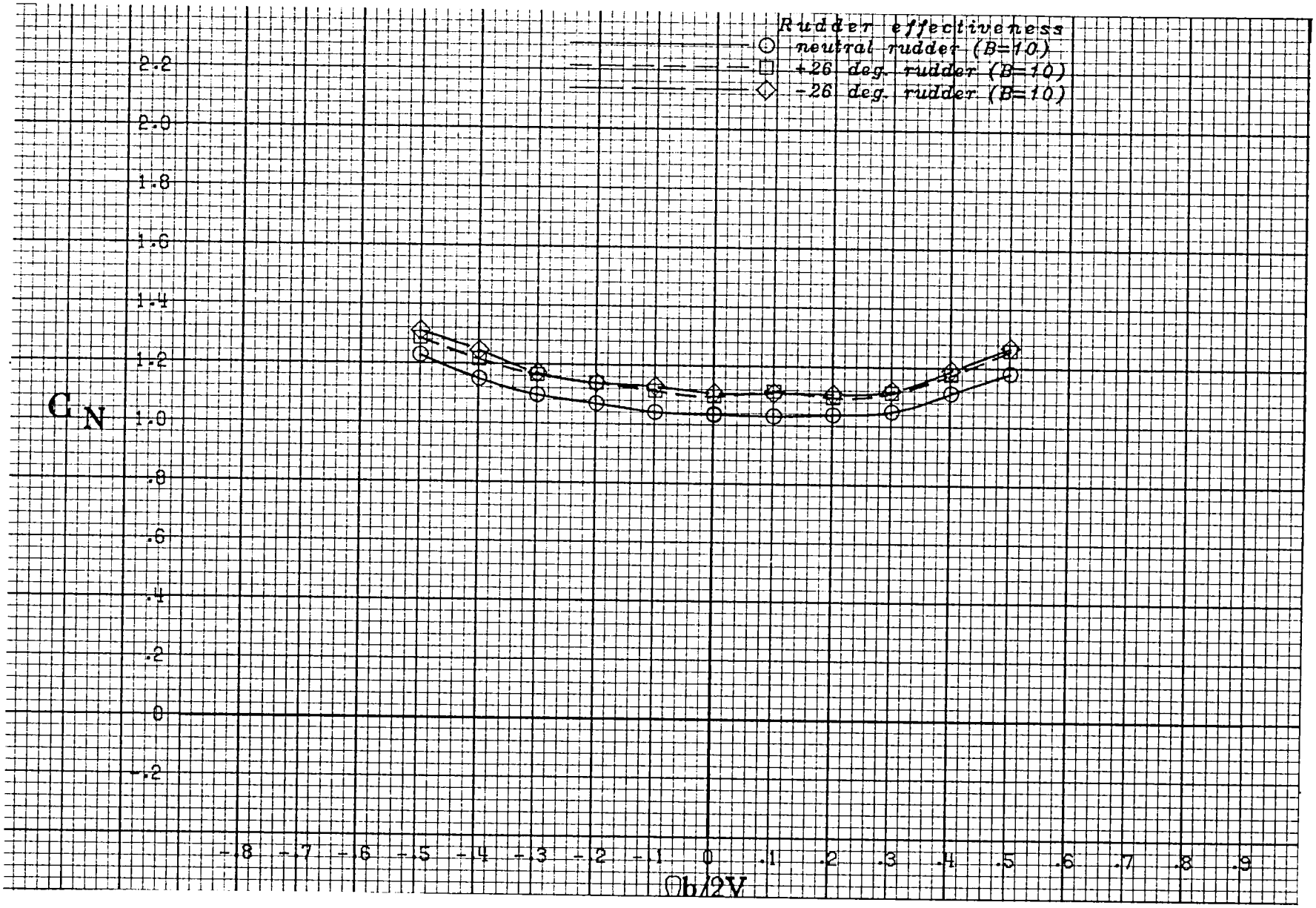

(d) α = 35 deg.

Figure A 16 .- Continued.

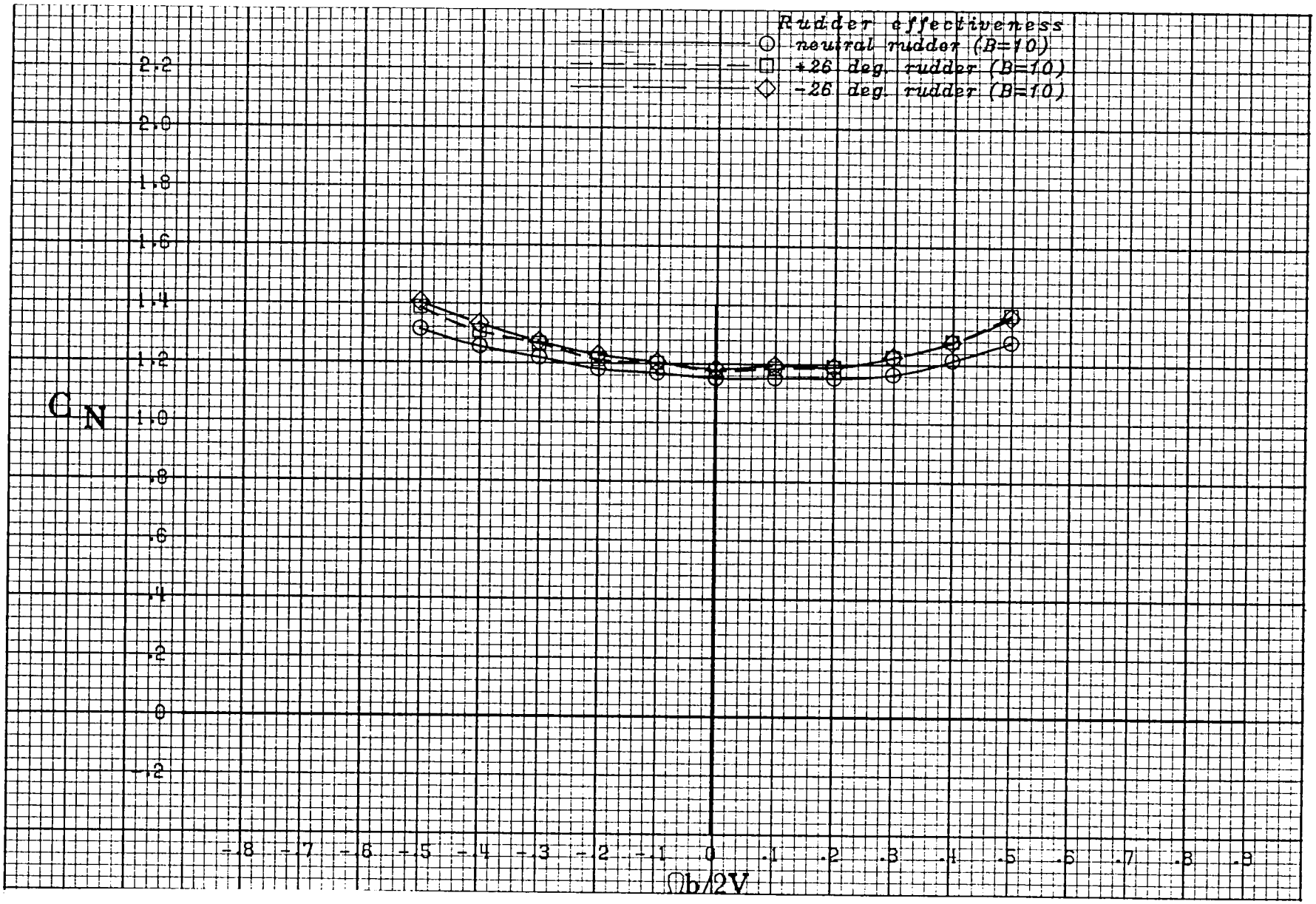

(e) α = 40 deg.

Figure A 16 .- Continued.

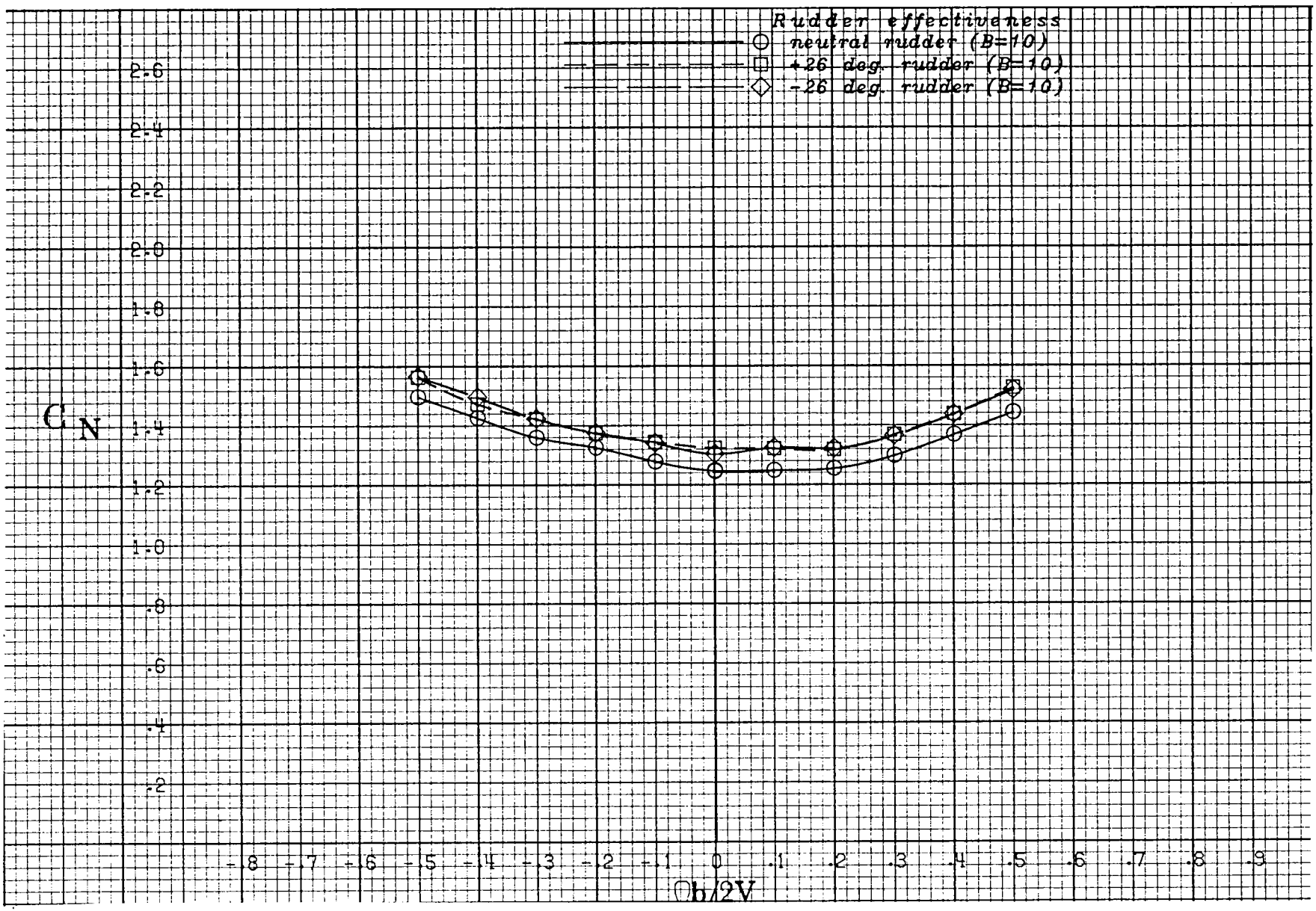

(f) α = 50 deg.

Figure A 16 .- Continued.

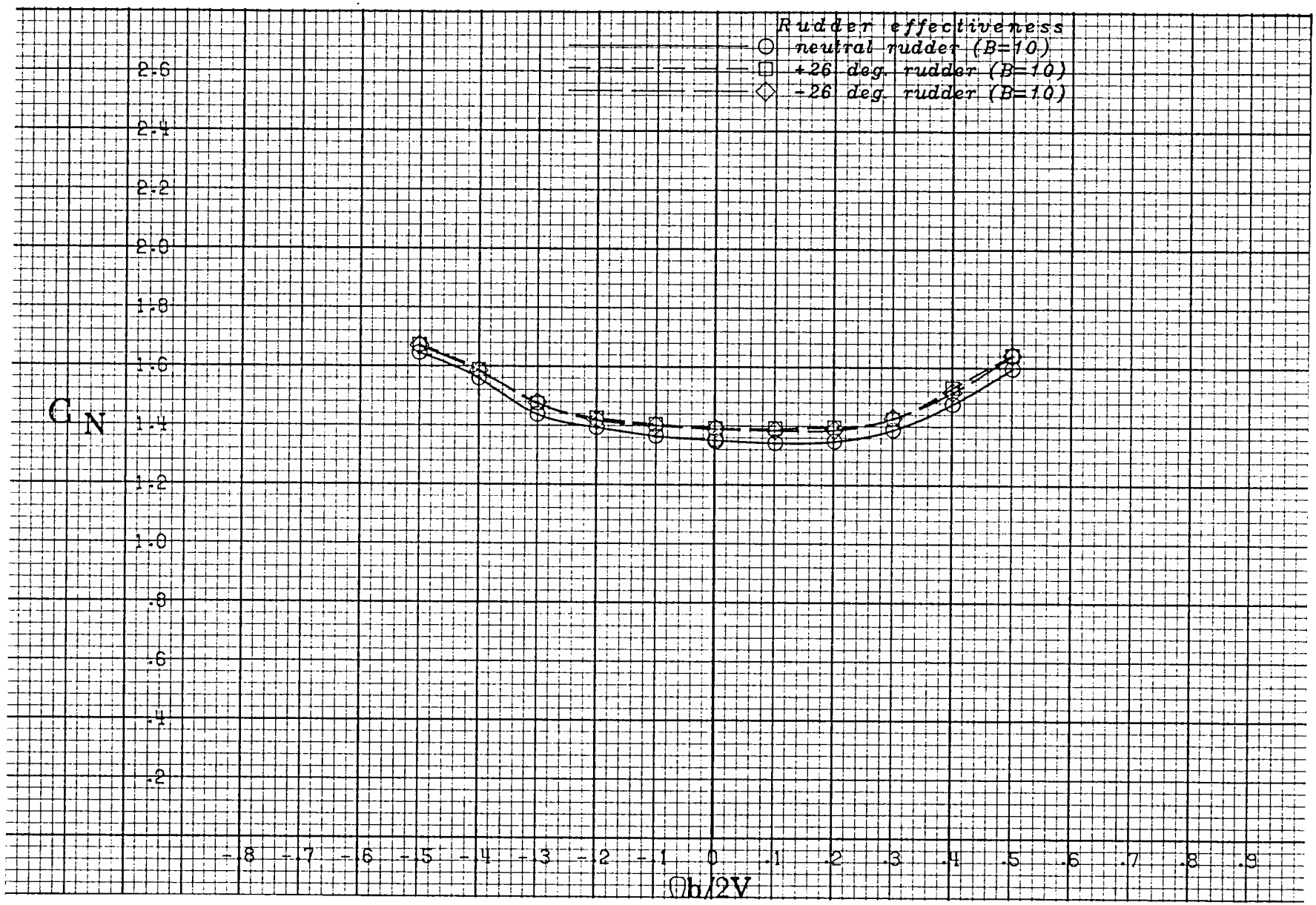

(g) α = 60 deg.

Figure A 16 .- Continued.

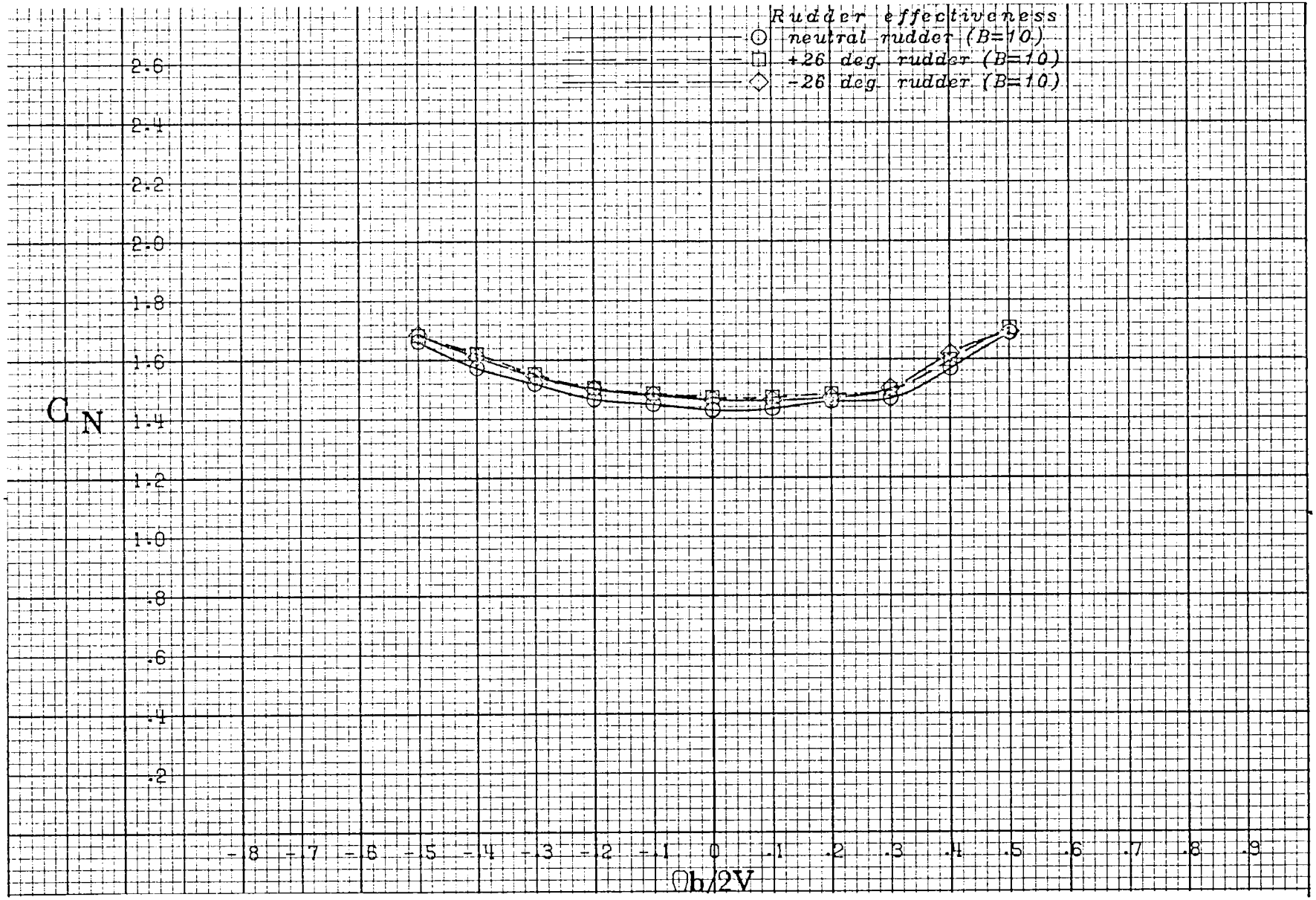

(h) α = 70 deg.

Figure A 16 .- Continued.

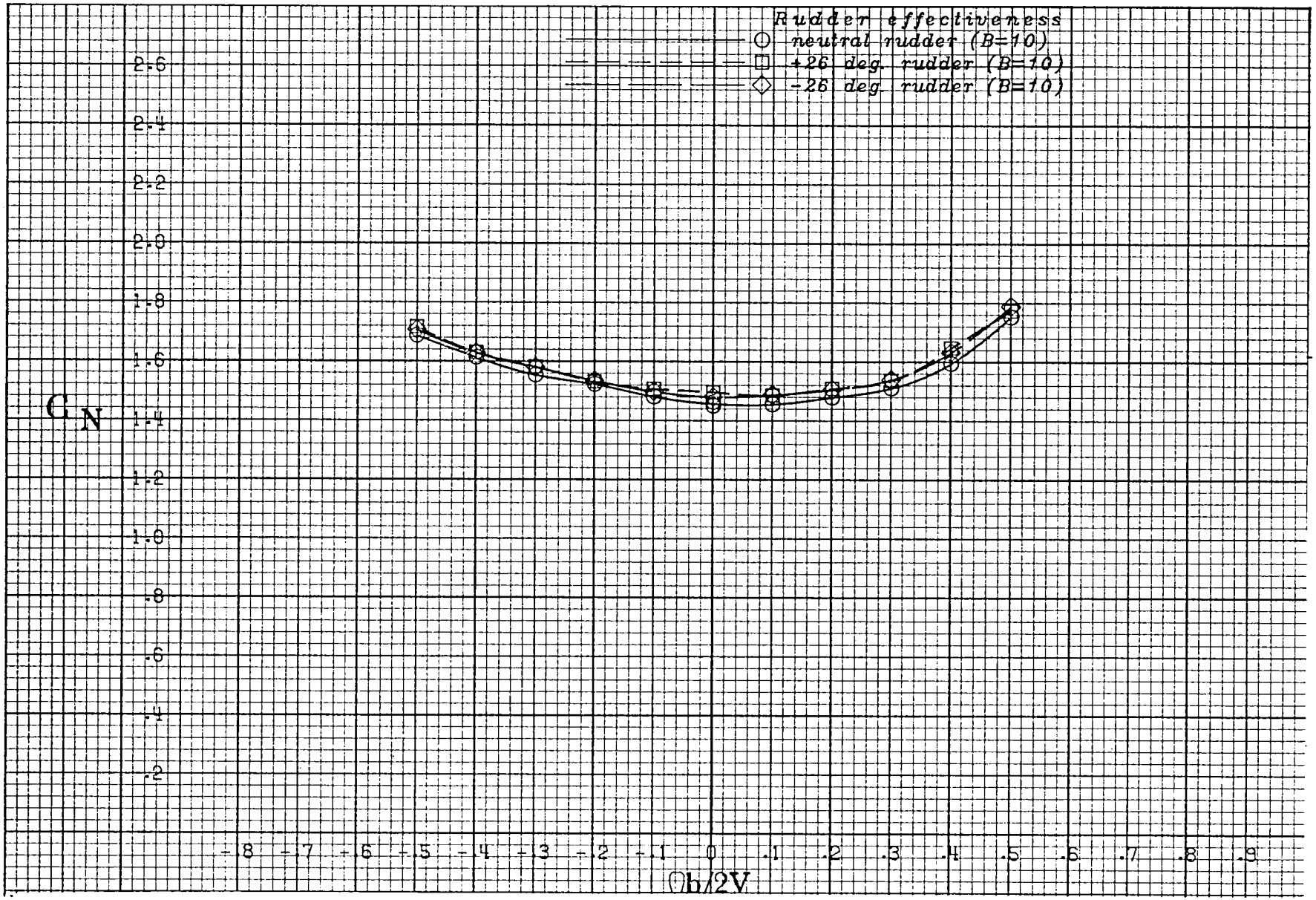

(i) α = 80 deg.

Figure A 16 .- Continued.

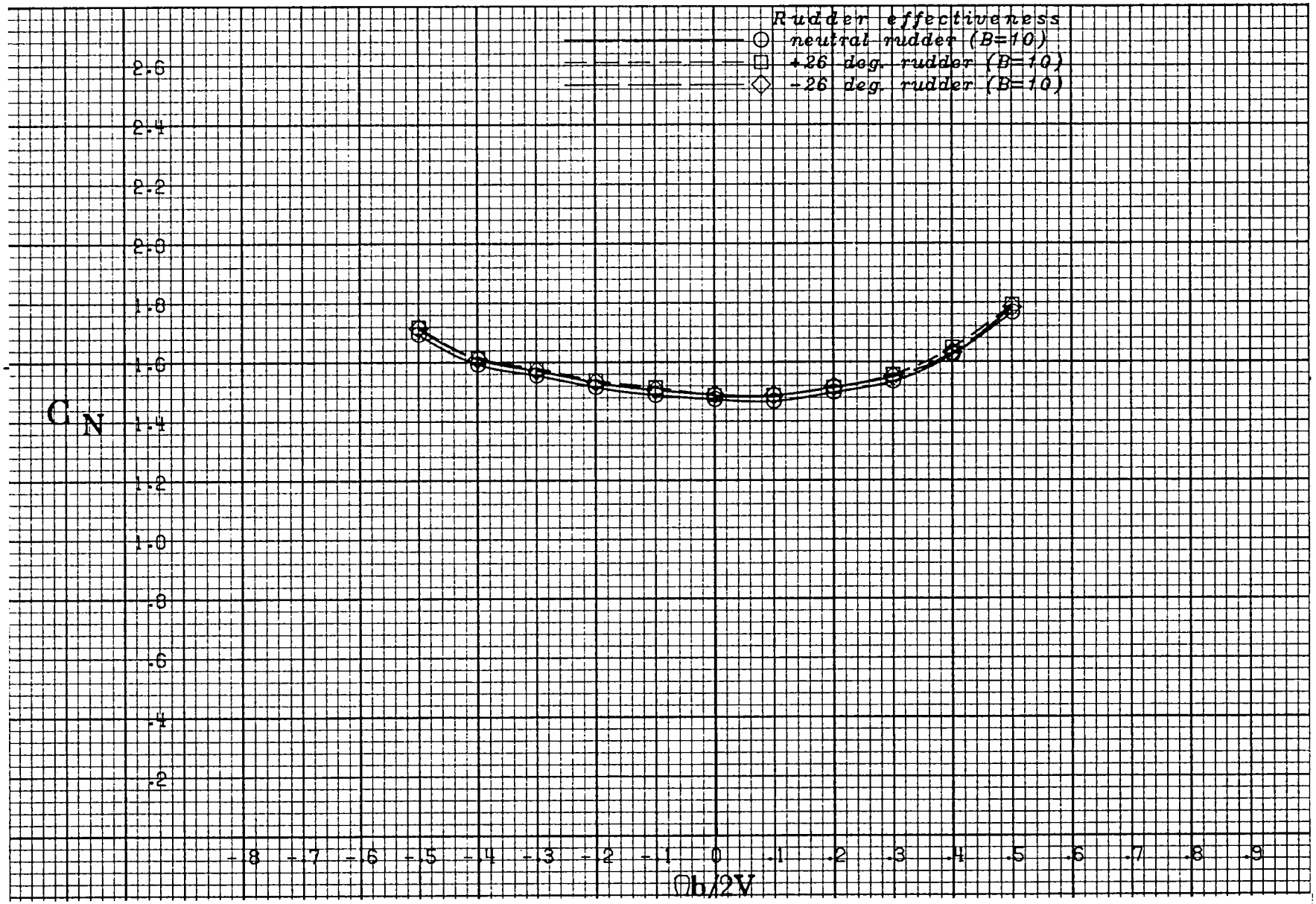

(j) α = 90 deg.

Figure A 16 .- Concluded.

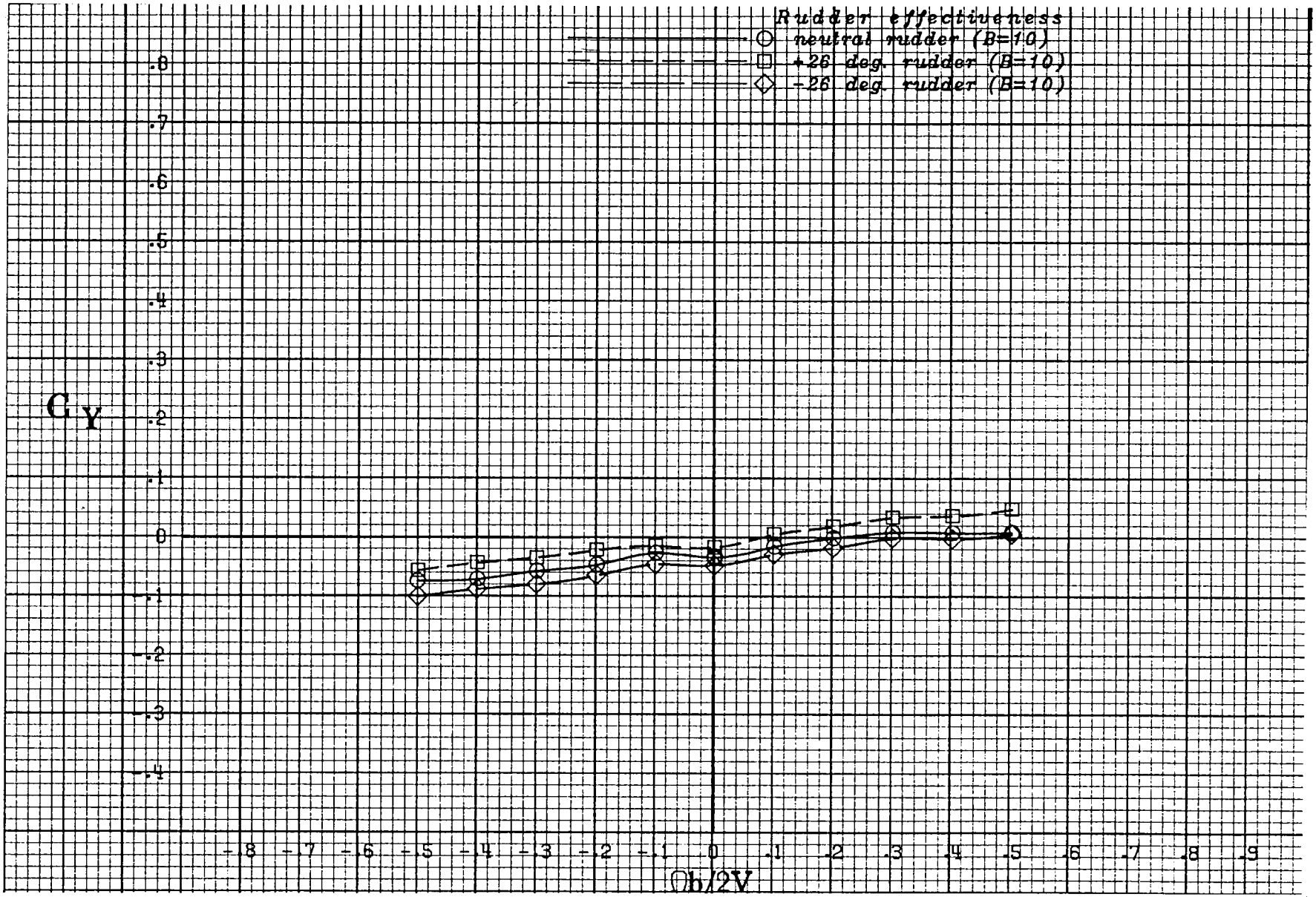

(a) α = 20 deg.

Figure A 17 .- Effect of rotation rate and rudder deflection on side-force coefficient for the basic configuration with neutral elevator and ailerons at +10 deg sideslip angle.

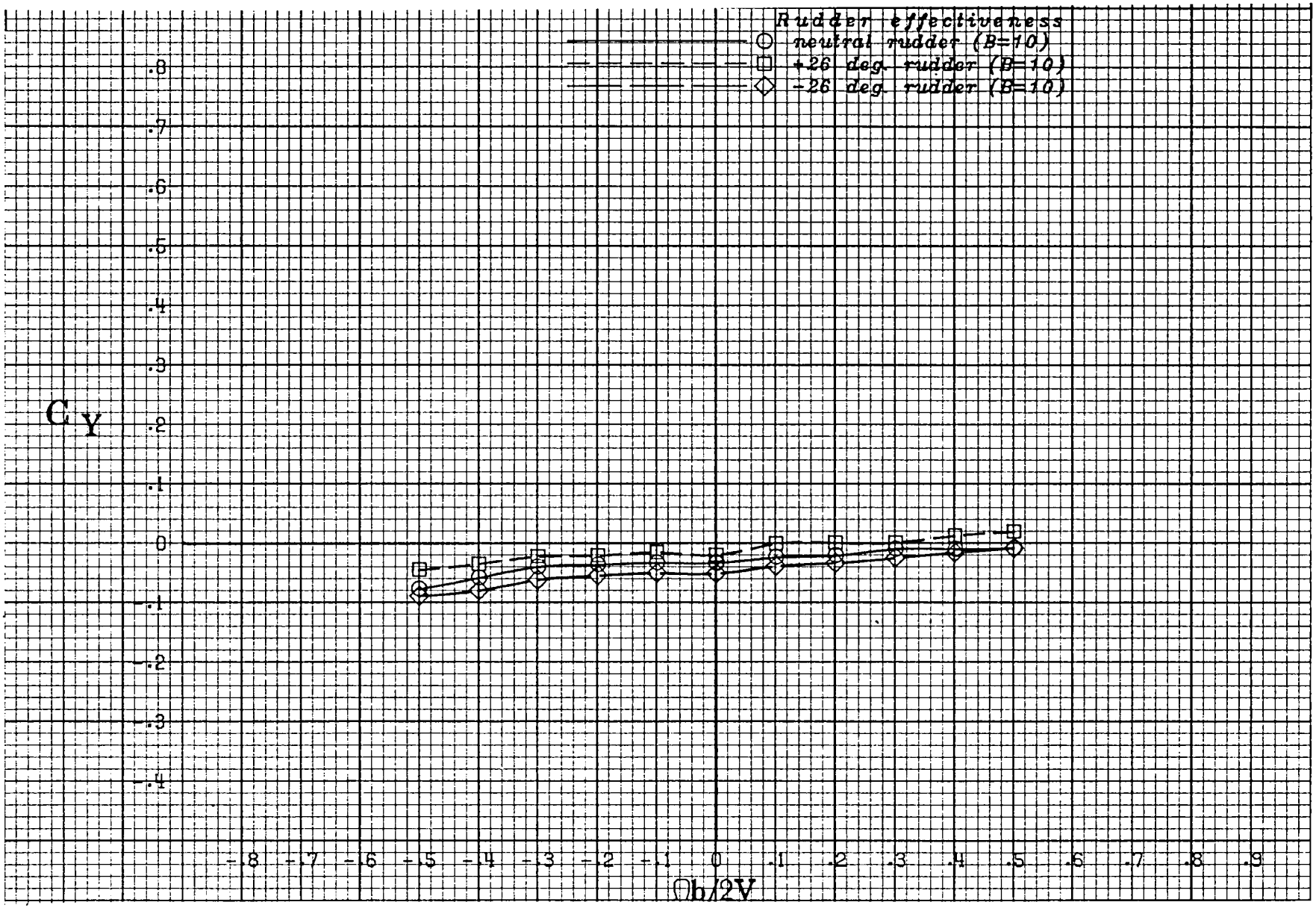

(b) α = 25 deg.

Figure A 17 .- Continued.

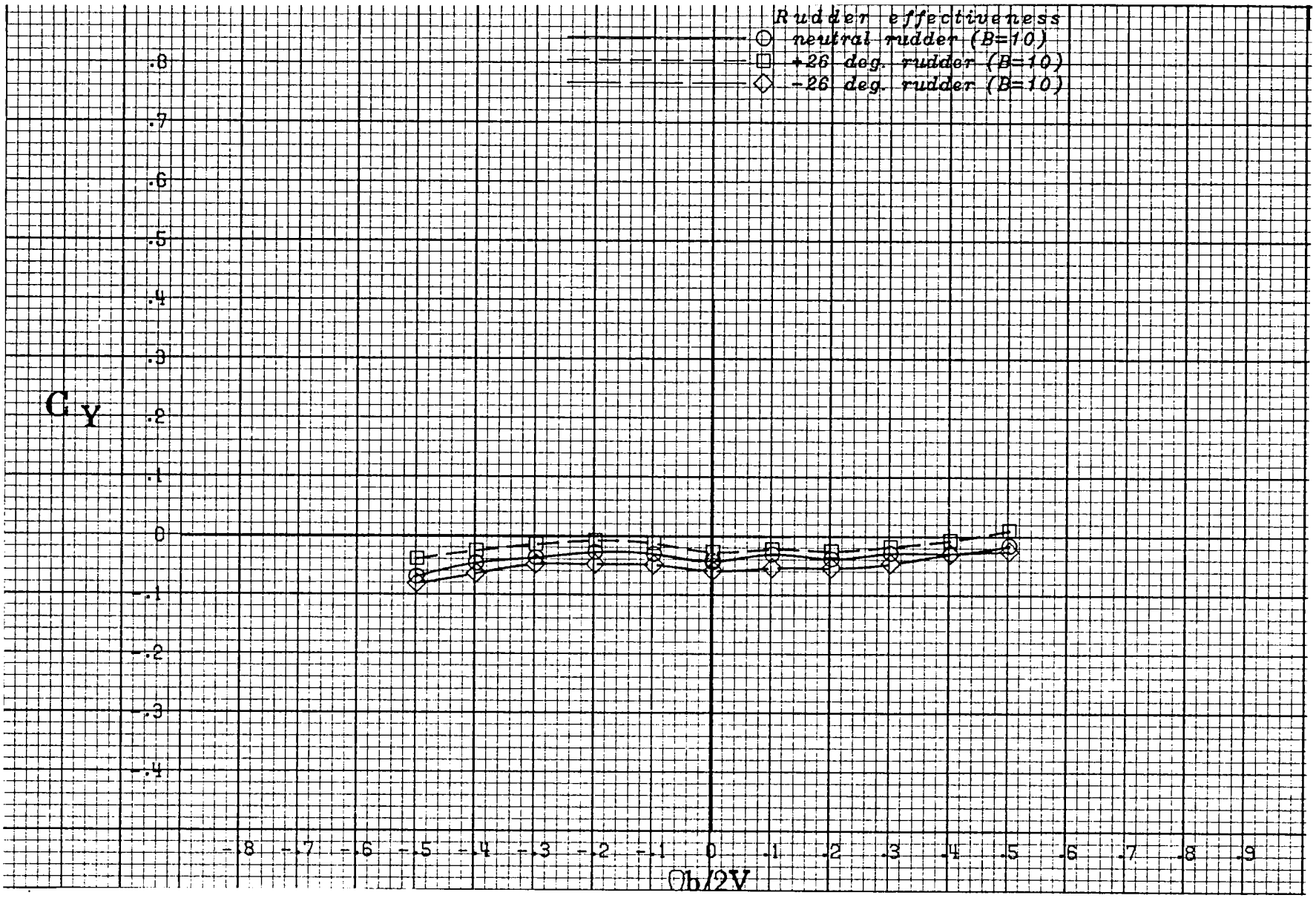

(c) α = 30 deg.

Figure A 17 .- Continued.

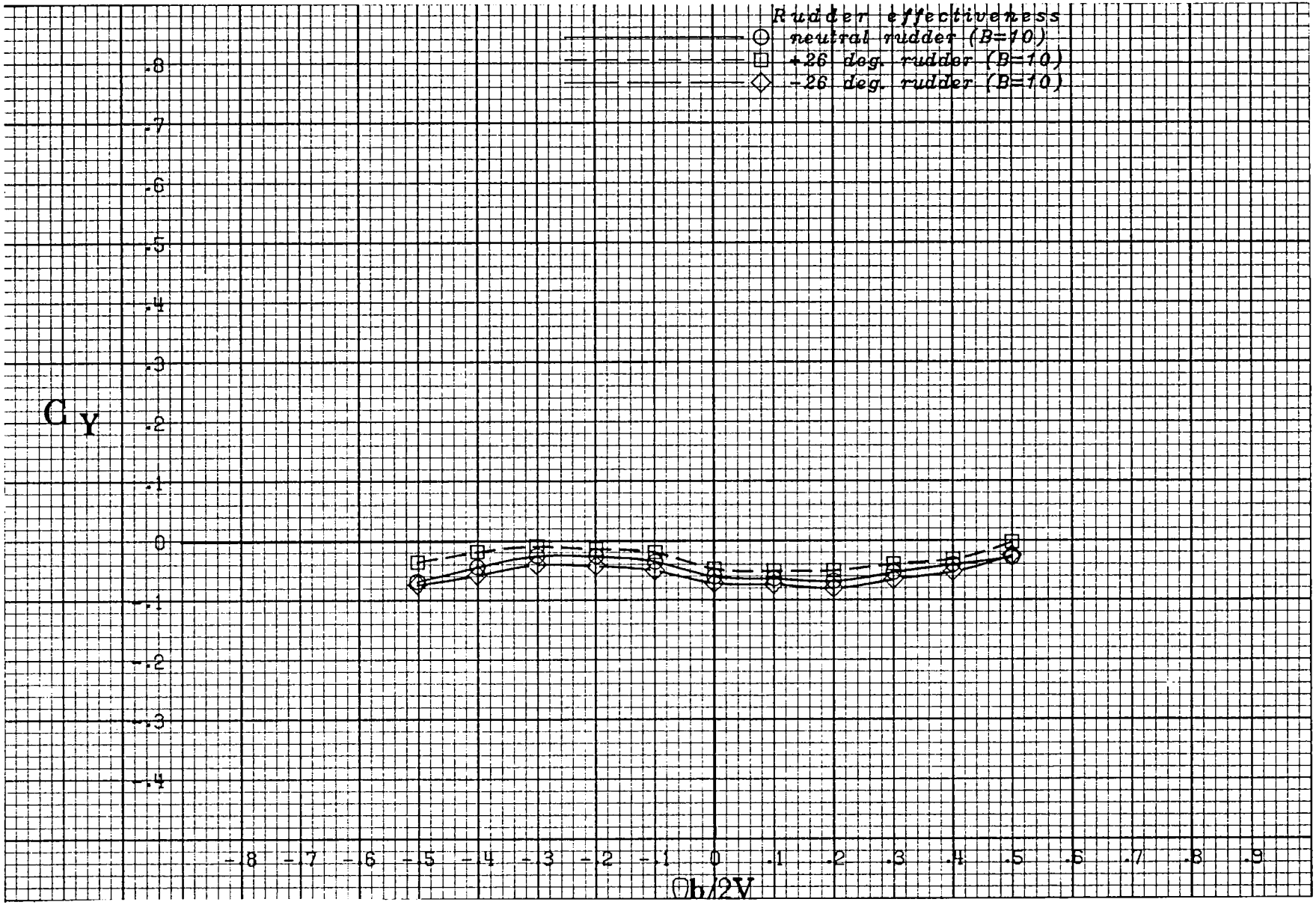

(d) α = 35 deg.

Figure A 17 .- Continued.

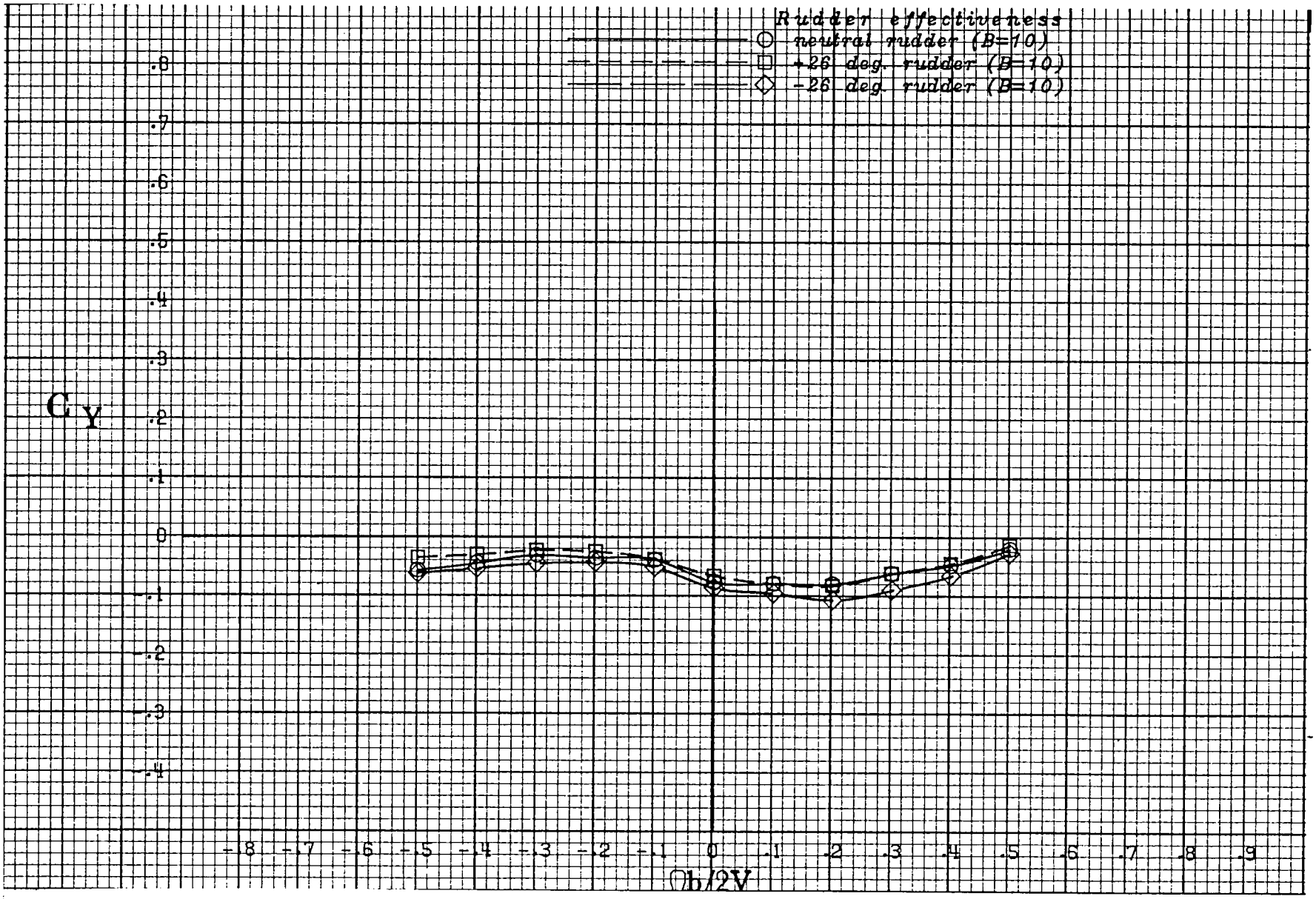

(e) α = 40 deg.

Figure A 17 .- Continued.

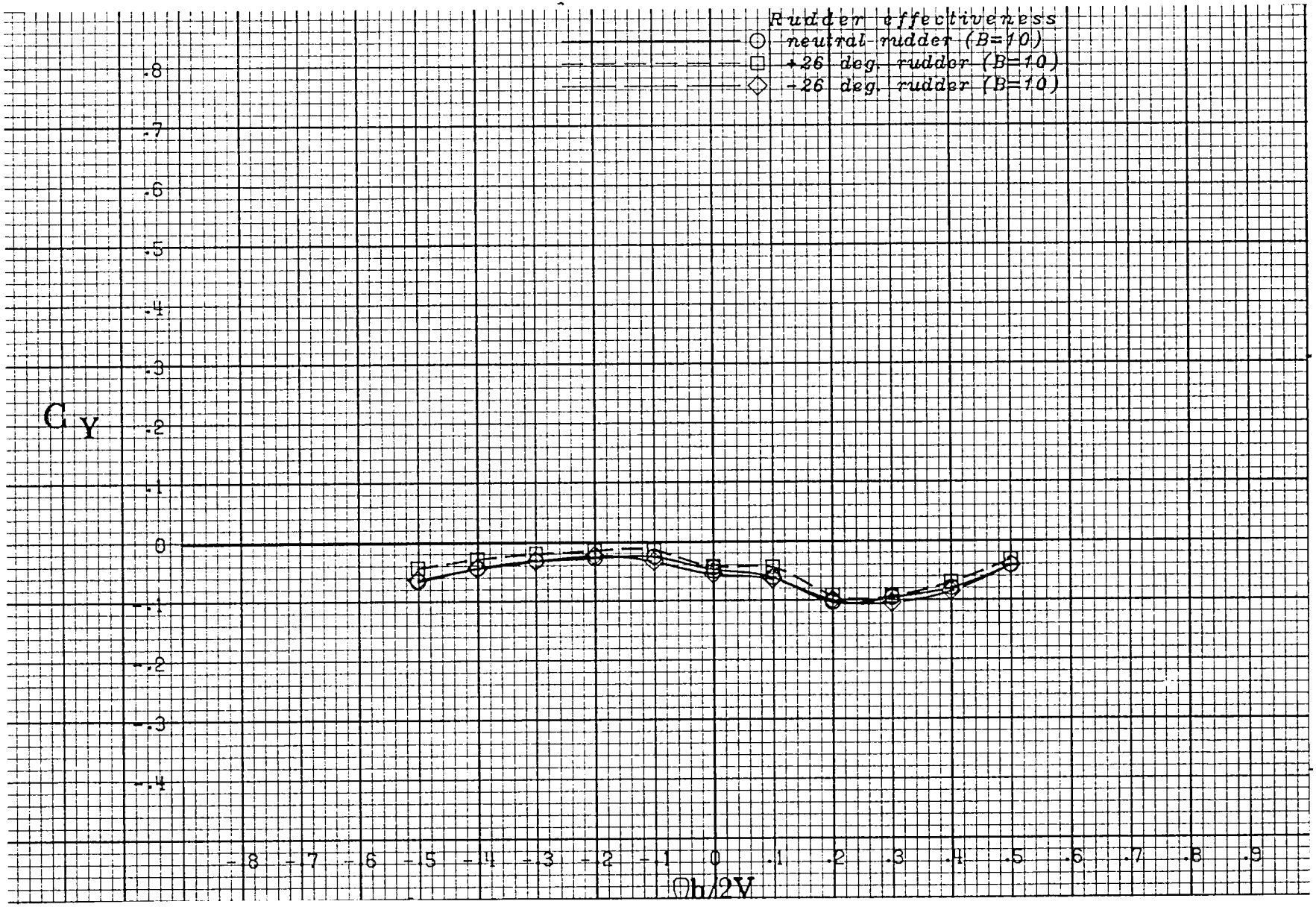

(f) α = 50 deg.

Figure A 17 .- Continued.

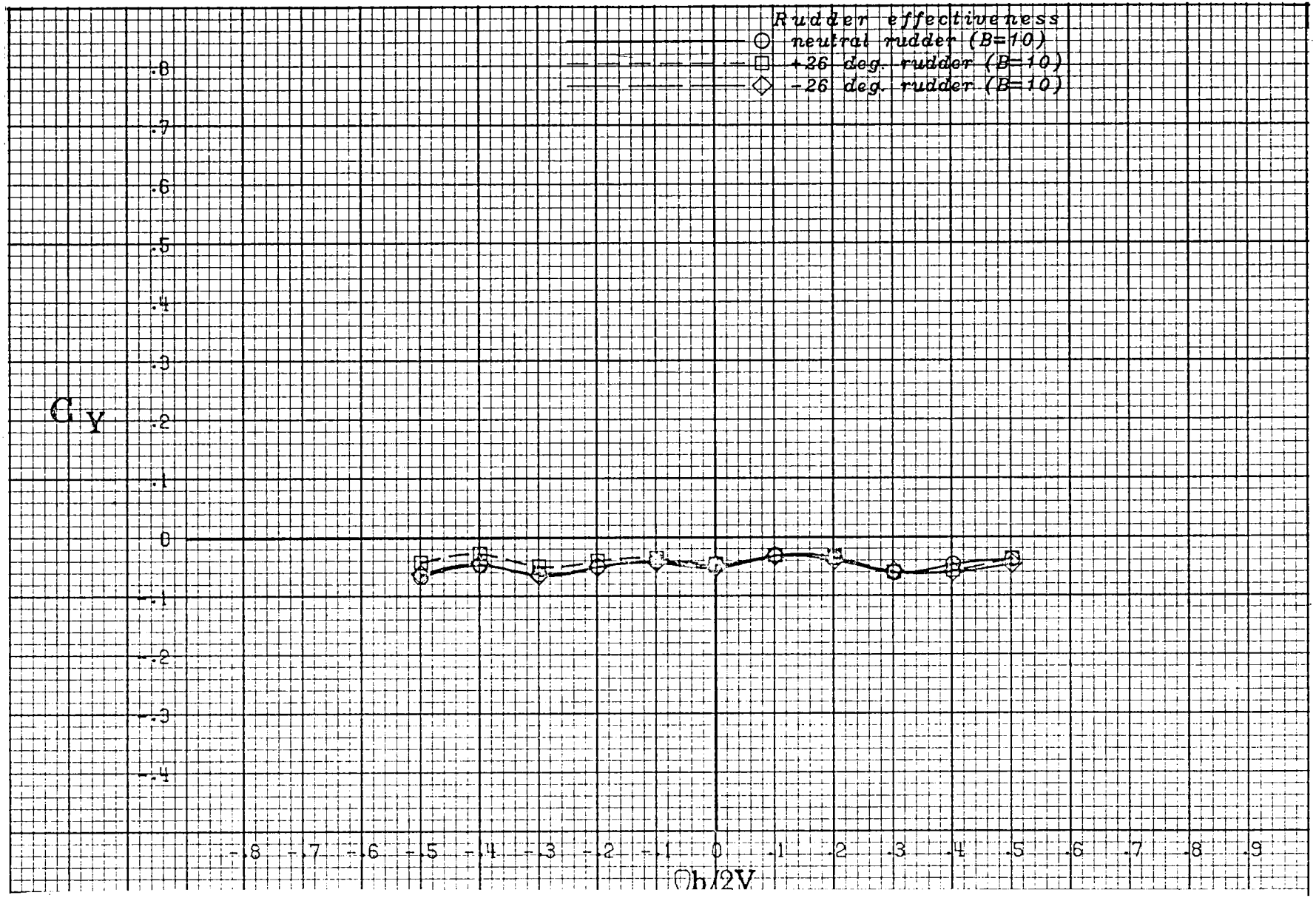

(g) α = 60 deg.

Figure A 17 .- Continued.

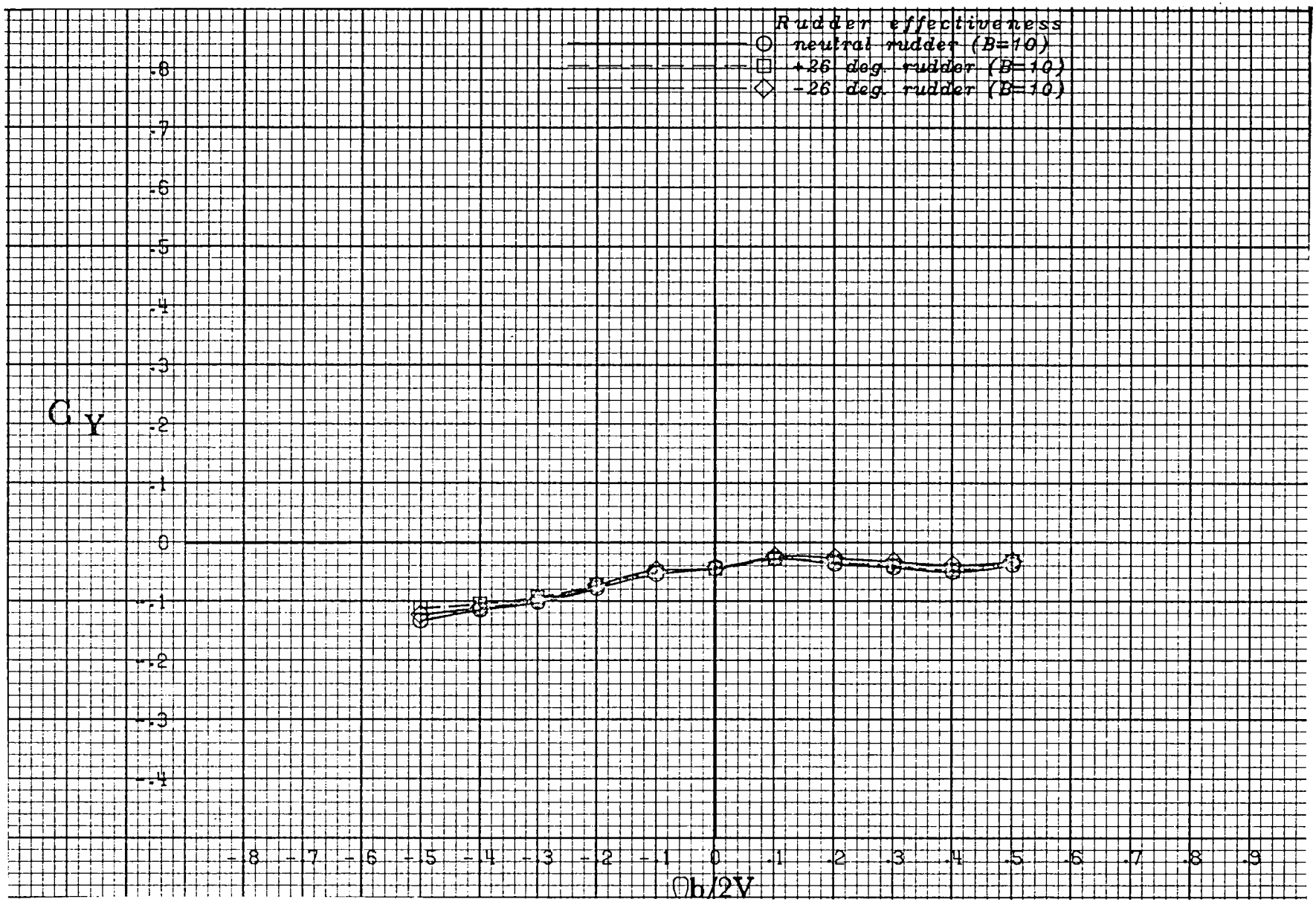

(h) α = 70 deg.

Figure A 17 .- Continued.

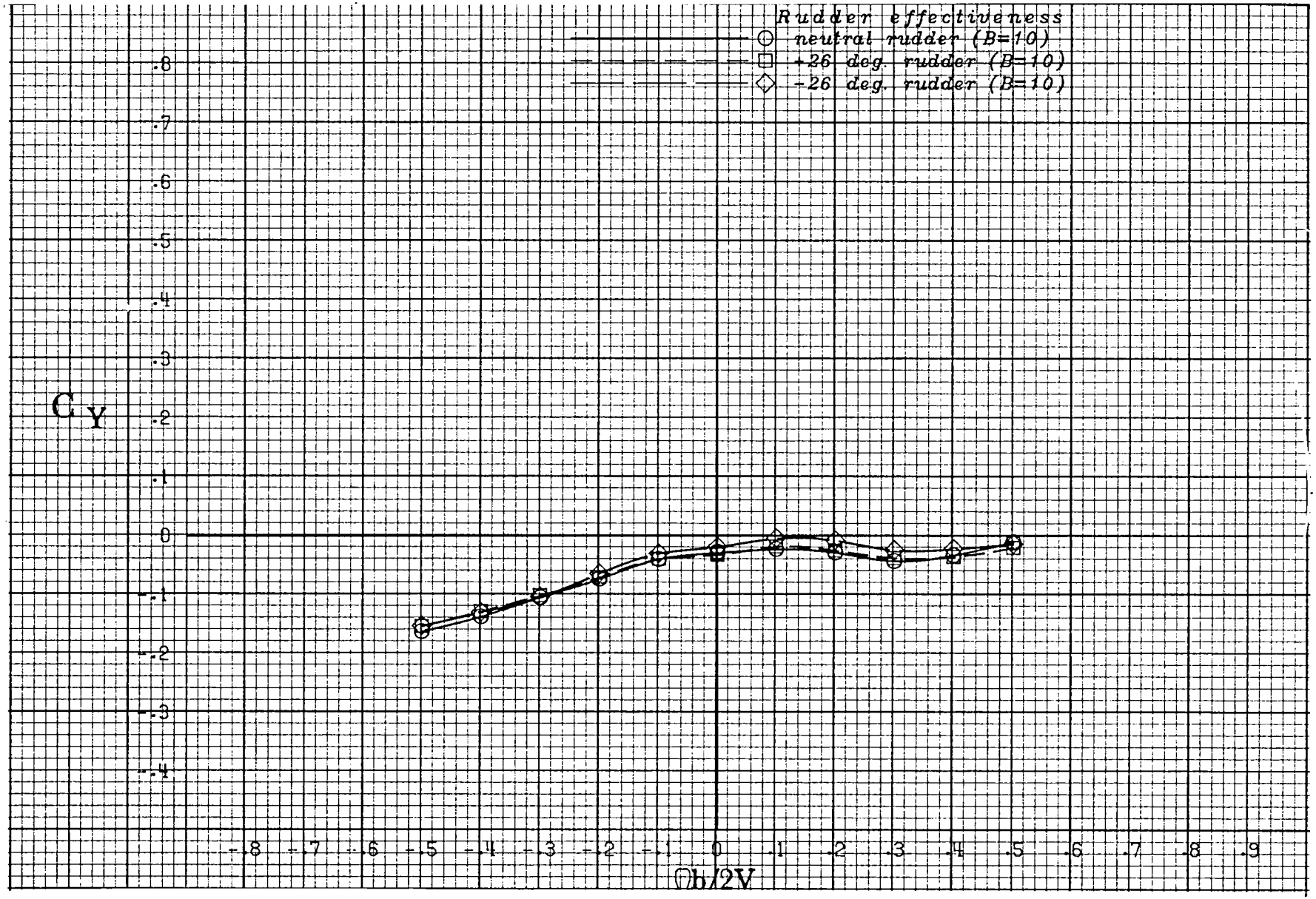

(i) α = 80 deg.

Figure A 17 .- Continued.

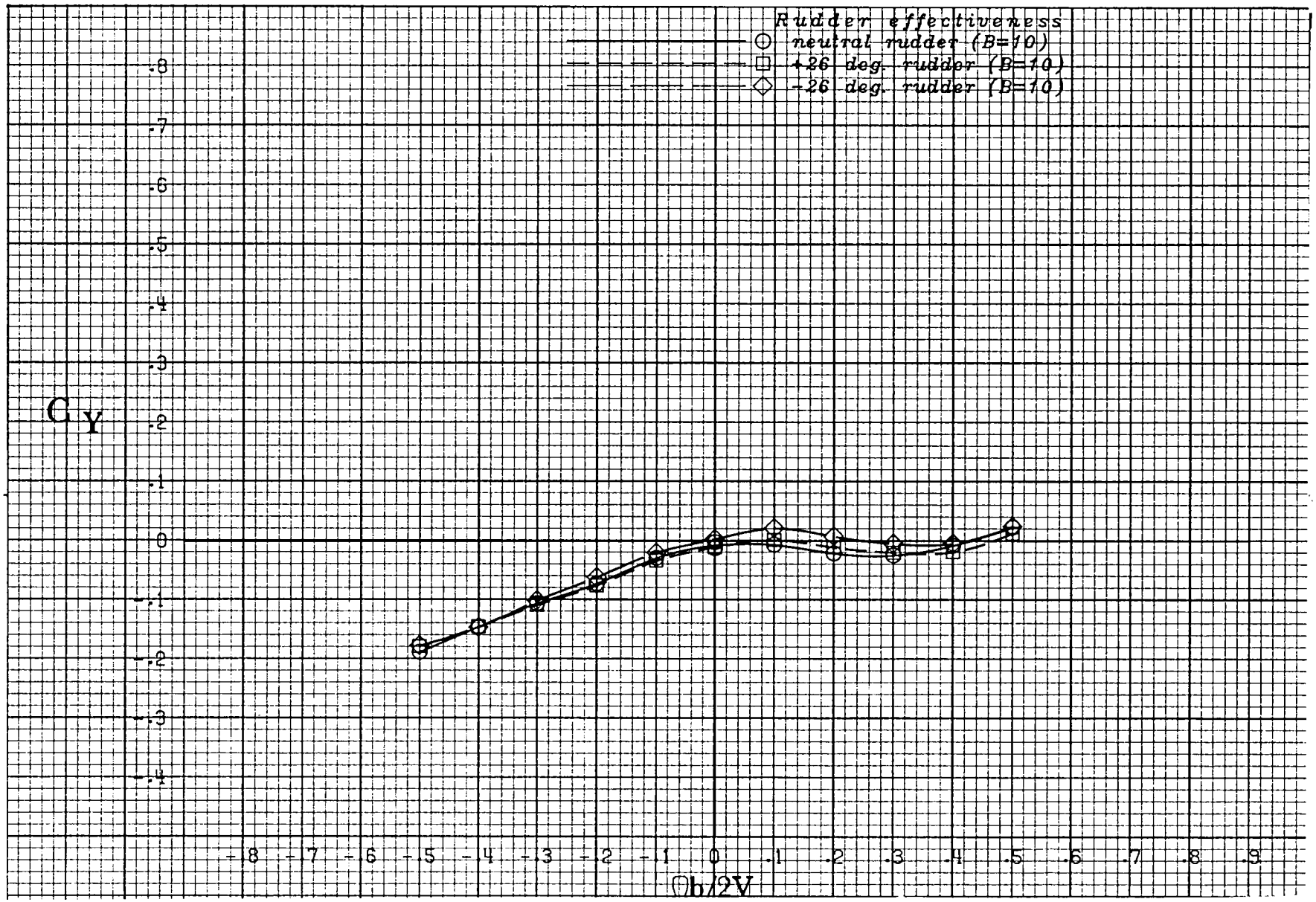

(j) α = 90 deg.

Figure A 17 .- Concluded.

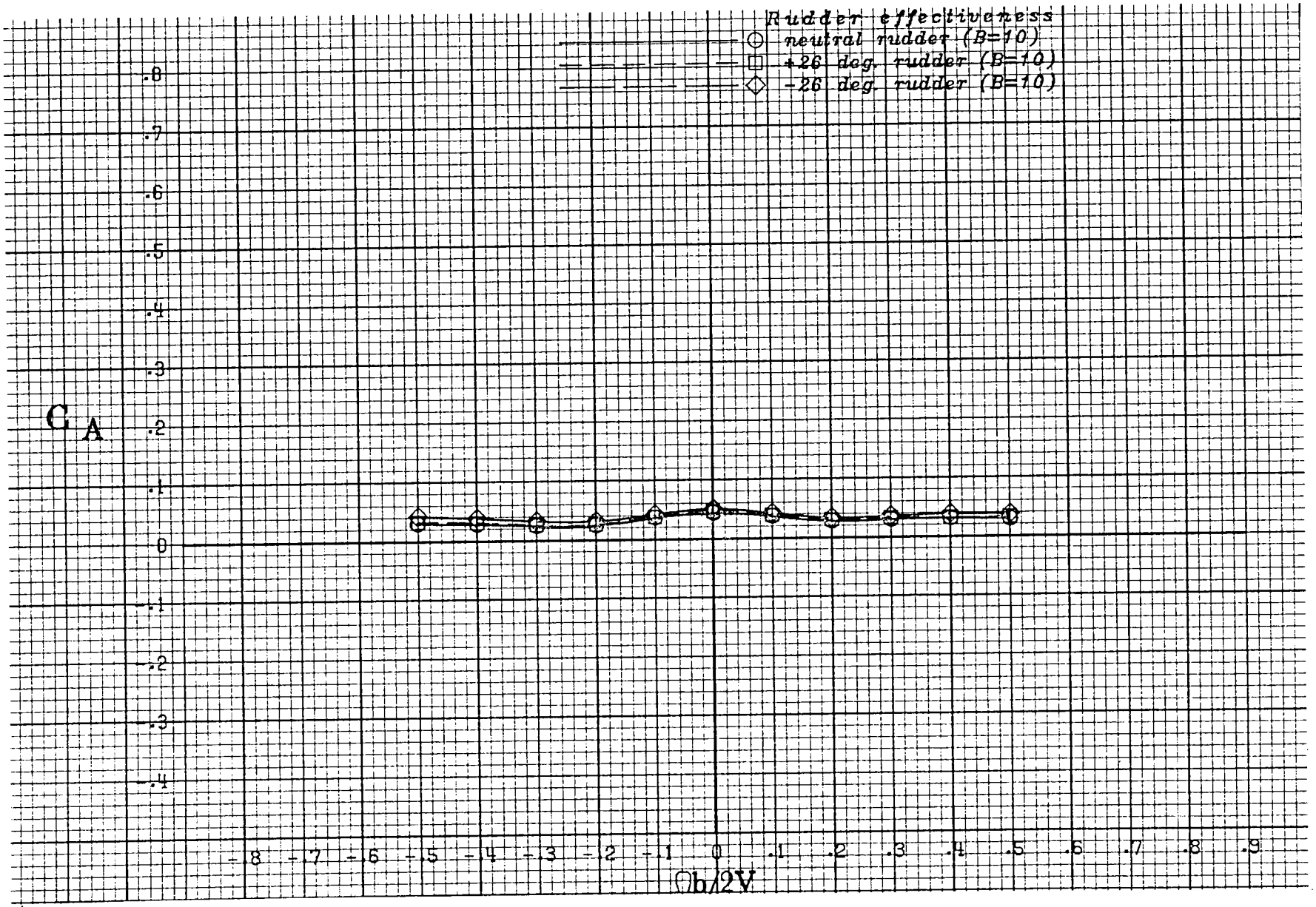

(a) α = 20 deg.

Figure A 18 .- Effect of rotation rate and rudder deflection on axial-force coefficient for the basic configuration with neutral elevator and ailerons at +10 deg sideslip angle.

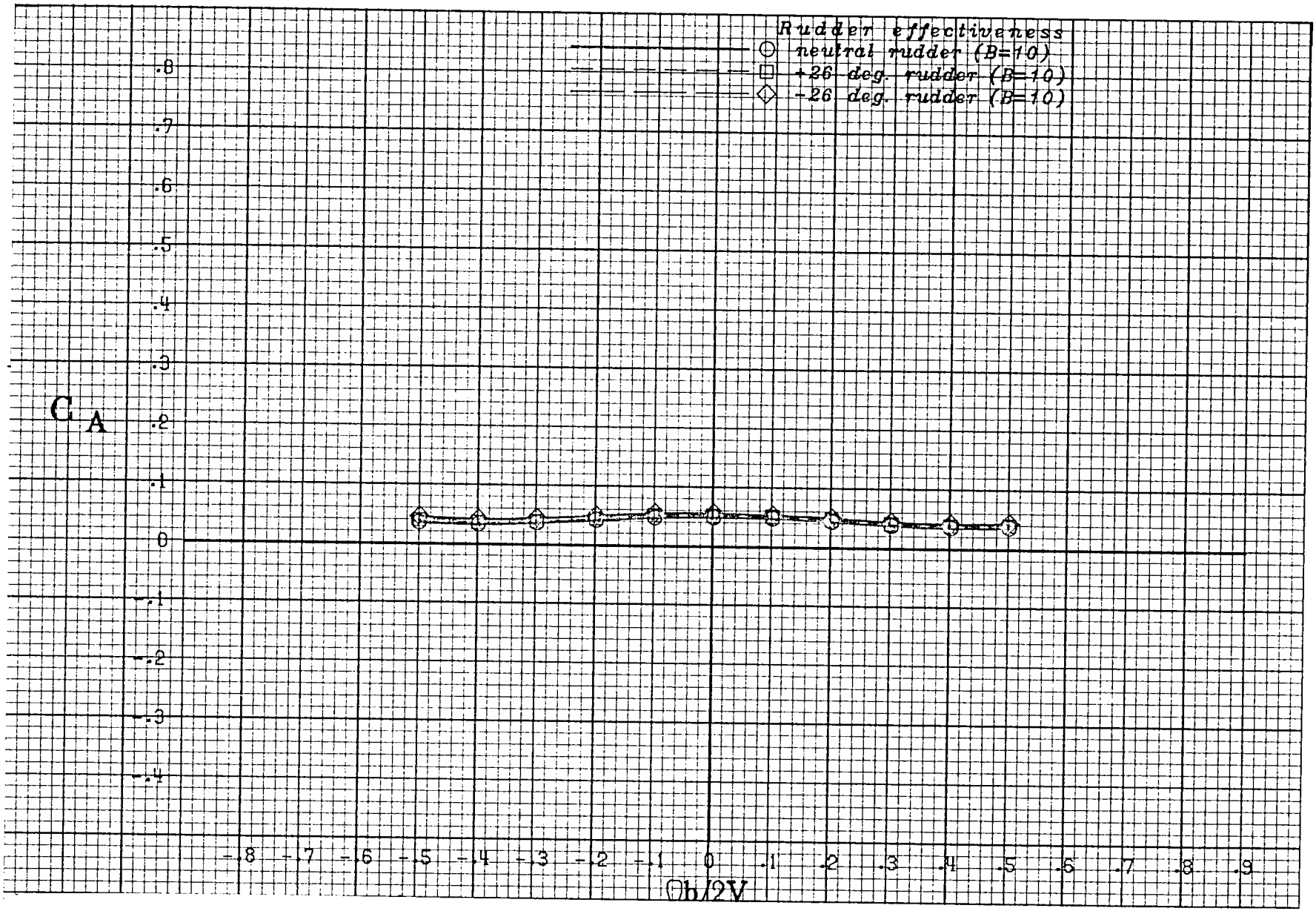

(b) α = 25 deg.

Figure A 18 .- Continued.

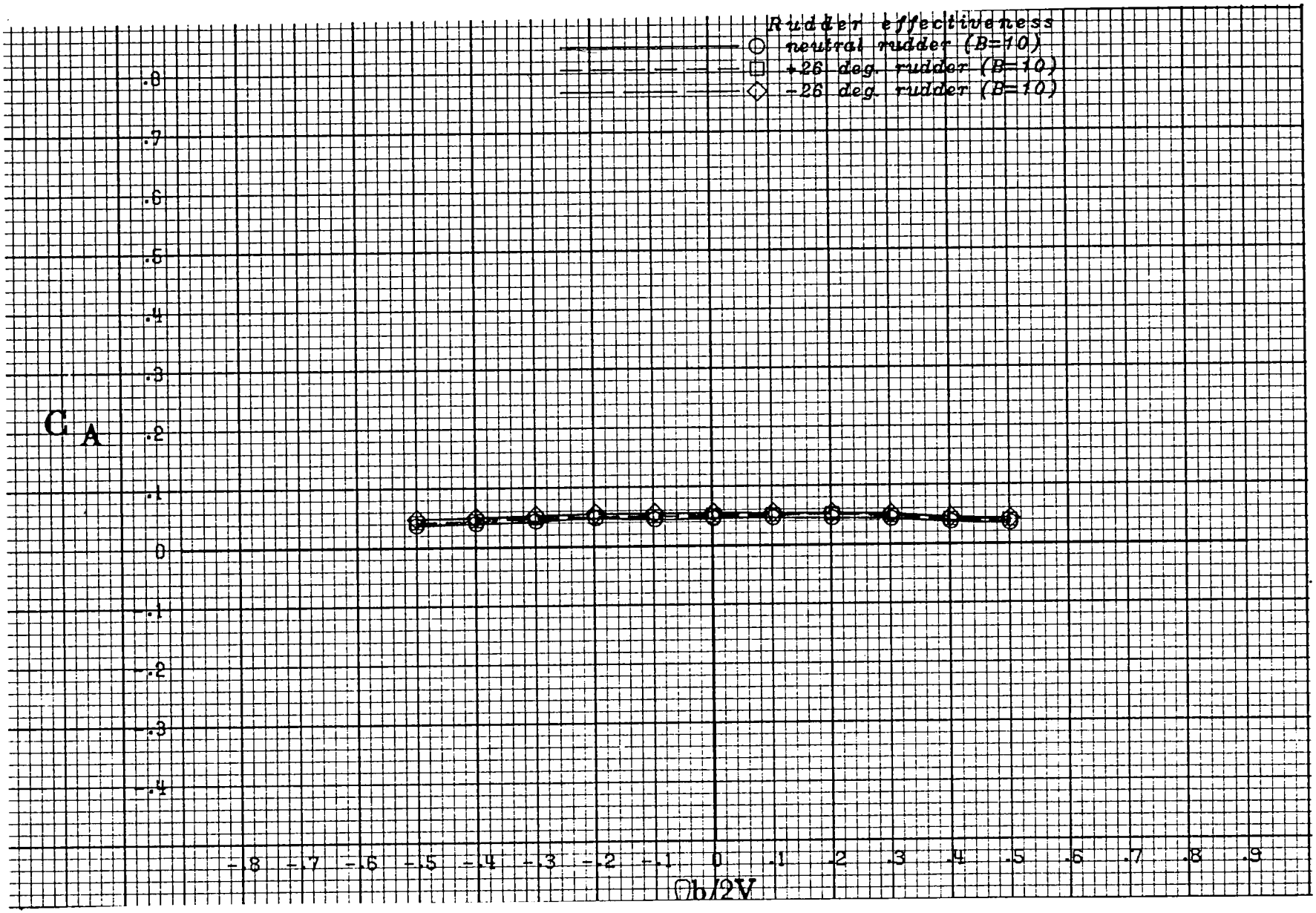

(c) α = 30 deg.

Figure A 18 .- Continued.

(d) α = 35 deg.

Figure A 18 .- Continued.

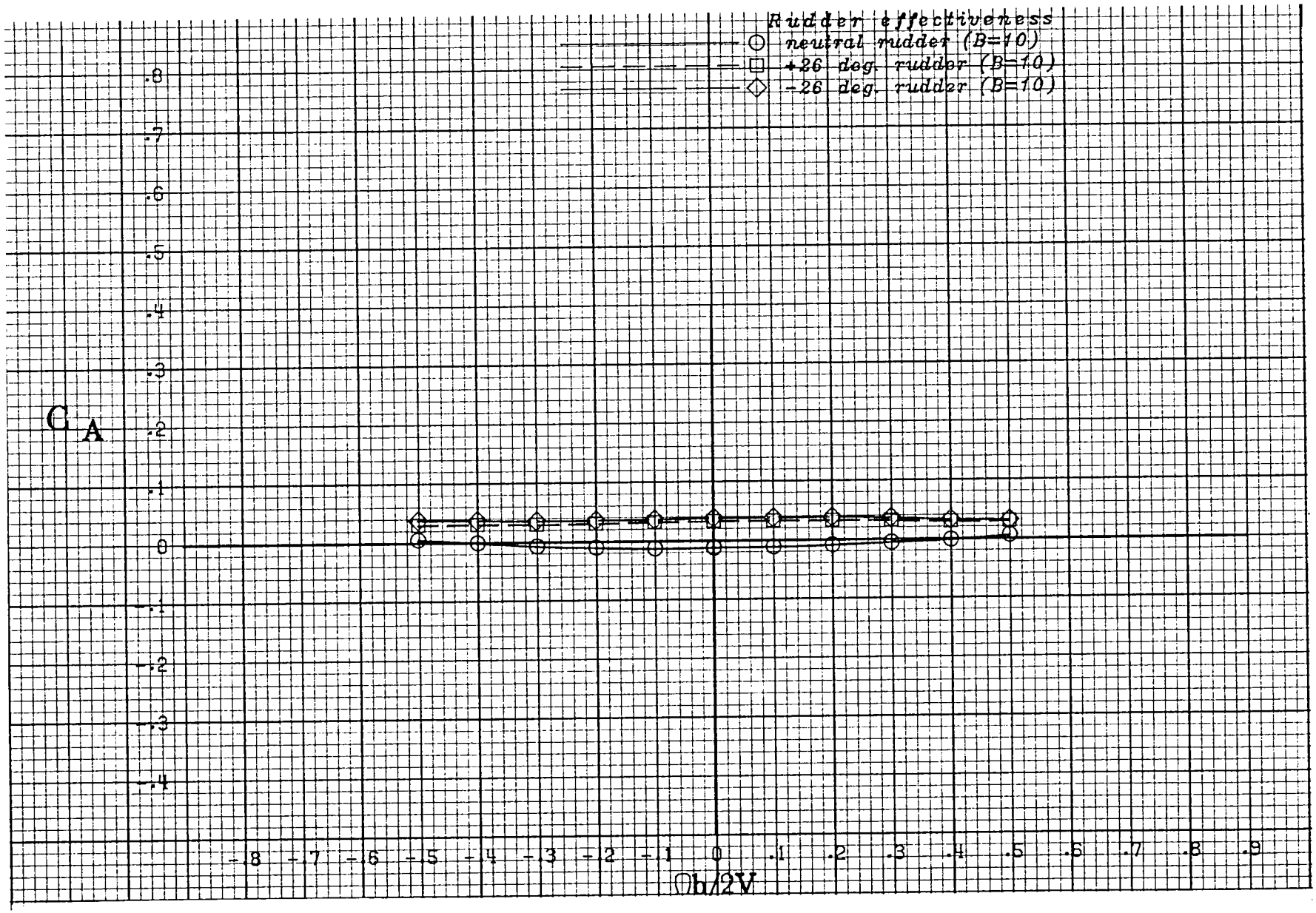

(e) α = 40 deg.

Figure A 18 .- Continued.

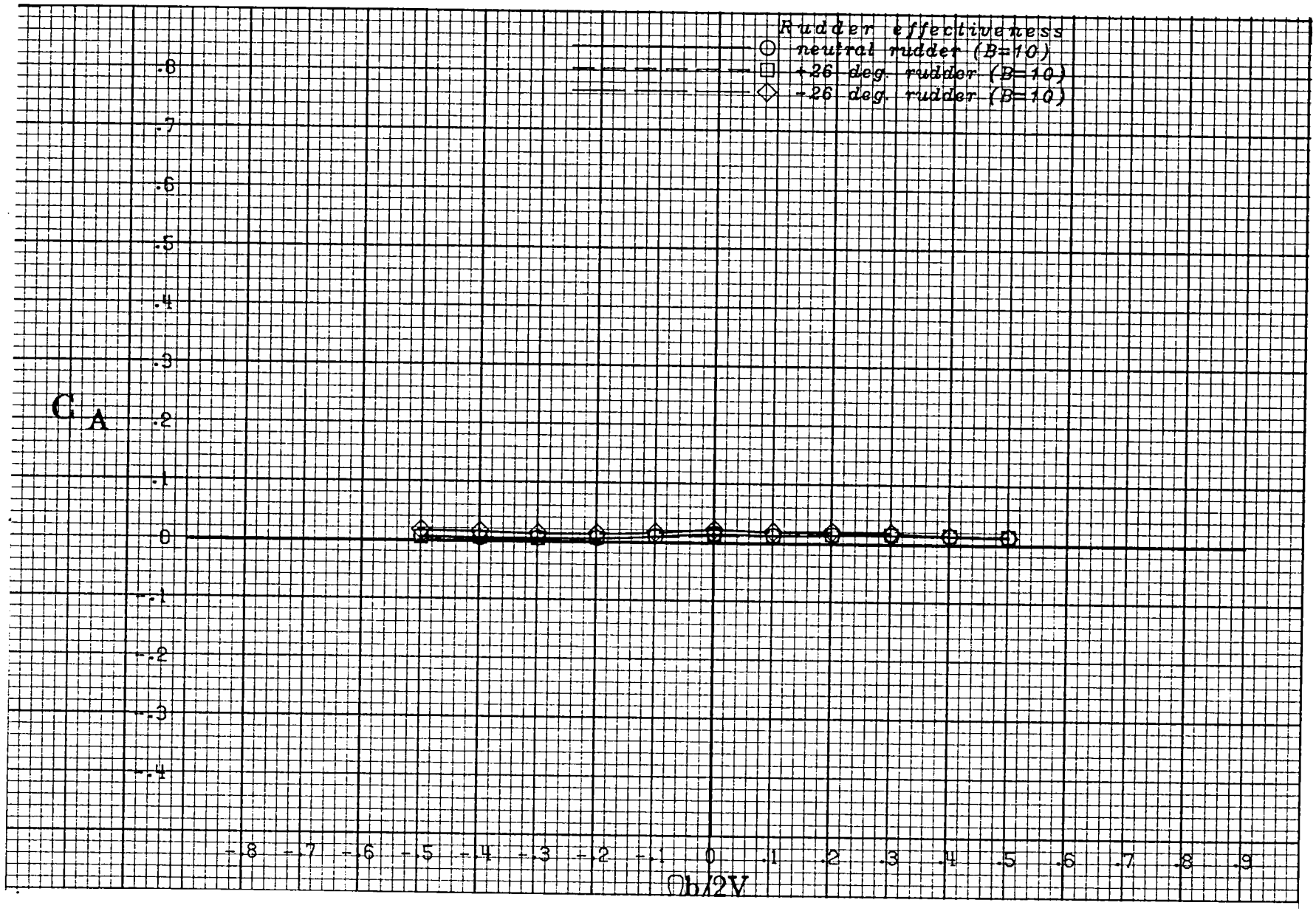

(f) α = 50 deg.

Figure A 18 .- Continued.

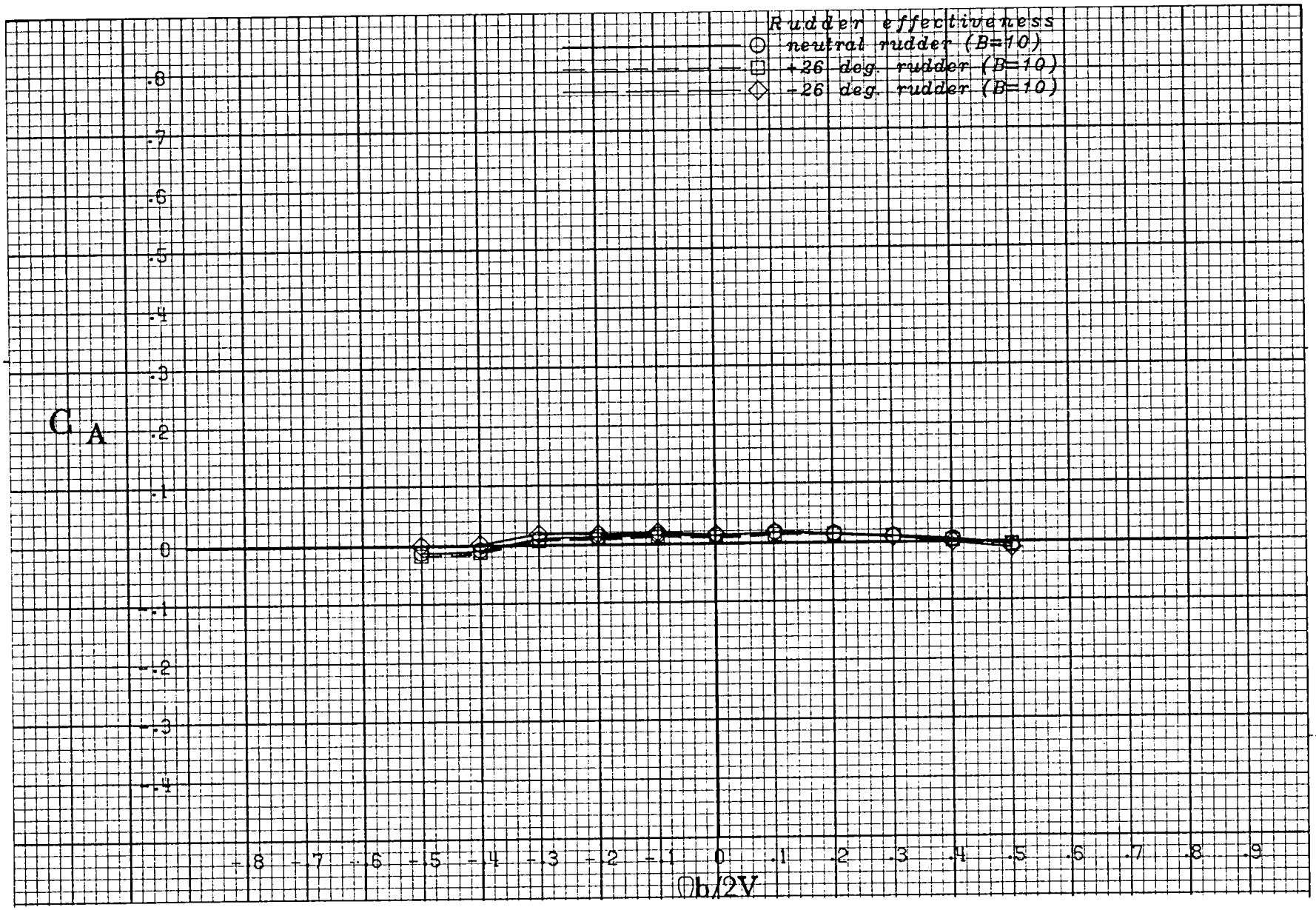

(g) α = 60 deg.

Figure A 18 .- Continued.

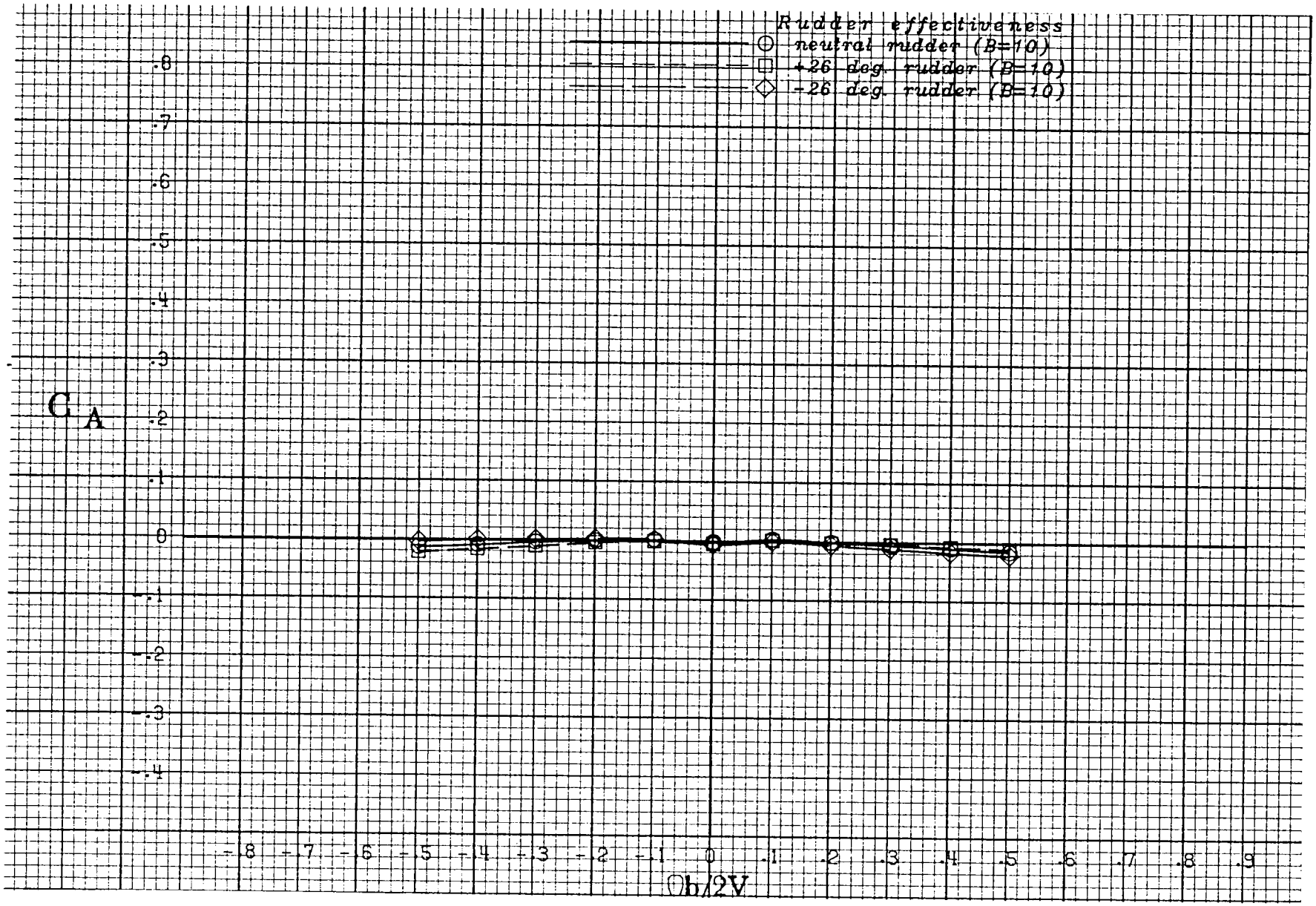

(h) α = 70 deg.

Figure A 18 .- Continued.

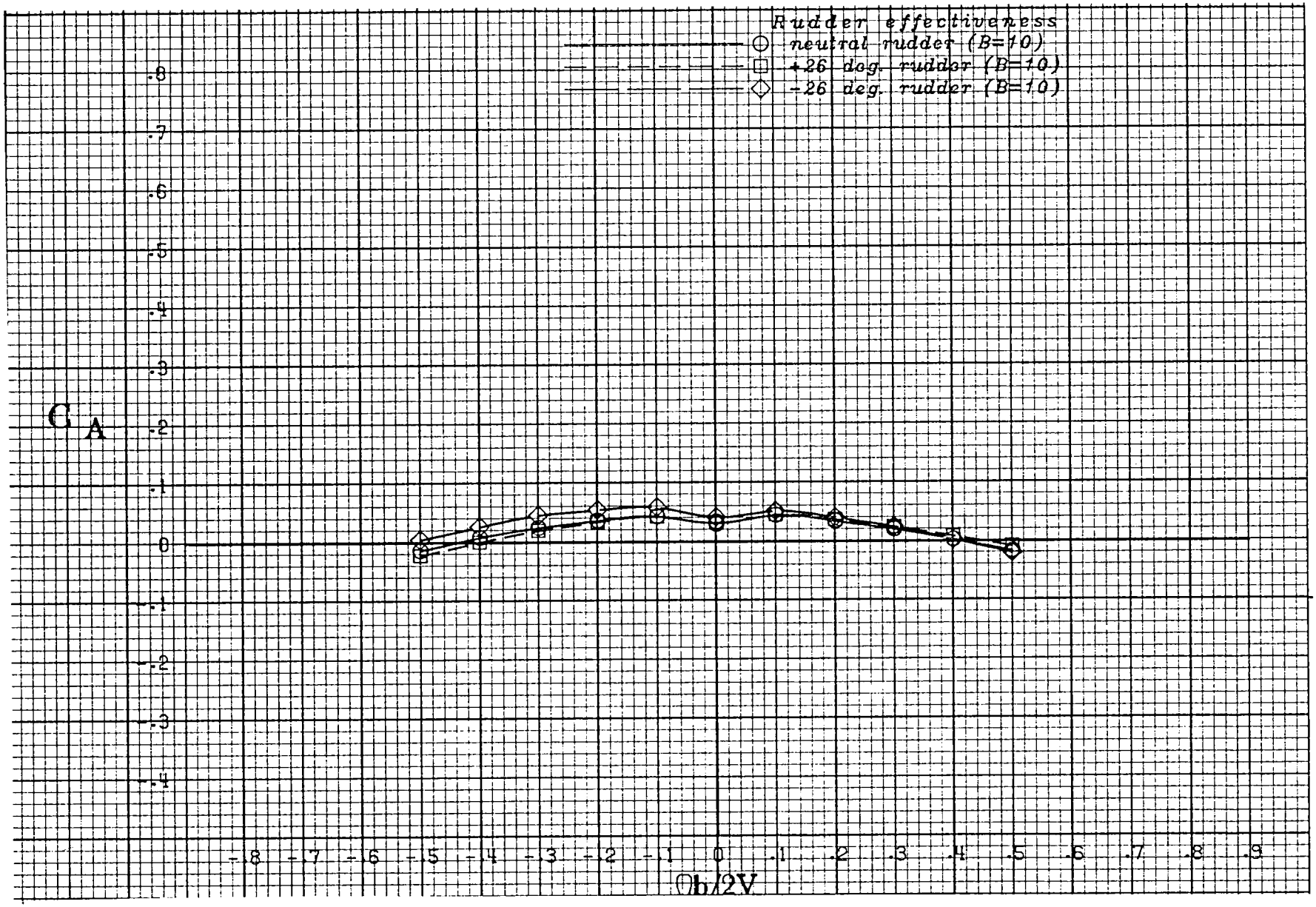

(i) α = 80 deg.

Figure A 18 .- Continued.

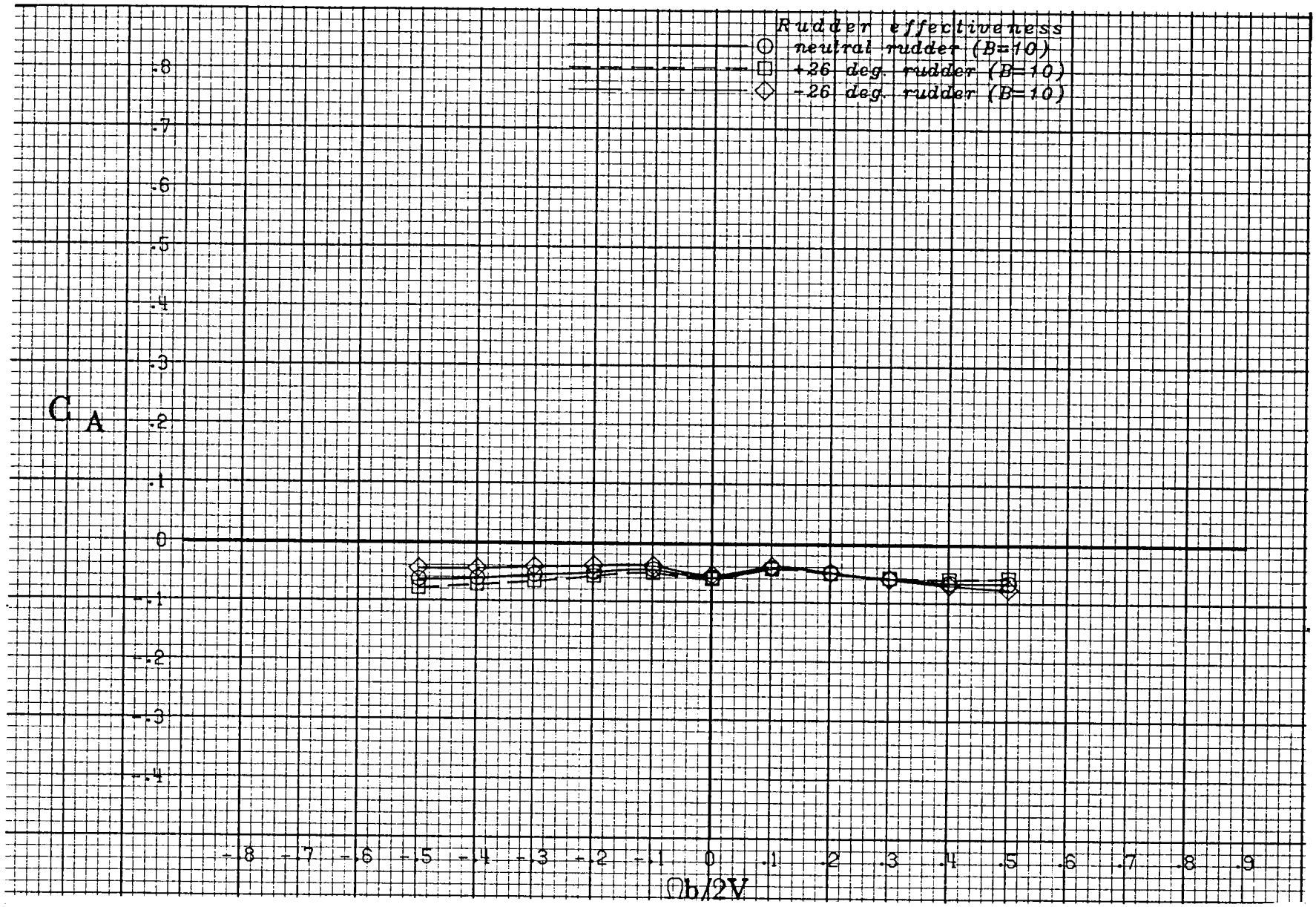

(j) α = 90 deg.

Figure A 18 .- Concluded.

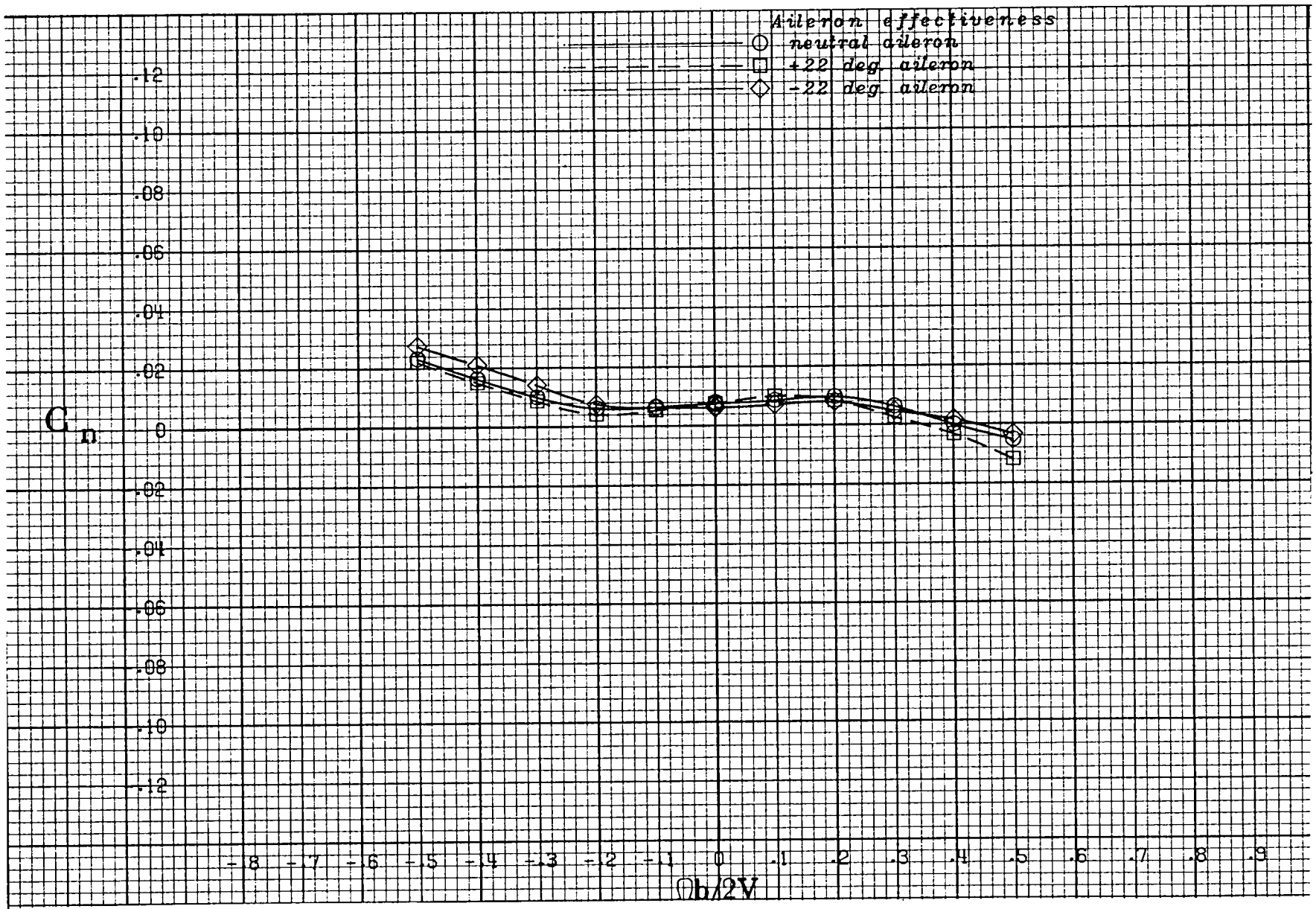

(a) α = 20 deg.

Figure A 19 .- Effect of rotation rate and aileron deflection on yawing-moment coefficient for the basic configuration with -10 deg elevator and -26 deg rudder at zero sideslip angle.

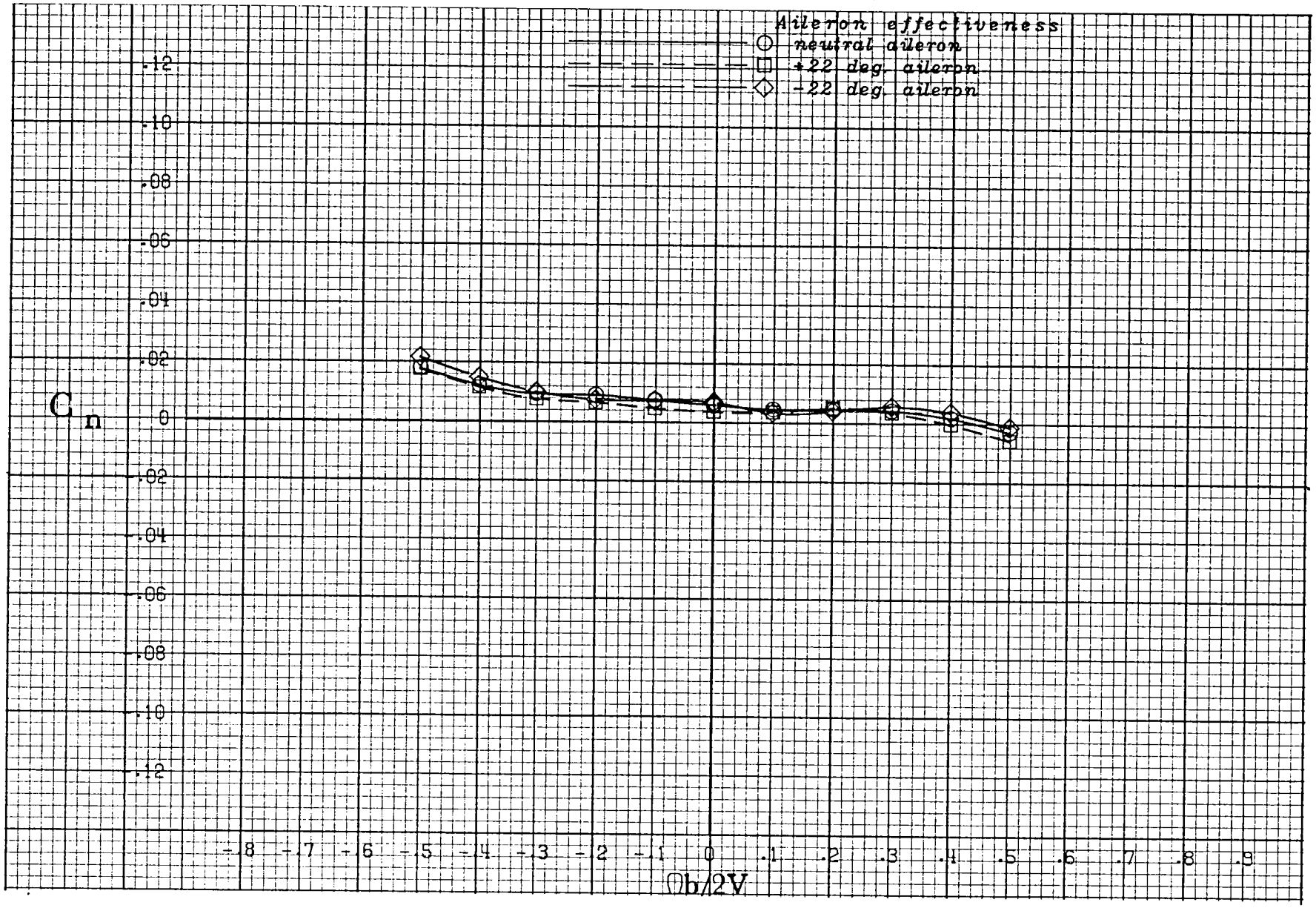

(b) α = 25 deg.

Figure A 19 .- Continued.

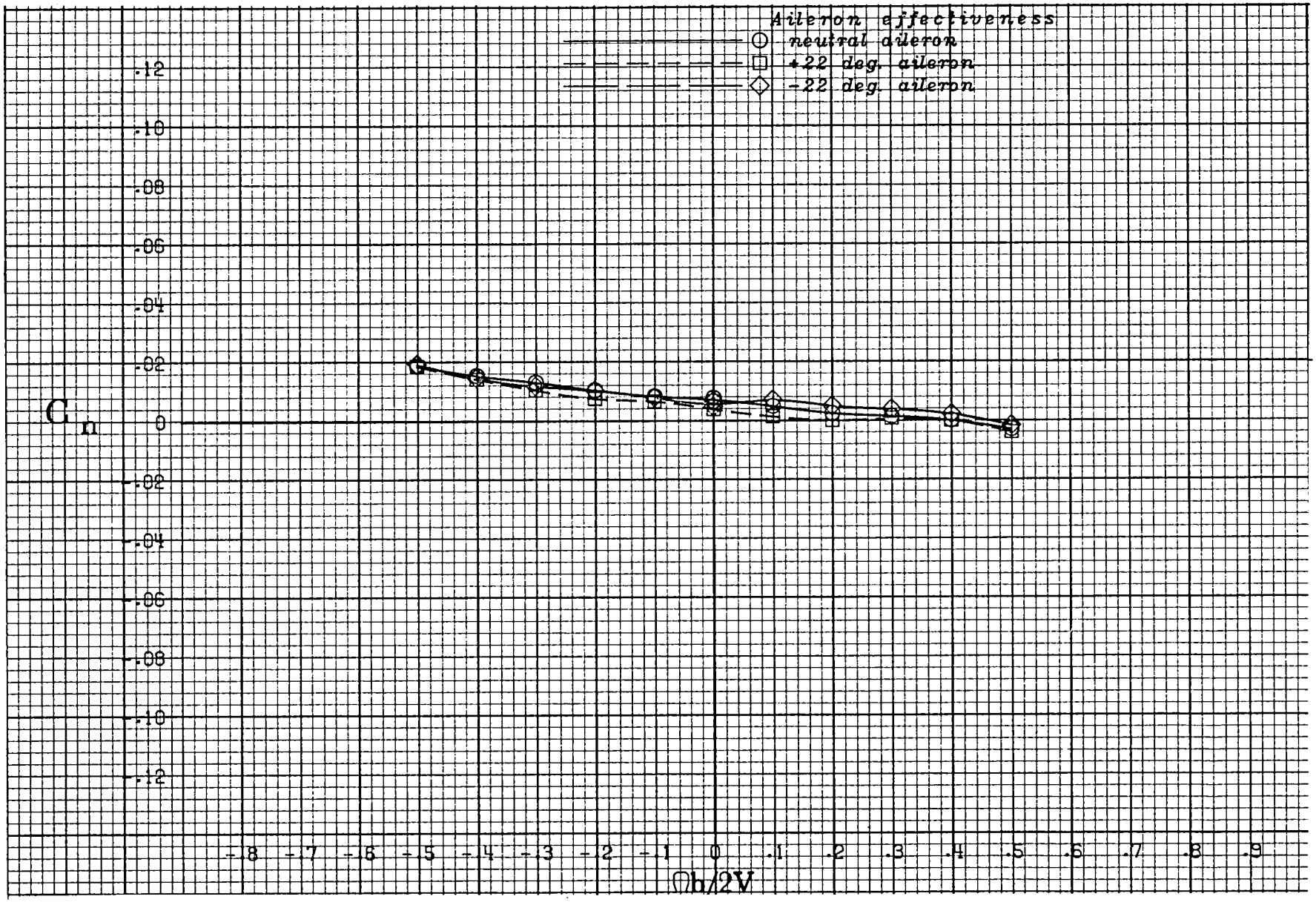

(c) α = 30 deg.

Figure A 19 .- Continued.

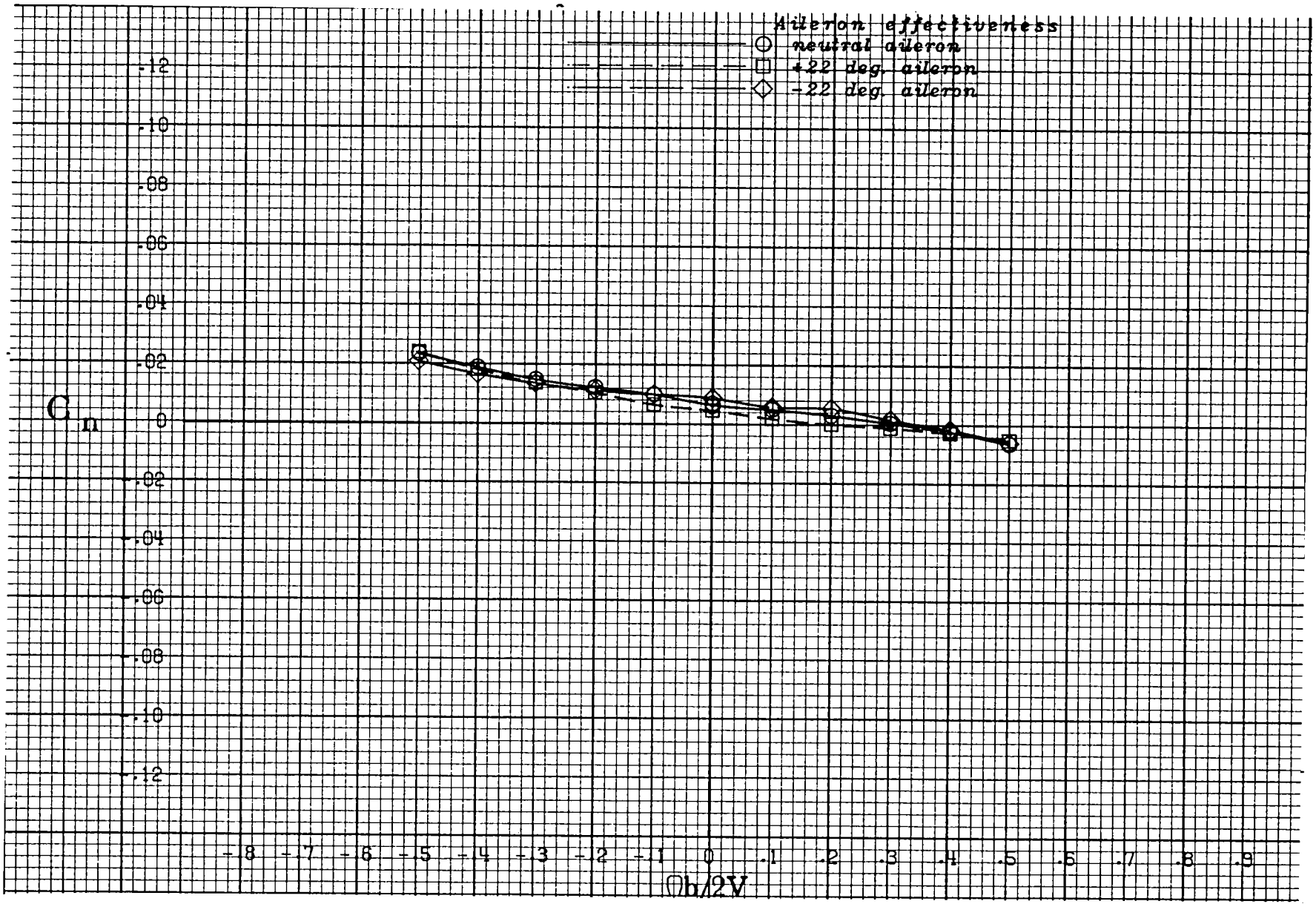

(d) α = 35 deg.

Figure A 19 .- Continued.

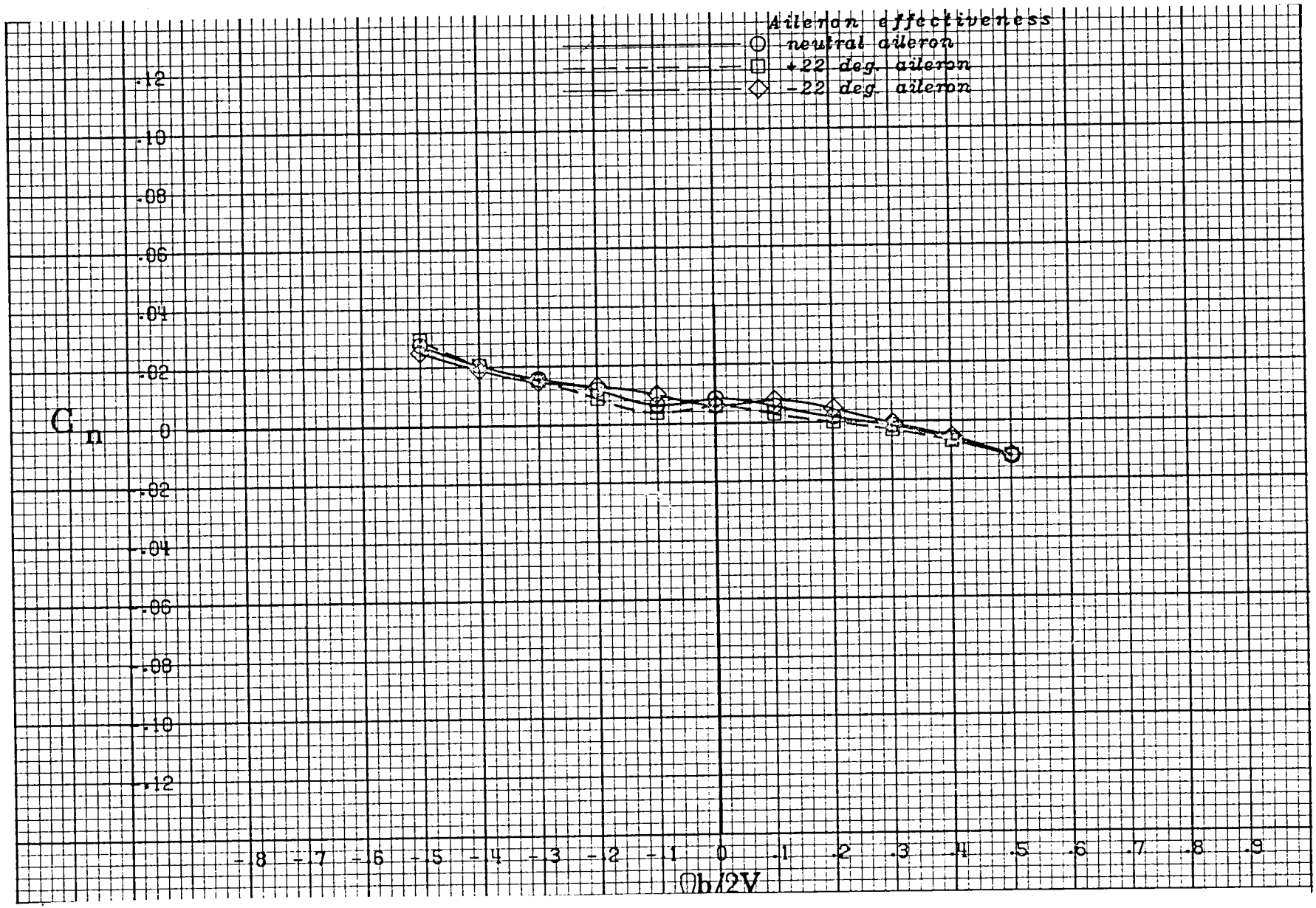

(e) α = 40 deg.

Figure A 19 .- Continued.

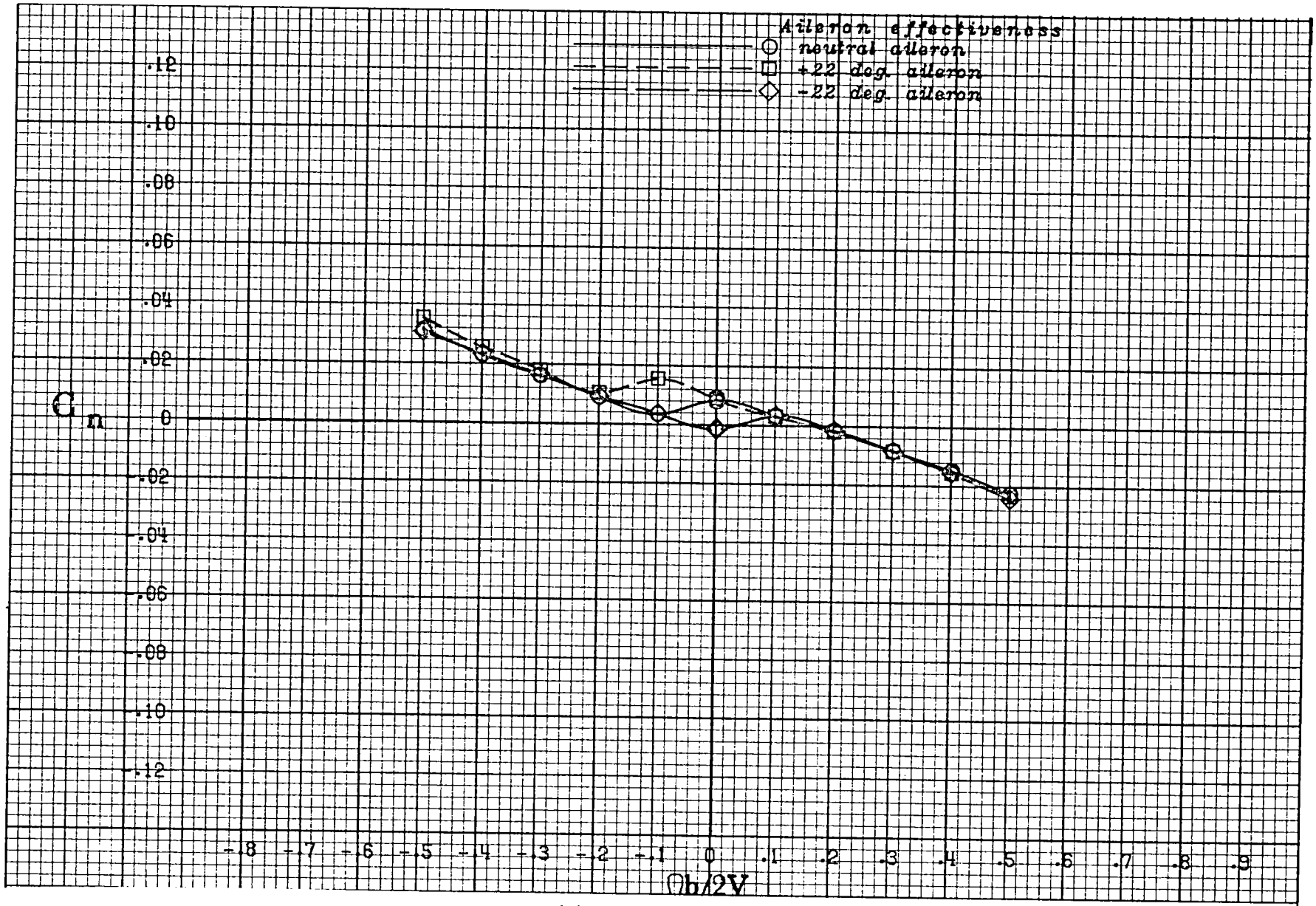

(f) α = 50 deg.

Figure A 19 .- Continued.

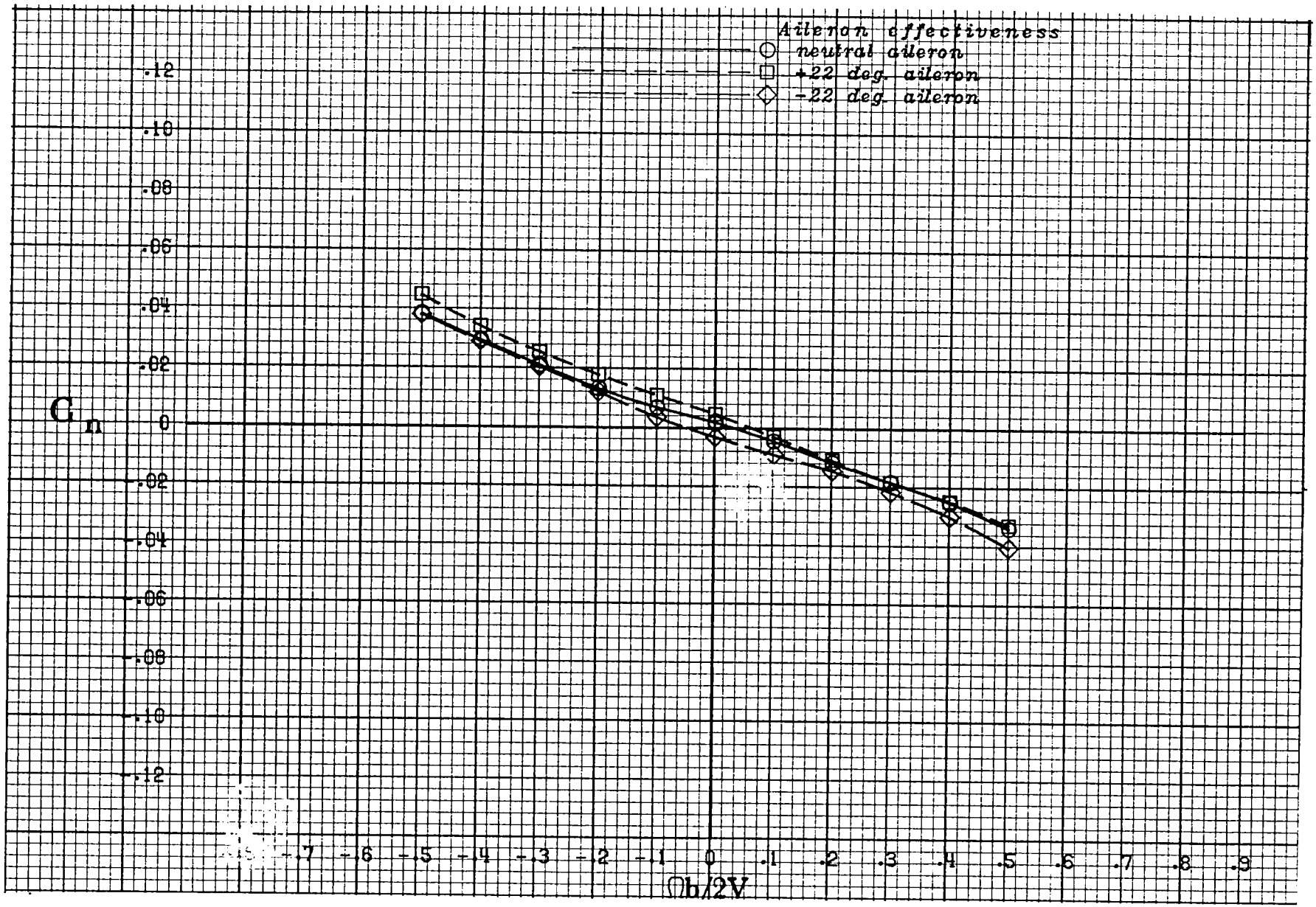

(g) α = 60 deg.

Figure A 19 .- Continued.

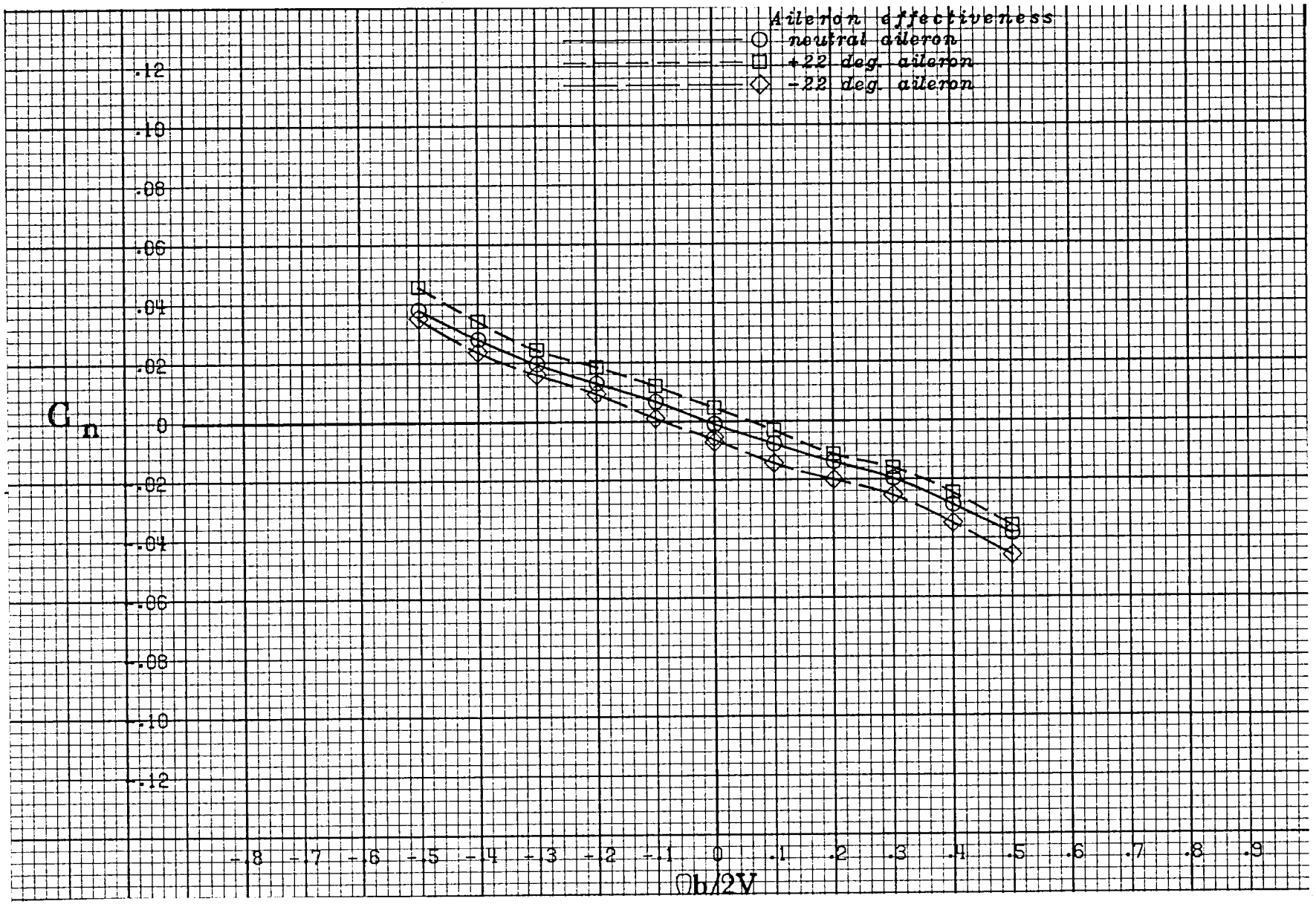

(h) α = 70 deg.

Figure A 19 .- Continued.

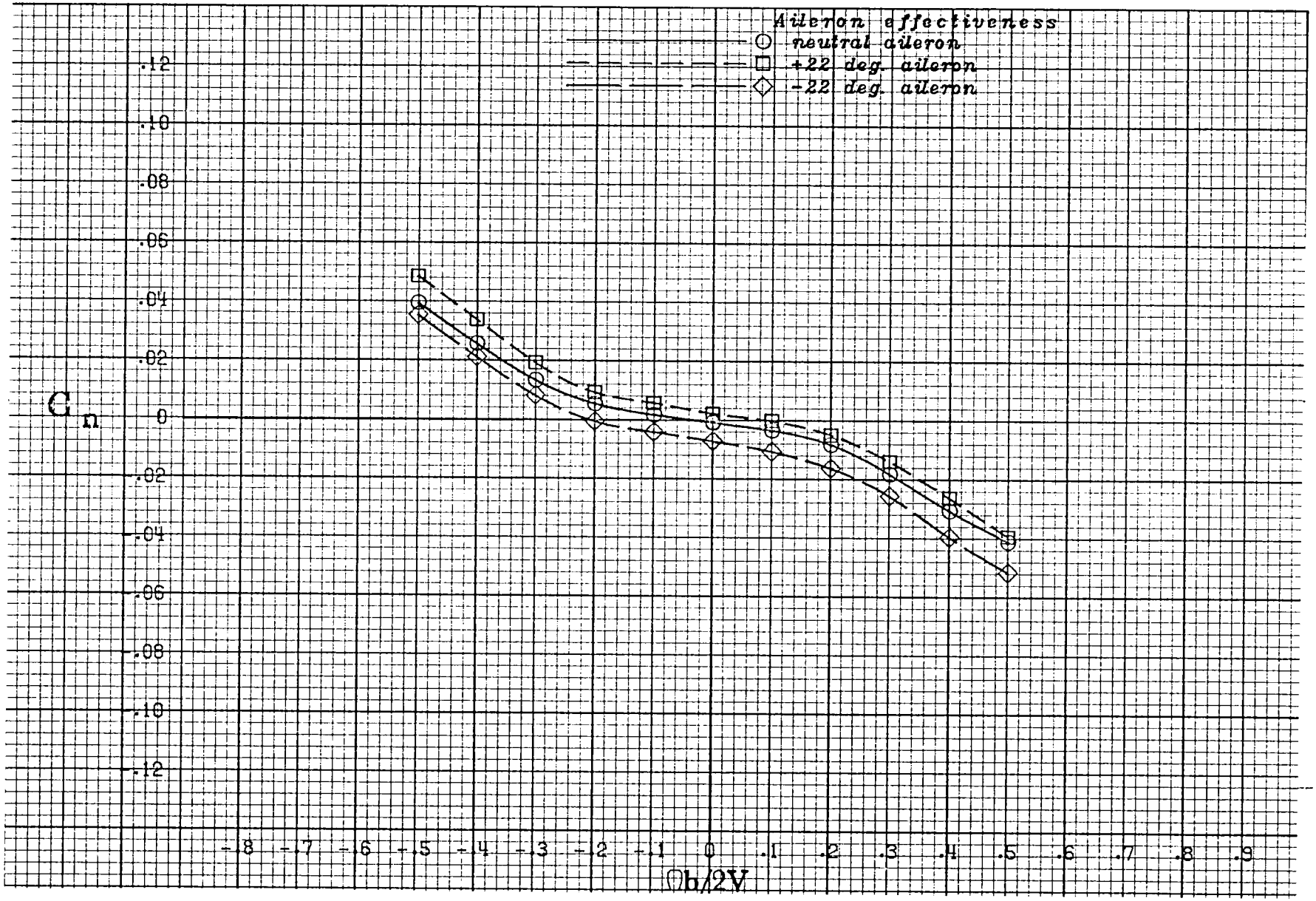

(i) α = 80 deg.

Figure A 19 .- Continued.

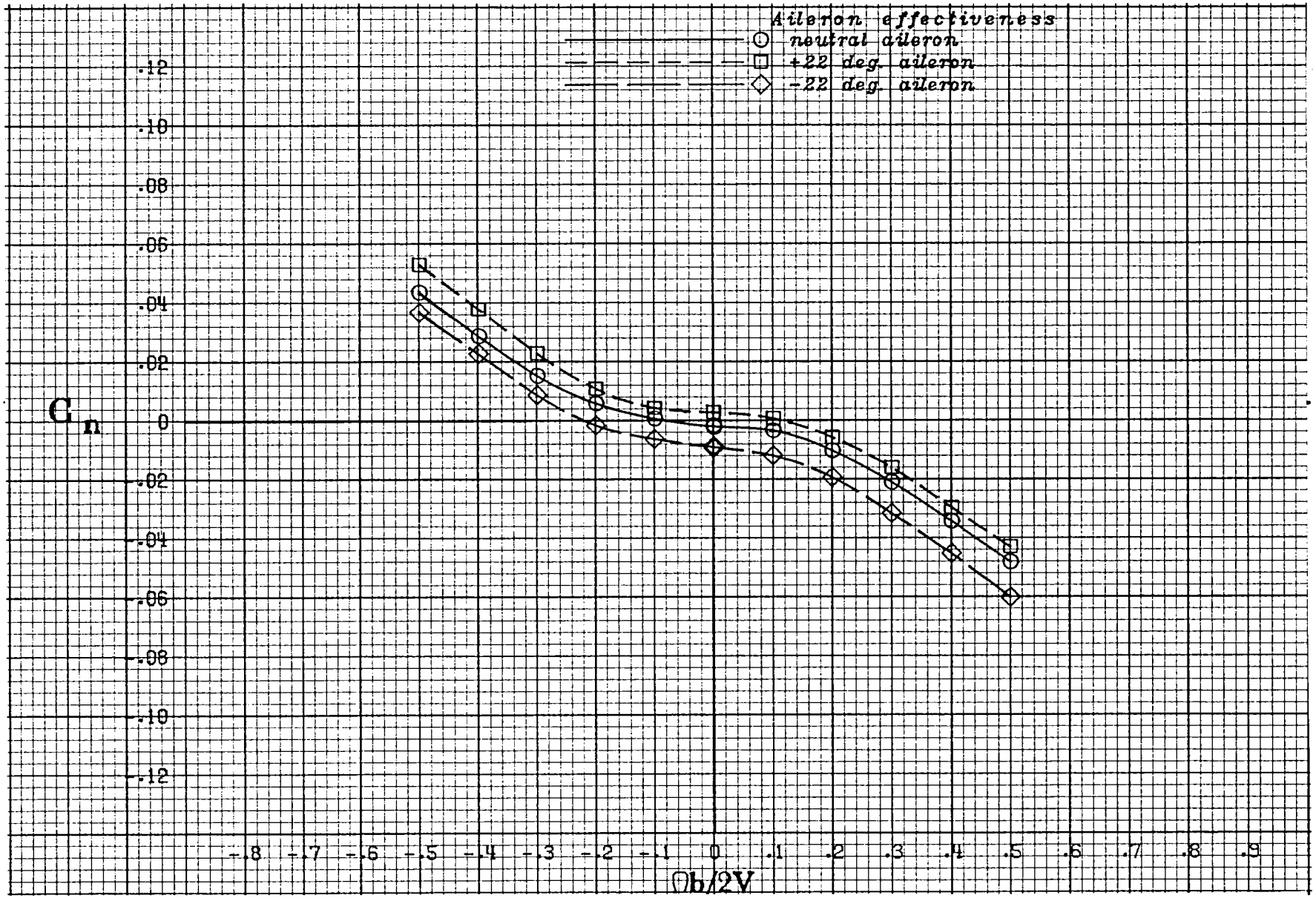

(j) α = 90 deg.

Figure A 19 .- Concluded.

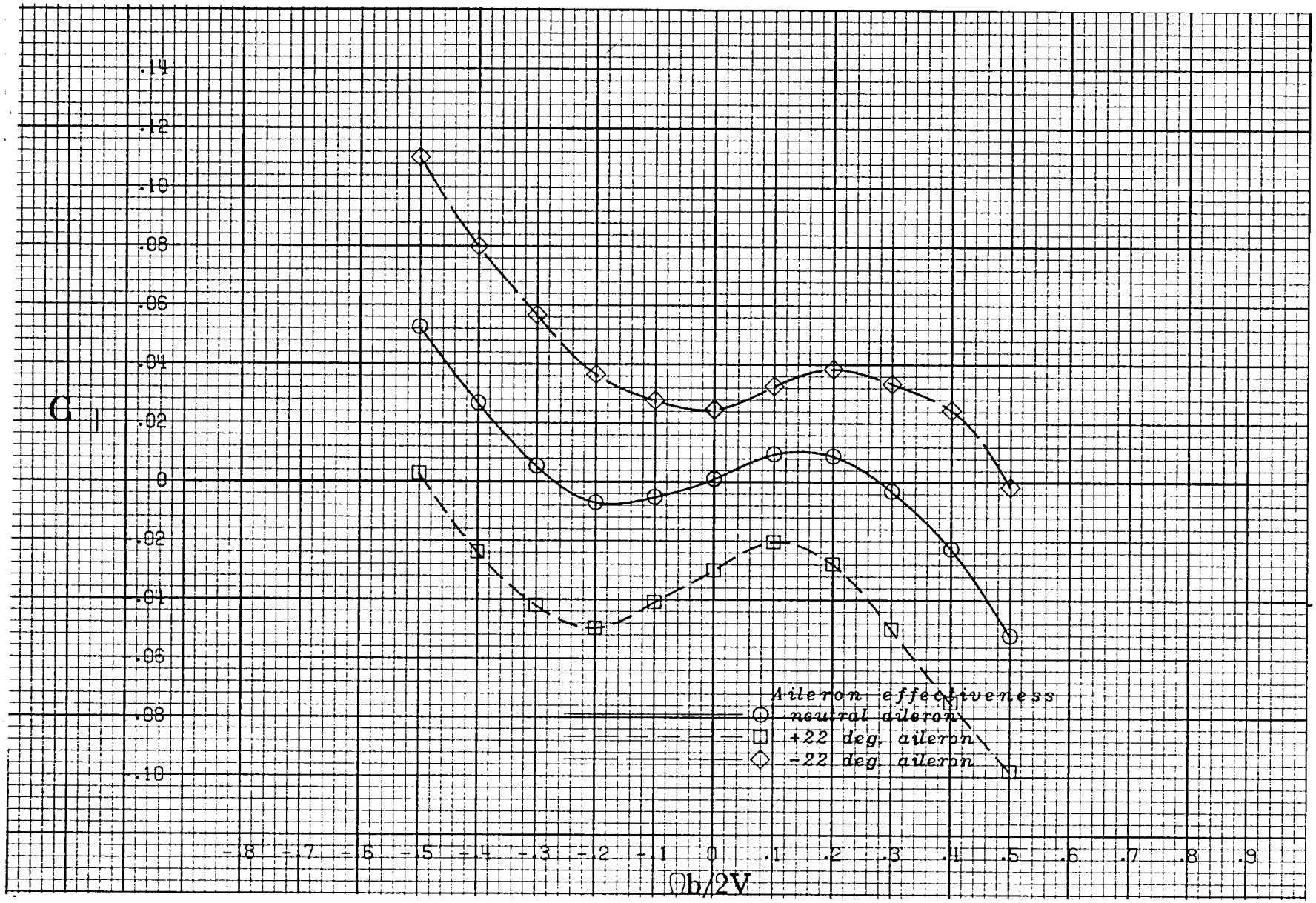

(a) α = 20 deg.

Figure A 20 .- Effect of rotation rate and aileron deflection on rolling-moment coefficient for the basic configuration with -10 deg elevator and -26 deg rudder at zero sideslip angle.

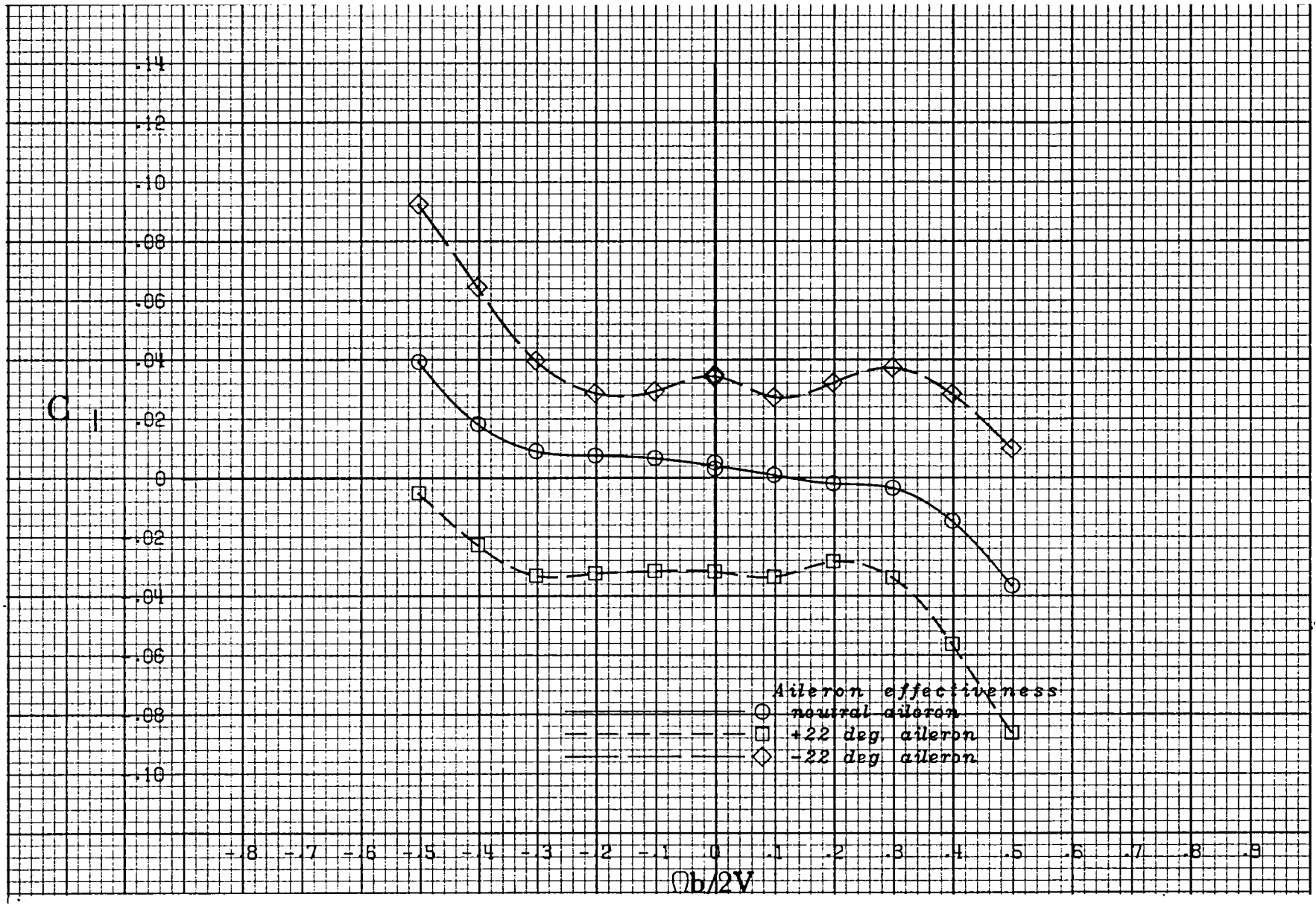

(b) α = 25 deg.

Figure A 20 .- Continued.

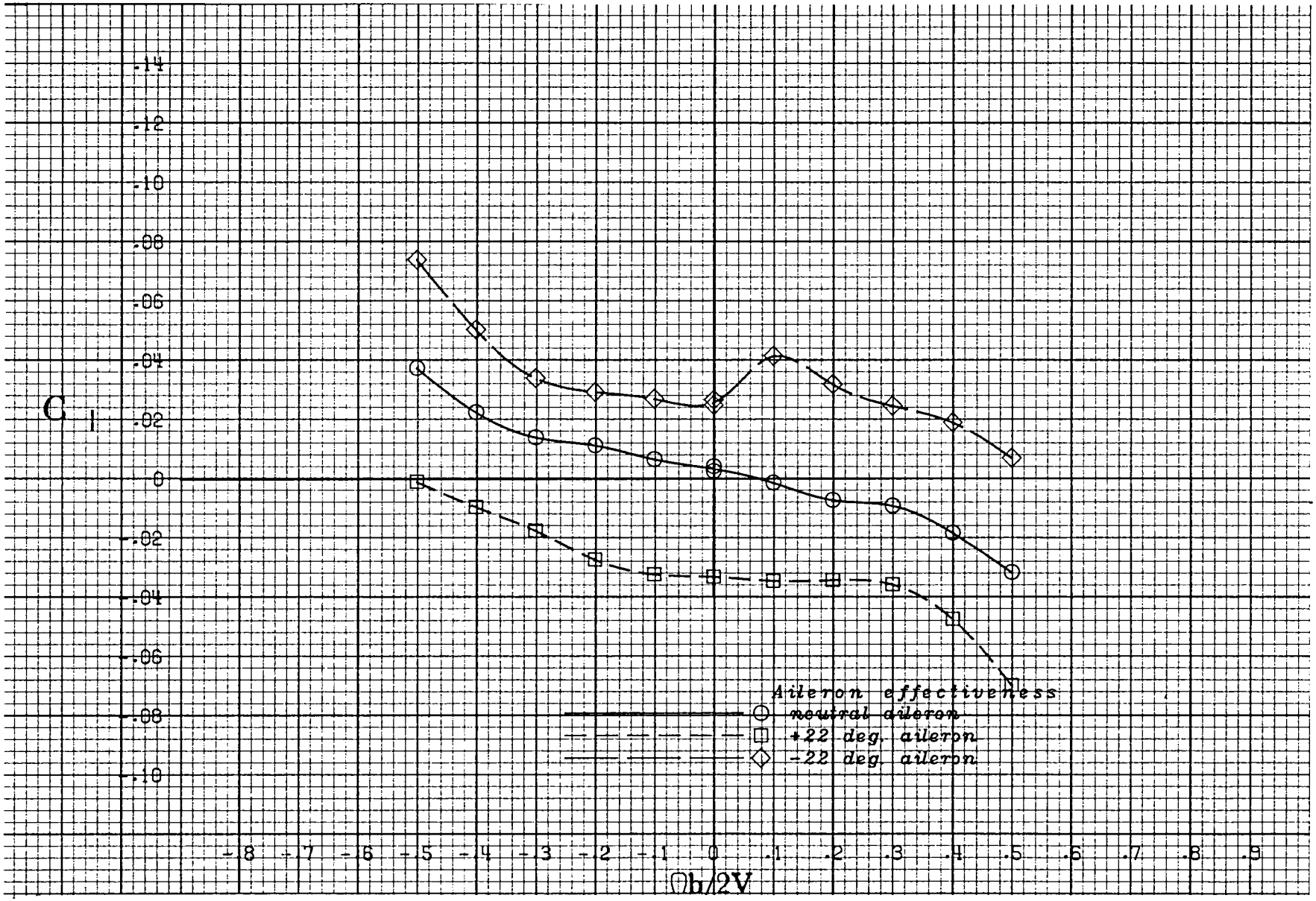

(c) α = 30 deg.

Figure A 20 .- Continued.

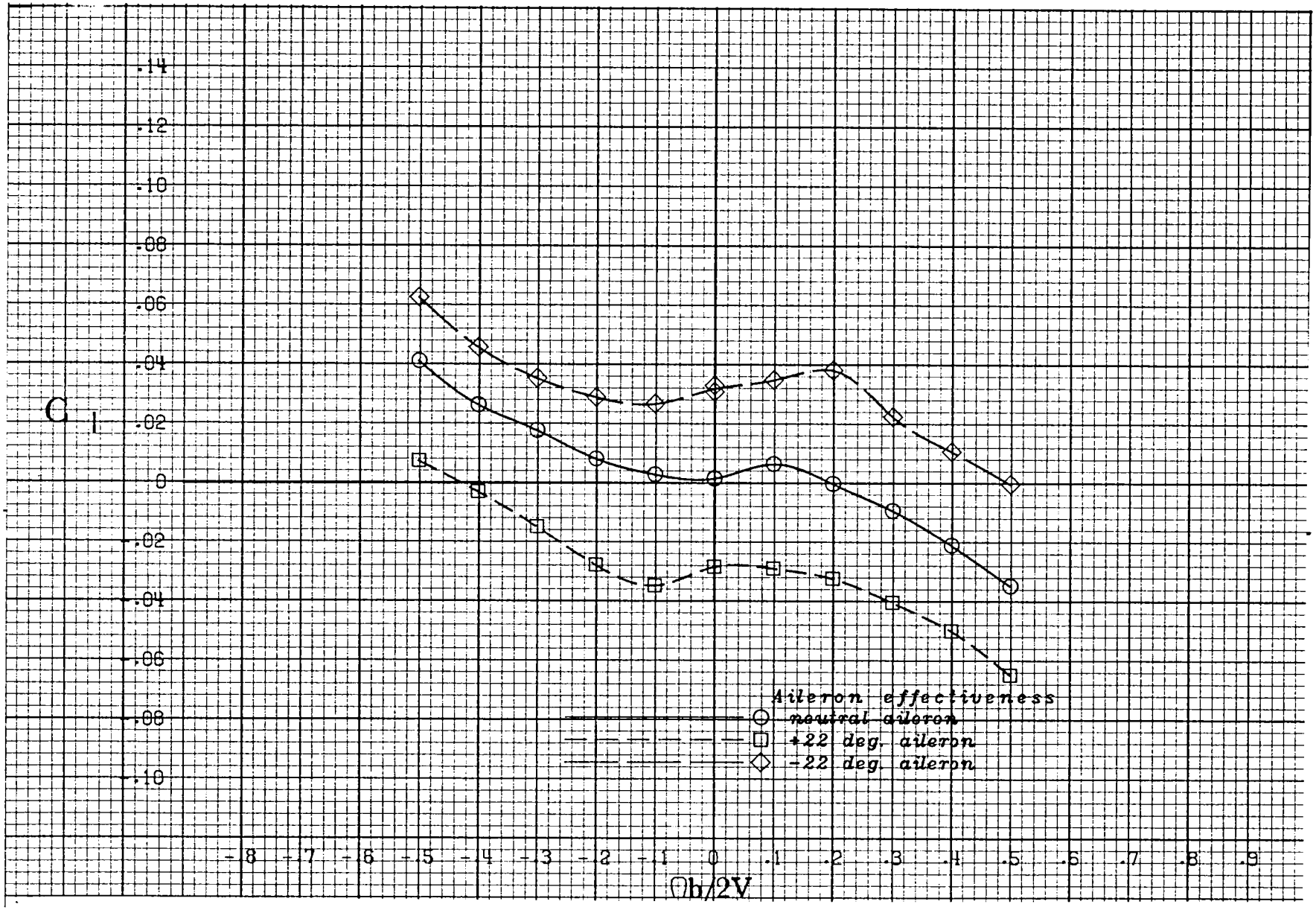

(d) α = 35 deg.

Figure A 20 .- Continued.

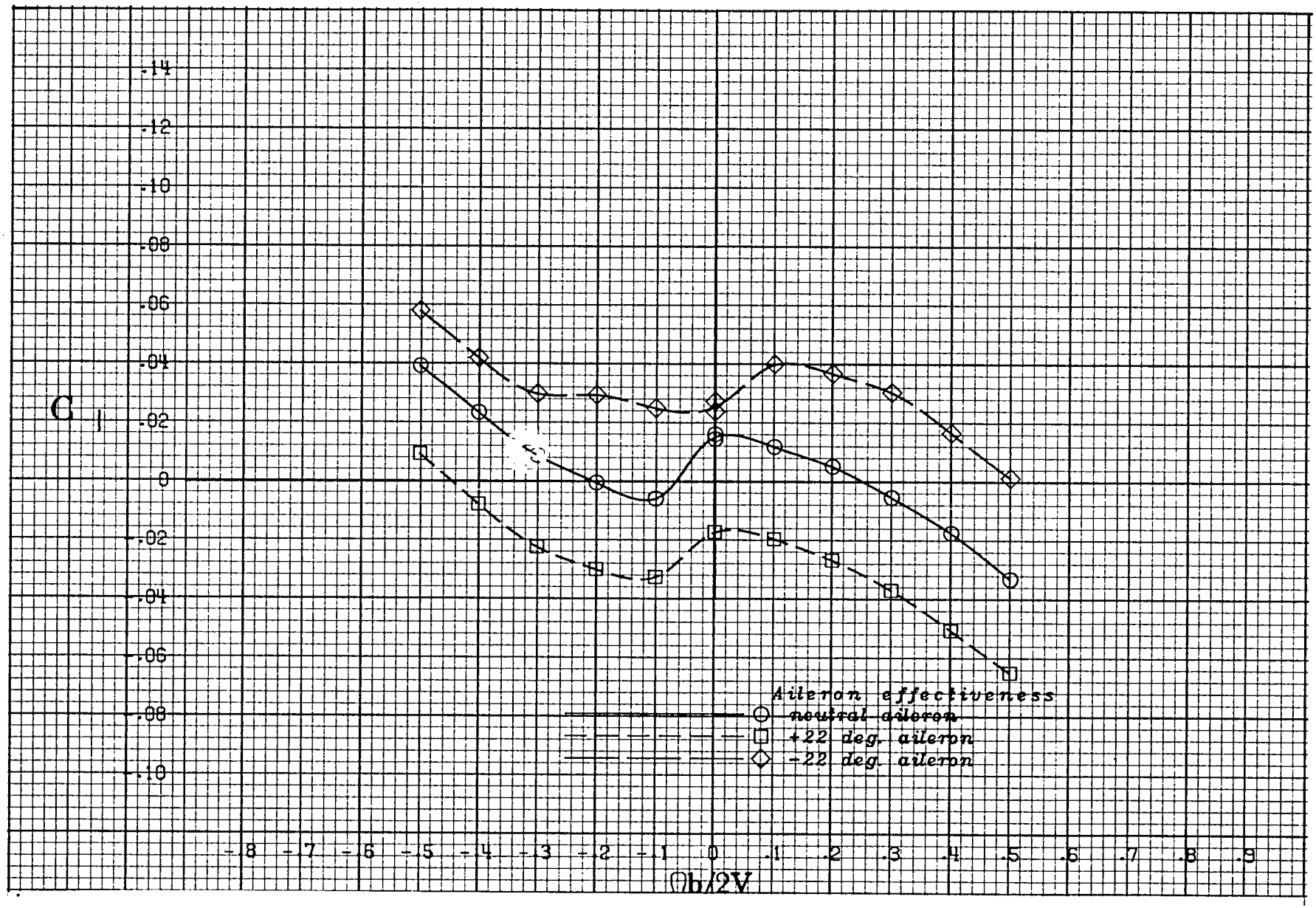

(e) α = 40 deg.

Figure A 20 .- Continued.

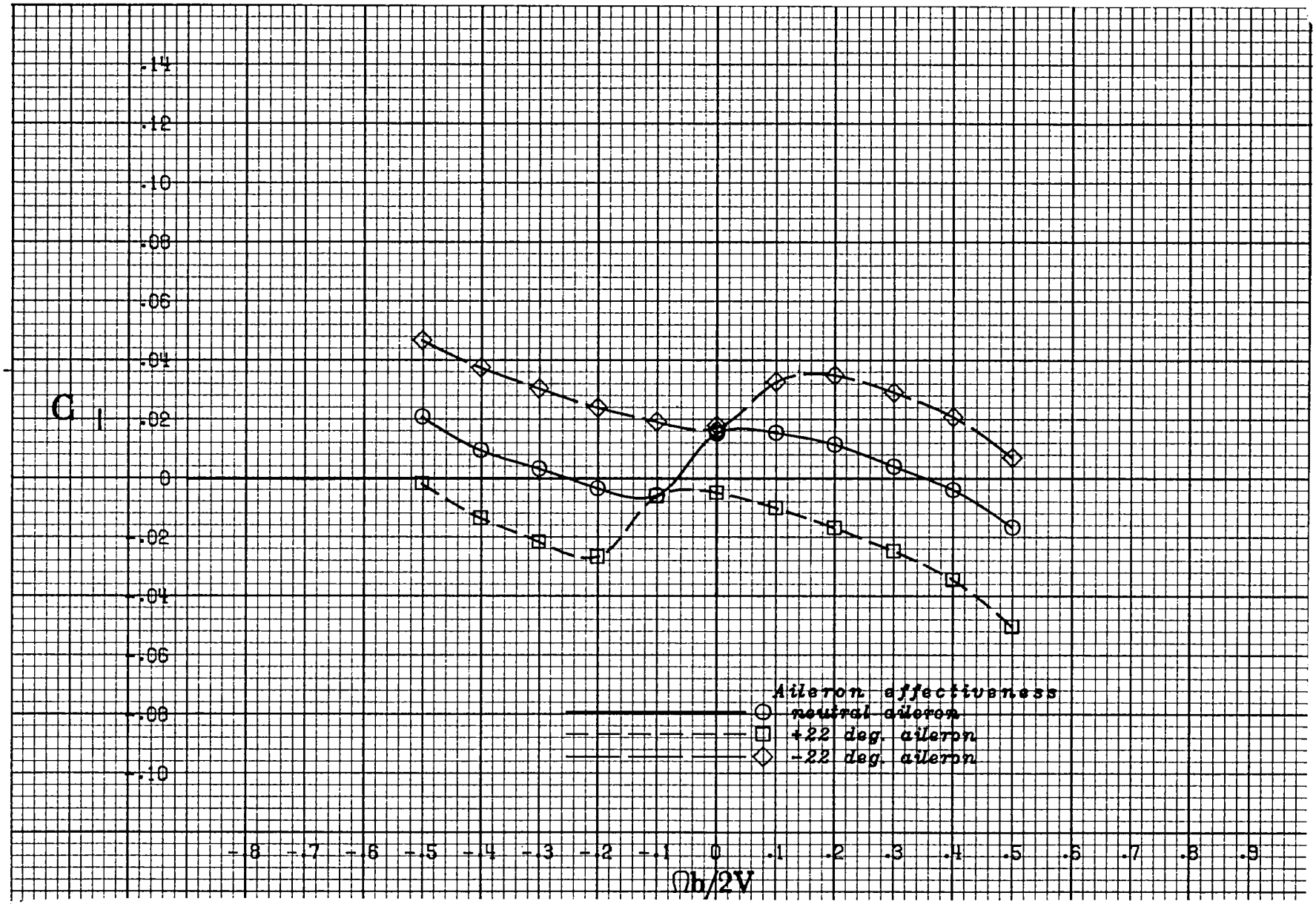

(f) α = 50 deg.

Figure A 20 .- Continued.

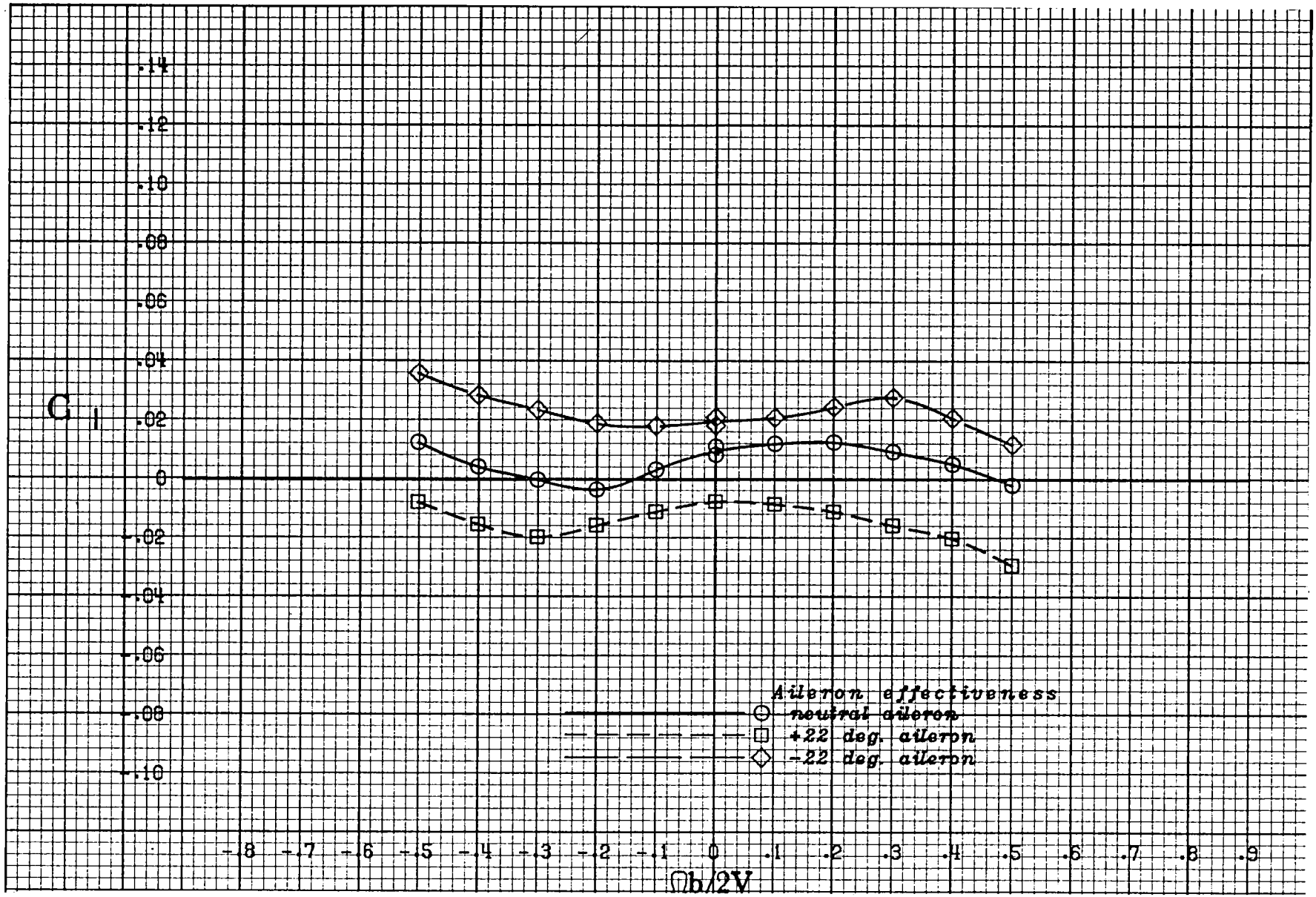

(g) α = 60 deg.

Figure A 20 .- Continued.

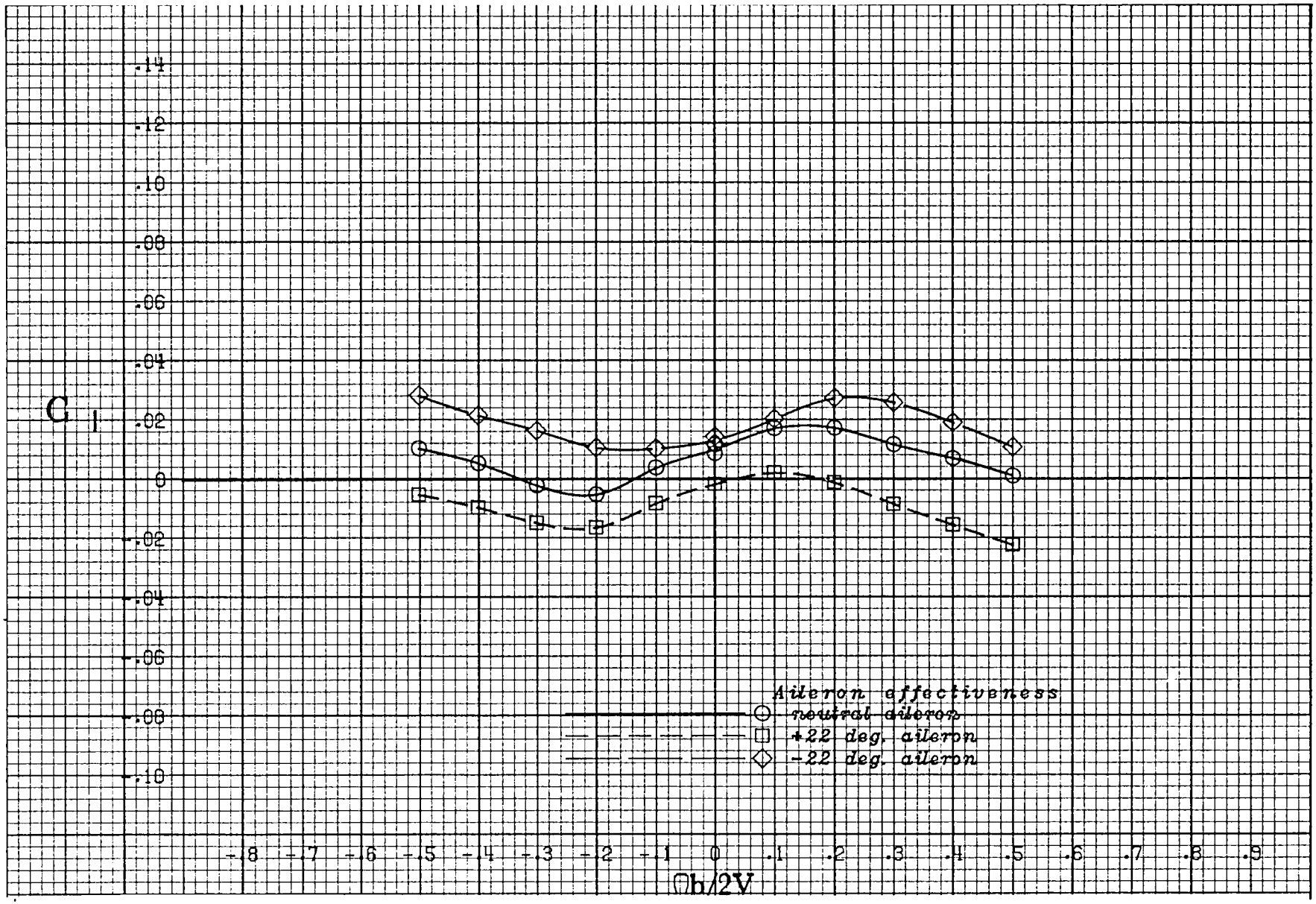

(h) α = 70 deg.

Figure A 20 .- Continued.

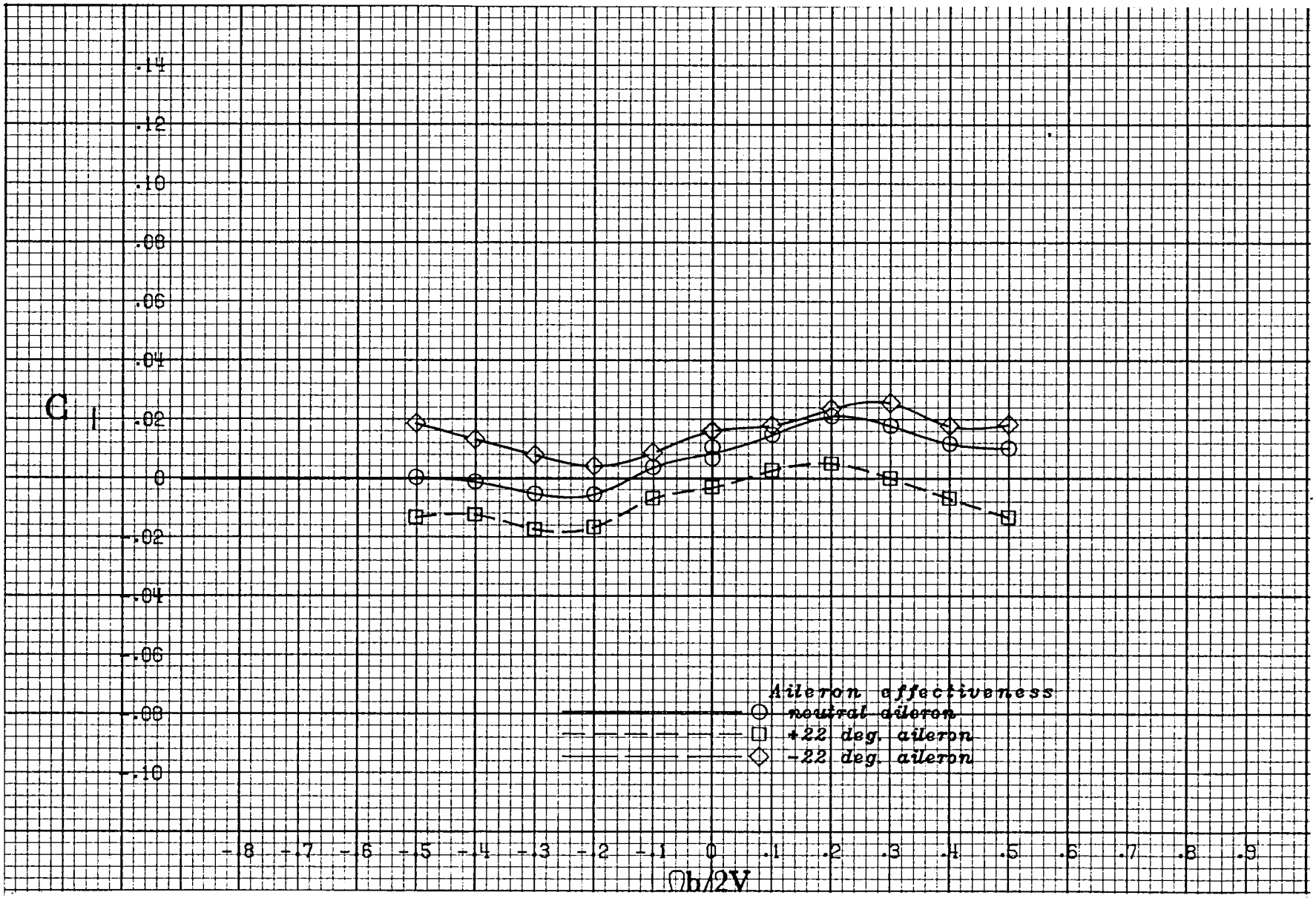

(i) α = 80 deg.

Figure A 20 .- Continued.

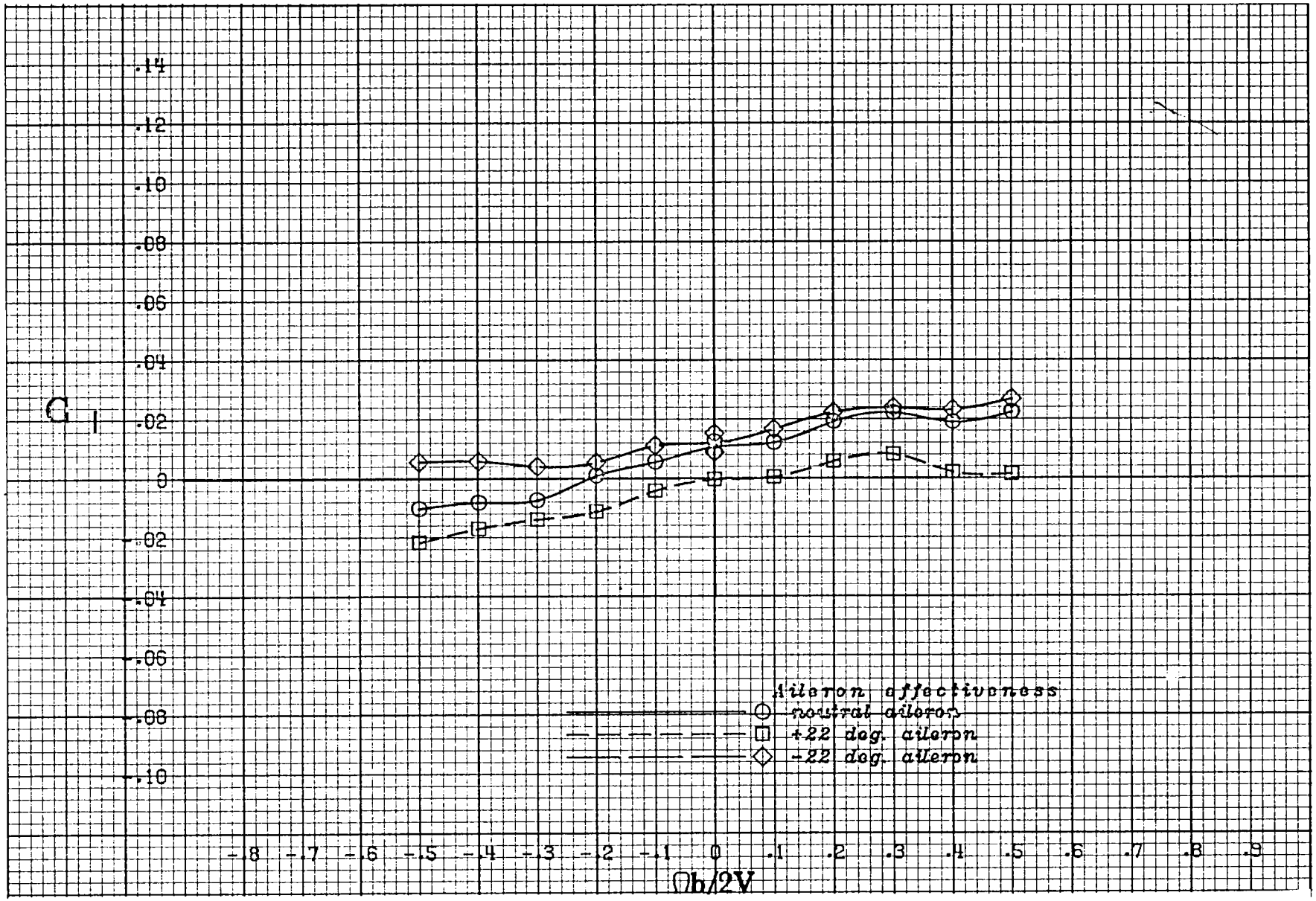

(j) α = 90 deg.

Figure A 20 .- Concluded.

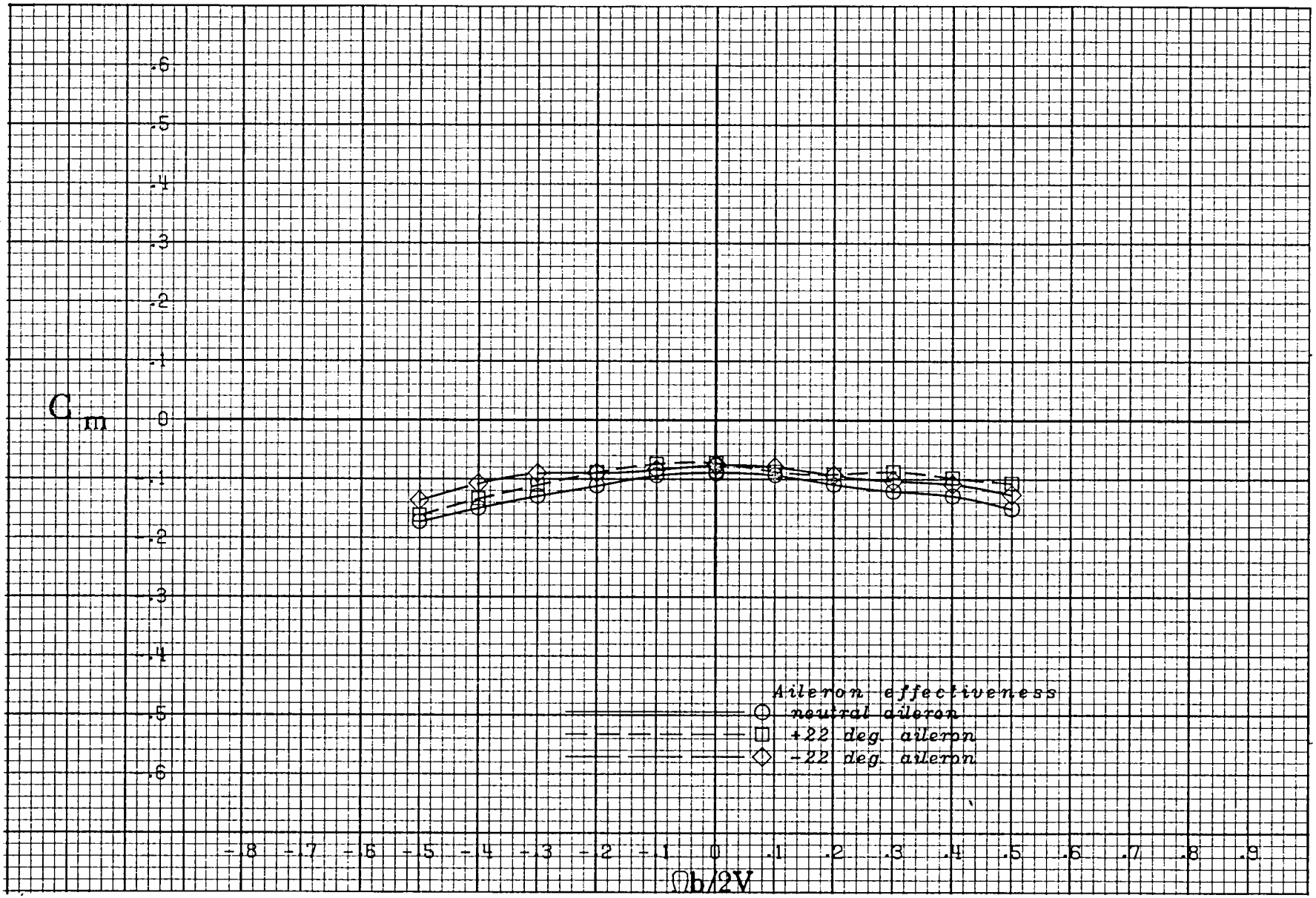

(a) α = 20 deg.

Figure A 21 .- Effect of rotation rate and aileron deflection on pitching-moment coefficient for the basic configuration with -10 deg elevator and -26 deg rudder at zero sideslip angle.

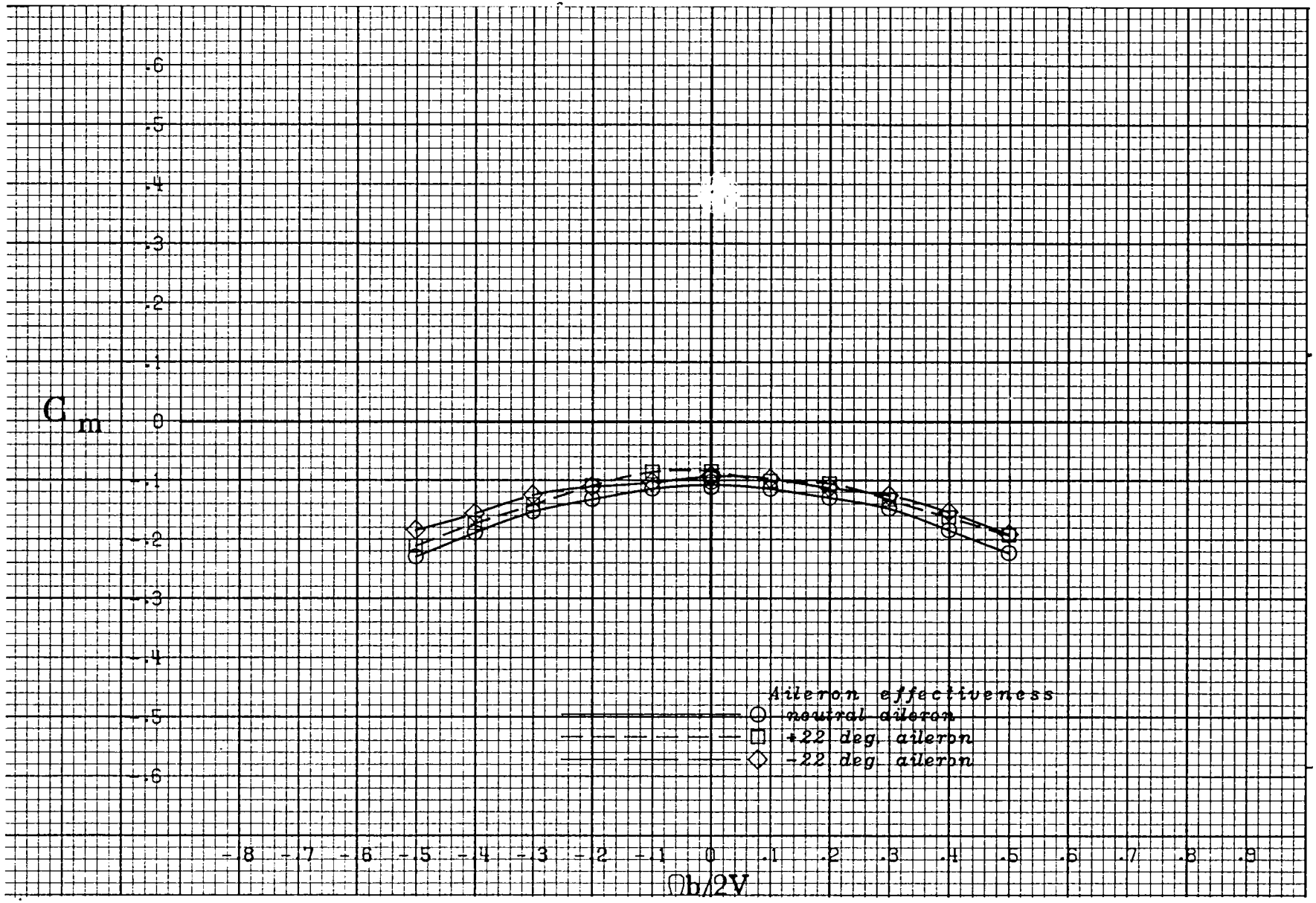

(b) α = 25 deg.

Figure A 21 .- Continued.

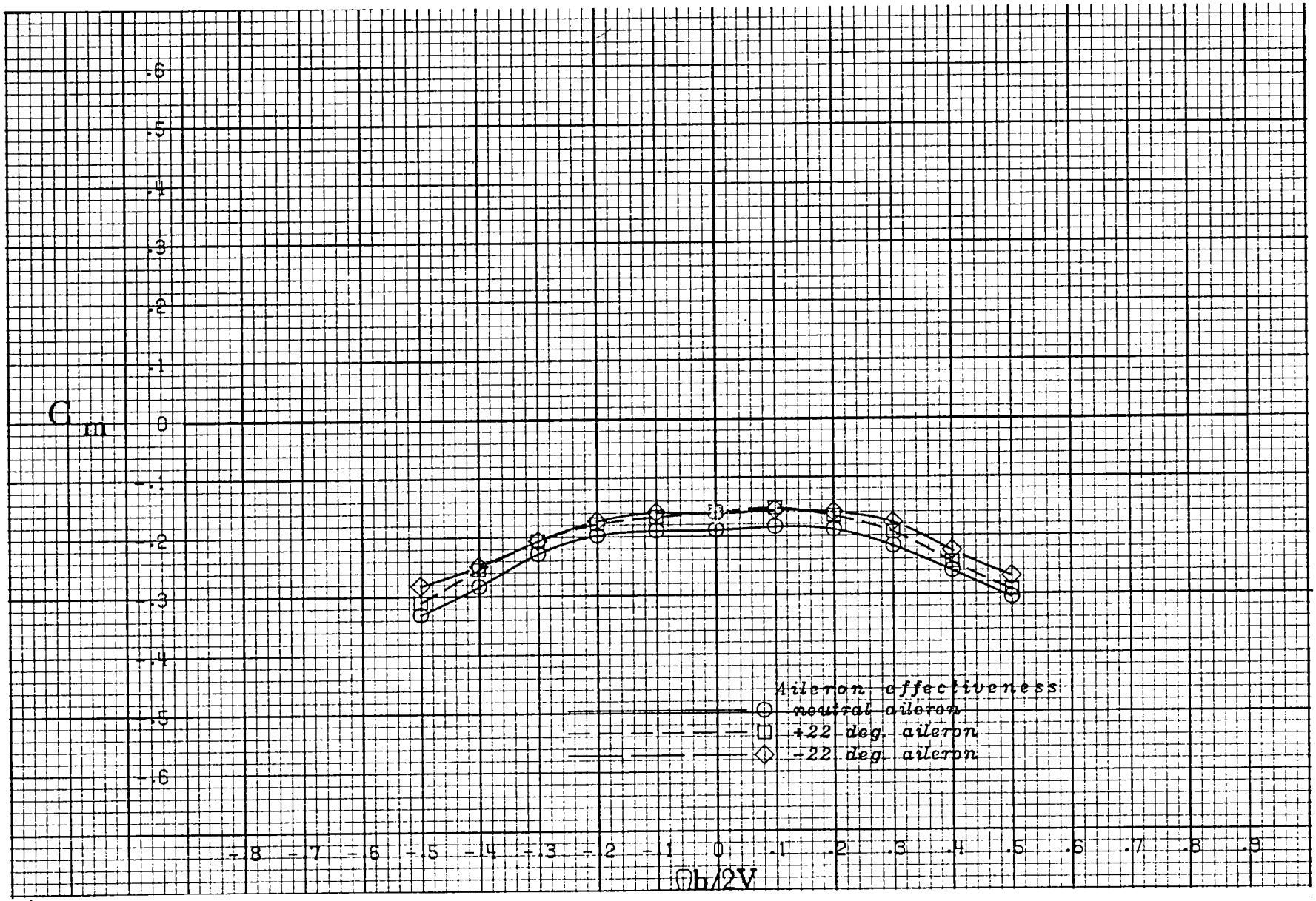

(c) α = 30 deg.

Figure A 21 .- Continued.

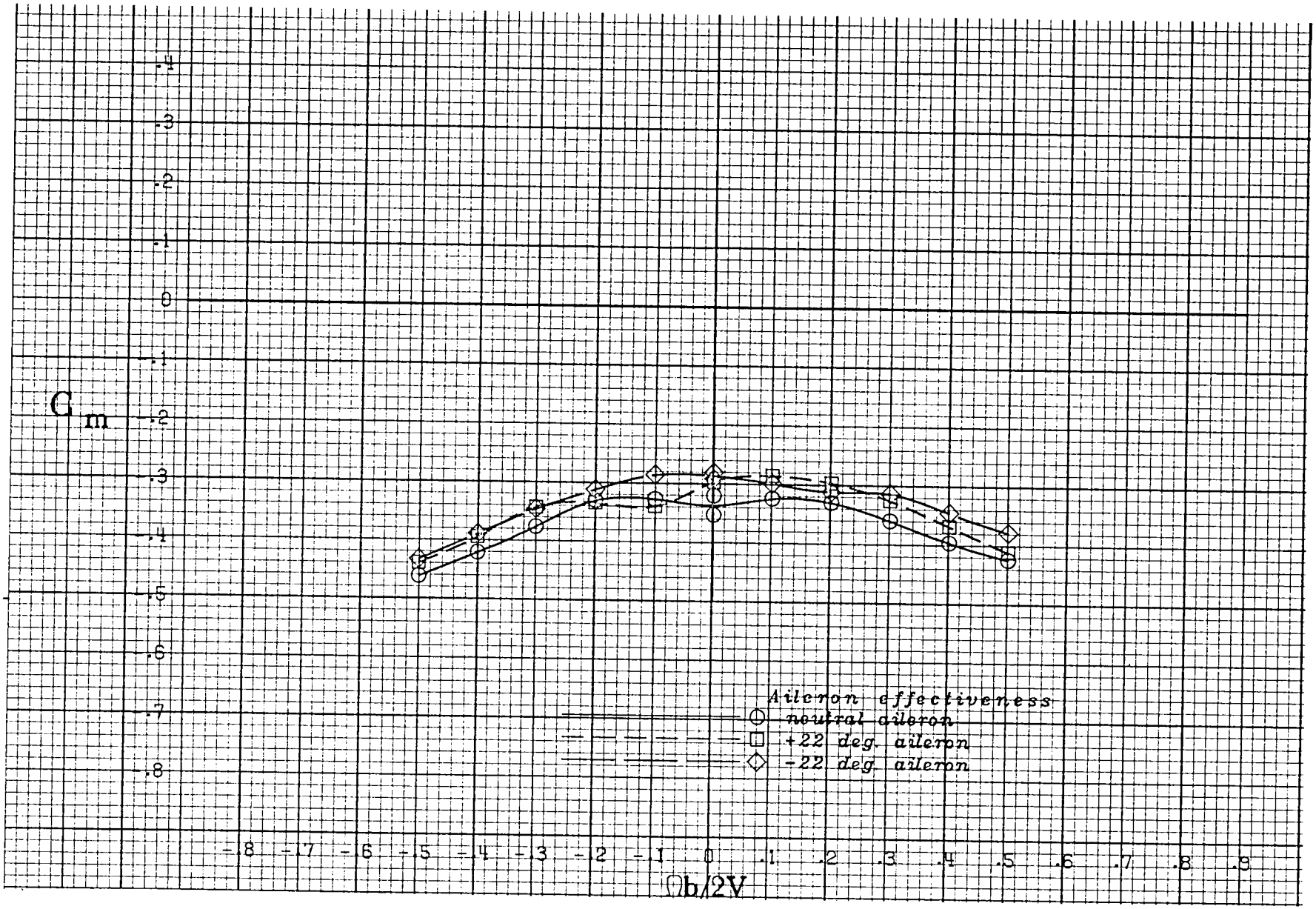

(d) α = 35 deg.

Figure A 21 .- Continued.

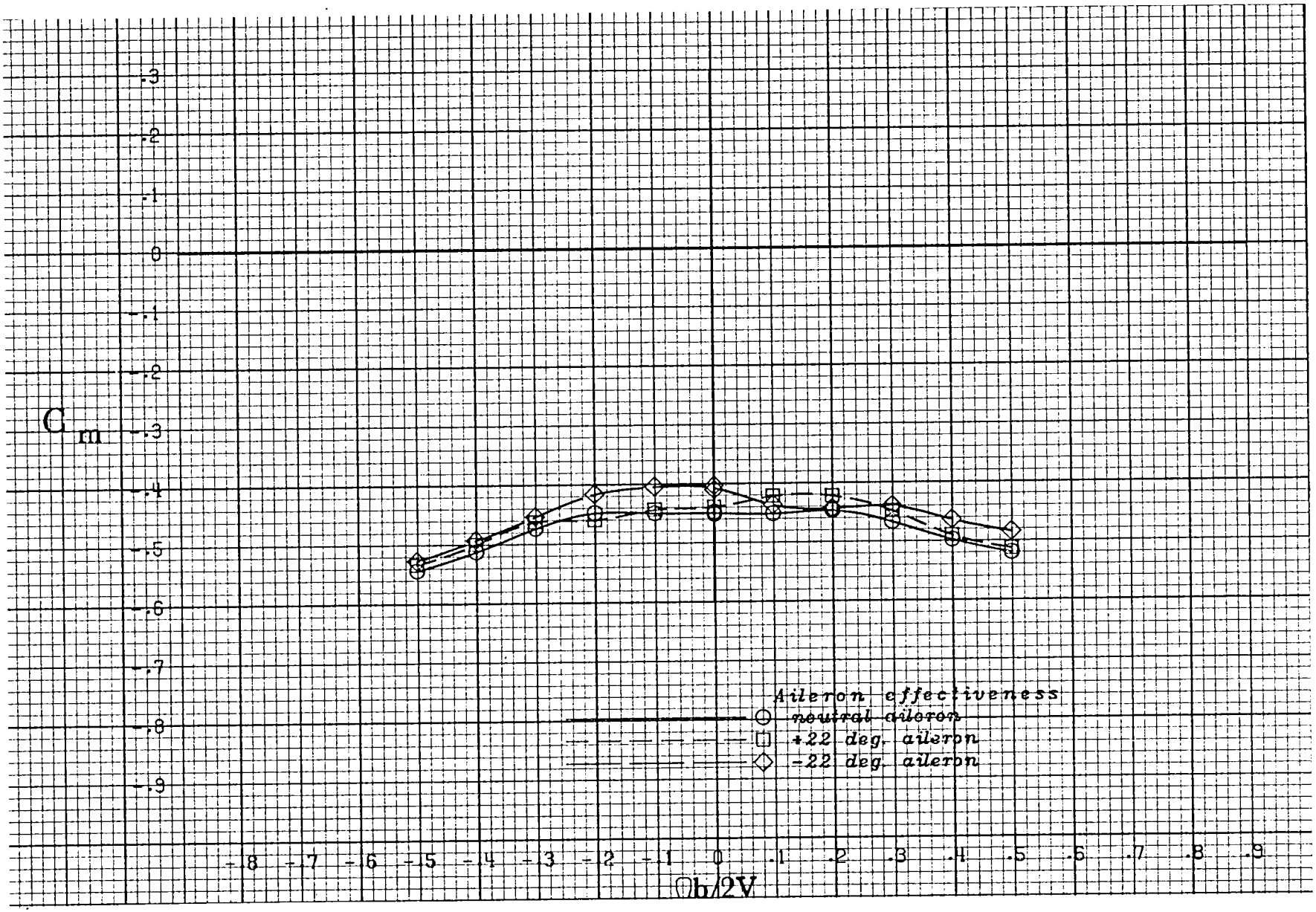

(e) α = 40 deg.

Figure A 21 .- Continued.

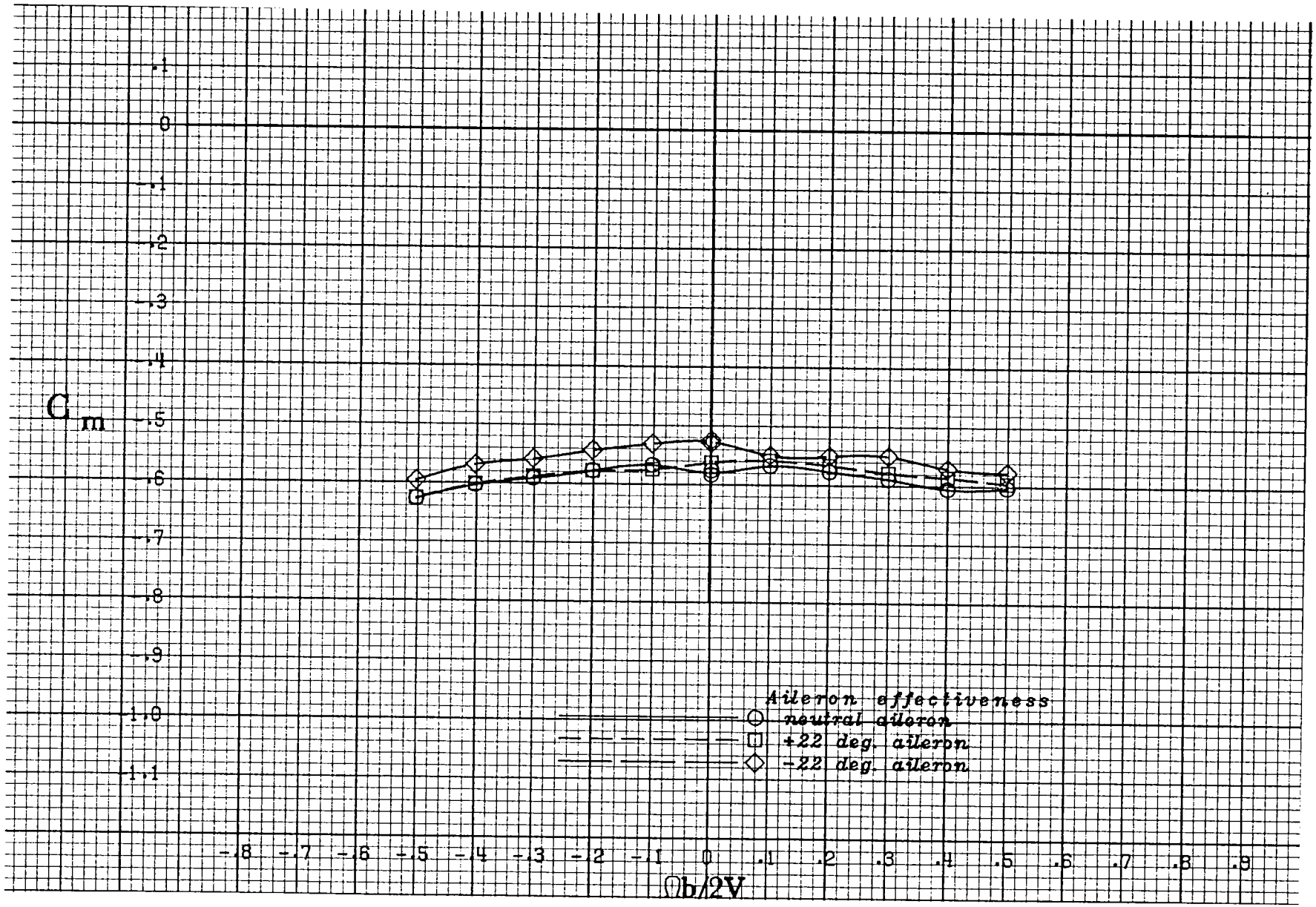

(f) α = 50 deg.

Figure A 21 .- Continued.

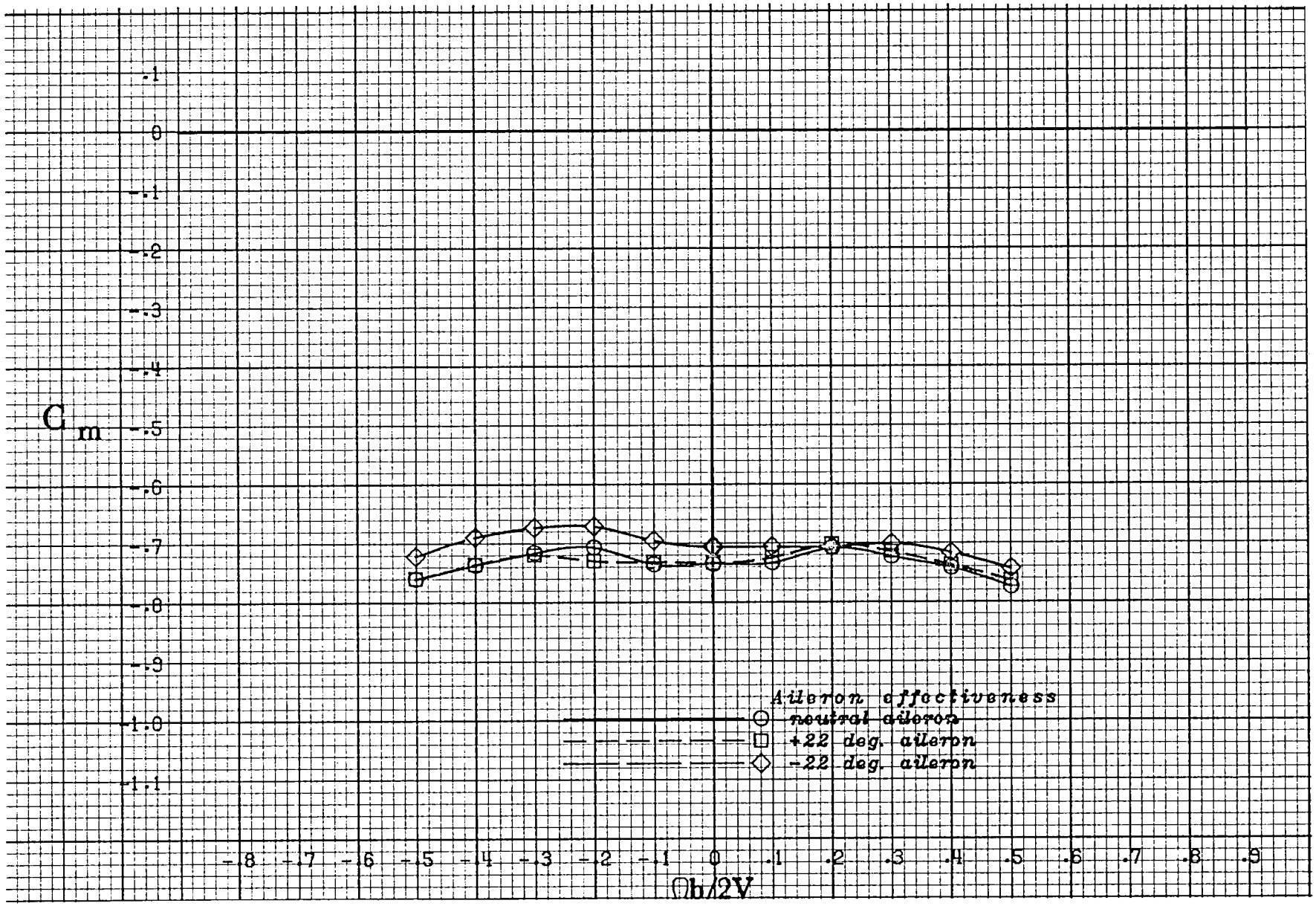

(g) α = 60 deg.

Figure A 21 .- Continued.

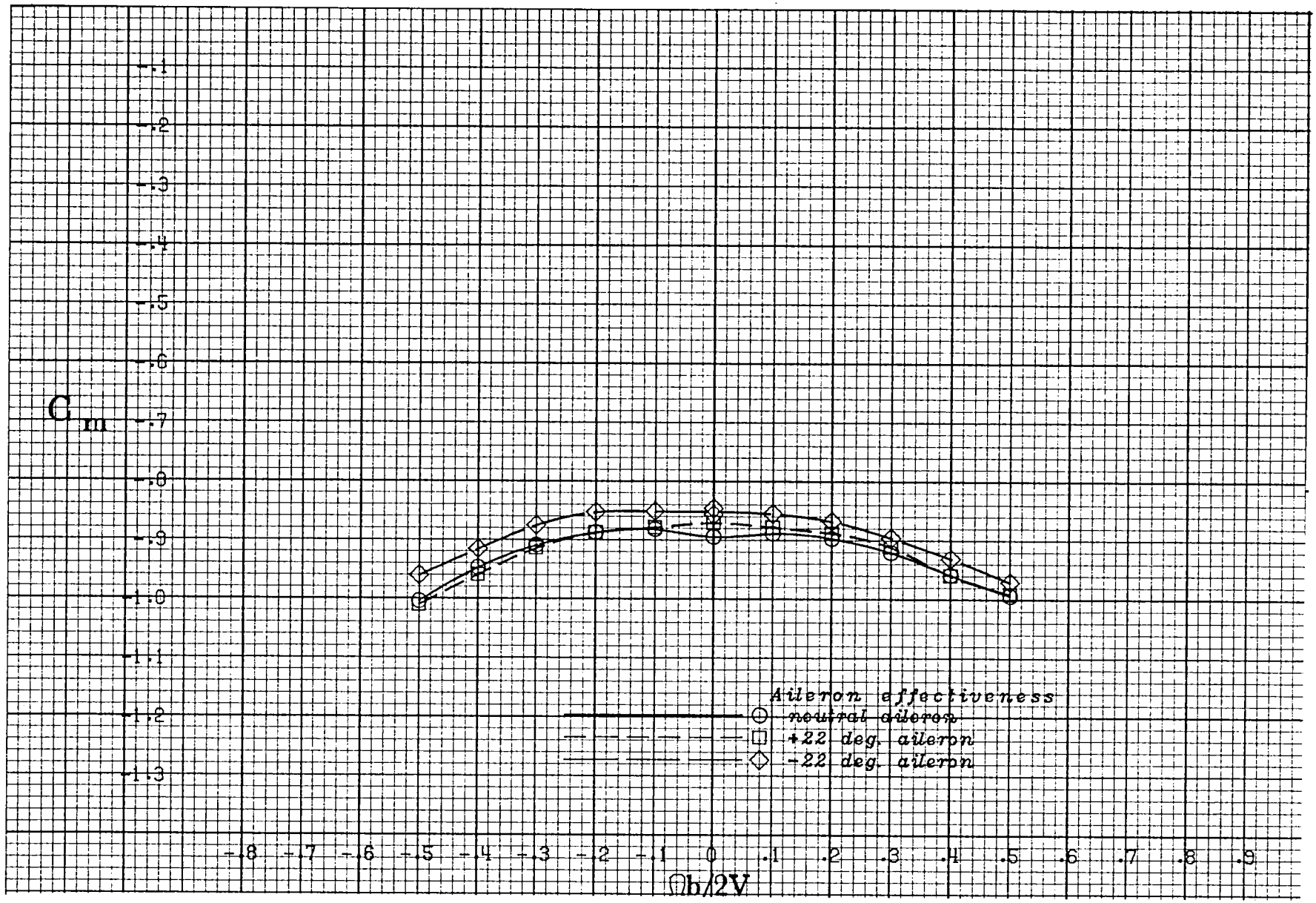

(h) α = 70 deg.

Figure A 21 .- Continued.

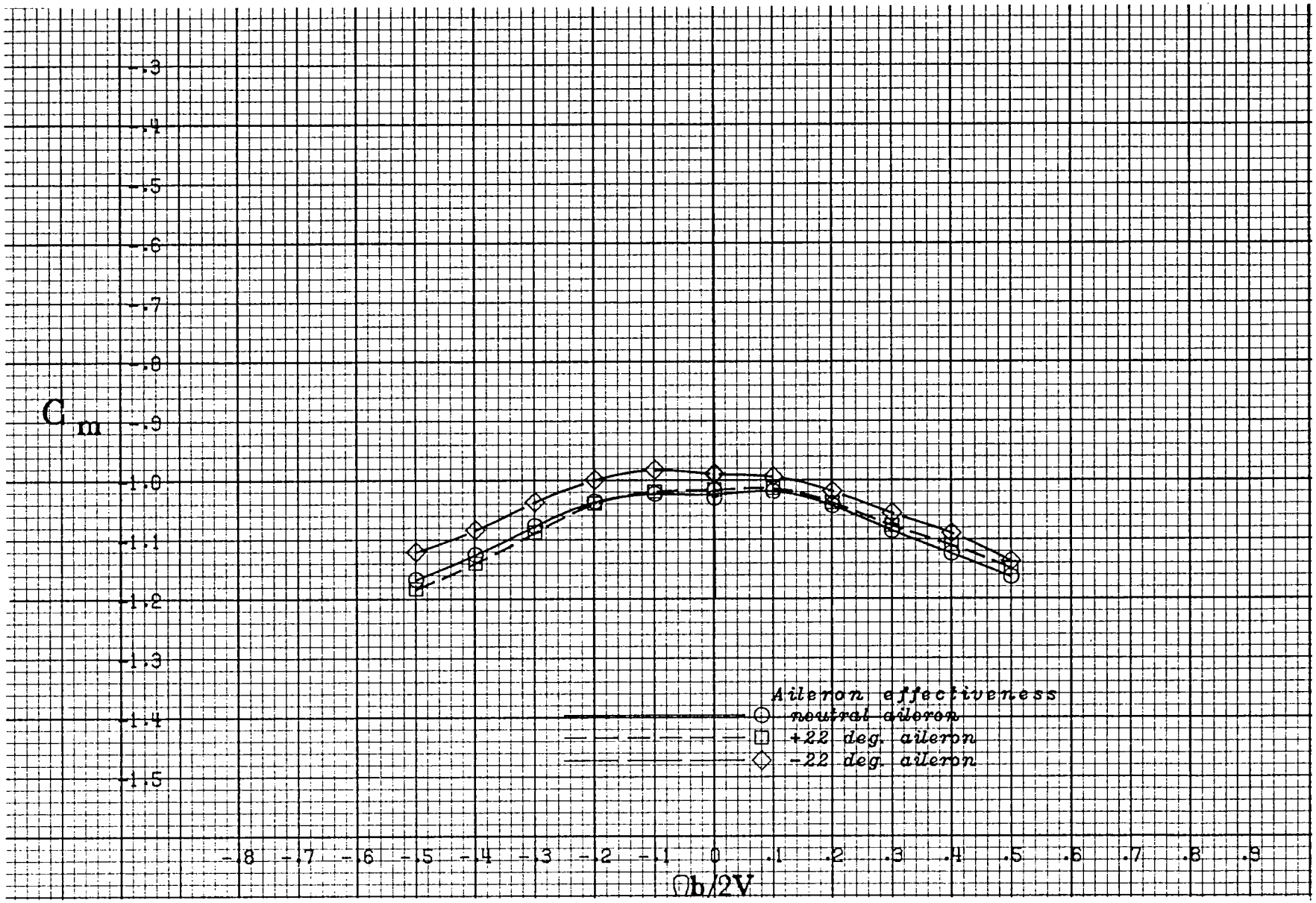

(i) α = 80 deg.

Figure A 21 .- Continued.

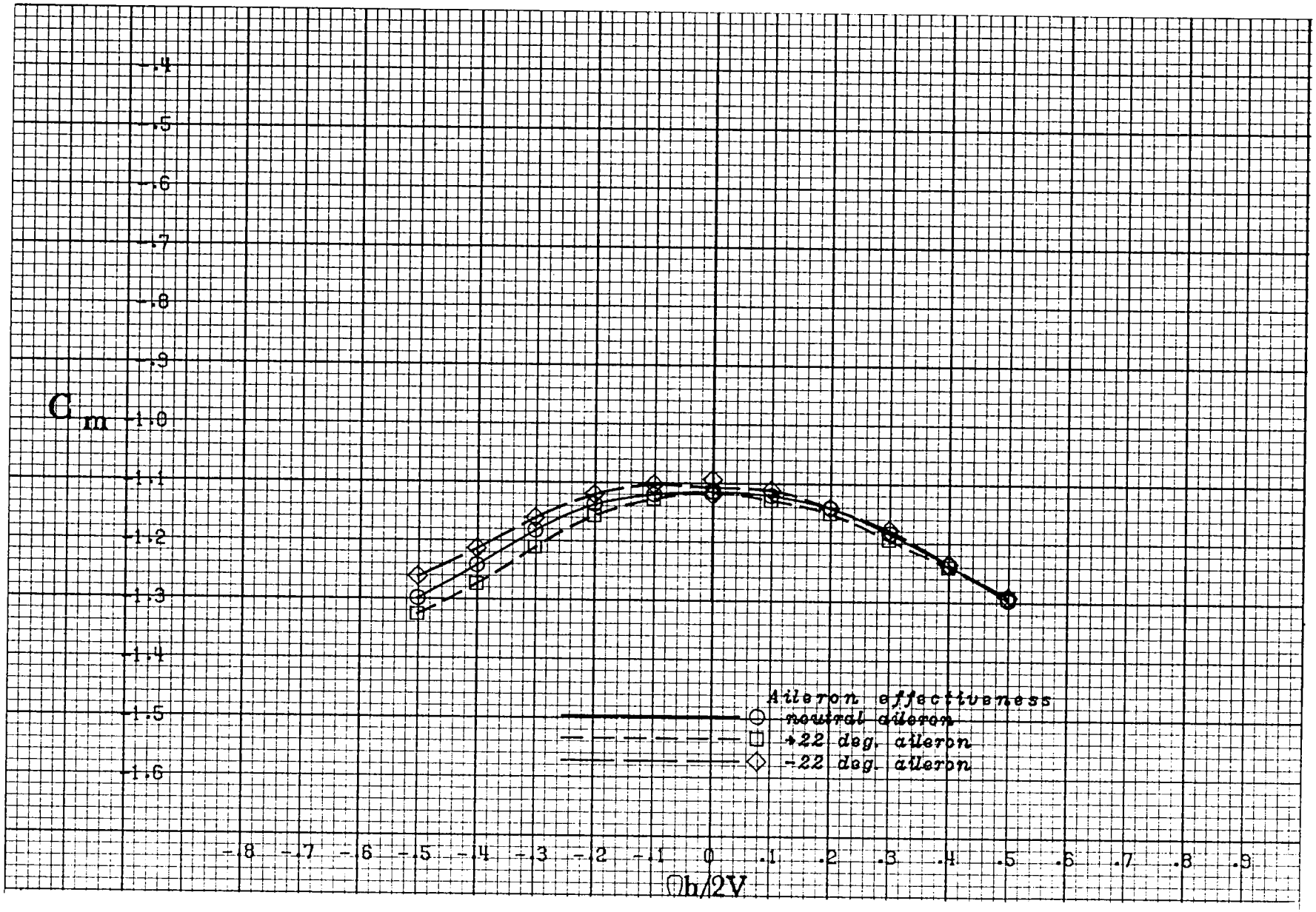

(j) α = 90 deg.

Figure A 21 .- Concluded.

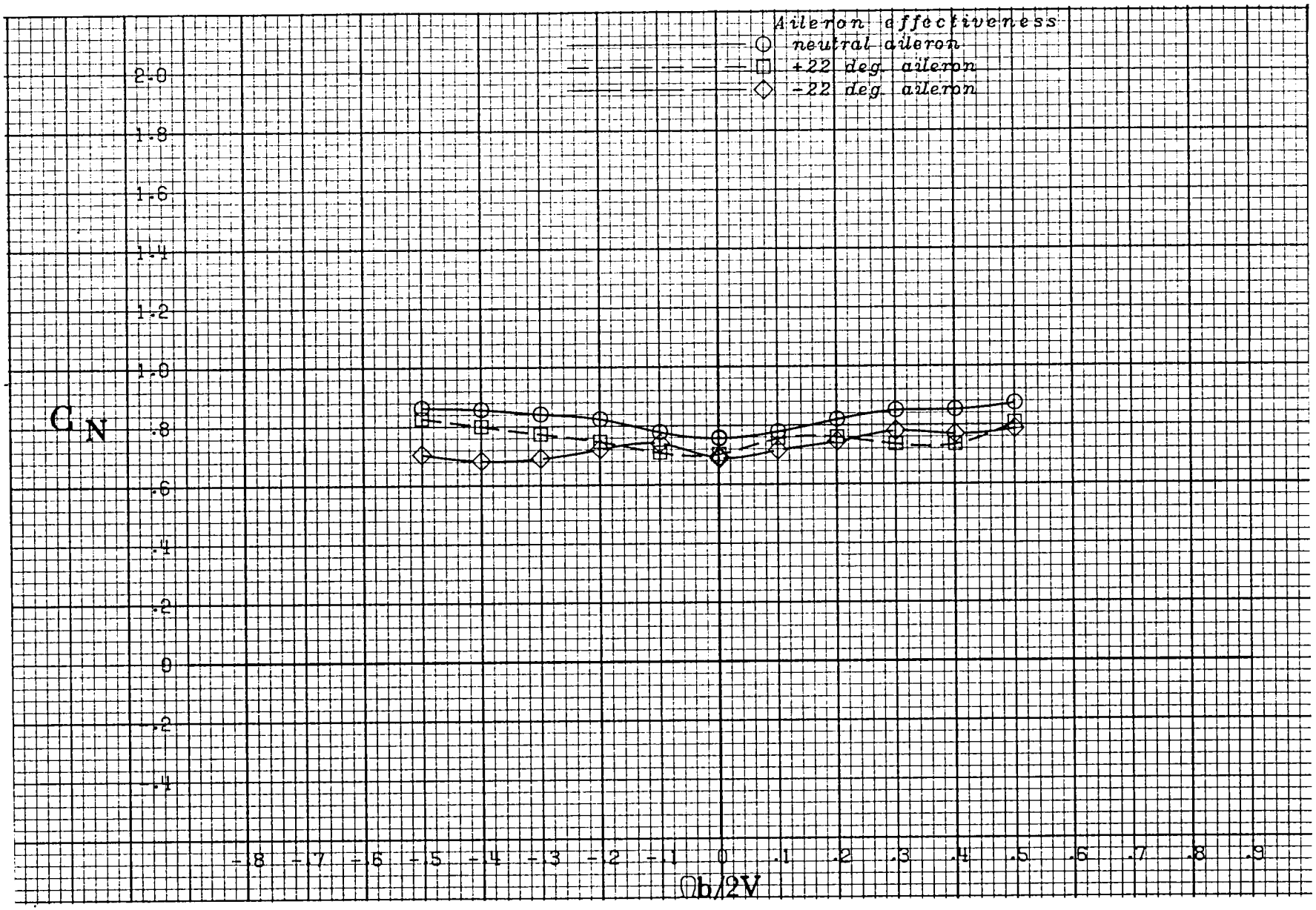

(a) α = 20 deg.

Figure A 22 .- Effect of rotation rate and aileron deflection on normal-force coefficient for the basic configuration with -10 deg elevator and -26 deg rudder at zero sideslip angle.

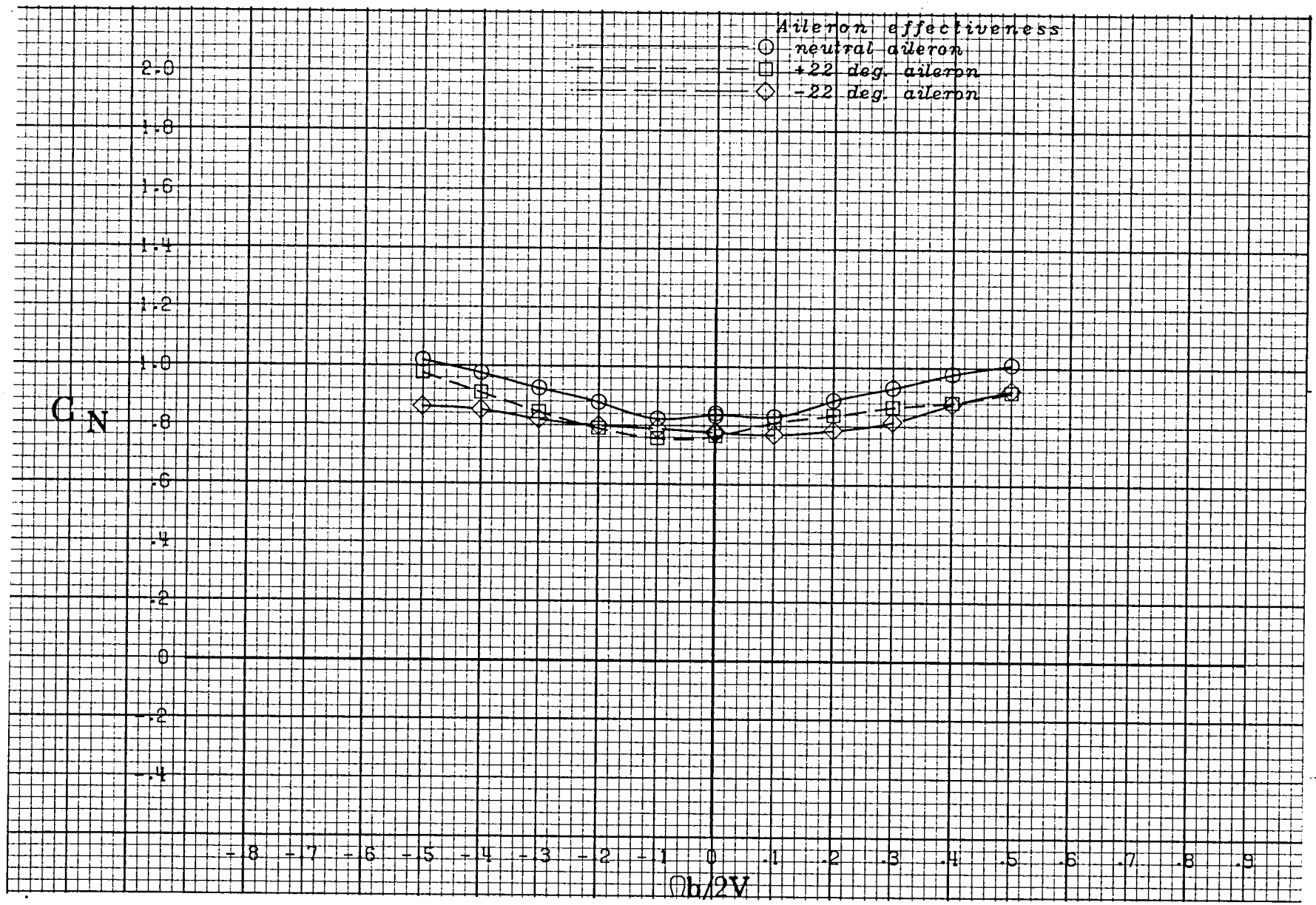

(b) α = 25 deg.

Figure A 22 .- Continued.

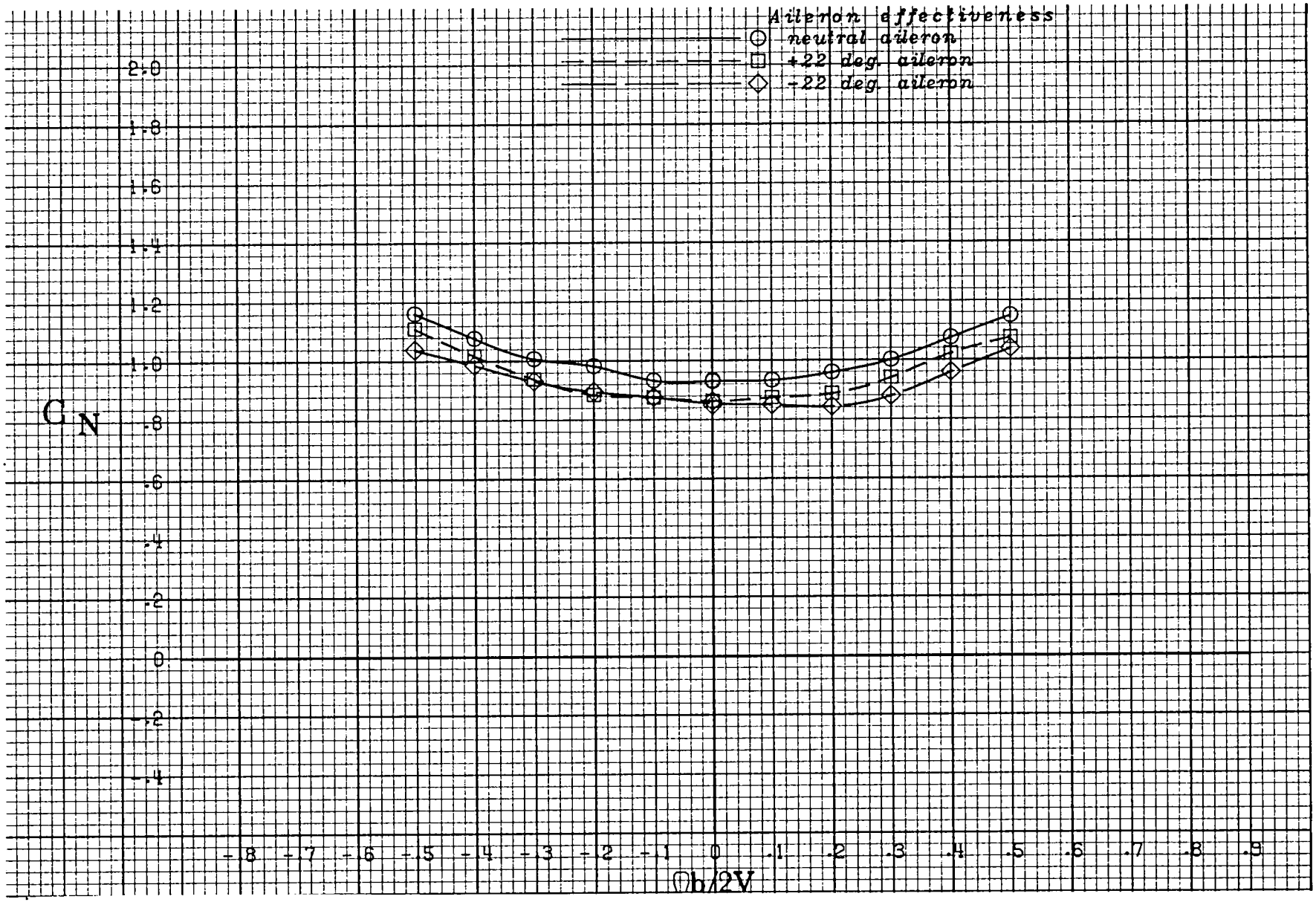

(c) α = 30 deg.

Figure A 22 .- Continued.

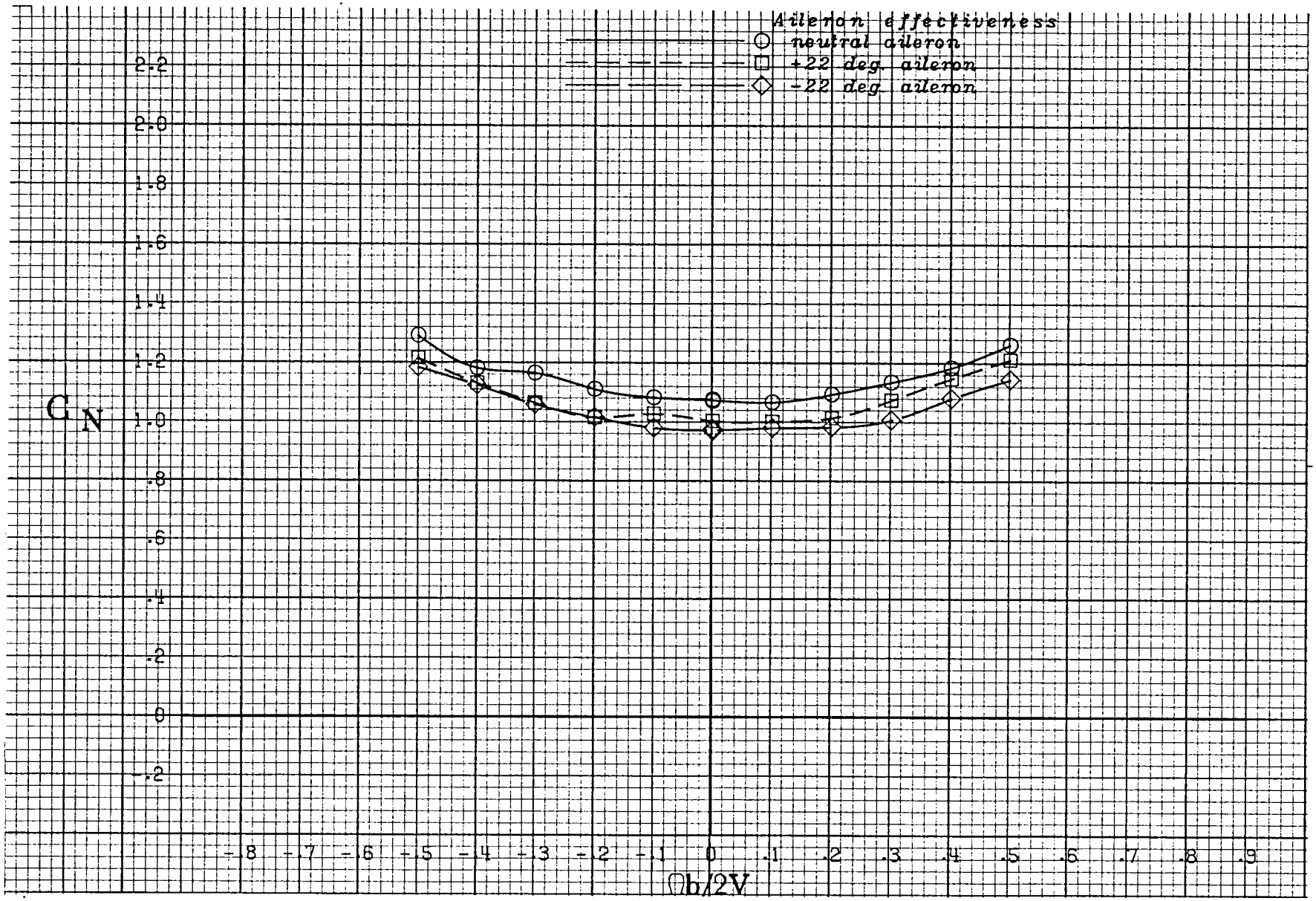

(d) α = 35 deg.

Figure A 22 .- Continued.

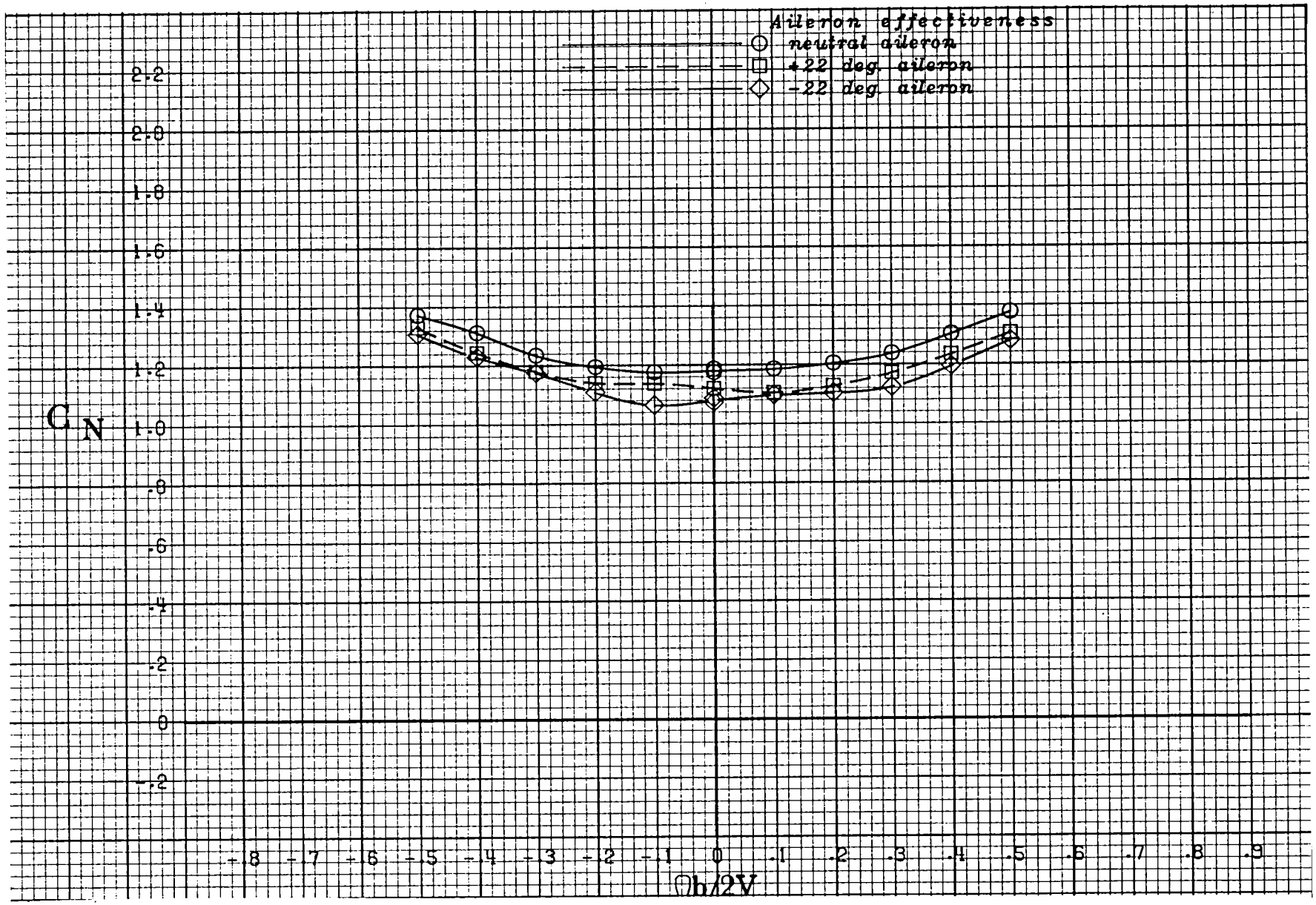

(e) α = 40 deg.

Figure A 22 .- Continued.

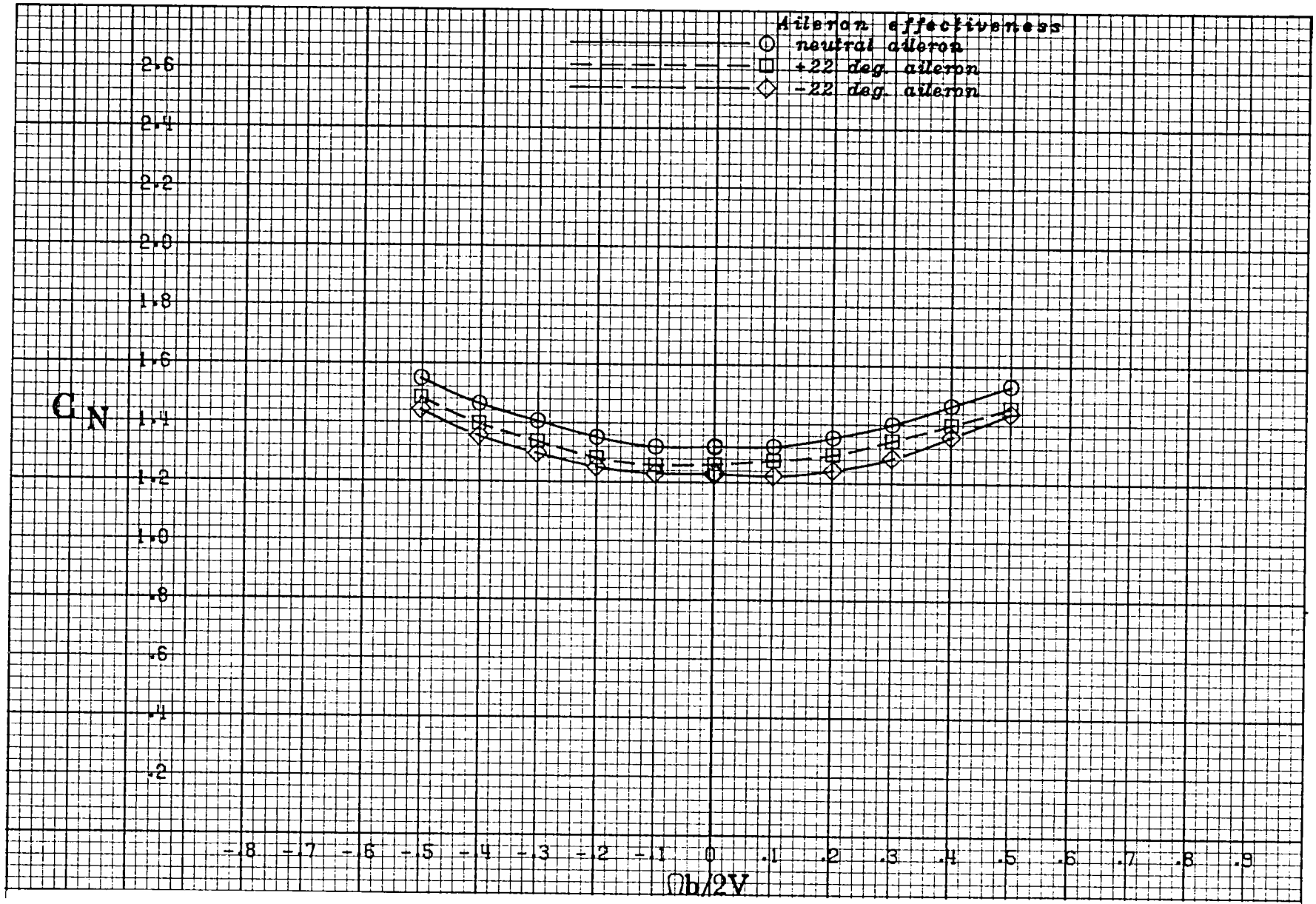

(f) α = 50 deg.

Figure A 22 .- Continued.

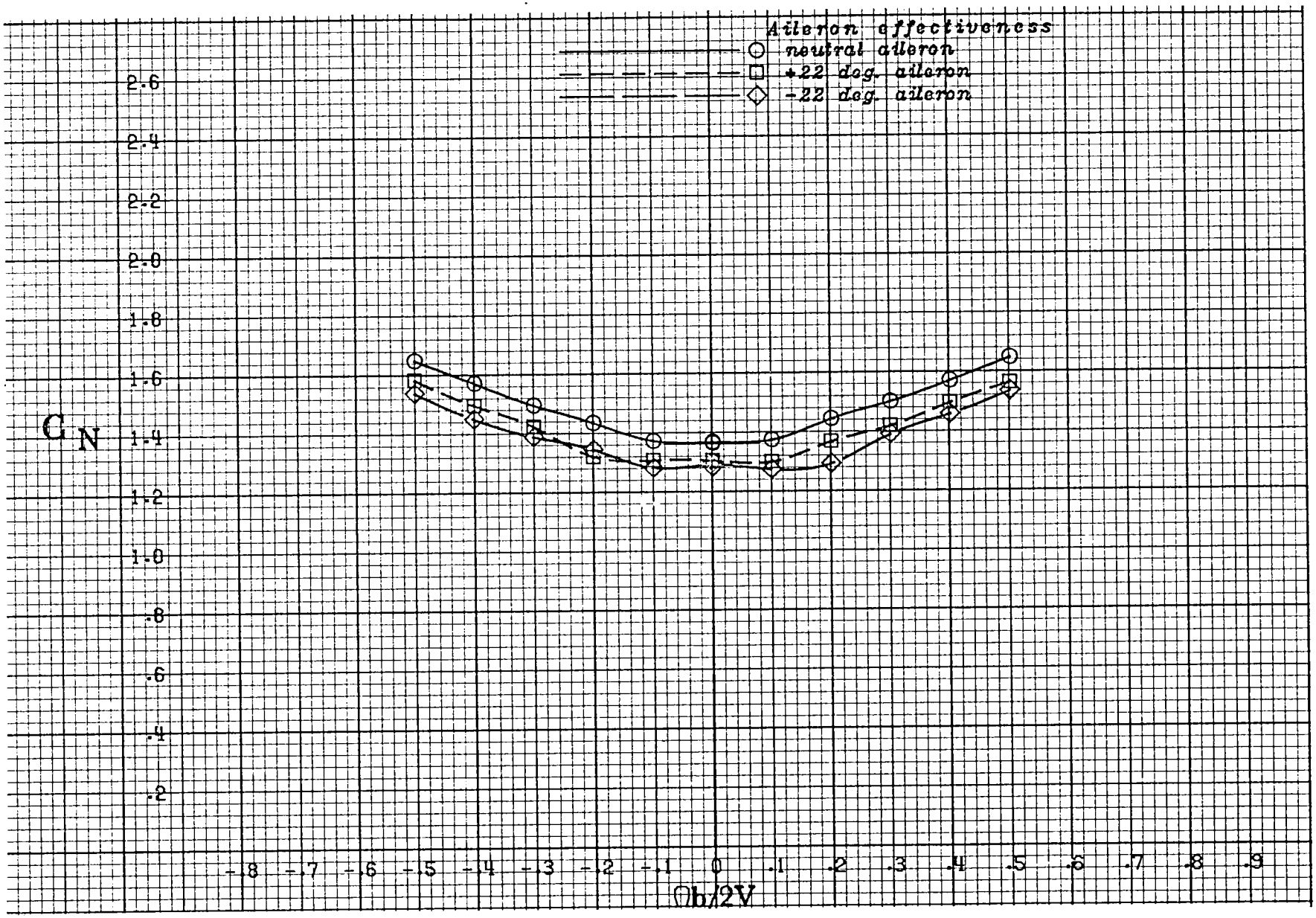

(g) α = 60 deg.

Figure A 22 .- Continued.

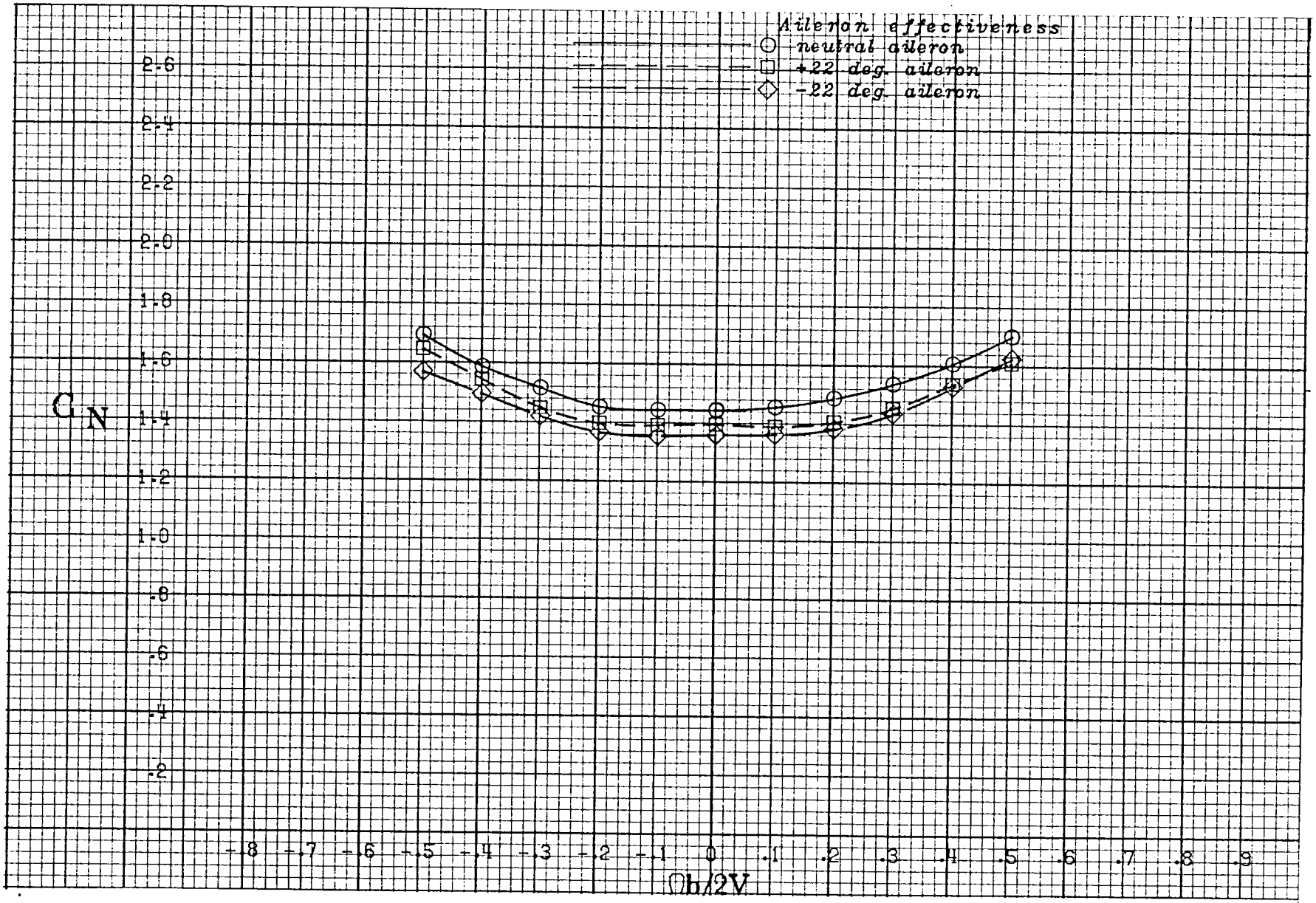

(h) α = 70 deg.

Figure A 22 .- Continued.

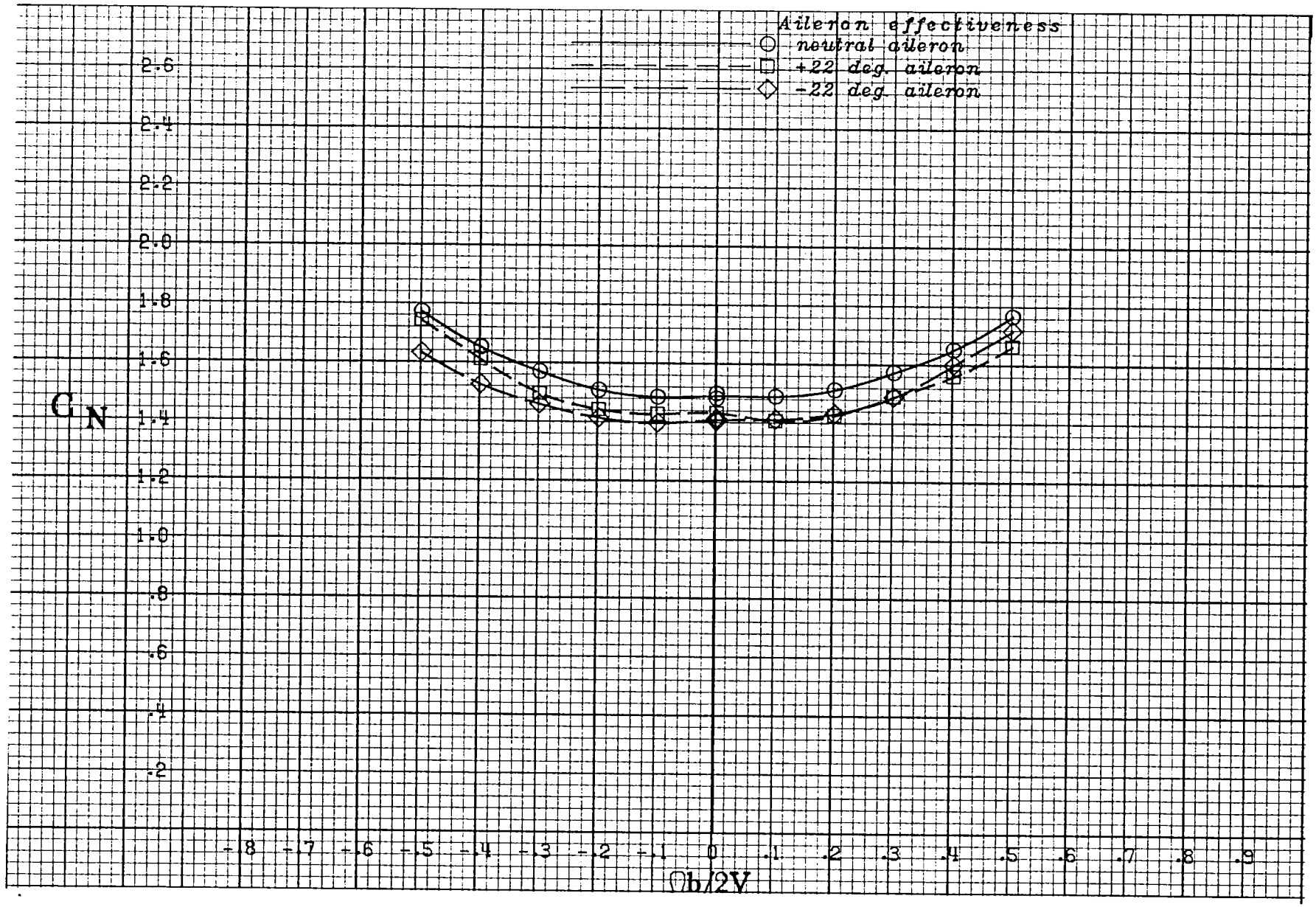

(i) α = 80 deg.

Figure A 22 .- Continued.

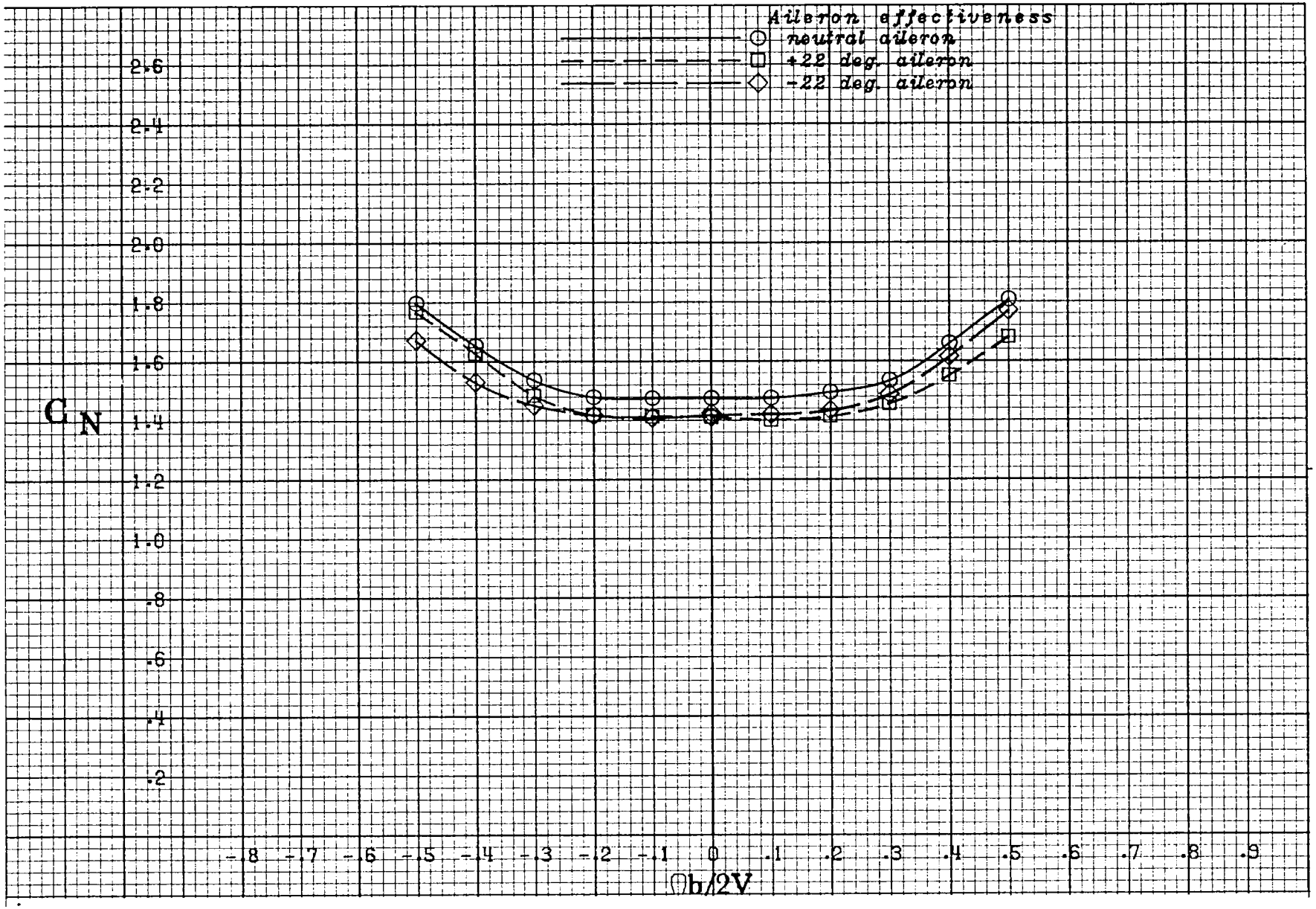

(j) α = 90 deg.

Figure A 22 .- Concluded.

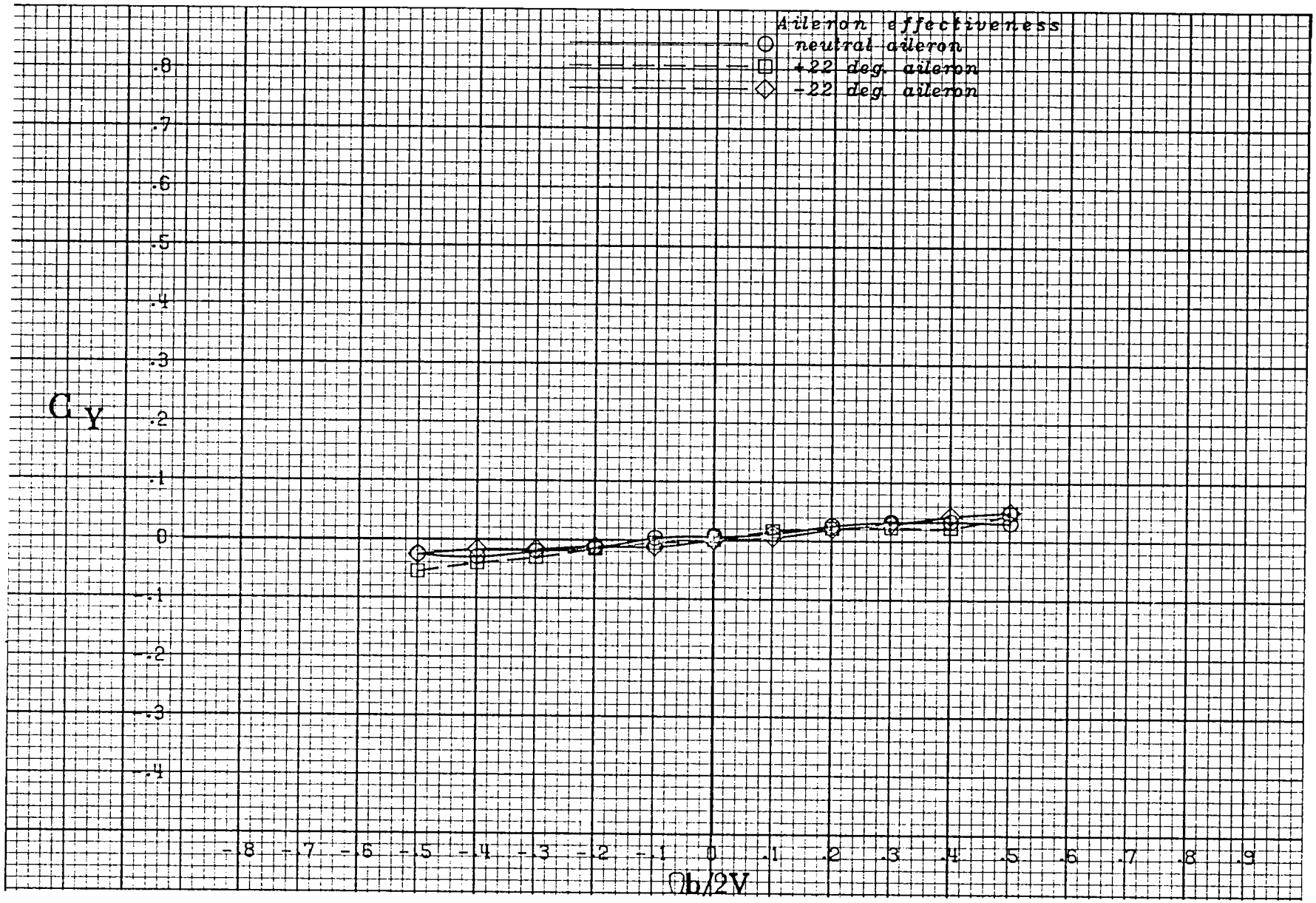

(a) α = 20 deg.

Figure A 23 .- Effect of rotation rate and aileron deflection on side-force coefficient for the basic configuration with -10 deg elevator and -26 deg rudder at zero sideslip angle.

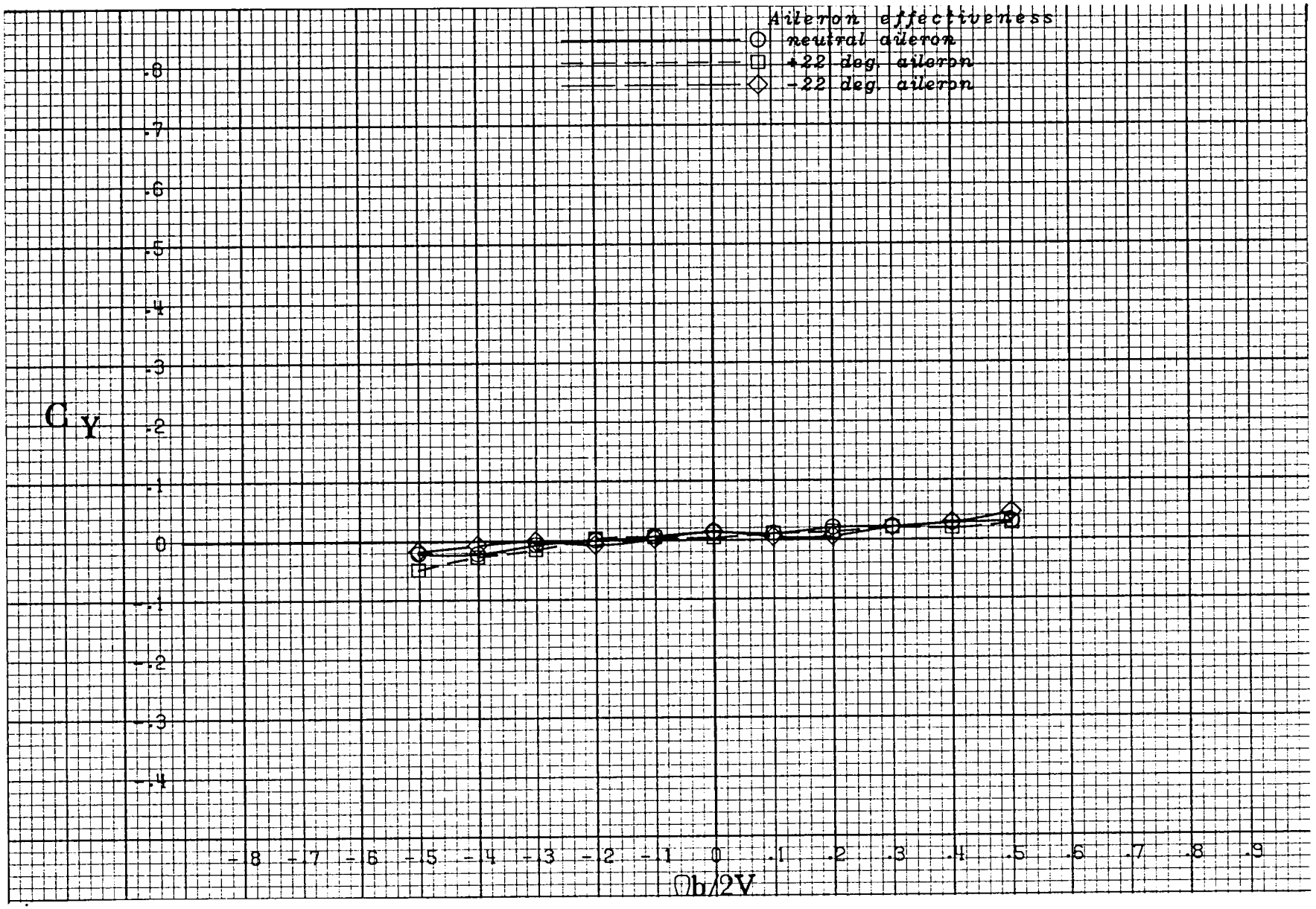

(b) α = 25 deg.

Figure A 23 .- Continued.

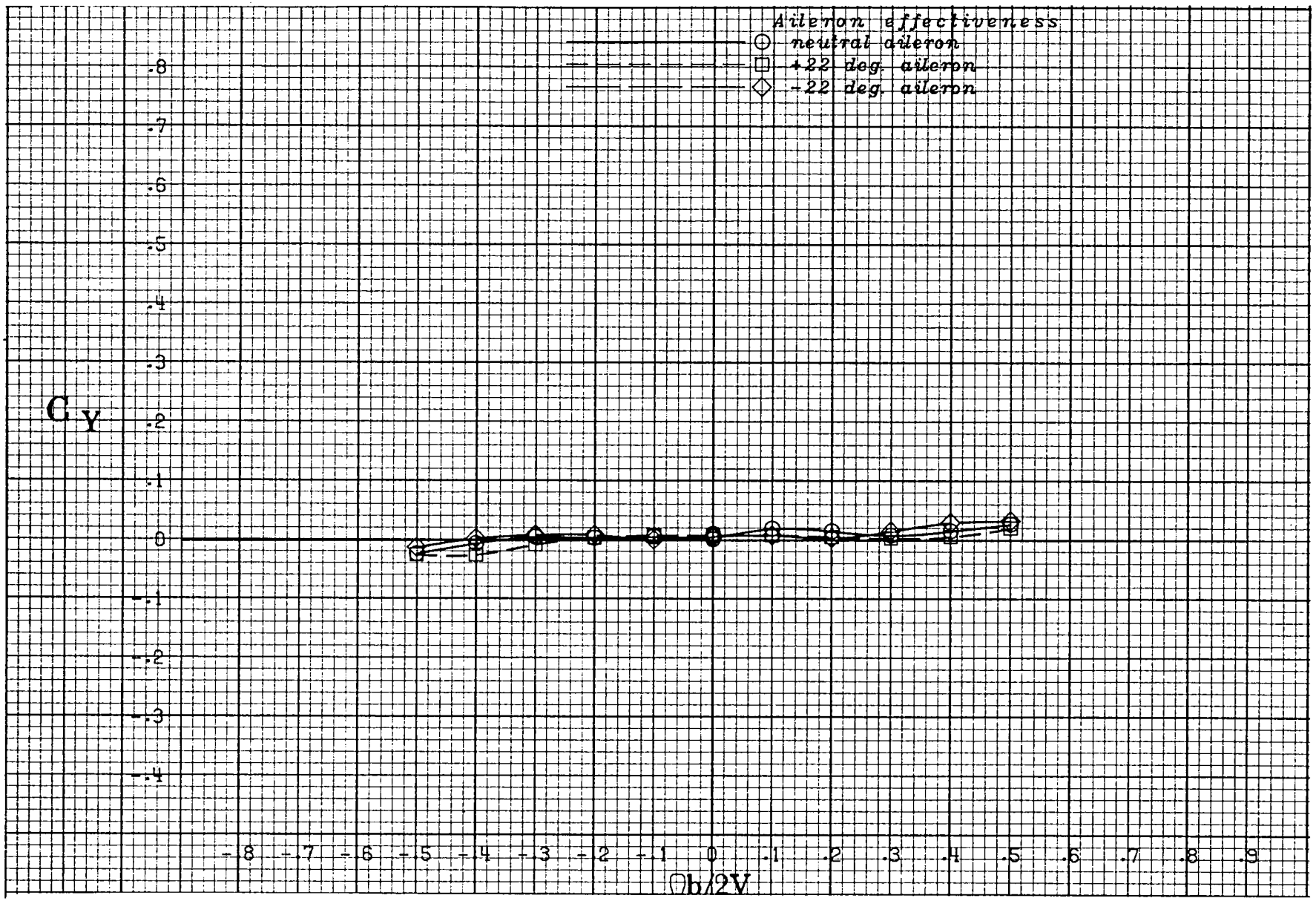

(c) α = 30 deg.

Figure A 23 .- Continued.

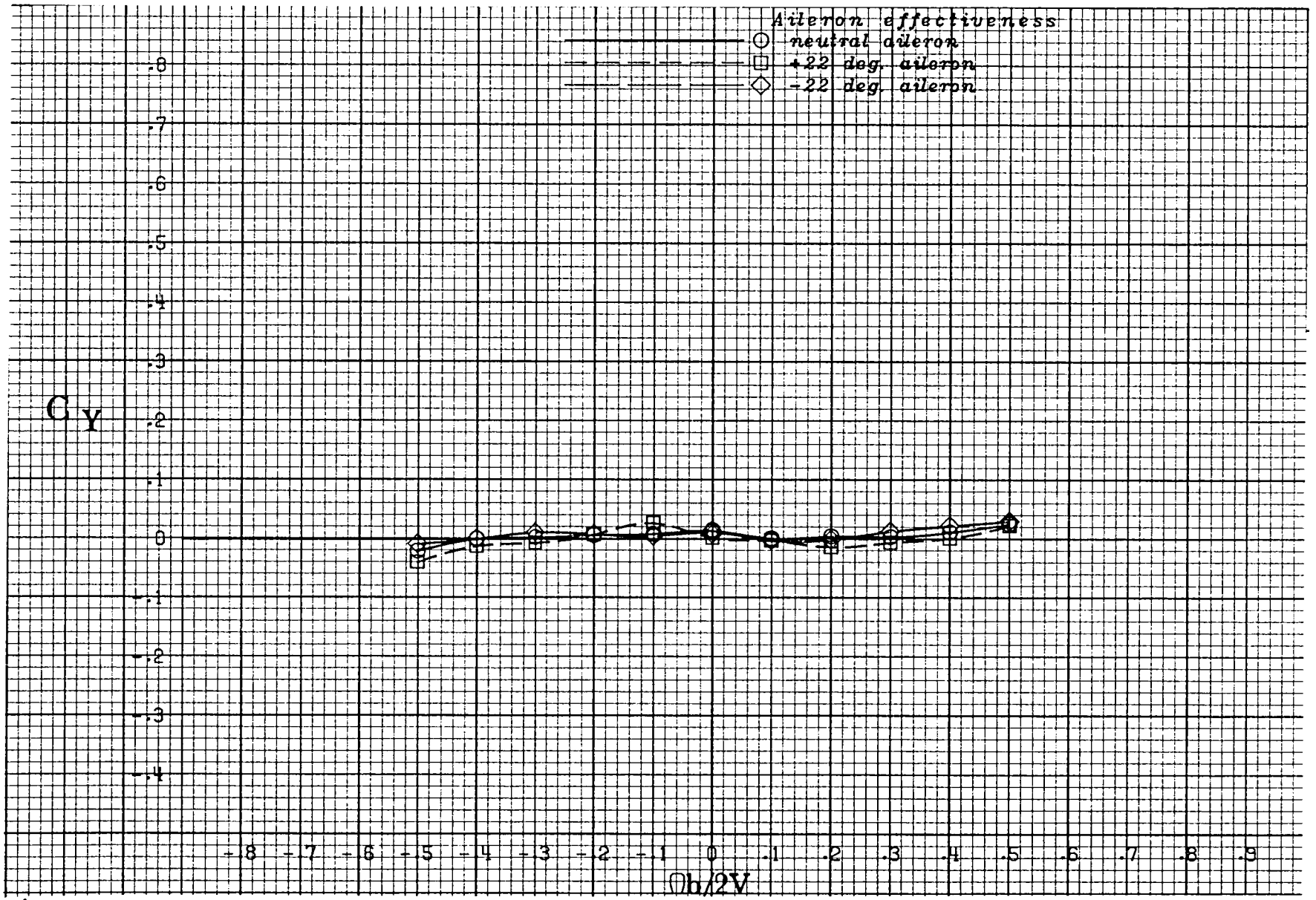

(d) α = 35 deg.

Figure A 23 .- Continued.

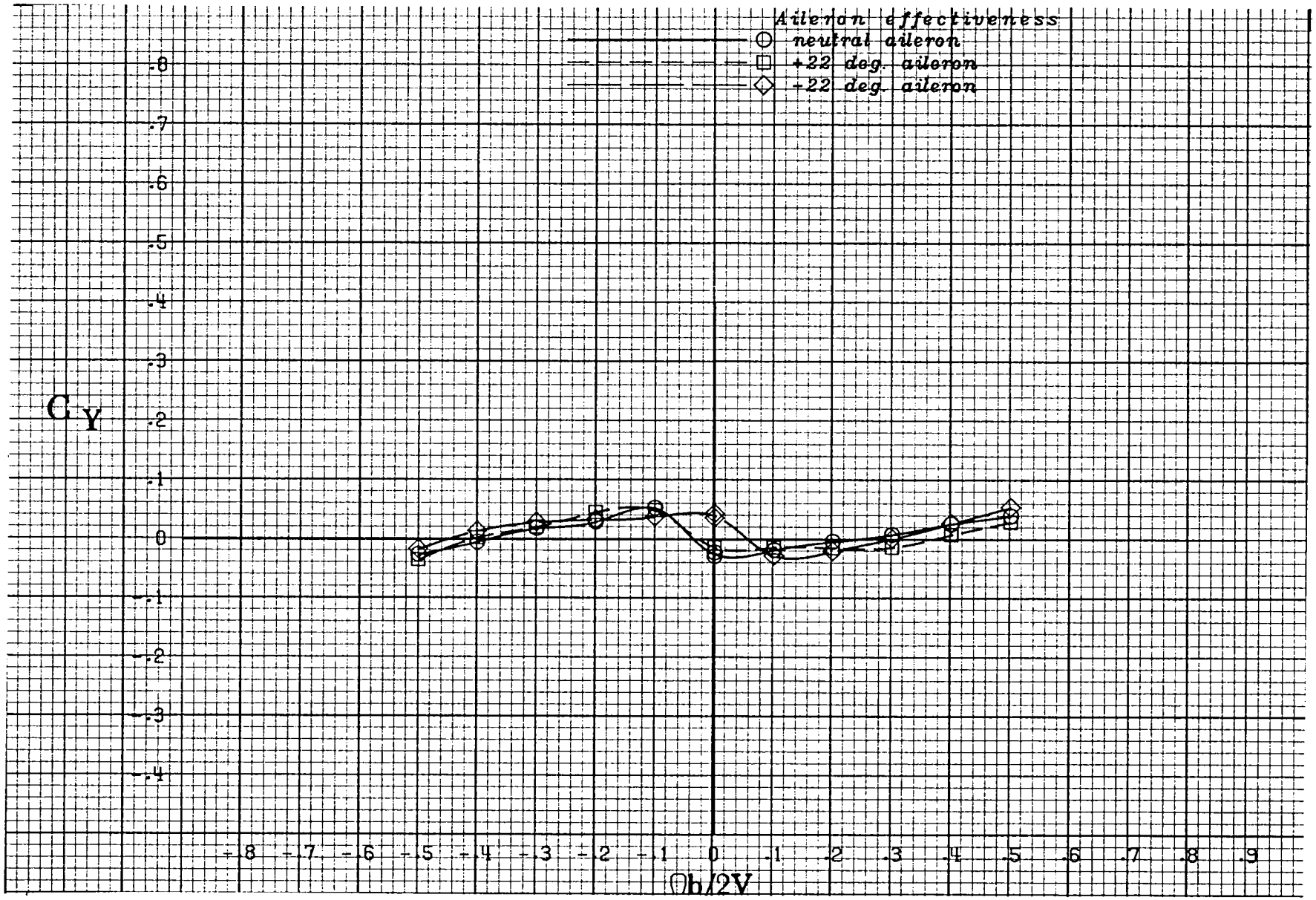

(e) α = 40 deg.

Figure A 23 .- Continued.

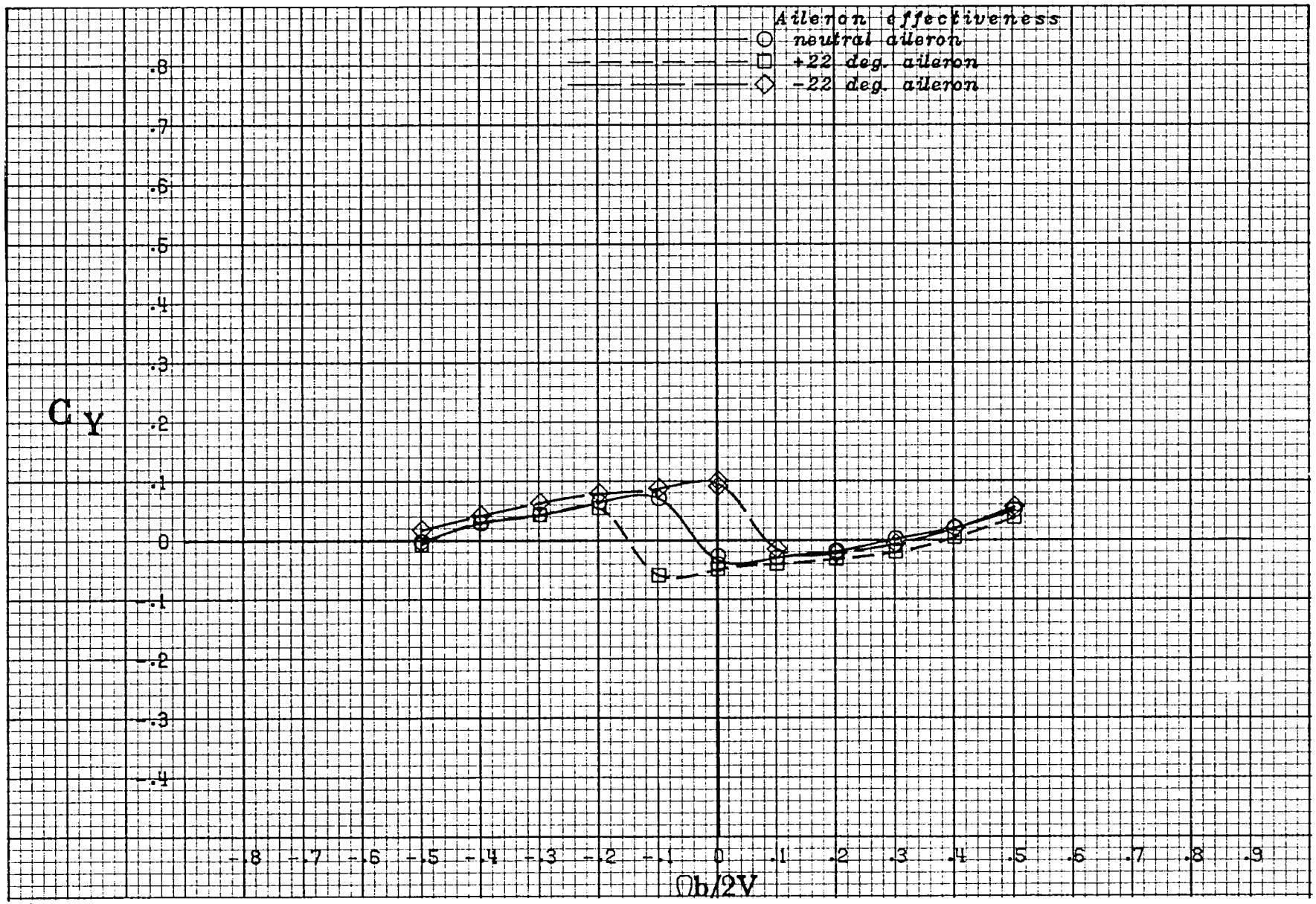

(f) α = 50 deg.

Figure A 23 .- Continued.

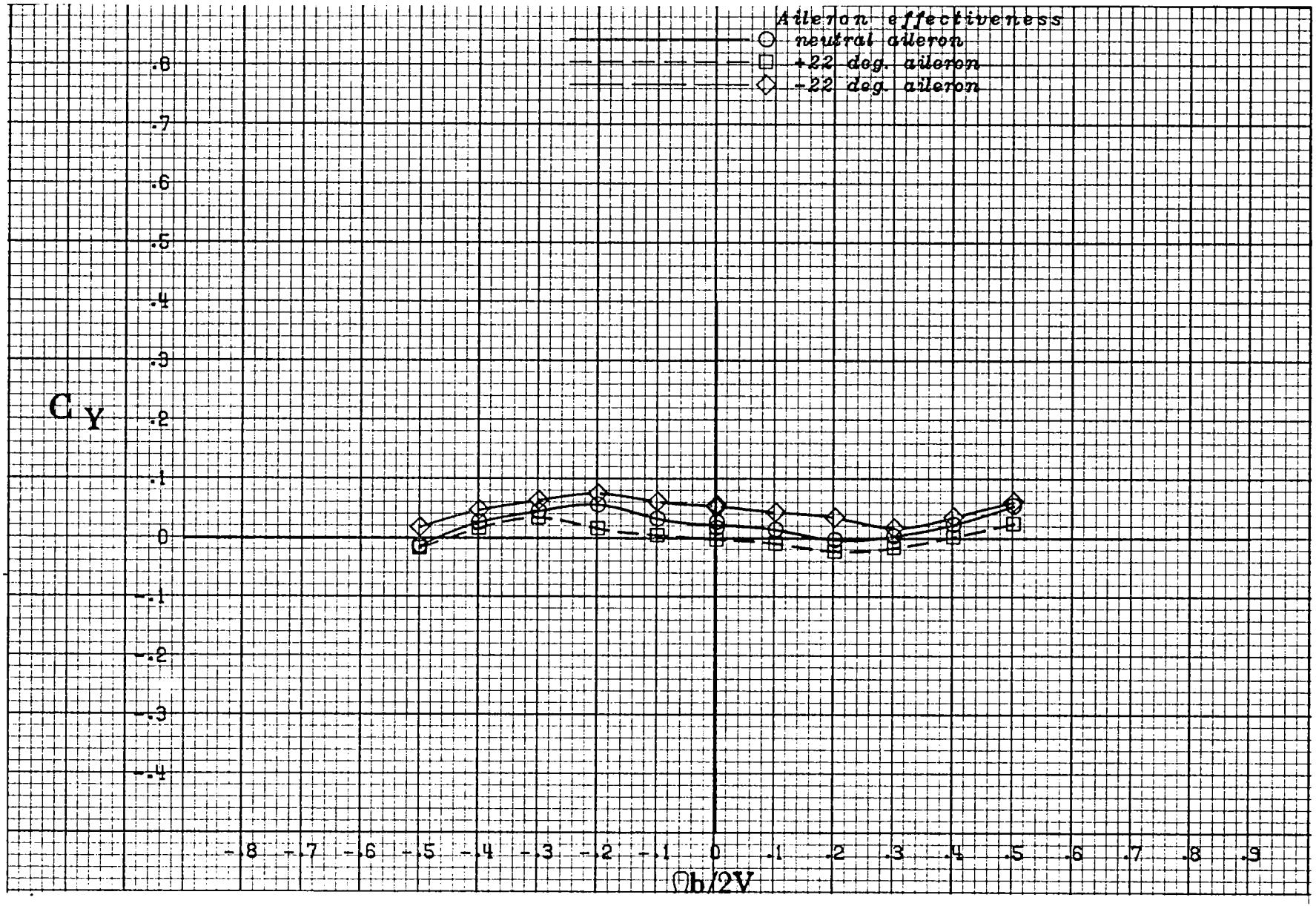

(g) α = 60 deg.

Figure A 23 .- Continued.

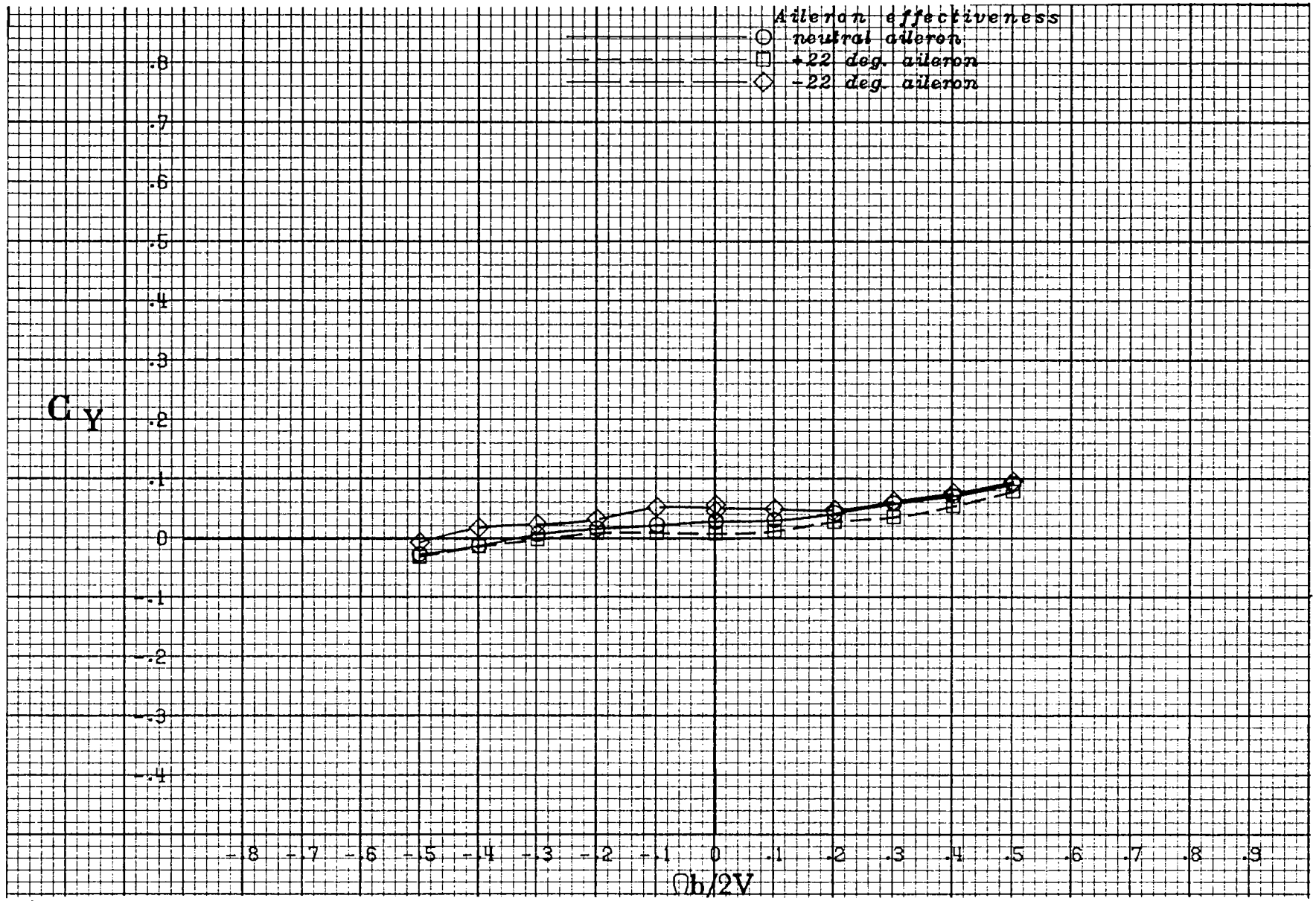

(h) α = 70 deg.

Figure A 23 .- Continued.

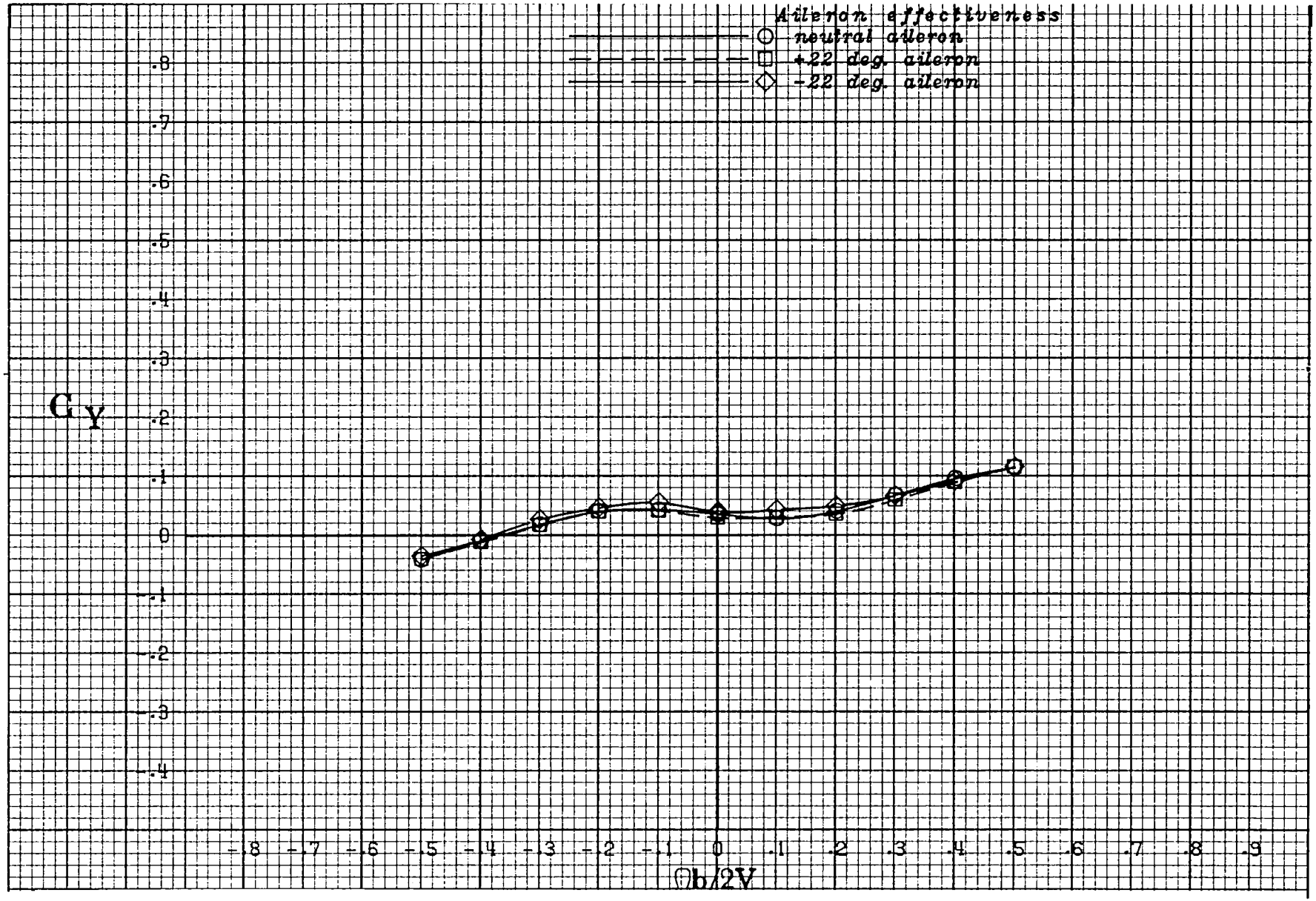

(i) α = 80 deg.

Figure A 23 .- Continued.

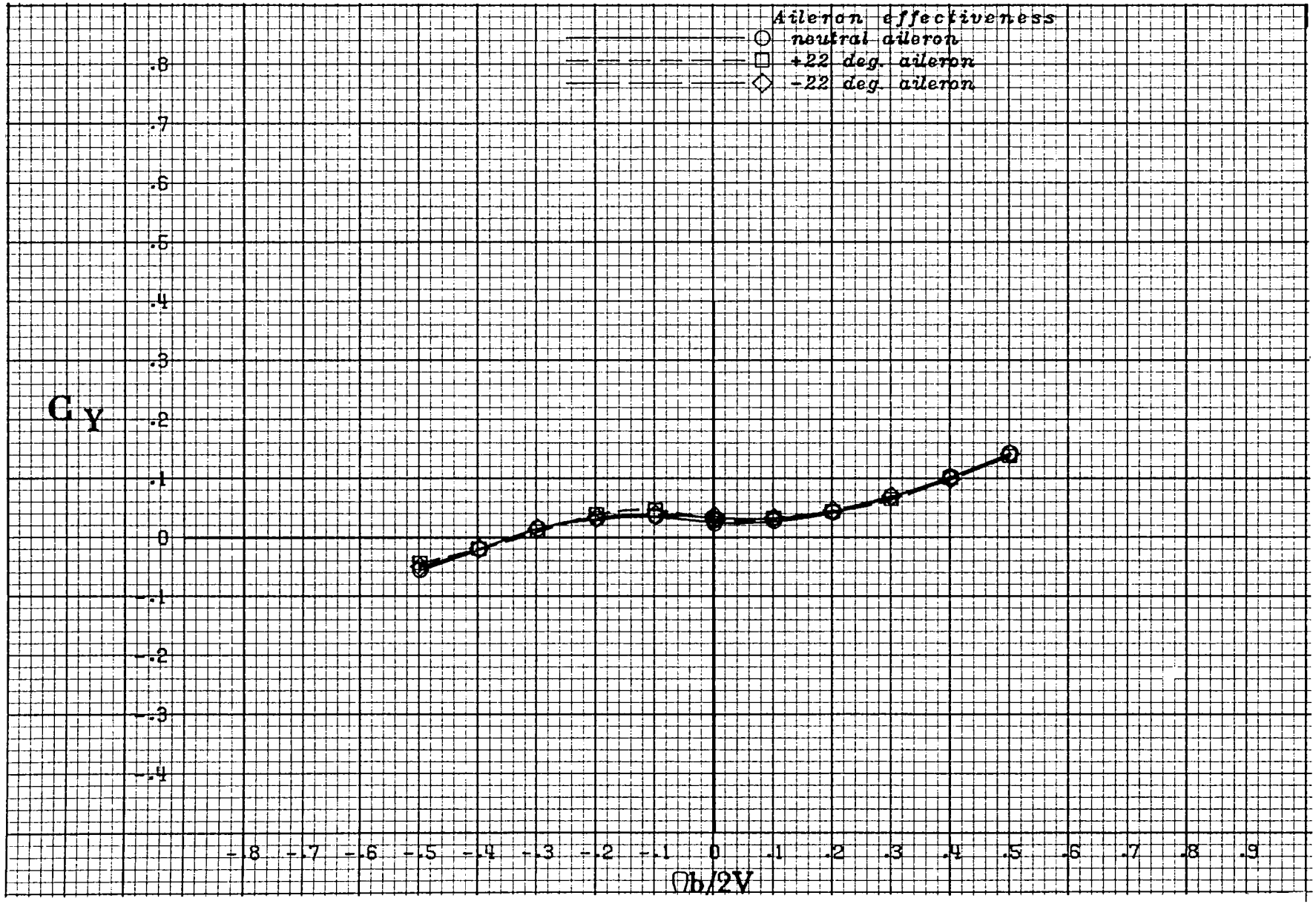

(j) α = 90 deg.

Figure A 23 .- Concluded.

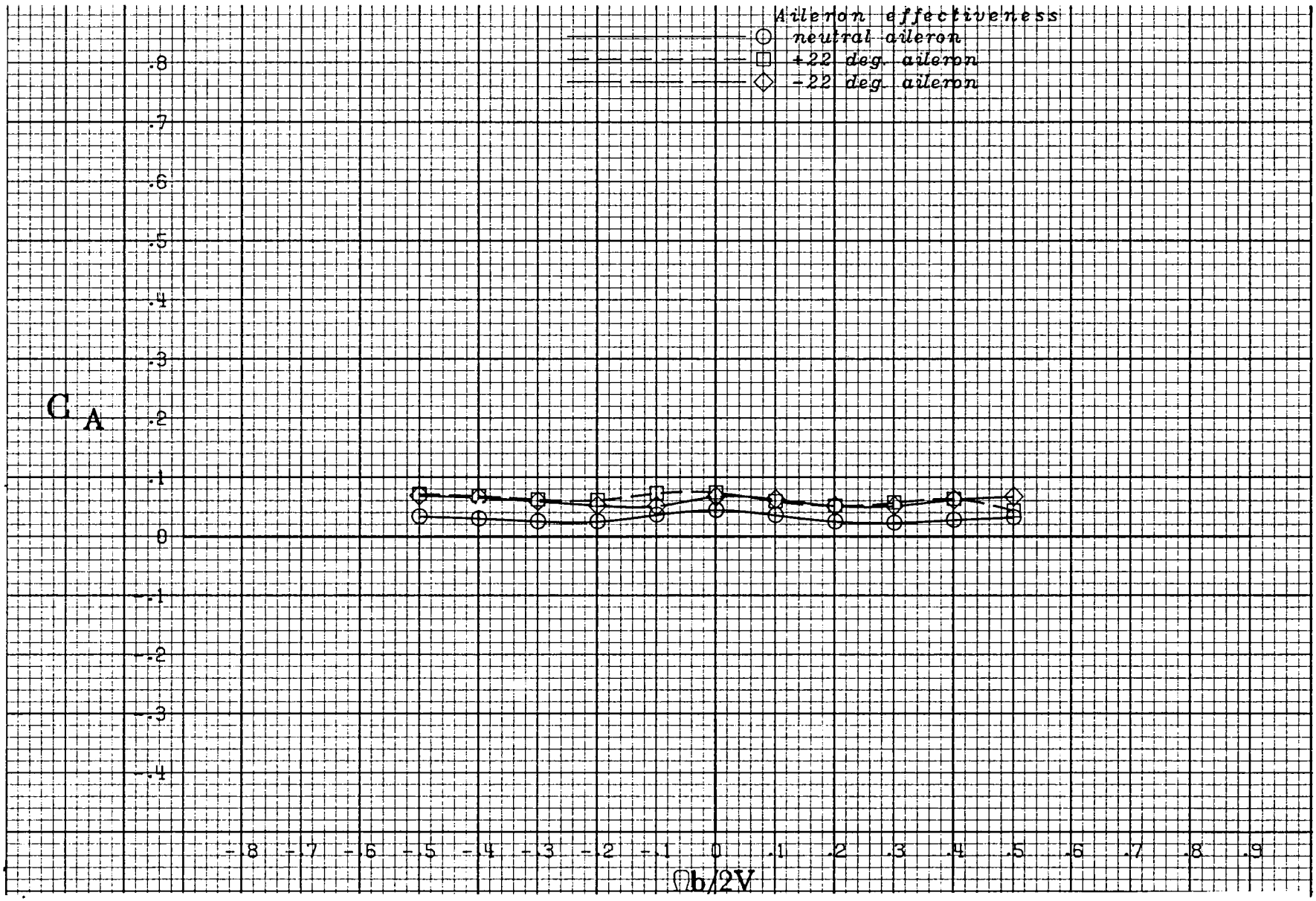

(a) α = 20 deg.

Figure A 24 .- Effect of rotation rate and aileron deflection on axial-force coefficient for the basic configuration with -10 deg elevator and -26 deg rudder at zero sideslip angle.

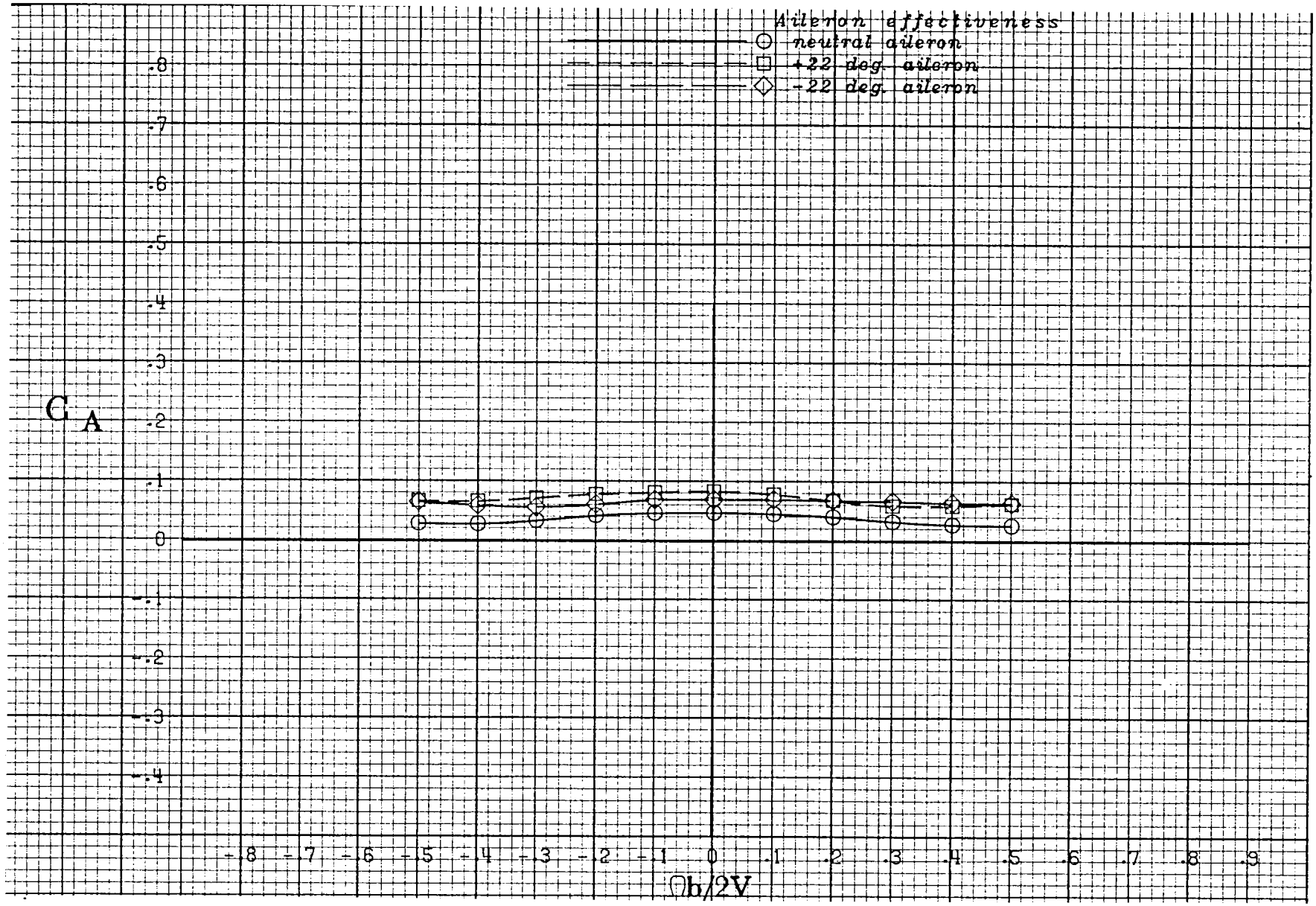

(b) α = 25 deg.

Figure A 24 .- Continued.

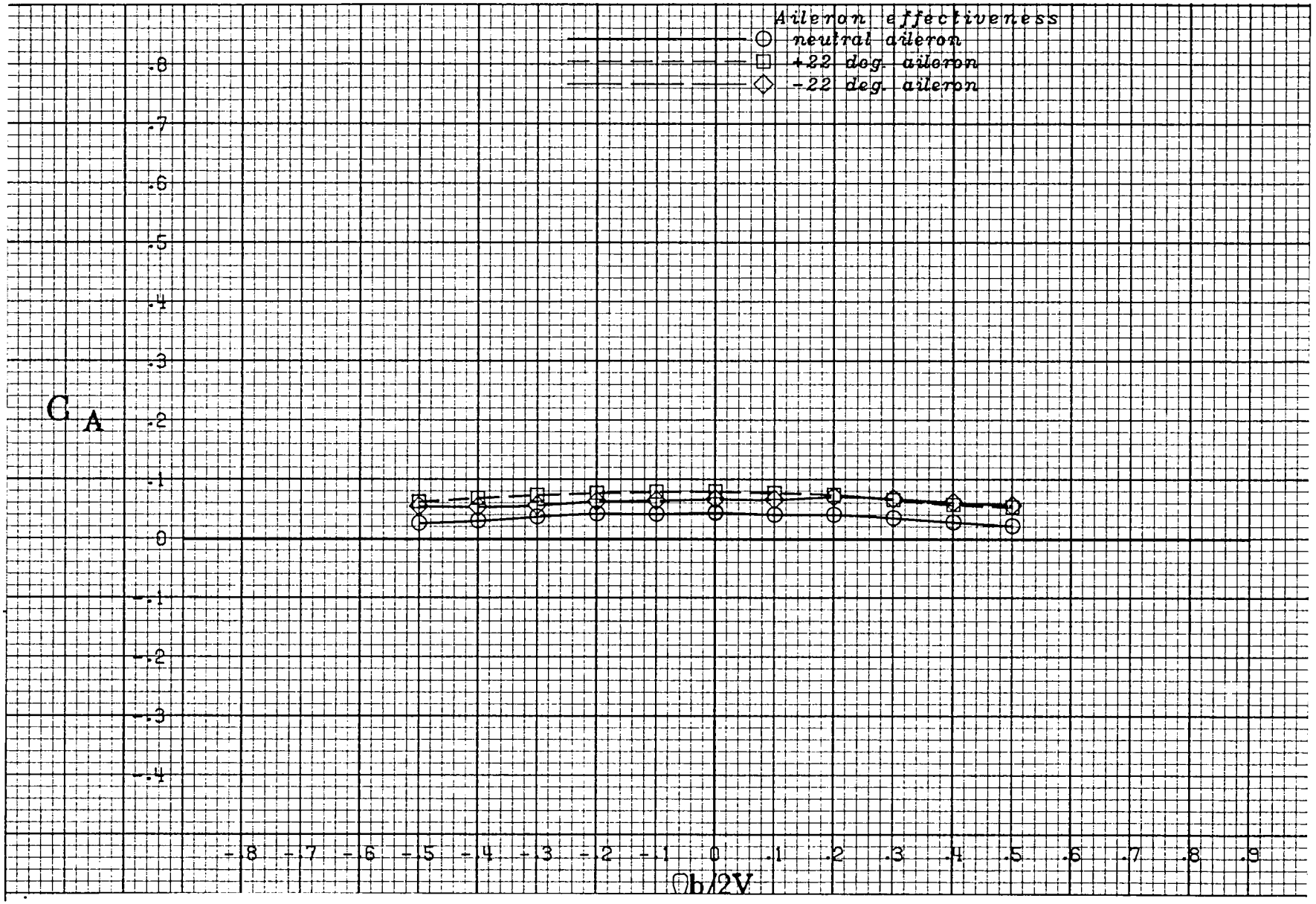

(c) α = 30 deg.

Figure A 24 .- Continued.

(d) α = 35 deg.

Figure A 24 .- Continued.

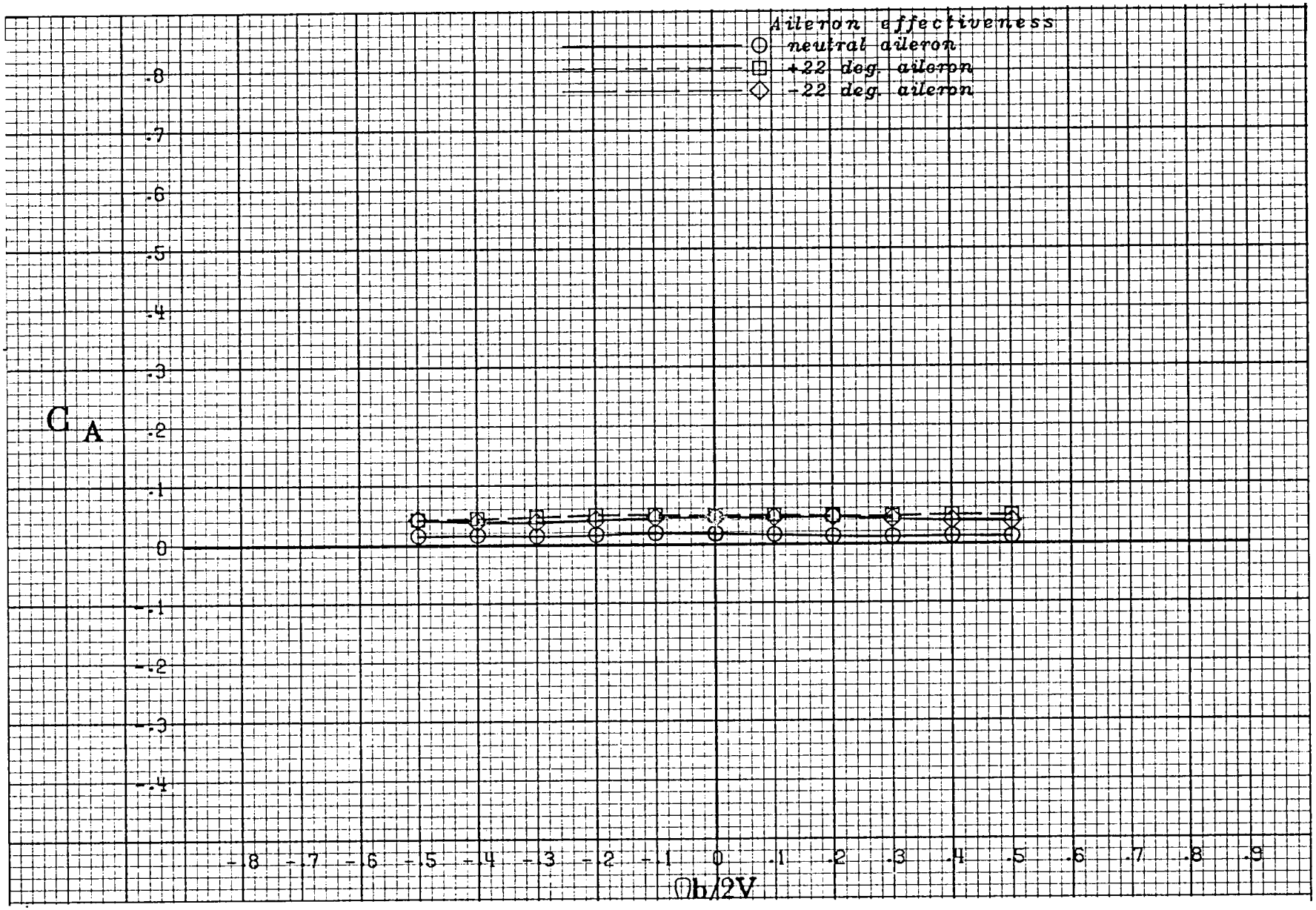

(e) α = 40 deg.

Figure A 24 .- Continued.

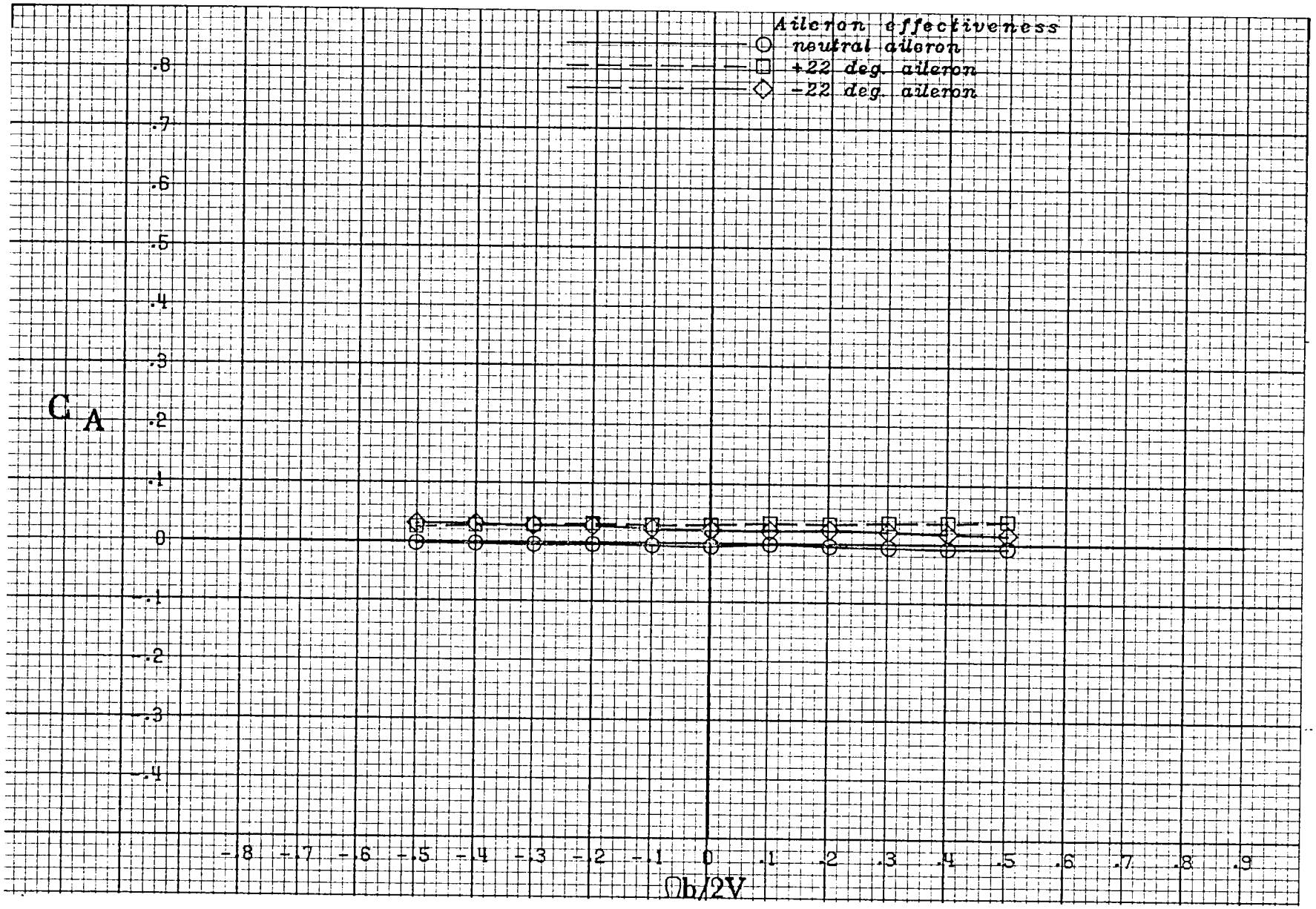

(f) α = 50 deg.

Figure A 24 .- Continued.

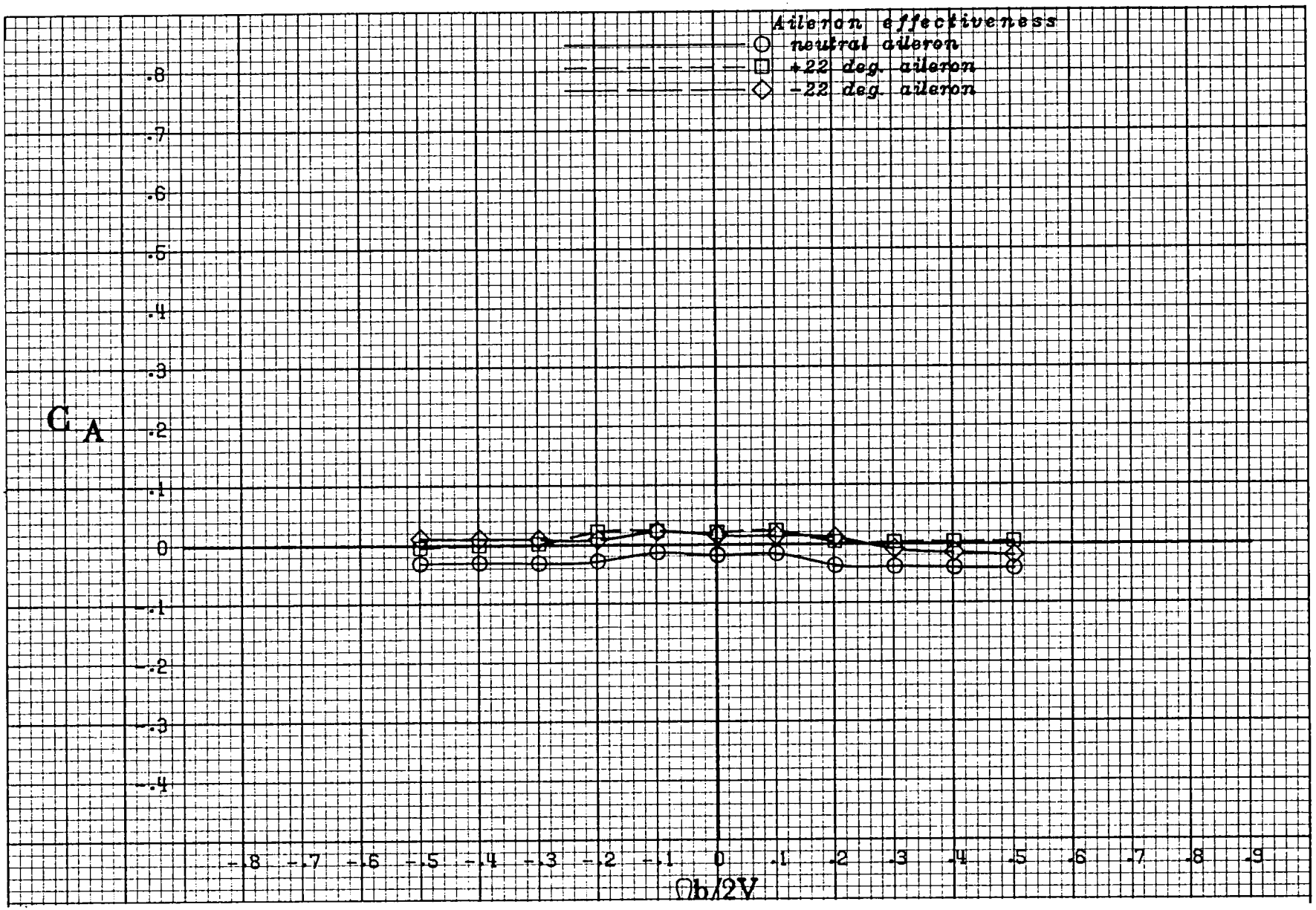

(g) α = 60 deg.

Figure A 24 .- Continued.

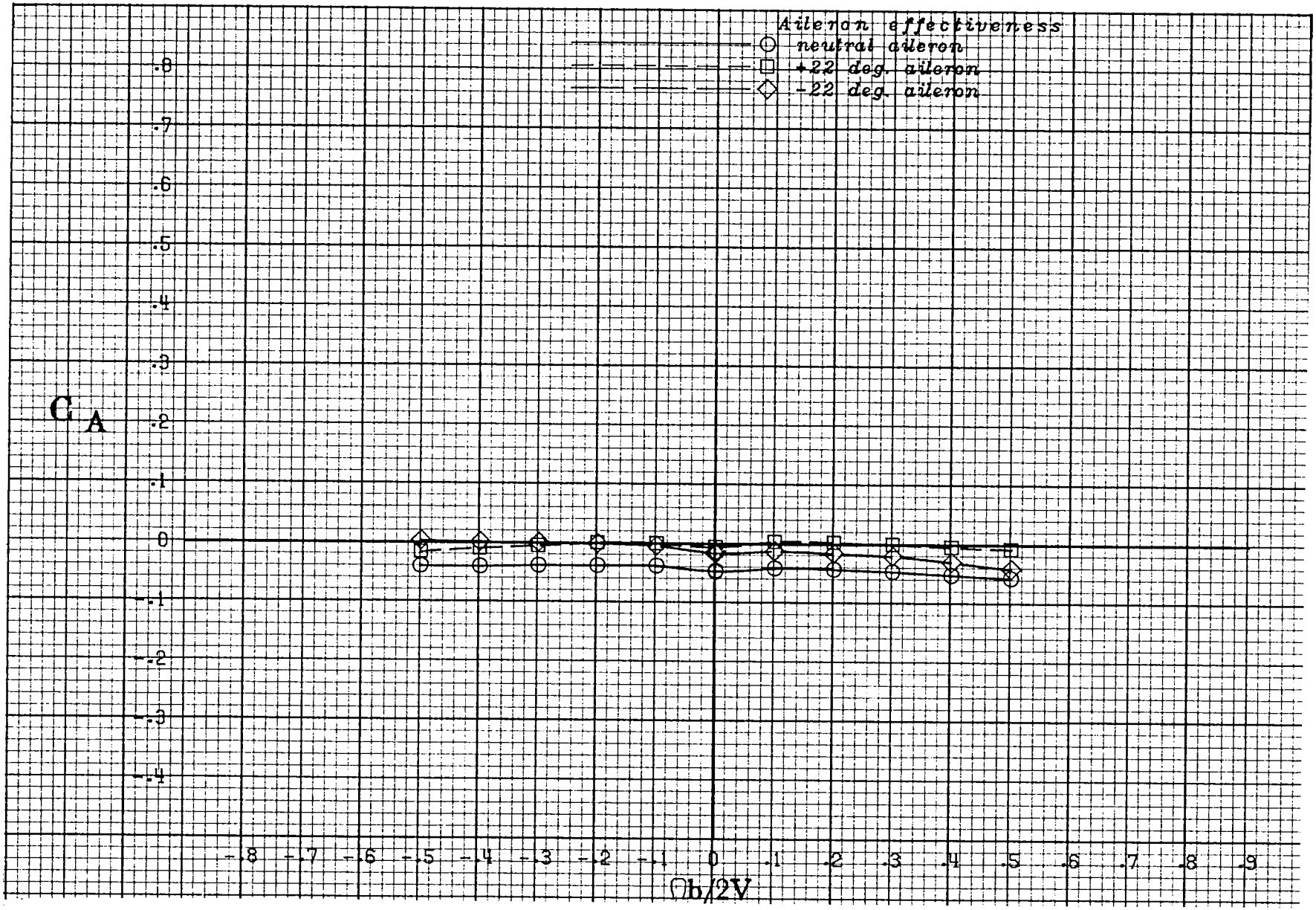

(h) α = 70 deg.

Figure A 24 .- Continued.

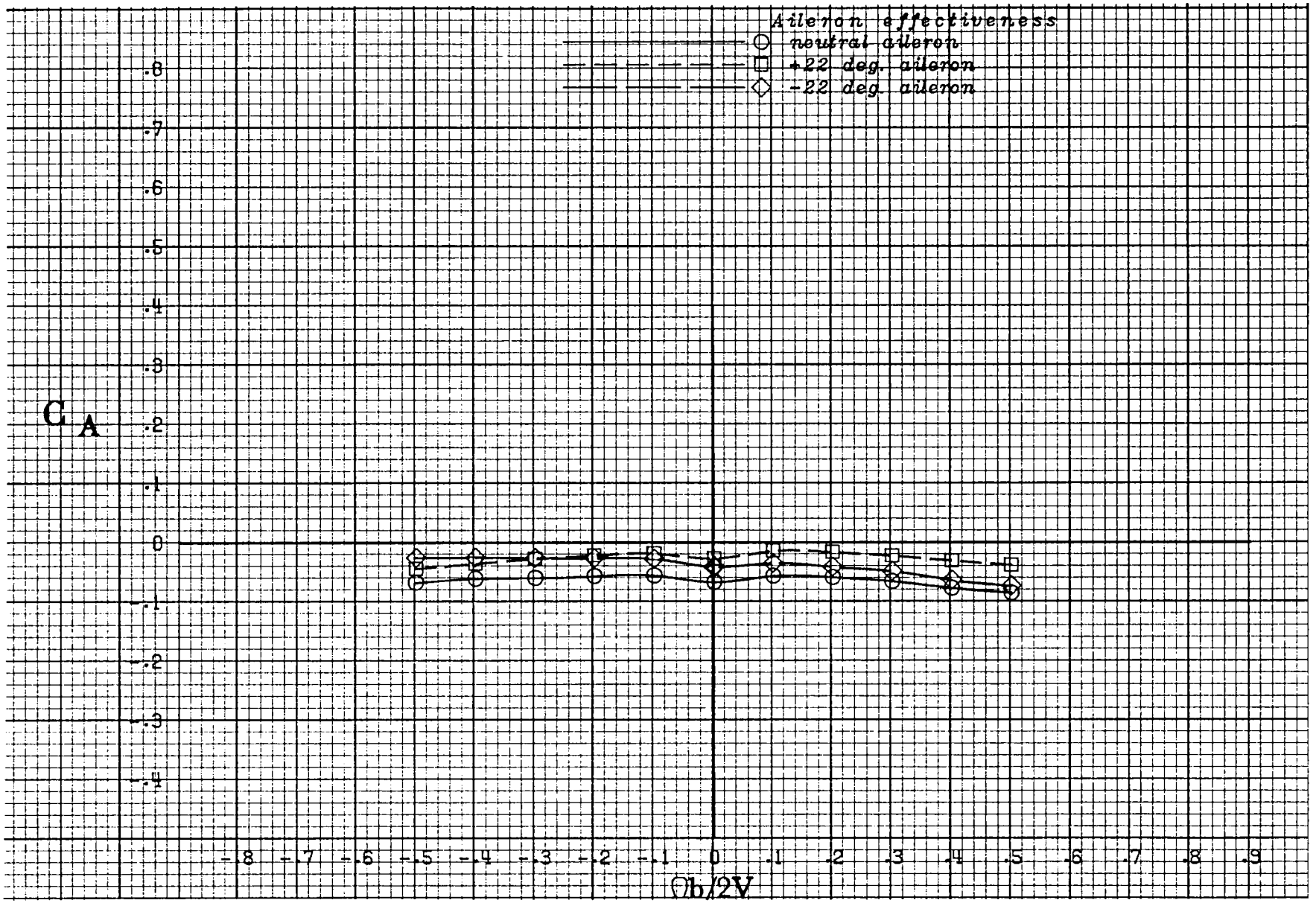

(i) α = 80 deg.

Figure A 24 .- Continued.

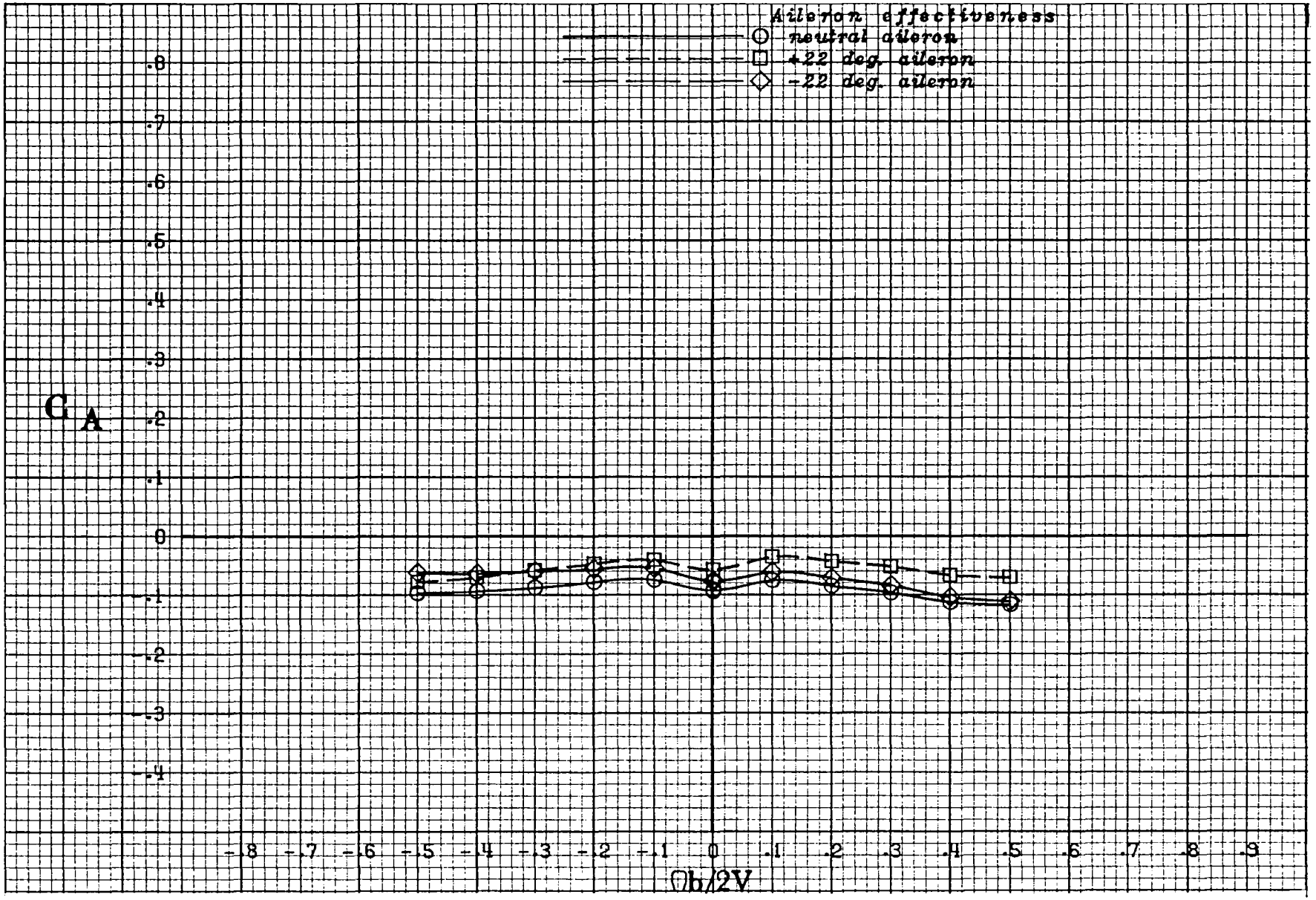

(j) α = 90 deg.

Figure A 24 .- Concluded.

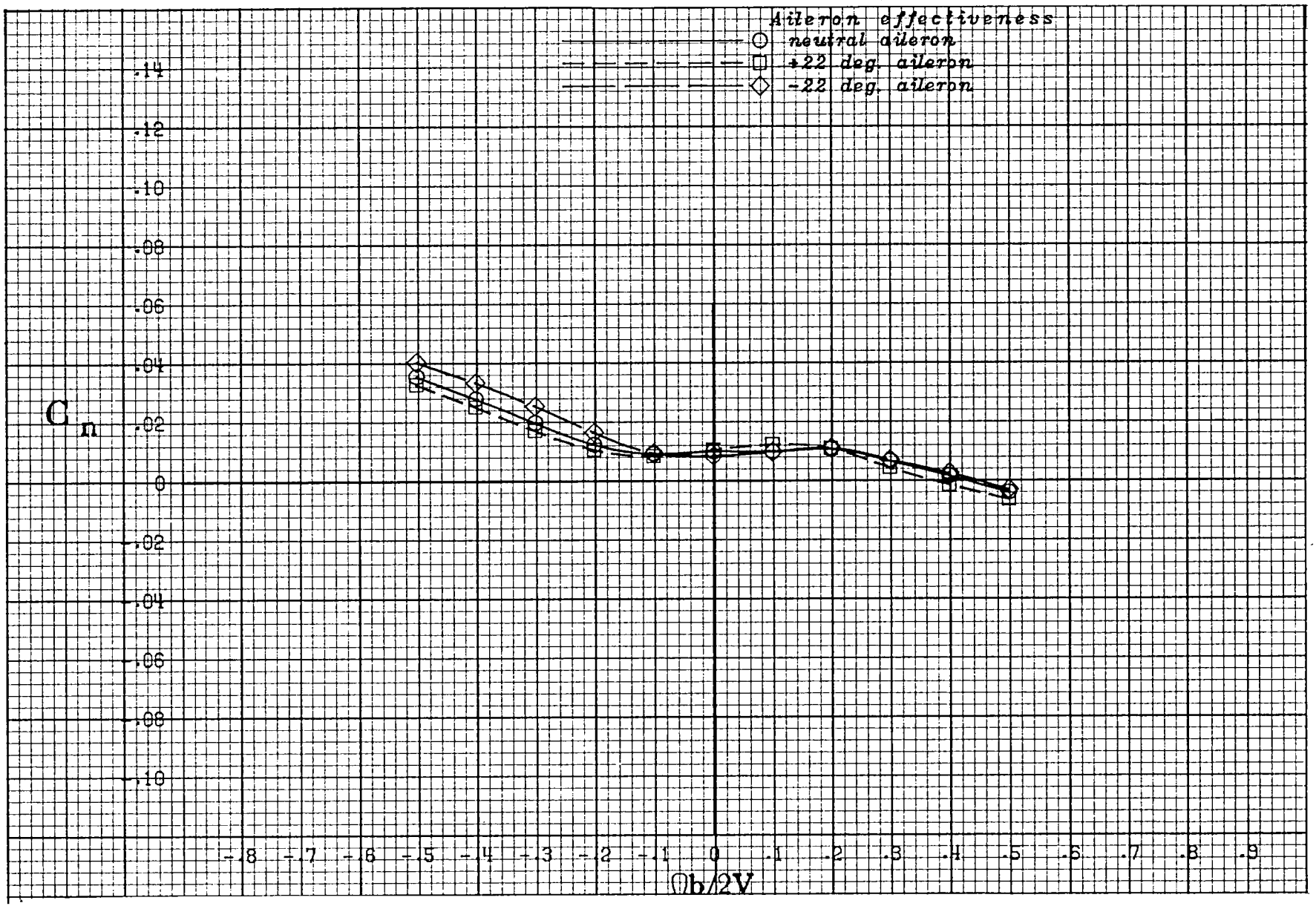

(a) α = 20 deg.

Figure A 25 .- Effect of rotation rate and aileron deflection on yawing-moment coefficient for the basic configuration with -10 deg elevator and -26 deg rudder at +10 deg sideslip angle.

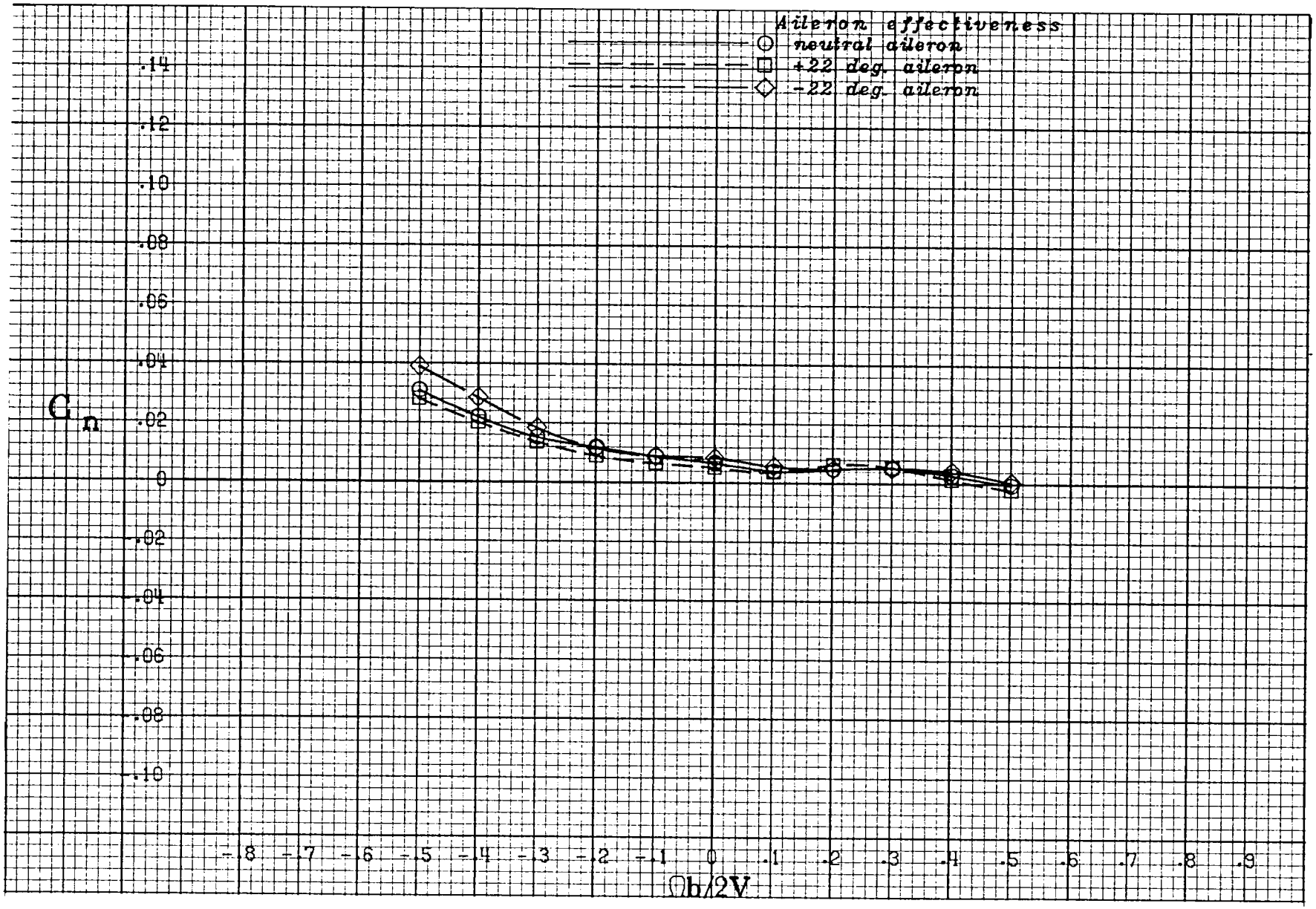

(b) α = 25 deg.

Figure A 25 .- Continued.

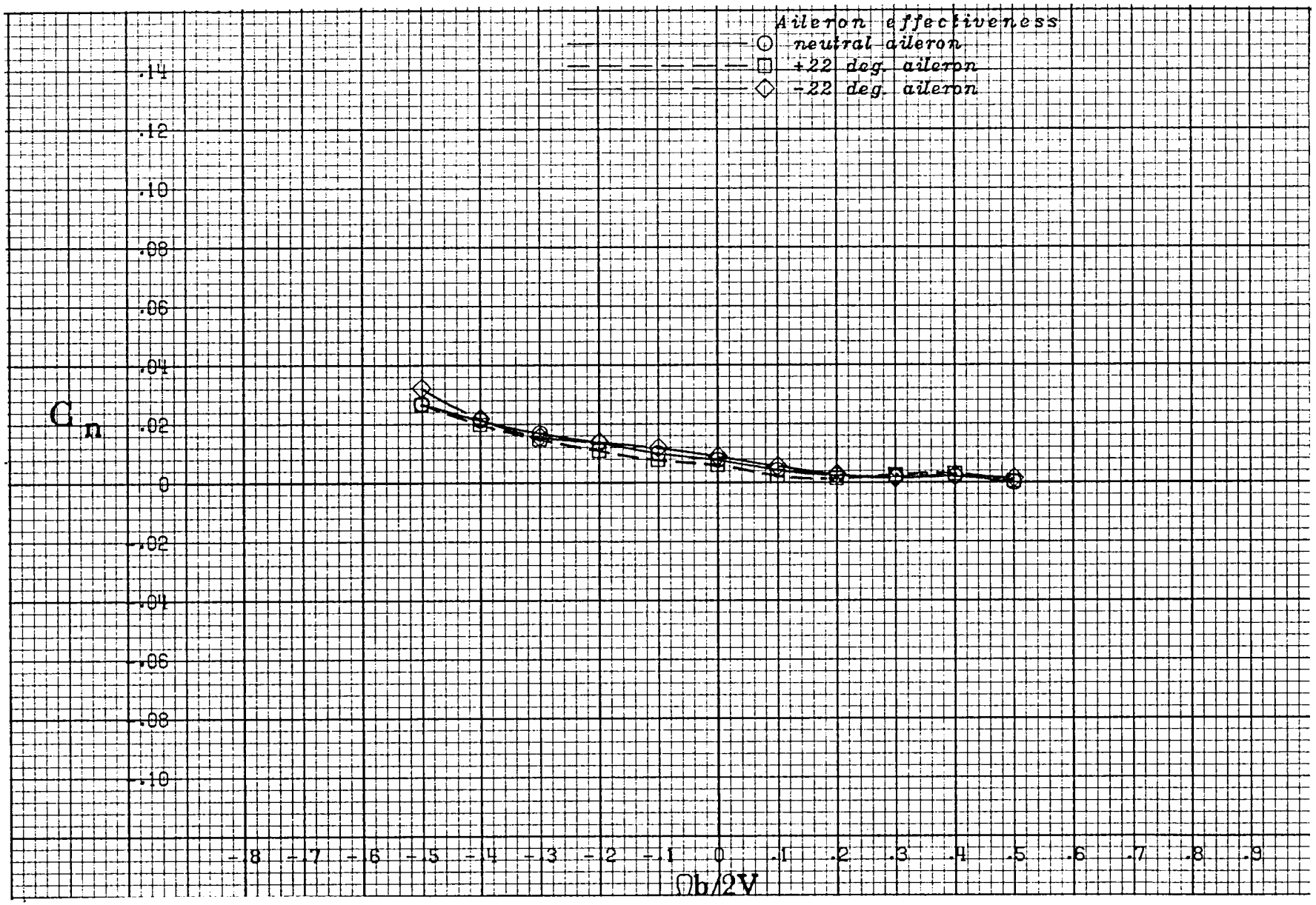

(c) α = 30 deg.

Figure A 25 .- Continued.

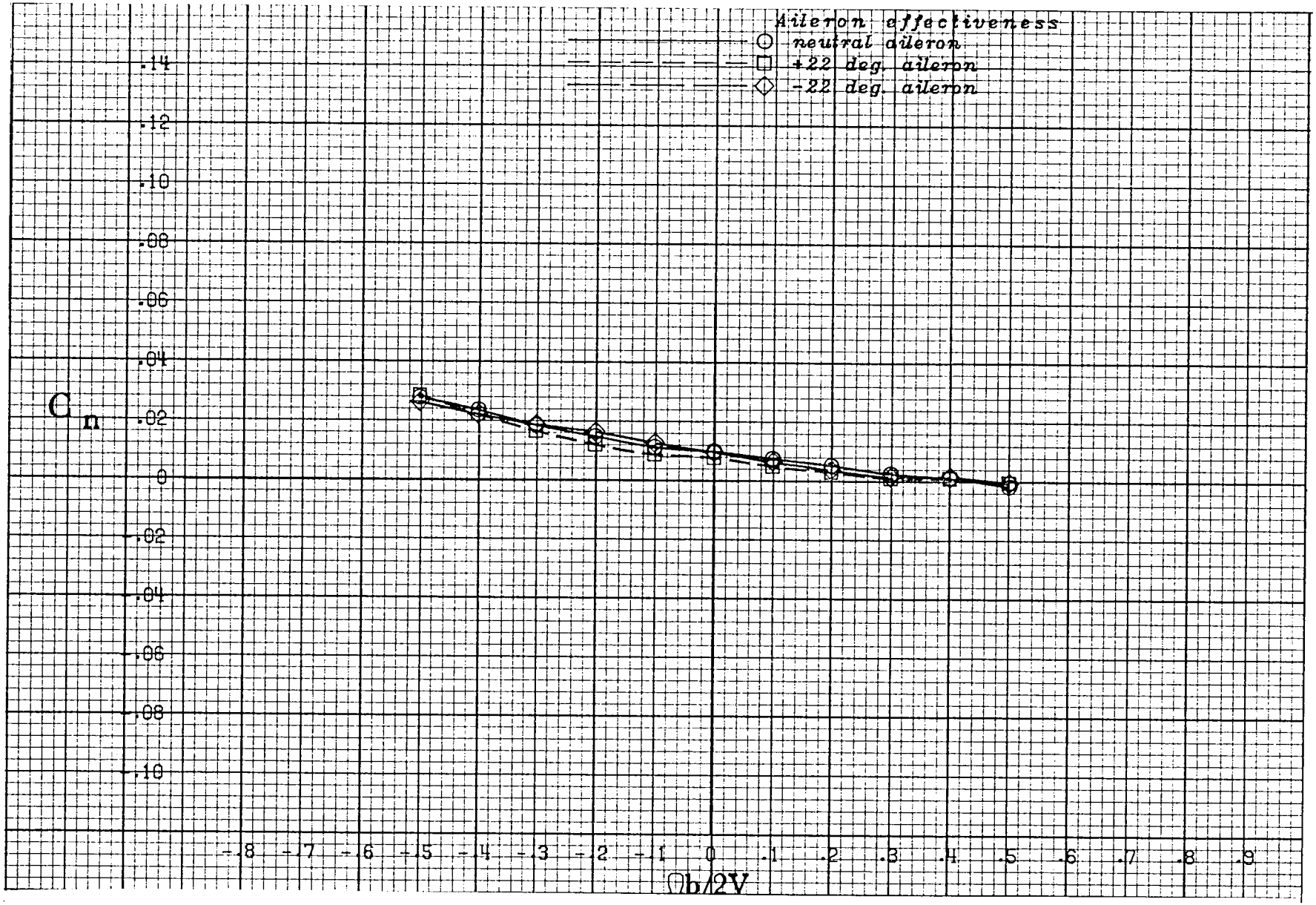

(d) α = 35 deg.

Figure A 25 .- Continued.

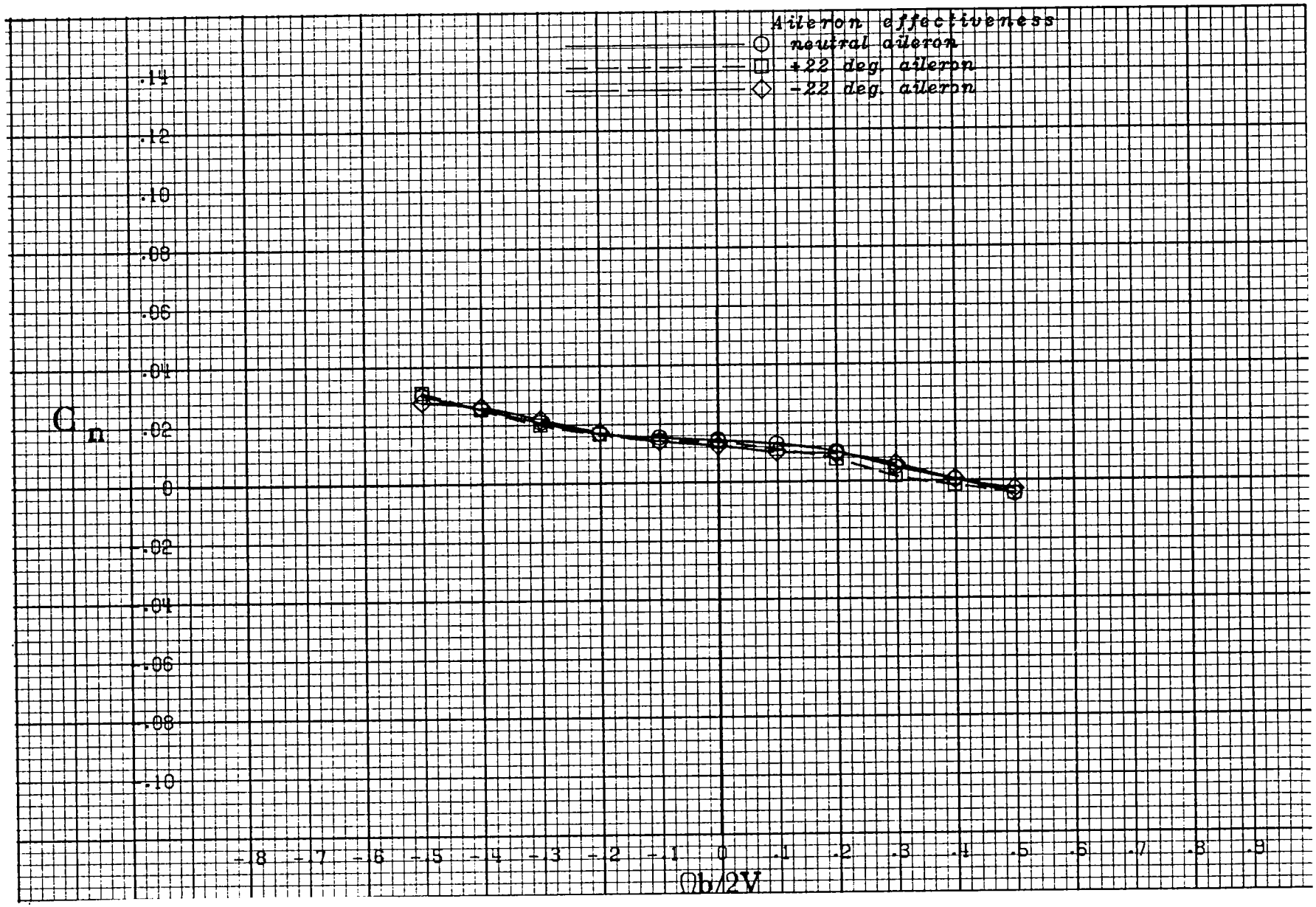

(e) α = 40 deg.

Figure A 25 .- Continued.

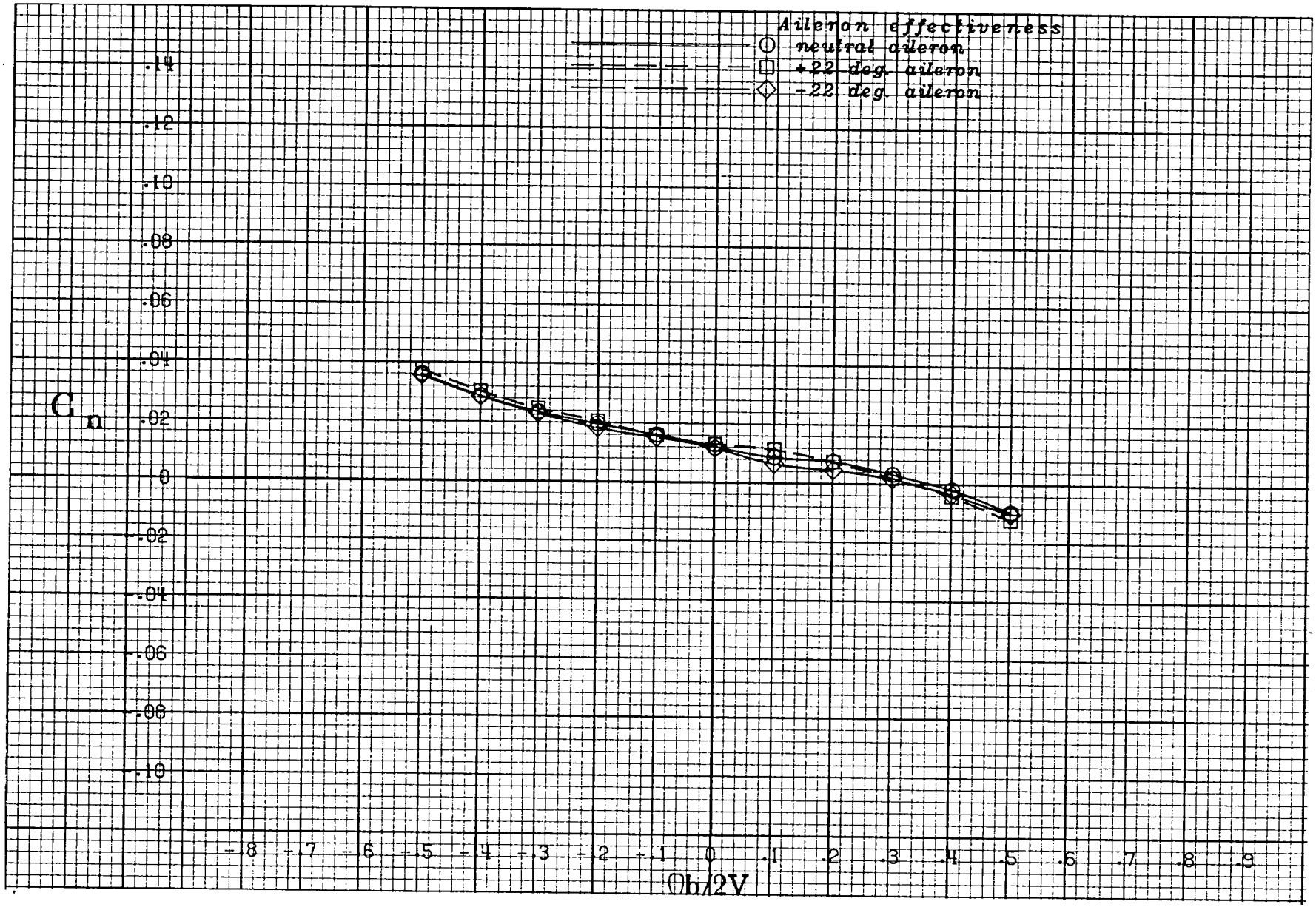

(f) α = 50 deg.

Figure A 25 .- Continued.

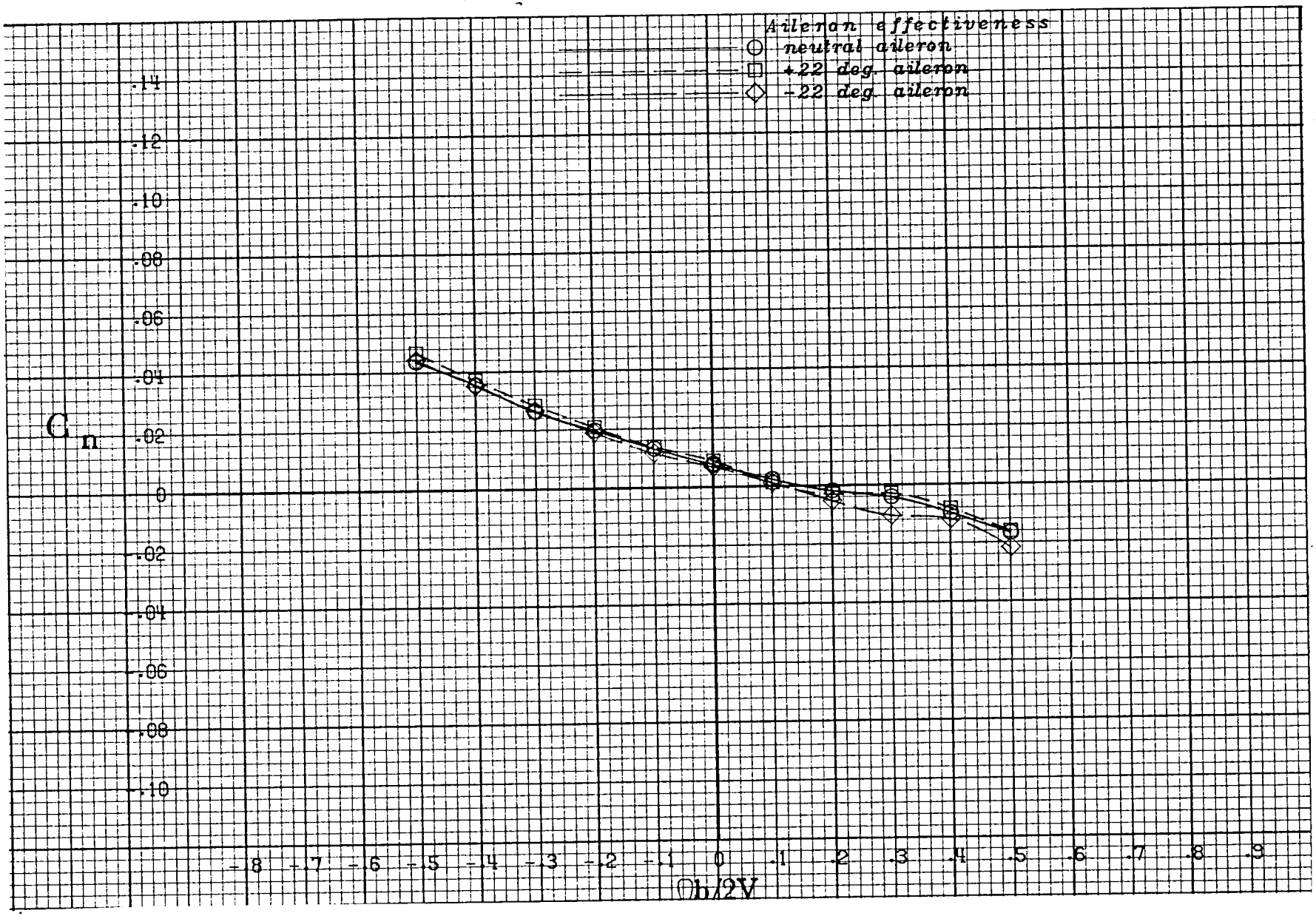

(g) α = 60 deg.

Figure A 25 .- Continued.

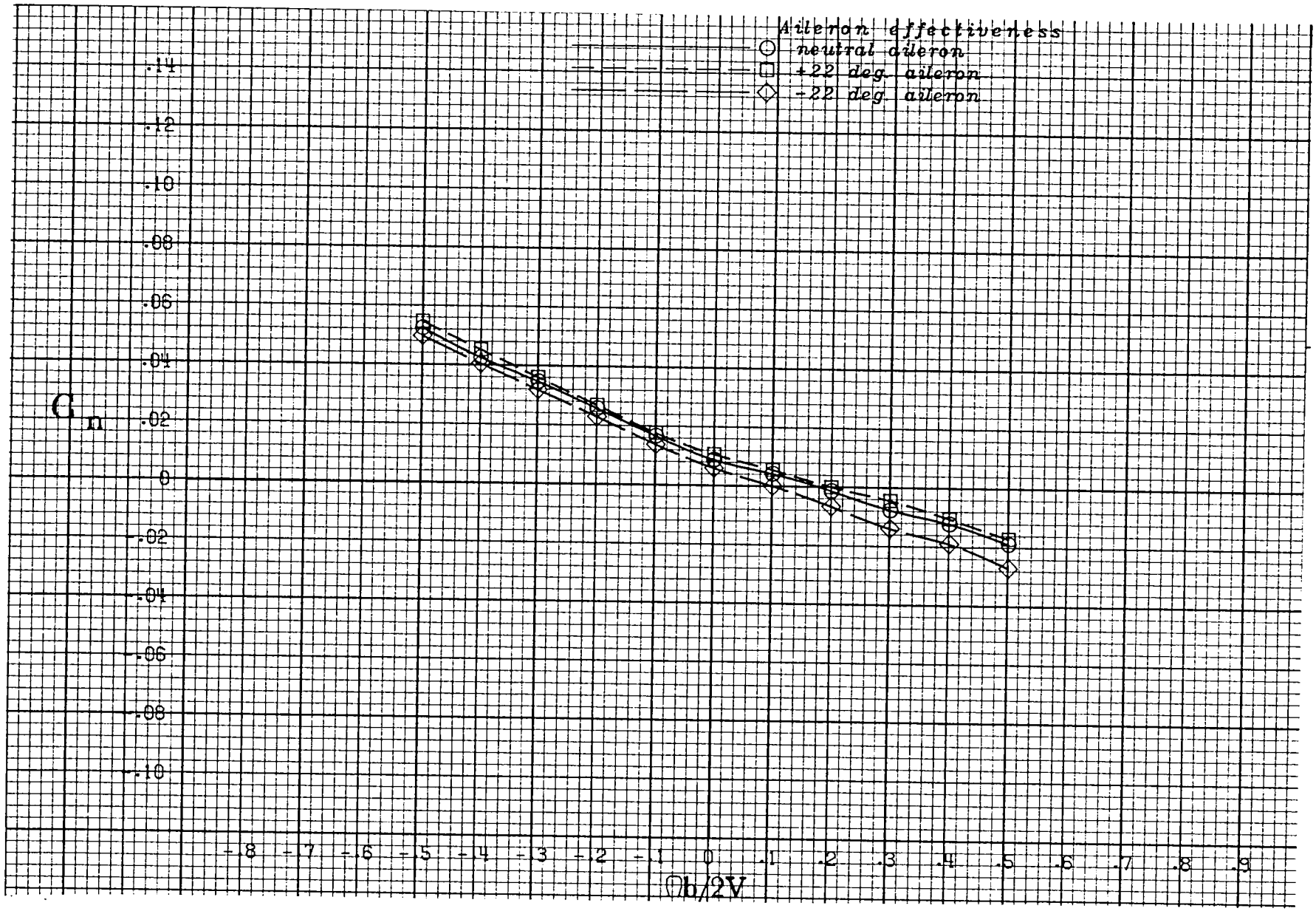

(h) α = 70 deg.

Figure A 25 .- Continued.

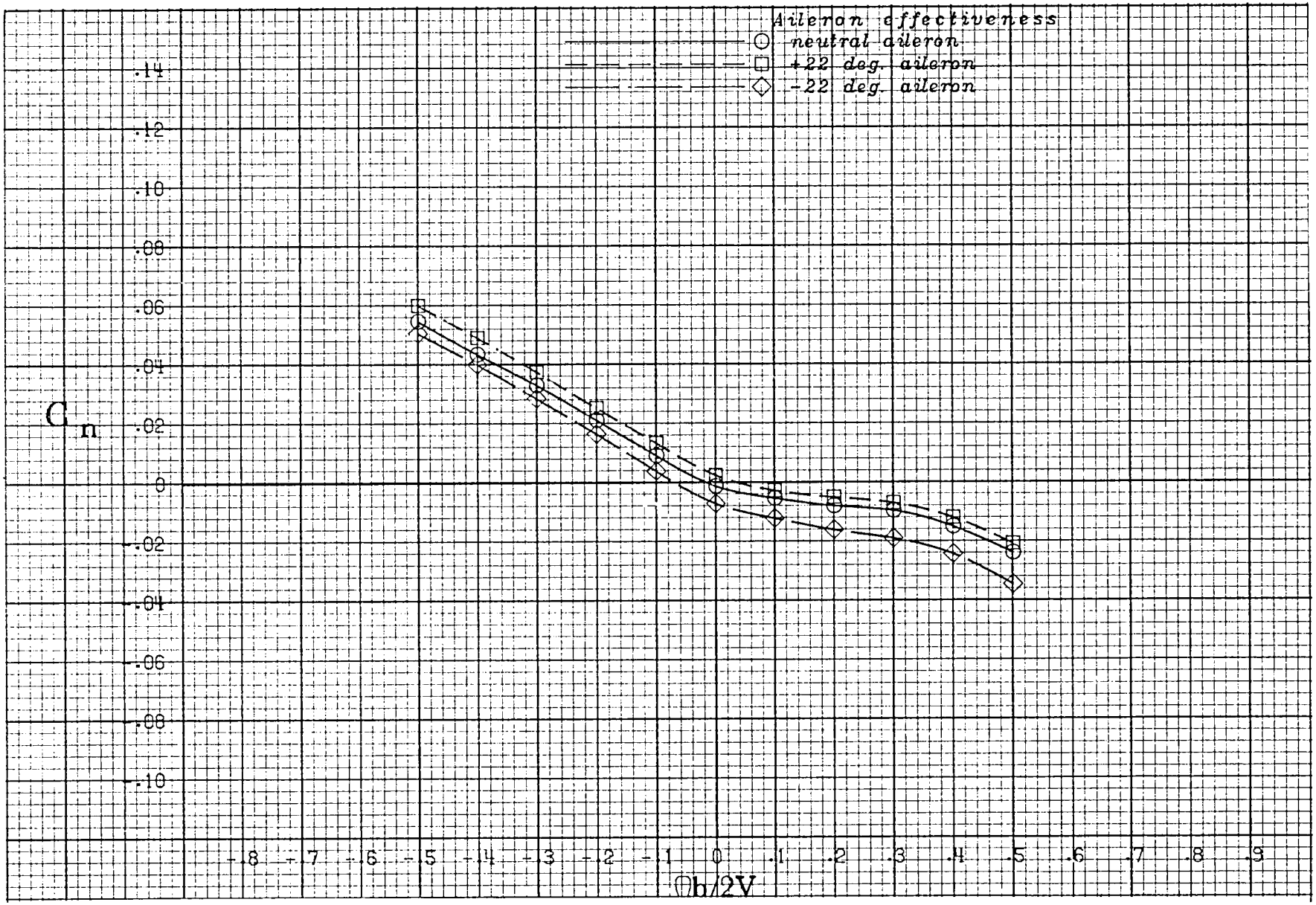

(i) α = 80 deg.

Figure A 25 .- Continued.

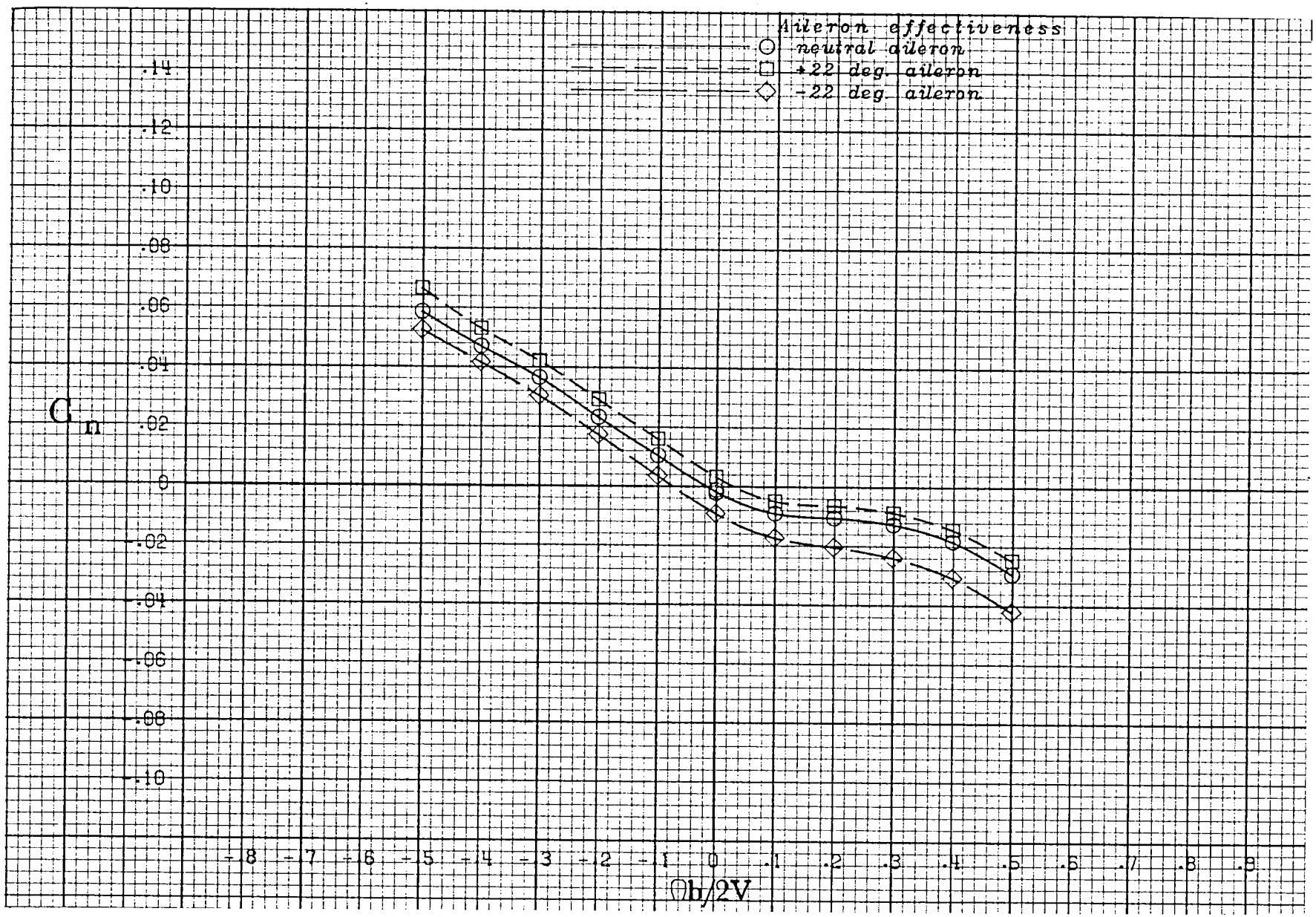

(j) α = 90 deg.

Figure A 25 .- Concluded.

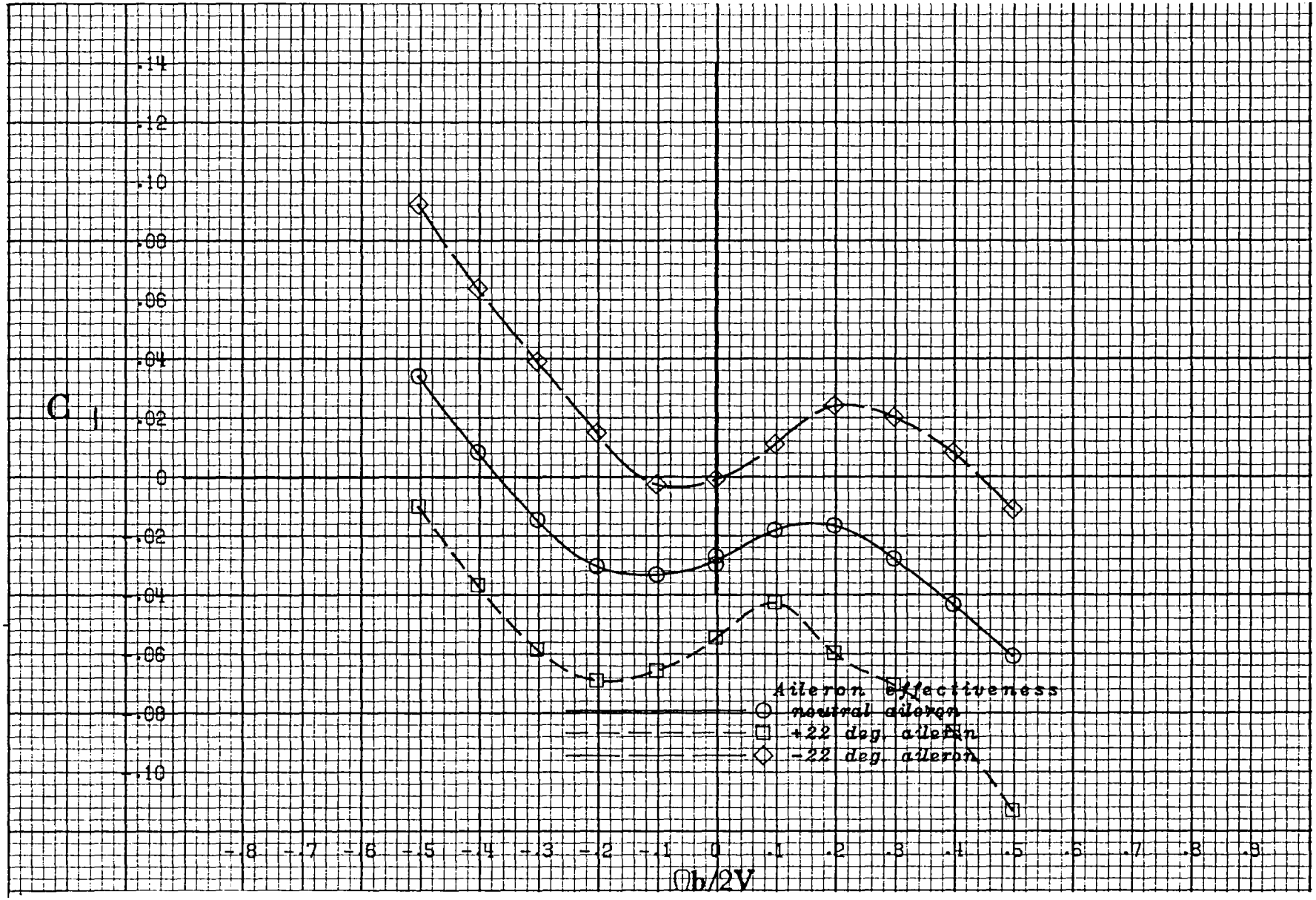

(a) α = 20 deg.

Figure A 26 .- Effect of rotation rate and aileron deflection on rolling-moment coefficient for the basic configuration with -10 deg elevator and -26 deg rudder at +10 deg sideslip angle.

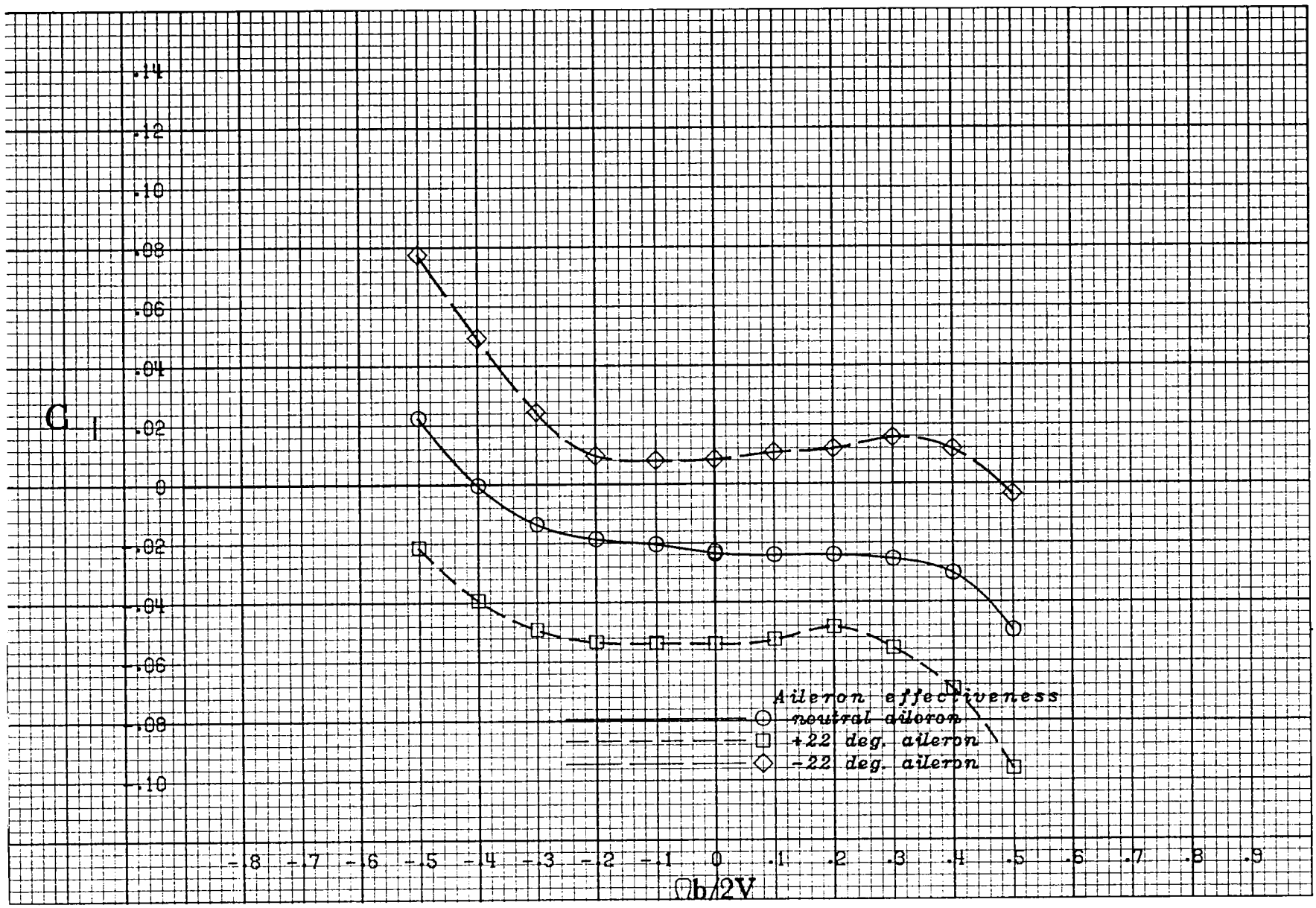

(b) α = 25 deg.

Figure A 26 .- Continued.

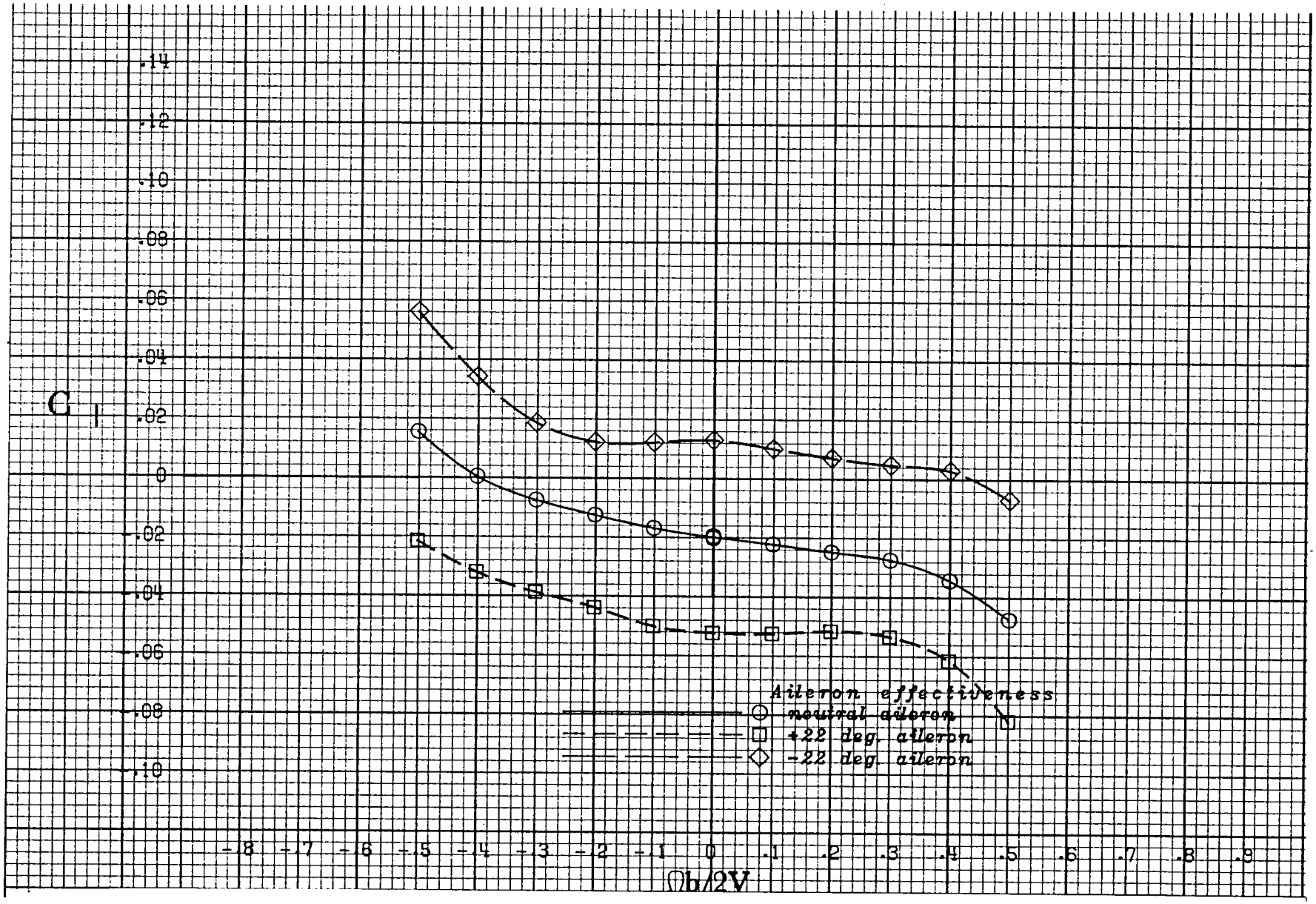

(c) α = 30 deg.

Figure A 26 .- Continued.

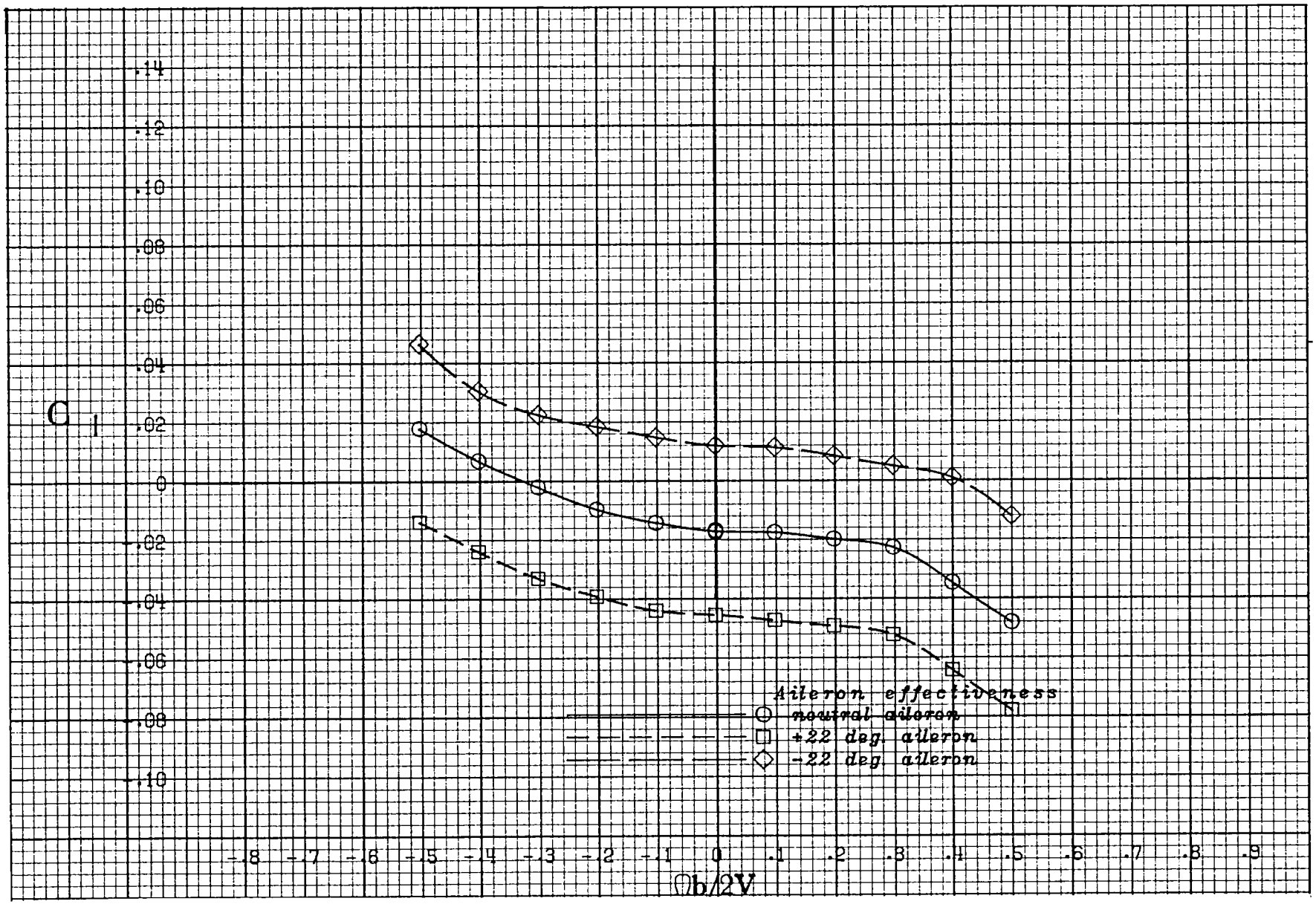

(d) α = 35 deg.

Figure A 26 .- Continued.

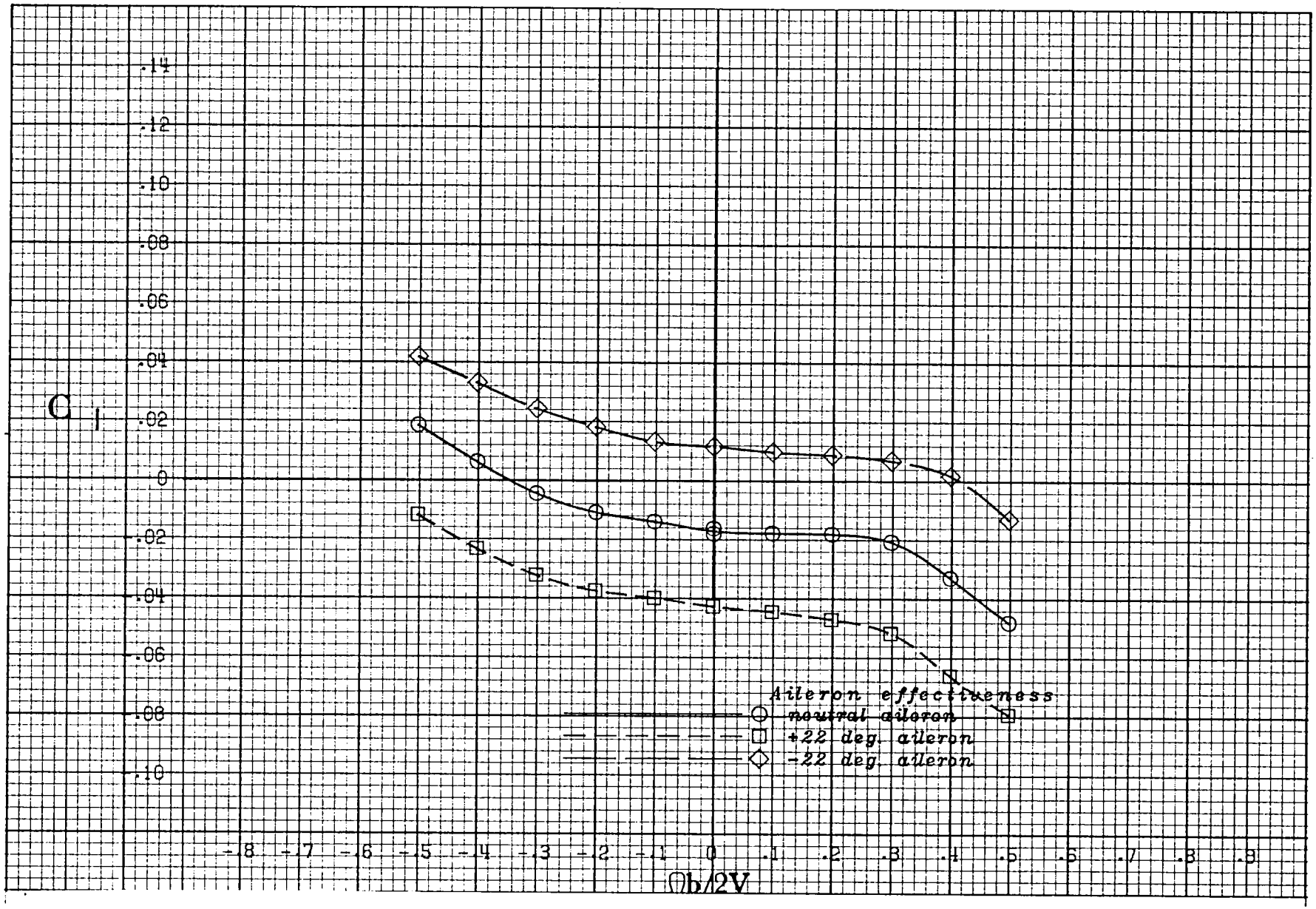

(e) α = 40 deg.

Figure A 26 .- Continued.

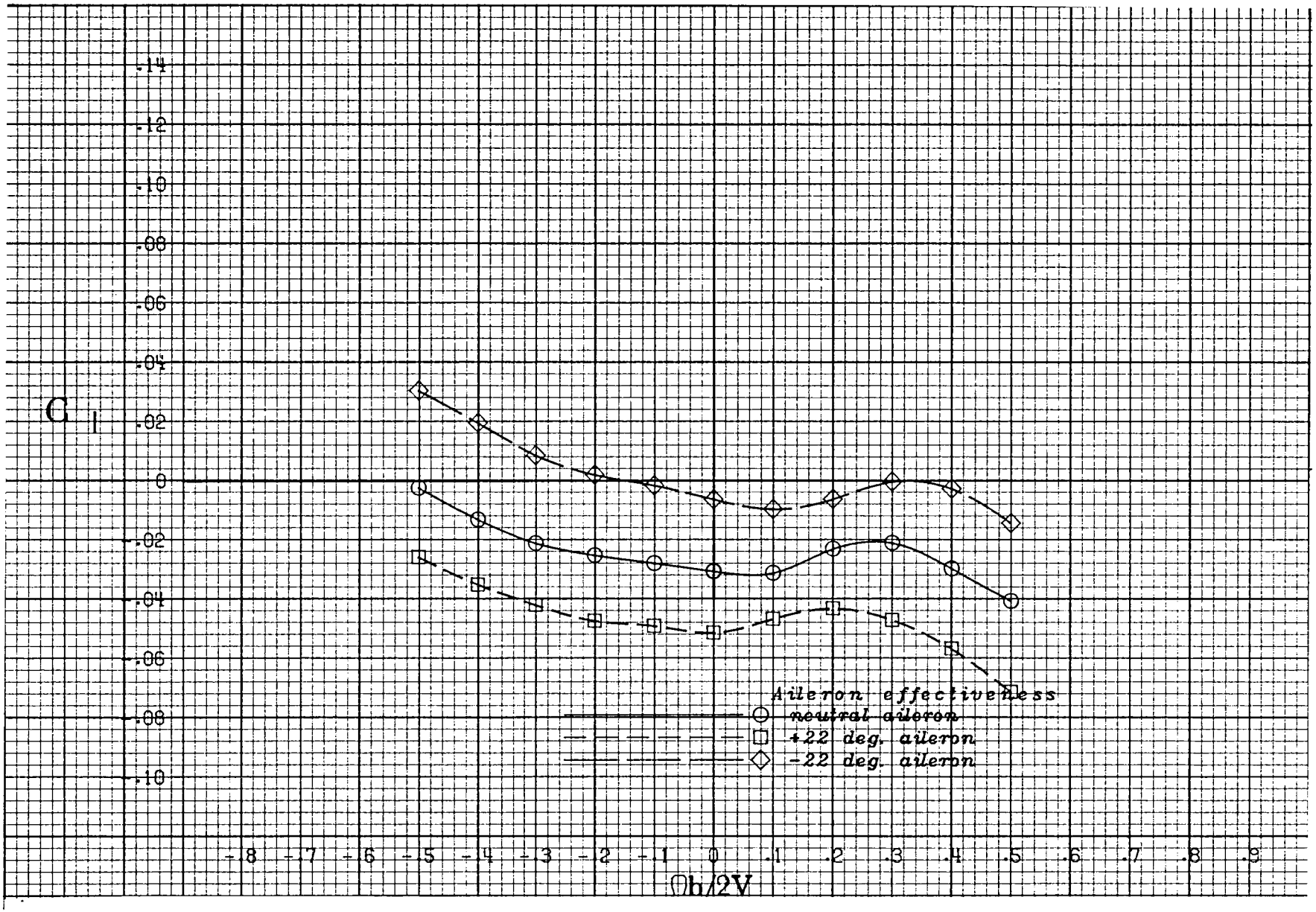

(f) α = 50 deg.

Figure A 26 .- Continued.

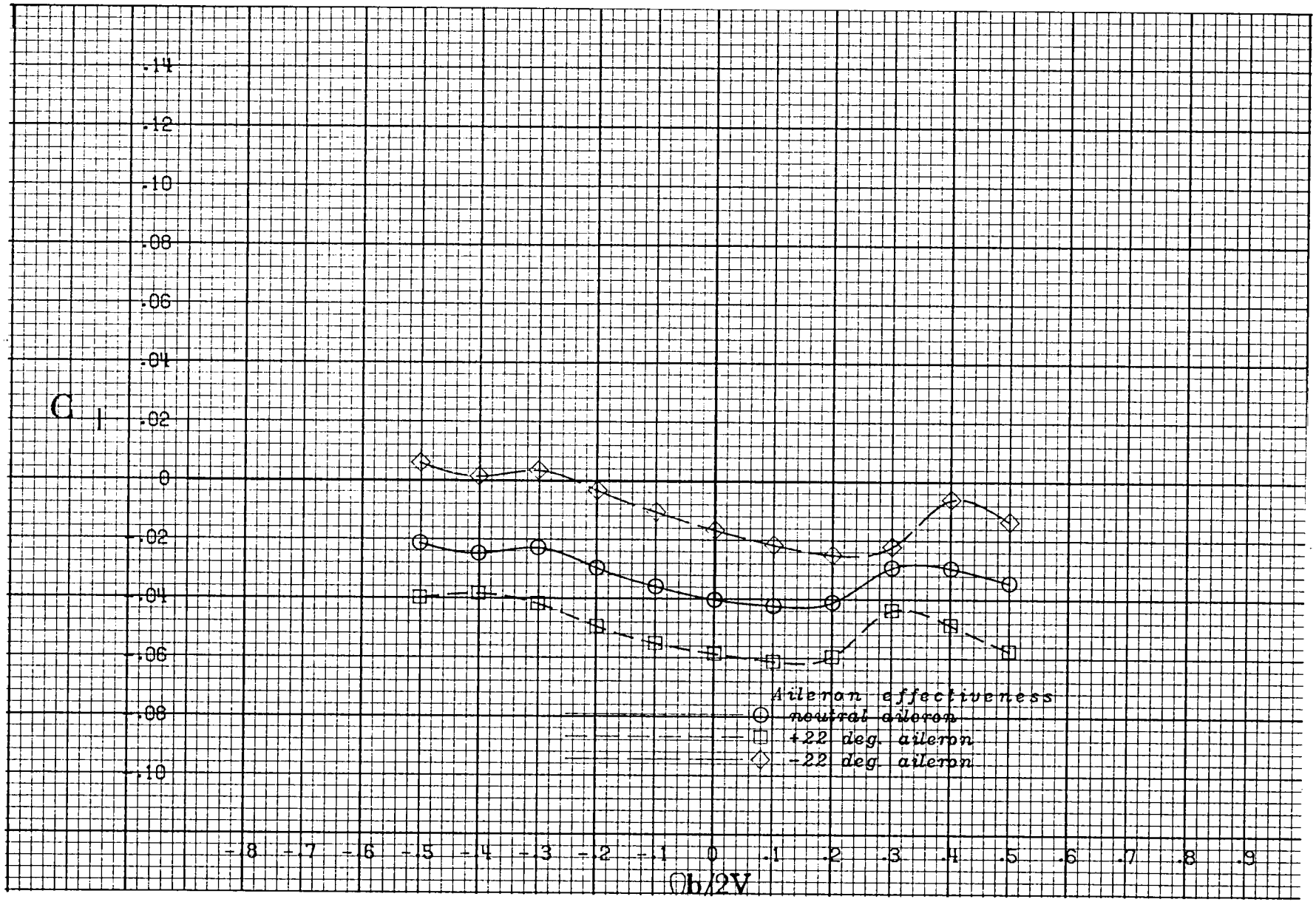

(g) α = 60 deg.

Figure A 26 .- Continued.

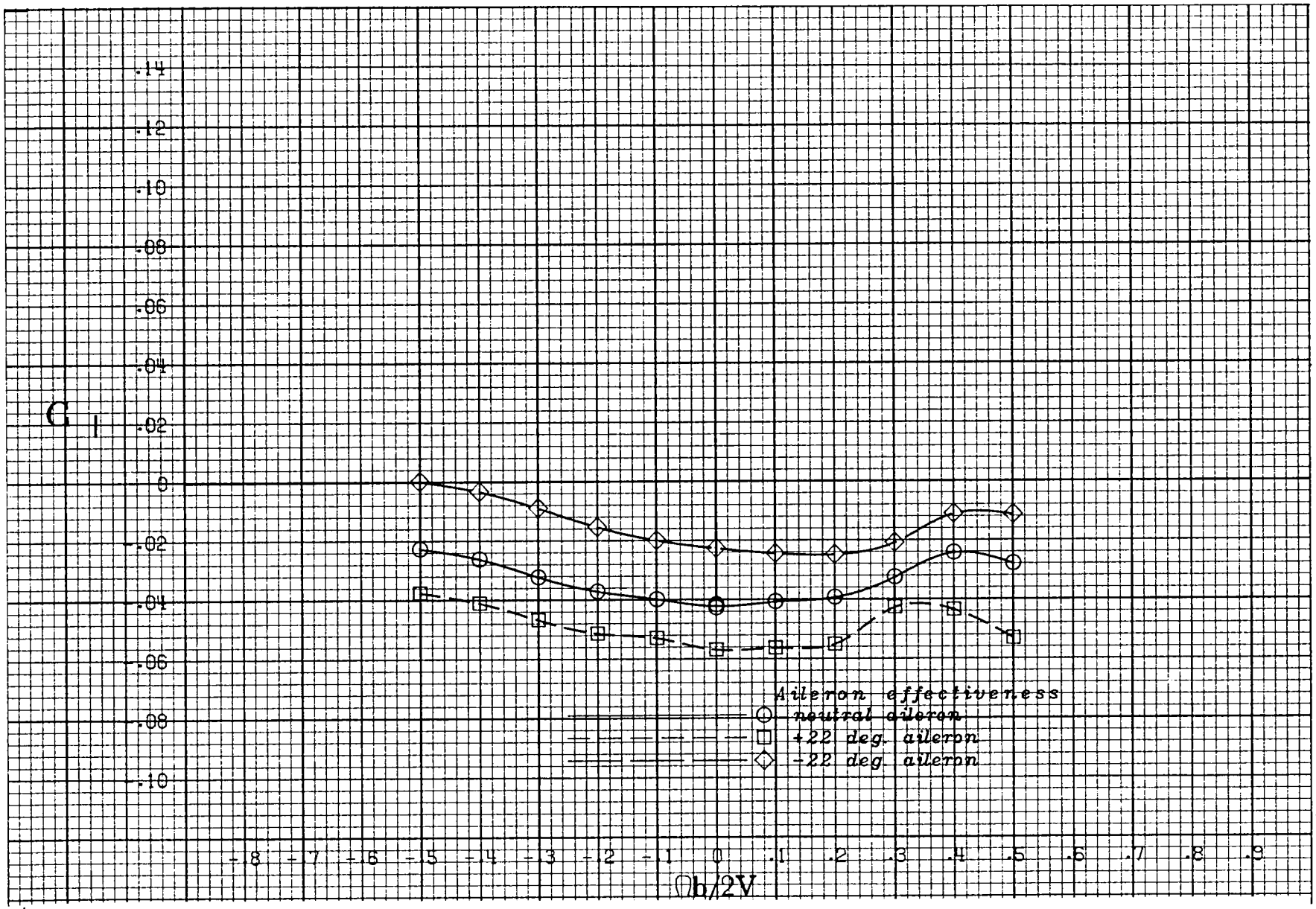

(h) α = 70 deg.

Figure A 26 .- Continued.

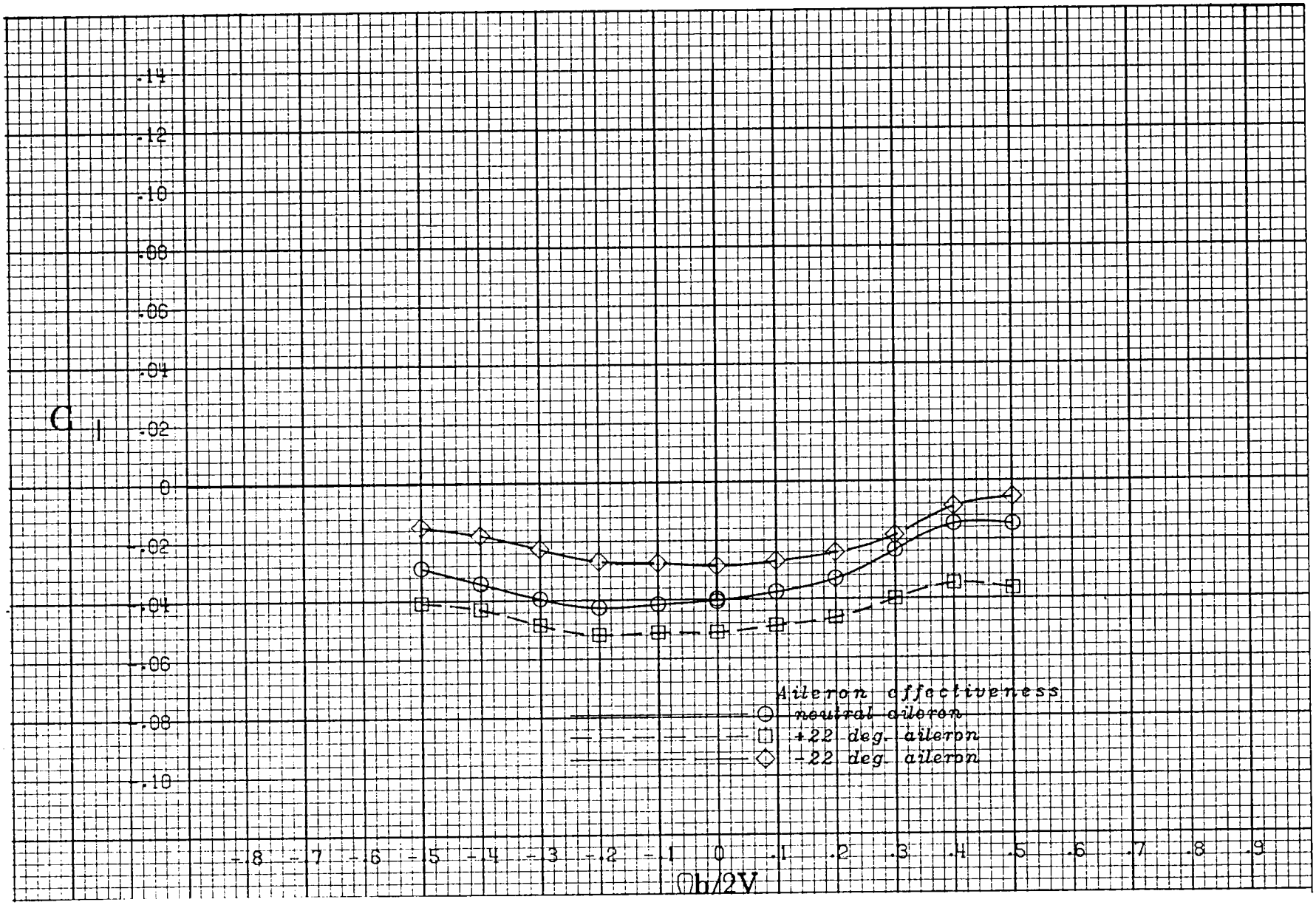

(i) α = 80 deg.

Figure A 26 .- Continued.

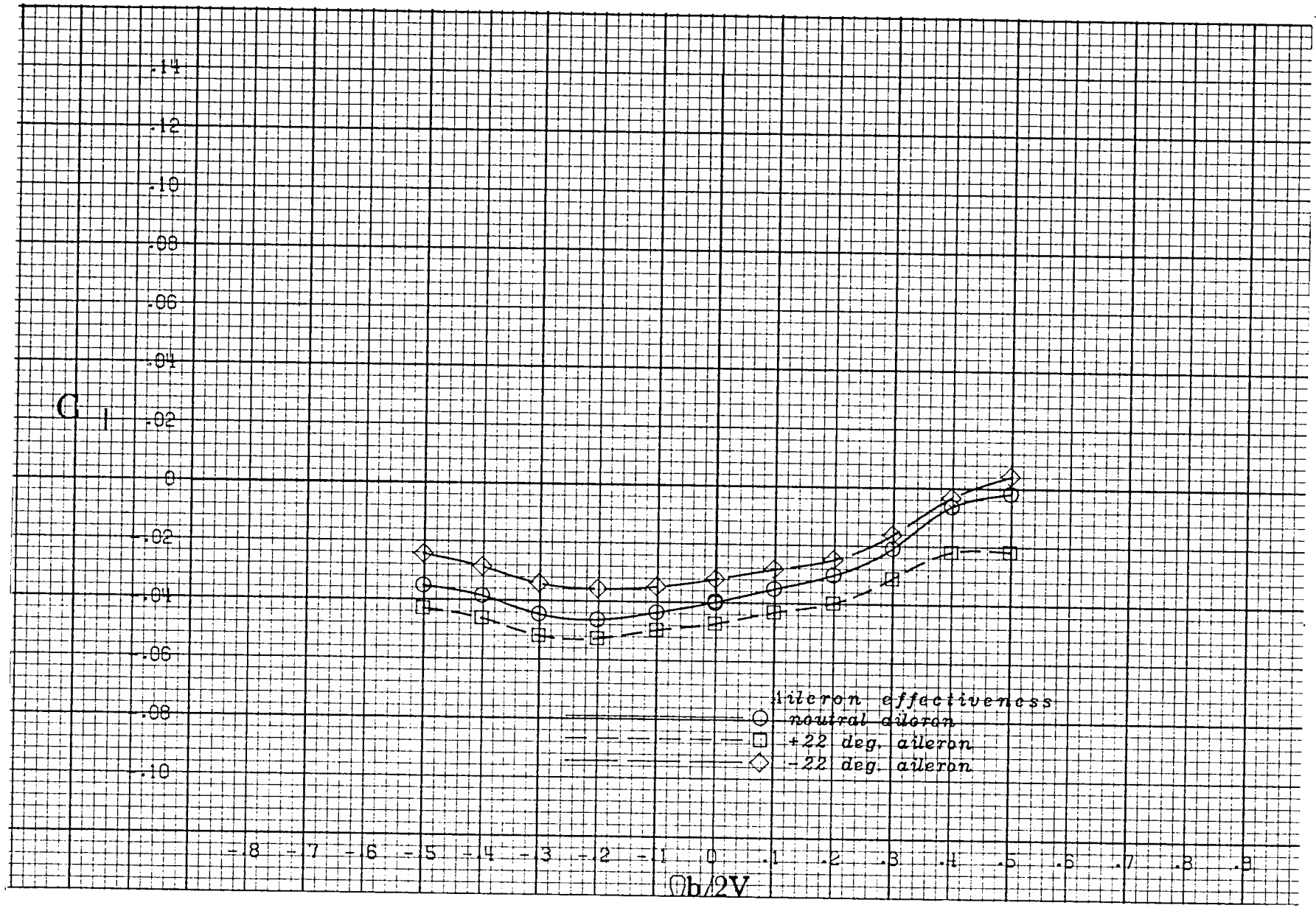

(j) α = 90 deg.

Figure A 26 .- Concluded.

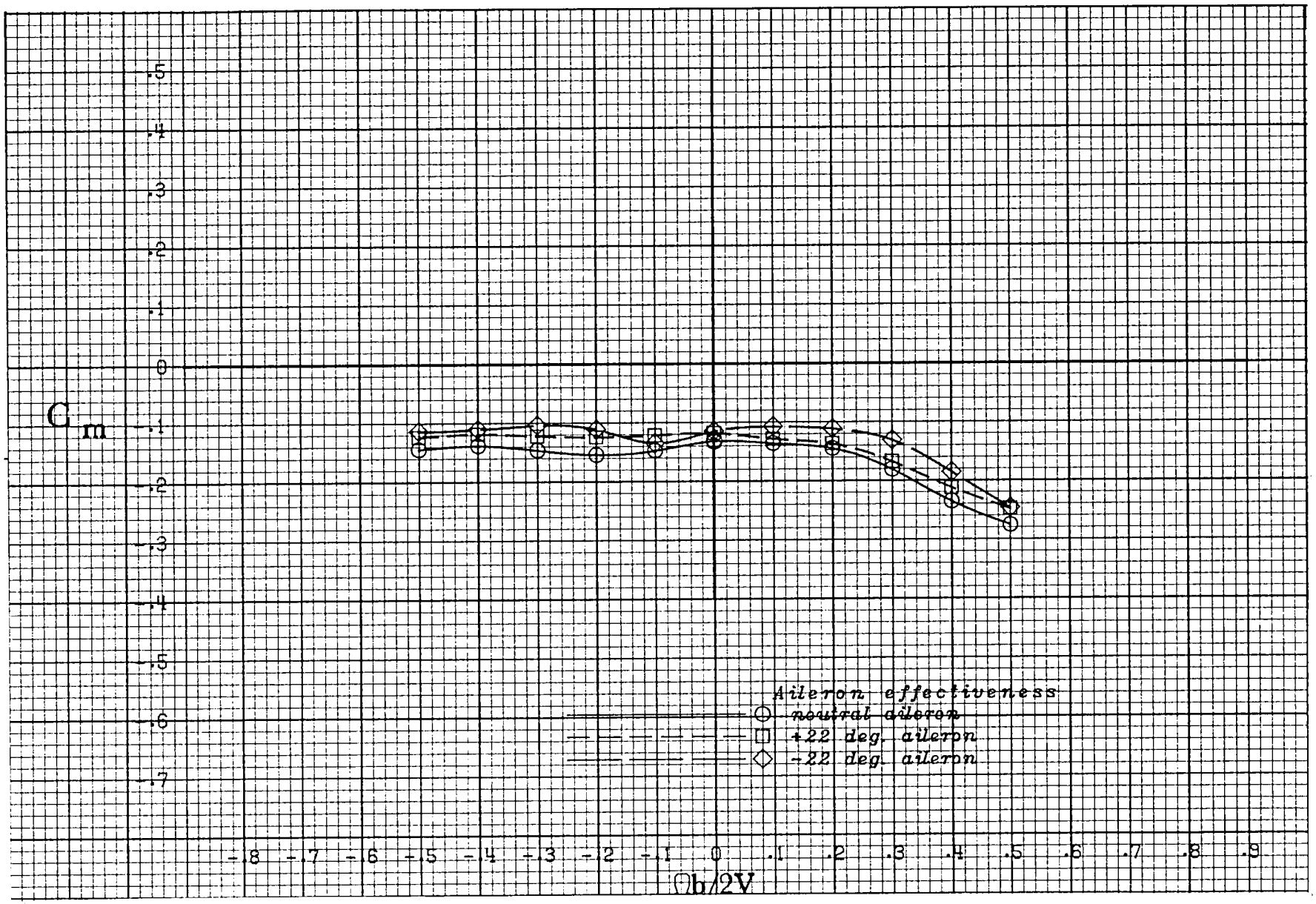

(a) α = 20 deg.

Figure A 27 .- Effect of rotation rate and aileron deflection on pitching-moment coefficient for the basic configuration with -10 deg elevator and -26 deg rudder at +10 deg sideslip angle.

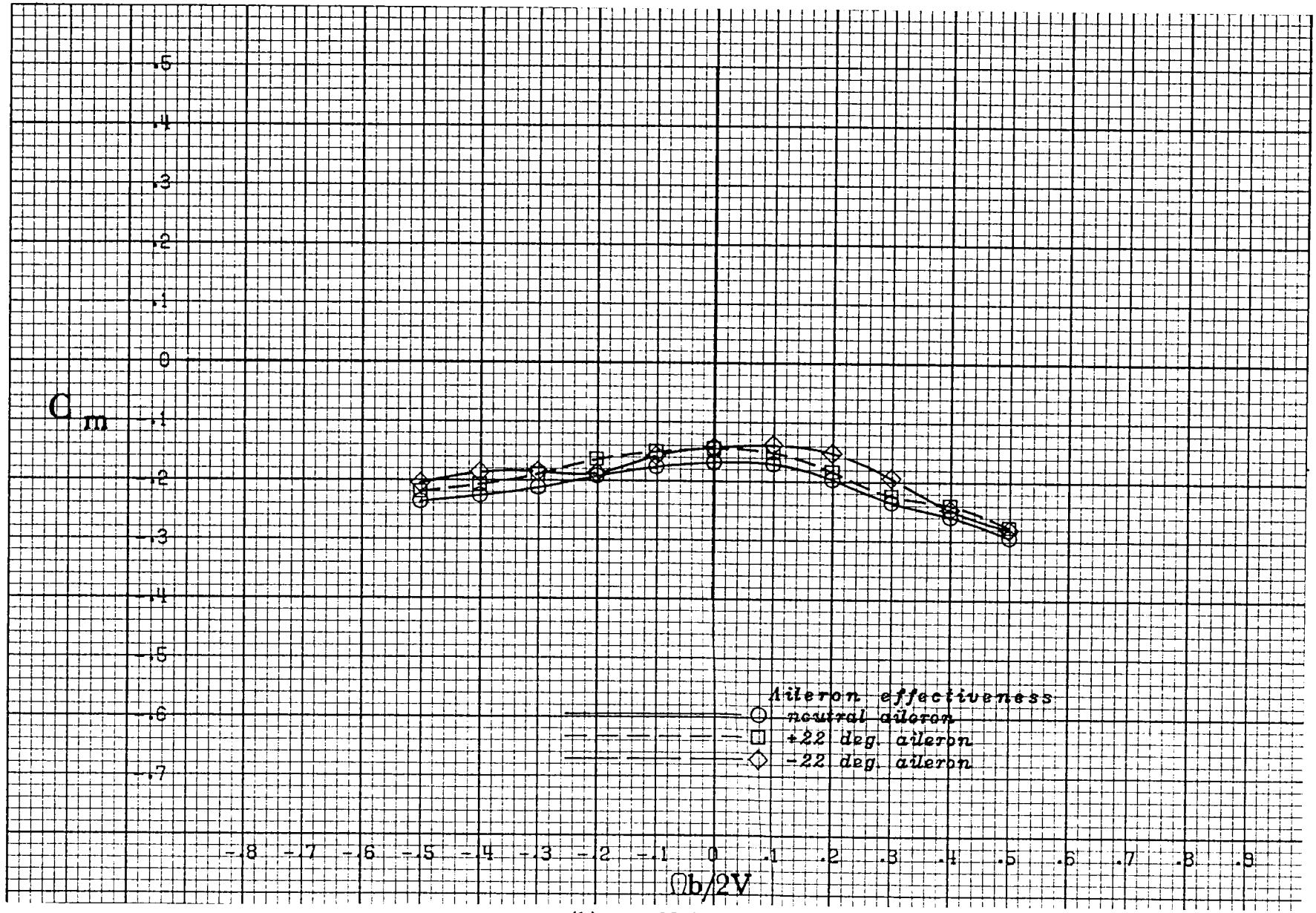

(b) α = 25 deg.

Figure A 27 .- Continued.

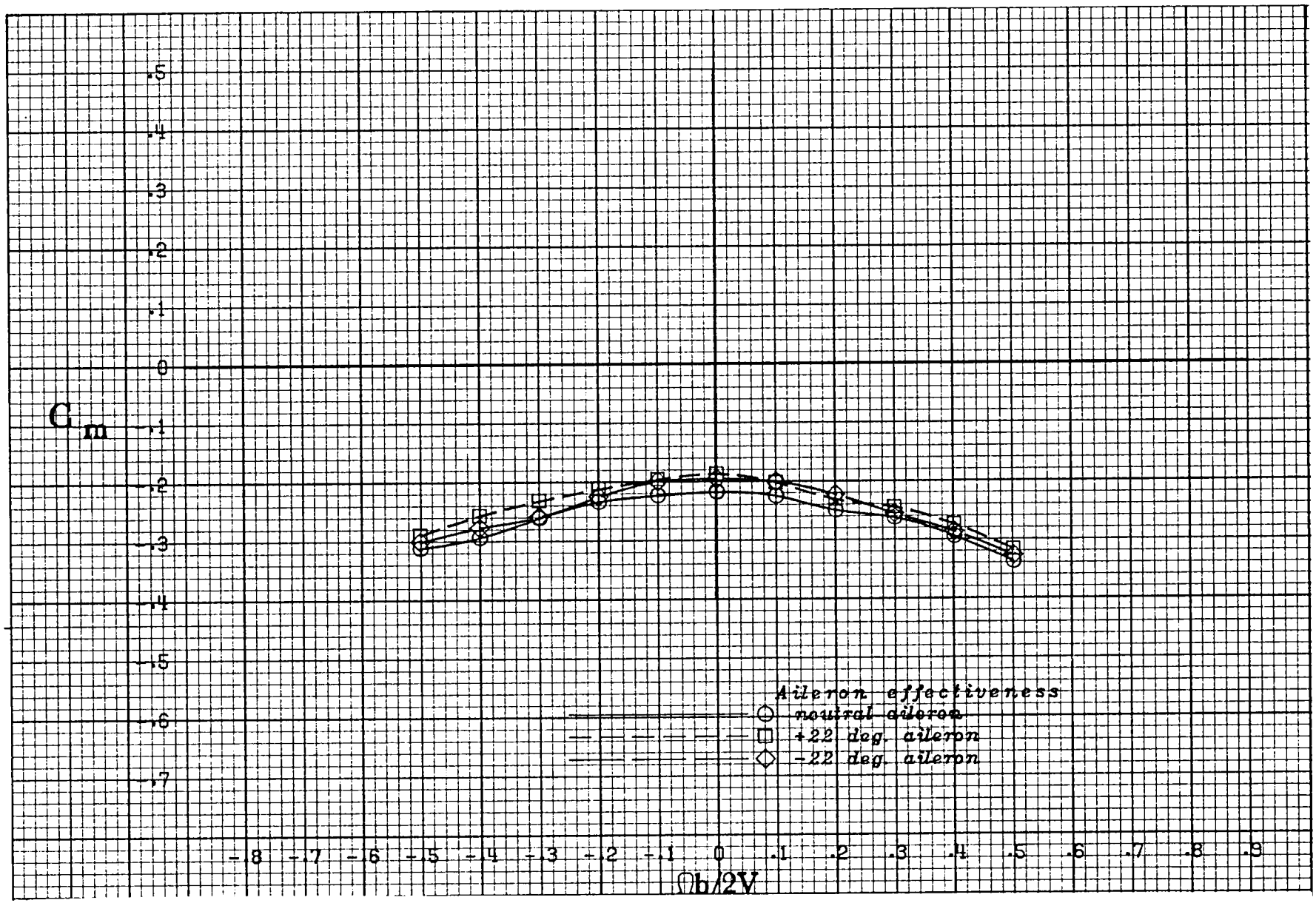

(c) α = 30 deg.

Figure A 27 .- Continued.

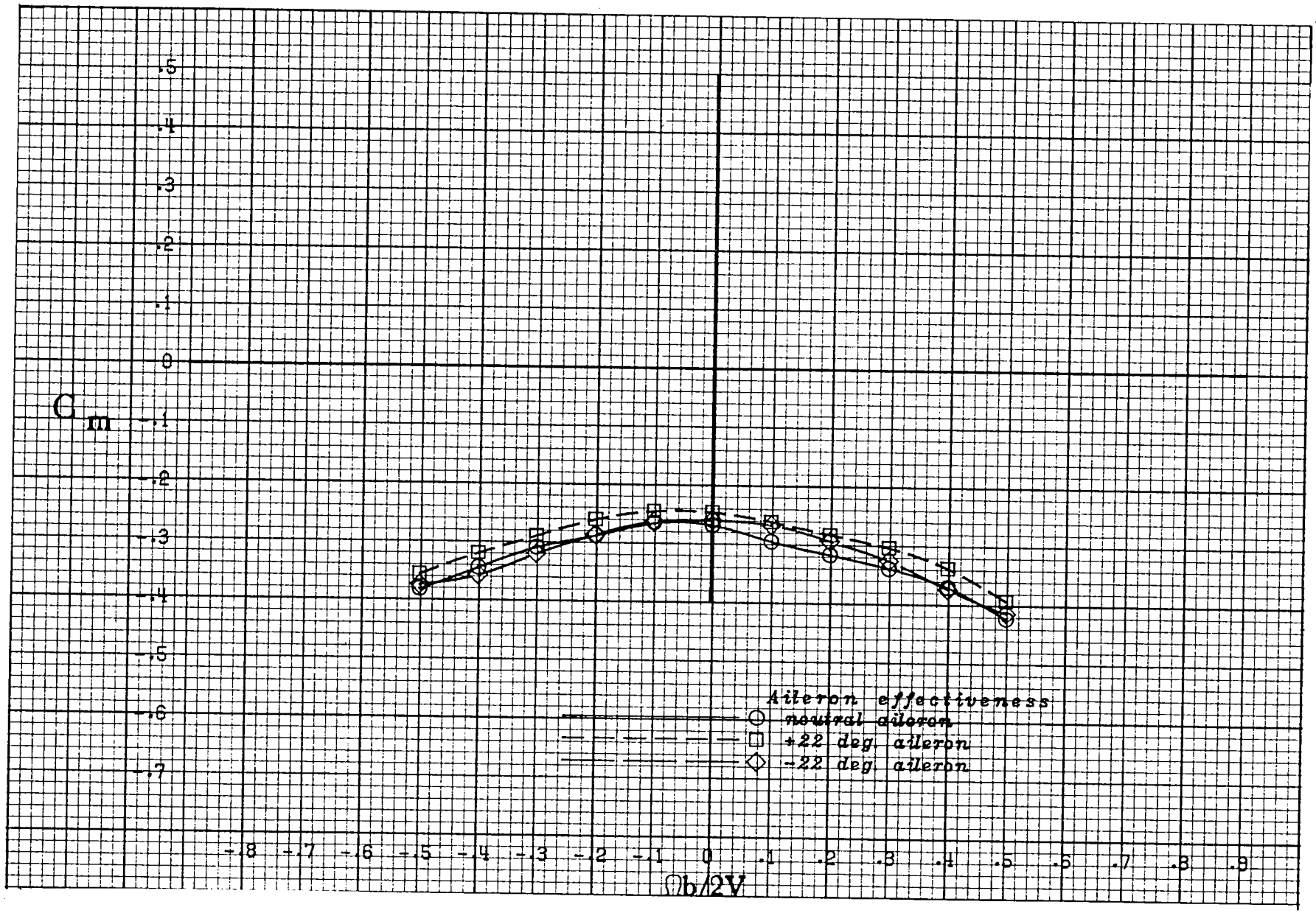

(d) α = 35 deg.

Figure A 27 .- Continued.

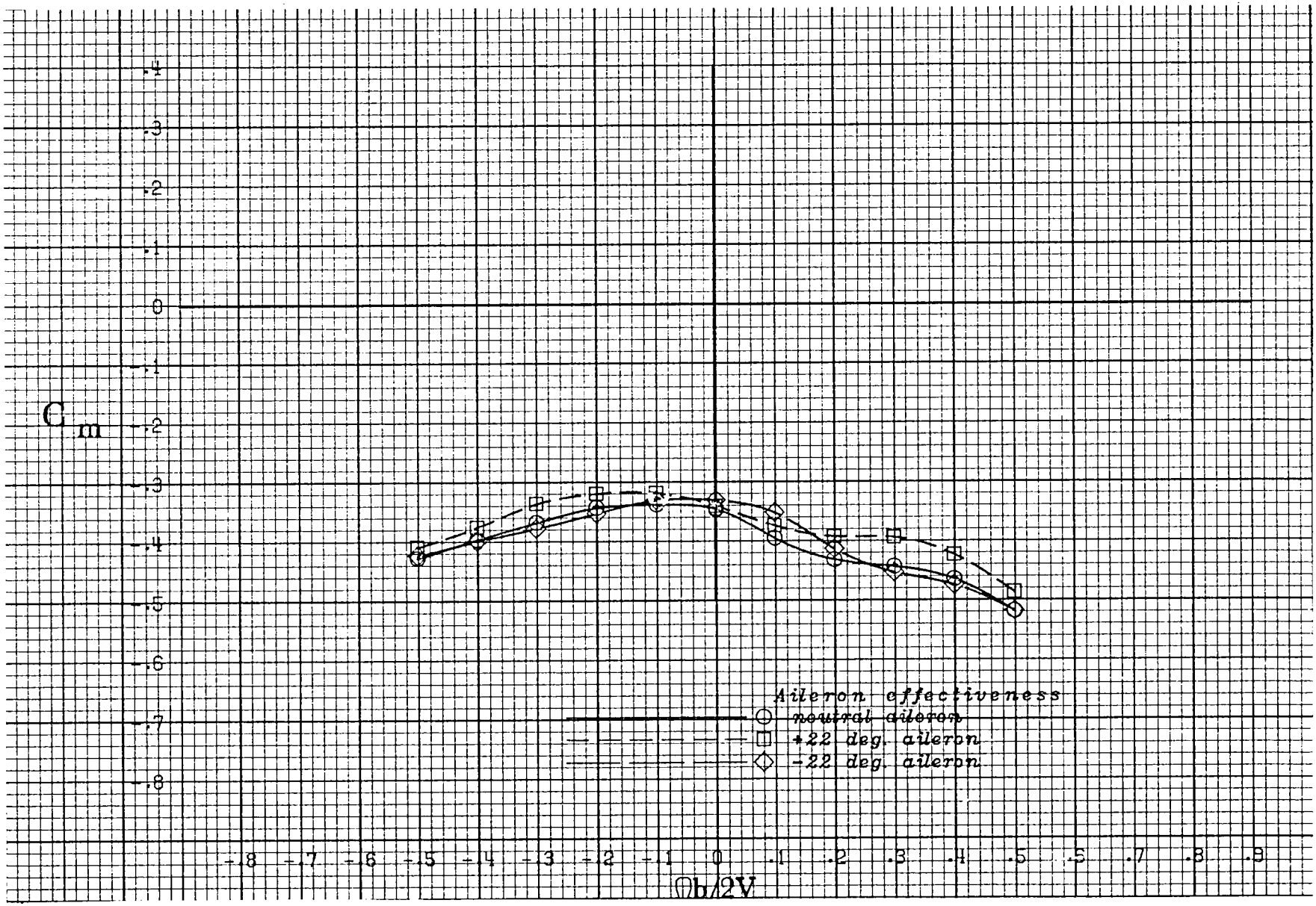

(e) α = 40 deg.

Figure A 27 .- Continued.

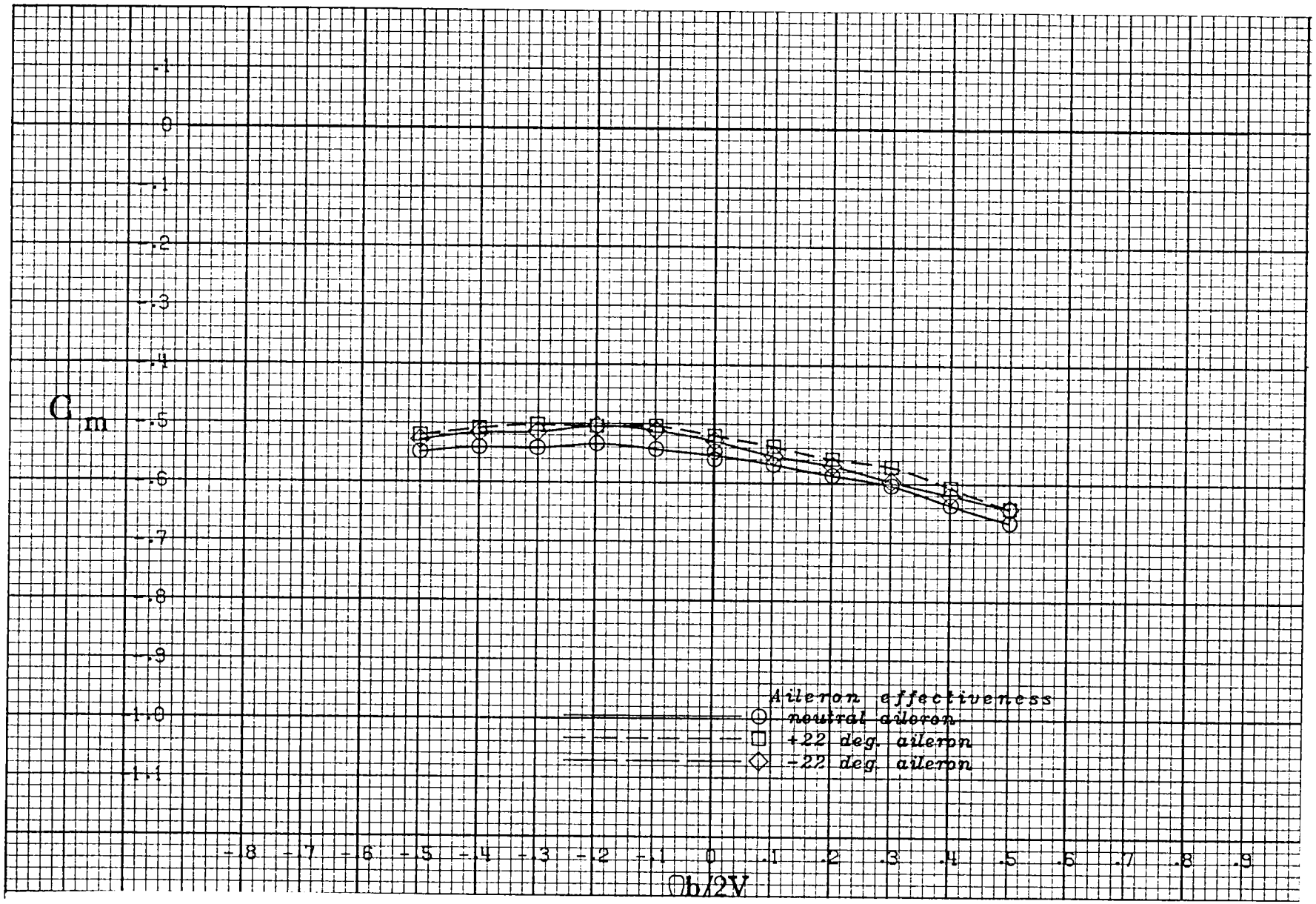

(f) α = 50 deg.

Figure A 27 .- Continued.

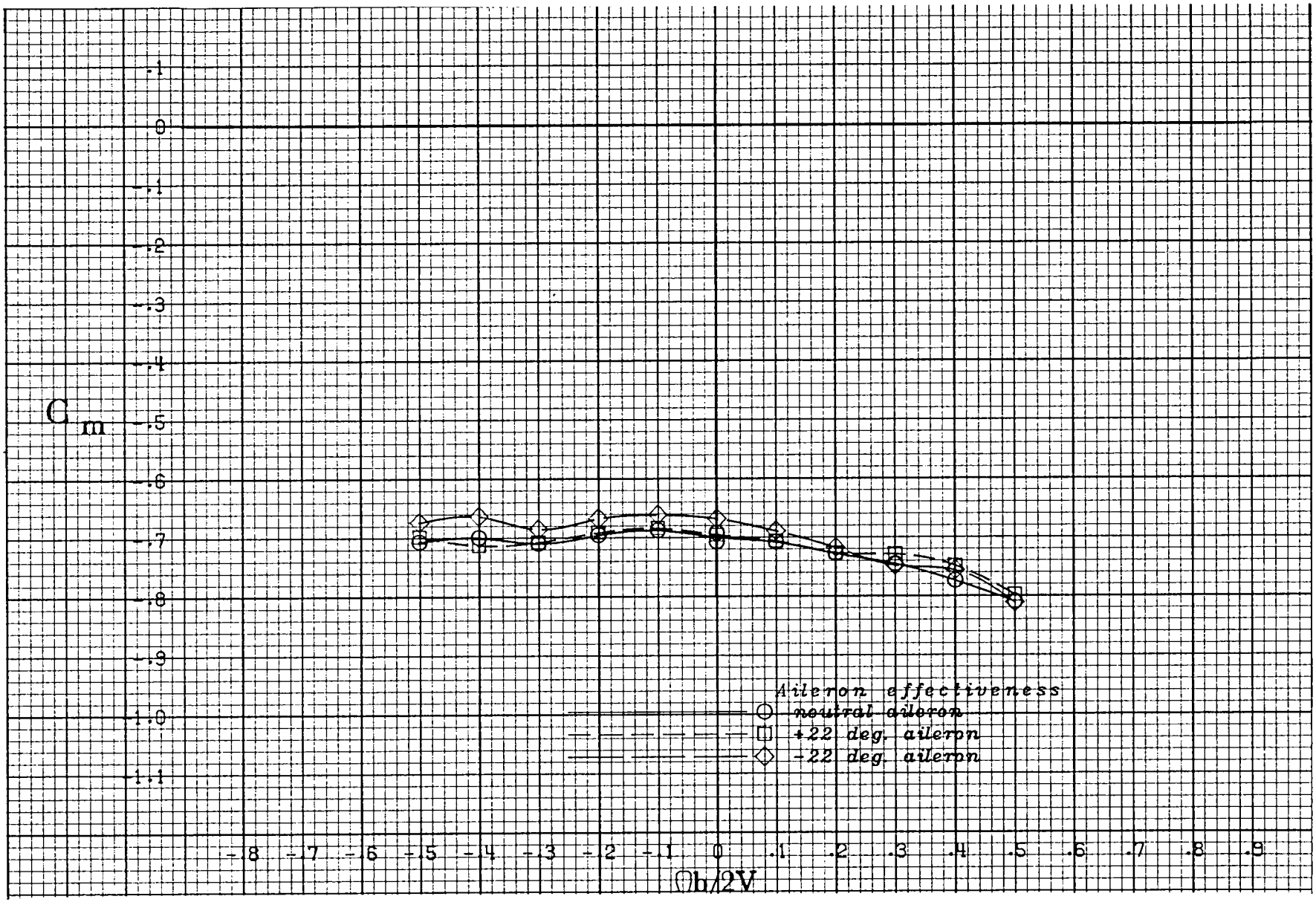

(g) α = 60 deg.

Figure A 27 .- Continued.

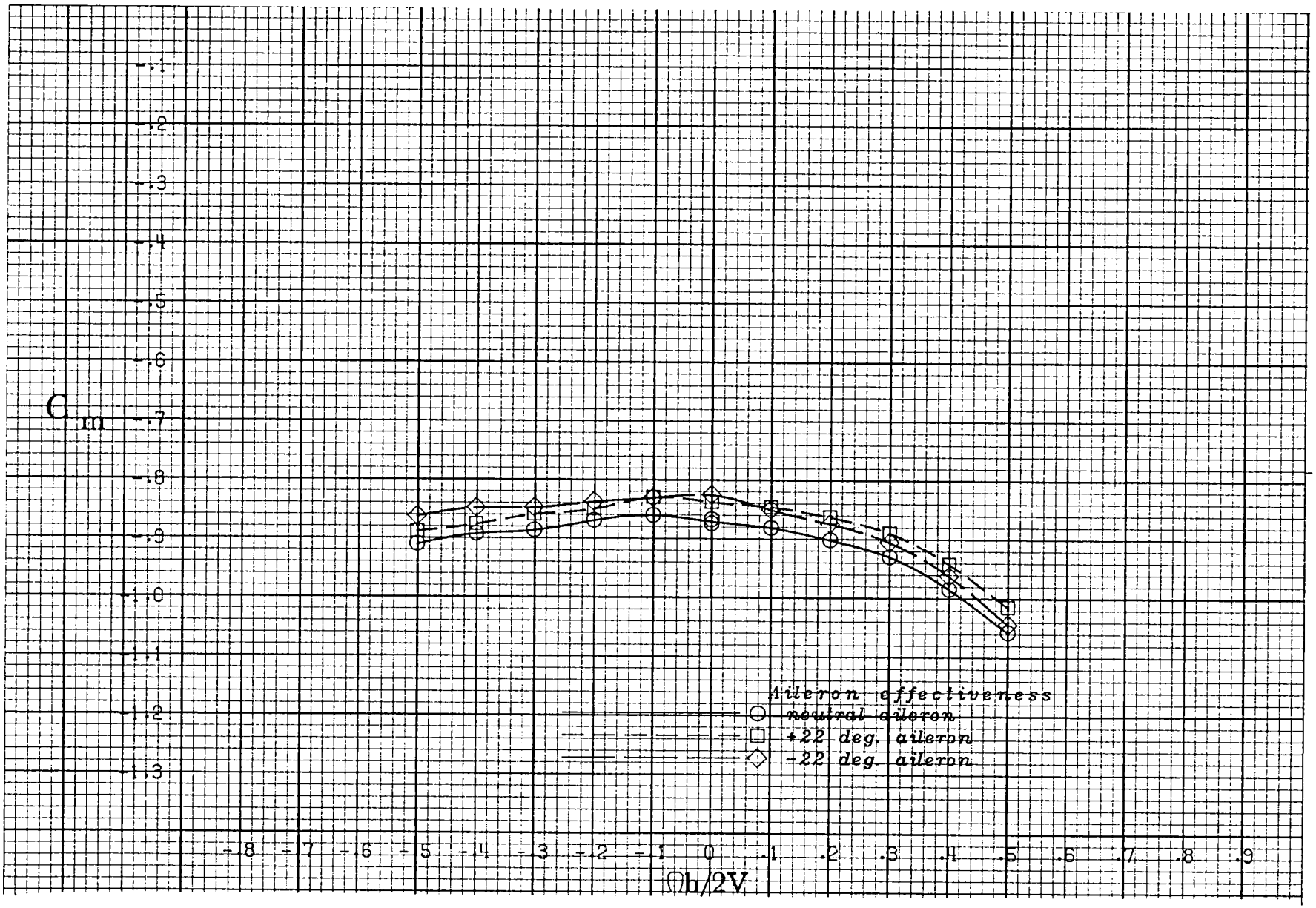

(h) α = 70 deg.

Figure A 27 .- Continued.

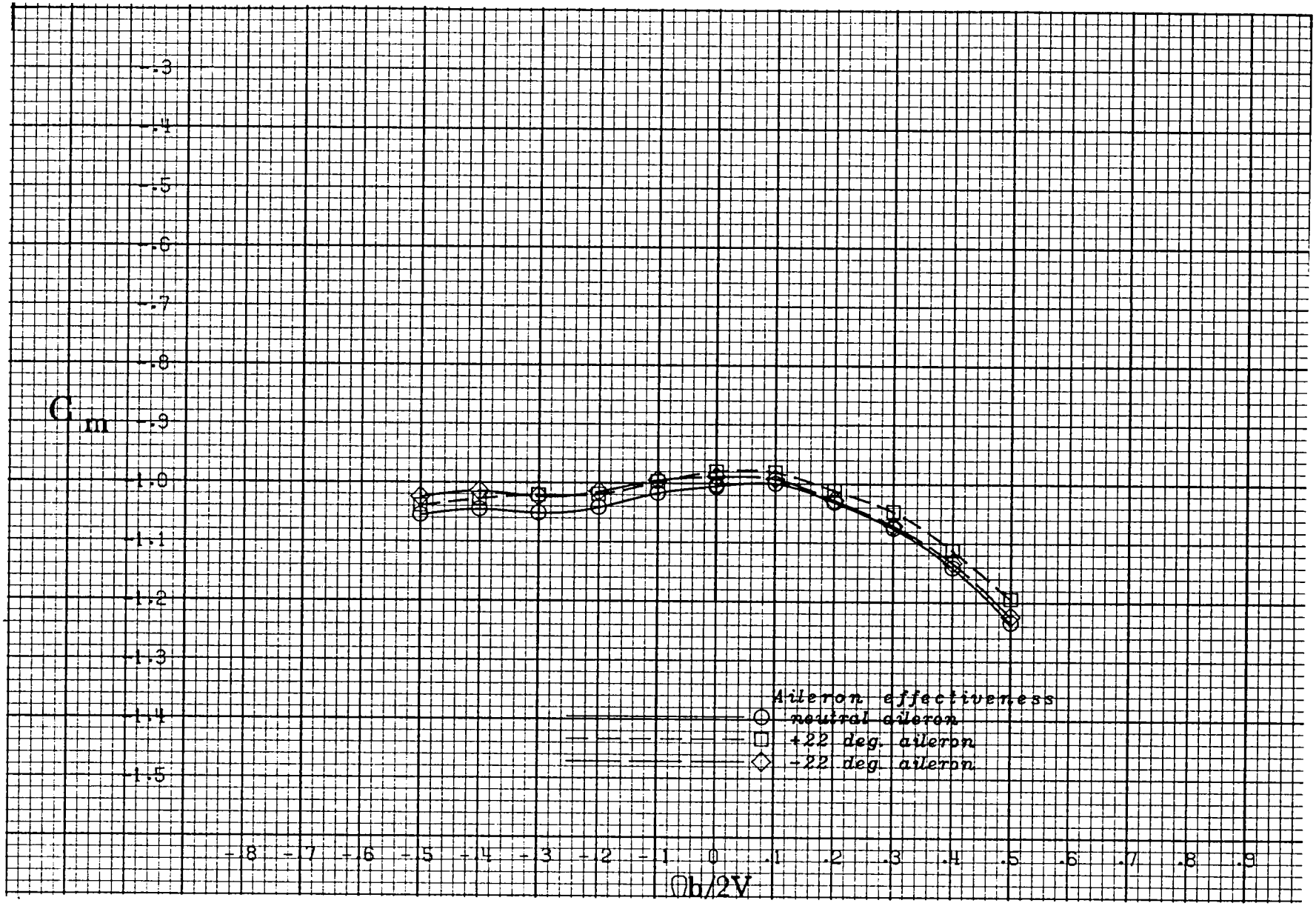

(i) α = 80 deg.

Figure A 27 .- Continued.

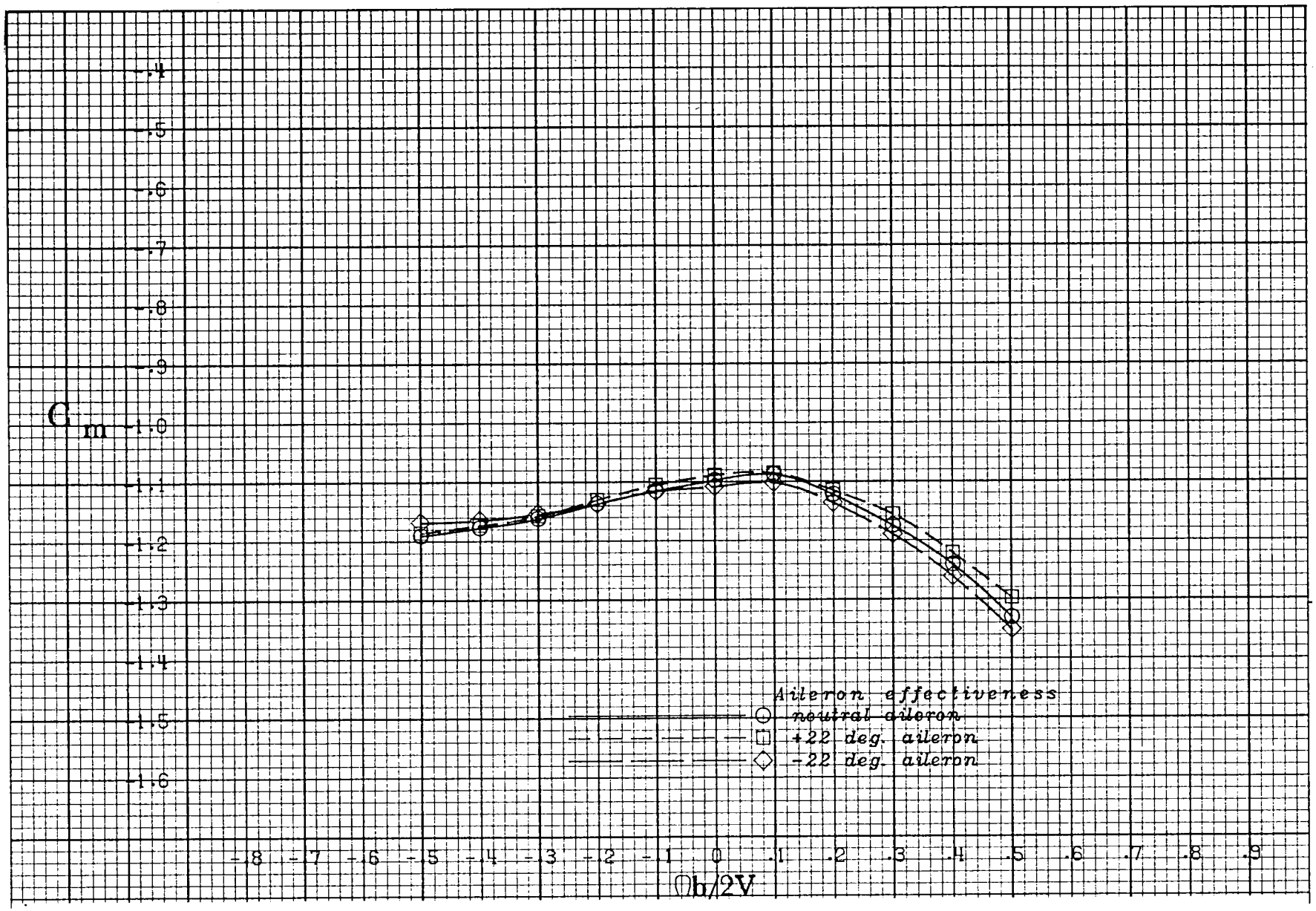

(j) α = 90 deg.

Figure A 27 .- Concluded.

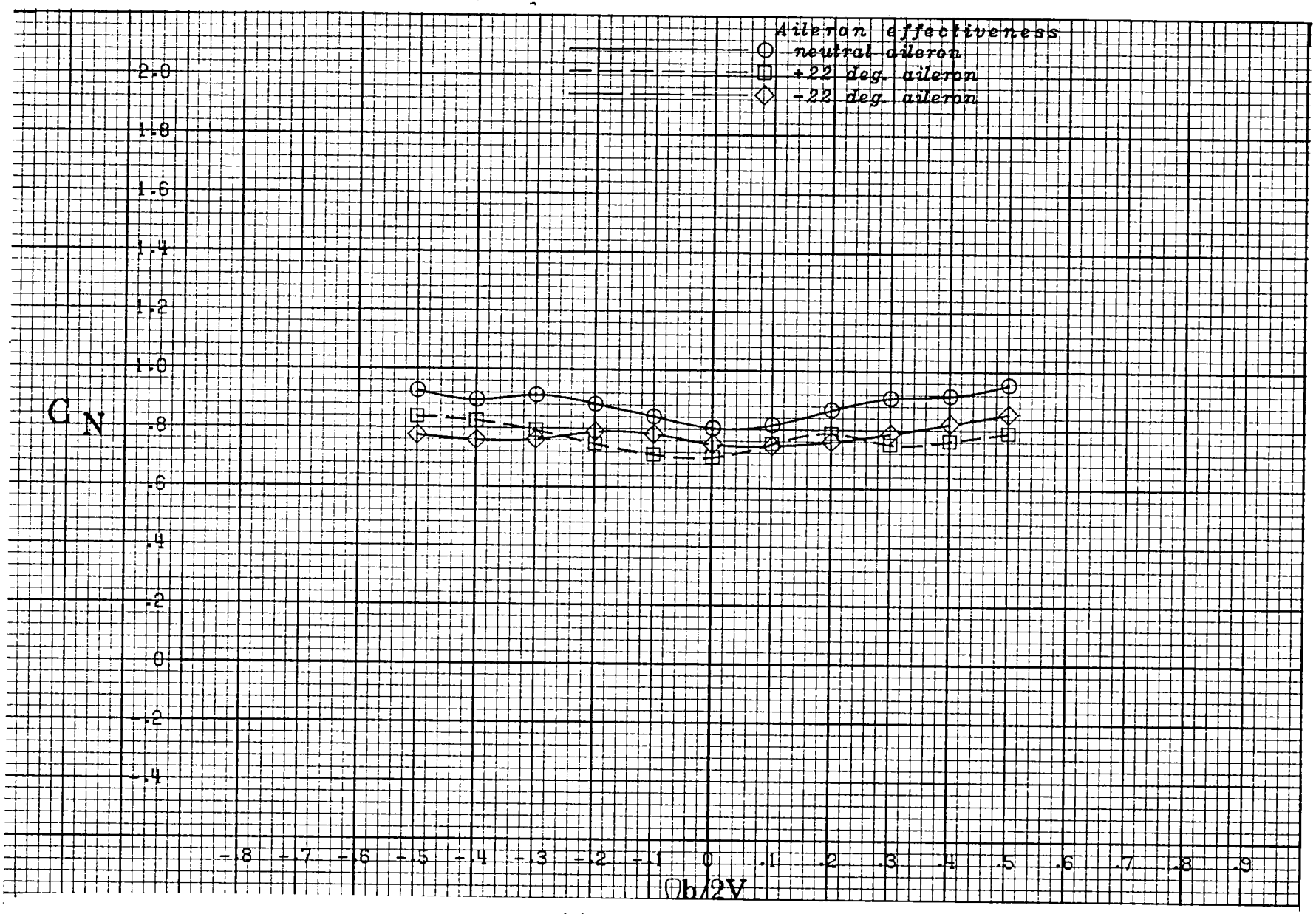

(a) α = 20 deg.

Figure A 28 .- Effect of rotation rate and aileron deflection on normal-force coefficient for the basic configuration with -10 deg elevator and -26 deg rudder at +10 deg sideslip angle.

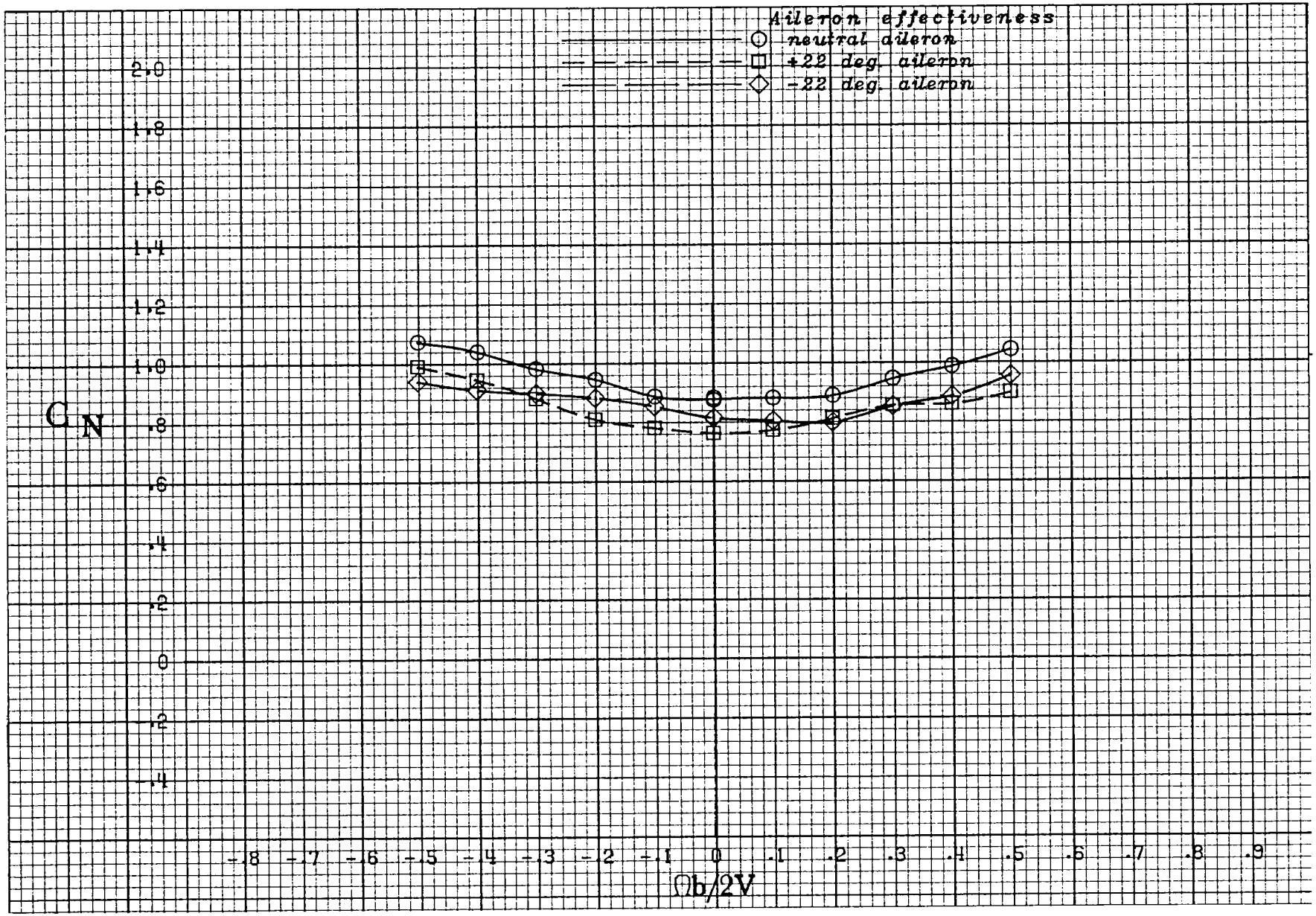

(b) α = 25 deg.

Figure A 28 .- Continued.

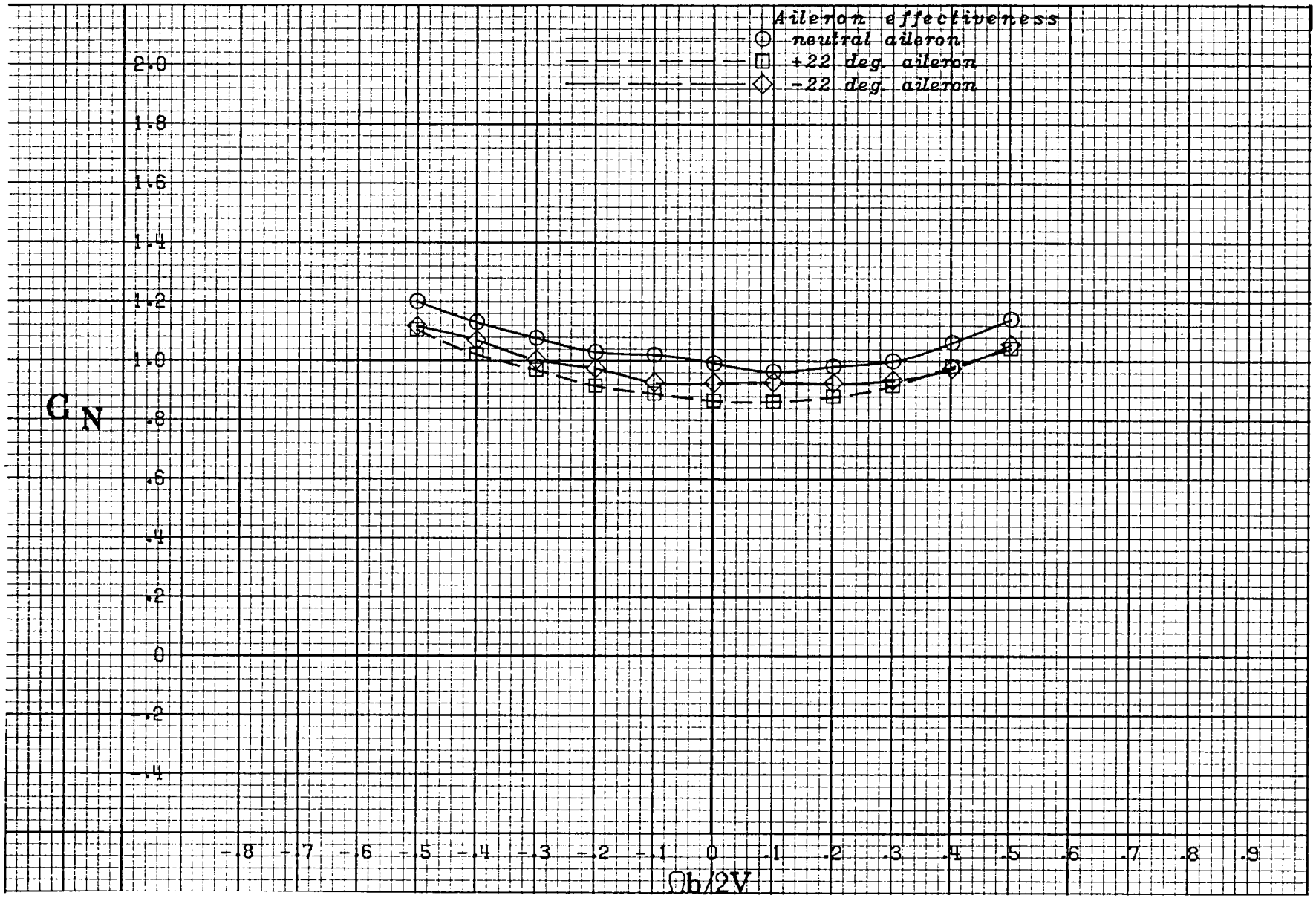

(c) α = 30 deg.

Figure A 28 .- Continued.

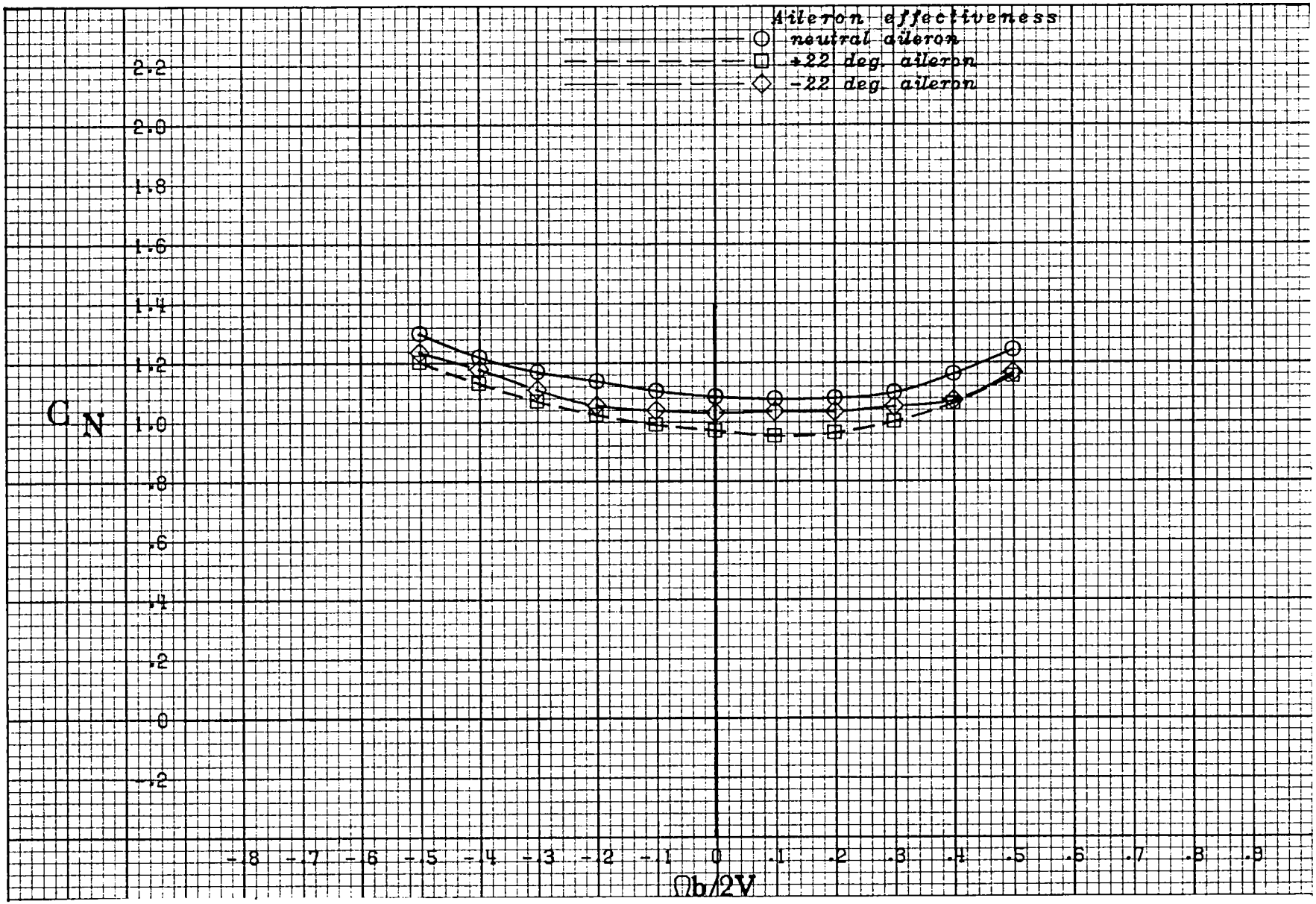

(d) α = 35 deg.

Figure A 28 .- Continued.

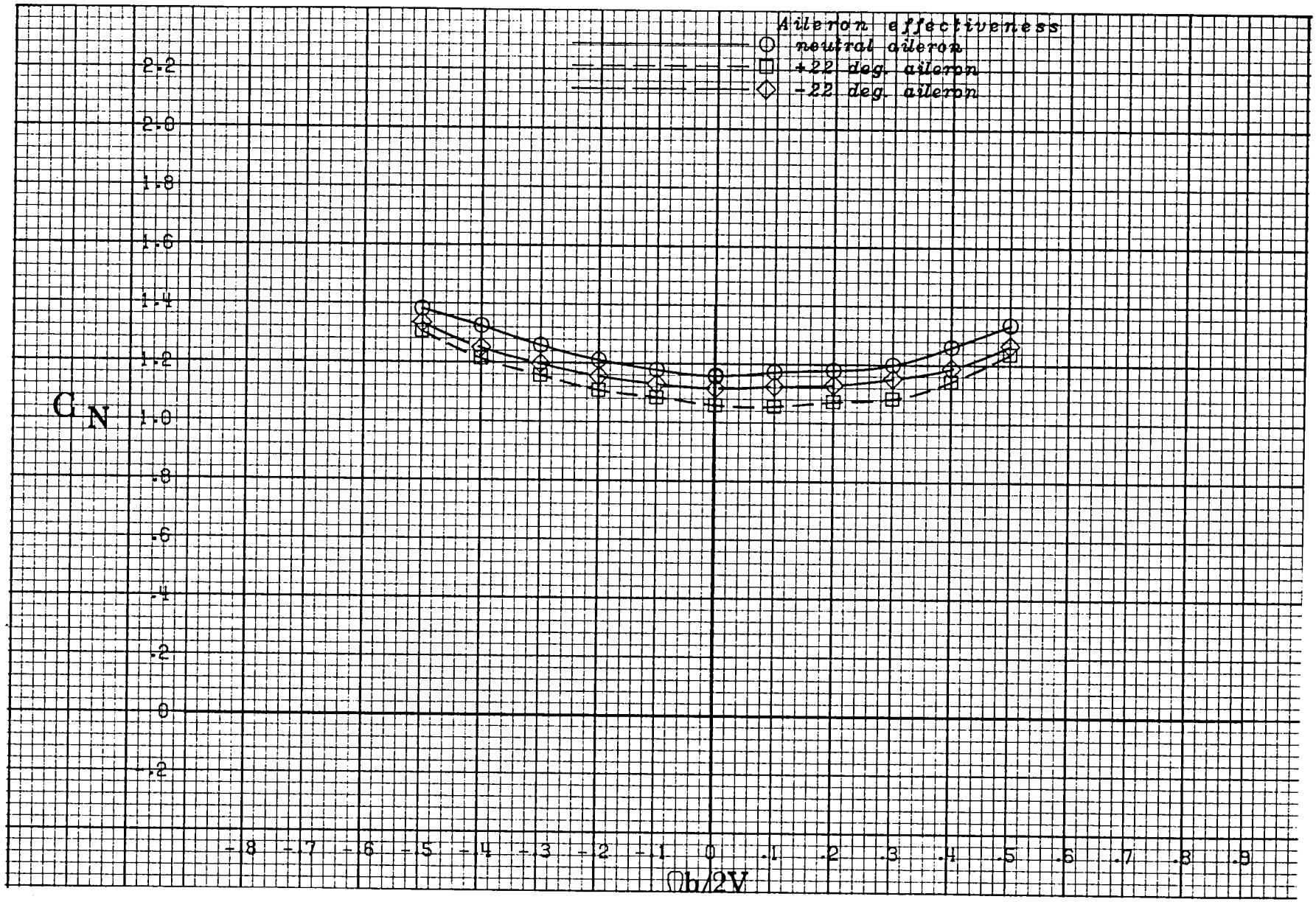

(e) α = 40 deg.

Figure A 28 .- Continued.

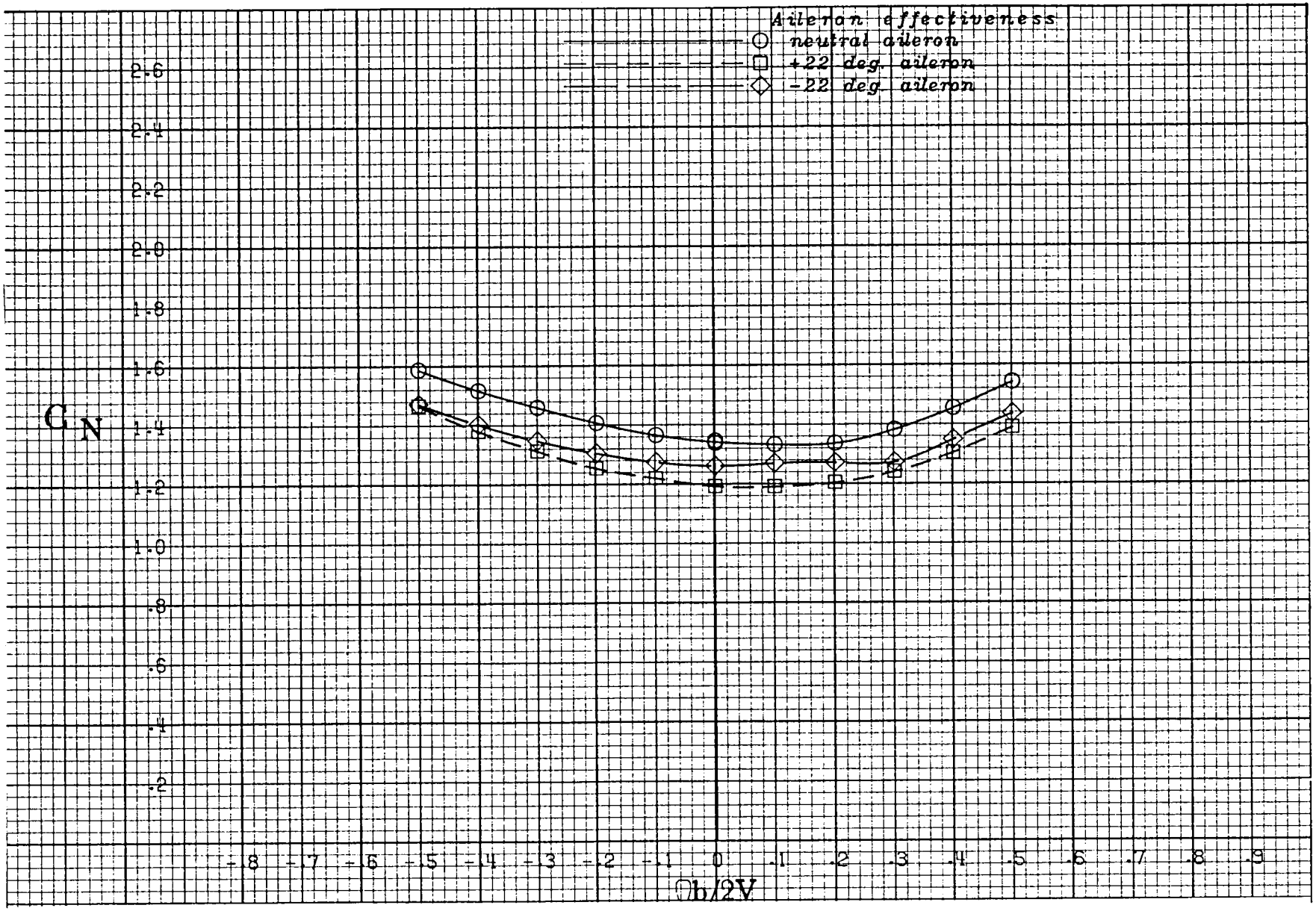

(f) α = 50 deg.

Figure A 28 .- Continued.

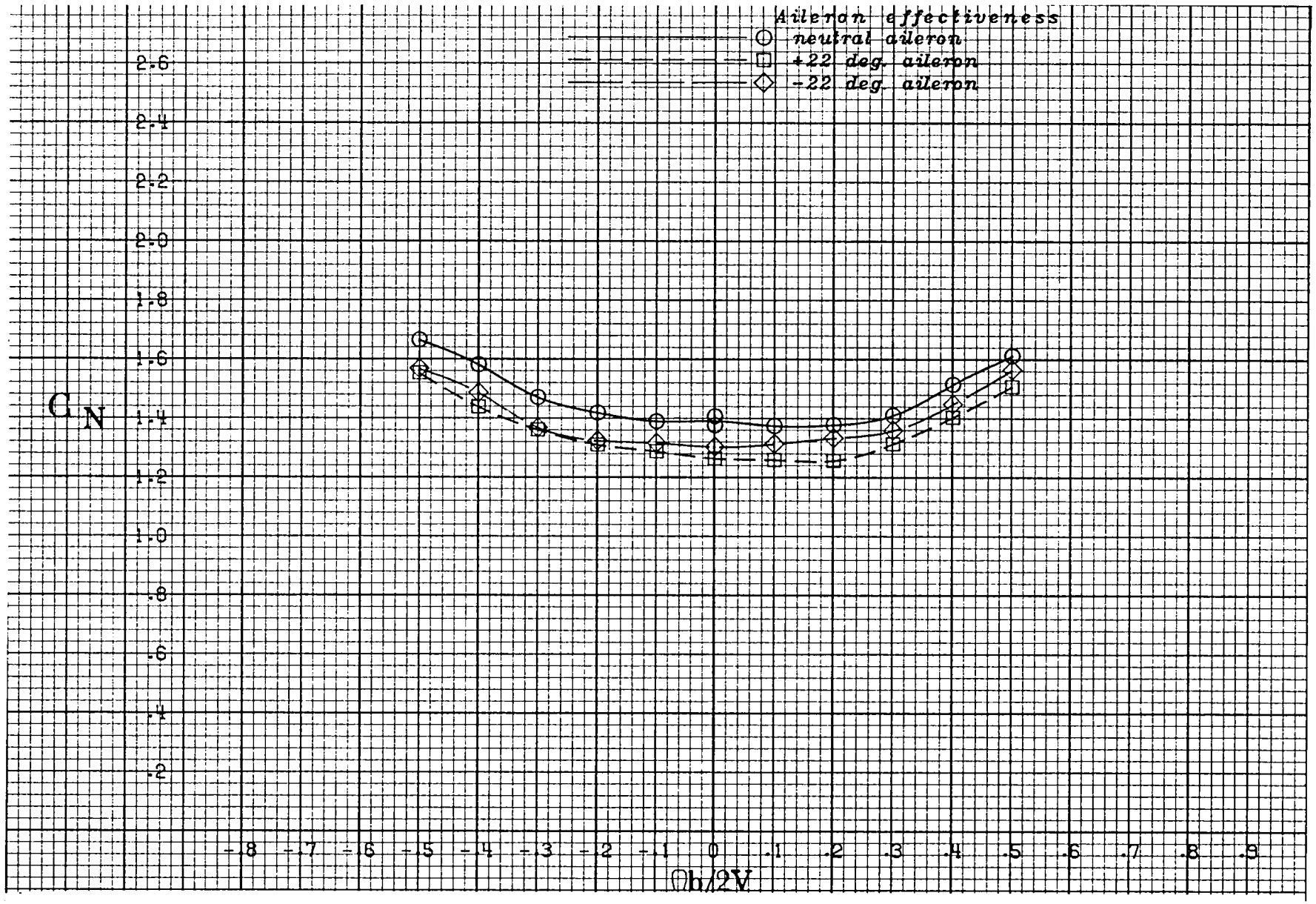

(g) α = 60 deg.

Figure A 28 .- Continued.

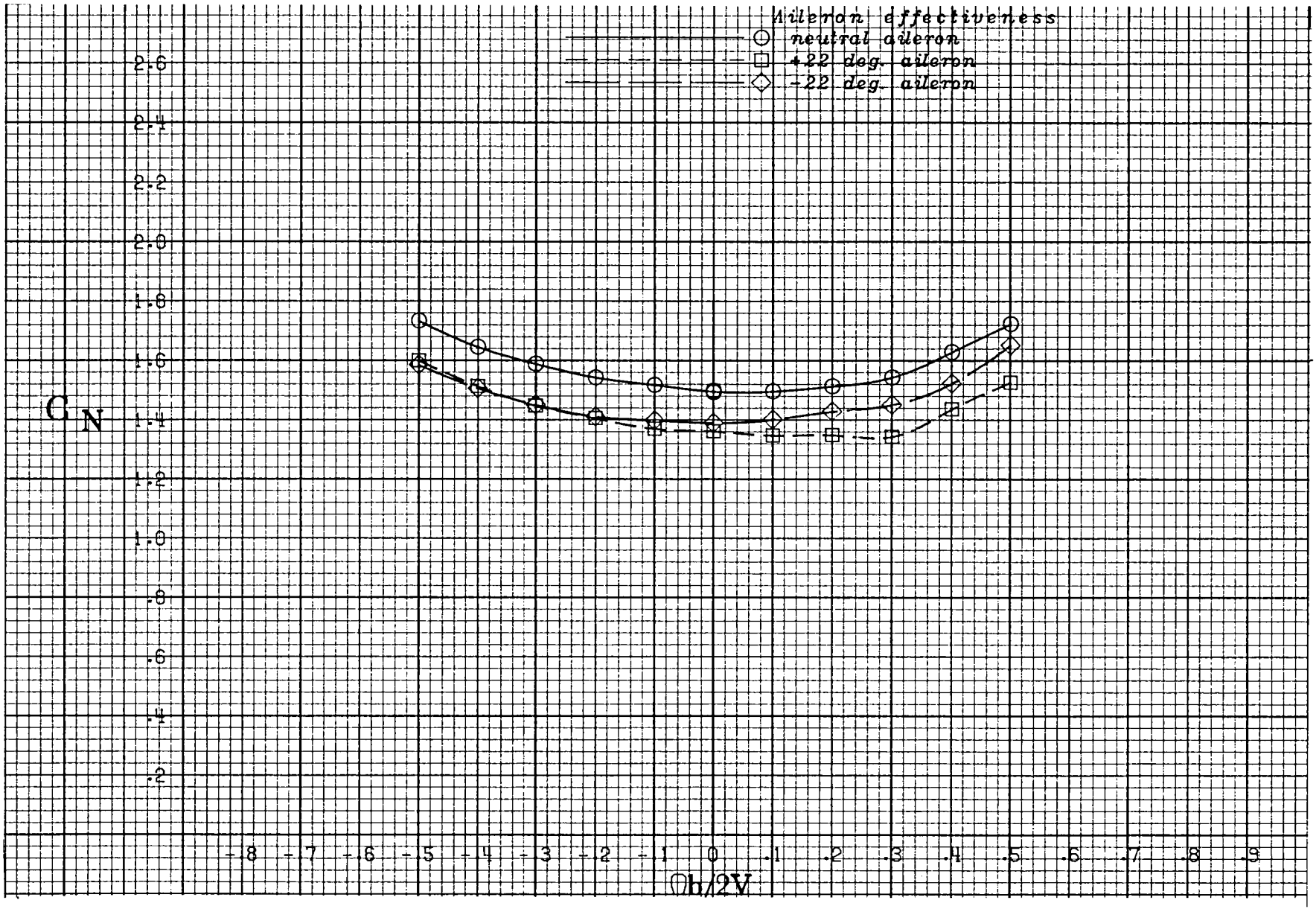

(h) α = 70 deg.

Figure A 28 .- Continued.

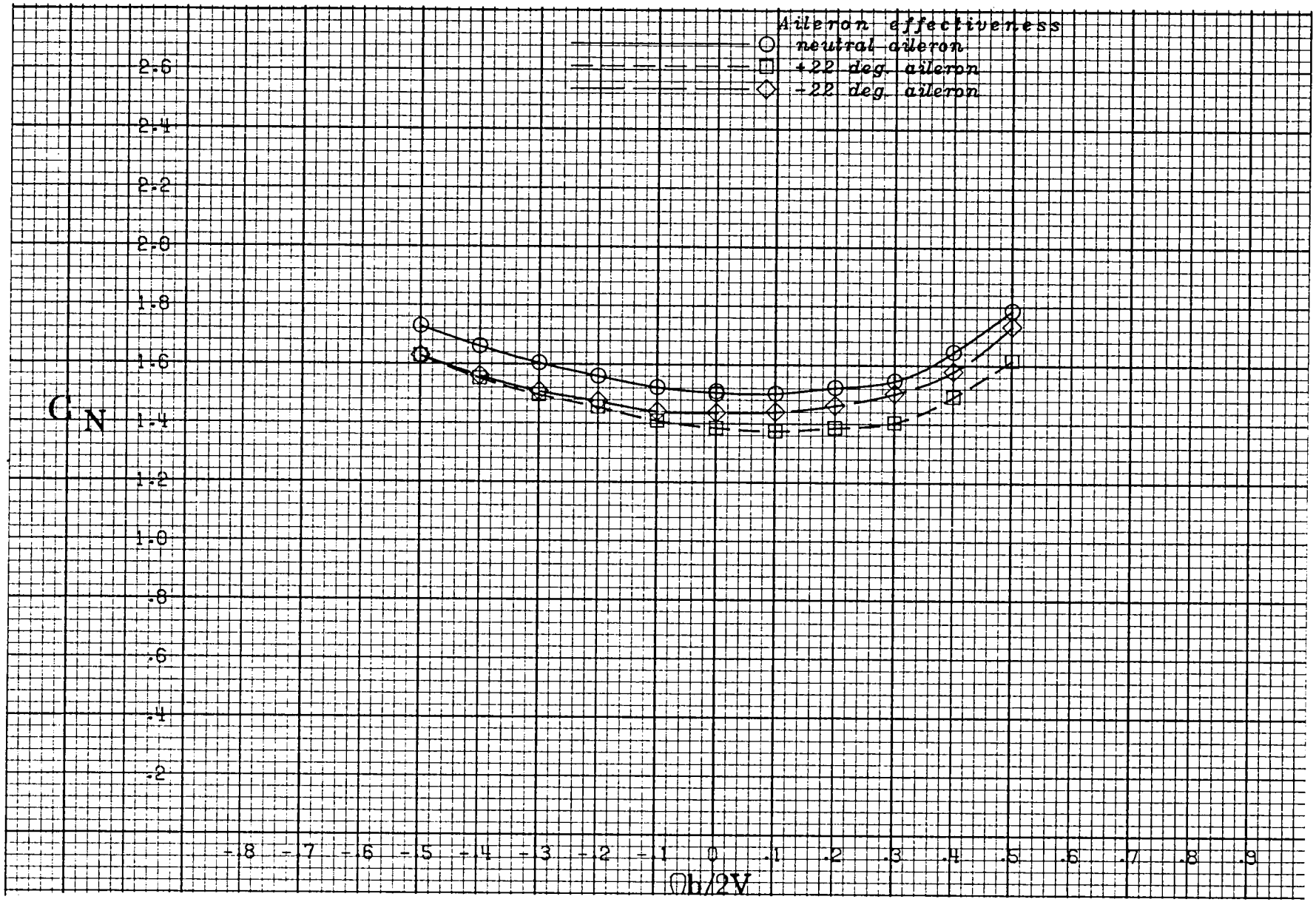

(i) α = 80 deg.

Figure A 28 .- Continued.

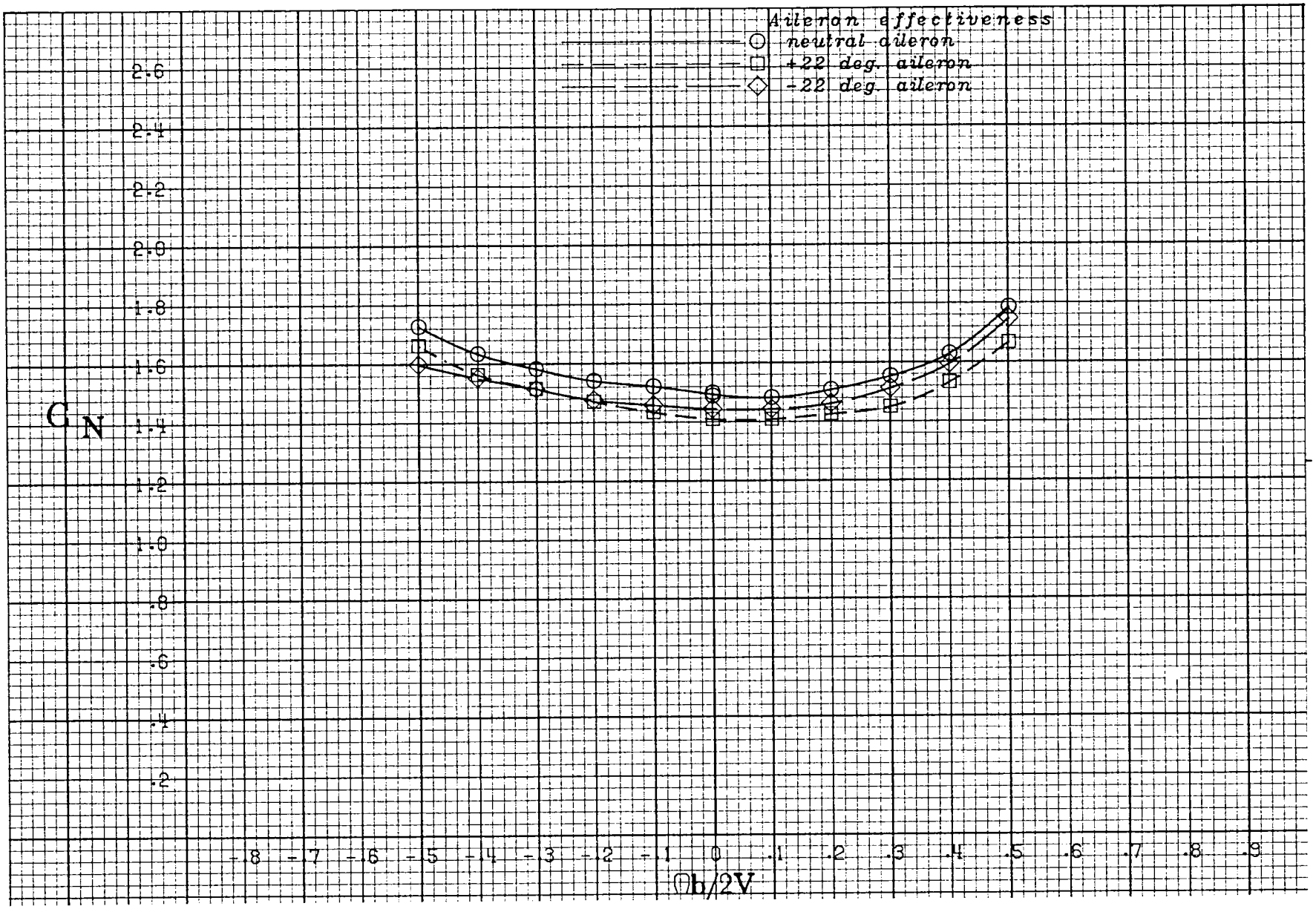

(j) α = 90 deg.

Figure A 28 .- Concluded.

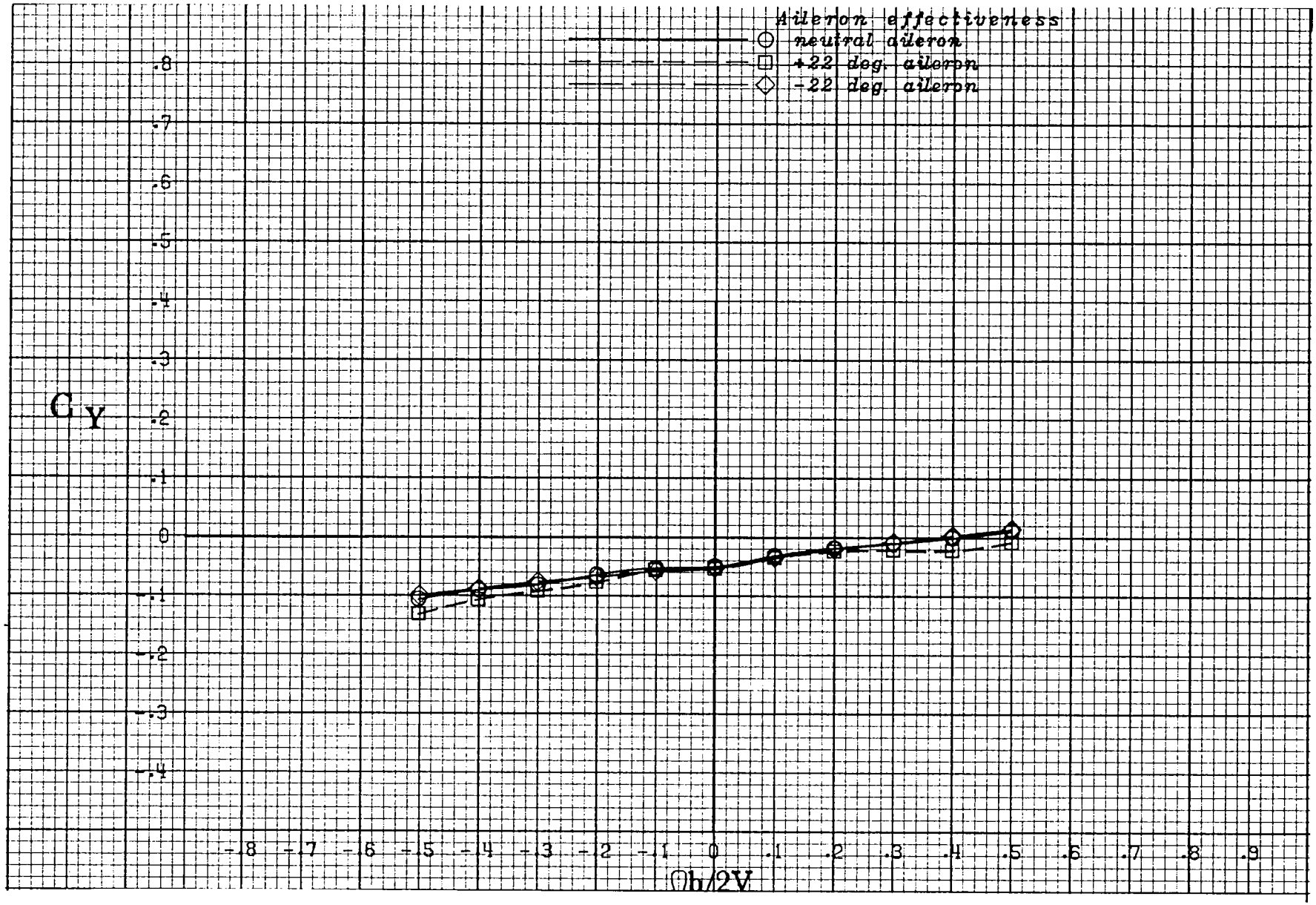

(a) α = 20 deg.

Figure A 29 .- Effect of rotation rate and aileron deflection on side-force coefficient for the basic configuration with -10 deg elevator and -26 deg rudder at +10 deg sideslip angle.

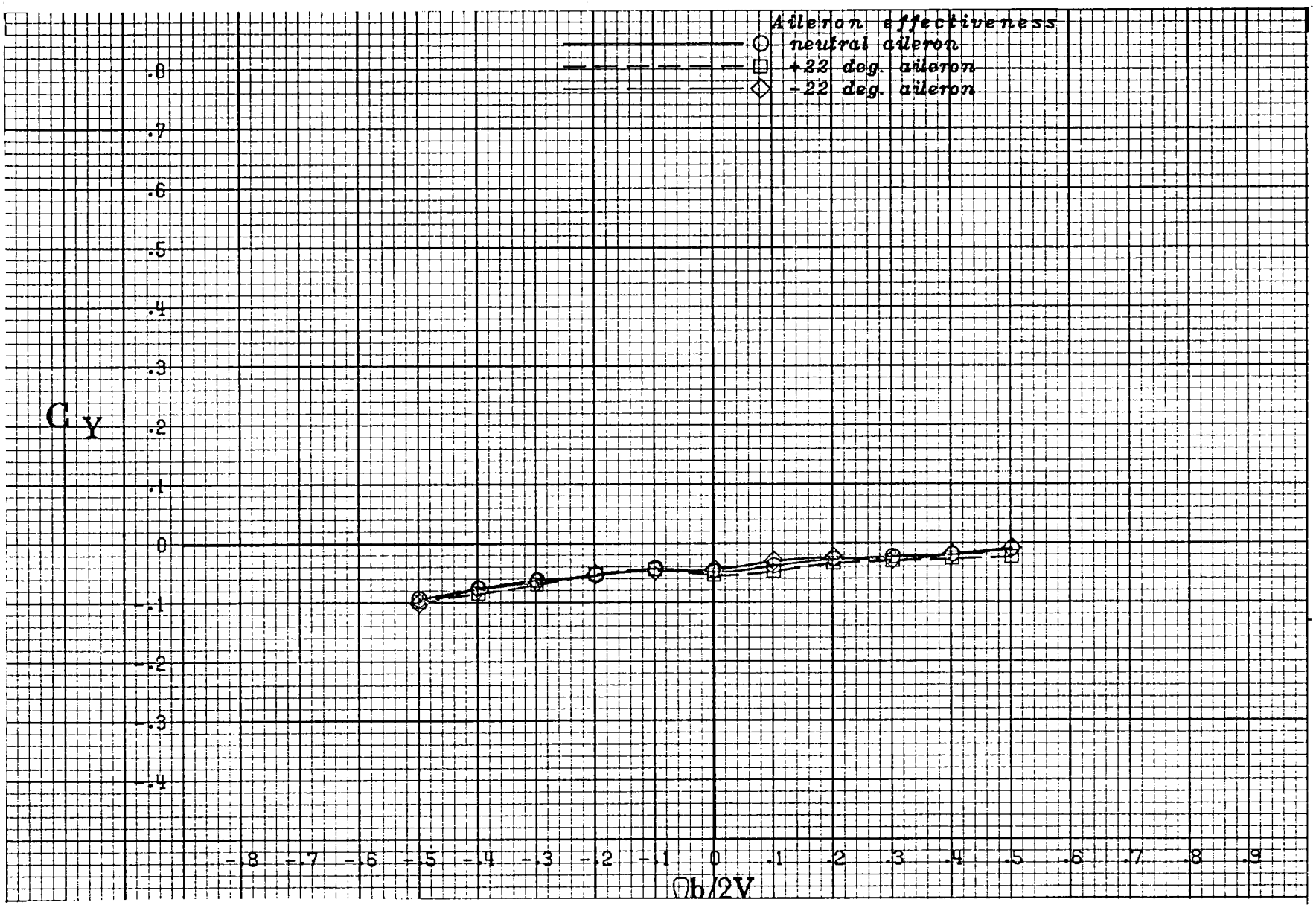

(b) α = 25 deg.

Figure A 29 .- Continued.

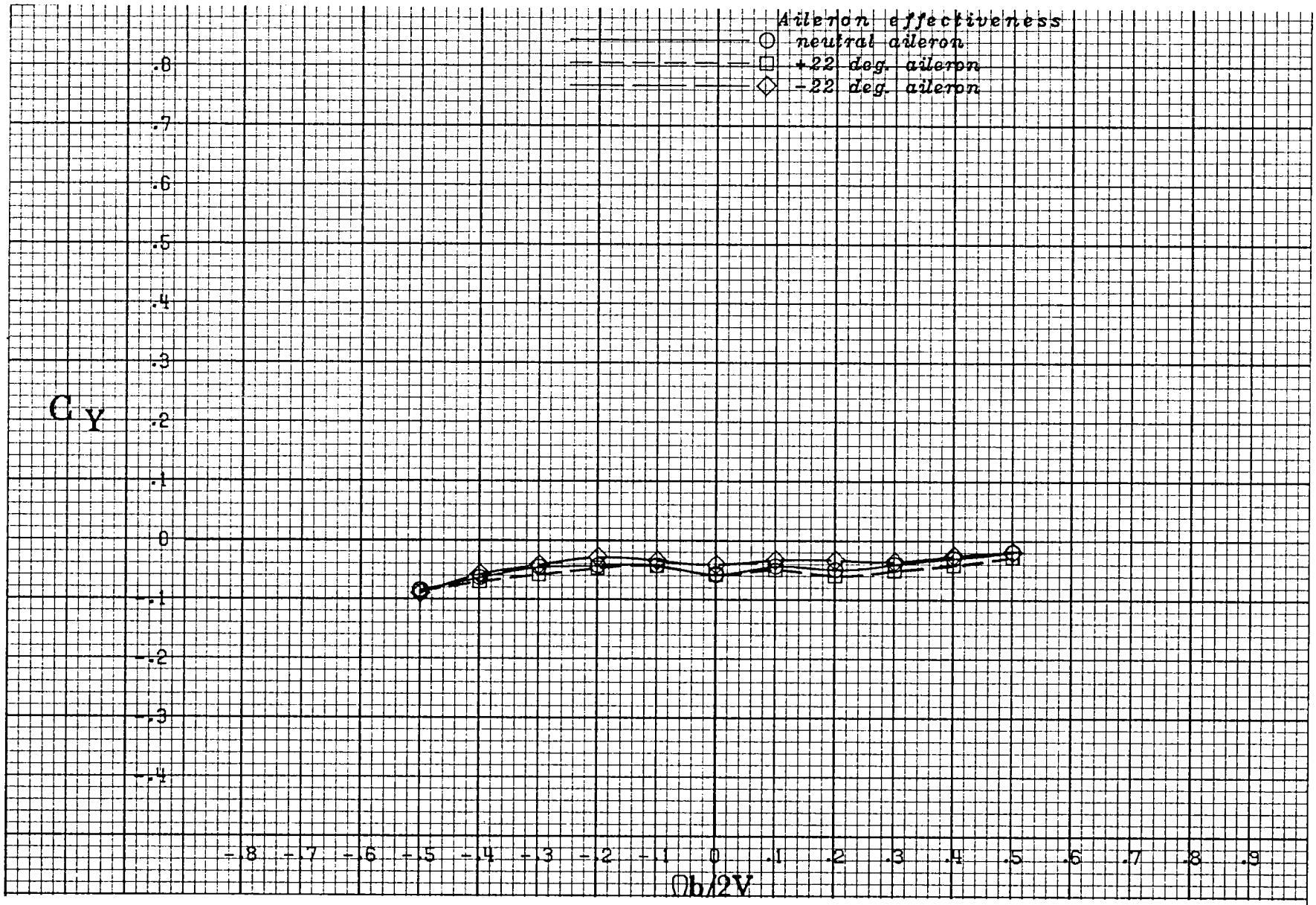

(c) α = 30 deg.

Figure A 29 .- Continued.

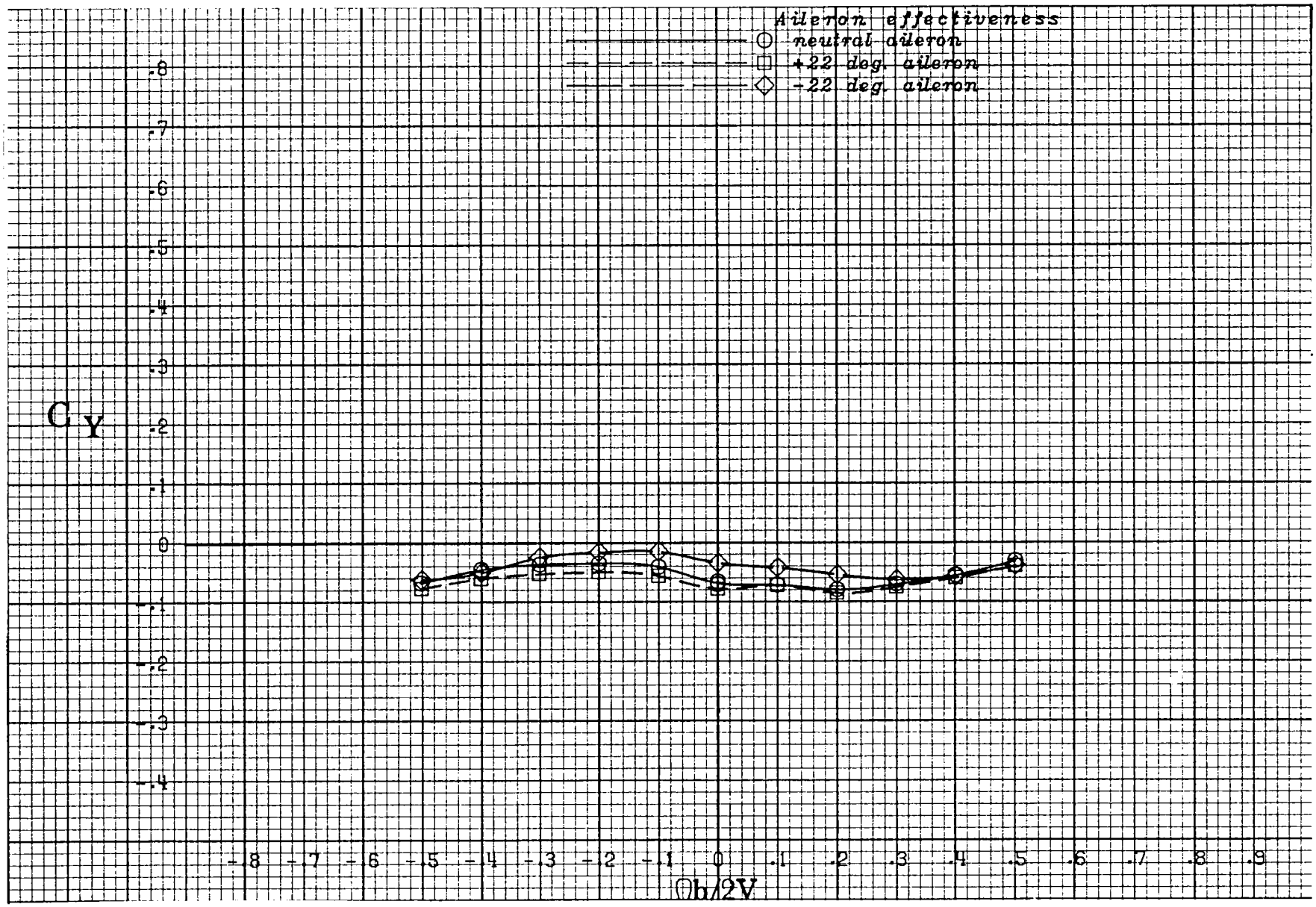

(d) α = 35 deg.

Figure A 29 .- Continued.

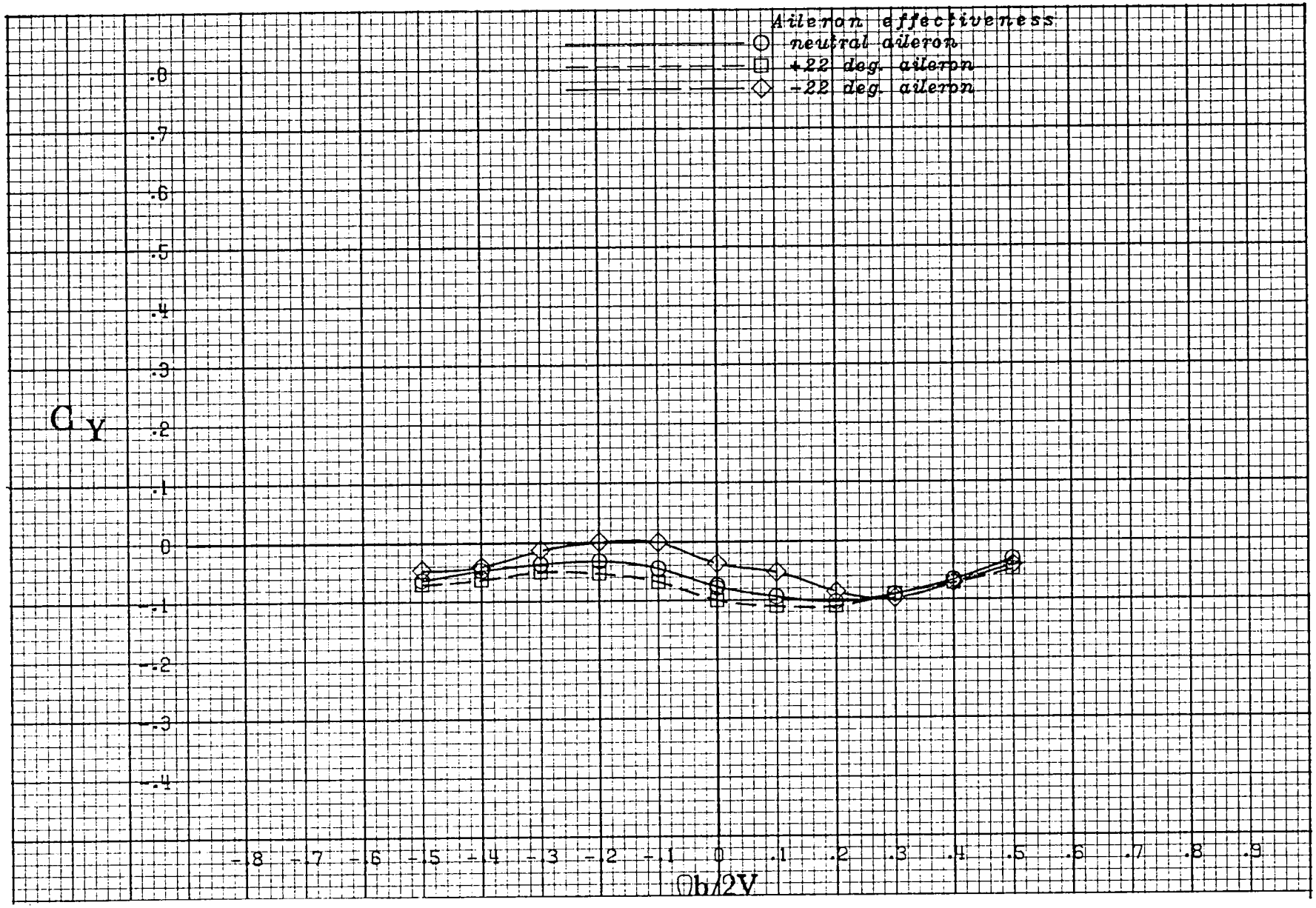

(e) α = 40 deg.

Figure A 29 .- Continued.

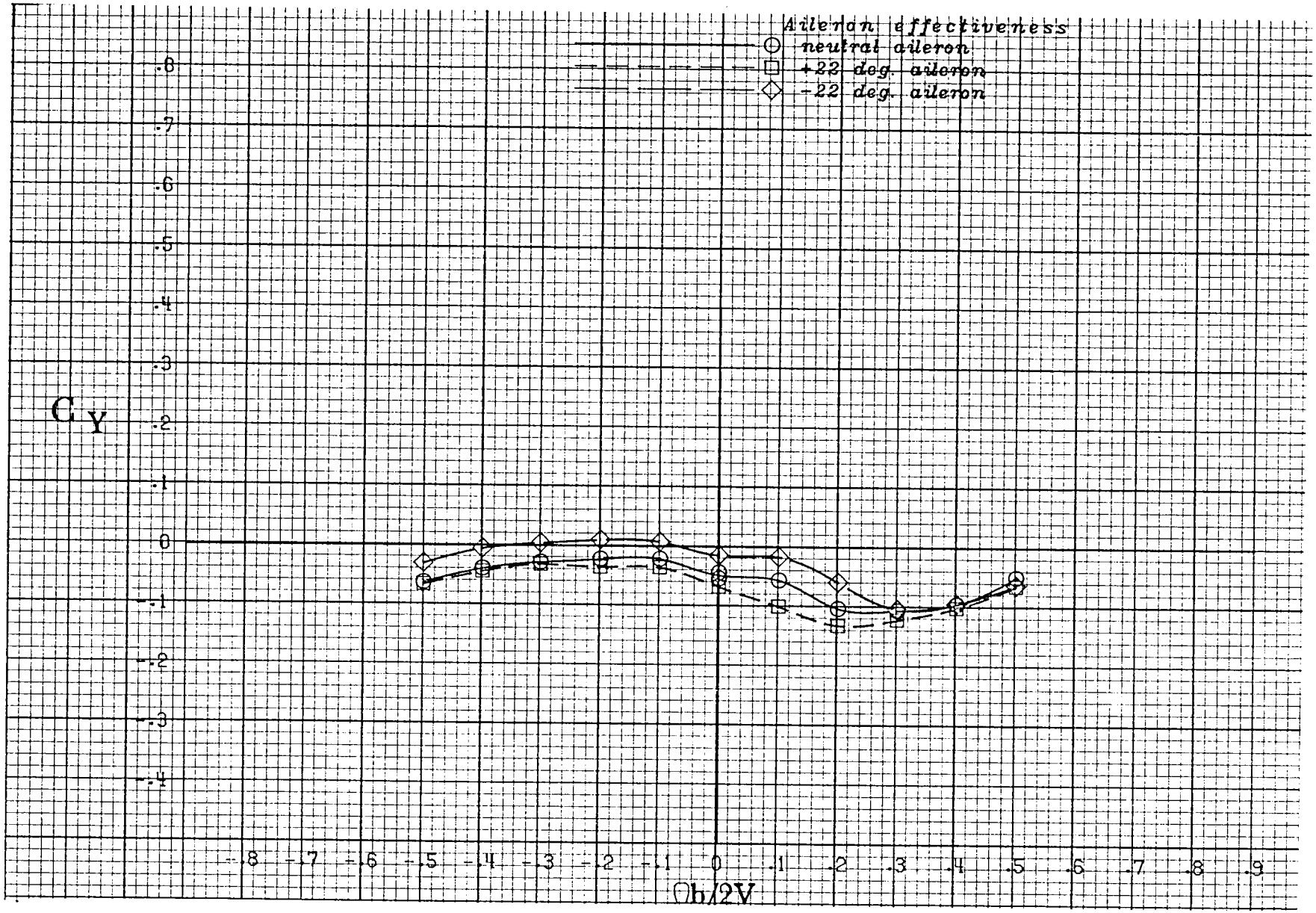

(f) α = 50 deg.

Figure A 29 .- Continued.

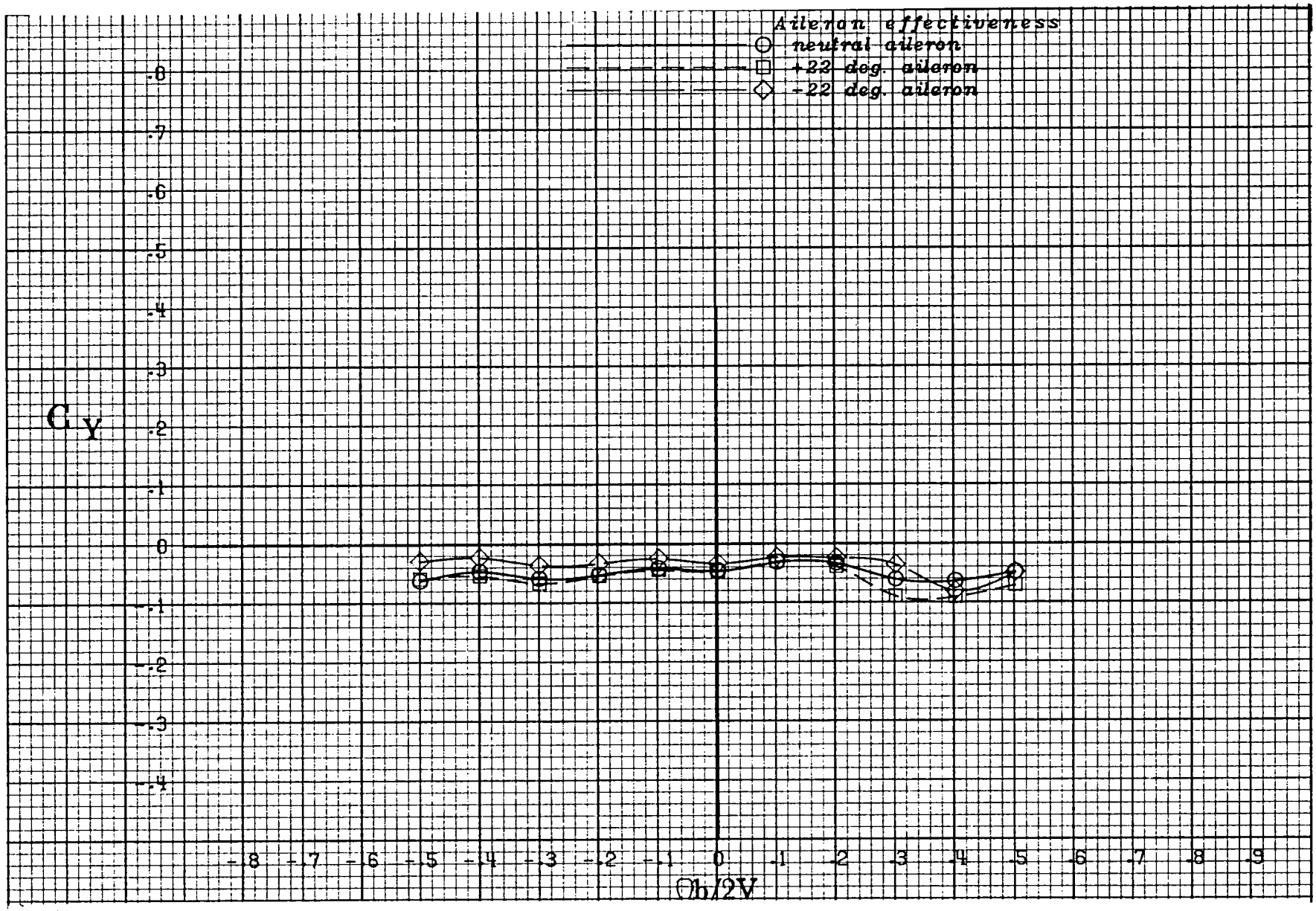

(g) α = 60 deg.

Figure A 29 .- Continued.

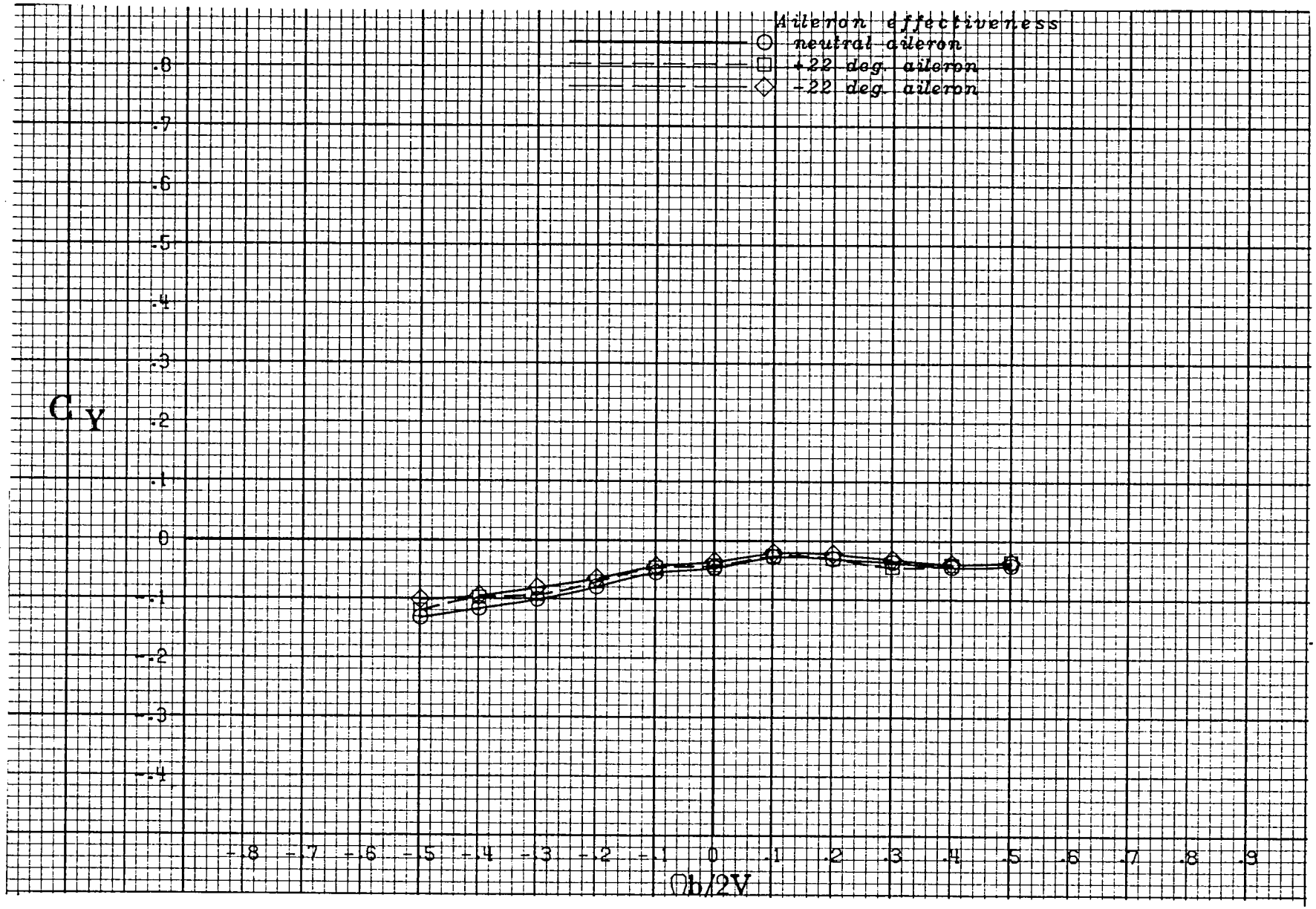

(h) α = 70 deg.

Figure A 29 .- Continued.

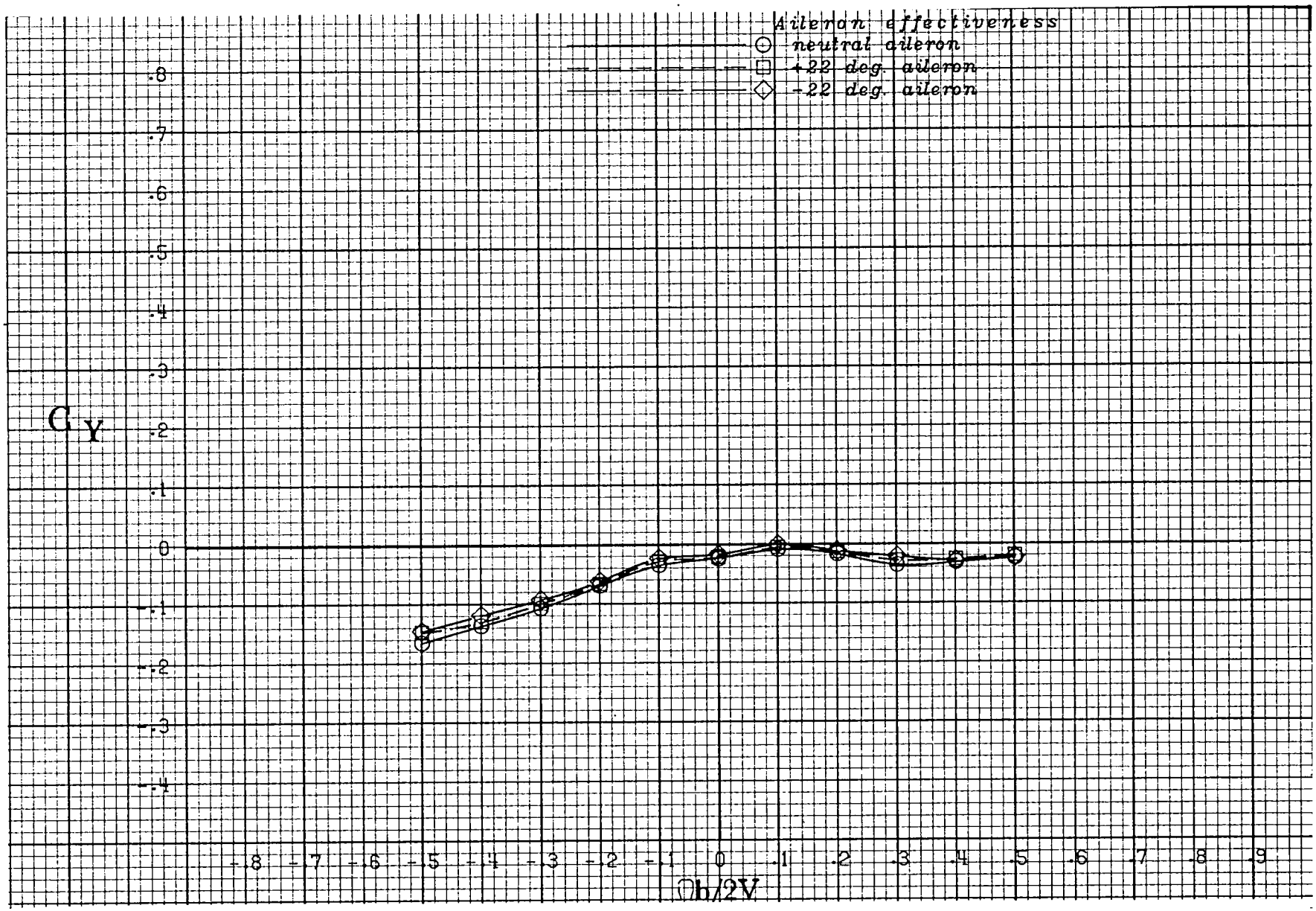

(i) α = 80 deg.

Figure A 29 .- Continued.

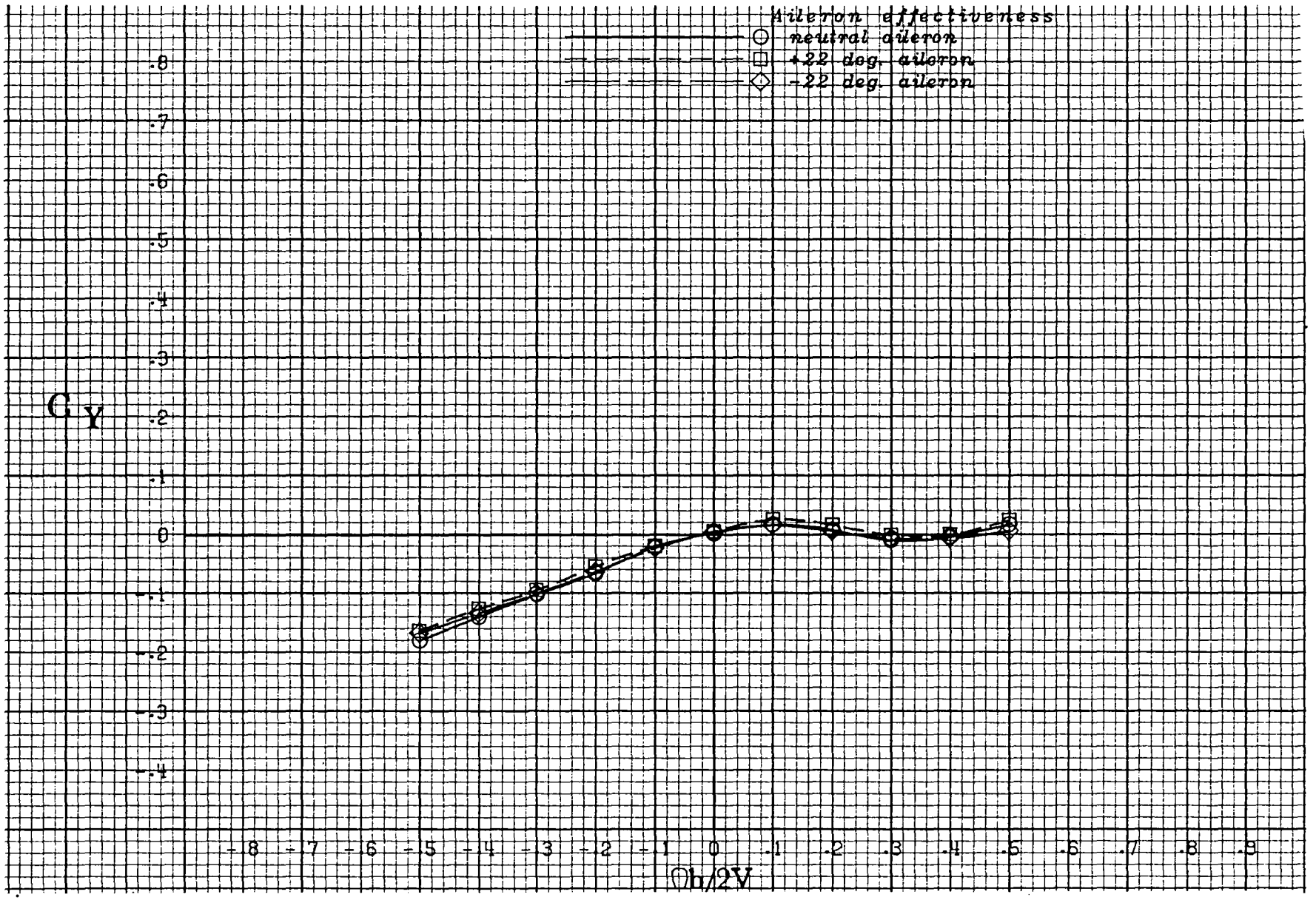

(j) α = 90 deg.

Figure A 29 .- Concluded.

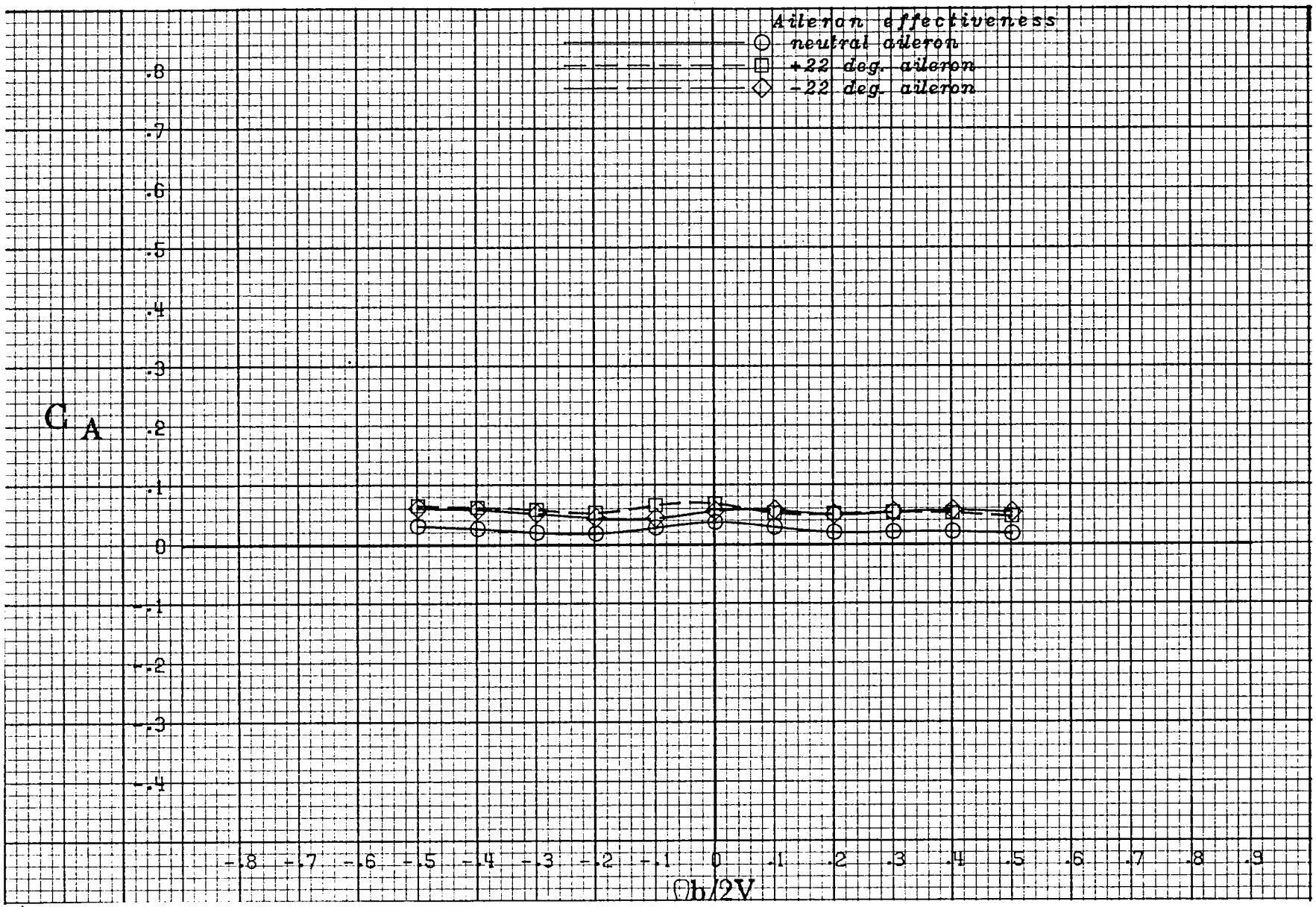

(a) α = 20 deg.

Figure A 30 .- Effect of rotation rate and aileron deflection on axial-force coefficient for the basic configuration with -10 deg elevator and -26 deg rudder at +10 deg sideslip angle.

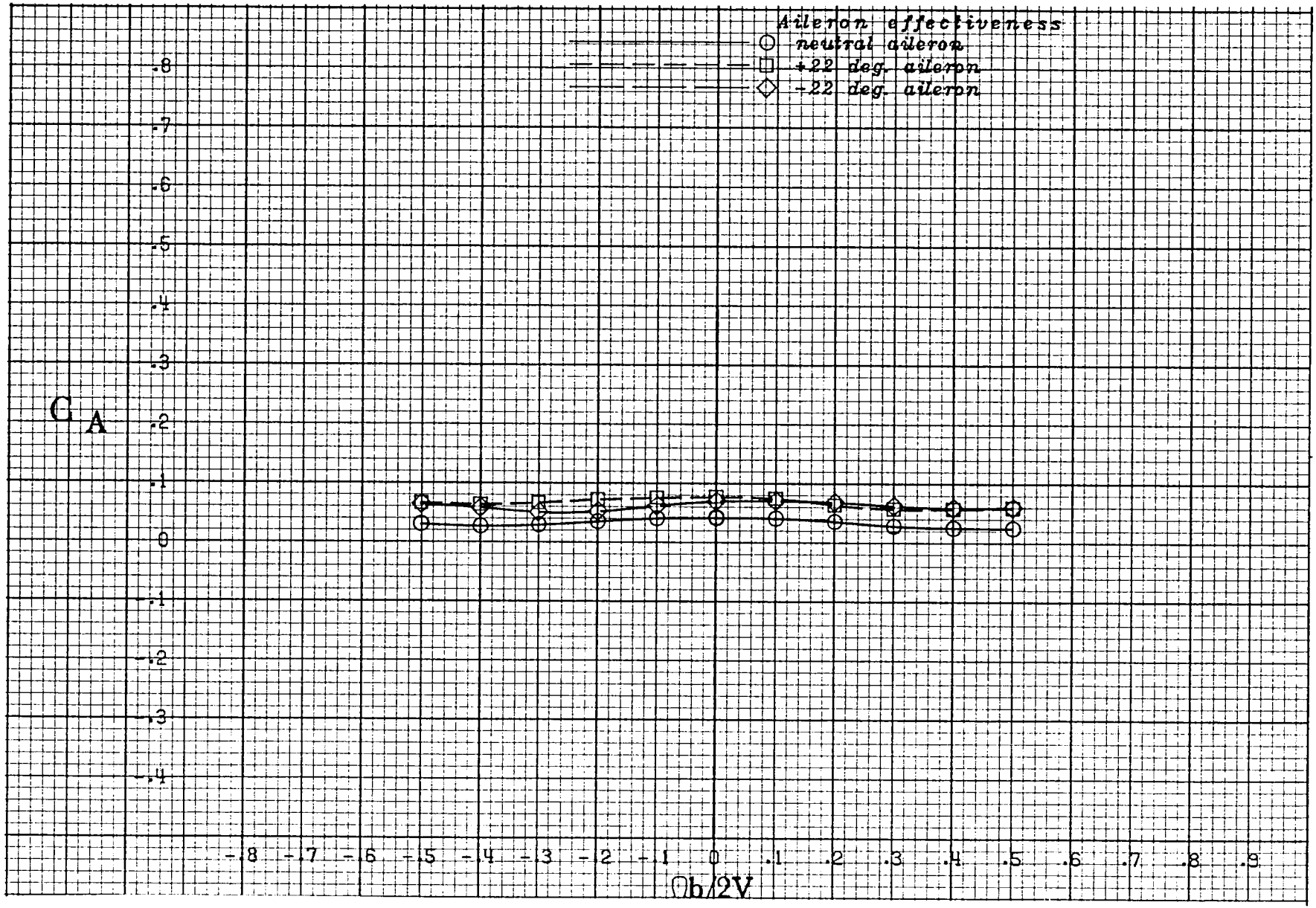

(b) α = 25 deg.

Figure A 30 .- Continued.

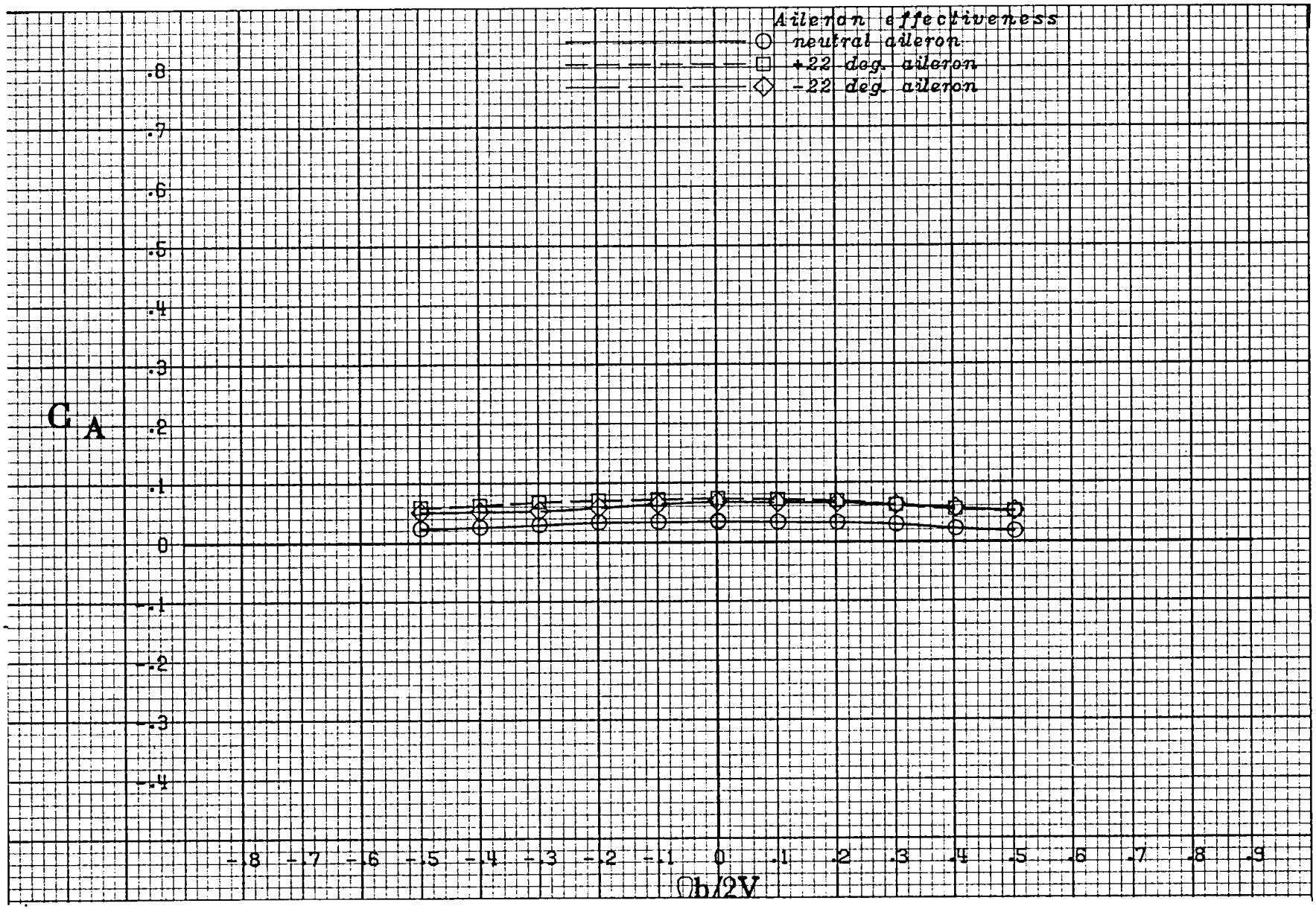

(c) α = 30 deg.

Figure A 30 .- Continued.

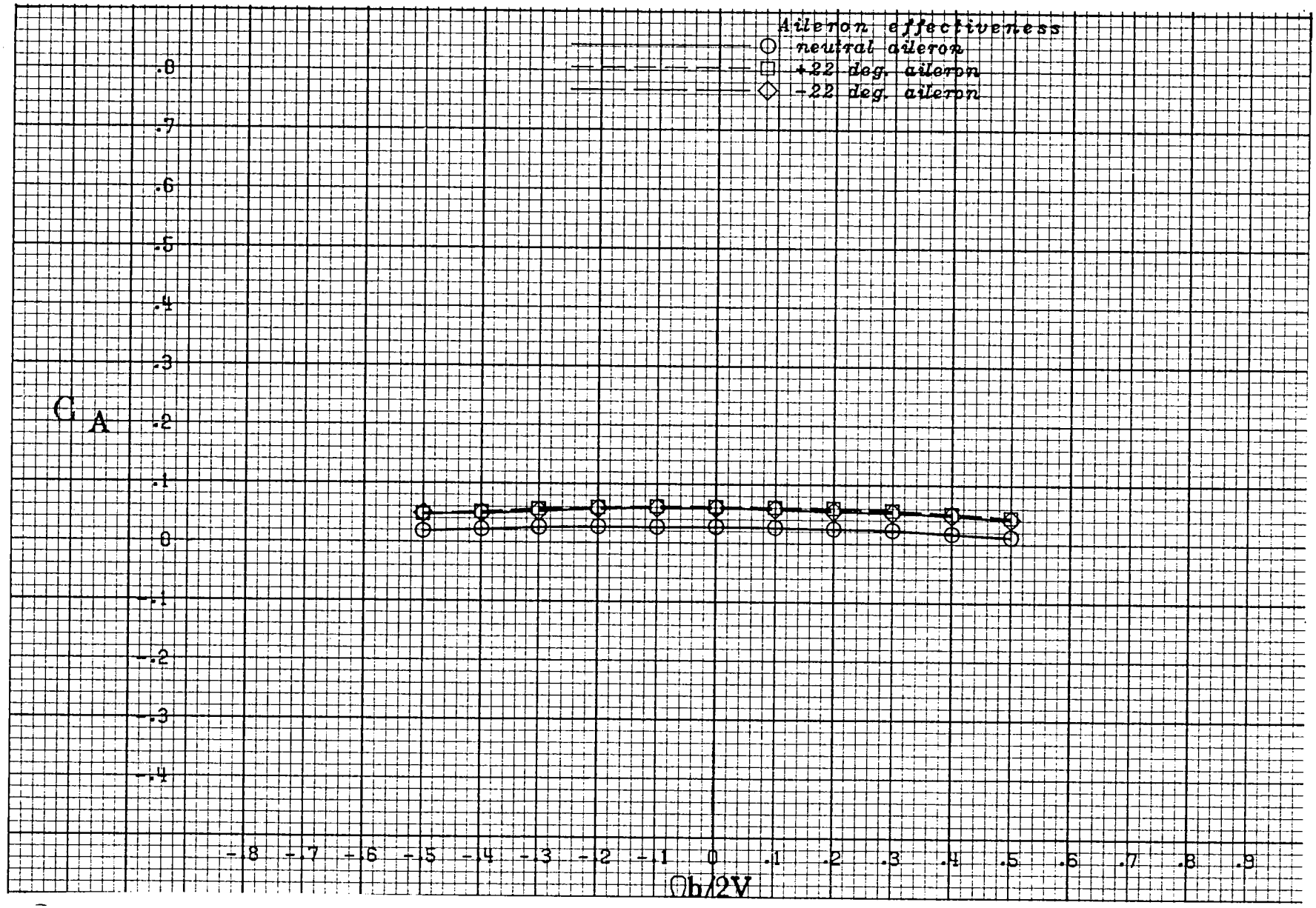

(d) α = 35 deg.

Figure A 30 .- Continued.

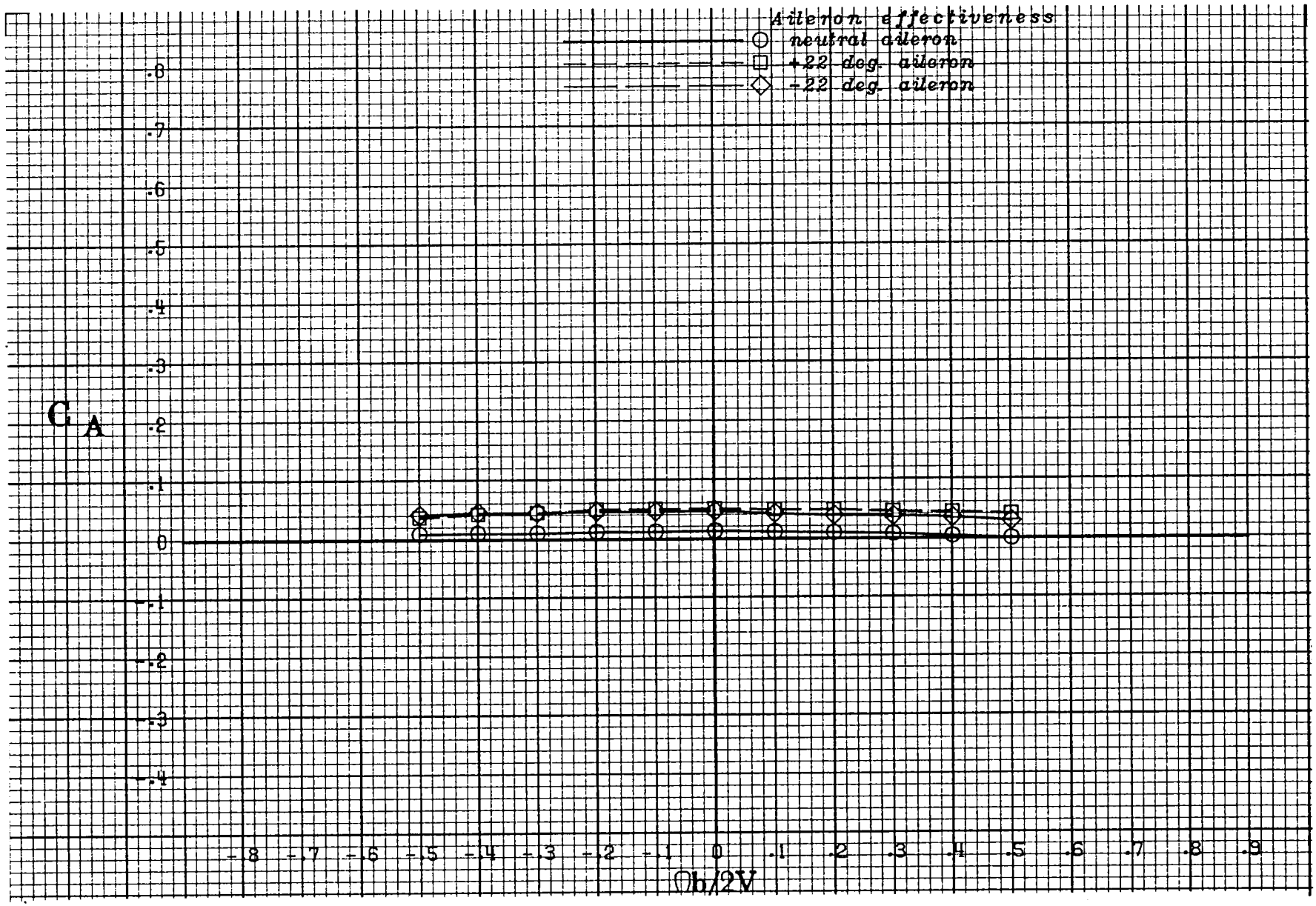

(e) α = 40 deg.

Figure A 30 .- Continued.

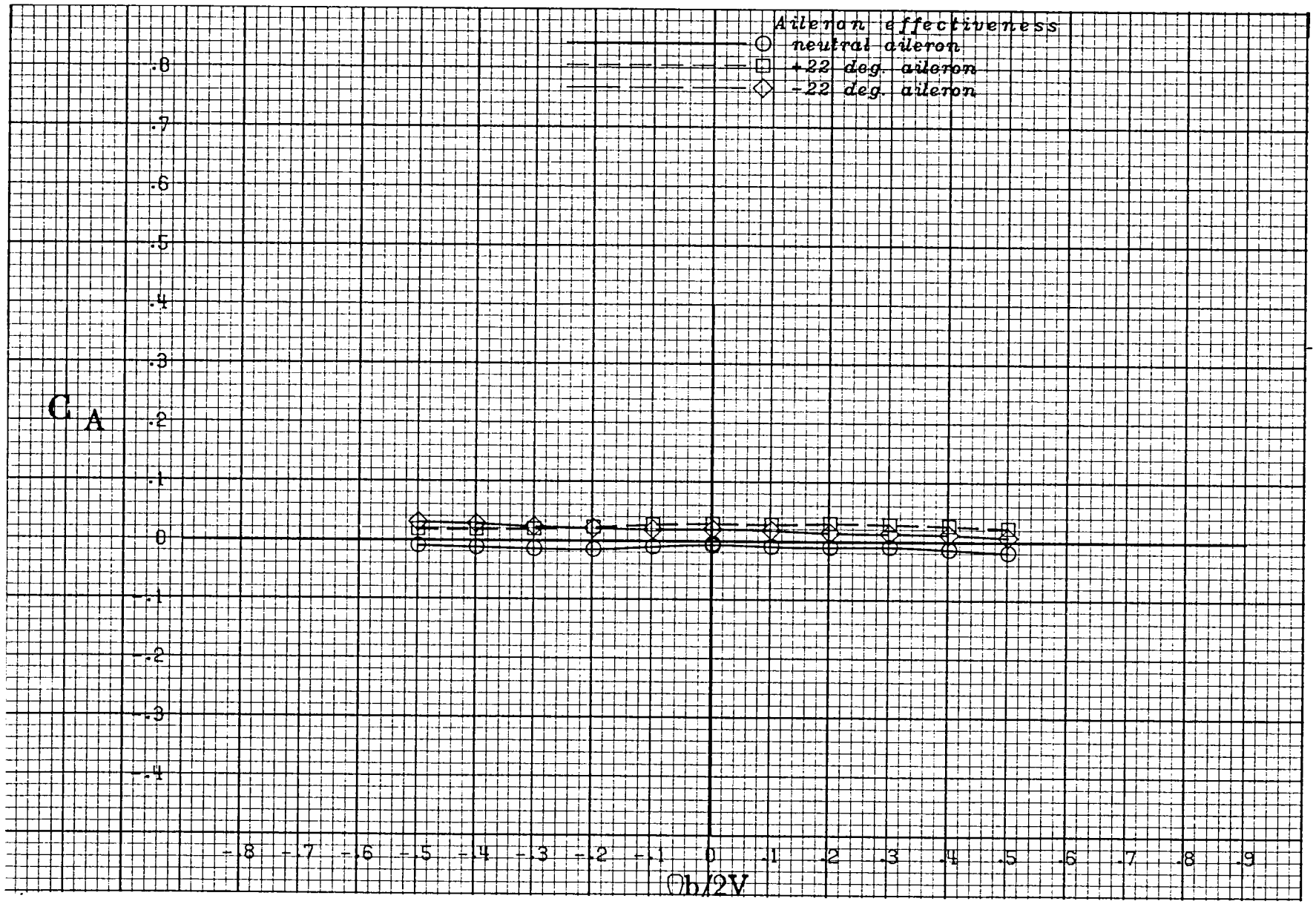

(f) α = 50 deg.

Figure A 30 .- Continued.

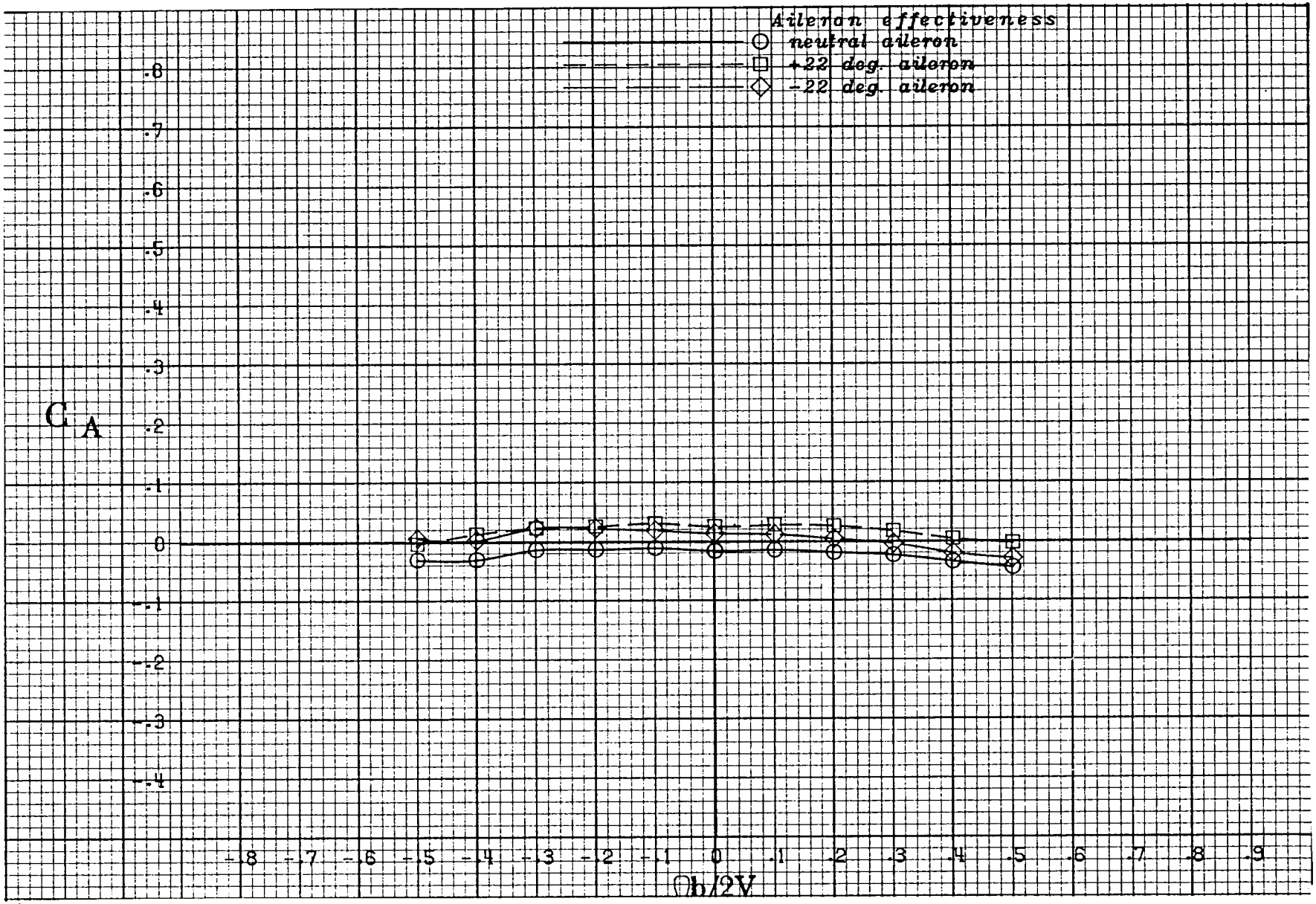

(g) α = 60 deg.

Figure A 30 .- Continued.

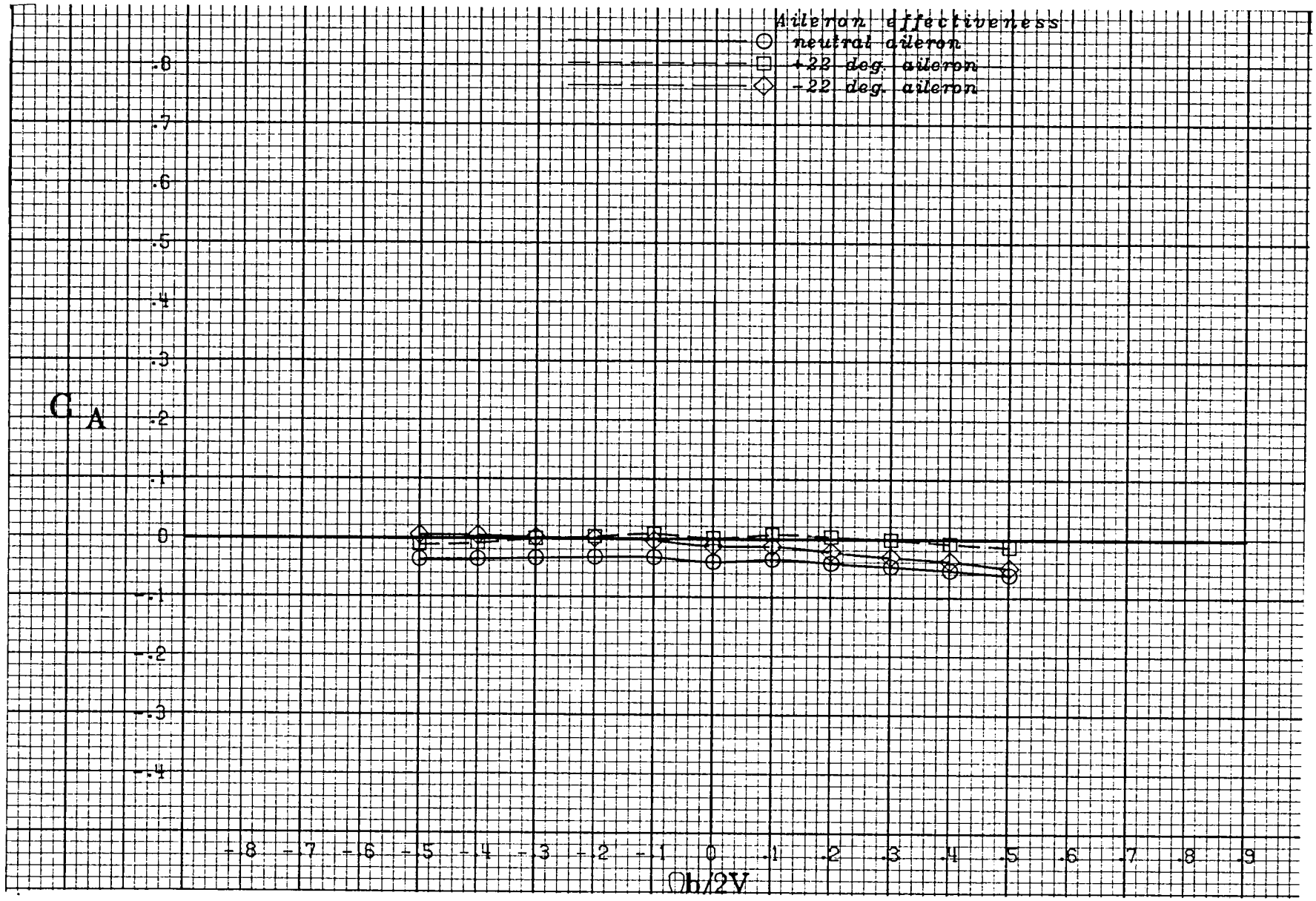

(h) α = 70 deg.

Figure A 30 .- Continued.

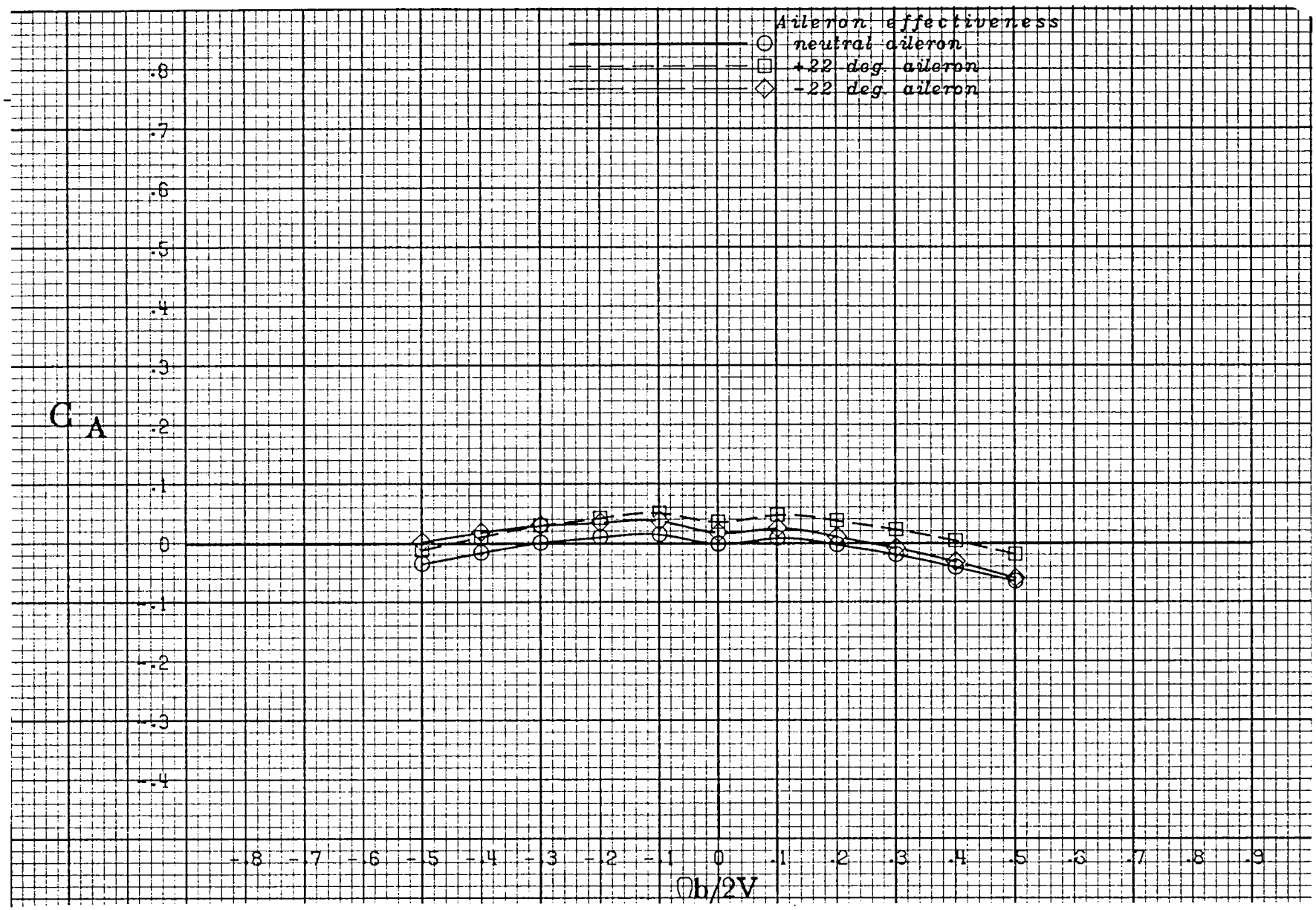

(i) α = 80 deg.

Figure A 30 .- Continued.

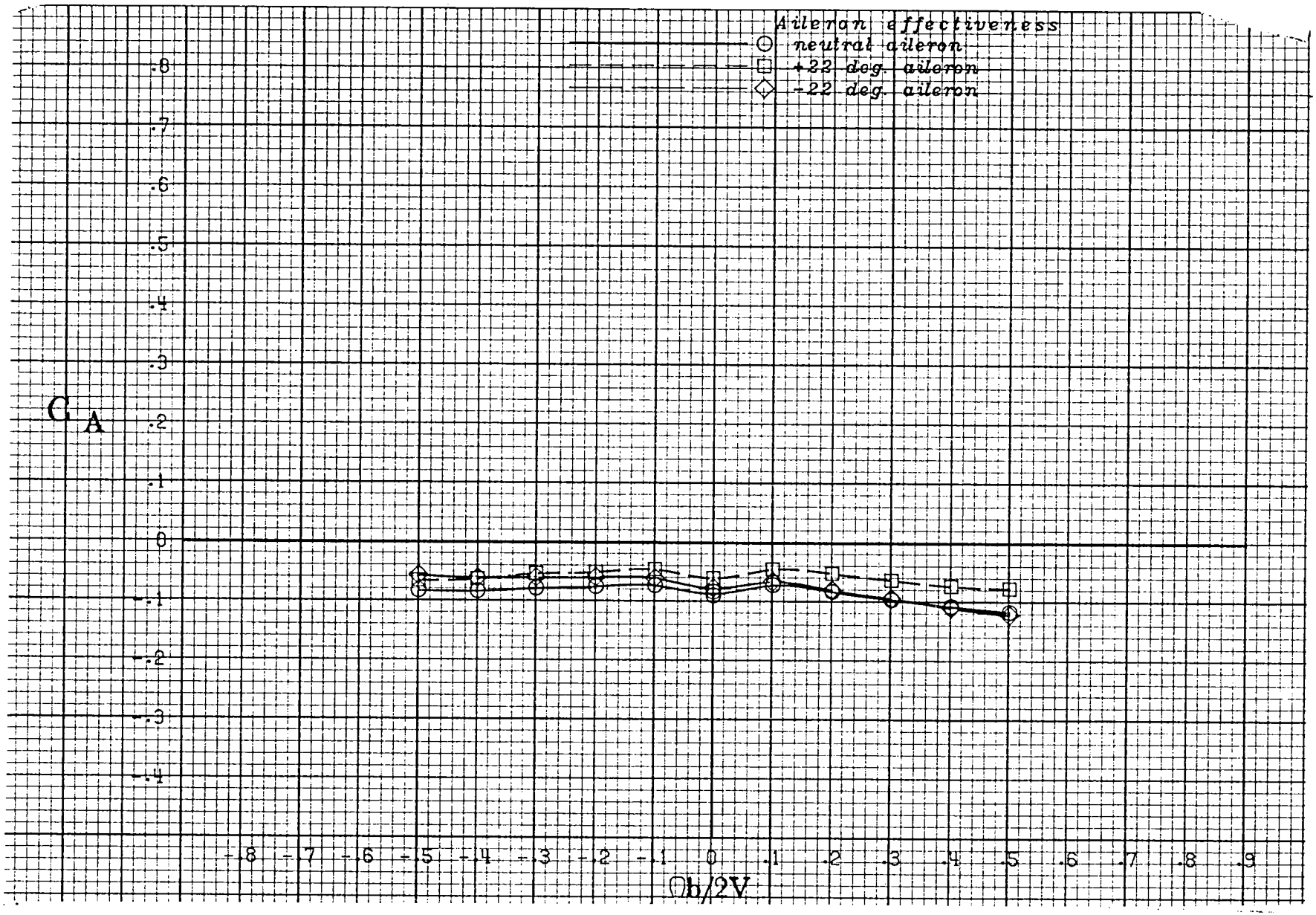

(j) α = 90 deg.

Figure A 30 .- Concluded.

1. Report No.	2. Government Accession No.	3. Recipient's Catalog No.
NASA CR-3248		

4. Title and Subtitle	5. Report Date
ROTARY BALANCE DATA FOR A TYPICAL SINGLE-ENGINE GENERAL AVIATION DESIGN FOR AN ANGLE-OF-ATTACK RANGE OF 20° TO 90°. III—Influence of Control Deflection on Predicted Model D Spin Modes	June 1984
	6. Performing Organization Code
7. Author(s)	8. Performing Organization Report No.
John N. Ralston and Billy P. Barnhart	
	10. Work Unit No.
9. Performing Organization Name and Address Bihrle Applied Research, Inc. 400 Jericho Turnpike Jericho, New York 11753	11. Contract or Grant No. NAS1-16205
	13. Type of Report and Period Covered Contractor Report
12. Sponsoring Agency Name and Address National Aeronautics and Space Administration Washington, D.C. 20546	14. Sponsoring Agency Code 505-43-13-01

15. Supplementary Notes

Langley Technical Monitor: James S. Bowman, Jr.

Topical Report

16. Abstract

The influence of control deflections on the rotational flow aerodynamics and on predicted spin modes is discussed for a 1/6-scale general aviation airplane model. The model was tested for various control settings at both zero and ten degree sideslip angles. Data were measured, using a rotary balance, over an angle-of-attack range of 20° to 90°, and for clockwise and counter-clockwise rotations covering an $\Omega b/2V$ range of 0 to 0.5.

17. Key Words (Suggested by Author(s))	18. Distribution Statement
General Aviation Spinning Rotary Balance High angle of attack wind tunnel data	Unclassified - Unlimited Subject Category 02

19. Security Classif. (of this report)	20. Security Classif. (of this page)	21. No. of Pages	22. Price
Unclassified	Unclassified	337	A15

N-305

For sale by the National Technical Information Service, Springfield, Virginia 22161

National Aeronautics and Space Administration

Washington, D.C.
20546

Official Business
Penalty for Private Use, $300

SPECIAL FOURTH CLASS MAIL
BOOK

Postage and Fees Paid
National Aeronautics and
Space Administration
NASA-451

NASA

POSTMASTER: If Undeliverable (Section 158 Postal Manual) Do Not Return